International Atomic Energy Agency

INDC(NDS)-151/L

INDC INTERNATIONAL NUCLEAR DATA COMMITTEE

PROCEEDINGS OF THE IAEA CONSULTANTS' MEETING ON NUCLEAR DATA FOR BORE-HOLE AND BULK-MEDIA ASSAY USING NUCLEAR TECHNIQUES

Krakow, Poland, 14 - 18 November 1983

Edited by

K. Okamoto

January 1984

IAEA NUCLEAR DATA SECTION, WAGRAMERSTRASSE 5, A-1400 VIENNA

Printed by the International Atomic Energy Agency
Vienna. Austria

January 1984
84-00755

PROCEEDINGS OF THE IAEA CONSULTANTS' MEETING ON NUCLEAR DATA FOR BORE-HOLE AND BULK-MEDIA ASSAY USING NUCLEAR TECHNIQUES

Krakow, Poland, 14 - 18 November 1983

Edited by

K. Okamoto

January 1984

Foreword

Nuclear techniques are now used as the basis for rapid identifications of many naturally occurring chemical elements on earth. In view of the current development of broad application of these techniques to exploration and exploitation of mineral resouces as well as for process and quality control in industry, and recognizing certain deficiencies in nuclear data needed for the reliable interpretation of analytical results of material exploration and assay, the International Nuclear Data Committee (INDC), at its last meeting in October 1981, recommended to the Agency to hold in 1983 a Specialists' Meeting on "Nuclear Data for Bore-hole and Bulk-media Assay Using Nuclear Techniques". Following this recommendation this Consultants' Meeting was convened by the Agency's Nuclear Data Section at the Institute of Physics and Nuclear Techniques of the Academy of Mining and Metallurgy at Krakow, Poland, from 14-18 November 1983. The meeting was attended by 27 nuclear geophysicists from 12 Member States representing the interest of relevant Government establishments, oil and other industrial companies, and academic institutes in the subject of the meeting.

The main objectives of the meeting was:

- to review the current requirements and status of nuclear (and atomic) data used in and required for the interpretation of analytical results of nuclear techniques applied to exploration, exploitation and processing of oil, gas, coal, ores and other mineral resources and materials;

- to identify the sources and assess the magnitude of uncertainties associated with the utilization and results of nuclear techniques such as neutron logging, γ-logging (including air-borne γ spectroscopy) X-ray analysis (X-ray fluorescence, energy dispersive X-ray fluorescence, X-ray diffraction, particle-induced X-ray emission), fission track method, activation analysis, analytical methods used in industrial process and quality control and other techniques and to compare quantitatively these methodical uncertainties with the uncertainties in existing nuclear data;

- to identify those nuclear techniques which are most suitable for developing countries and review the availability to these countries of nuclear (and atomic) data associated with these techniques;

- to formulate specific technical recommendations for needed future work after scrutinizing the nuclear (and atomic) data problems associated with the above-mentioned techniques.

The proceedings contain the review papers, the contributed papers presented at the meeting as well as the summary of the conclusions and recommendations of the meeting.

The Scientific Secretary of the meeting wishes to express his appreciation to the Polish authorities, the National Atomic Energy Agency and the Academy of Mining and Metallurgy in Krakow, for their kind assistance in the organization and preparation of the Meeting. His particular thanks and gratitude go to Prof. K. Przewlocki and his colleagues of the Institute of Physics and Nuclear Techniques of the Academy for their untiring help and excellent hospitality.

K. Okamoto
Scientific Secretary
of the Meeting
IAEA Nuclear Data Section

CONTENTS

Session V

APPENDICES

Appendix 1 (Contributed papers but not presented):

IAEA Consultants' Meeting on
Nuclear Data for Bore-hole and Bulk-media Assay Using Nuclear Techniques

Krakow, Poland
14 - 18 November 1983

Adopted Meeting Agenda

Monday, 14 November

Morning (10:00) Opening
Election of Chairman
Adoption of Agenda
Announcement

Session I: Introduction - Nuclear Data Requirement

[Review Talk]

1. "Introductory Talk" - some comments on the requirement for nuclear data in the earth science
   C.G. Clayton (AERE Harwell)

Session II: Nuclear technique application with emphasis on data requirement

[Review Talks]

1. "Nuclear data for oil and gas logging"
   R.L. Caldwell (Mobil Research & Development Corporation, Farmers Branch, Texas)

Afternoon

2. "Some application of atomic and nuclear methods in geology and mining"
   J. Csikai (Inst. Experimental Physics, Debrecen)

3. "Nuclear techniques in underground mining"
   K. Przewlocki (Inst. of Physics and Nuclear Techniques, AGH, Krakow)

[Contributed Papers]

4. "A case history of rock properties in an igneous metamorphic sequence"
   R. Peveraro (Britoil PLC, Glasgow)

Session III: Neutron techniques

[Review Talks]

1. "Remarks on some rock neutron parameters"
   J.A. Czubek (Institute of Nuclear Physics, Krakow)

Tuesday, 15 November
Morning (9:00)

2. "Recent progress in fast neutron activation cross section data"
   W. Michaelis (GKSS, Geesthacht)

3. "Nuclear petrophysics and interpretationally-metrological foundations of bore-hole radiometry"
   D.A. Kozhevnikov (Gubkin's Moscow Oil Chemical & Gas Industry Inst. Moscow)

[Contributed Papers]

4. "Silicon and aluminium determination in geological samples by 14 MeV neutron activation based on simple equipment"
   G. Pető (Inst. Experimental Physics, Debrecen)

5. "Measurements and calculations of neutron spectra in infinite media"
   S. Antkiw (Schlumberger-Doll, Ridgefield, Conn.)

6. "Application of the pulsed neutron-neutron method for determination of oil-water contacts in the bore-hole"
   Tran Dai Nghiep (Institute of Physics, Hanoi)

7. "Thermal neutron absorption cross-sections measured on rock samples and brines at the Institute of Nuclear Physics"
   J.A. Czubek (Institute of Nuclear Physics, Krakow)

8. "Calculation of neutron slowing down parameters and fast neutron spectra in rocks and soils"
   K. Morstin (Inst. of Physics and Nucl. Techniques, AGH, Krakow)

Afternoon

Session IV: γ-Measurement

[Review Talk]

1. "High resolution, low energy gamma-ray borehole spectroscopy"
   F.E. Senftle (US Geological Survey, Reston, Va)

[Contributed Papers]

2. "Gamma-ray spectrometry applied to down-hole logging"
   P. Dumesnil (Centre d'Etudes Nucléaires de Saclay)

3. "Lithological analysis of volcanic rock by the use of differential gamma-ray log"
   T. Itoh (JAPEX, Tokyo)

4. "Some comments on formation density measurement by gamma-ray interactions based on observations from Monte Carlo calculations"
   L.G. Sanders (AERE, Harwell)

5. "Airborne gammaspectrometry, evaluation and calibration"
   I. Wendt (Bundesanstalt für Geowissenschaften u. Rohstoffe, Hannover)

Wednesday, 16 November

Morning (9:00)

7. "Proposed potassium-uranium-thorium logging calibration facility for the petroleum industry"
   D.M. Arnold (Welex-A, Halliburton Co, Houston, Texas)
   -presented by R.L. Caldwell-

8. "Determination of the K_2O content of manganese ore by natural gamma-ray logging"
   J.A. Aylmer, C. Ceravolo, H. Charbucinski, P.L. Eisler and S.F. Youl (CSIRO, Melbourne)
   -presented by F.E. Senftle-

Session V: Others

[Contributed papers]

1. "A simple and rapid method of determining the thermal neutron absorption cross section of rocks"
   A. Kreft (Institute of Physics and Nuclear Techniques, AGH, Krakow)

2. "Experimental determination of photonuclear Yield excited by Bremsstrahlung with 20 MeV-Energy"
   E.R. Kartashev (the All-Union Inst. of Radiation Engineering, Moscow)

3. "On the sensitivity evaluation for on-stream elemental analysis using neutron and photoactivation techniques"
   E.R. Kartashev

Afternoon

Excursion to Salt Mine Wielitshka

Evening

Visit the Institute of Nuclear Physics.

Thursday, 17 November

Morning (8:30) & Afternoon

Session VI: Working Group Sessions

Preparation of Conclusions and Recommendations

Friday, 18 November
Morning (8:30)

Summary of Conclusions and Recommendations
Final Summary by Mr. Chairman (C.G. Clayton)
Closing
Visit to the Institute of Physics and Nuclear Techniques, Academy of Mining anbd Metallurgy

Chairmen of the Meeting:

C.G. Clayton (AERE, Harwell)

Chairmen of the Working Group Sessions

Group I "Applications" R. Peveraro (Britoil, Glasgow)

Group II "Microscopic Cross Sections" J. Csikai (Inst. Exp. Phys, Debrecen)

Group III "Macroscopic Data" J. Czubek (Inst. of Nucl. Phys. Krakow)

Group IV "Data Organization and Standards" R.L. Caldwell (Mobil Research & Development, Texas)

Scientific Secretary

K. Okamoto (Nuclear Data Section, IAEA)

Summary

Conclusions and Recommendations

IAEA CONSULTANTS MEETING ON NUCLEAR DATA FOR BOREHOLE AND BULK MEDIA ASSAY USING NUCLEAR TECHNIQUES

SUMMARY

A meeting of 27 specialist nuclear geophysicists representing 12 countries was held at the Institute of Physics and Nuclear Techniques of the Academy of Mining and Metallurgy at Krakow, Poland from 14th to 18th November, 1983.

Twentyfive papers were presented which dealt with the underlying science and technology of the application of nuclear techniques in minerals exploration, mining and process control. The papers were given by experts who were drawn from academic institutes of international reputation, from government establishments and from industry representing metalliferous minerals, oil producing and oil well logging companies. The topics discussed were a strong reflection of the continuing and important role of nuclear applications in the earth sciences and of the increasing number of techniques now available.

At the present time there is a growing need for accurate microscopic cross-section data for those nuclides and reactions which are required for the development of nuclear geophysical exploration methods and for on-line control and which have not yet entered into the sphere of interest of the nuclear energy industry.

In addition to a requirement for more accurate microscopic data, the interactions of neutrons and photons within rocks and ores can often be described conveniently by specific macroscopic parameters [such as neutron slowing down length (L_s) and thermal neutron macro absorption cross-section (Σ_a)] and these are becoming increasingly important, especially in the design of equipment and in the interpretation of data from a variety of measurement techniques. This situation is particularly true in the oil industry.

The major recommendations of the meeting can be summarised as follows:-

(i) Standard samples should be provided for an international intercomparison of methods of measuring the macro absorption cross-section (Σ_a) of rocks and the accuracy of each method of measurement should be established.

A special research project should be started to stimulate and co-ordinate the implementation of this intercomparison programme at different laboratories.

(ii) All available information on the measurement of Σ_a for rocks should be collected, together with existing data on other nuclear macro parameters and including a complete description of the rocks examined.

(iii) Computed macro parameters of synthetic rocks of increasing complexity should be accumulated using available and identified microscopic nuclear data.

(iv) An experimental program of benchmark measurements of neutron flux distributions in large simulated rock samples with well known constituents should be initiated. These measurements should be carried out under closely specified conditions of neutron source and rock configuration.

(v) There is an increasing requirement for more accurate neutron micro cross-section data (particularly fast neutron γ-ray production cross-sections) and support to implement this need is urgently required.

(vi) Urgent arrangements should be made to compile a catalogue of microscopic nuclear data specifically for use in nuclear geophysics.

Special attention was given to methods of analysing the mineral content of rocks by photo-neutron activation techniques. These techniques, which are currently being strongly investigated in the U.S.S.R. are a particular example of an area of application where more accurate nuclear data are required.

The importance of neutron sources is axiomatic in the field of nuclear geophysics. Whilst further attention to neutron-producing reactions and to the derivation of neutron energy spatial distributions, especially in a form suitable for bulk analysis is needed, it is recognised that compilation of such data is presently within the programme of the Nuclear Data Section of the I.A.E.A.

In conclusion it appears that nuclear geophysics is well established in the oil industry and is one of the most important disciplines underlying the continuing development of new techniques in oil well exploration and production. Its use in the wider field of minerals exploration, extraction and processing is increasing. Support for the above mentioned recommendations is thus strongly requested.

C.G. Clayton

Nuclear Geophysics Group,
AERE-Harwell.

OBSERVATIONS AND CONCLUSIONS

C.G. Clayton

OBSERVATIONS AND CONCLUSIONS

Following the formal presentation and discussion of the scientific papers, participants were separated into four groups each of which was given the task of commenting on specific aspects of the future needs for additional and more accurate data in nuclear geophysics.

The following is a summary of the conclusions.

MICROSCOPIC CROSS-SECTIONS

Much of nuclear geophysics is concerned with the interactions of neutrons and photons, and to some extent of primary and secondary ionising particles, in natural materials which have dimensions which are large compared with the mean free paths of the primary and secondary radiations.

Since one of the chief characteristics of natural materials is their elemental heterogeneity, which generally exists even in rocks of the same type, the problem of predicting the performance of equipment designed to respond to one or more analytes but which is also sensitive to other elements present in the rock matrix, is virtually impossible to any realistic degree of accuracy by referring solely to calibration measurements on 'standard' samples.

As a consequence of this situation the rôle of calculation in nuclear geophysics is vital and increasing, especially with the development of particle tracking programs and the decrease in size (and cost) of large memory computers.

It is axiomatic, therefore, that microscopic nuclear cross-section data on which many calculations depend should be available and accurate. Unfortunately this is not the case. Presently available nulcear data is a consequence of the growth of the nuclear power programme in which the requirements for nuclear data are somewhat different from those in nuclear geophysics. This point is developed in the introductory paper by Clayton et. al.

The requirement for more adequate nuclear data in nuclear geophysics has two principal origins. Nuclear data is needed to improve the accuracy of particle tracking programs and also to derive the precise yield of particular γ-rays on which calculations of the efficacy of analytical techniques depend.

Fortunately the sensitivity of particle tracking programs to uncertainties in the total and partial cross-sections of matrix elements can be examined by modified Monte Carlo programs and a series of investigations covering a range of typical operational situations and rock types is now required so as to give some guidance on the nuclear cross-section data which is in greatest need.

The requirement for γ-ray production data is easier to identify, although ranking the elements in order of urgency for new and more accurate data is difficult and subjective. In general, it is suggested that the most common elements should be considered first. There is a strong case for including most elements, ultimately, since those which are not of economic interest may occur as tracer elements to important minerals. Further consideration of this point is needed.

The following lists give some guidance to the present situation:

(i) Elements where no full evaluation is available

Ne, Zn, Ge, Tc, Pr, Er, Tm, Yb, Os, Ir, Hg, Tl, Po, At, Rn, Fr, Ra, Ac, Pa.

(ii) Fission product elements where some high energy data may be absent from evaluations

Se, Br, Rb, Sr, Ru, Pd, In, Sb, Te, I, Ba, La, Ce, Nd, Sm, Dy.

(iii) Elements for which the γ-ray production data are not yet evaluated

He, ^{11}B, Ne, Sc, Zn, Ge, Se, Br, Kr, Rb, Sr, Tc, Ru,
Rh, Pd, In, Sb, Te, I, Xe, Cs, Ba, La, Ce, Pr, Nd, Pm,
Sm, Te, Dy, Er, Tm, Yb, Lu, Os, Ir, Hg, Tl, Po, At,
Rn, Fr, Ra, Ac, Pa.

Among the neutron data the thermal neutron activation cross-sections are the most complete and accurate. For fast neutron energies the excitation functions even for the (n,p),(n,α) and (n,2n) reactions are often not sufficiently well known. There is a lack of data even around 14 MeV. For example, the integrated elastic scattering cross-sections have been determined directly for only 26 elements and the non-elastic cross-sections are known for about 50 per cent of the elements. Very few data are available for the neutron-induced γ-ray production and neutron emission cross-sections. There is a large spread in the available data on the (n,p), (n,α) and (n,2n) cross-sections.

For rocks in which there is a well developed thermal neutron flux and analysis by prompt thermal neutron capture γ-ray analysis is possible, thermal neutron γ-ray production cross-sections, apart from being generally available may not be required since on-site calibration of equipment is often possible using techniques which take account of variations in thermal neutron flux due to changes in formation density and moisture content, for example. However, the same situation does not prevail when analysis by fast neutron techniques have to be used, and this includes some common elements and important applications. One of the most pressing requirements, therefore, is to catalogue the specific γ-ray production cross-sections for (n,n'γ), (n,p) and (n,α) reactions from threshold energies to 20 MeV, in the first place for all common elements for which evaluated data does not presently exist.

Photonuclear cross-sections

There is increasing interest in the possibilities for using photonuclear reactions for minerals analysis both on-line and in borehole logging. Although significant development of equipment is required, especially for borehole logging, before a widespread application of photoneutron techniques can be contemplated, there now exists an important requirement for more accurate information on (γ,n) production cross-sections (initially to about 30 MeV) so that the analytical potential of these techniques for the analysis of natural materials in bulk can be evaluated.

Neutron targets

There are a number of important applications where the analysis of geological samples, such as drill core sections, requires an intense fast neutron flux for fast neutron activation analysis or, as an input to a moderator to produce an intense thermal neutron flux. Reactions such as $D(d,n)^3He$, $T(p,n)^3He$, $T(d,n)^4He$, $^7Li(p,n)^7Be$, $^9Be(d,n)^{10}B$ and $^{12}C(d,n)^{13}N$ are possible candidates. Although the neutron yields from these reactions are well documented, uncertainties in the thick target yields occur due to inadequate data on the variation of the stopping power of the ionised particle with energy in the target material. In addition, the integral neutron energy, space distributions for a range of target thicknesses are not available, although they are needed when irradiation of large volumes of rock is to be considered.

Atomic data

As well as a need for more accurate data on the stopping of energetic heavy ions in thick targets used for neutron production, as mentioned above, a similar requirement also exists in PIXE analysis. In addition, in this method there is also a need for more accurate data on ionisation cross-sections (especially for

X-rays near the absorption edges) and on the attenuation of low energy X-rays in the sample material.

MACROSCOPIC DATA

The very nature of the interaction of neutrons in bulk materials leads to a description of their gross behaviour by certain parameters which are defined in terms of the material composition and its physical properties (temperature, density, porosity, moisture content, for example) and one or more characteristics of the interaction mechanics. A list of the most important macro parameters in given in Table 1.

At the present time there is an urgent need in oil well logging for more accurate values of Σ_a of reservoir formation drill core samples as the accuracy of this parameter reflects directly on the accuracy of determining oil reserves.

There are several methods for measuring Σ_a of rock samples but most are still in the development phase and hence it is important for an early intercomparison of the various methods of measurement, based on a representative range of standard rock samples, to be undertaken as soon as possible.

There is also a need to acquire and catalogue the measured values of Σ_a for a wide selection of real rocks and at the same time to compare results with values computed from a careful analysis of the rock material.

For other macroscopic neutron parameters an intercomparison programme between the various calculational approaches, codes and nuclear data files and the existing experimental data would be valuable.

Although most of the current interest in macroscopic neutron parameters is for applications in the oil industry, it is forecast that similar needs will develop in other mineral industries as the impact of nuclear geophysics extends.

It is specifically recommended that the I.A.E.A. should:

(a) Provide standard samples for an international comparison of measured values of Σ_a for rock samples and establish the accuracy of each method of measurement.

(b) Collect all available measurements of Σ_a and other relevant nuclear data of rock specimens together with a complete description of the samples.

(c) Accumulate computed macroscropic data for synthetic rocks of increasing complexity.

(d) Initiate an experimental programme of benchmark measurements of neutron flux distributions in large simulated rock samples having a well known composition.

STANDARDISATION AND ORGANISATION OF NUCLEAR DATA

It is recognised that one of the deterrents to a wider application of nuclear techniques in minerals exploration, mining and processing is the difficulty of accessing particular nuclear data which is required in order to consider the viability of possible analytical techniques or to continue the development of a particular application. For macro transport parameters it is considered that there is merit in describing the experimental and calculational techniques used in their derivation.

Thus, there is a real need for a manual containing data relevant to nuclear techniques in nuclear geophysics. With such a manual available there should be a better chance of increasing the number and range of applications of nuclear geophysics by bringing opportunities for developing techniques and equipment more within the capability of the less sophisticated laboratories.

A possible skeleton for the contents of the proposal mannual is given below:

1. Gamma-ray production cross-sections

   (a) Tabulated data of cross-sections for the production of particular prompt and delayed γ-rays from thermal neutron capture.

   (b) Tabulated data and graphical displays of the cross-sections for the production of specific prompt and delayed γ-rays from (n,n'), (n,p), (n,α) and (n,2n) reactions, for example, from threshold energies to 20 MeV.

   (c) Tabulated yields of γ-rays from natural radioactive elements in parent-daughter equilibrium.

2. Photo-neutron production cross-sections

   Cross-sections and neutron energy spectra of (γ,n) reactions, tabulated in the first place up to an energy of 30 MeV.

3. Macro cross-sections and neutron transport parameters

   Values of macro cross-section and neutron transport parameters identified in Table 1 tabulated according to the lithological classification of a wide variety of rocks.

4. Gamma-ray transport parameters

   Tabulations of the following data:

   (a) Equivalent atomic number (Z_{eq}) of different rock types.

   (b) Mass attenuation co-efficients of γ-rays over an energy range from 0.1 MeV to 20 MeV in a range of typical types of rock.

   (c) Diffusion parameters for γ-rays over an energy range of 0.1 MeV to 20 MeV in a range of typical types of rock.

5. Neutron sources

Tabulations of:

(a) Isotopic neutron source data, including neutron energy spectra, lifetimes, specific activities and associated γ-ray yields.

(b) Accelerator neutron sources for particle and electron accelerators. Outline data of energy dependence of neutron yields and differential cross-sections for each reaction -

For (particle, n) sources to 5.0 MeV
For (electron, γ,n) sources to 30 MeV.

(c) Bibliography of sources of detailed data sets.

6. Description of experimental and computational methods for determining nuclear and petrophysical parameters of rocks

(a) Experimental techniques for methods of determining the parameters identified in Table 1; where relevant referring to range of application (rock type, depth of penetration, neutron source energy, etc.).

(b) Description of particle tracking programs for evaluating transport parameters of rocks.

(c) Outline description of deterministic calculations with emphasis on limitations imposed by boundary conditions for calculating nuclear and petrophysical parameters.

7. Bibliography of available nuclear data relevant to nuclear geophysical applications

C.G. Clayton

Nuclear Geophysics Group,
Nuclear Physics Division,
Harwell.

January, 1984

TABLE 1

NEUTRON MACRO PARAMETERS

Absorption cross-section	Σ_a
Transport cross-section	Σ_{tr}
Resonance absorption cross-section (atom density x resonance integral)	Σ_{I_o}
Fast neutron scattering cross-section	Σ_{sf}
Slowing-down power (average log. neutron energy decrement per collision (ξ) x macro fast scattering cross-section)	$\xi\Sigma_{sf}$
Moderating ratio	$\xi\Sigma_{sf}/\Sigma_{a,2200}$
Neutron slowing down length	L_s
Neutron diffusion length	L_D
Neutron migration length	M
Neutron slowing down time	t_s
Neutron flux decay time	
Neutron spectra	
Neutron-induced γ-ray spectra	

REVIEW PAPERS

SOME COMMENTS ON THE REQUIREMENT FOR NUCLEAR DATA IN THE EARTH SCIENCES

C.G. Clayton
B.H. Patrick
L.G. Sanders
M.G. Sowerby

Nuclear Physics Division, AERE-Harwell,
Didcot, Oxon, U.K.

ABSTRACT

The increasing application of nuclear techniques in the earth sciences, and especially the use of particle tracking codes, has focussed attention on the need for more accurate nuclear data and for data which particularly refer to elements of interest in the analysis of rocks and ores.

The present paper gives a brief summary of the current and potential requirement for nuclear data in nuclear geophysics and an indication of several important areas where better data would be valuable.

1. INTRODUCTION

The role of nuclear techniques in the earth sciences is well established and there is continual advancement, both in the range of applications and in the breadth and intensity of the underlying science and technology. The most outstanding successes have been recorded in the oil industry, especially from the efforts of international companies and dedicated national institutes. Applications in the coal and metalliferous and non-metalliferous mining industries, though considerably smaller, nevertheless show significant promise for the future.

Underlying these advances are the various nuclear energy establishments and academic institutes which have a responsibility for acquiring nuclear data, and specialised international agencies with a particular function in compiling and disseminating available information.

The continuing development of the application of nuclear techniques in the earth sciences, and in particular the relatively recent use of large computational programs, now poses the important question as to whether or not nuclear data requirements are being adequately satisfied by existing data evaluation programmes directed towards nuclear energy.

The problem of appraisal is not a simple one as the subject requires examination from the point of view of the range of applications in the earth sciences (some of which are widely divergent), the variety of techniques in use, the measurement accuracy required and various features of instrument design and use, for example. However, even from elementary considerations, it soon becomes apparent that, apart from micro cross-section data, there are a variety of 'macro' data which need to be evaluated in order to progress a more effective use of these techniques. In this category we can include the use of neutron migration lengths as link parameters in the design of porosity probes in oil well logging and the use of λ_o values (λ_o = total epithermal neutron flux per unit lethargy interval and unit thermal flux) to describe the shape of the neutron spectrum in different types of rock. In some cases the required parameter is well-defined but there are several options to the method of measurement and a systematic comparative study has yet to be made. This is the current situation in determining the macro absorption cross-section of rock samples.

A somewhat different example of a requirement for nuclear data arises from the lack of information on the effective moderating power of different configurations of irradiation cells in which, for example, rock specimens of different sizes can be placed prior to activation analysis. Optimisation data giving the moderating powers of different media for distributions of discrete isotopic neutron sources, or for an accelerator neutron target are not generally available.

The requirement for more data of this kind is not an academic one. At the present time the development and application of nuclear techniques and associated equipment in the earth sciences is mainly within the direction of specialised laboratories. It is axiomatic that the full extension of nuclear geophysics will only be achieved when the scientific bias in the subject moves more clearly into the area of a well documented technology. This implies that documentation must be relevant, complete and simple.

There are several examples of nuclear techniques being used routinely to determine non-nuclear data and it seems not inconsistent to include these within the scope of this topic. Probably the best known examples are the measurement of bulk density by (γ-γ) techniques and porosity and soil moisture by (n,n) methods.

Consideration of the availability and need for micro cross-section data inevitably leads to a comparison with data requirements in the nuclear energy field and some important similarities and differences can readily be established.

(i) The range of elements of interest in the nuclear energy industry is narrower than in the earth sciences where nearly all the elements in the Periodic Table may be encountered.

(ii) In general, in the earth sciences, applications concern elemental analysis and evaluation of bulk parameters. A wide variety of nuclear techniques are candidates for use. Neutron reactions which produce γ-rays are particularly important with point energy γ-ray production cross-sections being required. In contrast, in reactor core calculations and in shielding design, interest in γ-ray production is largely confined to estimates of the total energy dissipated.

(iii) In the earth sciences the dimensions of samples encountered for analysis vary from small (compared to mean free path lengths of particles and photons) to very large and include a wide range of source-detector configurations.

(iv) Also, the requirement for microscopic cross-section data is fairly strongly linked to the particular analytical technique. For example, there is only a weak demand for more data in energy dispersive X-ray fluorescence analysis whilst with (n,γ_{prompt}) techniques nuclear data appears to be a more important requirement in fast neutron than in thermal neutron reactions.

(v) The development and increased use of particle tracking and linked computer programs to evolve neutron and γ-ray flux and energy distributions for realistic rock formations and measurement configurations has placed increased emphasis on the accuracy of nuclear data, especially where calibration facilities and bench-mark measurements are not valid. Whilst this is a similar demand to that in the nuclear energy area, the data requirements may be different.

(vi) The use of sealed and continuously pumped ion accelerators in the earth sciences appears likely to increase in the future. Sealed neutron tubes which are used routinely in oil well logging will undoubtedly find a wider application if acceptable tube lifetimes can be obtained. Accelerators are currently being considered for analysing large geological samples (to give better representation of the mineral content of a potential ore body) and for ore sorting. In both types of application extensive data on neutron space and energy distributions is required to permit efficient large volume irradiation to be obtained.

Although dissimilarities in application between requirements in nuclear energy and in the earth sciences point to different needs and presentation of nuclear data, it is fortunate that much of the required micro data has been evaluated and recommended values are available in computer based files. A few comments on the organisational structure relating to the evaluation and dissemination of microscopic nuclear data are worthwhile.

An international network of four data centres (Table 1) now exists to collect experimental and evaluated data and a Computer Index of Nuclear Data (CINDA)(1) is available which lists the literature and computer files on microscopic neutron data. CINDA 83 (1977-1983) also contains a useful list of neutron data handbooks covering neutron-induced reactions, decay properties and photon-induced reactions. Another useful index on computer files is the Index to Large Evaluated Data Files(2). The published list is now somewhat out of data but a current list can be obtained from the Data Centres.

Nuclear structure and decay data can also be important and these are evaluated and disseminated by the International Nuclear Structure and Decay Data Network which is co-ordinated by the Nuclear Data Section of the International Atomic Energy Agency. An up-to-date list of compilations and evaluations in this area is available(3).

Although much of the data for earth science applications may have been derived and in some cases assessed to provide recommended values, it may not be in an appropriate form for use. Much experimental data have been obtained by techniques which were adequate to meet original requirements, but which are generally unsatisfactory for present needs. For example, γ-ray spectra derived by using NaI(Tl) scintillators are often of little value for interpreting spectra obtained using Ge detectors.

There is now a wealth of expertise around the world on the assimilation and evaluation of nuclear data and it is vital that this is consulted before new data is adopted for uses for which it was not initially designed. There are many examples where unsuitable and inaccurate data have been incorrectly used. Many countries have Nuclear Data Committees(4) and it is strongly recommended that the members of these committees should be consulted wherever appropriate.

It is well outside the scope of the present paper to give a detailed review of the degree of fulfilment and the future requirement for data in the earth sciences. Comment has therefore been restricted to the more obvious areas where improved data might seem to lead to an increased probability of effectiveness and acceptance of nuclear techniques.

2. MICROSCOPIC CROSS-SECTION DATA

The need for accurate data on micro cross-sections varies greatly according to the technique and the area of application. In general, accurate micro data is required to assist basic calculations on the expected performance of measuring equipment and to allow the transfer of well identified results from calibration and bench-mark experiments to real measurement situations.

The requirement is more intense when penetrating radiations are used and when the analytical model does not allow calibration standards: though there are exceptions to this generalisation.

Three simple examples will illustrate the point:-

(i) In energy dispersive X-ray fluorescence analysis, interpretation of the observed spectra may be difficult due to matrix or particle-size effects, for example, but this is a problem of the technique. Experimental results can usually be reliably compared with the data obtained from a set of accurately prepared samples. Better fluorescence yield or absorption cross-section data is then of little value. Within the range of applications presently encountered, the role of calculation to determine yield results is generally minor.

(ii) The situation in proton-induced X-ray emission (PIXE) analysis is somewhat different. With thin samples the incident protons suffer a negligible energy loss and so an approach similar to that referred to above is possible; calibration requiring merely the bombardment of thin single-element standards to obtain a calcellation of ionization cross-section and other parameters between specimen and standard. However, in the analysis of thick samples the X-ray yield is the integral of intensities reaching the detector from successive interactions along the ion track and when the composition is complex and X-ray attenuation coefficients are large the use of standard materials is no longer reliable.

An assessment of the uncertainties when using PIXE for thick sample analysis has recently been carried out(5) in which experimental aspects such as current integration and detector efficiency and the data base of proton stopping powers, ionization cross-sections and X-ray attenuation coefficients have been considered. Overall errors in thick target yields from uncertainties claimed by authors from commonly used ancillary data sets is estimated to lie between 10% and 15% and this result is supported by independent measurement of trace element concentrations in two light matrices of known composition.

An analysis of the origin of uncertainties in thick sample PIXE analysis has recently been published by Campbell et al(6) and Table 2, reproduced from their paper, lists various causes of uncertainty and their possible magnitude. It appears that more accurate values of L sub-shell cross-sections and low energy X-ray attenuation coefficients, especially near absorption edges is required.

(iii) In multi-element analysis of coal by (n,γ_{prompt}) techniques, *it can be shown(7) that, with some generally* acceptable assumptions, the concentrations of virtually all the important elements except oxygen can be determined by measuring the γ-ray intensities from thermal neutron capture. Perturbations in thermal neutron flux are unimportant if the material is intimately mixed and a 1/v cross-section is assumed. However, to include oxygen which is important in achieving the full applicational viability of the technique, the γ-ray yield from the $^{16}O(n,n'\gamma)$ reaction is used and linked to the observed thermal neutron derived γ-ray spectrum through, for example, the $^{28}Si(n,n'\gamma)$ and $^{28}Si(n,\gamma)$ or the $^{12}C(n,n'\gamma)$ and $^{12}C(n,\gamma)$ reactions. Invariance in the fast neutron spectrum throughout the differing operational conditions is thus invoked. In calculating the probable accuracy of a potential operational measurement system, a knowledge of the relevant $(n,n'\gamma)$ cross-sections for yield of identified γ-rays for point neutron energies from the lowest reaction threshold to the highest source energy is required.

This latter example illustrates a more general situation in bulk materials analysis when both thermal and fast neutron reactions might be considered. In rocks which are highly moderating and all significant elements can be determined by thermal neutron capture reactions, variations in thermal neutron flux are either unimportant or can be allowed for by calibration. In a calculational approach to the same situation uncertainties in the cross-sections of matrix elements also tend to be unimportant since the consequent uncertainties in thermal neutron flux affect all nuclides equally. However, when prompt γ-rays from fast neutron interactions offer the main analytical route, calculation of the analytical precision of the measurement then requires the availability of accurate nuclear data, since the γ-ray yield is a strong function of neutron energy and the neutron energy spectrum may vary for a variety of reasons, such as change in composition and variation in the (low) hydrogen content. Fast neutron techniques are required for analysis when:-

(i) They are the only techniques available for determining the concentration of a particular analyte.

(ii) *The rock formation is weakly moderating, and*

(iii) One or more elements are present in the rock with total thermal neutron capture cross-sections sufficiently high to form a strong thermal neutron sink. This situation tends to occur in seabed analysis. Chlorine is the critical element which not only provides the sink but, in addition, chlorine γ-rays tend to dominate the γ-ray spectrum.

The use of fast neutron activation analysis of selected elements at low concentration in some rock types has focussed attention both on the purity of available neutron source spectra and on the accuracy of the initial yield from threshold reactions.

The analysis of gold in the ppm range in quartzites by the reaction $^{197}Au(n,n'\gamma)^{197m}Au \rightarrow$ 279 keV γ-rays, $T_{\frac{1}{2}}$ = 7.8s is a particular example. The cross-section for this reaction and for the $^{28}Si(n,p)^{28}Al \rightarrow$ 1779 keV γ-rays, $T_{\frac{1}{2}}$ = 2.3 min and the $^{27}Al(n,p)^{27}Mg \rightarrow$ 1014 keV and 844 keV γ-rays, $T_{\frac{1}{2}}$ = 9.46 min reactions which are potentially interfering are displayed in Fig. 1. Since the aluminium concentration may be 5 x 10^4 times and the silicon concentration 5 x 10^5 times greater than the gold concentration, an accurate knowledge of the source neutron spectrum is clearly desirable to avoid significant interference. An upper energy limit to the source neutron spectrum which is below the $^{28}Si(n,p)$ threshold is required, but some overlap of the $^{27}Al(n,p)$ reaction may be acceptable in order to maximise γ-ray yield from the gold. In such a situation accurate information on the shape of the $^{27}Al(n,p)$ cross-section at the threshold energies is desirable. It is not presently available. It is, of course, precisely in this region where measurement of the cross-section is difficult.

The reactions $D(d,n)^3He$, $T(p,n)^3He$ and $^7Li(p,n)^7Be$ are possible candidates for neutron sources for use in the above application. Although the neutron yields from these reactions are well documented, the integral neutron energy, space distributions for a range of target thicknesses are not available, but they are needed when irradiation of large volumes of rock is considered.

Although, in general, techniques can be identified in which there is a need for micro cross-section data, the question must be asked of how accurate the data needs to be and whether or not the requirement is specific to a particular elemental matrix and analytical problem. Fortunately the means of answering these questions is now available in the sensitivity option to the MCBEND(8) Monte Carlo code known as DUCKPOND(9). Sensitivity coefficients may be requested for any type of collision or partial cross-section and with any nuclide at any energy. However, to keep the number of sensitivity coefficents finite, constraints must be specified for the uncertainties on the nuclear data. As the codes can cope with highly complex geometrical configurations, sensitivities to uncertainties in partial cross-section data can be examined in accurate models of real measurement situations.

2.1 Some examples of the availability of nuclear data

In general, the requirement for nuclear data arises from a need to:-

(i) predict neutron flux and energy distributions, and

(ii) derive specific γ-ray yields.

To meet the first requirement it is necessary to provide data in a computer compatible format which present all significant neutron cross-sections over the entire energy range of interest, e.g. from 10^{-4} eV to ∿20 MeV. Such data are available in evaluated data libraries where, for each nuclide, experimental data have been assembled to form a recommended ('evaluated') data set. In many cases gaps in the experimental data have been filled by calculation.

It is not possible to judge quantitatively whether or not available files are of good quality, but it is possible to judge whether data which might be required are available or missing.

To do this we have organised the evaluated data into two main categories:-

(i) full evaluations which give all significant cross-sections, and

(ii) gamma-ray production cross-sections.

It is most convenient if all data are given in the same evaluation, but at the present time only the more recent files in the ENDF/B series [versions 4 and 5] and files in the ENDL Library normally give γ-ray production cross-sections. Since ENDF/B files are in the most widely used format these are the ones referred to in Table 3 where it can be seen that for Z=1 to Z=92 there are at least 19 and maybe up to 35 elements for which there are no full evaluations (although 8 of these do not occur naturally) and there are a total of 45 elements where γ-ray production data are not evaluated.

A detailed analysis of the data content for each nuclide is outside the scope of this paper, but an indication of the range of information available can be obtained by examining a few elements which have different relevance in earth science applications. As examples we examine the status of the cross-sections of carbon, silicon, zinc and fluorine.

(i) Carbon

The ENDF/B-5 file on carbon (MAT 1306) contains data on γ-rays produced by neutron capture and by inelastic scattering.

(n,γ) The thermal neutron capture γ-ray spectrum is given and assumed to be applicable at all neutron energies up to 20 MeV. Primary γ-rays are identified and provision is made to increase their energies in line with the kinetic energy of the incoming neutron so as to conserve total energy. The assumption that the γ-ray spectrum from thermal capture can be used at all neutron energies is probably satisfactory as the capture cross-section is thought to be 1/v up to at least 1 keV and in any case is generally very small ($\lesssim$0.1 mb) above that energy.

(n,n'γ) The cross-section for the production of the 4.44 MeV γ-ray from the first excited state of ^{12}C is given as a function of neutron energy from the threshold energy to 20 MeV. The data shown in Fig. 2, are based on measurements by Morgan et al$^{(10)}$ using a NaI(Tl) scintillation detector with an overall uncertainty of $\sim$10%. Angular distribution data for the 4.44 MeV γ-ray are also given in the form of Legendre coefficients at a number of neutron energies between the threshold and 20 MeV.

It is concluded that the data on γ-ray production are probably adequate for most applications in the earth sciences.

It is likely that the situation regarding the neutron energy dependence of the capture spectrum as assumed for carbon is a common one and applies to many of the elements listed in Table 3 for which capture spectrum data are given. The assumption that the thermal spectrum is valid at all neutron energies may be adequate for some earth science studies, but it could lead to problems where significant resonance capture occurs.

(ii) Silicon

Silicon is an important element in earth science applications and the evaluation in the ENDF/B-4 Library (MAT 1194) contains a considerable quantity of γ-ray production data.

(n,γ) Neutron capture γ-ray spectra are given for all energies up to 20 MeV. Between 10^{-5} eV and 50 keV, the evaluated data are based on several measurements in Maxwellian thermal neutron spectra. From 50 keV to 1 MeV, the spectrum adopted has its origins in a measurement by Lundberg and Bergqvist$^{(11)}$ using a NaI(Tl) detector to study fast capture above 1 MeV neutron energy. Between 1 and 20 MeV, the photon spectrum is assumed to be the average of those selected for the two lower energy regions. In each of these three neutron energy ranges, photon intensities are given for 42 discrete γ-rays with energies from 0.752 to 10.61 MeV. These spectra cover the most important γ-rays above 0.5 MeV emitted following capture in silicon.

The assumption that the thermal neutron capture γ-ray spectrum applies to energies as high as 50 keV is probably acceptable for present applications as resonance neutron capture is small and there are few resonances below 10 keV. The capture cross-section is therefore likely to be close to 1/v in the low energy region.

(n,n'γ) Up to 3 MeV incident neutron energy, production cross-sections are given for 7 discrete γ-rays ranging in energy from 0.755 to 2.425 MeV. It is not clear whether the data were obtained from experimental measurements or from calculation. Above 3 MeV, the total γ-ray production cross-section is provided as a function of neutron energy and, at each of the specified energies, a γ-ray spectrum is given in 50 keV energy bins. These data were obtained from nuclear model calculations using a Hauser-Feshbach code and including direct interactions.

At first sight, spectra summed over 50 keV intervals may seem to be unsuitable for application in which high resolution Ge detectors are used. However, such data may be adequate in situations where a single γ-ray dominates an energy bin. This may be the case for the strong 1.779 MeV γ-ray from the first excited state in ^{28}Si. It is to be noted that the intensity of the 1.75-1.80 MeV bin is always at least 10 times greater than that in neighbouring bins and frequently more than 100 times greater. However, it must be remembered that the data are from calculations, probably not backed up by experiment, and it is doubtful if such calculations are accurate to better than 100% for the production of a particular γ-ray.

The cross-section for the production of the 1.779 MeV γ-ray is given in Fig. 3.

($n,n'\alpha\gamma$) The ($n,n'\alpha$) reaction in silicon sometimes leaves the residual nucleus in an excited state giving rise to a prompt γ-ray which may be useful as a signiture of the element. The threshold for the reaction is $\sim$10 MeV. Total γ-ray production cross-sections are given at a number of neutron energies between threshold and 20 MeV. At each energy, a photon energy spectrum is given in 50 keV bins. However, as the possible number of γ-rays which can be emitted is limited to only a few, the spectra effectively give data on discrete energy γ-ray emission. The statistical model was used to calculate the cross-sections for leaving the ^{24}Mg nucleus in the various possible excited states and then the experimentally known γ-ray decay branching ratios used to estimate the γ-ray intensities. The uncertainty in the γ-ray production cross-sections then arises almost entirely from the calculation of the cross-sections for feeding the excited states, the magnitude of the uncertainty being $\sim$100% or higher.

($n,n'p\gamma$)
($n,\alpha\gamma$)
($n,p\gamma$)
The evaluated data for these reactions are specified in an exactly analogous way to those for the ($n,n'\alpha\gamma$) reaction.

In all the above reactions, the photons are assumed to be emitted isotropically.

Summarising, it can be seen that much of the data for γ-ray production from silicon rely on calculations using nuclear models and it remains to be seen if the data are of sufficient accuracy for earth sciences use.

The need to use calculated data is likely to be quite common, being the only source for many of the elements given in Table 3 as having ($n,n'\gamma$) cross-sections.

(iii) Zinc

Zinc is an example for which no full evaluation of even the cross-sections of the natural element exists. In fact, this situation appears, from information in the Index to Large Evaluated Data Files, to be true for all the stable isotopes of zinc. Table 3 indicates that there are at least 19 elements in this category. For many of these, there are almost certainly measurements of the total and partial cross-sections which could form the basis of an evaluation, with theory being used to fill in the missing data. The absence of such an evaluation presumably indicates that the need has not arisen in the nuclear industry. Since zinc is not an uncommon element and has wide industrial use, there seems to be a strong case for undertaking a more complete evaluation.

(iv) Fluorine

Fluorine is an example of an element which can be identified by decay γ-rays emitted by a radioactive residual nucleus produced by charged particle emission following a fast neutron interaction. The most commonly used γ-rays are the 1.357 MeV emitted from the decay of ^{19}O($T_{\frac{1}{2}}$ = 26.9s) produced by the ^{19}F(n,p) reaction, and the 6.13 MeV γ-ray from ^{16}N decay ($T_{\frac{1}{2}}$ = 7.13s) following the ^{19}F(n,α) reaction. If it is desired to estimate the yield of these γ-rays by calculation, then clearly one needs to know the ^{19}F(n,p) and ^{19}F(n,α) cross-sections as a function of neutron energy and the γ-ray branching ratios of the residual nuclei. It is probably safe to assume that the latter are known with sufficient accuracy and the main error in the yields arises from uncertainties in the cross-sections if we neglect the effect of other materials present.

The cross-sections for (n,p) and (n,α) reactions are given in the ENDF/B-4 evaluation (MAT 1277) as a function of neutron energy from the threshold energies up to 20 MeV. In both cases, the evaluations were based on curves drawn through the available data, which exhibit structure, supported by theoretical calculations which agree with the gross structure up to 16 MeV. The cross-sections are shown in Fig. 4.

2.2 Some comments on the accuracy of available nuclear data

It is very difficult to make any general statement on the accuracy of available data as uncertainties vary depending on a number of factors, especially the historical importance of the data. Nevertheless, the question is sufficiently relevant to justify some comment, but it must be emphasised that the uncertainties quoted below are mainly guidelines and the situation for particular nuclide interactions may be different.

The nuclear data in the evaluated files can be divided into two broad categories:-

(i) One for which experimental measurements exist, and

(ii) One for which measured data are scarce, or not available.

In case (i), the uncertainties in the data are related to uncertainties in the measurements and each case has to be considered individually.

Thermal neutron capture γ-ray spectra fall into this category, data being available for a considerable range of elements. In (ii), theoretical models must be used to provide the required values and in this case it is possible to make some general comments on achievable accuracies.

As calculations are frequently used to derive fast neutron interaction data, particularly production cross-sections for specific γ-rays, we shall concentrate on that process, paying most attention to inelastic scattering.

Neutron reactions up to a few MeV at least are dominated by compound nucleus effects and in these cases the statistical model is widely used. At higher neutron energies pre-equilibrium effects begin to play a significant role and appropriate models are now being developed to deal with this situation.

In the compound nucleus region, the total inelastic cross-section can be calculated to within ∿20%. For specific levels, which may have vibrational or rotational characteristics, requiring the use of coupled channel codes, the uncertainty could rise to ∿40%. If correlations between the entrance and exit channels are present (which means that the compound nucleus model does not apply) then an additional uncertainty of ∿50% might be included. These figures are applicable when some level density information is available for both the compound and residual nuclides, but if systematics have to be used for this information, then the uncertainties might be larger.

The γ-ray production cross-sections depend on the decay of the residual excited states as well as on the cross-sections for formation of those states. If we are interested in a particular γ-ray, then the cascade of γ-rays must be taken into account and here model dependent selection rules can come into effect. This may introduce uncertainties by factors of 2 or 3, or even more. If many levels contribute to the cascade, the uncertainty due to statistical effects will be reduced.

As those energies where only a few low lying excited states participate, the γ-ray branching ratios may be known quite accurately from experiment. In these cases, the uncertainty in the production of a particular γ-ray will arise entirely from uncertainties in the inelastic cross-sections for feeding those states.

Another way of approaching the calculational problem is to consider the fact that the compound nucleus formation cross-section can be estimated to ∿ 10% up to the highest neutron energies required in the present area of applications. The compound nucleus cross-section is composed of only compound elastic, inelastic and capture processes at energies below (n, charged particle) or (n,2n) reaction thresholds, if fission is ignored. In the MeV region, neutron capture cross-sections are small and, therefore, if knowledge of the elastic scattering cross-section exists, the compound nucleus formation cross-section can be used to provide details of the total inelastic cross-section. If the production of a discrete energy γ-ray is required, then the remarks above also hold.

At neutron energies where pre-equilibrium effects are present, then the calculational problem is even more acute than when the compound nucleus model can be used. Parameters for the pre-equilibrium model are generally obtained by fitting to measured data and in many of the cases of interest in the earth sciences, such data do not exist.

The calculation of (n, charged particle) cross-sections followed by prompt γ-rays will suffer from the same problems as in inelastic scattering, but in addition the characterisation of the Coulomb barrier particularly near threshold will introduce another uncertainty. It seems likely that the estimation of cross-sections to specific excited states could be in error by a factor two. If then the γ-ray branching has to be estimated from calculation, the uncertainty in the production of discrete γ-rays will be further increased.

Thus, it is unlikely that even in the most favourable situation, the cross-section for production of a discrete γ-ray is known to better than 10%. Where calculations have to be used, the achievement of 20% accuracy will be possible in only a few cases and in the remainder, errors of 50% or even factors of several times may be more typical.

3. DATA RELATING TO NEUTRON REACTIONS IN BULK MEDIA

The interpretation of neutron interactions in bulk media underlies much of the effort now being devoted to extending the application of neutron techniques in the earth sciences.

If the formation parameter to be determined is the only variable then calibration is relatively simple and the response of a probe, for example, can generally be established for a range of the parameter of interest. However, when there are several independent variables calibration and interpretation becomes a major problem and strong perturbations in neutron flux, energy distributions can be expected. Typical perturbating factors include:-

(i) variations in rock type

(ii) variations in density

(iii) changes in formation fluid and fluid content

(iv) the occurrence of strong neutron absorbers, and

(v) the effect of the measuring device itself and the dimensions and condition of the access hole.

A purely analytical approach to resolving the effect of such massive influences on the neutron field is virtually impossible for realistic situations, but a quasi-theoretical approach based on known values for macro neutron parameters of rocks (such as slowing down length, diffusion length, absorption and scatter cross-sections) offers a possible route to success and an important contribution in this area has recently been developed by Czubek(12).

An alternative approach is to use Monte Carlo and coupled programs, which have the advantage of allowing consideration of realistic situations, to determine the effect of each parameter on instrument response and thence to establish the corresponding relationships between the various parameters. The end point of this in oil-well logging, for example, is to build-up a set of departure curves. Along with suitable bench-mark experiments and calibration data (and with other operational data often available from core analysis, e.g.) a closer approach to formation evaluation can generally be obtained.

Whichever approach is adopted, a catalogue of information on macro neutron interaction data is extremely valuable, both in helping to steer an approach to interpretation and in carrying out a preliminary assessment of the potentially best approach to resolving a particular problem in formation evaluation.

In this paper we have limited our comments to the more important neutron parameters and their value in some common rock types. We believe that a more comprehensive catalogue would be valuable.

3.1 Nuclear properties of some formations

3.1.1 Standard rocks

The average values of elemental abundancies in some typical rocks are given in Table 4 and their nuclear characteristics in Table 5 in which the the macro cross-sections and other parameters are also defined. It is evident that the rocks have macro absorption cross-sections $\sim 1 \times 10^{-2}$ cm^{-1} and macro scattering cross-sections ~ 1 cm^{-1}. Compared with these rocks, pure water has large absorption and scattering properties, though still of the same order. For sea water the absorption increases by several times while there is little change of scattering.

The penultimate column of Table 5 is a measure of the "slowing-down power" (product of macro fast scattering cross-section and average logarithmic energy decrement ξ per collision). This indicates how well the material moderates neutrons: water is seen to be much more proficient than dry rock. But an intense thermal neutron group is not built up if, on being moderated, the neutrons are rapidly absorbed. A well-moderated neutron spectrum therefore occurs if high slowing-down power is accompanied by low thermal neutron absorption. The parameter which characterises this principle is the "moderating ratio" defined by $MR = \xi\Sigma_{sf}/\Sigma_{a.2200}$.

If MR is in excess of about 10 the spectrum can be accepted as "well-moderated". Table 5 thus illustrates the high moderating ratio of pure water and the smaller value of sea water. Moreover it can be expected that, in some dry or very low porosity rocks, the neutron spectrum will be "hard" (poorly moderated) and that the influence exercised by the epithermal group should then be considered.

3.1.2 Average dry rocks

If the typical dry mixes of Table 4 are used to calculate nuclear characteristics some of the relative contributions of the individual nuclides can be deduced and these are set out in Tables 6 and 7. Most of the large contributions to absorption in Table 6 are to be expected; for example Fe in all cases, Si in all except limestone, and Ca in limestone. Also K can contribute strongly, particularly in granite.

Hydrogen is of special interest in dry rocks, since its abundance is uncertain and variable while its contribution to nuclear characteristics can be significant. This applies especially to the slowing-down power (Table 7); for the shale example (0.28 wt% H) the hydrogen contributes over 76%. For all the dry rocks there are small contributions to the slowing-down power (<4%) from anything other than O, Si, C, H and, with the exception of limestone, O and H are the main contributors.

3.1.3 Additional neutron absorbers

The rocks of Table 5 have relatively low absorption cross-sections. In practice, neutron absorption maybe enhanced by additional rock-forming elements and by the possible presence of low abundance high absorbers (neutron poisons) such as B and Gd.

Absorption in the dry sandstone of Table 4 exceeds the value for pure silica, weight for weight, by 71%. For dry limestone and calcite the corresponding figure is 23%. The effects of neutron poisons can be even greater. In calcite, say, the enhancement of thermal neutron absorption by 5 ppm Gd is 35.9% and by 75 ppm B it is 121%.

An analysis of rock constituents to determine the thermal neutron absorption is not an easy task. However, Monte Carlo studies are often conducted with precise knowledge of simulated rock, since this is assigned by the user, and can be employed to investigate the significance of uncertainties relating to the constituents of actual rocks. In addition, for computer experiments which are intended to simulate a particular real formation of which samples are available, it is usually not necessary to analyse for very low abundance elements in order to provide sufficient data for the slowing-down energy region. To do so would not significantly affect the macro scattering cross-section and the resonance escape probability is high.

This would apply to a neutron poison such as Gd which has a very high thermal neutron absorption cross-section, but not a resoance integral to match. A 1/v absorber such as B can prove to be an exception. Its resonance integral is about the same as that of Gd but its atom number density in rock can be much higher. These points are illustrated in Table 8.

For the thermal group good values of macro absorption and total cross-sections can be derived by the pile-oscillator technique and used directly as input for a Monte Carlo computation. To employ this technique only small formation samples are required since the sample macro neutron cross-section would normally be ∿0.5-1.0 cm^2 corresponding to ∿200g of rock for an absorption measurement. At increased cost smaller sample sizes can easily be handled.

3.2 Neutron flux distributions

Of primary interest in bulk minerals analysis is the derivation of neutron flux spatial distributions from which other differential or integral data may be calculated. An example is given in Fig. 5 which shows the computed radial distributions of thermal neutrons for a point monoenergetic source in pure-water saturated sandstone at four values of porosity. Data of this kind provide a useful indication of the penetration of neutron flux and the relative detector countrates to be expected at different distances from the source. The cross-over regions are evident where the flux is the same for two quite different porosities.

Thermal neutron flux distributions for a point ^{252}Cf source in pure water and in sea water are displayed in Fig. 6. The flux depression due to chlorine in the sea water is clearly seen.

The next step in formulating a more realistic picture of neutron flux distributions is to add a borehole and the effect of this is shown in Fig. 7 for a ^{252}Cf source and a coal described in Table 9. The high thermal neutron flux when the borehole is water-filled is clearly evident as is the significant decrease when the ash content is increased from 10% to 40% ash.

3.3 Characteristic lengths in neutron transport

Evaluations of characteristic lengths are of assistance in identifying the spatial regions having most influence on the response of a neutron logging tool. Moreover, the results can be used to support the development of expressions for neutron flux distributions which provide interpolation of Monte Carlo results and a physical understanding of the transport processes involved. Neutron characteristic lengths are of special interest in oil-well logging for appraisals of the performance of tools which are designed to be insensitive to borehole effects and to be responsive mainly to the neutron transport properties of the formation. A good example is the dual-spaced thermal neutron porosity tool, for which the near/far detector count-ratio is expected to respond in this manner(13).

If it can be stablished for a given logging tool that the response bears a one-to-one relationship with some neutron parameter which characterises the formation, then a powerful predictive and diagnostic method becomes available. The computation of actual tool response is normally not possible by deterministic methods and is relatively expensive by Monte Carlo techniques. If tool response can be deduced from an easier computation, namely of a characteristic neutron parameter, then time and cost are reduced and the results apply to all similar tools.

If tool response can be related to a neutron characteristic length of the formation then computations of the latter allow response to be predicted in a wide variety of formations. This approach opens the way to rapid studies on the magnitudes of response perturbations, such as excavation effects and low concentration thermal neutron poisons.

3.3.1 Slowing-down length

In general, theoretical expressions for neutron slowing-down lengths are not in good agreement with experiment or are burdensome to evaluate. But a slowing-down length can be defined in terms of the second spatial moment of the flux at the final energy region. If in some way a neutron spatial flux distribution $\phi(s)$ is derived the nth moment of the flux is given by

$$\overline{s^n} = \int_{s=0}^{\infty} s^n \phi(s)dV \bigg/ \int_{s=0}^{\infty} \phi(s)dV \qquad (1)$$

where s is the distance co-ordinate from the source to a field point and dV is a volume element at distance s. The first moment is thus the average crow-flight distance a neutron travels from source to absorption and the second moment is the corresponding mean square distance.

To accord with the form for characteristic lengths which appears in simple theories, the square of the slowing-down length $L_s(E)$, from some initial source energy to a final energy E, is defined by

$$2L_s^2(E) = z^2 = \int_{s=0}^{\infty} z^2\phi(E,z)dz \bigg/ \int_{0}^{\infty} \phi(E,z)dz \qquad (2)$$

in terms of an infinite plane source, or

$$6L_s^2(E) = r^2 \int_{0}^{\infty} r^4\phi(E,r)dr \bigg/ \int_{0}^{\infty} r^2\phi(E,r)dr \qquad (3)$$

in terms of a point source.

Using these definitions $L_s(E)$ may be evaluated if $\phi(E,r)$ is determined by experiment or from Monte Carlo computations.

3.3.2 Diffusion length

For a source-free medium, in which the diffusion coefficient is not directionally dependent, the diffusion equation reduces to the standard wave-equation

$$\nabla^2 \phi_{th} = \phi_{th}/L^2 \qquad (4)$$

where the diffusion length L makes its appearance as a derived quantity. In this way

$$L = \sqrt{D_{th}/\Sigma_{a,th}} \approx \sqrt{\lambda_{tr,th}/3\Sigma_{a,th}}, \qquad (5)$$

where D_{th} is the diffusion coefficient and $\lambda_{tr,th}$ the transport mean free path for thermal neutrons.

If L is derived experimentally, from a neutron flux distribution which is assumed to be a solution of equation (4), then it is "that diffusion length which gives the best fit of the experimental flux distribution to the corresponding diffusion theory solution". There is not a unique definition of "best fit". Unequivocally, if the thermal neutron flux distribution from a thermal neutron source is derived from Monte Carlo computer experiments, then, by substituting the thermal flux in the integrals of equations (2) and (3),

$$2L^2 = z^2 \qquad (6)$$

for an infinite plane thermal neutron source, and

$$6L^2 = r^2 \qquad (7)$$

for a point thermal neutron source.

3.3.3 Migration length

The migration length (M) describes the net effect of slowing-down and thermal diffusion. It may be defined by equations similar to (2) and (3), for a fast source, but with $\phi(E)$ replaced by ϕ_{th}. The relationship connecting the characteristic lengths is found to be

$$M^2 = L_s^2(E_c) + L^2 \qquad (8)$$

where E_c is a suitable "thermal cut-off energy" chosen to separate the slowing-down and thermal energy regions.

For Monte Carlo computations of neutron characteristic lengths plane geometry is the most convenient choice, an infinite plane source being postulated and neutrons tracked in the positive z region. The relevant plane spatial regions are split into volume elements and average fluxes are then derived for each element. A compromise must therefore be selected in the trade-off between spatial resolution and statistical accuracy. On using equation (2) to compute second spatial moments from Monte Carlo flux averages it is also necessary to consider the appropriate z value to use with each average flux when replacing the integrals with summations. This necessarily involves some assumption about the form of the spatial flux variation.

Here the arithmetic mean z value has been used for each segment and all the runs have been conducted for a choice of geometrical conditions under which this approach is valid. These conditions were studied before the runs were performed in order to establish the criteria for choosing the z increments. It is most important to ensure that the flux nowhere decreases by a large factor over a single grid width in any region which makes a significant contribution to the second moment summation.

A Monte Carlo program was used to compute thermal neutron fluxes, and the fluxes in a narrow energy band (0.1-0.5 eV) just above thermal. Each flux output was used as input to a second program which converts the integrals of equation (2) into summations, deriving slowing-down length with the 0.1-0.5 eV flux group and migration length with the thermal flux group.

The relationship between migration length and porosity for a calcite pure water mixture with full and partial saturation is displayed in Fig. 8. It is noteworthy that there is a minimum in the value of migration length in the partially saturated case at about 75% porosity.

The relationship between near/far count ratio, for the simple configuration of a thermal neutron probe shown in Fig. 9, and neutron migration length in a wide range of formation conditions is illustrated in Fig. 10. The results are remarkably close to a smooth curve considering that the plot includes dry rocks, pure water, strongly saline pore fluids and rock poisoned with gadolinium and boron.

For probes which behave in this manner, and there is evidence that others do so, Monte Carlo computations can be used to establish characteristic length equations. When this is done for a variety of formation types the results are permanently available for applications such as the interpolation of experimental values of probe response, or the derivation of partial-saturation effects, even if new responses have to be derived because of a change in tool design.

For a particular type of pore fluid and matrix rock, having only one variable (e.g. porosity), probe response must be a smooth function of neutron characteristic length. The more variables which can be added (e.g. rock constituents, pore fluid salinity), while still retaining a smooth curve, the greater the range of applicability of a set of derived data, such as partial-saturation effects.

3.4 Neutron spectra

Neutrons having energies above thermal can make a significant contribution to neutron detector countrate or to the rate of production of γ-rays from a particular element. Three features controlling these rates can be identified:-

(i) the magnitude of the epithermal relative to the thermal flux;

(ii) the energy distribution of the epithermal flux;

(iii) the yield of γ-rays from the analyte arising from epithermal interactions.

The importance of (i) is self-evident but must be related to (ii) since the interaction cross-sections in the epithermal region are often strongly energy dependent, exhibiting resonances at well-defined energies (at least up to the energy region where the resonances are so closely-spaced that they can no longer be resolved). Point (iii) must be examined for each analyte; special γ-rays can be expected following neutron absorption in an element but the relative intensities of the γ-rays may be different for thermal neutron absorption and resonance absorption, in the latter case according to the particular resonance.

3.4.1 Relationship between thermal and epithermal reaction rates

In well-moderated spectra the epithermal flux usually varies inversely as the neutron energy (1/E spectra) and effective cross-sections are available in the form of resonance integrals which already contain the 1/E weighting. For such a spectrum the differential epithermal flux may be written

$$\phi_e(E) = \lambda/E,$$

or, in terms of the total thermal flux,

$$\frac{\phi_e(E)}{\phi_{th}} = \phi_{eo}(E) = \lambda_0/E \qquad (9)$$

$\phi_{eo}(E)$ being the corresponding normalised epithermal flux. If N_a is the number density of interacting atoms the epithermal absorption rate is given by

$$RR_e = N_a \int_{E_c}^{\infty} \phi_e(E)\sigma_a(E)dE = \phi_{th}\lambda_0 N_a I_0 \qquad (10)$$

where the resonance integral I_0 is defined by

$$I_0 = \int_{E_c}^{\infty} \sigma_a(E)\frac{de}{E} \qquad (11)$$

the lower energy limit E_c being a convenient thermal cut-off, generally 0.5 eV.

Calling $N_a I_0$ the macro resonance integral Σ_{I_0}, the total reaction rate becomes

$$RR_t = RR_{th} + RR_e = \phi_{th}(\Sigma_{th} + \lambda_0\Sigma_{I_0}). \qquad (12)$$

By definition, λ_0 characterises the epithermal neutron spectrum in being independent of the absolute value of the thermal flux, for the total flux ϕ_t up to energy $E_0 (E_0 > E_c)$ is given by

$$\phi_t = \phi_{th} + \int_{E_c}^{E_0} \phi_e(E)dE = \phi_{th}\left[1 + \lambda_0 \log\frac{E_0}{E_c}\right] \qquad (13)$$

It also follows from this model of the neutron spectrum that in any epithermal energy interval, E_1 to E_2, the flux is $\lambda_0 \log(E_1/E_2)$. Since $\log(E_1/E_2)$ is the "lethargy" interval, λ_0 is seen to be "the flux per unit lethargy interval normalised to unit thermal flux".

At first sight it may be confusing to note that the resonance integral I_0 of equation (11) has an infinite upper limit, whereas the total epithermal flux component equation (13) increases without limit as the upper limit E_0 increases. In fact I_0 contains the epithermal "shape" factor 1/E, and the generally decreasing trend in $\sigma_a(E)$, with increasing E, leads to decreasing contributions to the integral.

Epithermal reaction rates can be calculated from tabulated values of I_0 if λ_0 is constant and is known. Depending on the analyte and the hardness of the spectrum, epithermal reactions can make an important contribution. But the value of λ_0 can vary with position in the sample and with the nature of the sample. Further, the effective value of λ_0 may vary according to the energy band to which it refers. Although these considerations may appear unpromising, the problems are not severe when proper account is taken of those volume elements and energy regions which contribute most to detector countrate. The Monte Carlo results provide the necessary information on neutron spatial and energy distributions while a considerable amount of supporting nuclear data is already available on individual resonances.

A typical plot of λ_0 values for a point ^{252}Cf source in pure water is given in Fig. 11. Severe departures from the I/E form are observed very close to the source where source neutrons have experienced too few collisions to be well-moderated. In the spatial groups at 6-8 cm and 10-15 cm the spectrum has stabilised to 1/E although above 100 keV the influence of source neutrons is apparent. The spectral form for sea water is given correspondingly in Fig. 12. Whilst the 1/E form is generally maintained, some spectral hardening is evident by virtue of the chlorine present in the sea water.

By contrast Fig. 13 shows the spectral form for a point 1 MeV monoenergetic source in pure water saturated granite of 5% porosity. It is seen that the 1/E slowing down distribution does not establish itself at distances from the source below about 30 cm. At this distance the spectrum is relatively hard being approximately 10 times greater than that for pure water and a ^{252}Cf source (Fig. 11).

The effect of introducing a water-filled borehole can be seen in Fig. 14 which relates to zero-porosity basalt and a point ^{252}Cf source on the borehole axis. As in the case above, the spectrum does not stabilise until distances of about 30 cm from the source have been reached. However, unlike the previous case the near 1/E distribution builds-up by increasing intensity at the low energy end as the distance from the (moderating) water in the borehole increases. The result is a very hard spectrum with $\lambda_0=0.4$. In this case the borehole diameter is not large enough to give good moderation near its outer edge and the 1/E spectrum has to be developed further out.

In contrast to the above, in a plane perpendicular to the borehole axis (Fig. 15) and at a distance of 30-35 cm (approx. the distance of detector spacings), a 1/E distribution exists even close to the borehole. Many of the neutrons in this plane have suffered multiple collisions in the borehole fluid.

3.5 Measurement of the macroscopic absorption cross-section of rocks

At the present time there is considerable interest in the measurement of the macroscopic thermal neutron absorption cross-section of specimens of oil reservoir rock formations in order to assist in the interpretation of pulsed neutron and compensated steady-state neutron logs. In particular it is important to identify the presence of neutron poisons within the volume of formation being interrogated by the logging tool.

Several methods of measuring the macro absorption cross-section based on a pulsed neutron source(14-16) have been described. The method of Antonov et al(14) requires a special calibration curve which has to give the same value of the transport cross-section as that of the sample, whereas the method of Allen and Mills(15) requires the elemental composition in order to calculate the transport cross-section. Czubek et al(16) describe a method which is independent of the transport cross-section but at the present time requires a spherical sample with a volume of about 500 cm^3. Some further information on the accuracy of this method would be valuable.

Harris et al(17) have described the use of the Pile Oscillator Method to measure the absorption cross-section of some common geological materials. For rock samples weighing about 100g a relative accuracy of about ±10% in the macro absorption cross-section is claimed. The same technique is being used at A.E.R.E. Harwell(18). The precision of this method is generally within ±1% and the calibration technique is currently being developed to achieve an accuracy within the ±10% band.

Tittle and Crawford(19) have recently described a relatively simple steady-state method of determining the thermal neutron absorption cross-section which requires samples of mass about 0.5 to 1 kg, the sample being immersed in water during the measurement. The neutron source is 1 Ci ^{239}Pu-Be emitting $\sim 10^6$ n/s. A comparison of results with the method of Allen and Mills for four rocks with absorption cross-sections covering the range 6.2 to 16.1 c.u. showed variations between 9.3% and 20.9%.

There seems little doubt but that the Pile Oscillator Method should give the most accurate results, provided proper attention is given to correction factors arising from, for example, variations in sample size and neutron scattering. However, a suitable reactor is not always accessible and development of other techniques is to be encouraged. An intercomparison of results from a representative range of samples would be a valuable exercise.

4. BENCH-MARK CALIBRATION AND MONTE CARLO CALCULATIONS

The current practice of calibrating neutron and γ-ray borehole logging probes (and on-line monitoring equipment) generally relies on the use of one or more test facilities, constructed from natural or quasi-natural formations, to give the response of the equipment under known conditions. The interpretation of the response under operational conditions from the response under the conditions at calibration is a separate matter. But generally the accuracy with which operational responses can be deduced tends to be dependent on the divergence of the formation lithology and other formation factors from that of the test facility. The closer the calibration conditions are to the operational situation, the more accurate the interpretation.

To meet the widely different operational conditions encountered in practice, a number of test facilities are generally constructed. The overall test installation then becomes complex and expensive. In addition, when the test facilities are constructed from natural materials the neutron transport parameters of those facilities may be in doubt. In other words, the calibration is not conducted under well-defined conditions.

Now that Monte Carlo and coupled codes are becoming more generally available and more able to cope with realistic, complex situations an alternative approach to calibration can be considered. The basis of this philosophy is the construction of a limited number of calibration facilities which are composed of elemental materials (such as aluminium and carbon) and compounds (such as water and selected hydrocarbons) whose purity can be accurately established; especially since any impurities might be expected to be uniformly disseminated, unlike the situation with natural materials. By using a modular construction for such a facility it would be a simple matter to introduce porosity in a controlled manner.

In practice a tool to be calibrated would be inserted into each of the facilities and its response measured. In parallel, the response would also be calculated from the known nuclear parameters and dimensions of the test facilities and from the design of the tool. From present experience excellent agreement would be expected. From this information, the response in any of a series of operational environments circumscribing those anticipated operationally, could be predicted. Used in this way, the Monte Carlo code could be regarded as a transfer standard.

Implicit in this suggestion is that accurate nuclear data would be available relevant to the varietv of techniques which might be used, the materials of the tools and the elemental constituents of the rock formations encountered. However, as can be seen from Section 2.1 complete data requirements are not available for all elements and where data are available they may not have the accuracy required.

5. NUCLEAR TECHNIQUES FOR DERIVING NON-NUCLEAR DATA

An important application of nuclear techniques is in the determination of the bulk density of oil- and gas-bearing formations and coal deposits and minerals streams during plant processes control. Density determination is also often required as a correction factor on the measurement of certain other parameters, such as soil moisture.

Several papers have dealt with the fundamental aspects of the technique(20-22) whilst recent constributions have focussed on instrument design factors(23,24) and on the effect of borehole conditions.

The basic relation underlying formation density measurement is given by

$$\rho_e = \rho_b A_v \sum_i w_i \left[\frac{Z_i}{A_i}\right]$$

where ρ_e is the electron density, ρ_b is the formation bulk density, A_v is Avogadro's Number and w_i is the wt. fraction of the ith element of mass number A and atomic number Z.

The basic assumption underlying the technique is that by ensuring that the measuring equipment is sensitive only to Compton interactions(and hence to ρ_e) ρ_b can be estimated reliably provided $[Z/A]$ is constant. The effects of variation in the γ-ray energy spectrum due to changes in formation atomic number, source energy and detector threshold energy have been well developed(21,22) for systems in which $[Z/A]$ is constant and for these situations accurate results can be obtained providing the environmental conditions are well defined.

However, this is not always the case, especially in coal deposits where the hydrogen concentration between shales and different types of coal may vary significantly.

The magnitude of the independent effects of variation in hydrogen content for point source, infinite volume and for realistic borehole logging configurations is now being studied and the results of the first phase of this programme is reported on at this conference(25).

The measurement of formation porosity in oil well logging is of fundamental importance and both steady-state and pulsed neutron techniques are in use. Data interpretation is extremely difficult since, until recently, it has not been possible to isolate the effect of each perturbing parameter. However, the recent application of Monte Carlo and coupled computer codes(26) in this field is helping to resolve this problem and significant progress is being made; at least in the direction of obtaining a better understanding of the problem. A full discussion of the problem of formation porosity measurement is well beyond the scope of this paper.

6. CONCLUSIONS

(i) Although there are a number of techniques now in use which do not appear to have a significant demand for additional microscopic nuclear data, several important areas of application can be identified where there is a need for improved data. For some elements of interest in the earth sciences evaluated data listings are not yet available.

(ii) The demand for more accurate micro data is most intense in (n,γ) analytical applications and originates from the increased use of computational methods in feasibility and design studies. The need is likely to increase as benchmark calibration and coupled computational techniques are more widely accepted.

(iii) Sensitivity codes are now available which can be used to establish the significance of uncertainties in micro cross-section data in a wide range of applications. However, this approach requires evaluated uncertainties for the nuclide cross-sections and at the present time this information is available for only a limited number of nuclides.

(iv) The increasing use of neutron techniques for the analysis of bulk materials has indicated the need for a better understanding of the role of neutron transport and neutron spectrum hardness parameters in formation evaluation and instrument design.

(v) Nuclear techniques have an established function in the measurement of particular non-nuclear data, such as bulk density and formation porosity. Continuous development of these techniques is required to support the breadth of applications.

REFERENCES

(1) CINDA, a Computer Index of Neutron Data. (IAEA, Vienna, Austria). CINDA-A (1935-1976) Vol. 1, $Z \leqslant 50$ (1979)
CINDA-A (1935-1976) Vol. 2, $Z \geqslant 51$ (1979)
CINDA 83 (1977-1983). (1983)

(2) Index to Large Evaluated Data Files available from NEA Data Bank. (NEA Data Bank, Gif-sur-Yvette, France, 1981).

(3) LORENZ, A. Compilations and Evaluations of Nuclear Structure and Decay Data (Issue No. 5), Report INDC(NDS)-112/LNQ (I.A.E.A., Vienna, 1980).

(4) 1983 Compilation of National Nuclear Data Committees, Report INDC(Sec)-86/UN (I.A.E.A., Vienna, 1983).

(5) CLAYTON, E. Uncertainties in theoretical thick target PIXE yields. Nucl. Instr. and Meth. 191, 567 (1981).

(6) CAMPBELL, J.L., COOKSON, J.A. and PAUL, H. Uncertainties in thick-target PIXE analysis. Nucl. Instr. and Meth. 212, 427 (1983).

(7) WORMALD, M.R. and CLAYTON, C.G. In-situ analysis of coal by measurement of neutron-induced prompt γ-rays. Int. Jnl. Appld. Radn. and Isotopes, 34, 71 (1983).

(8) BENDALL, D.E. and BRISSENDEN, R.J. MCBEND Programme Users Guide, COSMOS Ref. set. Doc/147 (1980).

(9) HALL, M.C.G. DUCKPOND: A perturbation Monte Carlo and its applications. NEA Specialists' Meeting on Nuclear Data and Bench-marks for Reactor Shielding, Paris 27-29 October (1980).

(10) MORGAN, G.L., LOVE, T.A., DICKEN, J.K. and PEREY, F.G. Gamma-ray production cross-sections of tantalum and carbon for incident neutron energies between 0.007 and 20 MeV. Oak Ridge National Laboratory Report ORNL-TM-3702 (1972).

(11) LUNDBERG, S.B. and BERGQVIST, I. Gamma-rays from neutron resonance capture in Mg, Si, P and S. Physica Scripta, 2, 265 (1970).

(12) CZUBEK, J.A. Remarks on some rock neutron parameters. Inst. Nucl. Physics. Report No. 1222/AP, Krakow, Poland (1983).

(13) ALLEN, L.S., TITTLE, C.W., MILLS, W.R. and CALDWELL, R.L. Dual-spaced neutron logging for porosity. Geophysics 32, 60 (1967).

(14) ANTONOV, A.V., GRANATKIN, B.V. MERKULEV, A.Yu., MILLER, V.V. and SHIMELEVICH, Yu.S. The use of a pulsed neutron generator to determine neutron diffusion parameters of rocks and fluids. Radioisotope Instruments in Industry and Geophysics, 2, 139 (I.A.E.A., Vinenna, 1966).

(15) ALLEN, L.S. and MILLS, W.R. Measurement of thermal neutron absorption cross-section of rock samples by a pulsed source method. Log Analyst 16, 10 (1875).

(16) CZUBEK, J.A., DROZDOWICZ, K., KRYNICKA-DROZDOWICZ, E., IGIELSKI, A. and WOZNICKA, V. Measurement of the thermal neutron absorption cross-section of rock samples. Int. J. Appld. Radn. and Isotopes, 31, 143 (1983).

(17) HARRIS, J.M., McDANIEL, P.J., WIDMAN, D.H. and MILSAP, D.A. Thermal neutron absorption reactivity measurements of selected geological materials. SPWLA 24th Annual Logging Symposium, Paper VV, 2 (1983).

(18) SANDERS, L.G. Unpublished.

(19) TITTLE, C.W. and CRAWFORD, G.W. Measuring the thermal neutron absorption cross-section of rocks. Log Analyst, 24, No. 3.12 (1983).

(20) TITTMAN, J. and WAHL, J.S. The physical foundations of formation density logging (Gamma-Gamma) Geophysics, 30, 284 (1965).

(21) CZUBEK, J.A. Physical possibilities of gamma-gamma logging. Radioisotope Instruments in Industry and Geophysics, 2, 249 (I.A.E.A., Vienna, 1966).

(22) CZUBEK, J.A. Advances in gamma-gamma logging. Int. J. Appld. Radn. and Isotopes, 34, 153 (1983).

(23) WOOLSON, W.A. and STAGGS, V.E. Monte Carlo analysis of rugosity effects on gamma-gamma logs. Science Applications Inc., Palo Altos, Calif., U.S.A. Report GJB-39 (1982).

(24) BORSARV, M., CHARBUCINSKI, J. and EISLER, P.L. Design and development of borehole logging probes for density determinations in shallow rough boreholes. Log Analyst, No. 2, 3 (1983).

(25) CLAYTON, C.G., SANDERS, L.G. and KEMSHELL, P.B. Some comments on formation density measurement by gamma-ray interactions based on observations from Monte Carlo calculations. Paper presented at I.A.E.A. Meeting on Nuclear data for borehole and bulk media assay using nuclear techniques. Krakow, Poland (1983).

(26) SANDERS, L.G. The application of Monte Carlo computations to formation analysis by neutron interactions. Int. J. Appld. Radn. and Isotopes, 34, 173 (1983).

TABLE 1

International Data Centres for the collection and distribution of neutron cross-section data*

Data centre	Address	Countries served
U.S. National Nuclear Data Center	Brookhaven National Lab., Upton, New York, 11973, USA.	USA Canada
NEA Data Bank	B.P. 9, F-91190 Gif-sur-Yvette, France.	Western Europe Japan
USSR Centr PO Jadernym Dannym	Fiziko-Energeticheskij Institut, Obninsk, Kaluga Region, USSR.	USSR
IAEA Nuclear Data Section	Wagramerstrasse 5, PO Box 100, A-1400 Vienna, Austria.	Rest of world

*There are also a number of data centres which consider:-

(a) Nuclear structure and decay data

(b) Charged particle nuclear data

(c) Photonuclear data.

Details of these can be obtained from the data centres in the table.

TABLE 2

Sources of uncertainty in thick-target PIXE analysis using thick standards

Ionization cross-section	K_α X-rays. $20<Z<50$, $<\pm2\%$: $Z<20$, 53%. L_α X-rays. $66<Z<92$, 56%.
Attenuation coefficient	±5% for μ/ρ >300, falling to <1% for μ/ρ <20; double these uncertainties near absorption edges.
Stopping power	∿1%
Current integration	≦1% for currents >10 na
Dead time	≦1% should be possible
Spectrum unfolding	<1-100%
Tilt of specimen	0-1.72% per 1° of tilt, depending on μ/ρ
Surface roughness	assessment required
Secondary fluorescence	assessment required

TABLE 3

Availability of neutron cross-section data

Element	Full evaluation available(a)	γ-ray production data represented in evaluation(b)			Comments(b)(c)
		(n,γ)	(n,n'γ)	others	
1 H	ENDF/B5	✓			
2 He	ENDF/B4				
3 Li A= 6	ENDF/B5	✓	✓		
A= 7	ENDF/B4	✓	✓		
4 Be	ENDF/B4	✓		✓	
5 B A=10	ENDF/B5	✓	✓	✓	
A=11	ENDF/B4				
6 C	ENDF/B5	✓	✓		
7 N A=14	ENDF/B4	✓	✓	✓	
8 O A=16	ENDF/B4	✓	✓	✓	
9 F	ENDF/B4	✓	✓	✓	
10 Ne	-				
11 Na	ENDF/B4	✓	✓		
12 Mg	ENDF/B4	✓	✓	✓	
13 Al	ENDF/B4	✓	✓	✓	
14 Si	ENDF/B4	✓	✓	✓	
15 P	ENDL-82	✓			MT=3
16 S	ENDL-82	✓			MT=3 95%
17 Cl	ENDF/B4	✓	✓		MT=3
18 Ar	ENDL-82	✓			MT=3
19 K	ENDF/B4	✓	✓	✓	
20 Ca	ENDF/B4	✓	✓	✓	
21 Sc	JENDL-2				
22 Ti	ENDF/B4	✓			MT=3
23 V	ENDF/B4	✓		✓	MT=3
24 Cr	ENDF/B4	✓			MT=3
25 Mn	ENDF/B4	✓	✓		MT=3
26 Fe	ENDF/B4	✓	✓		MT=3
27 Co	ENDF/B4	✓			MT=3
28 Ni	ENDF/B4	✓			MT=3
29 Cu	ENDF/B4	✓			MT=3
30 Zn	-				
31 Ga	ENDL-82	✓			MT=3
32 Ge	-				
33 As	ENDL-82	✓			
34 Se	ENDF/B4*				99.1%
35 Br	ENDF/B4*				100%
36 Kr	ENDF/B5				100%
37 Rb	ENDF/B4*				100%

cont'd.,

TABLE 3 cont'd.,

Element	Full evaluation available(a)	γ-ray production data represented in evaluation(b)			Comments(b)(c)
		(n,γ)	(n,n'γ)	others	
38 Sr	ENDF/B4*				99.4%
39 Y	ENDL-82	✓			
40 Zr	ENDL-82	✓			MT=3
41 Nb	ENDL/B5	✓			MT=3
42 Mo	ENDF/B4	✓			MT=3
43 Tc					Not naturally occurring
44 Ru	ENDF/B4*				80%
45 Rh	ENDF/B5				
46 Pd	ENDF/B4*				99%
47 Ag	ENDL-82	✓			MT=3 100%
48 Cd	ENDL-82	✓			MT=3
49 In	ENDF/B4*				95.7%
50 Sn	ENDL-82	✓			MT=3
51 Sb	ENDF/B4*				100%
52 Te	ENDF/B4*				99.9%
53 I	ENDF/B5*				
54 Xe	ENDF/B5				100%
55 Cs	ENDF/B5				
56 Ba	ENDF/B4*				99.8%
57 La	ENDF/B4*				99.9%
58 Ce	ENDF/B4*				99.4%
59 Pr	ENDF/B5				
60 Nd	ENDF/B4*				100%
61 Pm					Not naturally occurring
62 Sm	ENDF/B4*				96.9%
63 Eu	ENDL-82	✓			MT=3
64 Gd	ENDL-82	✓			MT=3
65 Tb	ENDF/B5				
66 Dy	ENDF/B4*				99.8%
67 Ho	ENDL-82	✓			MT=3
68 Er	-				
69 Tm	-				
70 Yb	-				
71 Lu	ENDF/B4				100%
72 Hf	ENDL-82	✓			
73 Ta	ENDF/B4	✓			MT=3 100%
74 W	ENDL-82	✓			MT=3
75 Re	ENDL-82	✓			MT=3 100%
76 Os	-				
77 Ir	-				
78 Pt	ENDL-82	✓			MT=3

cont'd.,

TABLE 3 cont'd.,

Element	Full evaluation available(a)	γ-ray production data represented in evaluation(b)			Comments(b)(c)
		(n,γ)	(n,n'γ)	others	
79 Au	ENDL-82	✓			MT=3
80 Hg	-				
81 Tl	-				
82 Pb	ENDF/B4	✓			MT=3
83 Bi	ENDL-82	✓			MT=3
84 Po					Product of actinide decay
85 At					"
86 Rn					"
87 Fr					"
88 Ra					"
89 Ac					"
90 Th	ENDL-82	✓		✓	MT=3 Th-232 only
91 Pa					Product of actinide decay
92 U		✓		✓	MT=3 100%

Summary

Elements where no full evaluation is available:-

Ne, Zn, Ge, Tc, Pm, Er, Tm, Yb, Os, Ir, Hg, Tl, Po, At, Rn, Fr, Ra, Ac, Pa.

Fission product elements where some high energy data may be absent from evaluation:-

Se, Br, Rb, Sr, Ru, Pd, In, Sb, Te, I, Ba, La, Ce, Nd, Sm, Dy.

Elements where γ-ray production data are not evaluated:-

He, B-11, Ne, Sc, Zn, Ge, Se, Br, Kr, Rb, Sr, Tc, Ru, Rh, Pd, In, Sb, Te, I, Xe, Cs, Ba, La, Ce, Pr. Nd, Pm, Sm, Tb, Dy, Er, Tm, Yb, Lu, Os, Ir, Hg, Tl, Po, At, Rn, Fr, Ra, Ac, Pa.

/Footnotes ...

Footnotes to Table 3

(a) Evaluations given contain all significant cross-sections over the energy range $\sim 10^{-4}$ eV to ~ 20 MeV except where marked with an *. Evaluations marked with an * come from a fission product library and may not contain all significant cross-sections, particularly at high energies.

ENDF-4 and 5 evaluations come from the U.S.A. Evaluated Nuclear Data File versions 4 and 5.

JENDL-2 evaluations come from the second version of the Japanese Evaluated Nuclear Data Library.

ENDL-82 evaluations come from the 1982 version of the Evaluated Nuclear Data Library of the Lawrence Livermore Laboratory in the U.S.A.

(b) The γ-ray production cross-sections described in column 3 may not cover the complete energy range where they are significant. An entry of MT=3 in column 4 of the Table indicates that additional data are provided in which the photon production cross-sections from more than one reaction type are lumped together.

(c) Where the files described under column 2 are for isotopes, the percentage of the natural element covered by these is given in column 4.

TABLE 4

Average values of the elemental abundances (wt %) for typical rocks. Values refer to the dry (no moisture) condition, summing to 100% for each column

Element	Sandstone	Shale	Limestone	Granite	Basalt
Oxygen	51.58	49.90	48.24	48.61	44.65
Silicon	36.74	27.53	3.18	33.69	23.76
Aluminium	2.49	8.79	0.90	7.33	7.44
Iron	1.56	4.82	1.68	1.90	9.00
Calcium	3.93	1.57	34.02	0.95	7.45
Sodium	0.30	1.19	0.05	2.28	1.65
Potassium	1.08	2.99	0.47	4.52	0.68
Magnesium	0.70	1.60	0.58	0.31	3.82
Titanium	0.15	0.47	0.03	0.22	1.22
Phosphorus	0.03	0.07	0.07	0.08	0.10
Manganese	0.02	0.07	0.06	0.05	0.13
Carbon	1.36	0.72	10.67	0.03	0.03
Hydrogen	0.06	0.28	0.05	0.03	0.07

TABLE 5

Macroscopic parameters of zero-porosity rocks, pure water and sea water

Material	$\Sigma_{a,th}$ ($10^{-2}.cm^{-1}$)	$\Sigma_{s,th}$ (cm^{-1})	Σ_{I_o} ($10^{-2}.cm^{-1}$)	Σ_{sf} (cm^{-1})	$\xi\Sigma_{sf}$ (cm^{-1})	Moderating Ratio (MR)
Sandstone	0.6264	0.2869	0.3711	0.2743	0.0466	6.59
Shale	1.044	0.3646	0.6300	0.3108	0.1047	8.89
Limestone	0.7174	0.3111	0.4008	0.3008	0.0486	6.00
Granite	1.002	0.2671	0.5995	0.2604	0.0364	3.22
Basalt	1.456	0.3062	0.9040	0.2904	0.0500	3.04
Pure water	1.968	2.212	1.000	1.492	1.381	62.21
Sea water	2.199	1.412	1.412	1.486	1.370	41.06

$\Sigma_{a,2200}$	macroscopic neutron absorption cross-section at 2200 m/sec neutron velocity;
$\Sigma_{a,th}$	macroscopic thermal neutron absorption cross-section (averaged over standard temperature Maxwell distribution);
$\Sigma_{s,th}$	macroscopic thermal neutron scattering cross-section;
Σ_{I_o}	macroscopic resonance absorption cross-section (atom density x resonance integral);
Σ_{sf}	macroscopic "fast" neutron scattering cross-section (constant cross-section epithermal energy region;
ξ	average logarithmic neutron energy decrement per collision;
$\xi\Sigma_{sf}$	slowing-down power;
MR	moderating ratio ($\xi\Sigma_{sf}/\Sigma_{a,2200}$).

TABLE 6

Relative contributions of elements in typical rocks to total macroscopic cross-sections (moisture excluded)

Element	% of $\Sigma_{a,th}$ (thermal neutron absorption)					% of Σ_{I_o} (resonance neutron absorption)				
	Sandstone	Shale	Limestone	Granite	Basalt	Sandstone	Shale	Limestone	Granite	Basalt
Oxygen	0.19	0.10	0.15	0.12	0.08	0.42	0.22	0.35	0.25	0.16
Silicon	45.92*	18.87*	3.39	27.47*	13.74*	45.98*	18.53*	3.60	27.23	13.12*
Aluminium	4.66	9.01†	1.44	8.94†	6.44†	6.56†	12.45*	2.14	12.47*	8.64†
Iron	15.63*	26.42*	14.35*	12.42*	41.71*	16.11*	26.78*	15.69*	12.67*	41.01*
Calcium	9.25†	2.03	68.29*	1.46	8.11†	8.11†	1.74	63.51*	1.27	6.79†
Sodium	1.52	3.30	0.22	7.52†	3.86	1.70	3.62	0.26	8.33†	4.12
Potassium	12.73*	19.32*	4.72	34.74*	3.71	10.83*	16.13*	4.26	29.27*	3.01
Magnesium	0.40	0.50	0.28	0.11	1.00	0.45	0.56	0.34	0.13	1.09
Titanium	4.19	7.20†	0.71	4.01	15.77*	3.90	6.57†	0.71	3.69	14.00*
Phosphorus	0.04	0.05	0.08	0.07	0.06	0.03	0.04	0.07	0.06	0.05
Manganese	1.06	2.04	2.72	1.73	3.19	2.13	4.01	5.78†	3.44	6.11†
Carbon	0.08	0.02	0.57	0.00	0.00	0.07	0.02	0.50	0.00	0.00
Hydrogen	4.34	11.09*	3.08	1.14	2.34	3.72	9.33†	2.80	1.20	1.91

* (>10%). † (5-10%).

TABLE 7

Relative contributions of elements in typical rocks to total slowing-down power (moisture excluded)

Element	% of $\xi\Sigma_{sf}$				
	Sandstone	Shale	Limestone	Granite	Basalt
Oxygen	48.40	19.03	42.43	60.90	42.00
Silicon	6.66	2.03	0.54	8.16	4.32
Aluminium	0.33	0.47	0.11	1.30	0.99
Iron	0.36	0.45	0.36	0.58	2.07
Calcium	0.48	0.08	3.90	0.16	0.91
Sodium	0.12	0.19	0.02	1.19	0.65
Potassium	0.07	0.08	0.03	0.39	0.04
Magnesium	0.26	0.24	0.20	0.15	1.43
Titanium	0.02	0.02	0.00	0.03	0.14
Phosphorus	0.01	0.01	0.02	0.03	0.02
Manganese	0.00	0.00	0.00	0.00	0.01
Carbon	2.82	0.61	20.77	0.08	0.06
Hydrogen	40.47	76.78	31.62	27.02	47.34
O + H	88.87	95.81	74.05	87.92	89.34

TABLE 8

Nuclear characteristics of two neutron poisons found in rocks

	Gadolinium	Boron
$\sigma_{a,2200}$ (barns)	49.600	759
I_o (barns)	390	341
Σ_{I_o} (cm)	2.02×10^{-5}*	3.86×10^{-3}**

* at 5 ppm in calcite.

** at 75 ppm in calcite,

For calcite: $\Sigma_{I_o} = 3.27 \times 10^{-3}$ cm.

TABLE 9

Characteristics of the two coals referred to in Fig. 7

Weight fractions			Porosity	Bulk density g/cm^3	Relative atom density (%)						Thermal neutron macro. cross-section (cm^{-1})	
Ash	Moisture	Sulphur			C	H	O	N	Si, Al, Fe	Cl	Total	Absorption
0.1	0.1	0.01	0.4	0.82	45.62	42.85	9.18	0.83	0.51	0	1.0402	0.9406×10^{-2}
0.4	0.1	0.01	0.4	0.82	36.65	38.74	16.13	0.66	2.61	0	0.7475	0.9203×10^{-2}

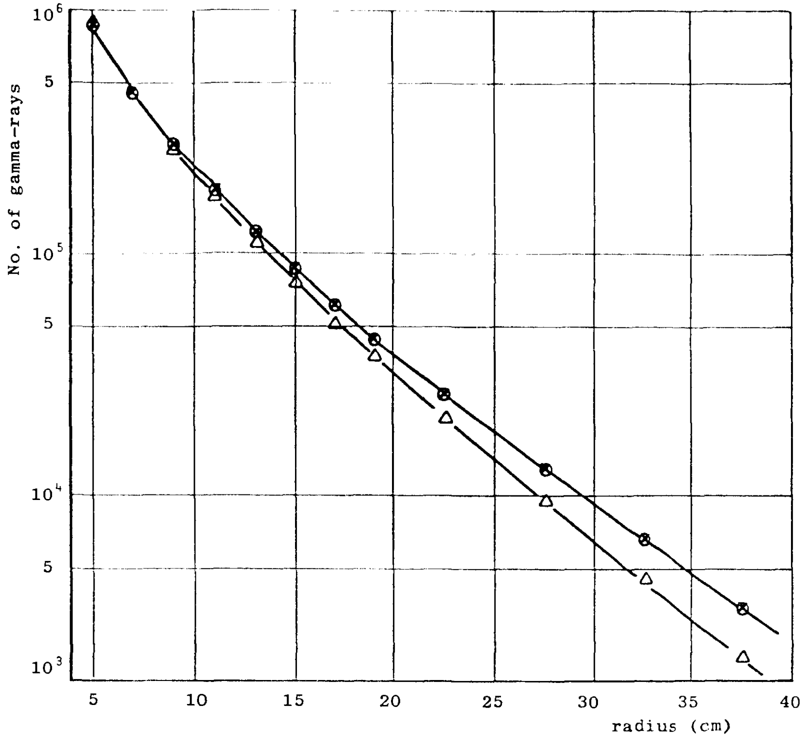

FIG. 1. Variation of gamma-ray intensity with radius.

Gamma-ray energy range from 100 keV to 660 keV

x - pure carbon

O - carbon + 0.2 wt.% zirconium

Δ - carbon + 20 wt.% hydrogen.

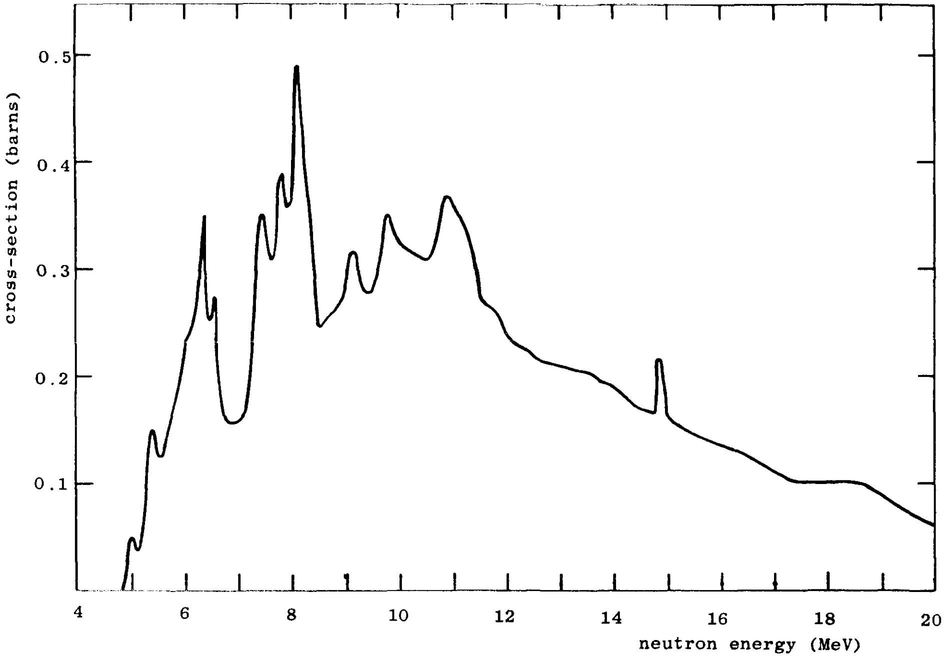

FIG. 2. The cross-section for production of the 4.44 MeV γ-ray from carbon as a function of neutron energy, taken from ENDF/B-5 (MAT 1306).

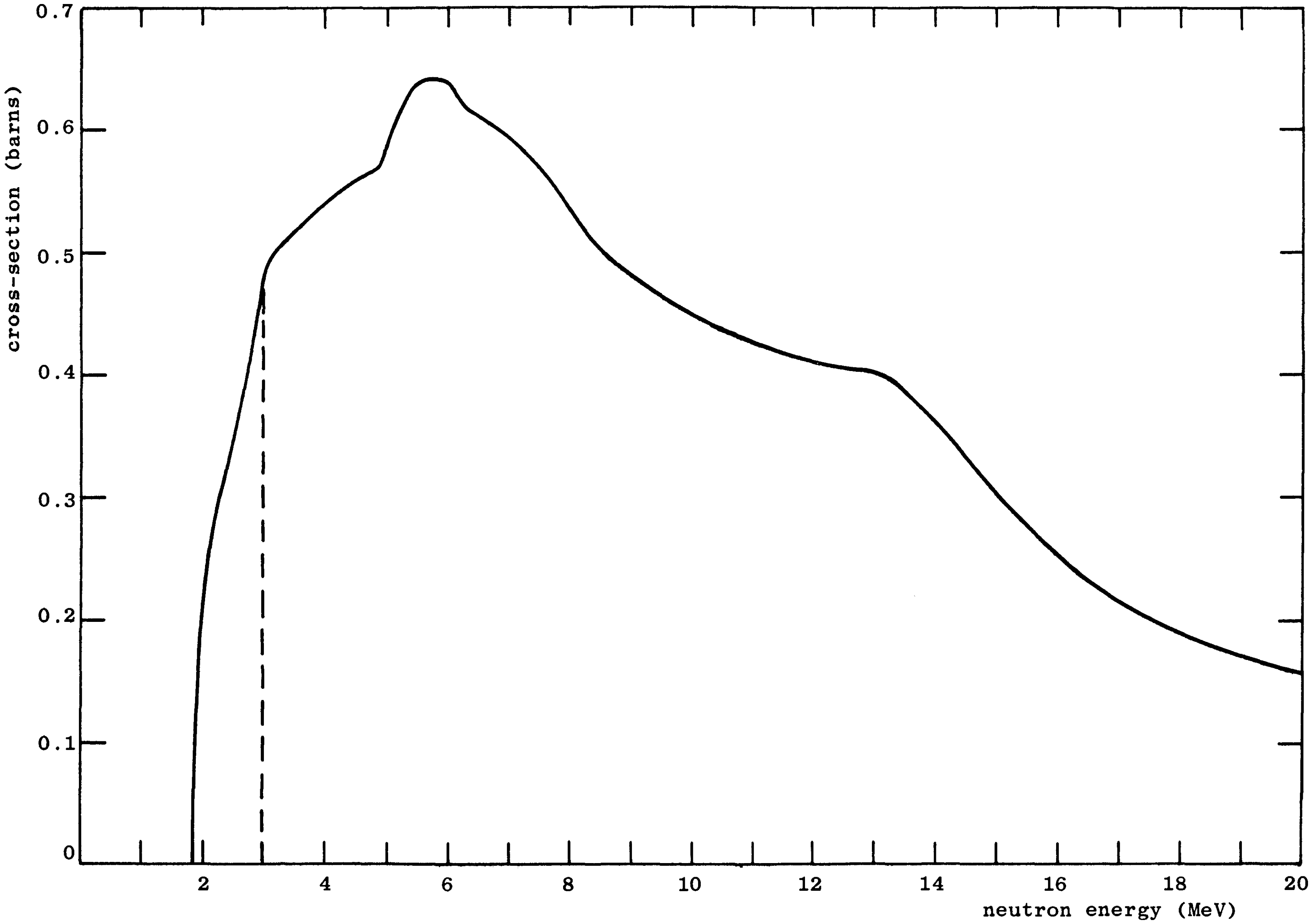

FIG. 3. The cross-section for the production of the 1.779 MeV γ-ray from silicon as a function of neutron energy, taken from ENDF/B-4(MAT 1194). Below 3 MeV, the data are for the discrete energy γ-ray, and above that neutron energy, the cross-section values are for the production of all γ-rays in the energy interval from 1.75 to 1.80 MeV.

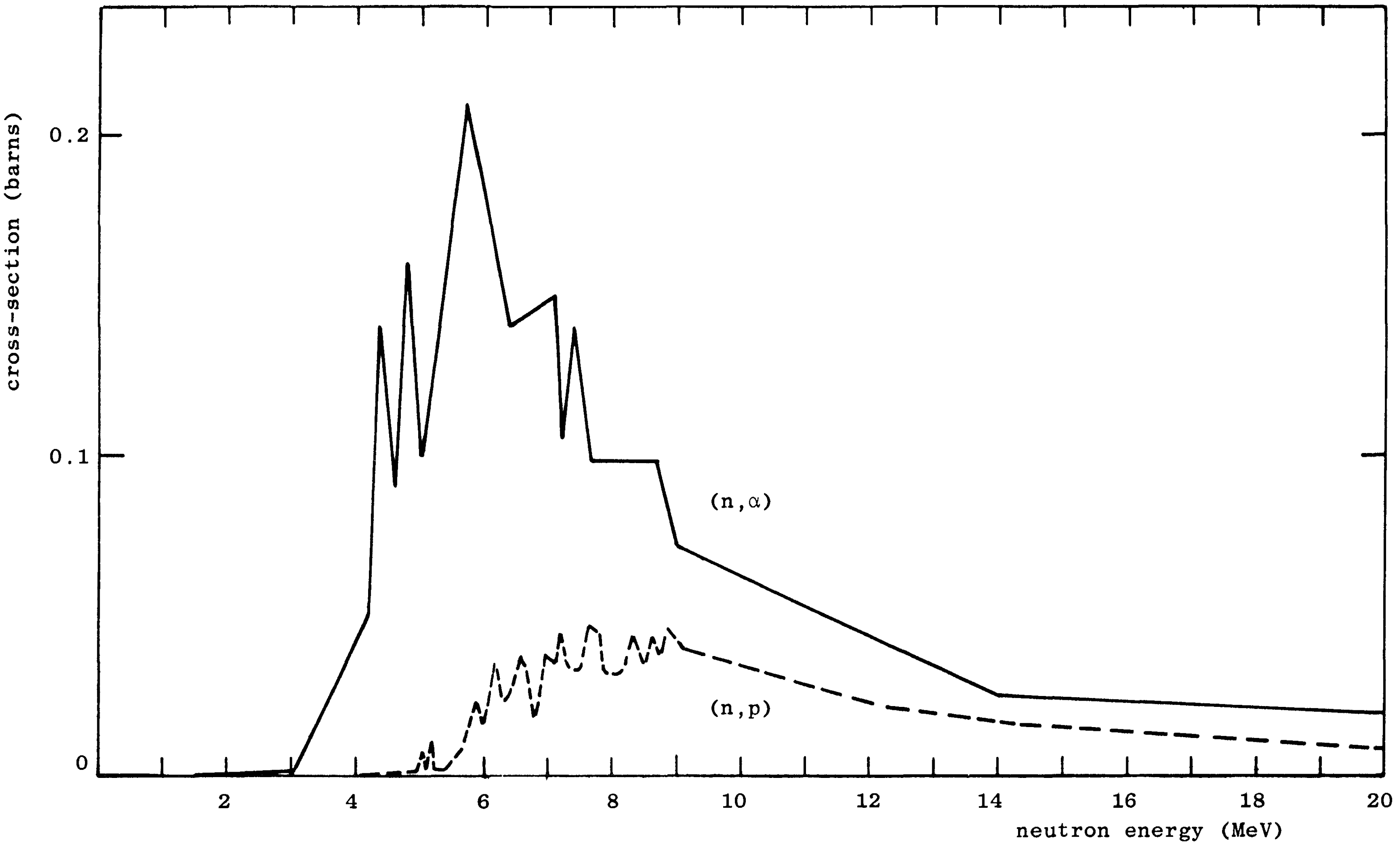

FIG. 4. The (n,α) and (n,p) cross-sections of fluorine as a function of neutron energy, taken from ENDF/B-4(MAT 1277).

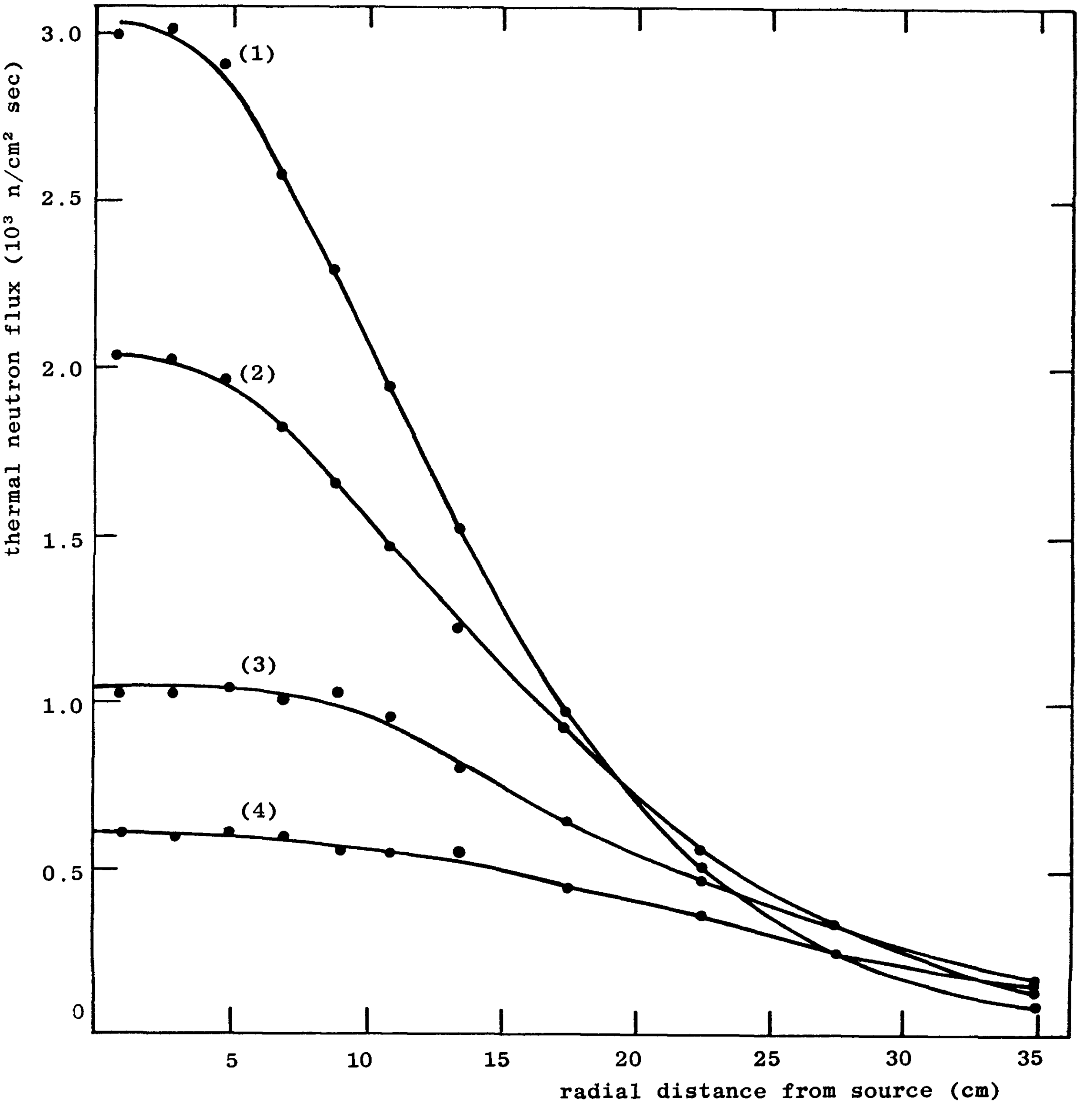

FIG. 5. Radial distribution of thermal neutron flux. Formation: sandstone (Table 6), pure-water saturated. ρ_g = 2.575 g/cm^3. Geometry: point source in infinite medium. Source energy; 1.25 MeV monoenergetic (10^6 n/s). Porosity: (1) 30%; (2) 20%; (3) 10%; (4) 5%.

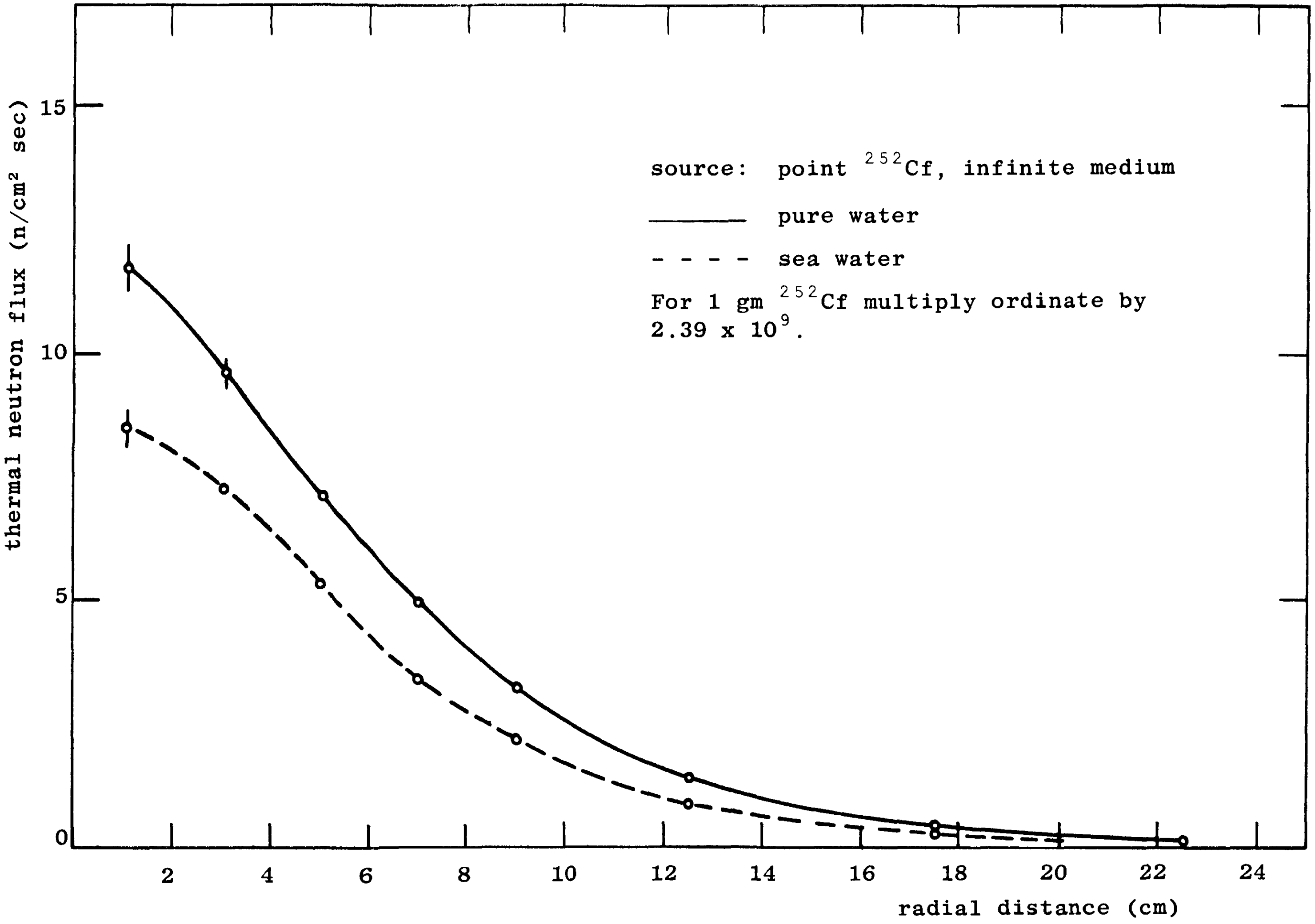

FIG. 6. Radial distribution of thermal neutron flux.

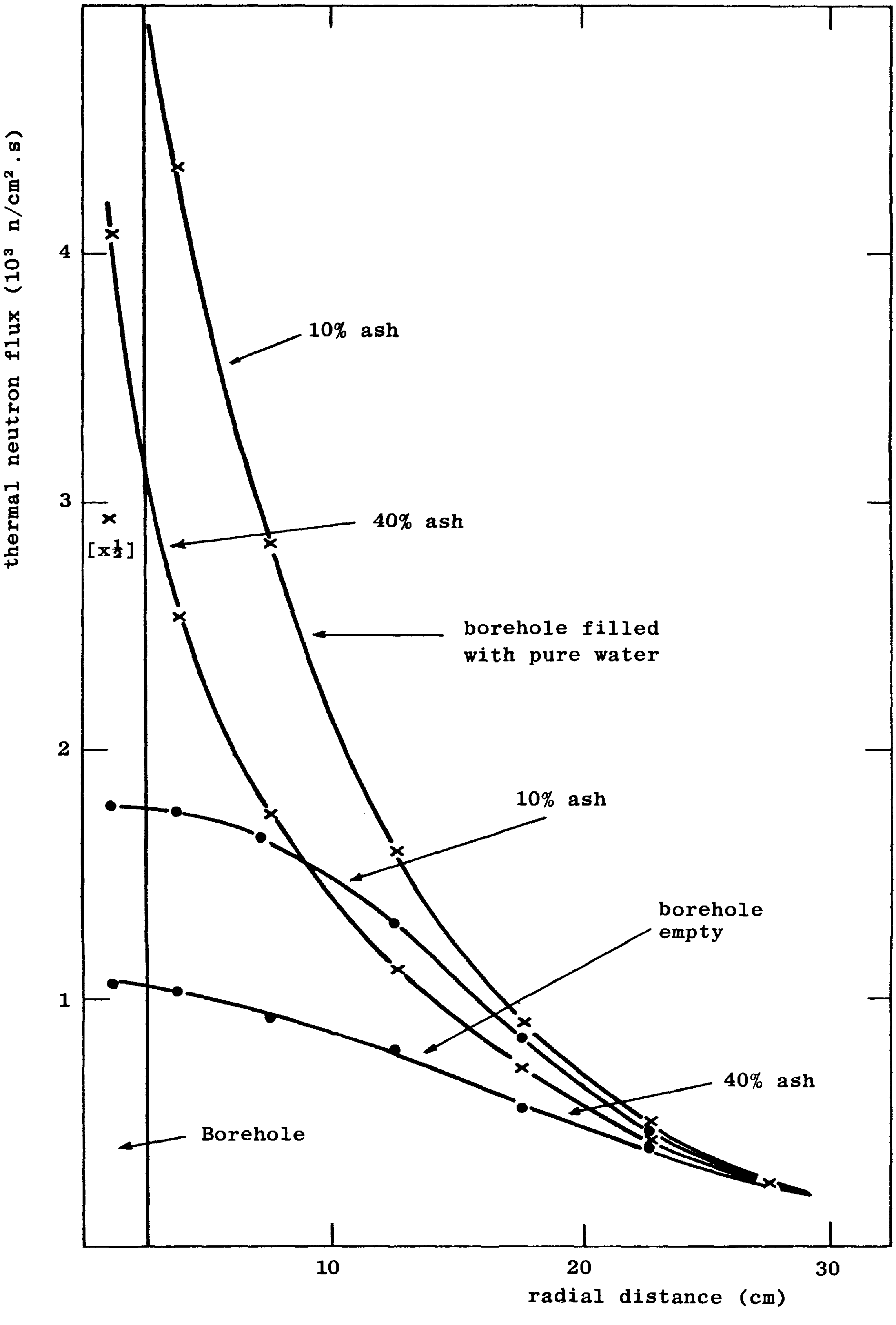

FIG. 7. Radial thermal neutron flux distribution averaged over z=0 to z=5 cm. Point source ^{252}Cf, 1 x 10^6 n/s.

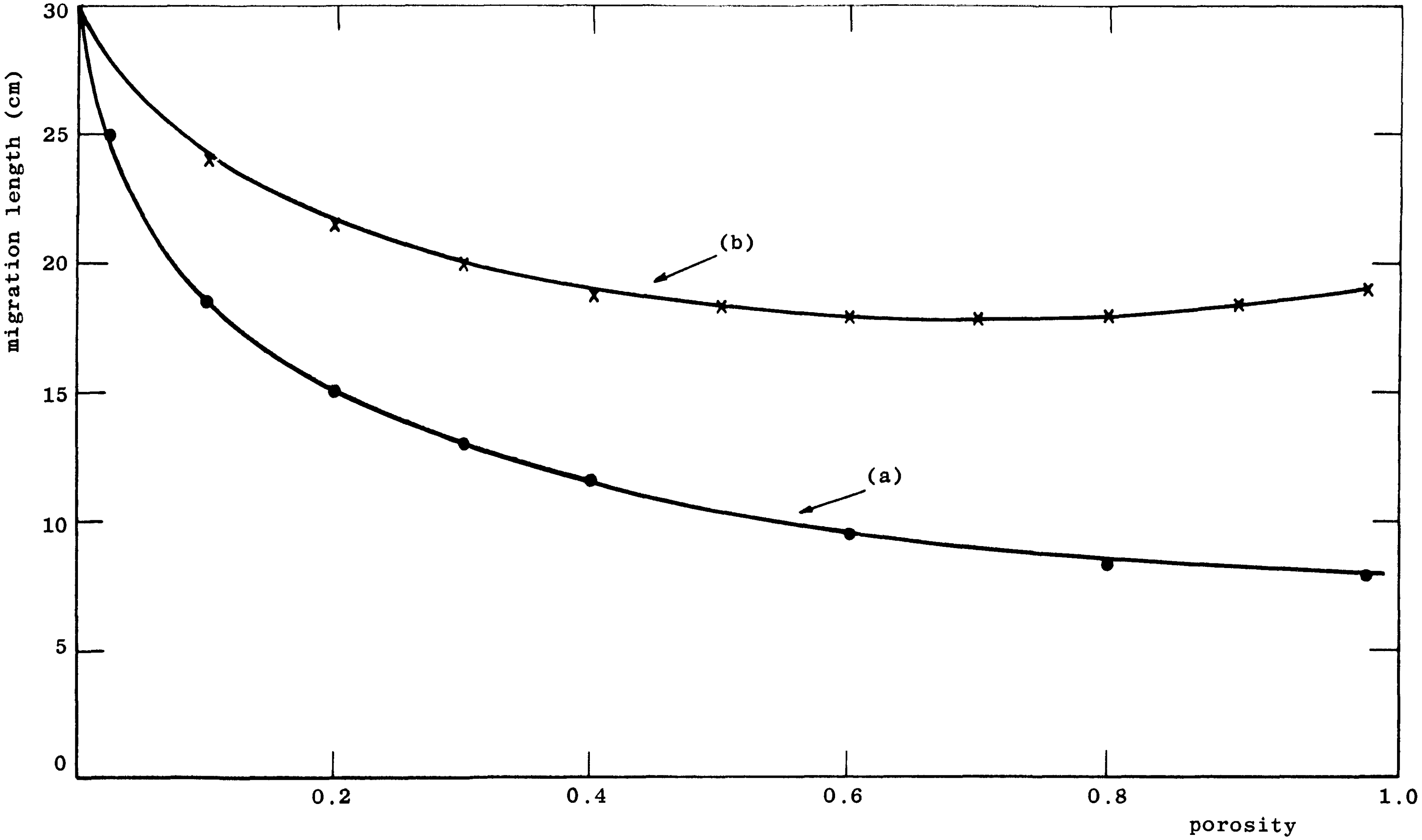

FIG. 8. Dependence of neutron migration length on porosity for a calcite-pure water saturated formation (a) and a calcite-pure water partially saturated formation (b) - saturation factor 0.4372. Source: ^{241}Am/Be.

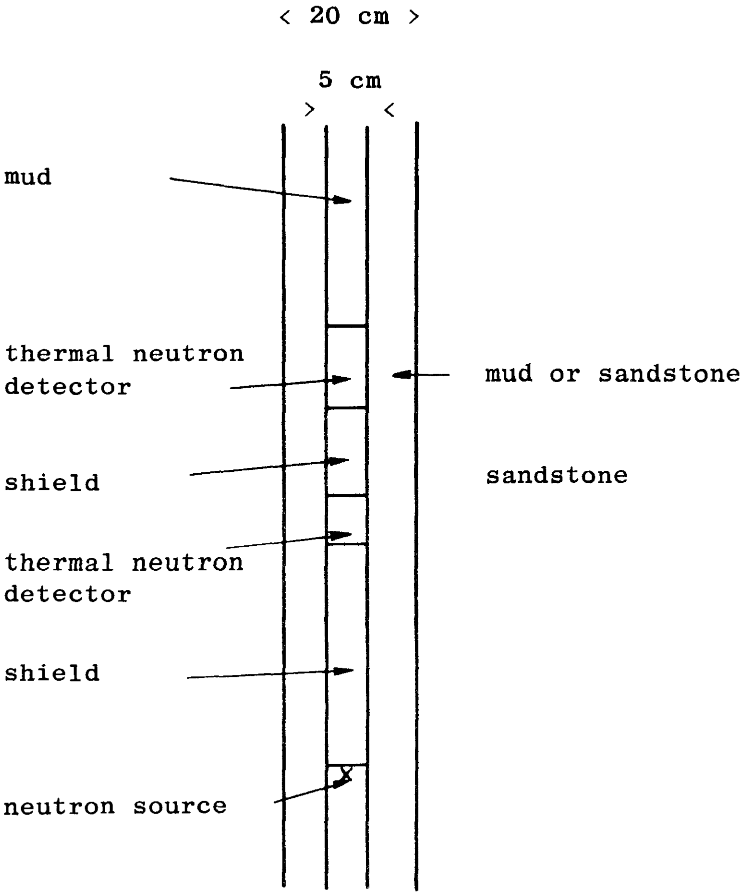

FIG. 9. Simple probe simulation for Monte Carlo studies on dual-spaced neutron porosity logging.

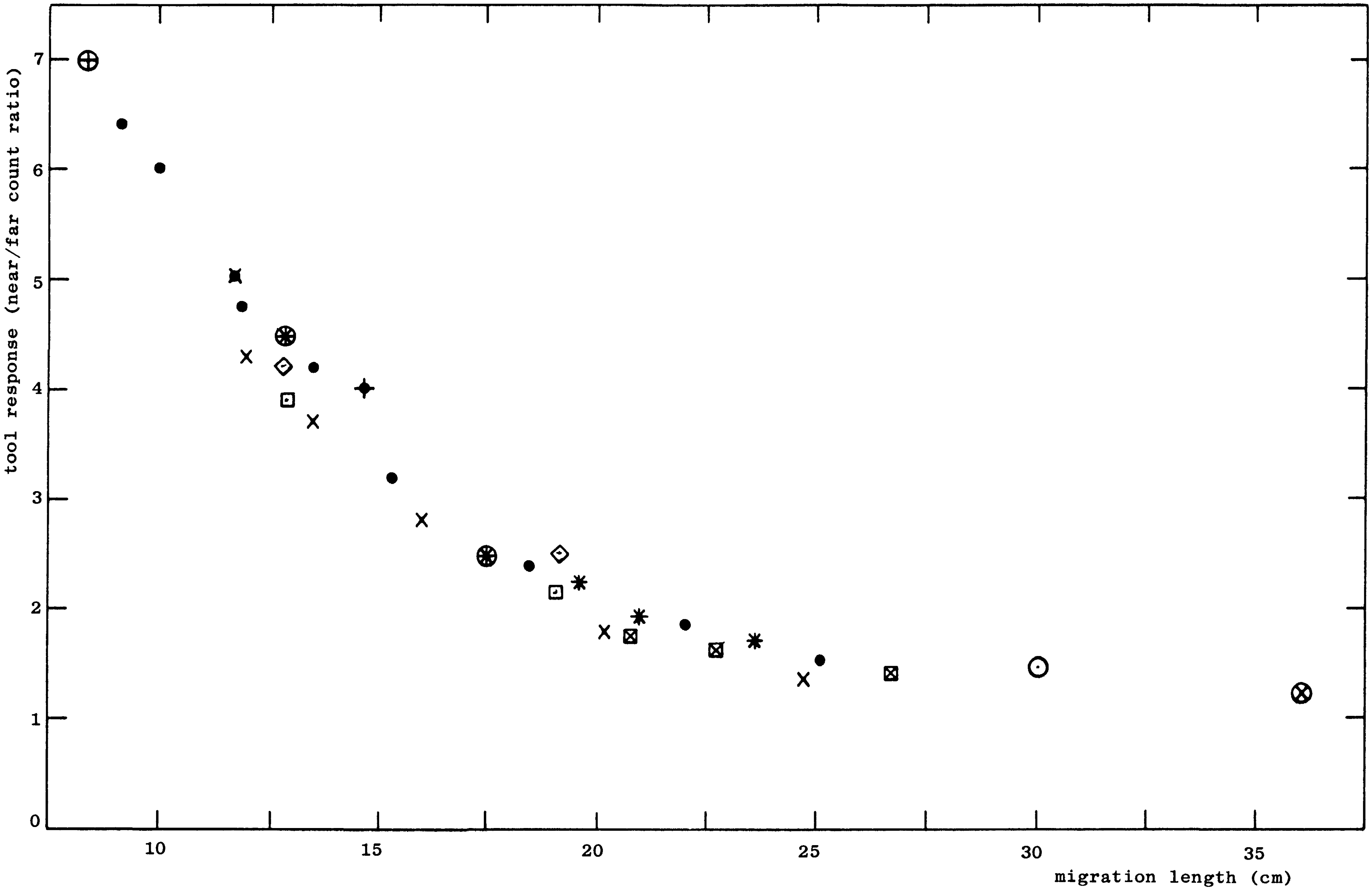

(see over page for caption and key to Fig. 10)

FIG. 10. Variation of near/far count-ratio for thermal neutrons with formation migration length.

KEY

Matrix	Pore fluid	Porosity	Saturation factor	Symbol
Calcite	-	0.0	-	⊖
Calcite	pure water	0.025-0.8	1.0	•
Calcite	pure water	0.1-0.3	0.437	*
Calcite (+5 ppm Gd +74 ppm B)	pure water	0.1-0.3	1.0	⊛
Silica	-	0.0	-	⊗
Silica	pure water	0.05-0.4	1.0	x
Silica	pure water	0.1-0.3	0.437	⊠
Silica	salt water (125 kppm)	0.1-0.3	1.0	⊡
Silica	salt water (250 kppm)	0.1-0.3	1.0	◈
None	pure water	-	1.0	⊕

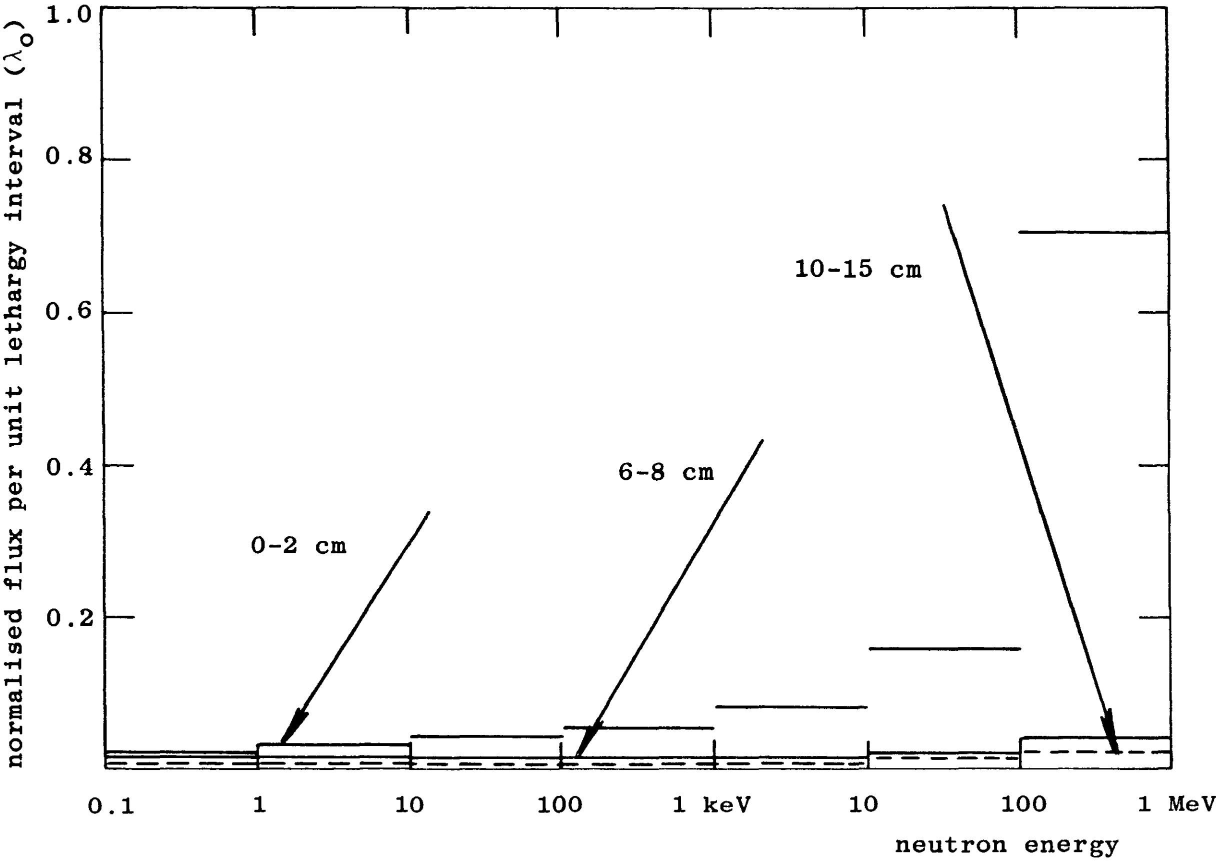

FIG. 11. Neutron spectra for point ^{252}Cf source in pure water.

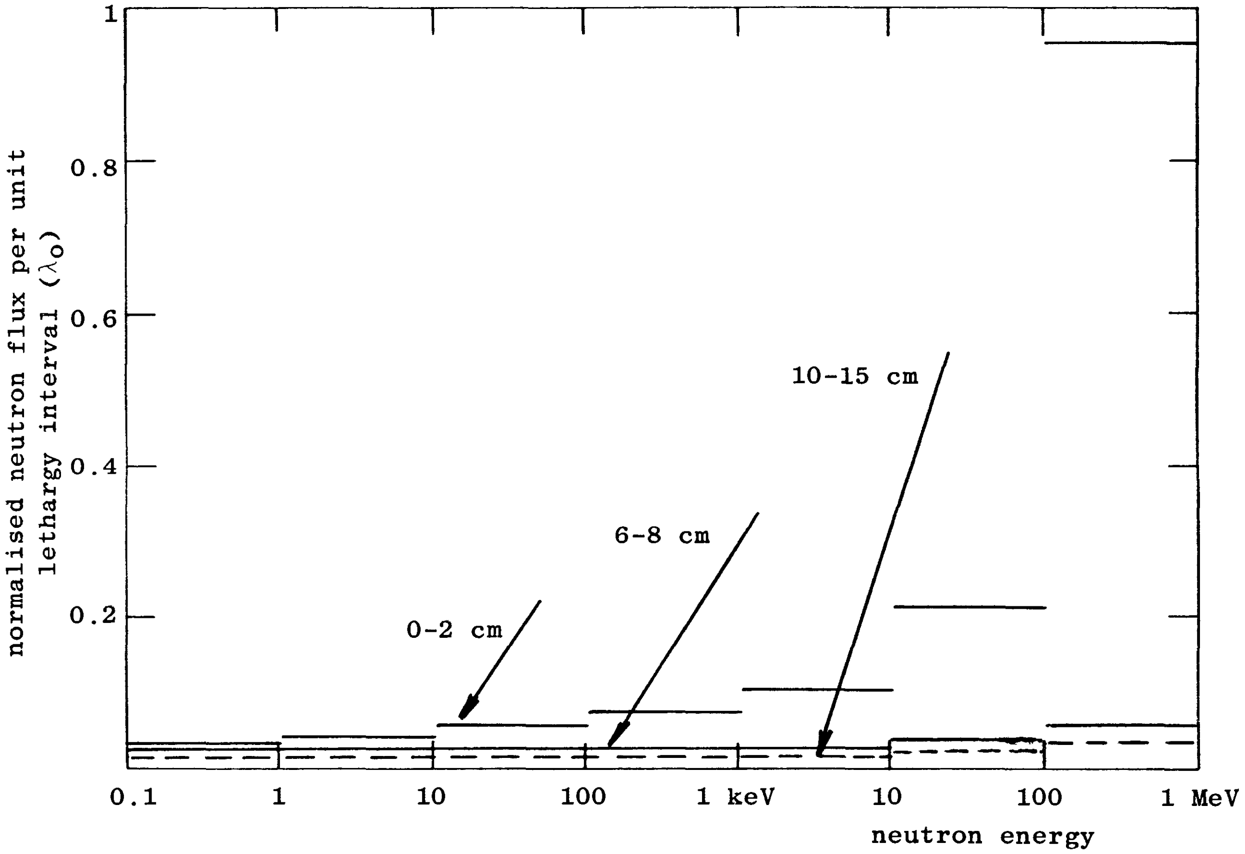

FIG. 12. Neutron spectra for point ^{252}Cf source in sea water.

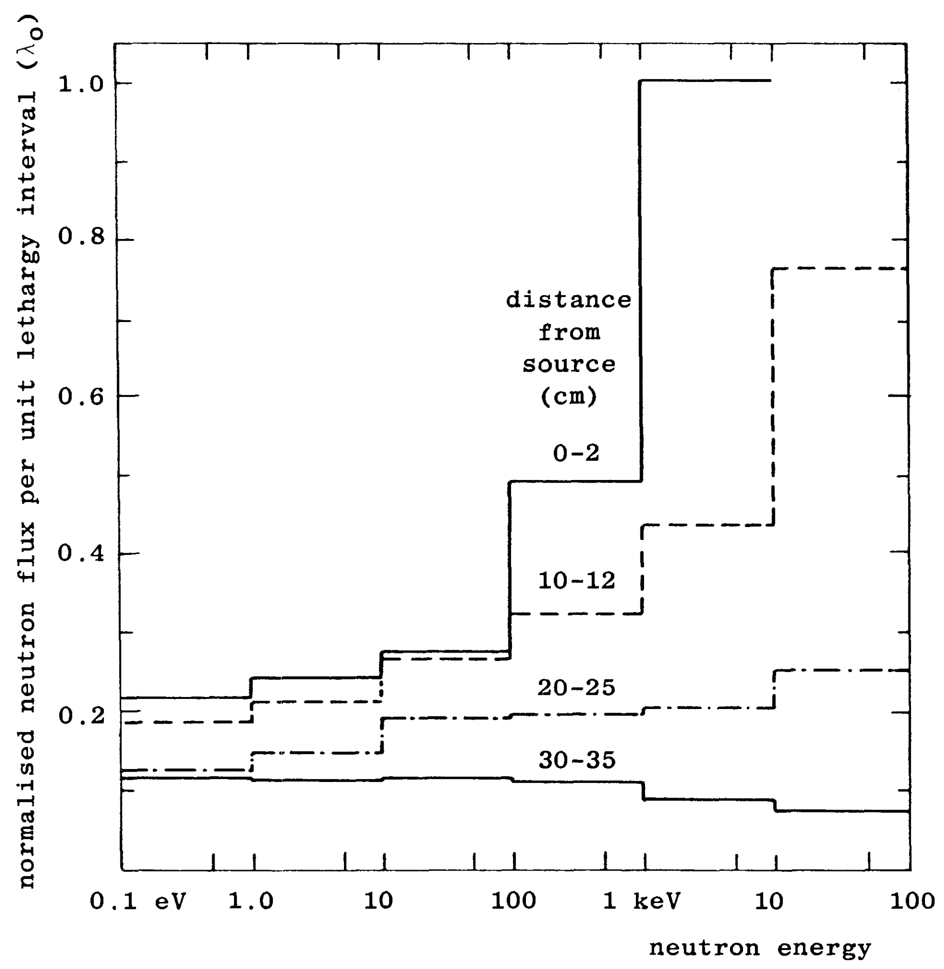

FIG. 13. Neutron spectra in pure water saturated granite (normalised to unit thermal flux). Geometry: point source in infinite medium; Source: monoenergetic, 1 MeV; Porosity: 5%.

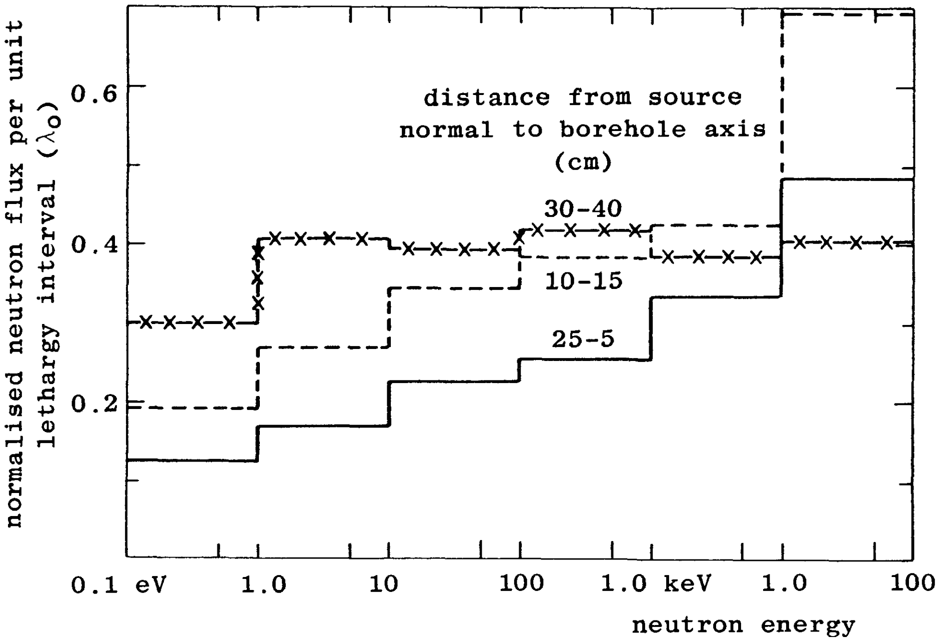

FIG. 14. Effect of pure-water filled borehole on neutron spectra in zero-porosity basalt (normalised to unit thermal flux). Geometry: point source on axis of pure-water filled 5 cm diameter borehole in infinite formation; Source: ^{252}Cf.

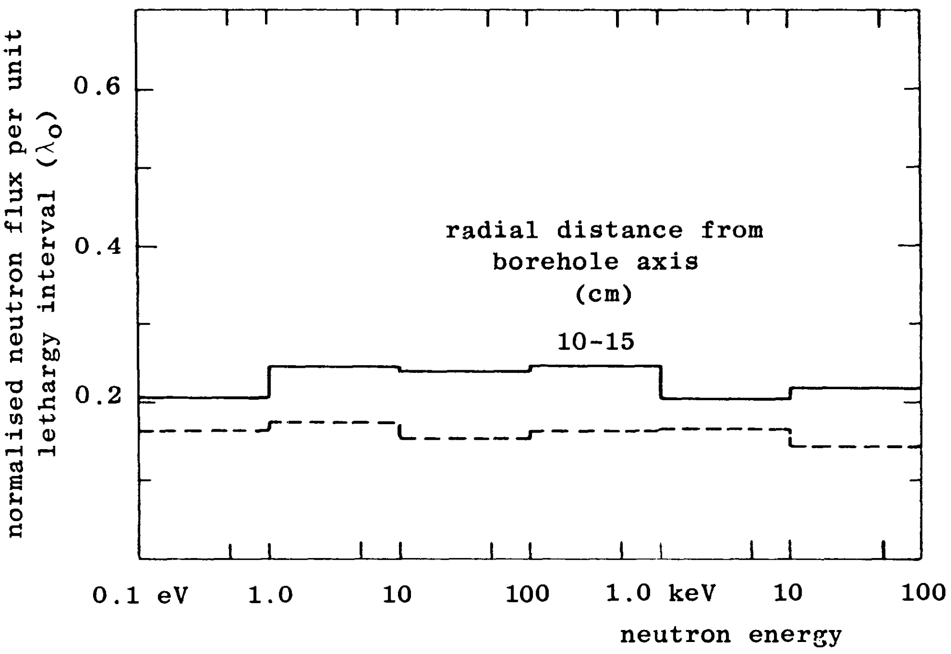

FIG. 15. Effect of pure-water filled borehole on neutron spectra in zero-porosity basalt. (Plots are for z-plane at 30-35 cm from source along borehole axis.)

NUCLEAR DATA FOR OIL AND GAS LOGGING

L.S. Allen, R.L. Caldwell, W.R. Mills
Mobil Research and Development Corporation
Farmers Branch, Texas 75234

ABSTRACT

The widespread use of nuclear logs for qualitative and semi-quantitative analyses of rock formations is well established. In the petroleum industry, a primary use of nuclear data is for calculation of reserves of oil and gas. For this and other purposes, quantitative data from nuclear logs and from the laboratory analysis of rock and fluid samples are necessary. To achieve quantitative determination of rock properties, including density, porosity, fluid saturation and rock matrix, the nuclear logs must be well calibrated. This paper will present a review of the nuclear data requirements for providing accurate quantitative analyses of nuclear well logs. The requirements fall into two general categories: (a) measurement in the laboratory of the properties of rocks recovered in the drilling process with primary value being given to cores of the formations, and (b) calibration facilities for accurately determining the responses of commercial logging tools.

To interpret pulsed neutron capture logs quantitatively, one needs the macroscopic thermal neutron absorption cross section of the rock matrix. Current techniques for making these measurements are reviewed. The principal new porosity logging development is the use of two epithermal neutron detectors and two thermal neutron detectors. This combination improves gas identification and porosity determination in shaly formations. A facility for calibration of natural gamma ray and neutron porosity logging tools is available in the U.S. A new facility for calibrating natural gamma-ray spectral logs is planned in 1984. A facility for calibrating pulsed neutron logs is urgently needed.

Natural gamma-ray spectral logs are now offered by two companies and two additional companies plan to offer commercial service within a year. Spectral analysis of neutron induced gamma rays requires a much more complex system. Logs based on measurement of a broad spectrum of gamma rays induced by 14-Mev neutrons are now in experimental use. Future spectral gamma-ray tools will probably utilize gamma-ray detectors with greater efficiency than the commonly used sodium iodide scintillator.

NUCLEAR DATA FOR OIL AND GAS LOGGING

L.S. Allen, R.L. Caldwell, W.R. Mills

1. Introduction

The use of nuclear well logs in the petroleum industry has been well documented in papers presented at symposia sponsored by the International Atomic Energy Agency [1,2]. The widespread use of nuclear logs for qualitative and semi-quantitative analyses of rock formations penetrated by boreholes is well established. For many applications properly calibrated nuclear logs are commercially available for quantitative analysis of rock properties, including density, porosity, fluid saturation and rock matrix. This paper will present a review of the nuclear data requirements for providing accurate quantitative analyses of nuclear well logs. The requirements fall into two general categories:

(a) measurement in the laboratory of the properties of rocks recovered in the drilling process, with primary value being given to cores of the formations, and
(b) standardization and calibration facilities for determining the responses of commercial logging tools.

The principal new development of the past two years has been the increased use of natural gamma ray spectral logs to help solve petroleum exploration and production problems. There is an urgent need for an industry standard facility in which these tools can be properly calibrated with known concentrations of potassium, uranium and thorium in the ranges usually encountered in routine use of the tools for petroleum logging. It appears that such a facility will be built during the year 1984. The next most urgent need for the quantitative use of nuclear logs in the petroleum industry is a facility for calibration of pulsed neutron logging tools. A summary will be given of the status of pulsed neutron logging services and of nuclear data requirements for quantitative use of these logs.

2. Thermal Neutron Absorption Cross Section Measurements for Rock Samples

2.1. Introduction

In order to interpret pulsed neutron capture logs quantitatively, it is necessary to know the macroscopic thermal neutron absorption cross section of an earth formation's rock matrix and pore fluids. A technique for measuring the neutron absorption cross section of rocks was described by Allen and Mills in 1975 [3]. The method utilizes a measurement of the thermal neutron lifetime for a sample of crushed rock which has been saturated with ordinary water. The water not only prevents excessive neutron leakage from the experimental sample, but so dominates the diffusion coefficient of the rock-water mixture that only a crude estimate of the rock's composition is needed to produce an accurate value of rock cross section from the measured thermal neutron lifetime.

The method was applied to both igneous and sedimentary rock samples. The values obtained clearly show that most rocks contain enough strongly absorbing trace elements (such as boron) that their absorption cross section cannot be computed from a knowledge of the major and minor elements present in the sample. A need for good experimental values was thus established. Unfortunately, the experimental procedure requires approximately twenty pounds of crushed rock. This amount presents no problem for the outcrop rock samples the procedure was developed to process. But such an amount very often is a problem when relatively precious core material is to be analyzed.

2.2 An improved pulsed source technique

To completely eliminate the unknown diffusion coefficient of the rock matrix from the data analysis procedure, Czubek [4] has described the use of a series of pulsed neutron measurements involving reflected, spherical samples. Usually five different reflector sizes are used in the experiments; the spherical geometry was chosen to simplify the theoretical analysis. If the rock matrix cross section is not too small, ordinary water or plexiglass plastic is a good choice for the reflector material. For very small cross sections (roughly 5 capture units, or less), graphite may be preferred. Although good results can be obtained by this method for rock samples of the order of a few pounds, the necessity of repeated experiments often leads to two or three days of laboratory work to process a single sample.

2.3 Nuclear reactor measurements

The use of a low-power nuclear reactor to measure the absorption cross section of very small earth samples has been reported by Harris and McDaniel [5,6]. Only 100 grams of rock are needed for this technique. The reactor used in the experiments was the Advanced Reactivity Measurement Facility at the Idaho National Engineering Laboratory. This 40 watt swimming pool reactor has six sites in the reactor core where small samples can be inserted for exposure to neutron fields of different magnitudes. A measurement is made by inserting the unknown sample in each location and precisely measuring the reactivity change needed to restore criticality of the reactor. Calibration of the reactivity change is accomplished by the use of samples of known scattering and absorption cross sections. Good results are shown for eight test samples and three geological samples of known cross section.

2.4 A capsule source method

A very simple steady-state method has recently been proposed by Tittle and Crawford [7]. They employ a small proportional counter filled with helium-3 gas as the neutron detector. The detector is separated from a one-curie ^{238}Pu-Be neutron source by the experimental sample, a plastic bottle filled with 500 gms of crushed rock which has been saturated with ordinary water. All of these components are located at the center of a large water tank which serves as the moderator-reflector for the experiment. An empirical calibration curve of counting rate versus absorption cross section is used. The curve is developed by saturating clean silica sand samples with water containing various concentrations of boric acid. Corrections for porosity variations can be made if the sample significantly deviates from the 32% value obtained for the sand. Initial results indicate that the correction for lithology is small, but the effect is currently being investigated in greater detail. Since very small changes in counting rate must be reliably detected, a very stable counting system is essential for good results.

3. Calibration of Potassium, Uranium, Thorium Logs

Natural gamma ray spectral logs were initially used in minerals exploration and for correlation of formations in petroleum logging. More recently spectral gamma ray logs have been used for complex lithology identification, to estimate cation exchange capacities of shaly clastic rocks, to locate productive fracture systems in low permeability formations and to make quantitative determinations of micas and clays in sandstone formations. These and other applications depend on quantitative assessment of each of the three radioactive contents indicated by the logs: potassium (K), uranium (U), thorium (T). The logs are commonly referred to as K-U-T logs.

The United States Department of Energy has constructed K-U-T calibration pits at several sites in the U.S. These pits consist of several layers containing known amounts of potassium, uranium and thorium in sequence. The elemental concentrations and borehole diameters were designed specifically to represent conditions encountered in mineral exploration. These facilities are not the most satisfactory for calibrating tools used in petroleum logging where the concentrations of radioelements in sedimentary formations are much lower than in uranium or thorium ore deposits.

A facility specifically designed for use by the petroleum industry was proposed in 1980. Funds for its construction have been committed by the American Petroleum Institute and a large segment of the U.S. petroleum industry.

The following general considerations govern these pits:

a. The radiometric grades of the various zones in the pits and distribution of the radio-elements in each zone must be well defined. Hence, a thorough sampling and assaying program is intrinsic to the project.

b. The size of the "hot" zones in the facility must be large enough to exclude external radioactive source material from influencing measurements in the vertical center of any zone. Based on calculations and measurements performed by various groups, zone boundaries should be two feet from the detector. Since most detectors are about one foot long, the height of the hot zones should be five feet.

c. A zone with a mixture of K, U and Th at above normal concentrations should be available to test the spectral identification procedures used by the various service companies.

d. Low activity "barren" zones between the calibration zones will enable bed boundary effects to be assessed. This is in recognition of the difference in bed boundary effects due to the spectral differences of the three species. Barren zones should be made of the same materials as the hot zones except for the radioactive materials used to spike the hot zones.

e. Calibration zones will be placed in two pits to make the facility readily usable.

f. Logging tools with intense neutron sources or strong eccentering devices will be excluded from routine use in this facility. However, neutron tools may be run in the facility during the facility characterization process. A delay of several days should be enforced between the use of a neutron tool in the pit and any attempt to calibrate in the facility.

g. The facility should be kept under water at all times to inhibit radon migration through the cement. Radon migration would especially disturb the measurement of the uranium response.

Detail specifications of the physical geometry of the pits, considerations concerning the overhead crane facilities required to raise and lower logging tools into the pits, and the selection of materials to be used in constructing the zones are given in a paper by Arnold [8].

It should be noted here that natural gamma-ray spectral measurements can be carried out on sections of whole core by several commercial laboratories. Three facilities so equipped are Core Laboratories (Calgary, Alberta), Geo-Tech (Calgary) and Redwood Corex (Aberdeen, Scotland). At lease one major U.S. oil company (Marathon Oil) also operates a continuous core scanner of this type.

4. Pulsed Neutron Capture Logs

Thermal neutron die-away logs based on the die-away and capture of neutrons originating from a pulsed source of 14-Mev neutrons was first used in the U.S.S.R. and later in the U.S.A. With the capability of differentiating hydrocarbons from salt water through iron tubing and casing, this log has been used widely in the petroleum industry for about 20 years.

In the U.S., commercial services are offered by two companies: Dresser-Atlas, initially, and later Schlumberger. Two other U.S. companies are planning to offer pulsed neutron capture logging services within the next year: Welex - a Halliburton company and Gearhart Industries. The Welex tool will use a neutron generator manufactured by Kaman Sciences Corporation. The Gearhart tool will use neutron tubes and high voltage supplies of their own design, to be manufactured in a new facility near Alvarado, Texas.

4.1 Current status

It was noted in Section 2 that a quantitative interpretation of pulsed neutron capture logs cannot be made unless the macroscopic thermal neutron absorption cross section of all components of an earth formation is known. This statement presupposes, of course, that it is possible to determine the true macroscopic thermal neutron absorption cross section of the formation from the pulsed neutron capture log. To obtain such values, correction factors for neutron diffusion effects, borehole size, cement thickness and borehole fluid usually must be applied. Considerable insight into the importance and magnitude of these corrections has been provided by Preeg and Scott [9] using Monte Carlo simulations of Schlumberger's Thermal Decay Time log. They show, for example, that Monte Carlo calculations readily permit one to determine thermal neutron lifetimes for the individual zones (casing, cement, borehole fluid) which contribute to the overall lifetime measured by a gamma ray detector in the simulated sonde. Effects of porosity and bed thickness also are explored. Some modeling results have been confirmed by laboratory experiments. Perhaps the greatest value of these calculations is that they clearly show that departure curves can be used with confidence only over a limited range of borehole and formation capture cross sections.

An improved thermal neutron decay time logging system (known as the TDT-M) has been developed by Schlumberger [10] to provide both increased statistical precision and greater accuracy in the determination of thermal neutron lifetimes. The new system uses 16 time gates to span the neutron die-away spectrum. The time gates always have a fixed relative size but they are adjusted as a whole over four sets of values to accommodate changes in the thermal neutron lifetime. A ratio of counts recorded in two of the earlier gates to the counts recorded in either four or five of the later gates is empirically correlated with the true thermal neutron lifetime. The gate choices used in the ratio calculation depend on the indicated lifetime. For example, if the lifetime falls between 120 μs and 210 μs, the gates used in the numerator are 4 and 5, and the gates used in the denominator are 8, 9, 10 and 11. Gates 15 and 16 are always used to determine background. Results of the empirical fit are said to be good to an accuracy of ±1%. An improved neutron generator has also been introduced with the TDT-M system. Its output is approximately twice that of previous models using the same accelerating potential. The improved statistics provided by the new analysis system and increased neutron output allow the far-spaced gamma ray detector of the TDT-M to be used in the determination of thermal neutron lifetime. All previous TDT systems have been required to use the near-spaced detector. In general, neutron diffusion effects are smaller for the measurement made with the far-spaced detector, hence a more accurate capture cross section is obtained.

A new method of signal processing for pulsed neutron capture logging has been introduced recently [11,12]. Previous methods utilized counting rates observed in various time windows following a neutron generator burst; ratios of the counting rates have been used generally to estimate the decay constant or lifetime in a presumed exponential decay. In the new method the average time of occurrence of a detector pulse after a burst is measured. This time is measured with respect to the start of a time gate of width G and is related to the macroscopic absorption cross section Σ by

$$\langle t \rangle = \frac{1}{v\Sigma} - \frac{G}{e^{v\Sigma G} - 1}$$

where v is neutron speed. In comparison logging runs made in a borehole covering a depth interval of 1700 feet, the time average method yielded an average standard deviation of 0.85 c.u. (1 c.u. = 10^{-3}cm) for Σ, whereas the traditional two-gate method yielded a value of 1.25 c.u. The improved precision of the time average method is particularly noteworthy in zones with high Σ values.

A problem that has plagued pulsed neutron capture logging in the past is the determination of a formation Σ value when that value is comparable to or greater than the borehole fluid Σ value. A new approach to this problem involves the use of recording counting rates in a multiplicity of time gates and separately determining the formation and borehole fluid decay components [13,14]. The Thermal Multigate Decay (TMD) logging system utilizes two scintillation gamma-ray detectors. Capture gamma rays occurring between neutron bursts are measured in each detector for six time gates; background is also measured and subtracted. The count rate data from the time gates are processed using an iterative least-squares technique applied to a two-exponential model which decouples the formation and borehole decay components, yielding both formation and borehole capture cross sections. A ratio of count rates recorded in the two detectors is used to obtain formation porosity. Supplemental curves obtained with the TMD system can be used to identify intervals which have filtrate invasion or large washouts, and can also be used to monitor correct tool operation and data transmission. The borehole independent formation cross sections obtained with this technique can be used directly in calculating formation water saturation. The borehole cross sections, quality parameters, and ratios can be used to extract additional information about borehole salinity, fluid contacts, packers, cement conditions, gas or air in the borehole region, and other borehole related anomalies. This information can also be used to improve the estimate of formation porosity obtained with the TMD system, and to resolve gas from oil in the formation.

4.2 Calibration

In qualitative applications of pulsed neutron logs, systematic differences among measurements made by different logging tools are relatively unimportant. However, for accurate quantitative results pulsed neutron logging tools should be calibrated in a test facility whose physical properties are accurately established at time of construction. Preliminary specifications for such a facility to calibrate thermal neutron die-away tools have been determined for a proposal to the American Petroleum Institute for funding. The original specifications should be reexamined in view of the recent availability of tools for making induced gamma-ray spectral measurements. The intrinsic thermal neutron properties and a complete chemical analysis of such a facility should be established as accurately as possible and the facility should represent realistic conditions under which pulsed neutron logs are run.

The thermal neutron die-away log response is used to determine the macroscopic thermal neutron absorption cross section, Σ, of the formation, customarily given in capture units (c.u.). In commercial logging tools used in the U.S., this quantity is deduced from the observed die-away rate of gamma rays resulting from the capture of thermal neutrons. The value of the measured Σ depends on the porosity, ϕ, and the macroscopic cross sections of the rock matrix, Σ_{ma}, and the fluid, Σ_f, filling the pore space. The calibration facility for neutron die-away tools should consist of several simulated formations saturated with fluid. The values of Σ_{ma}, Σ_f, and ϕ must be accurately determined for each formation. The present API test pit for calibration of conventional neutron porosity tools (steady state capsuled neutron source) is not suitable for a neutron die-away calibration facility for several reasons:

a. Since the borehole in the pit is uncased and the vast majority of pulsed neutron logs are run in cased wells, the present facility is not representative of conditions under which the logs are run.

b. If the limestone in the pit is absolutely pure $CaCO_3$, the range of values of Σ in the water-saturated rock zones is too restricted 7-11 c.u.).

c. It is unlikely that the limestone is chemically pure $CaCO_3$. Many sedimentary rocks contain trace amounts of elements which are strong thermal neutron absorbers. Carbonates may contain a few parts per million of gadolinium and a few hundred parts per million of boron. The presence of a small amount of boron in the API test pits (not tested for at the time of construction) can lead to a large uncertainty in Σ_{ma}.

d. There appears to be no universally acceptable method of determining Σ_{ma} after construction of a facility is complete and all surplus rock material has been discarded, as is the case for the present API test pit. Σ_{ma} must be determined independently, either on the whole rock or on the cores. In the former case, of course, the measurement must be made before construction.

The proposed new calibration faciliy for pulsed neutron logging tools should consider the factors given in the report of the working group that prepared the API proposal submitted in 1977 [15]. Among these factors are:

1. Location - the new facility should be located at the University of Houston near the existing API pits for calibrating gamma ray and neutron porosity tools.
2. Desirable test pit parameters - among those that were considered are:
   (a) Number and type of rock matrices
   (b) Porosities
   (c) Size of pit
   (d) Types of saturating fluids
   (e) Borehole diameter
   (f) Cased or uncased borehole

3. Methods to be used to establish the significant intrinsic properties (Σ_{ma}, Σ_f, ϕ) of the formations.

In addition, a working group needs to be formed to reach recommendations concerning factors important to the calibration of induced spectral gamma-ray logging tools.

5. Improved Gamma-Ray Detectors for Logging

Historically, gamma-ray detectors used in petroleum logging have been ionization chambers, Geiger-Mueller counters, or scintillation counters (NaI and CsI). The scintillation counters used presently in conventional total-count gamma-ray logging are quite adequate for that application. Improved detectors are needed in two relatively new areas of logging: (1) elemental analysis by means of neutron-induced gamma-ray spectral logging, and (2) natural gamma-ray spectral logging. The first of these areas requires a high-resolution detector, while the second requires a detector with moderately good resolution but very high efficiency.

5.1 High resolution detectors

The desirability of, and the problems associated with, the use of a high-resolution detector (line-width $\leq$ 2 keV at energy 1 MeV) have been summarized previously [2]. Since that summary no publications have appeared in the open literature to indicate that the primary problem of maintaining the detector at a sufficiently low temperature for a sufficiently long time has been solved to permit logging under oil well conditions. There are indications that some wireline logging service companies are diligently working to overcome the engineering problems and to produce a viable logging service based on high-resolution gamma spectroscopy.

5.2 High efficiency detectors

Natural gamma-ray spectral logging has the potential for allowing several log interpretation problems to be solved [1]. In particular, the effects of clays and radioactive minerals on log response can be separated. Counting rates encountered in natural gamma-ray spectral logging tend to be quite low. Thus, a detector with the highest possible counting efficiency, consistent with sufficiently good spectral resolution, is highly desirable. The search for large volume, highly efficient gamma-ray detectors has been directed primarily toward scintillators having one or more elemental components with an atomic number substantially higher than that of NaI and having a density greater than that of NaI. The most promising candidates thus far are certain oxides, notably bismuth germanate ($Bi_4Ge_3O_{12}$) and cadmium tungstate ($Cd\ WO_4$). Of these, bismuth germanate, or BGO as it is commonly called, appears to be the most useful for borehole applications. Cesium iodide activated with sodium has also been seriously studied.

Table 1 shows a comparison of the properties of NaI (Tℓ), CsI(Na), BGO, and $Cd\ WO_4$. The density of BGO is about twice that of NaI or CsI, giving it a much greater stopping ability for gamma rays. On the other hand, the relative scintillation output of BGO is about an order of magnitude below that of NaI or CsI, which results in poorer energy resolution for BGO. A serious drawback to BGO for deep logging applications is its variation of light output and resolution with temperature. Fig. 1 shows this variation over a temperature range that is reasonable for the inside of a logging tool [16]. These data clearly indicate the need for temperature stabilization of a BGO detector and its photomultiplier tube if it is to be useful in deep logging operations.

Conaway, Killeen, and Hyatt [17] and Stromswold [18] have independently carried out experimental comparison studies involving scintillators. In each work NaI(Tℓ), CsI(Na), and BGO detectors of identical size were placed in probes designed for uranium logging in shallow boreholes. Conaway, et al, used a detector size of 19 mm dia. x 76 mm length; Stromswold used NaI(Tℓ) and BGO detectors that were 38 mm dia. x 76 mm length. Data were obtained in uranium calibration test pits located near Ottawa, Canada, and Grand Junction, Colorado, in the U.S. Both groups concluded that the use of BGO for spectral analysis resulted in a reduction of approximately 50% in statistical errors compared to a NaI detector of the same size. Under the same conditions CsI was better than NaI by 10-20%.

Borsaru, et al, [19] have carried out tests comparing 51 mm x 51 mm BGO and NaI(Tℓ) detectors in a logging probe suitable for obtaining natural gamma-ray spectra in shallow boreholes drilled through coal seams. One figure of merit used for comparison was the relative standard deviation for estimating net peak area in a spectrum. For peaks at 0.6 MeV (U + Th), 1.46 MeV (K), and 2.62 MeV (Th), the relative standard deviation for BGO averaged about one-half that for NaI(Tℓ).

5.3 Data requirements

In order to properly calibrate and interpret the data from logging tools using gamma-ray detectors for spectral measurements, in either a passive or an active mode, properly designed and accurately known calibration models are required. A planned calibration facility for natural gamma-ray spectral measurements was described in section 3. Similar models will be needed in the future for induced gamma-ray spectral measurements. It seems logical to construct models which have an accurately known value of thermal neutron absorption cross section and which also have accurately known amounts of key elements that are detected and measured in induced spectral logging. These elements include hydrogen, carbon, oxygen, silicon, aluminum, chlorine, calcium, and iron. Planning of a pulsed neutron capture logging calibration facility should include the above considerations.

In order for the quality of a natural or induced gamma-ray spectral logging service to be ascertained, spectral data should be obtained under known conditions and the method by which elemental compositions are deduced from the data should be specifically stated. This procedure should include the way in which data obtained under nonstandard borehole conditions are corrected to standard borehole conditions.

5.4. Data analysis

It is frequently of interest to determine the earth's specific radioactivity as a function of depth from a measurement of the gamma-ray intensity made in a wellbore. To make such a determination one must clearly know the response function of the logging sonde and appropriate corrections for all borehole parameters including size, casing weight, cement and drilling fluid. An equation relating the specific radioactivity $q(z)$ and the observed intensity $I_0(z)$ in terms of depth z can be written as follows:

$$I_0(z) = K_0 \; CF(R) \int_{-\infty}^{+\infty} \phi_0(z-z')\, q(z')\, dz'$$

where K_0 is a calibration constant, $CF(R)$ is a correction factor for the attenuation of gamma radiation in the drilling fluid, casing, etc. within the borehole of radius R, and $\phi_0(z-z')$ is a kernel giving the contribution of an infinitely thin layer at z' to the measured intensity at z. Although the equation relating $\rho(z)$ and $I_0(z)$ is difficult to manipulate for rigorous expressions of the kernel $\phi_0(z-z')$, a useful approximation has been proposed by Davydov [20], namely,

$$\phi_0(z-z') = (\alpha/2)\exp(-\alpha|z-z'|)$$

In this easily-manipulated expression α is a parameter which fits the shape of the assumed function to the true kernel. Czubek [21] has recently shown that kernels of the Davydov form can readily represent the true kernel for a variety of conditions, including c~~or~~ases where detectors of finite length are used. Care must be exercised, however, when the borehole conditions greatly differ from those for which α is calibrated. In such cases the simple multiplicative borehole correction factor $CF(R)$ may not be adequate.

6. Neutron Porosity Logging

The status of neutron porosity logging as of 1981 was reviewed in the IAEA symposium on industrial application of radioisotopes and radiation technology [1]. Work published since that time has been concerned mostly with improvements in the methodology or interpretation of dual-detector logging.

6.1. Dual-thermal neutron detector logging

Theoretical calculations have been carried out to study the effects of trace amounts of strong thermal neutron absorbers on the response of a dual-thermal neutron detector probe [22]. These calculations were made with a finite element, multi-group, P1, 3 dimensional neutron transport code called FEMP3D. Results of the calculations have been compared to data available in the literature on a dual detector probe. FEMP3D has been used to model probe response in various porosity-matrix environments, primarily low-porosity, shaly sandstones which are fully saturated with fluid, partially saturated, or gas invaded.

6.2. Dual-epithermal neutron detector logging

A new four-detector neutron porosity tool has been introduced recently [23]. The tool consists of two thermal neutron detectors spaced apart on one side of a 16 Ci AmBe source (4×10^7 n/s) and two epithermal neutron detectors spaced apart on the opposite side of the source. The pair of epithermal detectors is nearer the source than the pair of thermal detectors. A bowspring that spans the detector spread forces the tool into an eccentered position in the borehole.

The principle behind the configuration described above is as follows. Dual-thermal neutron detector logging, in the form in which it has been available from wireline logging service companies, has provided accurate values of porosity in formations with relatively small macroscopic thermal neutron absorption cross section, Σ_a. In general, porosity is overestimated in formations with large values of Σ_a. This is caused by the use of source-detector spacings that are too small. The addition of a pair of epithermal detectors provides a second porosity measurement. In clean formations the two porosity measurements should agree. In formations with large Σ_{ma} values, the porosity derived from the epithermal pair should read lower than that from the thermal pair and should agree with other log-derived porosity values (e.g., from the gamma-gamma density log). Thus the epithermal porosity, when used with the density-derived porosity, should provide better gas detection in shaly gas sands than the thermal porosity. Comparison of the epithermal-derived and thermal-derived porosities provides an indication of the amount of strong thermal neutron absorbers present in the formation. A serious disadvantage of the dual-epithermal detector method is that, due to the lower detection efficiency of epithermal compared to thermal detectors, counting rates can be quite low. Another disadvantage is that the straightforward method of obtaining porosity from the ratio of counting rates, as done in dual-thermal detector logging, has been abandoned for a more complicated and less scientifically appealing adaptive filtering technique applied to the individual epithermal counting rates.

A useful technique for visualizing and comparing the responses of dual-epithermal and dual-thermal neutron detector configurations has been found to be a logarithmic cross-plot of the far detector count rate against the near detector count rate [23,24]. Figure 2 shows cross-plots from reference 23 for dual-epithermal and dual-thermal configurations. The effects of varying borehole conditions can be shown on a "spine and ribs" plot, with the spine being provided by the plots in Fig. 2. An example is illustrated in Fig. 3 which shows the effect of different amounts of tool standoff. In addition to tool standoff, data have been obtained for various borehole diameters, mudcake thicknesses, mud weights, borehole and formation fluid salinities, temperatures, formation gas saturations, and formation matrix types.

Recent theoretical modeling calculations have been carried out on both dual-thermal and dual-epithermal neutron detector logging systems [25,26]. Ellis, et al, [25] used both a two-dimensional discrete ordinates code (DOT) and a three-dimensional Monte Carlo code (SAM-CE). Calculations were carried out to predict detector counting rates and ratios of count rates in laboratory models in which the borehole diameter, rock matrix type, tool standoff, and formation temperature were varied. Experimental data were obtained under the same model conditions. Agreement between the experimental and calculated results is reasonably good in most cases.

Ullo [26] has used a 2-D discrete ordinates code (DOT) to predict the effect of gas on dual-detector systems, in particular the magnitude of the so-called "excavation effect". Results of the calculations indicate that the difference between an apparent porosity based on the near-epithermal detector count rate and an apparent porosity based on the ratio of epithermal counting rates may have a greater sensitivity to the presence of gas than the customarily used difference in apparent porosities between the formation density log and the dual-thermal neutron detector log. This seems to be especially true in some invaded gas-bearing formations and in shaly sands.

Very recently it has been demonstrated [27] that dual-epithermal neutron detection may provide a more accurate measure of formation porosity in an air-filled borehole than does dual-thermal neutron detection. This is probably due in part to the use of source-detector spacings in commercial dual-thermal detector tools that are too small, with the result that the porosity sensitivity of the count rate ratio is considerably reduced because of the extended source of slowing-down neutrons along the borehole toward the detectors.

7. Induced Gamma-Ray Spectroscopy

Spectral analysis of gamma rays produced by neutron bombardment of formations have long been of interest as a basis for new neutron logging techniques. In recent years emphasis has been on gamma rays produced using a 14-Mev pulsed neutron source and a sodium iodide detector. With a pulsed source and time discrimination the measurement can be selective as to gamma rays from inelastic scattering or capture.

For about ten years carbon/oxygen logging has been a commercial logging service based on measurement of gamma rays from inelastic scattering of 14-Mev neutrons. Carbon/oxygen logging continues to be useful in special situations, primarily for the logging of cased holes to distinguish oil and water in formations having high porosity, low salinity water and no carbonate mineral in the matrix or where the amount of carbonate mineral present is precisely known.

A gamma ray spectroscopy tool (GST) which utilizes both inelastic and capture gamma rays was introduced in 1978. The spectra are used to provide ratios of counting raters attributed to various elements using a weighted least squares analysis of both inelastic and capture gamma rays. The various elemental ratios are used to infer oil saturation (C/O), water salinity (Cl/H), porosity (H/(Si + Ca)), and lithology (Si/(Si + Ca)) of the formation. Many of the elements used are also present in the casing, cement and borehole fluid and must be accounted for to make a proper interpretation of the spectral data. Many different borehole and formation conditions have been investigated in the laboratory to determine the effect on the spectral responses of changes in borehole geometry and elemental composition [28]. Correction for these environmental effects provides a more accurate interpretation of formation parameters. The GST logs provided by this relatively new tool provide a good start on achieving quantitative elemental analysis in the borehole.

REFERENCES

1. ALLEN, L. S., CALDWELL, R.L., "Use of nuclear technology in oil and gas exploration", Industrial Applications of Radioisotopes and Radiation Technology, IAEA-CN-40/100, Vienna (1982).

2. CALDWELL, R. L., MILLS, W. R., ORR, W. L., ALLEN, L. S., "Nuclear techniques in oil and gas exploration and production", Nuclear Techniques and Mineral Resources, IAEA-SM-216/100, Vienna (1977).

3. ALLEN, L. S., and MILLS, W. R., "Measurement of the thermal neutron absorption cross section of rock samples by a pulsed source method", *Log Analyst* *16* 1 (1975) 10.

4. CZUBEK, J. A., "A method for measurement of thermal neutron absorption cross-sections in small samples", *J. Physics D* *14* (1981) 779.

5. HARRIS, J. M. and McDANIEL, P. J., "Small sample thermal neutron cross section determination from reactivity measurements", Soc. Prof. Well Log Analysts, 23rd Annual Logging Symposium, 1982, paper HH.

6. HARRIS, J. M., McDANIEL, P. J., and WIDMAN, D. H., "Thermal neutron absorption from reactivity measurements of selected geological materials", Soc. Prof. Well Log Analysts, 24th Annual Symposium, 1983, paper VV.

7. TITTLE, C. W. and CRAWFORD, G. W., "Measuring the thermal neutron absorption cross section of rocks", *The Log Analyst* *24* 3 (1983) 12,

8. ARNOLD, D. M.," API ad hoc committee on K-U-T logging calibration; recommended calibration facility design", *The Log Analyst* *23* 2 (1982) 60.

9. PREEG, W. E. and SCOTT, H. D.," Computing thermal neutron decay time (TDT) environmental effects using Monte Carlo techniques", Soc. Pet. Eng. (SPE) Paper 10293 (1981).

10. HALL, J. E., JOHNSTONE, C. W., BALDWIN, J. L., and JACOBSON, L.A., "A new thermal neutron decay logging system - TDT-M", Soc. Pet. Eng. (SPE) Paper 9462 (1980).

11. RANDALL, R. R., FERTL, W. H., HOPKINSON, E. C., "Time derived sigma determination for pulsed neutron capture logging", Mid East Oil Conference, Bahrain, 1981, SPE 9614.

12. RANDALL, R. R., HOPKINSON, E. C., "Improved methods of signal processing for pulsed neutron capture logging", 22nd Annual SPWLA Logging Symp., 1981, McAllen, Texas, Paper JJ.

13. SCHULTZ, W. E., SMITH, H. D., VERBOUT, J. L., BRIDGES, J. R., "Experimental basis for a new borehole corrected pulsed neutron capture logging system (TMD)", 23rd Annual SPWLA Symp., Calgary, 1983 Paper CC.

14. SMITH, H. D., ARNOLD, D. M., PEELMAN, H. E., "Applications of a new borehole corrected pulsed neutron capture logging system (TMD)", 23rd Annual SPWLA Symp., Calgary, 1983, Paper DD.

15. MILLS, W. R., HOYER, W. A., TITTMAN, J. and WILSON, B. F., "A proposed calibration facility for pulsed neutron logging tools," *The Log Analyst* *18* 1 (1977) 3.

16. STROMSWOLD, D. C., private communication.

17. CONAWAY, J. G., KILLEEN, P. G., HYATT, W. G., "A comparison of bismuth germanate, cesium iodide, and sodium iodide scintillation detectors for gamma ray spectral logging in small diameter boreholes", Current Research, Part B, Geol. Surv. Canada, Paper 80-18, pp. 173-177 (1980).

18. STROMSWOLD, D. C., "Comparison of sodium iodide, cesium iodide, and bismuth germanate scintillation detectors for borehole gamma-ray logging", IEEE Trans. Nuc. Sci., NS-28:1, (1981) 290.

19. BORSARU, M., CERAVOLO, C., CHARBUCINSKI, J., EISLER, P., YOUL, S., "Comparative performance of BGO and Na(Tℓ) detectors for identifying coal sediments by gamma-ray logs", Eighth European Formation Evaluation Symposium, London (1983).

20. DAVYDOV, Yu. B., "One-dimensional inversion problem in borehole gamma logging", *Izveytya* *Vyssh*. *Uchebnykh* *Zaved*., *Geologia* i *Razvedka*, No. 2 (1970) 105.

21. CZUBEK, J. A., "Kernel functions in gamma-ray logs", Institute of Nuclear Physics Report No. 1197/AP (1982).

22. McDANIEL, P. J., HARRIS, J. M., WIDMAN, D. A., "A theoretical analysis of the effect of thermal neutron absorbers on dual-spaced porosity log measurements", 23rd Annual SPWLA Logging Symp., 1983, Calgary, Paper LL.

23. DAVIS, R. R., HALL, J. E., BOUTEMY, Y. L., FLAUM, C., "A Dual porosity CNL logging system", Soc. Pet. Eng. of AIME, 56th annual meeting, San Antonio, Texas, 1981, SPE 10296.

24. SCOTT, H. D., FLAUM, C., SHERMAN, H., "Dual porosity CNL count rate processing", Soc. Pet. Eng. of AIME, 57th annual meeting, New Orleans, Louisiana, 1982, SPE 11146.

25. ELLIS, D. V., ULLO, J., SHERMAN, H., "Comparison of calculated and measured responses of a dual-detector epithermal neutron porosity device", Soc. Pet. Eng. of AIME, 56th annual meeting, San Antonio, Texas, 1981, SPE 10294.

26. ULLO, J. J., "Response of the dual spacing neutron log (CNL) to gas", Soc. Pet. Eng. of AIME, 56th annual meeting, San Antonio, Texas, 1981, SPE 10295.

27. FLAUM, C., "Dual detector neutron logging in air filled boreholes", 23rd Annual SPWLA Logging Symp., 1983, Calgary, Paper BB.

28. SCHWEITZER, J. S., MUNENTE, R. A., HERTZOG, R. C., "Gamma-ray spectroscopy tool environmental effects", Soc. Pet. Eng., Paper 11144, SPE 57th Annual Fall Technical Conference, New Orleans, Louisiana, Sept. 1982.

Table 1. Characteristics of Scintillators

	NaI(Tℓ)	CsI(Na)	BGO	$CdWO_4$
Density (g/cm^3)	3.67	4.51	7.13	7.91
Decay time (μs)	0.23	0.64	0.30	5
Relative light output (%)	100	80	8	40

BGO (w/PMT) GAIN CHANGE AND RESOLUTION
versus
TEMPERATURE

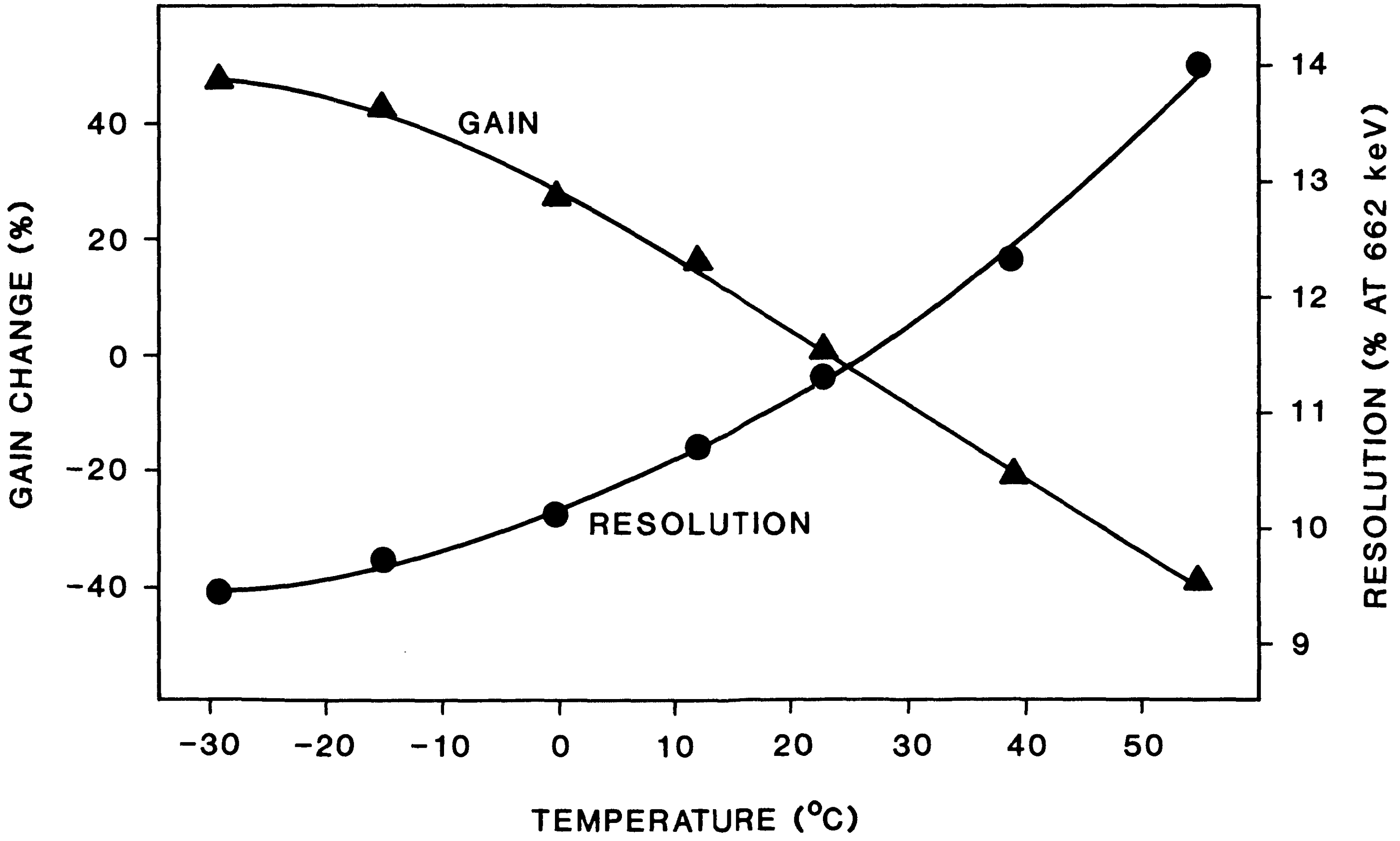

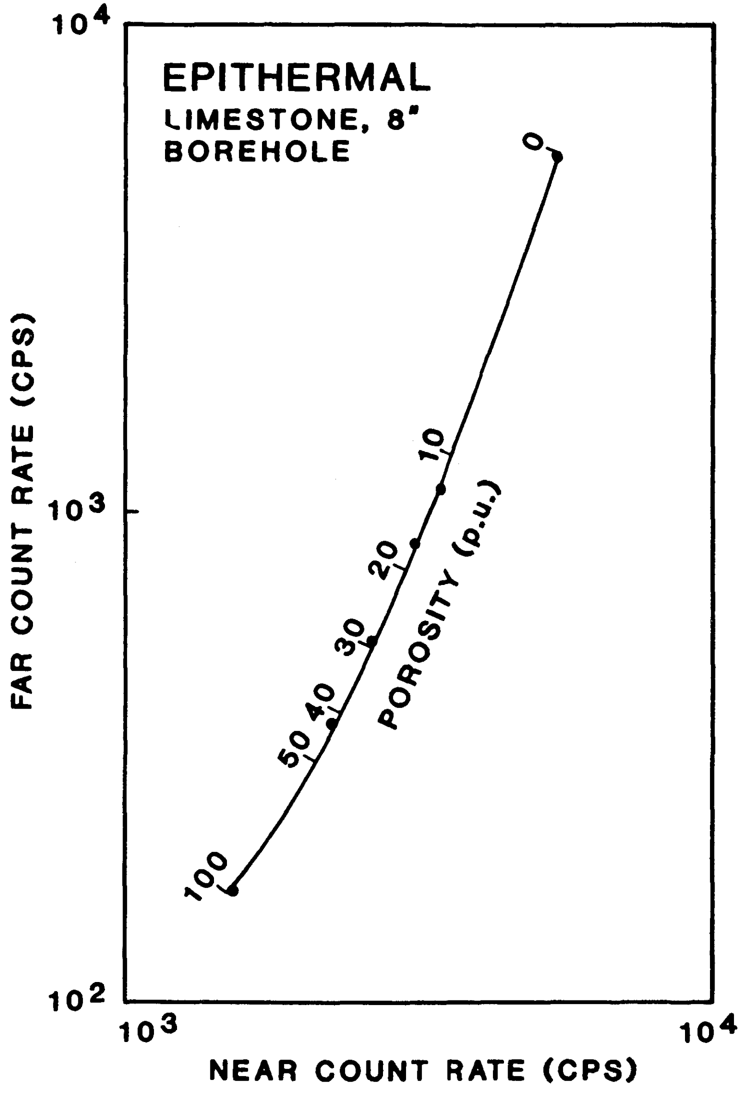
EPITHERMAL
LIMESTONE, 8" BOREHOLE
FAR COUNT RATE (CPS)
NEAR COUNT RATE (CPS)
10^4
10^3
10^2
10^3
10^4
0
10
20
30
40
50
100
POROSITY (p.u.)

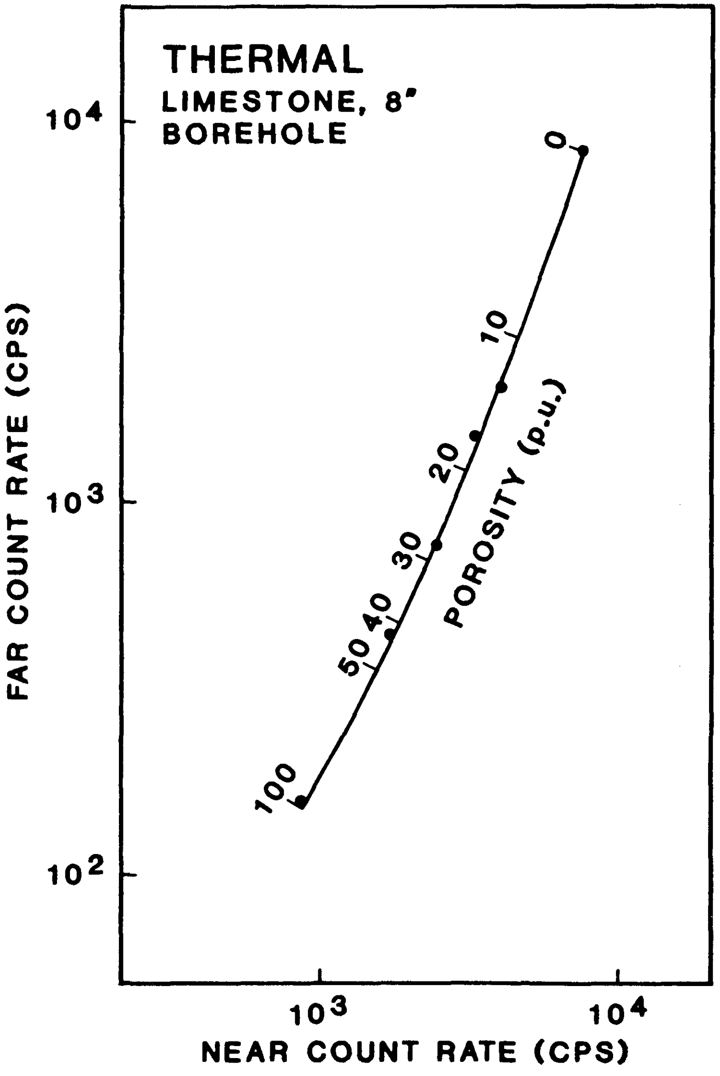
THERMAL
LIMESTONE, 8" BOREHOLE
FAR COUNT RATE (CPS)
NEAR COUNT RATE (CPS)
10^4
10^3
10^2
10^3
10^4
0
10
20
30
40
50
100
POROSITY (p.u.)

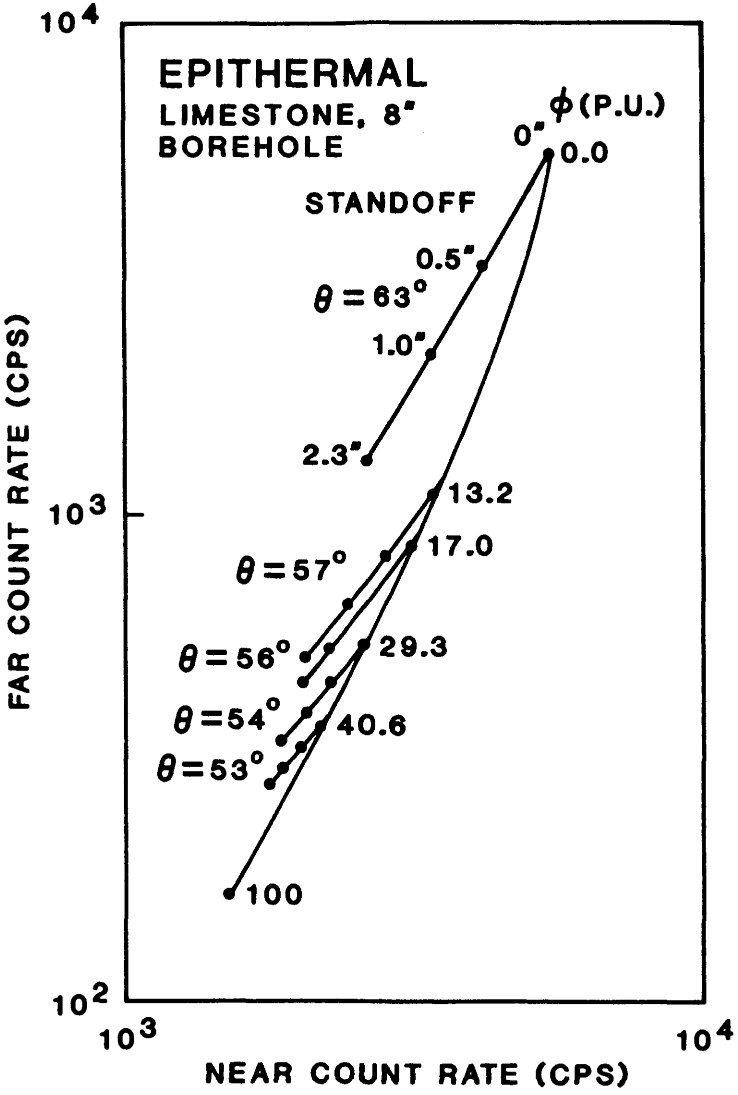
EPITHERMAL
LIMESTONE, 8" BOREHOLE
STANDOFF
φ (P.U.)
0"
0.0
0.5"
θ = 63°
1.0"
2.3"
13.2
17.0
29.3
40.6
100
θ = 57°
θ = 56°
θ = 54°
θ = 53°
FAR COUNT RATE (CPS)
NEAR COUNT RATE (CPS)
10^4
10^3
10^2
10^3
10^4

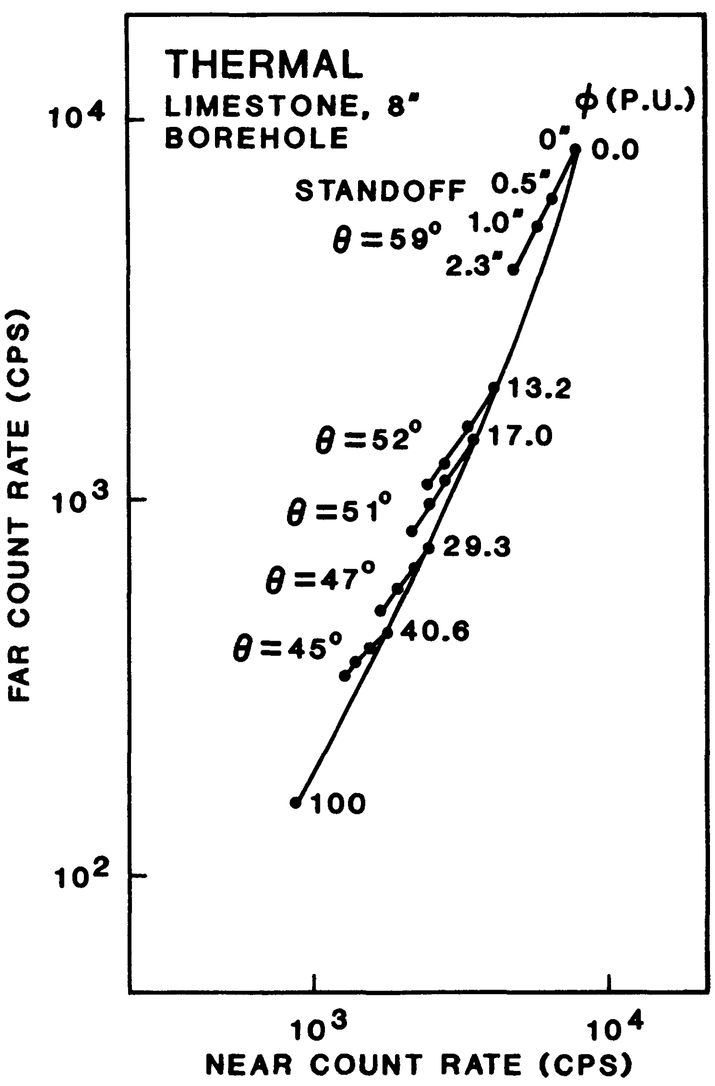
THERMAL
LIMESTONE, 8" BOREHOLE
STANDOFF
φ (P.U.)
0"
0.0
0.5"
1.0"
2.3"
θ = 59°
13.2
17.0
29.3
40.6
100
θ = 52°
θ = 51°
θ = 47°
θ = 45°
FAR COUNT RATE (CPS)
NEAR COUNT RATE (CPS)
10^4
10^3
10^2
10^3
10^4

IAEA CONSULTANTS' MEETING ON NUCLEAR DATA FOR BORE-HOLE AND BULK-MEDIA ASSAY USING NUCLEAR TECHNIQUES

Krakow, Poland 14-18 November 1983

SOME APPLICATIONS OF ATOMIC AND NUCLEAR METHODS IN GEOLOGY AND MINING*

J.Csikai, K.M.Dede, A.Deměny, G.I.Khalil**, N.K.Mumba***,
A.Pázsit, I.Szalóki, S.Szegedi

Institute of Experimental Physics, Kossuth University
4001 Debrecen, Pf. 105,Hungary

Abstract: For thé determination of major and trace elements in various geological samples the following atomic and nuclear methods have been used: X-ray fluorescence technique; thermal, resonance and fast neutron activation analyses including the on-stream measurements; pulsed neutron technique; delayed neutron detection; thermal neutron reflection and absorption; gamma spectrometry; detection of radon by track-etched technique; prompt radiation analysis; geological dating by spontaneous and neutron induced fission. The advantageous and disadvantageous of each techniques in comparision with other methods are discussed.

Special attention is paid to the atomic and nuclear data needed for the improvement of the methods mentioned above.

---

*This work was supported in part by the Ministry of Higher Education and the Hungarian Academy of Sciences.

**Permanent address: Alexandria University, Faculty of Science, Egypt.

***Permanent address: National Council for Scientific Research, Lusaka, Zambia

INTRODUCTION

The terrestrial crust consists of various types of rocks, which change slowly to soils, clays, sediments, etc. by erosion and sedimentation processes. The elements in terrestrial samples can be devided into four groups: major (>1.0 %), minor (0.01-1.0 %), trace (<0.01 %) and rare trace (<0.1 ppm). The major elements in most rocks types are as follows: Si, O, Al, Fe, Mg, Ca, Na, K, Ti and P. The concentrations of these elements in the well-known terrestrial rocks differ from 1 to 4 orders of magnitude, therefore, careful investigations are needed to develop the most suitable methods for the bore-hole and bulk-media assay. Fast, non-destructive methods are needed for the determinations of major constituents of rocks and the concentration of various elements in minerals, standard geological materials, processing solutions or slurries and ocean bottom cores. These methods should be applicable for sampling, in-situ and on-stream measurements. The main difficulty in the utilization of the atomic and nuclear methods for the chemical analysis of geological samples is in connection with the complexity of the matrices.

This paper briefly demonstrates a few methods used for the analysis of geological materials and gives some suggestions for the possible improvements of these techniques.

1. DETERMINATION OF MAJOR AND TRACE ELEMENTS IN CRUDE OILS BY NEUTRON ACTIVATION AND REFLECTION METHODS

The concentrations of major and trace elements in crude oils can give information on their quality and end-products, on the necessary refining and processing procedures as well as on the history of the oil fields [1]. The hydrogen content and the ratio of carbon to hydrogen are in connection with the concentration of aromatic components to the others which determines the calorific and economic values of oils.

Trace elements in crude oils are present in two distinct forms as metal-organic complexes and as solid and liquid suspensions. The separation of elements being in metal-organic complexes is a very difficult task. For this reason the in-situ determination of the concentration of these elements in crude oils would be very important in practice.

The concentrations of O, Na, Cl, V, Mn and Ni in crude oils of different origins were determined, using sampling (SNAA) and on-stream (ONAA) activation analyses. Samples were irradiated with thermal and fast neutrons produced by a 0.3 mg ^{252}Cf source and a 14 MeV generator. The H-content and the C/H atomic ratio have been determined by thermal neutron reflection method using an 18 GBq Pu-Be source.

An improved on-stream experimental arrangement developed for these measurements [2] is presented in Fig.1.

The nuclear data for reactions used in this investigations are summarized in Table 1.

Table 1

Element	Reaction	Half-life	Cross-section (b)	E_γ (keV)
V	$^{51}V(n,\gamma)^{52}V$	3.77 m	4.88	1434
Na	$^{23}Na(n,\gamma)^{24}Na$	15.0 h	0.53	1368
Cl	$^{37}Cl(n,\gamma)^{38}Cl$	37.3 m	0.43	1642
Mn	$^{55}Mn(n,\gamma)^{56}Mn$	2.58 h	13.3	846
Ni	$^{64}Ni(n,\gamma)^{65}Ni$	2.56 h	1.49	1482
O	^{16}O n,p ^{16}N	7.3 s	9×10^{-5}	6100 7100

For the determination of hydrogen content in crude oils and the ratio of carbon to hydrogen a method based on the thermal neutron reflection was developed [3]. The reflection coefficient (β) of thermal neutrons as a function of reflector thickness shows saturation at about 8 cm if a point source and a detector is placed onto the free surface of a semi-infinite moderator (see Fig.2.). It was found that the relative excess in the counting rates in the presence of sample depends linearly on the hydrogen content of sample: $\eta = (I-I_o)/\rho I_o$, where I and I_o are the counting rates with and without sample and ρ is the density of the sample. At zero hydrogen content we have the value for the matrix. In Fig. 3. the η and the $\rho\eta$ values are shown as a function of hydrogen concentration for hydrocarbons and oil in different matrixes, respectively.

The following general conclusions can be drawn from the analysis of the data obtained for oils from Iraq, USSR and Hungary:

- Vanadium content higher than 50 ppm can easily be measured by the on-stream method in continuous flow, during the exploitation. For the other elements a concentration of ten times higher than the detection limits can be determined also in-situ condition.
- The concentrations of Ni, Mn, Na and Cl vary in a wide range even for the same field.
- The trace elements are more sensitive to the quality of crude oil than the H and C/H values.

For the improvement of the NAA and NRM some new procedures should be developed, in addition to complete the available nuclear data. These are as follows:

1) Cross sections of the possible interfering reactions for the estimation of their contribution to the peak area.

2) Determinations of gamma spectra for elements irradiated and measured in the same circumstances as the samples to study the possible overlapping of the peaks and to select the most suitable gamma lines for the investigations.

3) Determination of average neutron flux for absorbing samples of unknown compositions.

4) Effect of the matrix on the reflected neutrons, i.e. on the η value.

5) Method for the determination of the flux albedo of neutrons for heterogeneous media.

6) Cross section curves for $^{13}C(p,n)^{13}N$ and $^{12}C(p,\gamma)^{13}N$ secondary reactions are needed to control the neutron reflection method used for the determination of C/H value.

The absolute interfering reactions and the overlapping gamma lines are summarized in Table 2. For the determination of isotopes producing interfering gammas a resolution of ± 10 % and ± 0.3 % was accepted for NaI and Ge(Li) detectors, respectively, and an interval of $T_{1/2}/3$ - $3T_{1/2}$ was chosen. In the case of oxigen the bias level was taken at 3.5 MeV. The data in Table 2. show that the number of interfering gamma lines can be significantly decreased if a Ge(Li) detector is used. Before using the neutron activation analysis the composition of the sample should be determined by a fast qualitative method as the X-ray fluorescence technique to estimate the possible disturbing reactions and gamma lines. In the case of typical geological samples placed into a mixed neutron field and measured with a NaI detector, the preliminary estimation of the composition is indispensable. This concerns for the drilled samples, too, before the well-logging method is applied. For NAA generally 14 MeV neutrons, as well as (α,n) and ^{252}Cf sources are used. If the amount of sample is small, the necessary corrections can be estimated in the knowledge of the spectrum averaged cross sections. However, for the borehole and bulk-media assay the unfolding of the neutron spectra is indispensable using the threshold foil technique. The accurate data for the average cross sections give a possibility to check the reliability of the excitation functions of threshold reactions applied for unfolding the spectra.

Table 2

Element	Reaction	Absolute interfering reaction	Interfering isotopes by gammas	
			NaI	Ge(Li)
V	$^{51}\mathrm{V}(n,\gamma)^{52}\mathrm{V}$ E_γ=1.44 MeV	$^{52}\mathrm{Cr}(n,p)^{52}\mathrm{V}$; $^{53}\mathrm{Cr}(n,np)^{52}\mathrm{V}$; $^{55}\mathrm{Mn}(n,\alpha)^{52}\mathrm{V}$	^{40}Cl, ^{50}Sc, ^{58}Mn, ^{68}Cu, ^{74}Ga, ^{84m}Br, ^{86}Br, ^{93}Sr, ^{138m}Cs, ^{152}Pm, ^{89m}Zr, ^{91m}Mo, ^{101}Mo, ^{102}Tc, ^{164m}Tb, ^{196}Ir	^{74}Ga, ^{138m}Cs, ^{152}Pm, ^{154}Pm, ^{164}Tb
Na	$^{23}\mathrm{Na}(n,\gamma)^{24}\mathrm{Na}$ E_γ=1.3685; 2.7541 MeV	$^{24}\mathrm{Mg}(n,p)^{24}\mathrm{Na}$; $^{27}\mathrm{Al}(n,\alpha)^{24}\mathrm{Na}$	^{48}Sc, ^{57}Ni, ^{69}Ge, ^{72}Ga, ^{77}Ge, ^{82}Br, ^{93m}Mo, ^{96}Nb, ^{101}Pd	^{77}Ge
Cl	$^{37}\mathrm{Cl}(n,\gamma)^{38}\mathrm{Cl}$ E_γ=1.6422; 2.1676 MeV	$^{41}\mathrm{K}(n,\alpha)^{38}\mathrm{Cl}$; $^{38}\mathrm{Ar}(n,p)^{38}\mathrm{Cl}$	^{34}Cl, ^{39}Cl, ^{44}K, ^{62}Co, ^{78}As, ^{83}Se, ^{84}Br, ^{87}Kr, ^{91}Mo, ^{94}Y, ^{98}Nb, ^{101}Mo, ^{104}Tc, ^{105}Cd, ^{116m}In, ^{133}Te, ^{134}I, ^{138}Cs	^{158}Eu
Ni	$^{64}\mathrm{Ni}(n,\gamma)^{65}\mathrm{Ni}$ E_γ=1.4816 MeV	$^{65}\mathrm{Cu}(n,p)^{65}\mathrm{Ni}$; $^{68}\mathrm{Zn}(n,\alpha)^{65}\mathrm{Ni}$	^{78}As, ^{87}Kr, ^{92}Y, ^{95}Ru, ^{93m}Mo, ^{98}Nb, ^{105}Cd, ^{106m}Rh, ^{112}Ag, ^{116m}In, ^{117m}Cd, ^{129m}Ba, ^{132}I, ^{134}I, ^{142}La, ^{150}Pm, ^{183}Hf	^{93m}Mo, ^{117m}Cd

Element	Reaction	Absolute interfering reaction	Interfering isotopes by gammas	
			NaI	Ge(Li)
Mn	$^{55}\mathrm{Mn}(n,\gamma)^{56}\mathrm{Mn}$ $E_{\gamma}=0.8469$ MeV	$^{56}\mathrm{Fe}(n,p)^{56}\mathrm{Mn}$; $^{57}\mathrm{Fe}(n,np)^{56}\mathrm{Mn}$; $^{59}\mathrm{Co}(n,\alpha)^{56}\mathrm{Mn}$	$^{71m}\mathrm{Zn}$, $^{69}\mathrm{Zn}$, $^{78}\mathrm{As}$, $^{92}\mathrm{Y}$, $^{95}\mathrm{Ru}$ $^{96m}\mathrm{Tc}$, $^{98}\mathrm{Nb}$, $^{105}\mathrm{Ru}$, $^{106m}\mathrm{Rh}$, $^{116m}\mathrm{In}$, $^{117m}\mathrm{Cd}$, $^{123}\mathrm{Xe}$, $^{127}\mathrm{Sn}$, $^{129m}\mathrm{Ba}$, $^{132}\mathrm{I}$, $^{134}\mathrm{I}$, $^{142}\mathrm{La}$, $^{145}\mathrm{Pr}$, $^{150}\mathrm{Pm}$, $^{183}\mathrm{Hf}$, $^{195m}\mathrm{Ir}$, $^{196m}\mathrm{Ir}$	$^{134}\mathrm{I}$, $^{145}\mathrm{Pr}$
O	$^{16}\mathrm{O}(n,p)^{16}\mathrm{N}$ $E_{\gamma}=6.13$ MeV	$^{19}\mathrm{F}(n,\alpha)^{16}\mathrm{N}$; $^{15}\mathrm{N}(n,\gamma)^{16}\mathrm{N}$	$^{11}\mathrm{Be}$, $^{30}\mathrm{Al}$, $^{76}\mathrm{Ga}$, $^{86}\mathrm{Br}$	

Present status of 14 MeV cross sections is discussed in Ref. [4] and recommended values are given e.g. in Refs. [5, 6, 7]. Only a few spectrum averaged cross sections are available for the radioactive (α,n) sources in comparision with those determined for ^{252}Cf neutrons [8,9]. Results obtained in Debrecen are summarized in Table 3.and 4. for Pu-Be [10] and ^{252}Cf [11] sources, respectively. In Table 5 the measured and calculated $\langle\sigma\rangle$ values are given using different $\sigma(E)$ sets. The accuracies of the measured data do not give a possibility to check the evaluated cross sections given in the ENDF/B-IV and ENDF/B-V.

Table 3

Element	Reaction	$T_{1/2}$	E [keV]	C.S. [mb]	Method
Al	^{27}Al(n,p)^{27}Mg	10 m	840	24 ± 3.4	4πβ gamma, β
Si	^{28}Si(n,p)^{28}Al	2.3 m	-	54 ± 11	β
P	^{31}P(n,p)^{31}Si	2.6 h	-	90.4 ± 10	β
Se	^{76}Se(n,γ) + ^{77}Se(n,n')^{77m}Se	17.7 s	161	413 ± 87	gamma
Br	^{79}Br(n,n')^{79m}Br	4.8 s	210	139 ± 22	gamma
	^{79}Br(n,γ)^{80m}Br	4.4 h	-	38 ± 8	β
	^{79}Br(n,γ)^{80m}Br	17.6 m	-	69 ± 14	β
Sr	^{86}Sr(n,γ) + ^{87}Sr(n,n')^{87m}Sr	2.8 h	388	42 ± 7	gamma
Y	^{89}Y(n,n')^{89m}Y	16 s	910	365 ± 75	gamma
Cd	^{110}Cd(n,γ) + ^{111}Cd(n,n')^{115m}Cd	49 m	247	123 ± 18	gamma Ge(Li)
In	^{115}In(n,n')^{115m}In	4.5 h	335	150 ± 19	gamma Ge(Li)
	^{115}In(n,γ)^{116m}In	54 m	-	136 ± 27	β
I	^{127}I(n,γ)^{128}I	25 m	-	95 ± 19	β
Ba	^{134}Ba(n,γ) + ^{135}Ba(n,n')^{135m}Ba	28.7 h	268	237 ± 40	gamma
	^{136}Ba(n,γ) + ^{137}Ba(n,n')^{137m}Ba	2.6 m	662	139 ± 28	gamma
Hg	^{198}Hg(n,γ) + ^{199}Hg(n,n')^{199m}Hg	43 m	158	143 ± 33	gamma Ge(Li)
Au	^{197}Au(n,n')^{197m}Au	7.4 s	279	710 ± 140	gamma
	^{197}Au(n,γ)^{198}Au	2.7 d	411.8	130 ± 20	Ge(Li)
Pb	^{204}Pb(n,n')^{204m}Pb	67 m	336	< 31	gamma

Table 4

Reaction	C.S. [mb]	Reaction	C.S. [mb]
^{27}Al(n,p)^{27}Mg	4.84	^{58}Ni(n,p)^{58}Co	118.8
^{28}Si(n,p)^{28}Al	7.12	^{64}Zn(n,p)^{64}Cu	41.3
^{32}S(n,p)^{32}P	68.4	^{84}Sr(n,γ)^{85m}Sr	35.4
^{46}Ti(n,p)^{46}Sc	13.6	^{93}Nb(n,α)^{90m}Y	0.028
^{47}Ti(n,p)^{47}Sc	19.4	^{113}In(n,n')^{113m}In	164.3
^{54}Fe(n,p)^{54}Mn	87.8	^{181}Ta(n,γ)^{182}Ta	89.25
^{56}Fe(n,p)^{56}Mn	1.40	^{197}Au(n,γ)^{198}Au	77.0

Table 5

Reaction	Measured	Calculated Origin of $\sigma(E)$	
		ENDF/B-IV	ENDF/B-V
^{197}Au(n,γ)	76.2-95.5	79.91	76.50
^{46}Ti(n,p)	12.4-13.8	12.52	13.46
^{47}Ti(n,p)	18.9-22.0	23.85	24.06
^{115}In(n,n')	186-201	175.5	181.9
^{56}Fe(n,p)	1.18-1.45	1.476	1.50
^{58}Ni(n,p)	95-118.8	115.0	116.5

A simple experimental method has been developed for the determination of the average activating thermal neutron flux $\bar{\varphi}$ for extended absorbing samples [14]. In the case of unknown matrix compositions the selfshielding and flux depression factors cannot be calculated using the relationships given in the literature [12, 13]. It was found that the flux distribution $\varphi(x)$ in an absorbing sample can be well described by the following polynomial:

$$\varphi(x) = (ax^2+bx+c)^{-1}$$

where x is the distance from the surface of the sample, a,b and c are constants which can be determined from the measured data. The activity A(x) of a non-absorbing detector foil, e.g. $^{65}Cu(n,\gamma)$, is proportional to the value of $\varphi(x)$ function at a distance x. The average flux within the sample can be calculated by the following relation:

$$\bar{\varphi} = \frac{1}{d}\int_0^d \varphi(x)dx$$

So, to the determination of $\bar{\varphi}$ the flux should be measured only in three points inside the sample e.g. at x=d/4, d/2 and 3d/4.

The unperturbated flux density φ_o must be measured in these positions, too, by the same detector without sample. For the ratio of the fluxes we have:

$$\bar{\varphi}/\varphi_o = \bar{A}/A_o \text{ and so } \bar{\varphi} = \varphi_o\bar{A}/A_o.$$

The activity A_s of an unknown sample is given by the well known expression:

$$A_s = \bar{\varphi}_s\sigma n(1-e^{-\lambda t}).$$

A typical experimental arrangement is shown in Fig. 4. for the determination of $\varphi(x)$.

The same procedure is recommended for samples investigated by neutron reflection method to get information on their absorbing properties.

In the case of fast neutrons the removal cross sections can be used for the estimation of the average activating flux, for thin samples.

There is no reliable method for the determination of the activating flux in the resonance region for samples of unknown compositions.

The principle of the flux albedo based on the measurement of the activity of a thin foil with and without reflector has been introduced by Amaldi and Fermi [15]. This method was generalized for two media of different neutron diffusion properties [16] which is the most common case in the practice. The geometrical arrangements for the measurements of the albedo for homogeneous (β_o) and heterogeneous (β) media are shown in Fig. 5a and b. In both cases the Cd-difference method is used to eliminate the contribution of epithermal neutrons to the activities A^i.

For non-absorbing foil in arrangements a) and b) we have $\beta_o = 1-2A/A_\infty$, and

$$\beta = \frac{A_\infty - A' - A''(1+\beta_o)}{A' + A_\infty\beta_o}$$

respectively. If $\beta = \beta_o$, the expression obtained for heterogeneous medium will be the same as found for homogeneous one.

As it can be seen is Fig. 6. the values of β differ for various reflectors and reach a saturation at about 8 cm. No data are available for the reflection properties of rocks and minerals. Further investigations are needed to prove the possible use of the experimental albedo for complex matrixes and to explain its values by the diffusion theory.

The irradiation of various materials with fast neutrons the scattering and reactions can induce energetic charged particles such as protons, deuterons, tritons, alphas, etc. These charged particles can produce secondary reactions in various elements. Calculation of the yields of secondary reactions, data for the formation of charged particles, the reaction cross sections induced by charged particles, the secondary charged particle spectrum, the energy loss along the path are needed for various materials. The status of these data has been summarized by Lebedev and Nasyrov [17]. According to their comparision there are large discrepancies between the available experimental data and the calculated values.

In addition to the crude oils the oxigen contents have been determined for various rock samples collected from Hungary using cyclic activations with 14 MeV neutrons. The schematic drawing of experimental arrangement is shown in Fig. 7. Using powder samples of ~2.5 g and a total measuring time of 4 m, the reproducibility of the determination is ± 2 %. Among the investigated ten samples only in three cases are available chemical analysis. Results obtained with the two independent methods are in agreement within the 95 % confidence interval.

In spite of the comlexity of the geological materials a number of elements can be determined if the neutron activation analysis is combined with the radiochemical group-separation technique [20]. A compilation of gamma spectra for geological samples measured by Ge(Li) and NaI detectors with and without group-separations is strongly recommended.

2. BULK DETERMINATIONS OF URANIUM AND THORIUM

There are several fast, non-destructive nuclear methods which, in principle, are applicable for the determination of U and Th in rocks and minerals as well as for the exprolation of subsurface uranium [18]. The advantages and disadvantages of each method depend on the actual experimental conditions (age and type of rocks, composition of the matrix, penetrability of the soil environment, etc.). Before selection the method to be applied, the first part of the decay chain of ^{238}U should be considered, i.e.:

$$^{238}U \xrightarrow[4.5\ 10^{9}y]{\alpha} {}^{234}Th \xrightarrow[24\ d]{\beta^-} {}^{234}Pa \xrightarrow[\substack{1.2\ m\\ 6.7\ h}]{\beta^-} {}^{234}U \xrightarrow[2.5\ 10^{5}\ y]{\alpha}$$

$$\longrightarrow {}^{230}Th \xrightarrow[7.7\ 10^{4}\ y]{\alpha} {}^{226}Ra \xrightarrow[1.6\ 10^{3}\ y]{\alpha} {}^{222}Rn \xrightarrow[3.8\ d]{\alpha} \ldots\ldots$$

The intensity ratio of the 63 keV and 186 keV lines is sensitive to the equilibrium, because the 186 keV line is emitted both by the ^{226}Ra and the ^{235}U.

The following nuclear methods could complement the conventional procedures:

a) α-spectrometry with surface barrier Si detector to determine the ^{230}Th and ^{234}U by measuring the 4.62 MeV and 4.77 MeV alpha lines, respectively.

b) γ-spectrometry with HPGe or Ge(Li) to measure the 63 keV and 1 MeV lines from ^{234}Th and ^{234m}Pa, respectively.

c) Resonance neutron activation analysis by detection of 74.7 keV line from ^{239}U. If lead is present in the sample the contribution of its K_α fluorescence line to the peak area should be considered.

d) Detection of fragments from thermal and fast neutron fission of ^{235}U and $^{235,238}U$ + ^{232}Th, respectively, using the cadmium difference method.

e) Detection of K and L fluorescence lines using ^{114}Cd and ^{125}I, ^{241}Am sources for excitation, respectively.

f) Determination of the intensity ratio of the K-line and the Compton-scattered gammas using a ^{57}Co source. Using small angle scattering the uranium K -lines can be well separated from the Compton-scattered gammas (see Fig. 8.).

g) Detection of delayed neutrons from thermal and fast neutron induced fission of ^{235}U and $^{235,238}U$ + ^{232}Th, respectively.

h) Measurements of the time distribution of neutrons in rocks following a burst of fast neutrons.

i) Detection of Rn and Tn by track-etched technique for the determination of subsurface uranium.

Precise knowledge of the average range R of alphas and fission fragments for various samples is needed to improve the methods a) and d), respectively. The effective range of fragments in mg/cm^2 increases with increasing $\overline{Z}$. On the basis of the available data for R($\overline{Z}$) the precision of the determination of uranium below $\overline{Z}\sim 50$ is about 5 %, while above $\overline{Z}\sim 50$ no better than 20 % (see. Ref [19]).The ^{252}Cf fragment source would give a good possibility for the determination of the exact form of the R($\overline{Z}$) function. In the case of b), c), e) and f) the absorption coefficient $\mu(\overline{Z},E)$ and the fluorescence yield $\omega(\overline{Z},E)$ for various rocks and minarals should be determined as a function of energy, where $\overline{Z}$ is the average atomic number of the sample. The selfabsorption correction factor for gammas in the case of homogeneous source can be calculated for the given detector-sample geometry if the $\mu(\overline{Z},E)$ function is known [18].

For the determination of the average activating epithermal neutron flux within bulk samples a method similar to that developed for thermal neutrons is needed.

The delayed neutron technique based on a double transfer system (see Fig. 9.) to assure the simultaneous measurements of the standard and sample is sensitive and rapid for the determination of U and Th. Accurate nuclear data are needed only to estimate the effects of interferences. The major interference is the $^{17}O(n,p)^{17}N$ ($T_{1/2}$ = 4.2 s) reaction, however, the (γ,n) reactions on ^{2}H and ^{9}Be produced by high energy gammas from $^{16}O(n,p)^{16}N$ ($T_{1/2}$ = 7.35 s, E_γ = 6.13 MeV) and $^{19}F(n,\alpha)^{16}N$ processes can contribute to the yield of delayed neutrons. For the determination of this correction the flux distribution and the excitation function should be known, i.e. the reaction rate curve $R = \phi(E)\sigma(E)$ in each point of the bulk sample. The exact knowledge of the cross section curve for $^{16}O(n,p)^{16}N$ reaction renders it possible the accurate determination of oxigen in various geological samples, too.

If Li, B, Cd and Gd is present in large abundance, the thermal neutron depression and selfshielding corrections cannot be neglected for a real sample of unknown composition.

The improvement of the pulsed neutron method needs the accurate knowledge of the diffusion parameters, the slowing down length and the resonance integrals for typical rock samples.

The method for measuring integrated subsurface radon concentrations based on the track-etched technique is widely used. A typical photograph on alpha particle tracks from Rn in LR-115 detector is shown in Fig. 10. For the accurate determination of the distance of the uranium deposit from the surface the following data should be determined for the actual soil and rock layers: the velocity of transport and diffusion constants for radon; the energy-range relation for alphas in air having different humidity.

3. FISSION TRACK DATING

The ^{238}U decays by spontaneous fission, leaving tracks in geological samples (apatite, zircon, mica, glass, tektites, sphene, whitlokite, etc.) and so, by measuring both the natural track abundance and the uranium content the age of minerals can be determined [19]. The spontaneous track density ϱ_s is proportional to the decay constont λ_{sf}, the time over the tracks have been stored T and the concentration of ^{238}U atoms N_8:

$$\varrho_s \propto N_8\lambda_{sf}T.$$

For the determination of uranium content the sample is exposed with thermal neutrons which can only cause fission of ^{235}U. The induced track density is proportional to the number of ^{235}U atoms N_5, the neutron fluence $F = \phi t$, and the fission cross section of ^{235}U with thermal neutrons σ_5:

$$\varrho_i \propto N_5\sigma_5F.$$

From these expressions we have

$$T = \frac{\varrho_s N_5\sigma_5 F}{\varrho_i N_8\lambda_{sf}} = 4.375\ 10^{-8}\ (\varrho_s/\varrho_i)F \text{ in year.}$$

A possible way for the separation of ϱ_i from ϱ_s is to change the etching time (see Fig. 11.). There are three assumptions in expression for T, namely the ranges of tracks from ^{235}U and ^{238}U are the same, i.e.: $R_5 = R_8$, the $\lambda_{sf} = 8.42\ 10^{-17} y^{-1}$, and that the concentration of ^{238}U does not change in time.

To improve this simple method used for geochronology the accuracy of the following atomic and nuclear data should be increased:

a) The lengths of etchable tracks of ^{235}U and ^{238}U fission fragments in various geological samples.
b) The value of λ_{sf}, for which the measured data varies from 5.3 $10^{-17}y^{-1}$ to 12 $10^{-17}y^{-1}$.
c) Nuclear data used for the determination of the average thermal neutron flux for a bulk media especially the $\sigma(n,\gamma)$ values for ^{51}V and ^{65}Cu.

4. APPLICATION OF PULSED NEUTRON TECHNIQUE FOR MEASURING THERMAL NEUTRON PARAMETERS IN NON-MODERATING MATERIALS

The methods for the determination of hydrogen content in geological formations and other matrixes by neutron reflection and absorption are based mostly on measuring the thermal neutron flux arised in the bulk material surrounding a fast neutron source. Reliable interpretation of the measured data requires information on the thermal diffusion parameters of the matrix consisting of non-moderating materials, too. These parameters generally cannot be unambiguously calculated from primary neutron cross section data, because of the possible occurence of trace elements of high thermal absorption cross section and bound hydrogen in form of crystal water. So, direct measurement of the thermal diffusion parameters for non-moderating materials is important also for geological applications. Therefore, it was desirable to develop rapid and reliable measuring procedures allowing to obtain the necessary data relating to the actual geological deposits instead of the compilation data files for elements and different kinds of minerals.Naturally,it would be useful to publish such type of data for mineralogically similar samples from different deposits. At present such a compilation is not available.

One of the well-known standard method for determining thermal diffusion parameters is the so called neutron pulse method, which consists in measuring the attenuation of the thermal flux in bulk samples following a fast neutron pulse. The method in its original form is applicable for moderating materials only. In our institute investigations are in progress to extend the neutron pulse method for non-moderating samples. The thermal neutron field is produced by a sandwich-like arrangement consisting of a thin moderator layer of known properties (such as water) surrounded by the investigated material, as shown by Fig. 12. The required parameters are determined by measuring the effect of the reflecting material on the decay time of the neutron pulse as a function of sample thickness.

Preliminary results indicate that the sensitivity of the method is acceptable if due attention is paid to reducing the background arised mainly by reflection of epithermal neutrons on the wall and other surrounding materials. The efficiency of the paraffin shielding combined with cadmium sheets is shwon in Fig. 13. The difference between the decay constants of the bare and reflected moderator is significant enough (see Fig. 14.) to allow the calculation of the diffusion parameters of the sample. Fig. 15. shows the result of a control measurement with a non-moderating material (iron) of well known diffusion parameters (thermal absorption and transport cross sections). The measured decay constants fit well to the theoretical curve calculated with the above parameters on the basis of diffusion theory.

Naturally, such measurements are of interest not only for geological applications but also in other fields, i.e. in studying building and structural materials.

The good agreement between the measured and calculated values for the decay constant of thermal flux shows the applicability of the diffusion theory in such cases and the reliability of the cross section data taken from the literature [21]. This method gives a possibility for the determination of the current albedo β for various materials. It was found that the β value is sensitive to the accepted diffusion length L.

Further investigations are needed to control the applicability of this method for the determination of diffusion parameters for elements and geological samples of unknown compositions.

5. APPLICATIONS OF REA METHOD IN BULK-MEDIA ASSAY

The X-ray fluorescence method has been used for the determination of chemical composition of drilled samples collected from 940-3300 m deep layers of the Hungarian territory east of the river Tisza. The experimental arrangement is shown in Fig. 16. Measurements were carried out in 3-5 points of the cylindrical surface. The concentrations of Cr, Mn, Fe, Cu, Zn, Rb, Sr, Y, Nb and Mo have been determined by the combination of the backscattering and "fundamental parameter" methods. The latter method, to take into account the matrix effect is based on the equation of Shiariwa and Fujino [22] which has the following form if two matrixes with known and unknown compositions are compared

$$C_x = C_s \frac{I_x}{I_s} \frac{g_{sE}}{g_{xE}} \frac{\mu_{M_1E} + \mu_{1x} \sin \Phi}{\mu_{M_oE} + \mu_{os} \sin \Phi}$$

where x, and s refer to the unknown and standard elements, M_1 and M_o are the unknown and known matrixes, I is the intensity of the fluorescence radiation, g is the efficiency of the excitation, μ is the absorption coefficient, Φ is the angle between the direction of the exciting radiation of E energy and the normal vector of the sample surface, C is the concentration.

The efficiency of the excitation can be given by [23] $g = \mu_{E\ photo} \cdot \omega KR$, where $\mu_{E\ photo}$ is the mass absorption coefficient for the photoelectric effect, ω is the fluorescence yield, $K = 1 - 1/r$ [24], where r is the absorption edge jump ratio, i.e. the ratio of the maximum and minimum values and R is the relative intensity of the measured line for a given shell. The values of $\mu_{M_1}E$ and $\mu_{M1}x$ absorption coefficients have been determined from the folloving expression

$$\mu = bZ^d,$$

while Z was deduced from the intensity ratio of the coherent and incoherent radiations scattered in backward direction accepting the relation [25]:

$$\frac{I_{coh}}{I_{incoh}} = aZ^n$$

where a, b, d, and n are fitted parameters, Z is the average atomic number.
In order to get information on the bulk-media the samples were homogenized and the concentrations of Ca, Fe, Zn, Zr, Mo, Pb, and the K, Cr, Mn, Cu, Ga, As, Rb, Sr, Y, Nb have been determined by additional and internal standard methods, respectively.

This experiment was devoted to the determination of the trace elements in rocks ($C < 0.1$ w%), therefore, the effect of secondary fluorescence could be neglected except for Cr because of the relatively high concentration of Fe (3-6 w%). For the determination of K and Ca ^{55}Fe, while for other elements ^{125}I exciting sources were used. The sensitivity of the determination of concentrations in our experiment as a function of atomic number is demonstrated in Fig. 17. for ^{125}I source of 110 MBq and $3\ 10^4$ s measuring time. The results obtained by the REA method in a few cases have been controlled by the NAA. As it can be seen in Fig. 18. the agreement between the data for Mn is acceptable, proving the possible use of the X-ray fluorescence technique for bulk-media assay if measurement is extended for a number of points of the surface.

The following expression was used for the determination of the concentrations of unknown elements using the internal standard method:

$$C_x = C_s \frac{I_x g_{sE}}{I_s g_{xE}} \frac{\mu_{ME} + \mu_{Mx} \sin \Phi}{\mu_{ME} + \mu_{Ms} \sin \Phi}$$

The error of this method consists of three sources: a) statistical and geometry (1-2 %), b) the mass absorption coefficient of the matrix, c) uncertainties of the fundamental parameters.

There are a number of experimental data and various formulae for the $\mu(Z,\lambda)$. The most well known are as follows:

A) $\mu(Z,\lambda) = a\lambda^3 + b\lambda^4 + \sigma_E\ Z(N/A)$ [26]
where $\lambda(\mathring{A}) = 12.3981/E(\mathrm{keV})$, σ_E is the Klein-Nishina cross section, A is the mass number and N is the Avogadro-number.

B) $\mu(Z,\lambda) = c\lambda^3 + d\lambda^4$

$\mu(Z,\lambda) = c\lambda(n-d \ln \lambda)$ [27]

C) $\mu(Z,\lambda) = cE_{AB}\lambda^n$ [28]

In the above formulae a, b, c, d and n are fitting parameters, while E_{AB} is the energy of the lower absorption edge.

D) Storm and Israel [29] has given different formulae for the cross sections of various interactions based on quantummechanical calculations. Further data are found in the Bertin's book [30].

The errors of absorption coefficients in the range of 1-100 keV are in the interval of 1-10 % depending on the energy and atomic number. The uncertainties around the absorption edges are higher than in other regions both for experimental data and analytical formulae resulting in a large error in the value of jump ratio r.

The dependence of the fluorescence yield on atomic number can be approximated by the following two formulae:

$$\omega = \frac{Z^4}{A+Z^4}, \qquad A = \begin{cases} 10^6 & \text{K series} \\ 10^5 & \text{L-series} \end{cases} \qquad [31]$$

$$\left(\frac{\omega}{1-\omega}\right)^{1/4} = A + BZ + CZ^3 \qquad [32].$$

There are large discrepancies in the ω values obtained by the various methods.

On the bases of the compiled data [33] published before 1971 the accuracies of ω_K and ω_L are 3-5 % and 10-15 %, respectively. The experimental data for ω belonging to the L-series cannot be approximated with the theoretical formulae.

A new compilation based on the data measured since 1971 would be necessary. The Table of Strom and Israel [29] for the relative intensities R based also on old data, measured before 1970.

For the improvement of the REA method the accuracy of the following atomic data should be increased: $\mu(Z,E)$; $\mu(Z,E)_{photo}$; $\omega(Z)_K$; $\omega(Z)_L$ and $R(Z)_{K,L,M}$.

REFERENCES

[1] H. Al-Shakristani, M.J. Al-Atyca, J. Radioanal. Chem., 14 (1973) 401.

[2] J. Csikai, S.M. Al-Jobori, Cs.M. Buczkó, S. Szegedi, J. Radioanal. Chem., 71 (1982) 215.

[3] S.M. Al-Jobori, S.Szegedi, Cs.M. Buczkó, Radiochem. Radioanal. Letters, 33 (1978) 133.

[4] J. Csikai, IAEA TECDOC-223. (1978) Vienna.

[5] S.M. Qaim, in Handbook of Spectroscopy, Vol. III. (1981) 141, CRC Press, Inc.

[6] V.M. Bychkov, V.N. Manokhin, A.B. Pashchenko, V.I. Plyaskin, INDC(CCP)-146/LJ, IAEA, Vienna (1980).

[7] Z.T. Bődy, J. Csikai, Atomic Energy Rev. 11 (1973) 153.

[8] K. Kobayashi, I. Kimura, W. Mannhart, J. Nucl. Sci. Technol. 19 (1982) 341.

[9] W. Mannhart, W.G. Alberts, Nucl. Sci. Eng. 69 (1979) 333.

[10] I. Józsa, G. Pető, J. Csikai, K.D. Vinh Long, ATOMKI Közlemenyek 16/4 (1974) 339.

[11] Z. Dezső, J. Csikai, Proc. Int. Conf. on Nucl. Data for Sci. and Techn., Antwerp, 6-10 Sept. p. 421 (1982).

[12] W. Bothe, Z. f. Phys., 120 (1943) 437.

[13] A. Sola, Nucleonics, 18 (1960) 78.

[14] Cs.M. Buczkó, A. Borbély, J. Radioanal. Chem. 42 (1978) 393.

[15] E. Amaldi, E. Fermi, Phys. Rev. 50 (1936) 899.

[16] J. Csikai, A.A. Haddou, L. Szabados, to be published.

[17] B.L. Lebedev, F. Nasyrov, INDC(CCP)-43/L IAEA (1974).

[18] A. Chouak, P. Vuister, G. Paic, M. Berrada, J. Csikai, J. of Radioanal. Chem. 45 (1978) 445.

[19] R.L. Fleischer, P.B. Price, R.M. Walker, Nuclear Tracks in Solids, Univ. of California Press, (1975).

[20] J.C. Laul, Atomic Energy Review, 17/3 (1979) 603.

[21] I. Lagner, J.J. Schmidt, D. Woll, Tables of evaluated neutron cross sections for fast reactor materials, KFK 750, EUR 3715e (1968).

[22] T. Shiariwa, N. Fujino, Jap. Journal of Applied Phys. 5 (1966)866.

[23] R.B. Shen, J.C. Russ, X-Ray Spectrometry 6 (1977) 56.

[24] A. Kuczomovo, Y-Ray Spectrometry 11 (1982) 112.

[25] H. Kunzendorf, Nucl. Instrum. Meth. 99 (1972) 611.

[26] J.A. Victoren, J. Appl. Phys. 19 (1948).

[27] M.A. Short, J. Taback, X-Ray Spectrometry 4 (1975) 119.

[28] J. Leroux, T.P Thinh, Revised Tables of X-Ray Mass Attennation Coefficients, Corporation Scientifique Claisse INC (1977).

[29] E. Storm, H.J. Israel, Nuclear Data Tables, Sec. A. 4 (1970) 565.

[30] E.P. Bertin, Principles and Practice of X-Ray Spectrometric Analysis, Plenum Press, New York (1975).

[31] N.A. Dayson, X-Ray Spectrometry 4 (1975) 90.

[32] J.W. Colby, Advances in X-Ray Analysis 11 (1968) 287.

[33] W. Bambynek, B. Crasemann, R.W. Fink, H.U. Freund, H. Mark, C.D. Swift, R.E. Price, P. Venugopalo Roo, Rev. Mod. Phys. 44 (1972) 716.

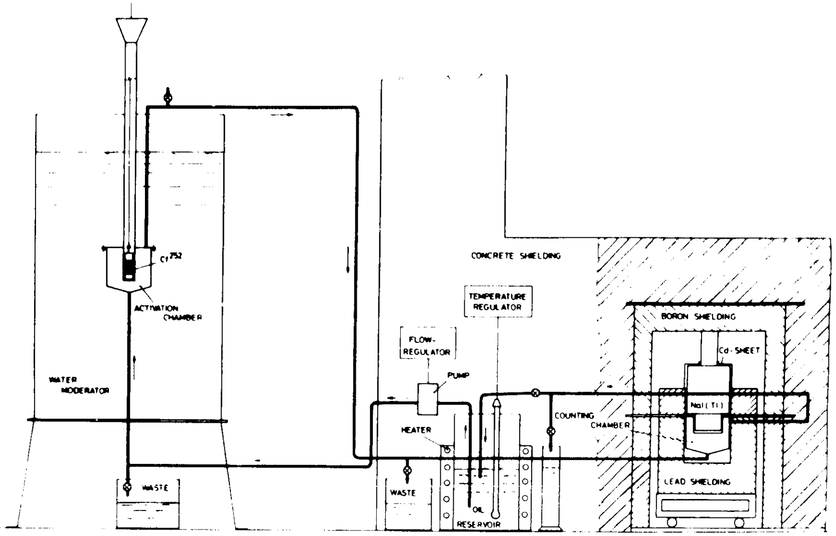

Fig. 1. On-stream measuring equipment

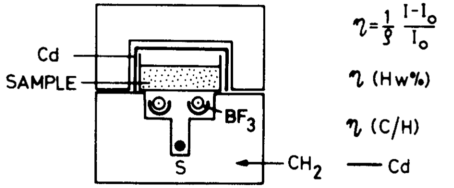

Fig. 2. Neutron reflection arrangement

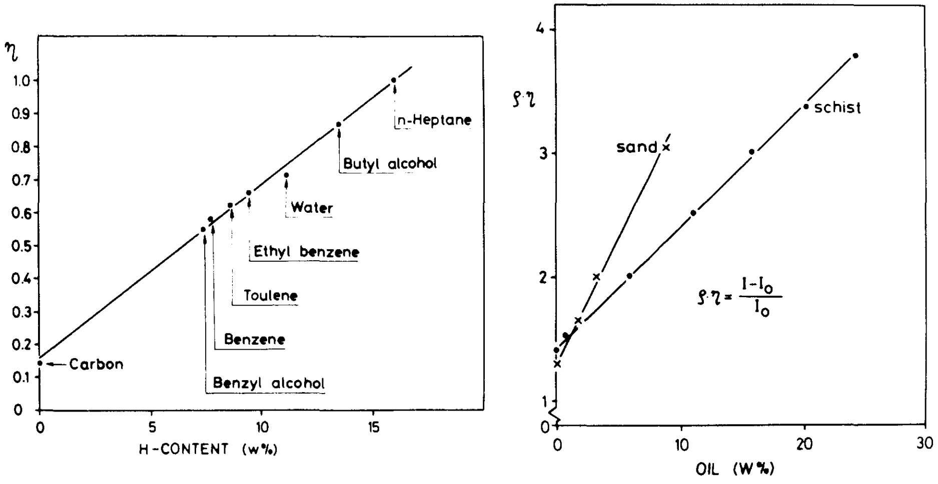

Fig. 3. Dependence of reflected neutrons on hydrogen and oil contents of different samples.

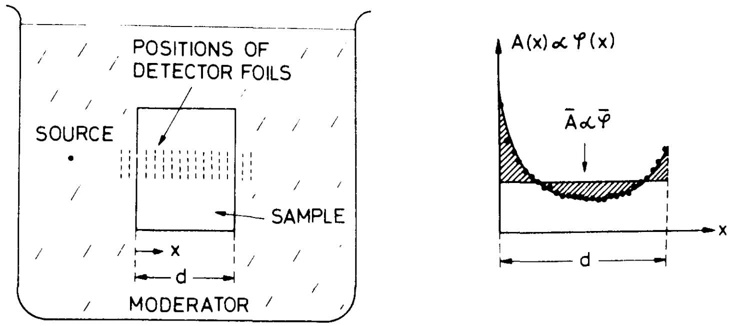

Fig. 4. Experimental arrangement for the determination of the average activating flux for a bulk-media.

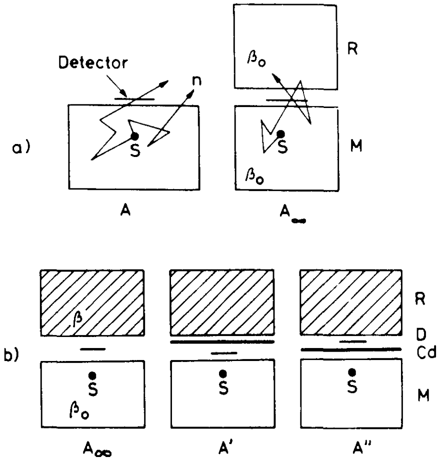

Fig. 5. Geometrical arrangements for the determination of flux albedo.

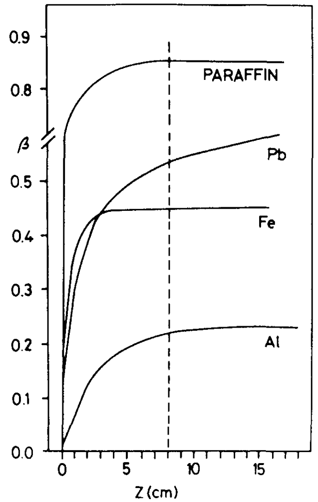

Fig. 6. Dependence of albedo from the reflector thickness and material.

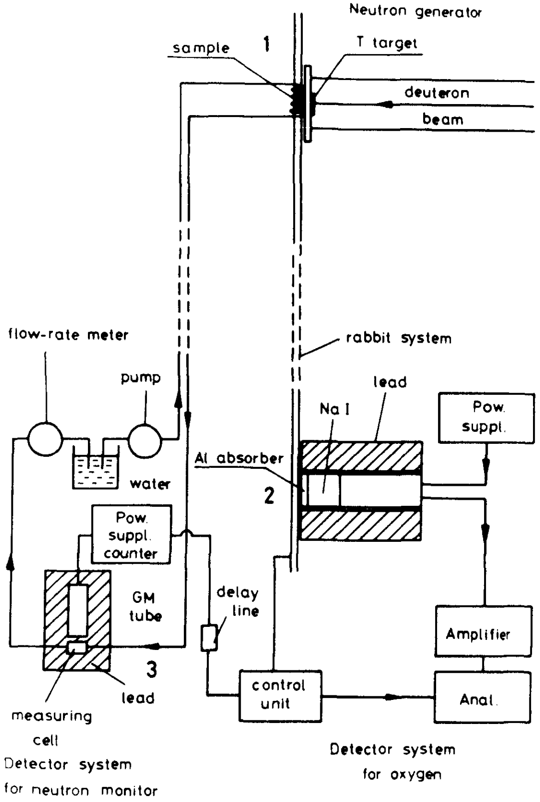

Fig. 7. Schematic view of experimental arrangement for the determination of oxigen.

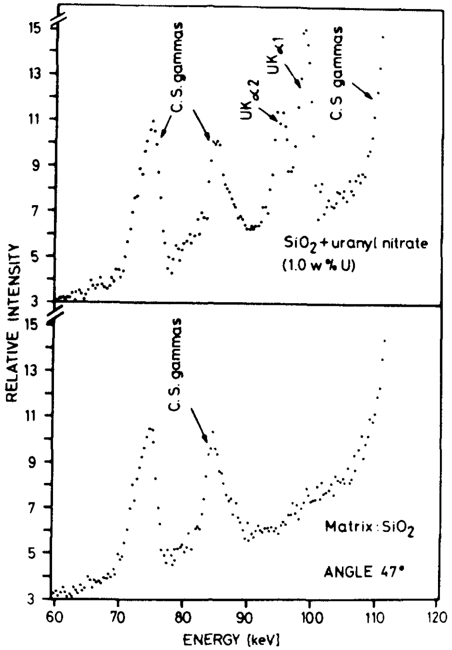

Fig. 8. X-ray spectra of uranium in SiO_2 matrix

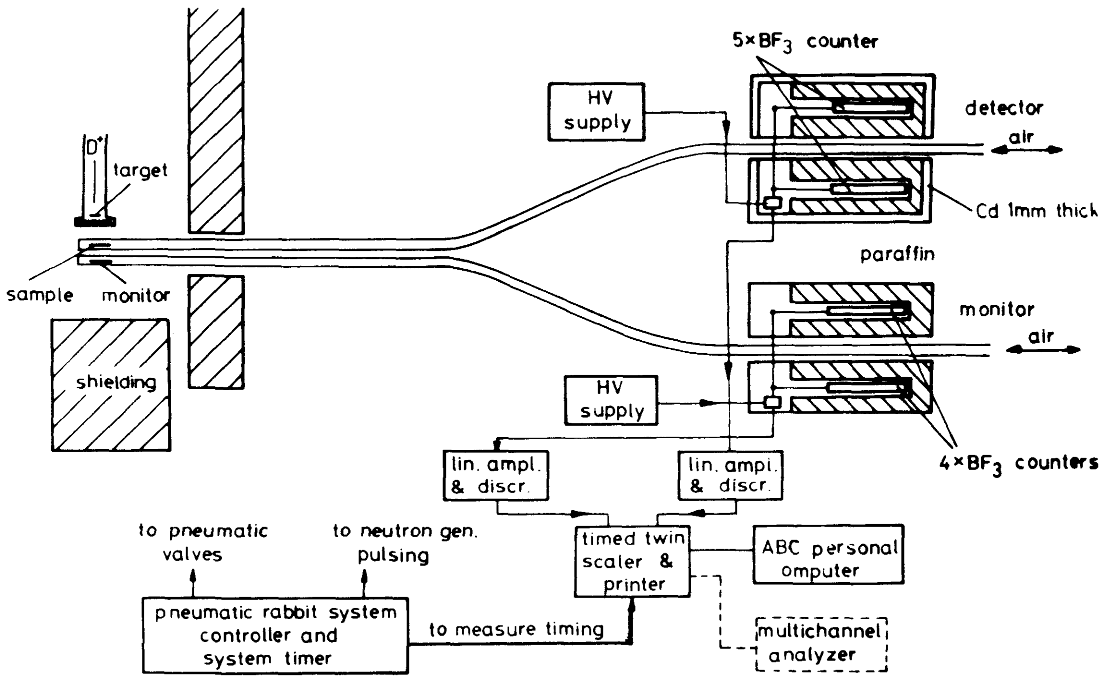

Fig. 9. Experimental arrangement for the determination of U by delayed neutrons.

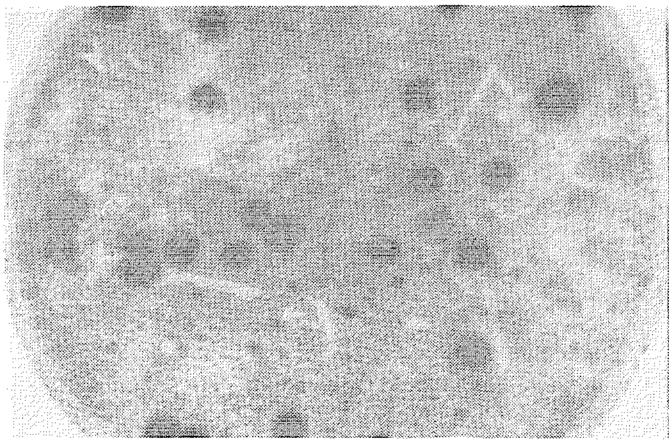

Fig. 10. Alpha particle tracks from Rn in LR-115 detector.

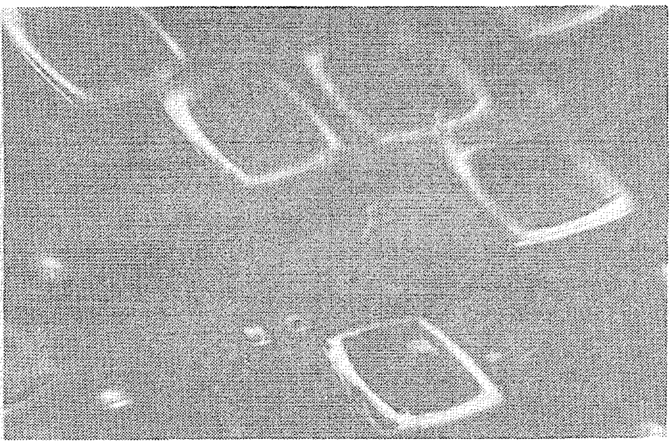

Fig. 11. Tracks in mica from spontaneous fission (large) and thermal neutron induced fission (small).

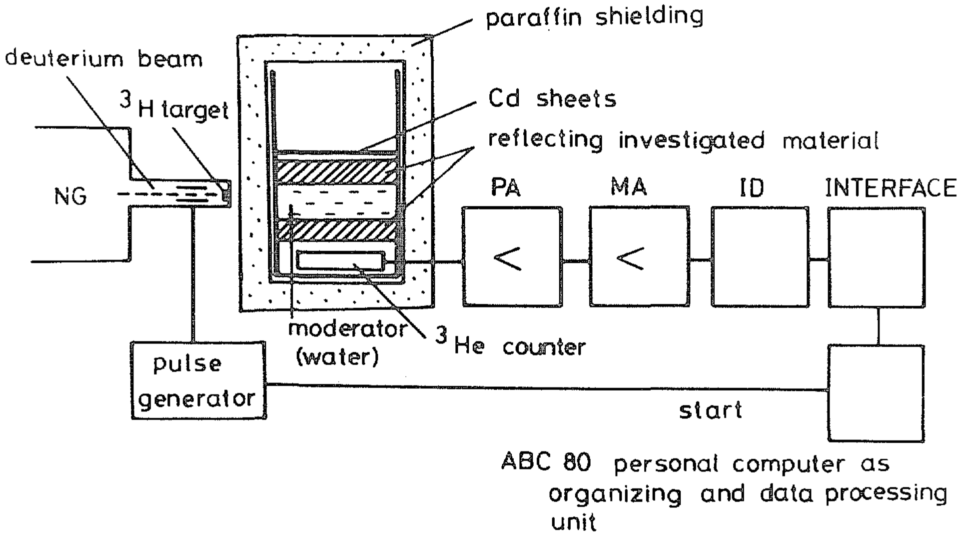

Fig. 12. Principle of pulsed neutron method for the measurement of diffusion parameters of non-moderator materials.

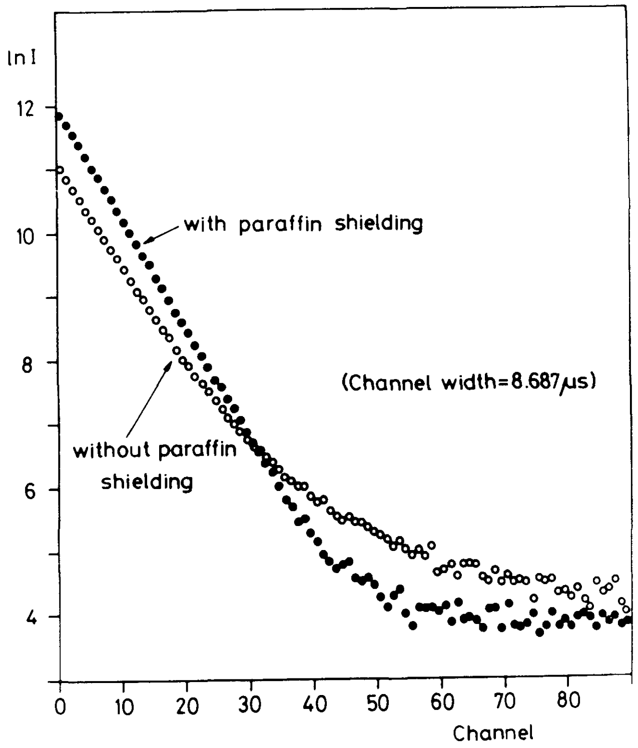

Fig. 13. Effect of shielding in pulsed neutron measurements.

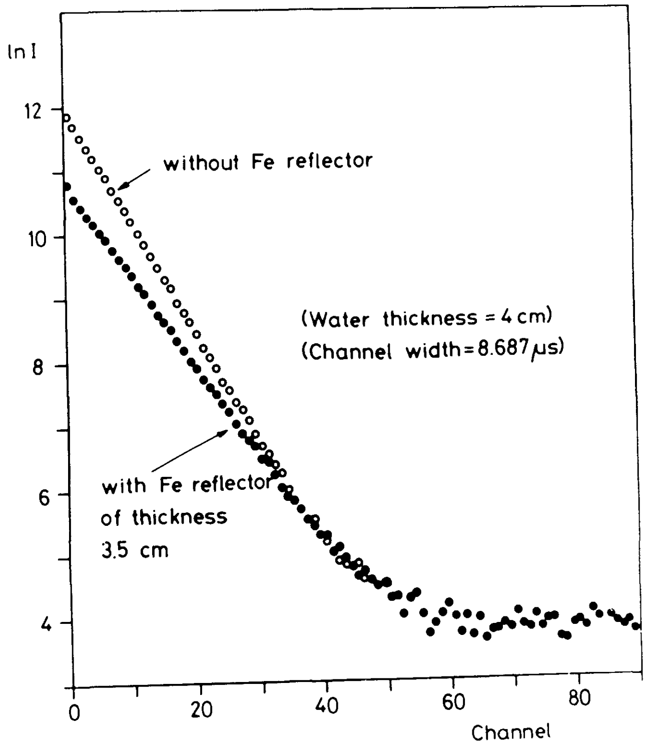

Fig. 14. Dependence of decay constant on the reflector material

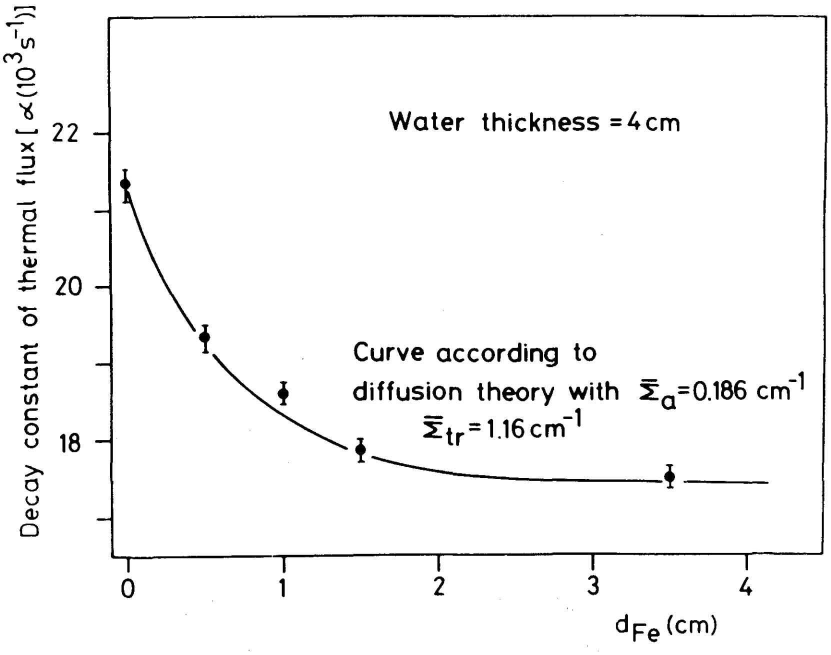

Fig. 15. Measured and calculated decay constants for iron.

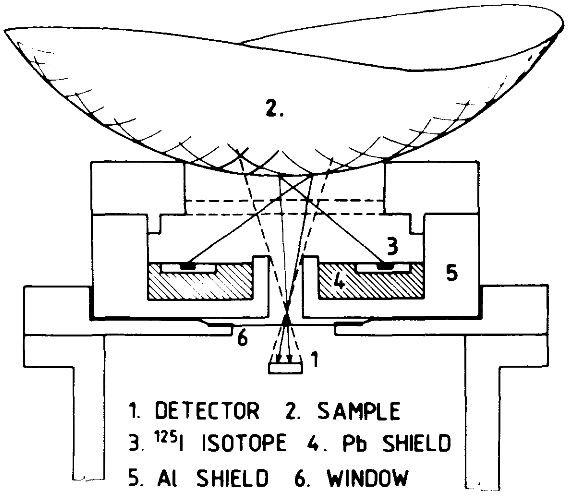

Fig. 16. Experimental arrangement for REA measurements of drilled samples.

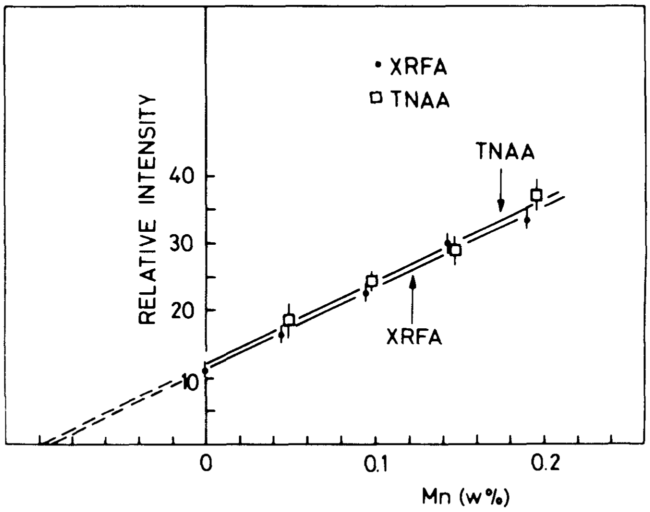

Fig. 18. Manganese content in a drilled sample measured by REA and NAA methods.

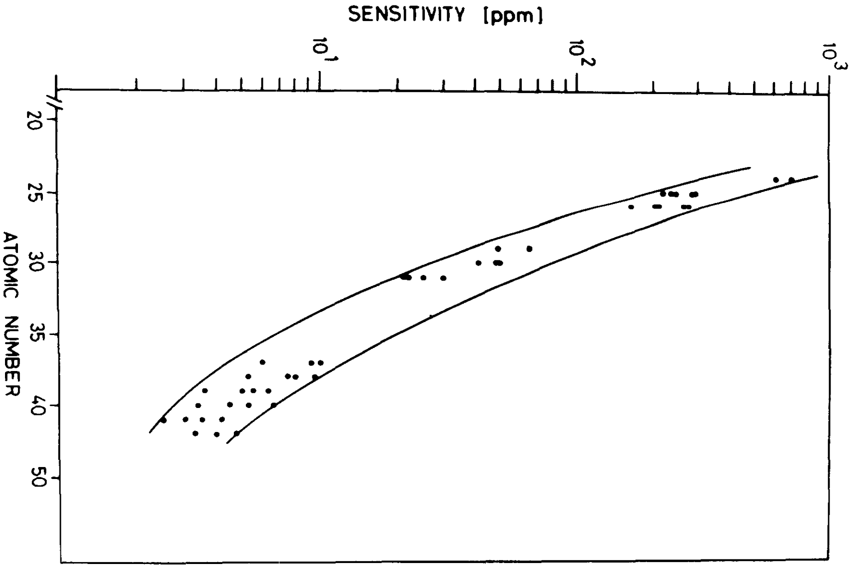

Fig. 17. The sensitivity interval of REA method as a function of Z number.

NUCLEAR TECHNIQUES IN UNDERGROUND MINING

K.Przewłocki
Institute of Physics and Nuclear Techniques
Academy of Mining and Metallurgy, Kraków

I. General review

Application of nuclear techniques in mining has a tradition which is over 25 years old. At the present one may distiguish the following four main directions of this application. These are:

1. Gamma switches widely applied in the control and automation of shaft stations, vertical transport in shafts, conveyor belts, coal-level gauges in the coal bunkers, etc. These are simple "yes" or "no" devices, placed in robust housings and operating with a high degree of reliability. They can be easily available comercially /1/.
2. Quantitative technological measurements: Although physical principles of the nuclear devices are simple, to standardize them properly and make them work in heavy mining conditions /dust, high humidity, large variations of the electric power supply, explosive atmosphere/ is not an easy task to do. This is why most of the methods proposed so far are still in the stage of implementation and only few such devices are produced at a large scale.
The following devices and/or techniques may be classified into this group:
   - $\gamma\gamma$ density gauges used in stowing-slurry control and in hydraulic transport of the coal output /2/;
   - nuclear logging of the inclined bore-holes of small dimensions, used in uranium- and potassium-mines /3/, /4/;
   - fast determination of the chemical composition of ores, based on the interaction of the nuclear radiation with mineral materials, performed in order to optimize mining exploitation, to control ore benification processes or used at the prospection stage. Attempts are also being made to apply these techniques for performing fast "in situ" analyses of the unprepared rock face for the chosen element content during exploitation /5/, /6/;
   - nuclear ash content gauges /7/;
   - belt weighers to measure and control mass flow in materials transport /1/;
   - continuous control of the mining atmosphere /8/;
   - coal/rock sensing gauges /gamma-gamma, or natural radioactivity measurements/ to control automatic coal-cutting machines /9/;
   - measurements of coal calorific value /10/, /11/.
3. Measurements of physical parameters of the underground environment

The main task in mining is to minimize the potential hazard which the human beings working underground are continuously faced with. Miners deal with the continuous environment in the form of gaseous, solid and liquid phases in which complex physical phenomena take place.

To recognize them properly one has to put out a lot of effort and sometimes apply sophisticated equipment, ideas and interpretation methods. As a rule these problems are rather of an unique nature; they are usually characteristic for a certain group of mines or even for one particular mine The following examples should be mentioned here:

- origin and age of the mining waters /12, /13/;
- diffusion of CO_2 and CH_4 in orogen;
- natural radioactive pollution in mines /14/;
- tracing of the mining atmosphere paths in mining works; detection of interconnections through the old gobs /15/;
- flow of unhomogeneous fluids /16/;
- cap rock thickness estimates /17/, /18/;
- determination of absolute age of rocks;
- parameters estimate of the deposited back fill /19/.

4. Radioactive waste disposal in the geologic formations

New kind of mining, connected with the problem of nuclear waste disposal is actually under development. New criterions lie at the base of this mining: effective heat dissipation in rock masses, and concept of the multiple geologic barrier, assuring no contact with groundwaters of the repositories within few hundred thousand years /20/, /21/.

Radioactive switches, level gauges, density gauges, belt weighers, ash content gauges - these are more or less developed and proved devices. Their further refinement depends mainly on the improvement of their reliability and the existing nuclear data are more or less sufficient for realization of these devices and they can hardly be a subject of any farther consideration in this context. On the other hand there is a variety of unique parameters of the undergorund envinroment which can be measured with the aid of a method derived from the nuclear techniques /22/, /23/. Some of those methods have met with success and are routinely used, some others not. E.g. measurements of the miuon penetration through the rock cap into the mining works. The phenomenom itself is certainly an interesting one and it has been under investigation for many years /17/. However, due to the complicated equipment involved and labour consumption the value of the final information for miners is smaller than its cost. The method has but weak chances to gain popularity.

II. Neutron Techniques

R.Cornuet in his summary of the IAEA Conference on Industrial Application of Radioisotopes and Radiation Technology held in Grenoble in 1981 said that in the light of the presented papers a growing attention is being paid to the application of neutron techniques in the industrial measurements. Their major advantage is the relatively great measurement range /from 0.2 to 1 meter/. However, in what concerns nuclear reactors and NAA /neutron activation analysis/ the experience gathered so far shows that the reactors are too expensive to be installed in industrial plants solely for the purposes of the NAA. It is rather preferred that the existing research reactors, if they are close enough to the mineral-processing factories or geologic units, should be used for this purpose /25/.

Cf^{252} and Pu^{239}+Be neutron sources are easily available and they may be used in the underground mining for logging /4/, /26/, moisture determination /27/ and ore analysis /28/. Application of the techniques using the isotope neutron sources is however limited because of the radiation hazards which become significant when a neutron source with the yield of 10^8 n/s or higher is used. As it has been stated in the above-mentioned summary availability of a cheap, remote-controlled, portable neutron generator of the sealed-tube type could greatly stimulate farther application of the neutron techniques in general and in the mining technologies in particular. Performing the so-called combined neutron experiment /29/ or using stationary neutron fields makes possible to determine such parameters as: calorific value of coal, hydrogen content in bulk media /31/ or to perform express analyses of rock face, core samples, etc.

Nuclear data wanted in this case will be the same as in the case of the neutron bore-hole logging.

III. Gas chromatographic analysers

Even though this method is not derived purely from the nuclear techniques the introduction of a standard gas chromatograph equipped with an ionisation chamber and a beta-source as the ioniser permits to increase significantly the sensitivity of the method /32/. This sensitivity is high enough to meet all the requirements necessary to control mining atmosphere, to analyse fire gases and to trace air paths through the old gobs /15/. Polish mining industry shows a continuously growing interest in these techniques. The method has proved to be useful also in the environmental physics /measurements of freon content, halogen compounds, pesticides, etc/ It may be mentioned here that external water pollution may also have some impact on the mining activity. In Poland a case has been reported when the polluted groundwater flew into a mine and there mixed with the high-quality water used even for drinking purposes, decreasing drastically quality of the latter /33/. In other cases radium-bearing waters presented some problems in mines, as they caused precipitation of radium salts in mining works. Ionisation chambers were used in this case to monitor the radon content in air /34/.

To refine this technique some atomic data concerning the cross sections for electron splitting out, resonance effects in certain molecules would be welcome, as well as data concerning recombination processes.

IV. Photoactivation analysis of ore samples

Modern linear accelerators, microtrons or betatrons are much cheaper than nuclear reactors and they may be considered as powerful sources of the hard bremsstrahlung radiation which may lead to various photonuclear reactions in the activated samples. More than 20 years of implementation of this technique in the mining industry proved that PAA /photoactivation analysis/ of sillicates is fast, reliable, relatively insensitive to impurities and it can be successfully used to control ore deposit exploitation and benefication of the ore output. Mass of the sample is ca 100 g /35/. The following photonuclear reactions may be considered as presenting some practical possibilities /table I/. Relatively high detectability limit in most cases exceeds even the industrial needs /tables II/.

PAA was found to be very useful in the copper industry where it got a large spread-out /37/.

Nuclear data concerning neutron cross sections and /n, α/, /n,p/, /n,2 α/ reactions are relatively well documented as NAA is a very popular technique, especially in the laboratory practice. This is not, however, the case of the photonuclear reactions. The giant resonances which are characteristic for this type of reactions are not known in such detailed fashion as the neutron resonances. Also the exact knowledge of the energetic tresholds for the photonuclear reactions, half-life periods of the decay products and cross sections for particular reactions would be welcome for the professionalists working with PNAA. For some reasons not enough attention has been paid so far to this field of research.

Fast instrumental analysis of sillicates is not an easy task to do. This draws the attention of some greater industrial laboratories to nuclear methods of analysis. In some cases XRF /X-ray fluorescence analysis/ and/or fast NAA may be used to resolve a specific analytical problem but sometimes PNAA will be preferred. The advantages of the latter are: low cost, speed /ca 5 min counting time/, relatively light samples /0.1 kg/, nondestructiveness, high detectability limit and practical insensitivity to such sample parameters as granulometric size, moisture content and technological impurities.

V. Radioactive waste disposal

It is well known that technology of the fuel processing is at the present time a subject to father improvement; volume of the HLW /high Level Waste/ tends to be lowered, which of course is accompanied by an increase of their activity. Nuclear data which can facilitate designing of the repositories in the opinion of different authors are:

- statistical output of the particular fission products and transuranians for different types of nuclear reactors;
- half-life periods for the radioactive decay and spontaneous fission processes;
- energy of electromagnetic and nuclear radiations;
- neutron output and spectrum of neutron energies;
- mechanism of the preferential release from the solid phase /36/ of the heavy nuclei which have undergone radioactive decay or spontaneous fission;

- recovery efficiency in the uranium-only reprocessing cycle, as the wastes arising from this process are known to be very efficient in heat generation /21/;
- output of the volatile radioactive products as it may cause the necessity of designing a proper ventillation system in the mining works;
- knowledge of geochemical mobility of different radioactive elements. Particular atoms which undergo radioactive decay may change their valencies and consequently their geochemical mobility. These last data are essential for determining the risk level connected with potential flooding and/or disruptive scenarios and for assesing the effectiveness of the geologic multibarrier concept.

Final remarks

As a conclusion one may express an opinion that there are at least few problems in underground mining where the availability of new nuclear /or atomic/ data may help to make a farther progress in mining technology.

Bibliography

1. J.F.Cameron "Relation between nuclear techniques and other prospecting and exploitation techniques" Nuclear Techniques in Geochemistry and Geophysics IAEA 1976.
2. K.Korbel, J.Lasa, K.Przewłocki "Die Dichtenkontrolle von Versatzmischungen mit Hilfe von Kernstrahlung" Freiberger Forschungshefte Heft C 174, 239, 1965.
3. M.Mięsowicz, L.Jurkiewicz, A.Mikucki "A GM-Counter apparatus for gamma ray well logging" Acta Geophysica Polonica 1, No. 3-4, 187, 1953.
4. J.Czubek, B.Dziunikowski, L.Jurkiewicz, J.Krzuk, J.Niewodniczański, T.Owsiak, K.Przewłocki, A.Zuber "Radioactive well logging in horizontal bore holes for potassium salts prospecting" Proceedings of the II U.N. Conference on the Peaceful Use of Nuclear Energy Geneva 1958, Paper P/1951.
5. C.G.Clayton "Some experience with the use of nuclear techniques in mineral exploration and mining" Nuclear Techniques in Geochemistry and Geophysics, IAEA 1976.
6. A.S.Sthan "Prospects for the use of photoactivation and radioisotopeexcited x-ray analysis in mineral exploration" /in Russian/, Nuclear Techniques in Geochemistry and Geophysics IAEA 1976.
7. C.G.Clayton "Use of nuclear techniques in on-stream analysis in mineral processing plants", Nuclear Techniques for Mineral Exploration and exploitation, IAEA 1971.
8. Y.G.Sevastianov "Mineral Exploration, mining and processing" International Atomic Energy Agency Bulletin 24, No. 4, 45, 1982.
9. J.F.Cameron "Review of some nuclear techniques used in mineral processing in the United Kingdom" Nuclear Techniques in Geochemistry and Geophysics, IAEA 1976.
10. M.R.Wormald, C.G.Clayton "In situ analysis of coal by measurement of neutron induced prompt gamma rays" Int. J.Appl Radiat. Isot. 34, No. 1, 71, 1983.
11. A.Kreft, E.Chruściel, B.Dziunikowski, J.Gyurcsak, S.Kalita, A.Lenda, W.Przybyłowicz, J.Woźniak "A system of integrated instrumental analysis of soft brown coals", submitted for publication in "Fuel".
12. A.Różkowski, K.Przewłocki "Application of stable environmental isotopes in mine hydrology taking Polish coal basins as an example" Isotope Techniques in Groundwater Hydrology, IAEA 1974.

13. A.Zuber, J.Grabczak, M.Kolonko Environmental and artificial tracers for inwestigating leokages into salt wines, Isotope Hydrology 1978 Vol. I, p.45 /IAEA, Vienna, 1979/.

14. I.Tomza "Analysis of the natural radioactivity in a coal mines" Ph. d. thesis /in Polish/, available in a Library of the Mine Mining Institut, Katowice, 1977.

15. J.Lasa "Progress in the practice of the electron capture detector" Chemia Analityczna, 24, 415, 1979.

16. W.Parzonka, K.Przewłocki, V.N.Pokrovska "Kinematic behaviour of polyfractional mixtures" Proceedings of the 6-th Int. Conf. "Hydrotransport 6" BHRA Canterbury 1979.

17. M.Mięsowicz, L.Jurkiewicz, J.M.Massalski "On some low ionising radiation observed by measurements of cosmic radiation at great depth" Phys. Rev. 77, 380, 1950.

18. O.A.Baikonurov "Methods of control of the physico-technical parameters in the underground ore mining" /in Russian/ Editor "Nauka" Alma - Ata 1979.

19. L.Barański, K.Przewłocki "Radiometric measurements of the bulk density and moisture content in a deposited back fill" Proceedings of the II Symposium of Soil Mechanics, Technical University Łódź 1979.

20. "Underground Disposal of Radioactive Wastes" Proceedings of the Symposium, Otaniemi 1979, IAEA 1980.

21. "Management of Commercially Generated Radioactive Waste" US Dept. of Energy, DOE"EIS-0046F vol. 1-3, 1980.

22. K.Przewłocki "Physical aspects of the application of nuclear techniques in mining exploitation", Nuclear Techniques in Geochemistry and Geophysics IAEA 1976.

23. V.G.Segalin "The use of radioactive isotopes for automatation of a coal industry" /in Russian/, Gostoptiekhizdat 1960.

24. R.Cornuet "Summary of the Conference", Industrial Application of Radioisotopes and Radiation Technology IAEA 1982.

25. J.W.Winchester "Activation analysis in mineral prospecting" Nuclear Techniques for Mineral Exploration and Exploitation IAEA 1971.

26. A.M.de Bourayne "L emploi des techniques nucleaires dans la prospection, l´extraction et le traintement du minerai d´ uranium" Industrial Application of Radioisotopes and Radiation Technology IAEA 1982.

27. "Commercial portable gauges for radiometric determination of the density and moisture content of building materials" Technical Reports Series No. 130 IAEA 1971.

28. A.Prądzyński "Photo nuclear and fast neutron activation analysis of copper in copper ores and flotation products" Nuclear Techniques and Mineral Resources, IAEA 1969.

29. R.L.Caldwell, W.R.Mills, L.S.Allen, P.R.Bell, R.L.Heath "Combination neutron experiment for remote analysis" Science 152, 3721, 457, 1966.

30. R.W.Tolmie, C.J.Thompson "Field equipment for neutron activation analysis" Nuclear Techniques and Mineral Resources. IAEA 1969.

31. E.Chruściel, J.Gyurcsak, R.Krasowski, A.Kreft, J.Woźniak "Determination of the asphalt content in bituminoys mixtures by neutron thermolisation" Nuclear Physics Methods in Material Research, 1980.

32. W.Babicz, E.Broś, J.Lasa, S.Nawrat, F.Sachs, J.Stobiński, I.Śliwka "Application of electronegative tracers to identification of the ventilation network in the underground mines" /in Polish/ Przegląd Górniczy, 34, No, 6, 255, 1983.

33. D.Różkowski private communicate.

34. V.V.Sulin "Gamma activation method of the determination of hydrogen and oxygen content in a samples of coal" /in Russian/ Iadernaia Giefizika, Niedra 1968.

35. V.I.Bielov, A.K.Bierzin, G.T.Vitozenc, V.V.Sulin "Results of use of the gamma activation method for the determination of oxygen and hydrogen content in a samples of coal" /in Russian/. Iadernaia Gieofizika Niedra 1968.

36. K.Kigoski "Alpha-recoil thorium-234: dissolution into water and the Uranium-234/Uranium-238disegnilibrium in nature", Science 173, 47, 1971.

TABLE I

NUCLEAR DATA OF SOME PHOTONUCLEAR REACTIONS

/V.V.Sulin "Basic prerequisites of the gamma activation method of the C and O determination in the samples of coals", /in Russian/
Nuclear Geophysics, Niedra, 1968/.

Activated isotope and abundance %	reaction	Energy, Mev		cross section mb	decay product	1/2	type of decay	Energy of MeV	
		treshold	giant resonance					particles	-quanta
C^{12} /98,89/	$(\gamma\ n)$	18,6	22,8	10,4	C^{11}	20,5 min	β^+	0,96	No
O^{16} /99,76/	$(\gamma\ n)$	15,6	21,9	14,0	O^{15}	2,03 "	β^+	1,73	No
Si^{28} /92,27/	$(\gamma\ n)$	17,14	20,9	21,0	Si^{27}	4,2 s	β^+	3,85	0,84; 1,01
Si^{29} /4,68/	$(\gamma\ p)$	12,8	19,6	31,0	Al^{28}	2,3 min	β^-	2,87	1,78
Si^{30} /3,05/	$(\gamma\ p)$	12,9	21,0	32,0	Al^{29}	6,6 min	β^-	2,5; 1,4	1,28; 2,43
N^{14} /99,63/	$(\gamma\ n)$	10,5	22,5	2,8	N^{13}	10,0 min	β^+	1,19	No
S^{32} /95,02/	$(\gamma\ n)$	14,7	20,1	15,0	S^{31}	2,6 s	β^+	4,42	1,27
P^{31} /100/	$(\gamma\ n)$	12,35	19,0	17,0	P^{30}	2,55 min	β^+	3,3	No
Fe^{54} /5,84/	$(\gamma\ n)$	13,8	17,7	67,0	Fe^{53}	9,0 min	β^+	2,6	0,37
Al^{27} /100/	$(\gamma\ n)$	12,8	19,6	8,0	Al^{26}	6,5 s	β^+	3,21	No
Ca^{40} /96,97/	$(\gamma\ n)$	15,9	19,6	15,0	Ca^{39}	0,9 s	β^+	5,5	2,5
Mg^{24} /78,6/	$(\gamma\ n)$	16,5	19,4	9,8	Mg^{23}	12 s	β^+	3,0	0,44
Mg^{26} /11,29/	$(\gamma\ p)$	14,3	22,0	25,0	Na^{25}	60 s	β^-	3,8; 2,8	0,98; 0,58; 0,40; 1,61
K^{39} /93,08/	$(\gamma\ n)$	14,5	19,3	11,2	K^{38} K^{38}	0,97 s 7,7 min	β^+ β^+	4,8 2,7	2,1

TABLE II

CHARACTERISTICS OF SOME WORKED OUT IN THE USSR METHODS OF PHOTOACTIVATION ANALYSIS OF THE MINERAL SAMPLES

/A.C.Sthan "Perspectives of application of gamma activation and XRF methods of analysis in the exploration of mineral raw materials" /in Russian/ Nuclear Techniques in Geochemistry and Geophysics IAEA, 1976

Samples	Type of accelerator	Detected element	Detection limit /weight %/
Copper ores	betatron 25 MeV	Cu	10^{-2}
Zinc-lead ores	betatron 30 MeV	Zn	10^{-2}
Polimetallic ores	intensive beam	Cu, Ba, F, Al, Mn, Sb	10^{-2} - 10^{-3} 10^{-3}
Titanium - zirkonium ores	betatron 25 MeV	Ti Zr	10^{-2} 10^{-3}
-"-	betatron 25 MeV	Hf	$5 . 10^{-3}$
Be - Mo - W ores	LAE-15	Mo	$2 . 10^{-3}$
Gold bearing ores	LAE-8	Au	$5 . 10^{-5}$

Remarks on some rock neutron parameters

Uwagi o neutronowych parametrach skał

Замечания об некоторых нейтронных параметрах пород

by

Jan A. CZUBEK
Inst. Nucl. Physics
ul. Radzikowskiego 152
31-342 Kraków, Poland

Working paper prepared for the IAEA
Consultants' Meeting on Nuclear Data
for Borehole and Bulk-Media Assay
Using Nuclear Techniques
14-18 November, 1983
Kraków, Poland

Abstract

Application of borehole neutron methods requires the knowledge of the proper calibration curves. An experimental procedure to get these curves is very complicated, difficult and expensive; the pure theoretical way (using the known neutron codes and neutron data files) is not satisfactory either. A compromise approach is to relate some integral neutron parameters of rocks (like slowing-down length, diffusion length, absorption cross-section, neutron lifetime, etc.) to the registered tool signal in a given rock medium. It is possible in this way to "translate" the calibration curves known in one type of lithology to another one. To be able to perform this "translation" a good knowledge of the rock neutron parameters is needed.

A method to calculate the thermal neutron parameters (absorption cross-section, diffusion coefficient and diffusion length) of rocks is given in the paper. It is based on a proper energy averaging of cross-sections for all rock matrix and rock saturating liquid constituents. Special emphasis is given to the presence of hydrogen. The diffusion lengths in different lithologies in function of the variable rock porosity have been calculated. An influence of the thermal neutron spectrum on the shape of the porosity calibration curves for the dual spacing neutron method is shown. This influence has been estimated on two porosity units, in average.

Magmatic rocks as a possible source of geothermal energy are now becoming a target of neutron loggings for the porosity determination. Here the knowledge of the slowing-down lengths is of a great importance in the problem of the estimation of the calibration curves. A semi-analytical approach to get this parameter is given in the paper. It was found, as far as concerns the slowing-down of fast neutrons, that all magmatic rocks behave as sandstone with, however, different content of bound water in the rock matrix and different rock matrix density.

Some neutron methods are based on the detection of epithermal neutrons. For theoretical considerations it is important to know the physical meaning of the registered signal: is it proportional to the epithermal neutron flux, or to the slowing-down density? From the discussion of experimental data reported in the literature it seems that it is the slowing-down density that is the physical quantity being measured. This conclusion has a very important practical implication - the porosity calibration curves depend upon the slowing-down length alone and are independent of the slowing-down cross-section for epithermal neutrons.

Streszczenie

Zastosowanie metod neutronowych w otworach wiertniczych wymaga znajomości poprawnych krzywych kalibracji. Otrzymywanie ich na drodze eksperymentalnej jest procedurą bardzo skomplikowaną, trudną i drogą; sposób czysto teoretyczny (wykorzystując znane kody neutronowe oraz biblioteki danych neutronowych) również nie jest zadowalający. Pośrednia droga polega na badaniu zależności mierzonego sygnału sondy w danym ośrodku skalnym od pewnych całkowych parametrów neutronowych skał (takich jak długość spowalniania, długość dyfuzji, przekrój czynny absorpcji, czas życia neutronów, itp.). Wykorzystując takie podejście jest możliwe dokonanie "tłumaczenia" krzywych kalibracji znanych w jednym typie litologii na inny. By dokonać jednak tego "tłumaczenia" wymagana jest dobra znajomość neutronowych parametrów skały.

W pracy została przedstawiona metoda obliczania parametrów skał dla neutronów termicznych (przekrój czynny absorpcji, współczynnik dyfuzji i długość dyfuzji) . Opiera się ona na właściwym uśrednianiu po energii przekrojów czynnych wszystkich składników skały oraz płynów ją nasycających. Specjalny nacisk położono na obecność wodoru. Obliczono długość dyfuzji w funkcji zmiennej porowatości dla dwudetektorowych sond neutronowych. wpływ ten został oceniony na dwie jednostki porowatości, średnio.

W ostatnich czasach skały magmowe, jako możliwe źródła energii geotermicznej, zaczęły być celem profilowań neutronowych. Znajomość długości spowalniania posiada tutaj podstawowe znaczenie dla zagadnienia krzywych kalibracji. Zostało w pracy przedstawione półanalityczne podejście do otrzymania tego parametru. Otrzymano, że wszystkie skały magmowe,jeśli chodzi o długość spowalniania prędkich neutronów, zachowują się jak piaskowce z różną jednak zawartością wody związanej oraz gęstością mineralogiczną.

Niektóre metody neutronowe opierają się na pomiarze neutronów epitermicznych. Dla rozważań teoretycznych ważna jest znajomość fizycznego znaczenia rejestrowanego sygnału: czy jest on proporcjonalny do strumienia neutronów epitermicznych, czy też do gęstości spowalniania? Z dyskusji danych eksperymentalnych podawanych w literaturze wynika, że to gęstość spowalniania jest właśnie tą mierzoną wielkością fizyczną. Ta konkluzja posiada duże praktyczne implikacje - krzywe kalibracji porowatości zależą tylko od długości spowalniania, nie są natomiast zależne od przekroju czynnego spowalniania dla neutronów epitermicznych.

Резюме

Применение нейтронных методов в скважинах требует информации об калибровочных кривых. Экспериментальный подход для получения этих кривых очень сложный, грмоздкий и стоит дорого; совсем теоретический (применяя известные нейтрнные коды и сборки нейтронных данных по сечениям) тоже неудобен. Удобный подход получается когда некоторые интегральные нейтронные параметры пород (как длина замедления, длина диффузии, сечение поглощения, длина жизни нейтронов, итд.) коррелируется с сигналом глубинного прибора в данной породе. Используя этот подход возможно "перевести" калибровочные кривые для одного типа литологии породы в другом. Но чтовы получить возможность такого "перевода" нужно в первую очередь искать нейтронные параметры пород.

В работе представлен метод вычисления параметров для тепловых нейтронов (сечение захвата, коэффициент диффузии и длина диффузии) в породах. Он базирует на соответствующим усреднению сечений по энергии для всех элементов породы и насысчающей её жидкости. Особое внимание придано на присутствие водорода. Вычислено длины диффузии в зависимости от пористости пород для различных литологии. Представлено влияние спектра тепловых нейтронов на форму калибровочных кривых для двойно-длинного нейтронного метода. Это влияние оценено на две единицы пористости, в среднем.

В последнее время применяется нейтронный каротаж для определения пористости в магматических породах которые очень перспективные как возможные источники геотермической энергии. Здесь очень важная для калибровочной кривой проблема длины замедления. Полутеоретический подход для определения этого параметра представлен в работе. Оказалось что все магматические породы, с точки зрения определения длины замедления, следуют песчаник но с различным содержанием химическо связаной воды и пористостю.

Некоторы нейтронные методы базируют на измерении надтепловых нейтронов. Для теоретических исследовании физический смысл регистрируемого сигнала очень важный: пропорциональный он надтепловому потоку нейтронов или плотности замедления? Из дискуссии экспериментальных результатов приведеных в литературе вытекает что имеется дело с плотностю замадления. Это замечание очень важно с практической точки зрения - калибровочные кривые для пористости зависят от длины замедления и независимые от сечения замедления для надтепловых нейтронов.

Notation index

A_i - atomic mass of the element "i"

D - diffusion coefficient for the neutron flux (cm)

$\bar{D}$ - energy averaged diffusion coefficient for the neutron flux (Eq.(2.5))

$\bar{D}_o$ - energy averaged diffusion coefficient for the neutron density (cm^2/s) (Eq.(2.26))

E - energy of neutron (eV)

$E_m = k.T_m$ - energy corresponding to the temperature T_m of the moderator

$E_n = k.T_n$ - energy corresponding to the energy of the neutron gas

$E_{th} = 0.0253$ eV - thermal neutron energy

$Ei(x)$ - integral exponential function (Eq.(2.36))

g_{tr} - Westcott coefficient for the transport cross-section (Eq.(2.9))

$J(\beta)$ - special function (Eq.(2.35))

k - Boltzmann constant

K - proportionality coefficient in effective neutron temperature formula (Eq.(2.7))

$L_d = (\bar{D}/\Sigma_a)^{1/2}$ - diffusion length of thermal neutrons (cm) (Eqs (2.42) , (2.43), (2.47))

L_i - diffusion length in the i-th diffusion slowing-down group (cm)

L_s - slowing-down length (cm) (Eq.(3.1))

$L_s(0.01)$ - slowing-down length corresponding to the $\rho_{0.01}$ (Eq.(3.12))

m_n - mass of neutron

m, b - parameters of the correlation line (Eq.(3.2))

m_1, b_1 - parameters of the correlation line (Eq.(3.12))

M - migration length of neutrons (cm)

M_x - molecular weight, x - index of material

$N_A = 6.022529\ 10^{23}\ mole^{-1}$ - Avogadro number

p_i - weight fraction of the element "i" in the rock matrix

p_W - weight fraction of the bound water in the rock matrix

$q(r,E)$ - slowing down density of neutrons (neutrons/cm^3/s//energy interval) (Eq.(4.1))

$\vec{r}$ - point at space

r - distance between two points

$r(a,b)$ - sample correlation coefficient between the variable "a" and "b"

$R(a,b)$ - true correlation coefficient between the variables "a" and "b"

R - signal furnished by the logging tool

t - time

T_m - temperature of the moderator (K)

T_n - effective neutron temperature (K) (Eq.(2.7))

v - neutron velocity (cm/s)

$\bar{v} = <1/v>$ - averaged neutron velocity (Eq.(2.4))

$\overline{\cos_{H_2O}(E)}$ -energy averaged cosine of the scattering angle of neutron on water molecule

H_2O - water content (in volume per cent) (Eq.(3.4))

α_1, β_1 - parameters of the correlation line (Eq.(3.7))

$\beta(T_n)$ - coefficient (Eq.(2.34))

$\gamma = 0.57721\ 56649$ - Euler constant (Eq.(A.2))

ξ = average neutron lethargy loss per collision

ρ - bulk density (g/cm^3) (Eq.(3.3))

ρ_M - rock matrix density (g/cm^3)

ρ_o - apparent rock matrix density (g/cm^3) when all bound water content is subtracted (Eq.(3.10))

ρ_x - density (g/cm^3) ; x - index of material

$\rho_{0.01}$ - apparent rock matrix density (g/cm^3) with one per cent (by volume) of water (Eq.(3.9))

$\sigma_a(E)$ - microscopic absorption cross-section (barn)

$\sigma_s(E)$ - microscopic scattering cross-section (barn)

$\sigma_{tr}(E)$ - microscopic transport cross-section (barn)

$\sigma^{H_2O}_{tr,1/v}(E_m)$ - microscopic transport cross-section of water molecule assuming its 1/v behaviour (barn)

Σ_a - absorption cross section (cm^{-1})

$\bar{\Sigma}_a$ - energy averaged absorption cross-section (cm^{-1})

Σ_{aM} - absorption cross-section of the rock matrix (cm^{-1})

Σ_{aW} - absorption cross-section of the fluid saturating the pore space (cm^{-1})

$\Sigma_{tr}(E)$ - transport cross-section (cm^{-1})

Σ_{trM} - transport cross-section of the rock matrix (cm^{-1}) (Eq.(2.32))

Σ_{trM}' - transport cross-section of the rock matrix when all bound water content is subtracted (cm^{-1}) (Eq.(2.31))

Σ_{trW} - transport cross-section of the fluid saturating the pore space (cm^{-1})

$\Sigma^{H_2O}_{tr,1/v}$ - transport cross-section of water assuming its 1/v behaviour (cm^{-1})

$\Sigma_s(E)$ - scattering cross-section (cm^{-1})

ϕ - porosity of the rock (in a fraction: $0 \leqq \phi \leqq 1$)

$\Phi(E)$ - neutron energy spectrum ($energy^{-1}$) (Eq.(2.8))

$\phi_o(\vec{r},t)$ - neutron flux (neutrons/cm^2/s)

$\phi(\vec{r},E,t)$ - neutron flux (neutrons/cm^2/s/energy interval)

$\phi_n(r)$ - epithermal neutron flux at the point "r" calculated for the n slowing-down diffusion groups (Eq.(2.50))

$\phi_{n+th}(r)$ - thermal neutron flux at the point "r" calculated for the n slowing-down diffusion groups (Eq.(2.53))

$\phi_e(r,E)$ - epithermal neutron flux (neutrons/cm^2/s/energy interval) (Eq.(4.1))

1. Introduction

The fundamental cause of the successful application of neutron methods for the well logging purposes is the diversity of the rock elemental composition. Rock constituents with cross-sections exhibiting different behaviours in function of neutron energy contribute in different proportions to the slowing-down, scattering and absorption of neutrons. This, in turn, gives different levels of epithermal or thermal neutron fluxes or originates different gamma ray spectra of radiative capture, activation or inelastic scattering of neutrons in the rock media. The occurrence of all these physical phenomena creates a possibility to relate the logging tool signal to such geological parameters as: rock lithology, porosity, grade of a given element, brine salinity, etc. There are several ways to get these relations which are called the calibration curves. The most popular, though not the easiest (and quite an expensive) one, is a purely empirical way, where the signal from the borehole tool is registered when the tool is located in different blocks of rock for which the geological parameters in question are well known. The opposite approach is purely theoretical. Starting from the knowledge of the elemental composition of the rock medium, the borehole and the logging tool construction, and using rather sophisticated neutron codes, together with neutron data files, one arrives at a calculation of the tool response in a given medium. Another, mixed approach is to relate the measured tool signal in a given rock medium to some integral neutron parameters of that medium like the slowing-down length, migration length, absorption cross-section, etc. This approach, when properly handled, permits to "translate" the tool calibration curves from one environment to another. It seems to be the optimum one in the actual state of the art as concerns the calibration of neutron probes. Its main difficulty, however, is the lack of good knowledge (and sometimes even of a proper definition) of the neutron parameters of the rock media. Few experimental data exist in this field, and the calculation methods are not always adequate. The present paper is a contribution to this subject.

2. Thermal neutron parameters of rocks

2.1. Definition of parameters

A large number of neutron logging methods are based on the detection of thermal neutrons. In the theoretical description of these methods, besides the fast neutron slowing-down problems, the diffusion of thermal neutrons in the rock-borehole systems has to be taken into account. This is usually approached by the diffusion equation:

$$\frac{1}{v}\,\frac{\partial \emptyset_o(\vec{r},t)}{\partial t} - D\,\nabla^2\,\emptyset_o(\vec{r},t) + \Sigma_a\,\emptyset_o(\vec{r},t) = 0 \quad , \qquad (2.1)$$

where the thermal neutron flux $\emptyset_o(\vec{r},t)$ (in neutrons/cm^2/s) at a given point $\vec{r}$ and time t is linked with the thermal neutron parameters of the medium: D - the diffusion coefficient (in cm) and the absorption cross-section Σ_a (in cm^{-1}) and with the velocity v of thermal neutrons. However, the notation of the diffusion equation in the form given by Eq.(2.1) is not exact. When one starts from the Boltzmann transport equation in the P1 diffusion approximation, solid angle integrated neutron flux $\emptyset_0(\vec{r},E,t)$ appears (E is here the energy of neutrons). For further considerations one has to assume the separability of space and time from the energy variables, thus

$$\emptyset_0(r,E,t) = \emptyset_0(r,t).\Phi(E) \quad . \qquad (2.2)$$

Here the energy spectrum $\Phi(E)$ has to be normalized to the unity. After the simple integration over the energy E one arrives at the equation:

$$\frac{1}{v}\,\frac{\partial \emptyset_0(\vec{r},t)}{\partial t} - \bar{D}\,\nabla^2\,\emptyset_0(\vec{r},t) + \bar{\Sigma}_a\,\emptyset_0(\vec{r},t) = 0 \quad , \qquad (2.3)$$

which formally has the same form as Eq.(2.1) except for the material parameters, which here are:

$$\frac{1}{\bar{v}} = <\frac{1}{v}> = \int_0^\infty \frac{1}{v}\,.\,\Phi(E).dE \qquad (2.4)$$

$$\bar{D} = \frac{1}{3}<\frac{1}{\Sigma_{tr}}> = \frac{1}{3}\int_0^\infty \frac{1}{\Sigma_{tr}(E)}\,.\,\Phi(E).dE \qquad (2.5)$$

$$\bar{\Sigma}_a = \int_0^\infty \Sigma_a(E).\Phi(E).dE \qquad (2.6)$$

which simply means that the parameters appearing in Eq.(2.1) as constants are now averaged over the energy spectrum $\Phi(E)$ existing in the medium.

In geophysical literature, even quite recent, this subtle difference between Eqs (2.1) and (2.3) is simply neglected (Scott et al., 1982, Edmundson and Raymer, 1979). Sometimes, more inquisitive authors use the following assumptions (Tittle, 1962):

1. The thermal neutron spectrum $\Phi(E)$ is of the Maxwellian type at the temperature equal to that of the moderator.
2. The absorption cross-section is energy dependent like $(E)^{-1/2}$, and
3. The scattering cross-section is energy independent.

The last assumption is almost true except for the hydrogen nuclei, which are usually bound in water (or oil) molecules in the geological environment. For these molecules the scattering Σ_s (or transport, Σ_{tr}) cross-section is energy dependent. As concerns the first assumption, one has to keep in mind that it is true in the non-absorbing medium only. What we propose here is to take into account the real energy spectrum $\Phi(E)$ of slow neutrons in each particular geological formation and to calculate all neutron parameters according to their definitions given by Eqs (2.4), (2.5) and (2.6), when the proper energy behaviours of the $\Sigma_{tr}(E)$ and $\Sigma_s(E)$ cross-sections are respected. The exact solution of the problem presented in such form is, of course, not possible without the knowledge of the neutron spectrum $\Phi(E)$. To solve this vicious circle we propose to use the idea of the effective neutron temperature T_n (Beckurts and Wirtz, 1964):

$$\frac{T_n}{T_m} = 1 + K\,\frac{\Sigma_a(T_m)}{\xi\Sigma_s(T_m)} \qquad (2.7)$$

to describe the behaviour of the slow neutron spectrum. Here T_m is the temperature of the moderator, $\xi\Sigma_s(T_m)$ is the slowing-down power of the medium at the temperature T_m and K is a constant. The constant K has been measured by different authors for pure materials like light water, graphite and beryllium. Guberman and Yakubson (1964) have measured the effective neutron temperature in rocks for a large range of variation of the ratio $\Sigma_a/\xi\Sigma_s$ (up to 6). According to their results we can calculate the value of the coefficient K in Eq.(2.7) as being equal to K = 2.2 . For light water Burkhart and Reichardt (1962) have measured the hardening of the neutron spectra and the K value from their data is K = 1.473.

Using the concept of the effective neutron temperature T_n one can assume that in the real conditions the energy spectrum of slow neutrons is of the Maxwellian type

$$\Phi(E).dE = \frac{E}{kT_n} \cdot e^{-E/kT_n} \cdot \frac{dE}{kT_n} \qquad (2.8)$$

taken just at the temperature T_n higher than that (T_m) of the moderator.

An example of the calculation of the neutron flux energy spectrum in limestone of the porosity 0 and 20 per cent saturated with fresh water is given in Fig. 2.1. The flux spectrum was calculated according to Eq.(2.8) at the moderator temperature 20° C for T_n calculated using Eq.(2.7). It is readily visible that for the zero porosity case the average neutron energy is much higher than for the 20 per cent porosity, and both are above the thermal neutron energy E_{th} = 0.0253 eV for this ambient temperature. These energy spectra are, according to Eq.(2.5), the weighting functions for the $1/\Sigma_{tr}(E)$ values needed for the calculation of the diffusion coefficient $\bar{D}$. The plots of the $1/\Sigma_{tr}(E)$ functions for both cases are also given in Fig. 2.1.

2.2. Parameters for light water

Petrie et al. (1957) have found, already many years ago, that the transport cross-section of light water and some hydrocarbons have nearly $1/\sqrt{E}$ behaviour. To get a better knowledge of this relationship we have calculated the Westcott coefficient, g_{tr}, (Beckurts and Wirtz, 1964) applied this time not to the activation cross-section but to the transport cross-section of light water:

$$g_{tr}^{H_2O} = \frac{2}{\sqrt{\pi}} \, \frac{1}{\sigma_{tr}^{H_2O}(E_{th})} \int_0^\infty \sigma_{tr}^{H_2O}(E).\Phi(E).dE \quad , \qquad (2.9)$$

where for the $\Phi(E)$ spectrum we have taken the Maxwellian one at the energy E_{th} = 0.0253 eV. To calculate the integral in Eq.(2.9) we have performed the following:

$$\int_0^\infty \sigma_{tr}^{H_2O}(E).\Phi(E).dE \approx \int_0^{0.8\ eV} \sigma_{tr}^{H_2O}(E).\Phi(E).dE =$$

$$\int_0^{0.8\ eV} \sigma_a^{H_2O}(E).\Phi(E).dE + \int_0^{0.8\ eV} \sigma_s^{H_2O}(E).[1 -$$

$$\overline{\cos_{H_2O}(E)}].\Phi(E).dE \quad , \qquad (2.10)$$

where $\sigma_a^{H_2O}(E)$ and $\sigma_s^{H_2O}(E)$ are the absorption and scattering cross-sections of the water molecules, respectively, and $\overline{\cos_{H_2O}(E)}$ is the average cosine of the scattering angle of slow neutron on the water molecule. The $\sigma_s^{H_2O}(E)$ values have been taken from the paper of Gotoh and Takahashi (1971) and the $\overline{\cos_{H_2O}(E)}$ values from that of Beyster (1968). The integration in the second integral on the right-hand side in Eq.(2.10) has been carried out numerically using the shape of the spectrum $\Phi(E)$ given by Eq.(2.8) with $T_n = T_m = 0.0253$ eV. The result was:

$$\int_0^{0.8eV} \sigma_s^{H_2O}(E).[1 - \overline{\cos_{H_2O}(E)}].\Phi(E).dE = 79.556 \text{ barn} \quad .(2.11)$$

For the light water molecule the value of σ_a at $E_{th} = 0.0253$ eV is

$$\sigma_a^{H_2O}(E_{th}) = 0.662 \text{ barn} \qquad (2.12)$$

(according to the data of Mughabghab and Garber, 1973) and has a $1/\sqrt{E}$ behaviour, i.e.

$$\sigma_a^{H_2O}(E) = 0.662\sqrt{E_{th}/E} \quad \text{barn} \qquad (2.13)$$

and

$$\int_0^{0.8\text{ eV}} \sigma_a^{H_2O}(E).\Phi(E).dE = 1.324 \int_0^{5.623} x^2.e^{-x^2}.dx \approx$$

$$\approx 1.324\sqrt{\pi}/4 = 0.587 \text{ barn} \quad . \qquad (2.14)$$

Finally the integral in Eq.(2.9) is:

$$\int_0^{\infty}\sigma_{tr}^{H_2O}(E).\Phi(E).dE = 80.143 \quad \text{barn} \qquad (2.15)$$

and because

$$\sigma_{tr}^{H_2O}(E_{th}) = 93.606 \qquad (2.16)$$

the Westcott coefficient, according to Eq.(2.9) is:

$$g_{tr}^{H_2O} = 0.9661 \quad . \qquad (2.17)$$

This value confirms that the transport cross-section of the water molecule can be considered as having nearly $1/\sqrt{E}$ behaviour.Under this assumption one takes

$$\sigma_{tr,1/v}^{H_2O}(E_{th}) = g_{tr}^{H_2O}.\sigma_{tr}^{H_2O}(E_{th}) = 0.9661 \times 93.606 =$$

$$= 90.43 \quad \text{barn} \qquad (2.18)$$

as the value of the transport cross-section at the thermal energy.

Another cross-section which is needed for further calculations is the slowing-down cross section of the water molecule at the thermal energy. This can be found using, for example, the Radkowsky model (cf. Soodak, 1962) which gives

$$\xi\Sigma_s^{H_2O}(E_{th}) = 44.1 \quad \text{barn} \qquad . \qquad (2.19)$$

These three cross-sections, Σ_a, $\Sigma_{tr,1/v}$ and $\xi\Sigma_s$ taken at the energy 0.0253 eV , together with the water molecule density

$$\rho_{H_2O} \cdot \frac{N_A}{M_{H_2O}} = 0.03343 \times 10^{24} \quad \text{molecules/cm}^3 \;, \qquad (2.20)$$

where ρ_{H_2O} is the density of water, N_A is the Avogadro number and M_{H_2O} is the molecular weight of water, give the macroscopic cross-sections and the effective neutron temperature T_n at the same energy which are listed in Table 2.1.

Table 2.1

Macroscopis cross-sections of water at energy 0.0253 eV. Density of water: $\rho_{H_2O} = 1$ g/cm^3.

$\Sigma_a^{H_2O}$	0.02213 cm^{-1}
$\Sigma_{tr,1/v}^{H_2O}$	3.023 cm^{-1}
$\xi\Sigma_s^{H_2O}$	1.474 cm^{-1}
$T_n/T_m = 1 + 1.473\,\Sigma_a/(\xi\Sigma_s)$	1.022115

It is easy now to calculate the thermal diffusion parameters for light water:

Diffusion coefficient, $\bar{D}$:

$$\bar{D} = \frac{1}{3} < \frac{1}{\Sigma_{tr}} > = \frac{1}{3.\Sigma^{H_2O}_{tr,1/v}(kT_n)} \int_0^\infty \sqrt{\frac{E}{kT_n}} \cdot \frac{E}{kT_n} . e^{-E/(kT_n)} . \frac{dE}{kT_n} =$$

$$= \frac{2}{3.\Sigma^{H_2O}_{tr,1/v}(kT_m).\sqrt{T_m/T_n}} \int_0^\infty x^4 . e^{-x^2} . dx =$$

$$= \frac{1}{\Sigma^{H_2O}_{tr,1/v}(kT_m)} \sqrt{T_n/T_m} . \sqrt{\pi}/4 = 0.148193 \text{ cm} . \qquad (2.21)$$

Absorption cross-section, $\bar{\Sigma}_a$:

Taking into account the energetic relations at $E_m = kT_m$ and $E_n = kT_n$ for the absorption cross-section

$$\Sigma_a(E) = \Sigma_a(E_m) . \sqrt{E_m/E} = \Sigma_a(E_m) . \sqrt{E_m/E_n} . \sqrt{E_n/E} =$$

$$= \Sigma_a(E_m) . \sqrt{T_m/T_n} . \sqrt{kT_n/E} \qquad (2.22)$$

one has

$$\bar{\Sigma}_a = \Sigma_a^{H_2O}(E_m) . \sqrt{T_m/T_n} . \int_0^\infty \sqrt{kT_n/E} . E/(kT_n) . e^{-E/(kT_n)} . dE/(kT_n) =$$

$$= \Sigma_a^{H_2O}(E_m) . \sqrt{T_m/T_n} . \int_0^\infty x . e^{-x} . dx =$$

$$= \Sigma_a^{H_2O}(E_m) . \sqrt{T_m/T_n} . \sqrt{\pi}/2 = 0.01940 \text{ cm}^{-1} . \qquad (2.23)$$

Finally the square of the diffusion length for water is:

$$L_d^2 = \bar{D}/\bar{\Sigma}_a = \frac{1}{2.\Sigma^{H_2O}_{tr,1/v}(T_m) . \Sigma_a^{H_2O}(T_m)} . (T_n/T_m) =$$

$$= 7.6392 \text{ cm}^2 \qquad (2.24)$$

which gives

$$L_d = 2.764 \text{ cm} .$$

Let us remark that the quantities directly measured in the pulsed neutron experiments are:

$$\overline{v\Sigma}_a = \bar{\Sigma}_a . < \frac{1}{v} >^{-1} = \bar{\Sigma}_a . \bar{v} \qquad (2.25)$$

and

$$\bar{D}_o = \bar{D} . \bar{v} , \qquad (2.26)$$

where, according to Eq.(2.4)

$$< \frac{1}{v} > = \frac{1}{\bar{v}} = \frac{\sqrt{\pi}}{2\sqrt{2\,kT_n/m_n}} = \frac{\sqrt{\pi}}{2\sqrt{2\,kT_m/m_n}\ \sqrt{T_n/T_m}} =$$

$$= \frac{\sqrt{\pi}}{2.v_{th}(E_m)} \sqrt{T_m/T_n} = (250973.5 \text{ cm/s})^{-1} =$$

$$= 3.9844847 \times 10^{-6} \text{ s/cm} , \qquad (2.27)$$

where the thermal neutron velocity at 20° C is

$$v_{th}(E_m) = \sqrt{2\,kT_m/m_n} = 2200 \text{ m/s} ,$$

where m_n is the mass of neutron. Finally, from Eqs (2.25) and (2.26) one has for water at 20° C

$$\overline{v\Sigma}_a = 4\,868.9 \text{ s}^{-1}$$

$$\bar{D}_o = 37\,192 \text{ cm}^2/\text{s} . \qquad (2.28)$$

These results are in a very good agreement with the experimental data (Czubek et al., 1980) .

2.3. Thermal neutron parameters of rock saturated with water

The main problem in the rock parameter calculations concerns the diffusion coefficient. Under the assumption of the $1/v$ behaviour for the σ_{tr} of the water molecule one can present the $\Sigma_{tr}(E)$ of the rock as:

$$\Sigma_{tr}(E) = (1-\emptyset)\cdot\Sigma_{trM} + \emptyset\cdot\Sigma_{trW}(E) =$$
$$= (1-\emptyset)\cdot\Sigma_{trM} + \emptyset\cdot\Sigma_{trW}(kT_n)\cdot\sqrt{kT_n/E} \quad , \qquad (2.29)$$

where $\emptyset$ is the rock porosity, Σ_{trM} is the transport cross-section of the rock matrix (considered here as being without any bound water content), and Σ_{trW} is the transport cross-section of the saturating liquid. If the liquid is simply fresh water, one has $\Sigma_{trW} = \Sigma^{H_2O}_{tr,1/v}$, if there is brine with some salinity or hydrocarbons, their Σ_{trW} should be calculated accordingly. In the case when the rock matrix contains the p_W weight fraction of the bound water and the rock matrix density is ρ_M , the transport cross-section of the rock matrix is

$$\Sigma_{trM}(E) = \rho_M\cdot N_A\cdot\sum_{i=1}^{n-1}\frac{\sigma^i_{tr}}{A_i}\cdot p_i + \rho_M\cdot N_A\cdot\frac{\sigma^{H_2O}_{tr}(E)}{M_{H_2O}}\cdot p_W \quad , \qquad (2.30)$$

where the first summation is going over all rock constituents but water (A_i and p_i are their atomic masses and weight fractions, respectively). Using the notation

$$\Sigma_{trM'}(E) = \rho_M\cdot N_A\cdot\sum_{i=1}^{n-1}\frac{\sigma^i_{tr}}{A_i}\cdot p_i \qquad (2.31)$$

one arrives at

$$\Sigma_{trM}(E) = \Sigma_{trM'} + \rho_M\cdot p_W\cdot\Sigma^{H_2O}_{tr,1/v}(E) \qquad (2.32)$$

which has to be inserted into Eq.(2.29) . Now, to calculate the diffusion coefficient $\bar{D}$ according to Eq.(2.5) one arrives at the expression:

$$\left\langle\frac{1}{\Sigma_{tr}(E)}\right\rangle = \frac{2}{(1-\emptyset)\cdot\Sigma_{trM'}}\int_0^\infty\frac{x^4\cdot e^{-x^2}}{x+\beta}\cdot dx \quad , \qquad (2.33)$$

where

$$\beta(T_n) = \frac{\emptyset(1-\rho_M\cdot p_W)+\rho_M\cdot p_W}{1-\emptyset}\cdot\frac{\Sigma^{H_2O}_{tr,1/v}(kT_n)}{\Sigma_{trM'}} \quad . \qquad (2.34)$$

The integral in Eq.(2.33) can be easily transformed into a set of known special functions, namely

$$J(\beta) = 2\int_0^\infty\frac{x^4\cdot e^{-x^2}}{x+\beta}\cdot dx =$$
$$= 1 - \frac{\sqrt{\pi}}{2}\beta + \beta^2 - \sqrt{\pi}\,\beta^3 + 2\,\beta^4\int_0^\infty\frac{e^{-x^2}}{x+\beta}\cdot dx =$$
$$= 1 - \frac{\sqrt{\pi}}{2}\beta + \beta^2 - \sqrt{\pi}\,\beta^3 + \beta^4\cdot e^{-\beta^2}\cdot\left[2\sqrt{\pi}\int_0^\beta e^{t^2}\cdot dt - \right.$$
$$\left. Ei(\beta^2)\right] \quad , \qquad (2.35)$$

where the integral exponential function

$$Ei(x) = \fint_{-\infty}^{x}\frac{e^t}{t}\,dt \quad , \qquad x > 0 \qquad (2.36)$$

is taken as the principal value of the integral. Both integrals in Eq.(2.35) can be expanded in the rapidly convergent series (cf. Appendix A) and the function $J(\beta)$ can be calculated using any programmable pocket calculator. The behaviour of the function $J(\beta)$ is the following:

$$\lim_{\beta\to 0} J(\beta) = 1 \qquad \lim_{\beta\to\infty} J(\beta) = 0$$
$$\lim_{\beta\to 0} \beta.J(\beta) = 0 \qquad \lim_{\beta\to\infty} \beta.J(\beta) = \frac{3\sqrt{\pi}}{4} \tag{2.37}$$

and the plots of the functions $\beta.J(\beta)$ and $J(\beta)$ are given in Fig. 2.2.

Finally for the diffusion coefficient $\bar{D}$ one has:

$$\bar{D} = \frac{1}{3}\left<\frac{1}{\Sigma_{tr}}\right> = \frac{1}{3(1-\varnothing)\cdot\Sigma_{trM}'}\cdot J[\beta(T_n)] \quad , \tag{2.38}$$

where

$$\beta(T_n) = \frac{\varnothing(1-\rho_M\cdot p_W) + \rho_M\cdot p_W}{1-\varnothing}\cdot\frac{\Sigma_{trW}(T_m)}{\Sigma_{trM}'}\cdot\sqrt{T_m/T_n} \quad . \tag{2.39}$$

The absorption cross-section $\bar{\Sigma}_a$ for rock is calculated in a similar way as for water (cf. Eq.(2.23)) , that is:

$$\Sigma_a(E) = (1-\varnothing)\cdot\Sigma_{aM}(E) + \varnothing\cdot\Sigma_{aW}(E) \quad , \tag{2.40}$$

where the indexes M and W refer to the rock matrix and to the saturating liquid, respectively, and the general behaviour of the absorption cross-section is given by Eq.(2.22) , which results in:

$$\bar{\Sigma}_a = [(1-\varnothing)\cdot\Sigma_{aM}(T_m) + \varnothing\cdot\Sigma_{aW}(T_m)]\cdot\sqrt{T_m/T_n}\cdot\sqrt{\pi}/2 \ . \tag{2.41}$$

Knowing $\bar{D}$ and $\bar{\Sigma}_a$ for a given rock saturated with water (or another liquid), the diffusion length L_d is calculated from the equation

$$L_d = (\bar{D}/\bar{\Sigma}_a)^{1/2} \quad . \tag{2.42}$$

The proper sequence of the calculation of rock thermal neutron diffusion parameters is as follows:

Starting from the elemental composition of the rock matrix we calculate, for the moderator temperature T_m, the values $\Sigma_{aM}(T_m)$, $\Sigma_{trM}'(T_m)$, $\xi\Sigma_{sM}(T_m)$. The input data for further calculation are: $\Sigma_{aW}(T_m)$, $\Sigma_{trW}(T_m)$, $\xi\Sigma_{sW}(T_m)$ - according to the data in Table 2.1 , next $\Sigma_{aM}(T_m)$, $\Sigma_{trM}'(T_m)$, $\xi\Sigma_{sM}(T_m)$, matrix density ρ_M, water content in the rock matrix p_W, and porosity $\varnothing$. Using these data one calculates $\Sigma_a(T_m)$ and $\xi\Sigma_s(T_m)$ for the entire rock which are next used to calculate the T_n/T_m ratio from Eq.(2.7). Next, the $\beta(T_n)$ value is calculated from Eq.(2.34) or (2.39) , and the $\bar{\Sigma}_a$ value from Eq.(2.41) . For a given value of $\beta(T_n)$ the function $J(\beta)$ is calculated from Eq.(2.35) . Once the $J(\beta)$ value is known, the diffusion coefficient $\bar{D}$ can be calculated from Eq.(2.38) and the L_d value from Eq.(2.42) . The whole sequence of calculations can be performed using a programmable pocket calculator of the type TI-59, for example. The program NEROTH for TI-59 which is calculating the $\bar{\Sigma}_a$, $\bar{D}$ and L_d values is available from the author on personal request.

2.4. Discussion of results

The experimental values of thermal neutron diffusion parameters for geological materials are almost unknown, except for a few values of the absorption cross-section of some rocks (cf. Czubek et al.,1982, 1983, Allen and Mills, 1975, Harris and McDaniel, 1982, Carre, 1968) and a single value of the diffusion length for the silica sand of the porosity 38.8 per cent saturated with fresh water which was measured by Tittle (1948). All other experimental data concern with water, graphite, beryllium or other nuclear materials. The value obtained by Tittle was $L_d = 5.416$ cm (without any remark concerned with the accuracy of that result) and was obtained as a difference between the migration length, M, and the slowing-down length, L_s, both values being calculated from the spatial distribution of the epithermal and thermal neutrons:

$$L_d = [\, M^2 - L_s{}^2]^{1/2} = [(966 - 790)/6]^{1/2} = 5.416 \text{ cm} . \quad (2.43)$$

The silica sand used by Tittle had the mineralogical density 2.66 g/cm^3. When one takes the mineralogical density of SiO_2 $\rho_{SiO_2} = 2.65$, one obtaines from the similitude principle that

$$L_{d1}[(1 - \phi_1)\cdot\rho_{M1} + \phi_1\cdot\rho_W] = L_{d2}[(1 - \phi_2)\cdot\rho_{M2} + \phi_2\cdot\rho_W] ,$$

where

$$\frac{\phi_1}{(1 - \phi_1)\cdot\rho_{M1}} = \frac{\phi_2}{(1 - \phi_2)\cdot\rho_{M2}} . \quad (2.44)$$

Here the indices 1 and 2 correspond to the case of the two mineralogical dinsities ρ_{M1} and ρ_{M2} of the same elemental composition. Thus, from Eq.(2.44) one has

$$L_{d2} = L_{d1}[\phi_1 + (1 - \phi_1)\cdot\rho_{M1}/\rho_{M2}] \quad (2.45)$$

valid for the porosity ϕ_2 given by:

$$\phi_2 = [(1 - \phi_1)\cdot\rho_{M1}/\phi_1/\rho_{M2} + 1]^{-1} \quad (2.46)$$

which gives in this case:

$$\phi_2 = 38.71 \% \text{ and } L_{d2} = 5.428 \text{ cm.}$$

The values of L_d for silica sands of different porosities saturated with fresh water are plotted in Fig. 2.3 for the case when the slow neutron spectrum has been taken into account (Eq.(2.42)) and when it has been ignored. In the latter case the L_d value has been obtained from the usual formula:

$$L_d = [\, 3\cdot\Sigma_{tr}(E_{th})\cdot \Sigma_a(E_{th})]^{-1/2} . \quad (2.47)$$

Tittle's data are also plotted (they have been calculated according to Eq.(2.47)) . The discrepancy between our (brocken curve) and Tittle's data is due to the differences in the microscopic cross-section used by him in 1948 and by us now.

It is well known from the well logging practice that real rocks always have higher absorption cross-section values than those calculated according to their elemental composition in major constituents. This is due to the presence of highly absorbing trace elements in the rocks. For the sandstone we have taken the matrix absorption cross-section $\Sigma_a(E_{th}) = 10$ c.u. (1 c.u. = 1 capture unit = 10^{-3} cm^{-1}) instead of 4.264 valid for SiO_2. The L_d values for such sandstone are also plotted in Fig. 2.3 for the two cases: with and without the slow neutron spectrum taken into account in the calculation. It is readily visible how important is the knowledge of the real $\bar{\Sigma}_a$ value of the rock to calculate the diffusion length L_d correctly.

For the three basic lithological types of sedimentary rocks, i.e. sandstone, limestone and dolomite, we have calculated the L_d values in function of their porosities for the case when the pore space is saturated with fresh water. The Σ_{aM} values taken for the calculation are those reported as typical of these rocks. The results are presented in Fig. 2.4. The L_d values calculated when the slow neutron spectrum has been taken into account are always larger than those when the slow neutron spectrum is ignored. The corresponding matrix densities taken for calculation were: 2.65 for sandstone, 2.72 for limestone and 2.85 for dolomite. The corresponding scattering cross-sections as well as the $\bar{\xi}$ and $\overline{\cos\theta}$ values have been calculated as for SiO_2, $CaCO_3$ and $CaMg(CO_3)_2$, respectively, where the cross-sections for these elements have been taken according to Mughabghab and Garber (1973).

What we have to emphasize here is that no experimental data directly confirm the validity of these results. Even the unique result of Tittle (cf. Fig. 2.3) is not precise enough to provide such confirmation. All we can do is to answer the problem: are the differences between the "spectrum" and "spectrumless" values of L_d significant for the neutron calibration curves? The answer can be furnished by the benchmark calculation.

2.5. Benchmark calculus

In order to find out how important are the differences observed in the L_d values depending upon whether or not the slow neutron spectrum has been taken into account, some simplified benchmark calculations have been carried out.

The calculations have been performed for a homogeneous (i.e. without borehole), infinite limestone medium using the multigroup diffusion approximation for the slowing-down process of fast neutrons. Instead of applying quite sophisticated neutron codes, like DOT, for example, (Engle, 1980) a particular model of the multigroup diffusion approximation has been developed for the benchmark calculation:

For the n slowing-down groups the diffusion length L in each group was equal $(L_1 = L_2 = \dots = L_n = L)$ and the down-scattering probability from the j-th group to the k-th group $(1 \leqq j < k \leqq n)$ was assumed constant for all groups below the neutron energy E_j, i.e. equal to $1/(n-j)$. Thus, for the j-th group the diffusion equation was:

$$D_j \nabla^2 \emptyset_j - \bar{\xi}\Sigma_{s,j}\, \emptyset_j + \frac{1}{n-(j-1)} \bar{\xi}\Sigma_{s,j-1}\, \emptyset_{j-1} + \\ + \frac{1}{n-(j-2)} \bar{\xi}\Sigma_{s,j-2}\, \emptyset_{j-2} + \dots + \frac{1}{n-2} \bar{\xi}\Sigma_{s,2}\, \emptyset_2 + \\ + \frac{1}{n-1} \bar{\xi}\Sigma_{s,1}\, \emptyset_1 = 0 \quad . \qquad (2.48)$$

Assuming

$$D_1 = D_2 = \dots = D_j = \dots = D_n = D \\ \bar{\xi}\Sigma_{s,1} = \bar{\xi}\Sigma_{s,2} = \dots = \bar{\xi}\Sigma_{s,j} = \dots = \bar{\xi}\Sigma_{s,n} = \bar{\xi}\Sigma_s \qquad (2.49)$$

the solution of the n diffusion equations of the type given above for the point isotropic source embedded in an infinte medium gives for the last n-th group:

$$\emptyset_n(r) = \frac{1}{4\pi L^3\, \bar{\xi}\Sigma_s} \; \frac{e^{-r/L}}{2^{2n-3}(n-1)} \cdot \\ \sum_{j=0}^{n-2} \left(\frac{2r}{L}\right)^j \sum_{t=0}^{n-2-j} \frac{2^{2t} \cdot {}^{n-2}b_t}{(n-2)!\,(n-1-t)!} \; \frac{(2n-2t-4-j)!}{j!\,(n-t-j-2)!} \quad , \qquad (2.50)$$

where

$${}^{n}b_k = {}^{n-1}b_k + n \cdot {}^{n-1}b_{k-1}$$

with $\qquad (2.51)$

$${}^{n}b_o = 1 \;,\; {}^{n}b_1 = \frac{n(n+1)}{2} \;,\; {}^{n}b_n = n!$$

and

$$L = L_s \left(1 + \sum_{i=1}^{n-1} 1/i \right)^{-1/2} \quad , \tag{2.52}$$

where L_s is the slowing-down length in a given medium.

We have called this model of the slowing-down process the multigroup diffusion proportional slowing-down model. The results of calculations according to this model are a very weak function of the total number n of diffusion groups, which is not the case when one uses the ordinary (we call it the uniform) multigroup diffusion model (cf. Beckurts and Wirtz, 1964). The whole derivation of this model will be published elsewhere.

When the $\emptyset_n(r)$ flux is taken as the epithermal neutron flux, the thermal neutron flux obtained from the diffusion equation is:

$$\begin{aligned} \emptyset_{n+th}(r) = {} & \frac{1}{4\pi \bar{\Sigma}_a} \, \frac{1}{L^2 L_d} \, \frac{1}{2^{2n-2}(n-1)} \cdot \\ & \left\{ \frac{r}{L} e^{-r/L} \sum_{j=0}^{n-2} \left(\frac{2r}{L}\right)^j G_{nj} \sum_{t=1}^{j+2} \frac{(j+1)!}{(j+2-t)!} \left(\frac{L}{r}\right)^t \cdot \right. \\ & \left[\frac{1}{(1+L/L_d)^t} - \frac{1}{(1-L/L_d)^t} \right] - \\ & \frac{L}{r} e^{-r/L_d} \sum_{j=0}^{n-2} 2^j (j+1)! \, G_{nj} \left[\frac{1}{(1+L/L_d)^{j+2}} - \right. \\ & \left. \left. \frac{1}{(1-L/L_d)^{j+2}} \right] \right\} \quad , \end{aligned} \tag{2.53}$$

where

$$G_{nj} = \sum_{t=0}^{n-2-j} 2^{2t} \frac{{}^{n-2}b_t}{(n-2)!\,(n-t-1)!} \, \frac{(2n-2t-4-j)!}{j!\,(n-t-j-2)!} \quad . \tag{2.54}$$

The calculations were performed for the L_s values obtained by Kreft (1974) for the Pu-Be neutron source in $CaCO_3$ of the matrix density 2.72. For thermal neutrons the $\Sigma_a(E_{th})$ was assumed equal to $\Sigma_a = 11.3$ c.u., which is still in the range observed for limestones (Wichmann et al., 1967). For such a value of Σ_a of the limestone matrix the L_d values are plotted in Fig. 2.4 for different porosities.

The benchmark calculation was carried out for the ratio $\emptyset_{n+th}(r_1)/\emptyset_{n+th}(r_2)$ obtained according to Eq.(2.53) . First, as an example, this ratio was calculated for $r_1 = 45$ cm and $r_2 = 60$ cm taking $n = 2$, 7 and 25 slowing-down groups. The result is presented in Fig. 2.5, where the weak sensitivity of the final result to the number of slowing-down groups is demonstrated (in the uniform slowing-down model the result depends much stronger upon the value of n) .

The ratio $\emptyset_{n+th}(r_1)/\emptyset_{n+th}(r_2)$ has been calculated for the two pairs of r_1, r_2 : $r_1 = 45$ cm/$r_2 = 60$ cm and $r_1 = 60$ cm/$r_2 = 75$ cm in function of the limestone porosity for the two different definitions of the L_d value - the one when the slow neutron spectrum is taken into account (Eq.(2.42)) and when it is ignored (Eq.(2.47)). The results are given in Fig. 2.6. The calculation was carried out for the value of $n = 7$ slowing-down diffusion groups. This kind of calculation approximates the dual spacing thermal neutron porosity tool. It is visible from Fig. 2.6 that the effect of the slow neutron energy spectrum is manifested in the difference of one to two porosity units on the calibration curve. For the same inter-detector distance (15 cm in this case) the shorter is the source-detector distance, the larger is the neutron spectrum influence on the porosity determination.

The theoretical flux ratio in an infinite medium depends upon the L_d, L_s, n, r_1 and r_2 values only. The experimental signals for such dual detector tools can also be presented as a univocal function of the migration length M (Scott et al., 1982) . This is presented in Fig. 2.7 , where the curves for $r_1 = 45$ cm and $r_2 = 60$ cm from Fig. 2.6 are plotted together with the Schlumberger data for a real probe. The r_1 and r_2 values for the Schlumberger data are unknown and in the real conditions the flux ratio is still altered by the detector efficiency ratio (the two detectors must not be alike) - thus the Schlumberger curve has been multiplied by a factor of two to reach a good scale for comparison. The curvature of our curve is greater than that of Schlumberger, which is in good agreement with the physics of the problem: the results obtained when the influence of the borehole is neglected always have higher sensitivity to the rock parameter variation.

Moreover, as is evident from the results given in Fig. 2.7, the incorrect calculation of the L_d value does not, practically, move the points out of the correct relationship: flux ratio vs migration length. For a given dual detector porosity probe such a curve can be considered as the universal calibration curve which can be used in different lithologies provided their neutron parameters are known. The slightly incorrect calculation of these parameters (as in the case of the calculation of the L_d value) does not change the correct interpretation provided that the same system of calculation of neutron parameters is always maintained for each lithology. However, for a pure theoretical calibration of a given probe using the theoretical value of the neutron flux, when the probe signal in a given lithology is related directly to the porosity, the L_d value has to be calculated correctly, as is visible from the results given in Fig. 2.6.

3. Slowing down of fast neutrons in magmatic rocks

3.1. Presentation of the problem

Magmatic rocks are becoming a more and more interesting environment as a potential (and/or in some sites, a real) source of geothermal energy, or as a host rock for radioactive waste disposal. The well logging service in these rocks, however, is not well developed so far. The main effort of logging companies being directed towards sedimentary series (petroleum and ore exploration), there is not one facility in the world for the calibration of neutron porosity tools in magmatic rocks. The design of such facility for this lithology is not an easy task, and it is quite expensive, too (Nelson et al., 1979, Baker et al., 1975) . What one has to do in such a situation is to adapt the porosity neutron calibration curves known for sedimentary series to magmatic ones. This can be done if all the neutron parameters for magmatic rocks are known, the slowing-down length, L_s, being the most important among them.

The experimental values of L_s for geological materials are not known (besides that of water) except those reported by Tittman (1955) for silica sand (SiO_2) and for pure limestone ($CaCO_3$), together with the one for 38.8 per cent water saturated silica sand mentioned earlier (Tittle, 1948).

In geophysical practice the L_s values are usually calculated using various neutron codes and the problem of which definition of the slowing-down length is the most proper one, i.e. neutron flux, neutron density, collision density or slowing--down density, is not entirely solved. What we are going to use is the flux neutron slowing-down length, L_s, the square of which is defined as:

$$L_s^2 = \frac{1}{6} \frac{\int_0^\infty r^2.\phi_0(r).4\pi r^2.dr}{\int_0^\infty \phi_0(r).4\pi r^2.dr} , \qquad (3.1)$$

where $\phi_0(r)$ is the flux of the slowed-down neutrons from a point isotropic fast neutron source in an infinite medium. The most convenient code to calculate this value is probably the one published by Kreft (1974). However, all codes calculating the L_s values have a common disadvantage: they require the knowledge of not only the elemental composition of the rock, but also of a large set of differential microscopic cross-sections of all kinds which are not always available. Moreover, the utilization of these codes requires quite sophisticated equipment run by highly educated specialists. On the other hand, what is needed in the geophysical field practice, is a simple and rapid algorithm which could permit to get the L_s values using as little input information as possible. To fulfil this requirement we have established a simple formula to evaluate the L_s parameter of magmatic rocks in the porosity range between 0 and 40 per cent when the matrix density and the content of water bound in the rock matrix are known (Czubek, 1981).

3.2. Derivation of algorithm

We have taken the averaged elemental analysis of 17 representative magmatic rocks reported by Daly (1933) in order to find their general behaviour as concerns the L_s values. These analyses are listed in Table 3.1. For some technical reasons

Table 3.1.

Index of magmatic rocks discussed in the present work

Our nomenclature	No of analysis and the rock nomenclature due to Daly (1933)	No of analysed samples (Daly, 1933)
1. Dunite	17. Dunite	10
2. Peridotite	76. Wehrlite	5
3. Pyroxenite	85. Diallagite	14
4. Gabbro	57. All gabbro	41
5. Basalt	58. All basalt	198
6. Diabase	90. Diabase	90
7. Diorite	125. Diorite, including 55 quarz diorites	125
8. Andesite	49. All andesite	87
9. Granodiorite	45. All granodiorite	40
10. Dacite	46. Dacite	90
11. Granite	4. Granite of all periods	546
12. Liparite	5. Rhyolite, including 24 liparites	126
13. Syenite	18. All syenite, including 5 "alkaline"	50
14. Trachyt	19. Tirachyts, as named by authors	48
15. Nepheline syenite	40. Nepheline syenite	43
16. Phonolite	41. Phonolite	25
17. Urtite	35. Urtite	3

the P_2O_5 content (very low, in fact) was neglected, the total was normalized to 100 per cent and the results were recalculated to get the elemental content (not in the form of oxides as in the original data) in weight per cent. These data, together with the rock matrix densities are listed in Table 3.2.

At our request Dr. Kreft has kindly calculated the L_s values for Am-Be source using his code in a broad range of porosities for all rocks listed in Table 3.2. We have found that for each type of the rock there is a perfect correlation between the L_s value and the total content of water according to the relation:

$$L_s \cdot \rho = m . \log_{10} H_2O + b \quad , \qquad (3.2)$$

where

$$\rho = (1 - \phi) \cdot \rho_M + \phi \cdot \rho_W \qquad (3.3)$$

is the bulk density of water saturated rock, and

$$H_2O = 100 . \phi + p_W \cdot \rho_M \quad (\%) \qquad (3.4)$$

is the water content in the volume per cent, where p_W is the weight per cent of the chemically bound water in the rock matrix. When one uses the data of Table 3.2 one has

$$p_W = H/0.1119 \quad , \qquad (3.5)$$

where H is the weight per cent of hydrogen in the rock matrix. The sample correlation coefficient $r(L_s \cdot \rho, \lg_{10} H_2O)$ for each type of rock from Table 3.2 in the range of porosities between 0 and 40 per cent is almost perfect (better than -0.9999 except for dacite: -0.99969, and urtite: -0.99953) though the pairs m,b for different types of rock are different. There is, however, a significant correlation between the m and b values for all the investigated rocks. This correlation is presented in Fig. 3.1, where the two regression lines are also given. The sample correlation coefficient is equal to:

$$r(m,b) = - 0.95525 \qquad (3.6.a)$$

which for $n = 17$ pairs of data gives a very narrow confidence belt for the true correlation coefficient: at the 95 per cent of the confidence level the true correlation coefficient R is within the limits

$$- 0.8775 \geqq R(m,b) \geqq - 0.9841 \quad . \qquad (3.6.b)$$

From the correlation in Fig. 3.1 one has:

$$m = - \alpha_1 . b - \beta_1$$

with

$$\alpha_1 = 0.373242 \quad [1/\lg_{10}(\%)] \qquad (3.7)$$

$$\beta_1 = 5.041956 \quad [g/cm^2/\lg_{10}(\%)]$$

and from Eq.(3.2) for $H_2O = 1$ per cent one has

$$b = L_s(0.01) \cdot \rho_{0.01} \quad , \qquad (3.8)$$

where the apparent bulk density of the rock containing one per cent (by volume) of water is:

$$\rho_{0.01} = \rho_o \, 0.99 + 0.01 \qquad (3.9)$$

with

$$\rho_o = \rho_M \cdot \frac{100 - p_W}{100 - p_W \cdot \rho_M} \quad , \qquad (3.10)$$

where ρ_o is an apparent rock matrix density without any water content.

The values of b, ρ_M and p_W being known for the rock in question, it was possible to establish the correlation between the $L_s(0.01) = b/\rho_{0.01}$ and $\rho_{0.01}$ values which is depicted in Fig. 3.2. Here the correlation is even more perfect than in Fig. 3.1 because the true correlation coefficient R at the 95 per cent confidence level is within

$$- 0.995 \leq R[L_s(0.01),\ \rho_{0.01}] \leq - 0.963 \qquad (3.11)$$

and the formula for $L_s(0.01)$ is:

$$L_s(0.01) = \frac{b}{\rho_{0.01}} = m_1 \cdot \rho_{0.01} + b_1 \qquad (3.12)$$

with

$$m_1 = - 5.974368 \quad cm^4/g$$

$$b_1 = 41.996607 \quad cm \quad .$$

Now, having set together Eqs (3.3), (3.4), (3.7), (3.9) and (3.12) we are able to calculate all data to get the L_s value from Eq.(3.2), which has the final form:

$$L_s = \frac{1}{(1 - \emptyset)\cdot\rho_M + \emptyset}\{- \beta_1 \cdot lg_{10}(100.\emptyset + p_W \cdot \rho_M) + (1 - \alpha_1)(0.99\ \rho_M \frac{100 - p_W}{100 - p_W \cdot \rho_M} + 0.01) \cdot [m_1\ (0.99\ \rho_M \frac{100 - p_W}{100 - p_W \cdot \rho_M} + 0.01) + b_1]\} \quad cm , \qquad (3.13)$$

where the four constants are:

$$1 - \alpha_1 = 0.626758$$

$$\beta_1 = 5.041956$$

$$m_1 = - 5.974368$$

$$b_1 = 41.996607$$

p_W is in the weigth per cent, ρ_M in g/cm^3 and $\emptyset$ is a fractional porosity $(0 \leq \emptyset \leq 1)$. The water density ρ_W was assumed equal to 1 g/cm^3.

We have compared the results obtained using Eq.(3.13) with those given by the neutron code of Kreft for all the rocks listed in Table 3.2 for 0, 20 and 40 per cent of the water saturated porosity. These results are presented in Figs 3.3, 3.4 and 3.5, respectively. Although the points, especially those for 20 and 40 per cent of porosity, are lying out of the bisectrix, the sample correlation coefficients between the L_s values according to Kreft (called $L_s(K)$) and those according to Eq. (3.13) (called $L_s(c)$) are 0.9962, 0.9949 and 0.9926 for 0, 20 and 40 per cent of porosity, respectively. The regression lines for the latter two cases deviate from the bisectrix, but when one compares the scales on both axes, one can find that this deviation does never exceed the four per cent of the relative value. For the 0 porosity case it is even better (except for urtite, where the deviation is also 4 per cent). These results permit us to extrapolate that when one uses Eq.(3.13) to calculate the slowing-down length L_s the parameter can be known with the same accuracy for all types of magmatic rocks encountered in the field practice.

4. Epithermal neutron porosity probes

4.1. Presentation of the problem

Some neutron porosity probes are equipped with epithermal neutron detectors (Tittman et al., 1966, Wood et al., 1971, Welex, 1968). Almost nothing is published on the design details of these tools, but it is obvious that the detectors should always be of some 1/v type covered by strong thermal neutron absorbers like cadmium. Sometimes, to increase the detection efficiency, some moderator can be inserted between the detector and the cadmium shield.

The main reason of the introduction of epithermal neutron detection to porosity tools was to decrease the influence of the lithology effects on the final interpretation results. While the experimental technique of the epithermal neutron log being relatively simple, the physical meaning of the measurement is not. What does the tool signal really mean?

In a weakly absorbing medium, as the geological formations always are, there is an obvious relationship between the epithermal neutron flux $\emptyset_e(r,E)$ and the slowing-down density $q(r,E)$ defined at a given point r and neutron energy E:

$$\emptyset_e(r,E) = \frac{q(r,E)}{\bar{\xi}\Sigma_s(E)} \quad . \qquad (4.1)$$

It is very little known what is really measured by the epithermal neutron tools in well logging: flux or slowing-down density? Usually, when one performs the numerical calculations, the epithermal neutron flux $\emptyset_e(r,E)$ is taken into account (Ellis et al., 1981) , sometimes, however, the slowing down density $q(r,E)$ is considered (Rathur and Grant, 1964).

Let us again take into account a very simple measurement situation, where the neutron source is embedded in an infinite and uniform geological formation without borehole. Within the n diffusion group slowing-down approximation, the slowing-down density is given by the term $\bar{\xi}\Sigma_s \cdot \emptyset_n(r)$ which, according to Eqs (2.50) and (2.52) , depends upon the L_s value only. Now we can consider the two alternatives: either the epithermal tool signal R in function of the porosity $\emptyset$ in a given lithology is proportional to the epithermal neutron flux $\emptyset_e(r)$, or it is proportional to the slowing-down density $q(r)$. The neutron energy E , at which both quantities are observed, can be fixed at the cadmium cut-off energy $E = E_{Cd} = 0.4$ eV.

4.2. Results of comparison

The microscopic slowing-down cross-section for the water molecule, according to the Radkowsky model (Soodak, 1962) at energy 0.4 eV is $\bar{\xi}\Sigma_s(H_2O) = 47$ barns. For SiO_2, $CaCO_3$ and $CaCO_3 \cdot MgCO_3$ which stand here for sandstone ($\rho_S = 2.65$), limestone ($\rho_L = 2.72$) and dolomite ($\rho_D = 2.85$) , the following slowing-down cross-sections in function of the porosity $\emptyset$ of the rock are obtained:

for sandstone

$$\xi\Sigma_s = 0.02825 + 1.543\,\emptyset \qquad (cm^{-1})$$

for limestone

$$\xi\Sigma_s = 0.037047 + 1.534\,\emptyset \qquad (cm^{-1}) \qquad (4.2)$$

for dolomite

$$\xi\Sigma_s = 0.043352 + 1.528\,\emptyset \qquad (cm^{-1}) \quad ,$$

where $\emptyset$ is a fraction $(0 \leqq \emptyset \leqq 1)$.

Let us suppose that the epithermal neutron tool signal R is proportional to the epithermal neutron flux $\emptyset_e$. Thus, multiplying R by the appropriate $\bar{\xi}\Sigma_s$ value for a given lithology and porosity, one has to get some value which should be proportional to the slowing-down density q. In that case the $R.\bar{\xi}\Sigma_s$ values in function of the appropriate slowing-down length L_s should be a univocal function independent of the lithology. We have taken the Schlumberger SNP calibration curves (Edmundson and Raymer, 1979) for which the results of such calculation are presented in Fig. 4.1. What is evident from these results, is that the $R.\xi\Sigma_s$ curves are different for different lithologies and, moreover, that they are not a monotonic function of the slowing-down length, which should occur if $R.\xi\Sigma_s$ is proportional to the slowing-down density q. Thus, the conclusion is that the measured epithermal neutron signal cannot be considered as being proportional to the epithermal neutron flux.

The second alternative is that the R values are directly proportional to the slowing-down density q. Thus, we have compared directly the signal R to the appropriate slowing-down length L_s. The resulting curves are much more free of the lithological effects (which was remarked by Edmundson and Raymer, 1979, too); this is shown in Fig. 4.2. One has to emphasize here that the R data have been taken from the published plots of the calibration curves (at the mesh points $\Delta\emptyset = 5\ \%$ between 0 and 40 per cent of porosity) and the L_s values are those published by Kreft (1974) for pure chemical compounds. Thus, we have some errors here induced by the digital evaluation of the analog plots, the possible differences in the matrix densities taken into account by Kreft and those of the calibration curves, and the differences between the real elemental compositions of rocks and those considered by Kreft. In spite of these sources of errors one can conclude that the relation R vs L_s is almost free of lithological effects. If the sources of errors are eliminated, this relationship would probably be more univocal.

To obtain an idea of the generality of our conclusion we have performed a similar comparison for the epithermal neutron calibration curves given by the Dresser Atlas (Wood et al., 1971) and Welex (Welex, 1968). All sets of data have been normalized to the same value in counts per second in limestone at 20 per cent of porosity (i.e. 269.9 cps for $L_s = 12.05$ cm in limestone). The results are plotted in Figs 4.3 and 4.4.

What can be deduced from these results is that as concerns the sensitivity of the porosity epithermal neutron tools, there are no evident differences among the probes. All of them have more or less the same slope vs porosity and similar lithology effects. Only towards very large slowing-down lengths (i.e. for very low porosities in the vicinity of 0 per cent) is the Schlumberger tool much more sensitive. The slope of the relationship cps vs L_s is related to the source-detector spacing. The slope being similar for all the considered probes implies that they have an identical, or almost identical value of this construction detail. An idea about the value of the source-detector distance can be deduced from an overlay of the curves in Figs 4.2, 4.3 and 4.4 with the theoretical relation $\xi\Sigma_s.\emptyset_n(r)$ vs L_s calculated according to Eq.(2.50) with an identical normalization (269.9 cps for $L_s = 12.05$ cm). The results of such calculations performed in the proportional slowing-down model for $n = 4$ slowing-down diffusion groups are presented in Fig. 4.5. The following source-detector spacings can be obtained:

for the Schlumberger tool: around 55 cm,
for the Dresser Atlas tool: between 50 and 55 cm,
for the Welex tool: between 45 and 53 cm.

A proper evaluation of these data should be made together with the discussion of particular properties of each sonde, keeping in mind that the plot in Fig. 4.5 is for an infinite, homogeneous medium without borehole, whereas the data in Figs 4.2, 4.3 and 4.4 have been obtained for real borehole conditions.

The fact that the epithermal neutron porosity tool signal is proportional to the slowing-down density is very important from the point of view of the porosity calibration curves in different lithologies. As long as the borehole conditions remain constant, the calibration curve in limestone, for example, can always be "translated" into the relationship: tool signal vs slowing-down length, as shown in Figs 4.2, 4.3 and 4.4 (calculating, however, the proper L_s values for each experimental point according to the given elemental composition of the rock). When one wants to obtain the porosity calibration curve for another lithology, in some magmatic rock, for example, it is sufficient to calculate the L_s versus porosity for that rock. A simple comparison of these L_s data for limestone and for magmatic rocks furnishes a lithology correction chart like the one presented, as an example, in Fig. 4.6.

5. Final remarks and conclusions

In the paper we have demonstrated the importance of the proper evaluation of the thermal neutron parameters of rocks in order to get the correct calibration curves for porosity determination using thermal neutrons. A special calculation procedure for these parameters has been established which takes into account the spectrum of slow neutrons existing in the rocks.

The slowing-down length of fast neutrons in magmatic rocks has been discussed and a very simple algorithm for its calculation has been found.

The discussion of the epithermal neutron signal of porosity tools results in the conclusion that it is proportional to the slowing-down density of neutrons in a given rock. This implies that it also is a univocal function of the slowing-down length L_s of neutrons in a given rock. Under this assumption it is now very easy to evaluate the lithological effects of the epithermal neutron tools.

All considerations of the rock neutron parameters presented here are based on some physical and theoretical speculations and there is a serious lack of experimental data in this field. This paper should be considered as a call for an experimental and research effort in methodology and experiments to obtain the neutron transport parameters for real rocks.

6. Acknowledgement

The author expresses his gratitude to Dr. A. Kreft from the Institute of Nuclear Physics and Techniques of the University of Mining and Metallurgy in Kraków for the calculation of the slowing-down lengths of magmatic rocks used in this paper. These slowing-down lengths have been calculated using the neutron code of Dr. Kreft.

7. References

Allen L.S. and Mills W.R., Jr. (1975): Measurement of the thermal neutron absorption cross-section of rock samples by a pulsed source method. The Log Analyst, 16, Jan.-Feb., 10-13.

Baker L.E., Baker R.P. and Hughen R.L. (1975): Report of the geophysical measurement in geothermal wells workshop. Sandia Lab. Rep. SAND 75-0608, Sept. 1975, Albuquerque, New Mexico.

Beckurts K.H. and Wirtz K. (1964): Neutron Physics. Springer Verlag, Berlin.

Beyster J.R. (1968): Neutron scattering from light water. Nucl. Sci. and Eng., 31, 254-271.

Burkhart K. and Reichardt W. (1962): Hardening of neutron spectra observed in water and solution of boron acid. Proc. Brookhaven Conf. on Neutron Thermalization, April 30 to May 2,1962, USAEC Rep. BNL-719 (C-32), 318-336 (vol.2).

Carre J.C. (1968): Mesure de la section de capture thermique des materiaux utilisés pour la fabrication des betons. CEA CEN Fontenay-aux-Roses, DEP/SEPP-GEP, Note MIN 105, Octobre 1968.

Czubek J.A. (1981): Some aspects on nuclear well logging in igneous rocks. Orkustofnun Rep. OS81009/JHD05, Reykjavik, June 1981, Iceland.

Czubek J.A., Drozdowicz K., Igielski A., Krynicka-Drozdowicz E., Sobczyński Z. and Woźnicka U. (1980): Thermal neutron diffusion parameters for light water. Nukleonika, 25, 657-666.

Czubek J.A., Drozdowicz K., Kranicka-Drozdowicz E., Igielski A. and Woźnicka U. (1982): Absorption cross-section for thermal neutrons measured on small rock samples. Acta Geophys. Polon., 30, 359-370.

Czubek J.A., Drozdowicz K., Krynicka-Drozdowicz E., Igielski A. and Woźnicka U. (1983): Measurement of the thermal neutron absorption cross-section of rock samples. Intern. Journ. of Appl. Radiat. and Isot., 34, 143 -151.

Daly R.A. (1933): Igneous Rocks and the Depth of the Earth. McGraw-Hill Book Co., Inc., New York and London.

Edmundson H. and Raymer L.L. (1979): Radioactive logging parameters for common minerals. The Log Analyst, 20, Sept.-Oct., 38-47.

Ellis D.V., Ullo J. and Sherman H. (1981): Comparison of calculated and measured responses of a dual-detector epithermal neutron porosity device. Paper SPE 10294 at 56-th Ann. Techn. Conf. of SPE of AIME, San Antonio, Texas, Oct.4-7.

Engle W.W., Jr. (1980): The method and application of discrete ordinates in low energy neutron-photon transport (ANISN, DOT). Part I: Methods. Lecture 3 in "Computer Techniques in Radiation Transport and Dosimetry", Edits W.R. Nelson and Th.M. Jenkins, Ettore Majorana Internat. Science Series, Plenum Press, New York and London, pp. 59-75.

Gotoh Yorio and Takahashi Hiroshi (1971): Slow neutron scattering by light and heavy water. Nucl. Sci. and Eng., 45, 126--140.

Guberman Sh.A. and Yakubson K.I. (1964): Possibility of application of thermal neutron temperature to the investigation of rocks. pp. 127-143 in "Problems of Nuclear Geophysics", Publ. House "Nedra", Moscow (in Russian).

Harris J.M. and McDaniel P.J. (1982): Small sample thermal neutron cross section determination from reactivity measurements. SPWLA 23-rd Ann. Logg. Symp. Trans., Paper HH, July 6-9,1982, Corpus Christi, Texas.

Kreft A. (1974): Calculation of the neutron slowing-down length in rocks and soils. Nukleonika, 19, 145-156.

Mughabghab S.F. and Garber D.I. (1973): Neutron Cross Sections. Vol. 1: Resonance Parameters. BNL Rep. BNL-325, Third edition, June 1973, BNL, Upton, N.Y.

Nelson P., Paulsson B., Rachiele R., Andersson L., Schrauf T., Hustrulid W., Duran O. and Magnusson K.A. (1979): Preliminary report on geophysical and mechanical borehole measurements at Stripa. Lawrence Berkeley Lab., Rep. LBL-8280, May 1979, Berkeley, Calif.

Petrie C.D., Storm M.L. and Zweifel P.F. (1957): Calculation of thermal group constants for mixtures containing hydrogen. Nucl. Sci. and Eng., 2, 728-744.

Rathur M.A.J. and Grant P.J. (1964): The age of Po-Be neutrons in water and in graphite. Brit. Journ. Appl. Phys., 15, 93-96.

Scott H.D., Flaum C. and Sherman H. (1982): Dual porosity CNL count rate processing. Paper SPE 11146 at 57-th Ann. Techn. Conf. of SPE of AIME, New Orleans, La., Sept. 26-29.

Soodak H. (Editor)(1962): Reactor Handbook, Vol. III, Part A: Physics.Interscience Publishers, New York.

Tittle C.W. (1948): The slowing down and diffusion of neutrons in hydrogeneous media. Ph.D. thesis, MIT, Cambridge, Mass.

Tittle C.W. (1962): How to compute neutron transmission and diffusion. Nuclear Chicago Corp., Techn. Bull. No 12.

Tittman J. (1955): Moderation of neutrons in SiO_2 and $CaCO_3$. Journ. Appl. Phys., 26, 394-398.

Tittman J., Sherman H., Nagel W.A. and Alger R.P. (1966): The sidewall epithermal neutron porosity log. Journ. Petrol. Technol., 18,1351-1362.

Welex (1968): Charts for the interpretation of well logs. Bull. A-133-476, Welex, Houston.

Wichmann P.A., Youmans A.H. and Hopkinson E.C. (1967): Advances in neutron lifetime logging. Journ. Petrol. Technol., 19, 479-486.

Wood R.D., Wichmann P.A. and Watt H.B. (1971): Gamma ray, neutron log. Dresser Atlas Technical Bull., Houston, Texas.

8. Appendix A

Evaluation of special functions

The special functions which appear in the formula for the $J(\beta)$ function (Eq.(2.35)) are: $Ei(\beta^2)$ and $\int_0^\beta e^{t^2}.dt$, where

$$Ei(x) = -\,-\!\!\!\!\!\!\int_{-x}^{\infty} \frac{e^{-t}}{t}.dt = -\!\!\!\!\!\!\int_{-\infty}^{x} \frac{e^{t}}{t}.dt \quad , \; x > 0, \qquad (A.1)$$

where the integral in Eq.(A.1) has to be taken as the principal value. According to Abramowitz and Stegun (1972) one has:

$$Ei(x) = \gamma + \ln x + \sum_{n=1}^{\infty} a_n \quad , \qquad (A.2)$$

where

$$\gamma = 0.57721\,56649 \qquad (A.3)$$

and

$$a_n = \frac{x^n}{n.n!} \quad , \qquad (A.4)$$

whereas an asymptotic expansion for $x \gg 1$ is:

$$Ei(x) \approx \frac{e^x}{x}\left(1 + \sum_{n=1}^{N} \frac{n!}{x^n}\right) \quad . \qquad (A.5)$$

Finally we have for the expression appearing in Eq.(2.35):

$$x^2\, e^{-x^2}\, Ei(x^2) = x^2\, e^{-x^2}(\gamma + \ln x^2) + e^{-x^2} \sum_{n=1}^{\infty} b_n \quad , \qquad (A.6)$$

where

$$b_n = \frac{x^{2n+2}}{n.n!} = b_{n-1}.x^2\left(\frac{1}{n} - \frac{1}{n^2}\right) \qquad (A.7)$$

and for $x \gg 1$:

$$x^2\, e^{-x^2}\, \mathrm{Ei}(x^2) \approx 1 + \sum_{n=1}^{N} g_n \quad , \qquad (A.8)$$

where

$$g_n = \frac{n!}{x^{2n}} = g_{n-1} \cdot \frac{n}{x^2} \quad . \qquad (A.9)$$

The second integral in Eq.(2.35) is:

$$x\, e^{-x^2} \int_0^x e^{t^2}\, dt = x^2\, e^{-x^2} \left(1 + \sum_{n=1}^{\infty} c_n \right) , \qquad (A.10)$$

where

$$c_n = \frac{x^{2n}}{(2n+1)\, n!} = c_{n-1} \cdot \frac{x^2 (2n-1)}{n(2n+1)} \qquad (A.11)$$

and for $x \gg 1$ the asymptotic expansion is:

$$x\, e^{-x^2} \int_0^x e^{t^2}\, dt \approx \frac{1}{2} \left(1 + \sum_{n=1}^{N} d_n \right) \quad , \qquad (A.12)$$

where

$$d_n = \frac{(2n-1)!!}{(2x^2)^n} = d_{n-1} \cdot d_1 \cdot (2n-1) \; . \qquad (A.13)$$

Reference

Abramowitz M. and Stegun I.A. (Editors): Handbook of Mathematical Functions with Formulas, Graphs and Mathematical Tables. Dover Publ., Inc., New York, 1972.

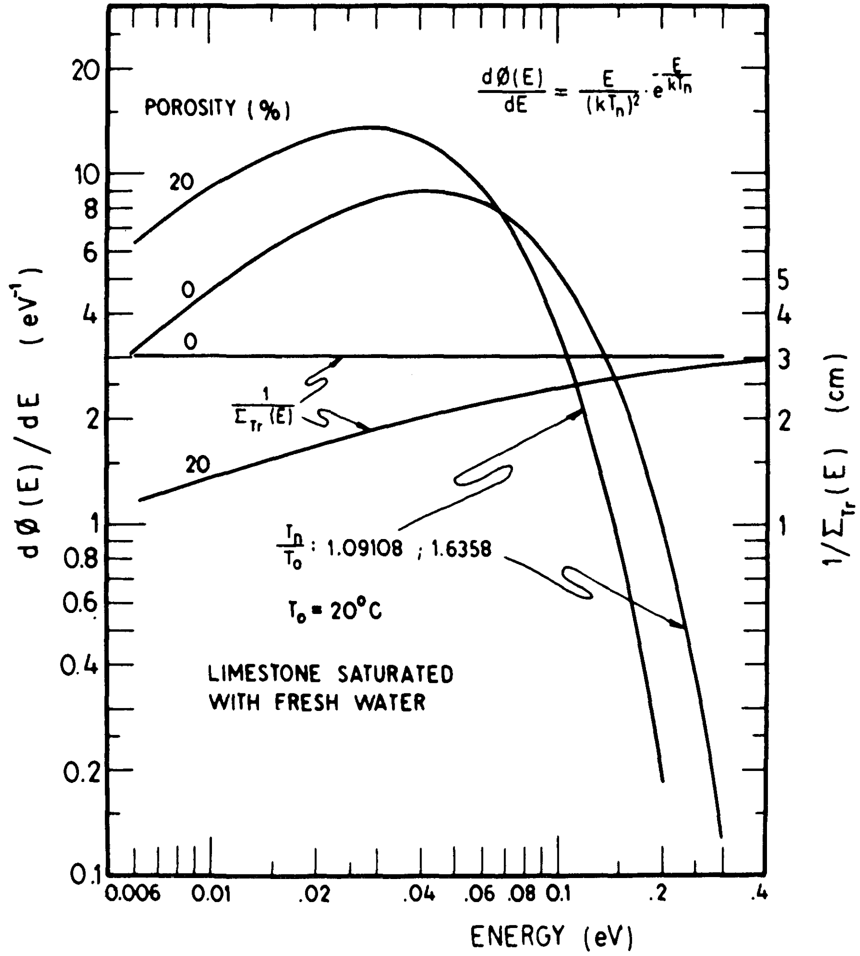

Fig. 2.1. Thermal neutron spectrum in limestone of the porosity 0 and 20 per cent saturated with fresh water.

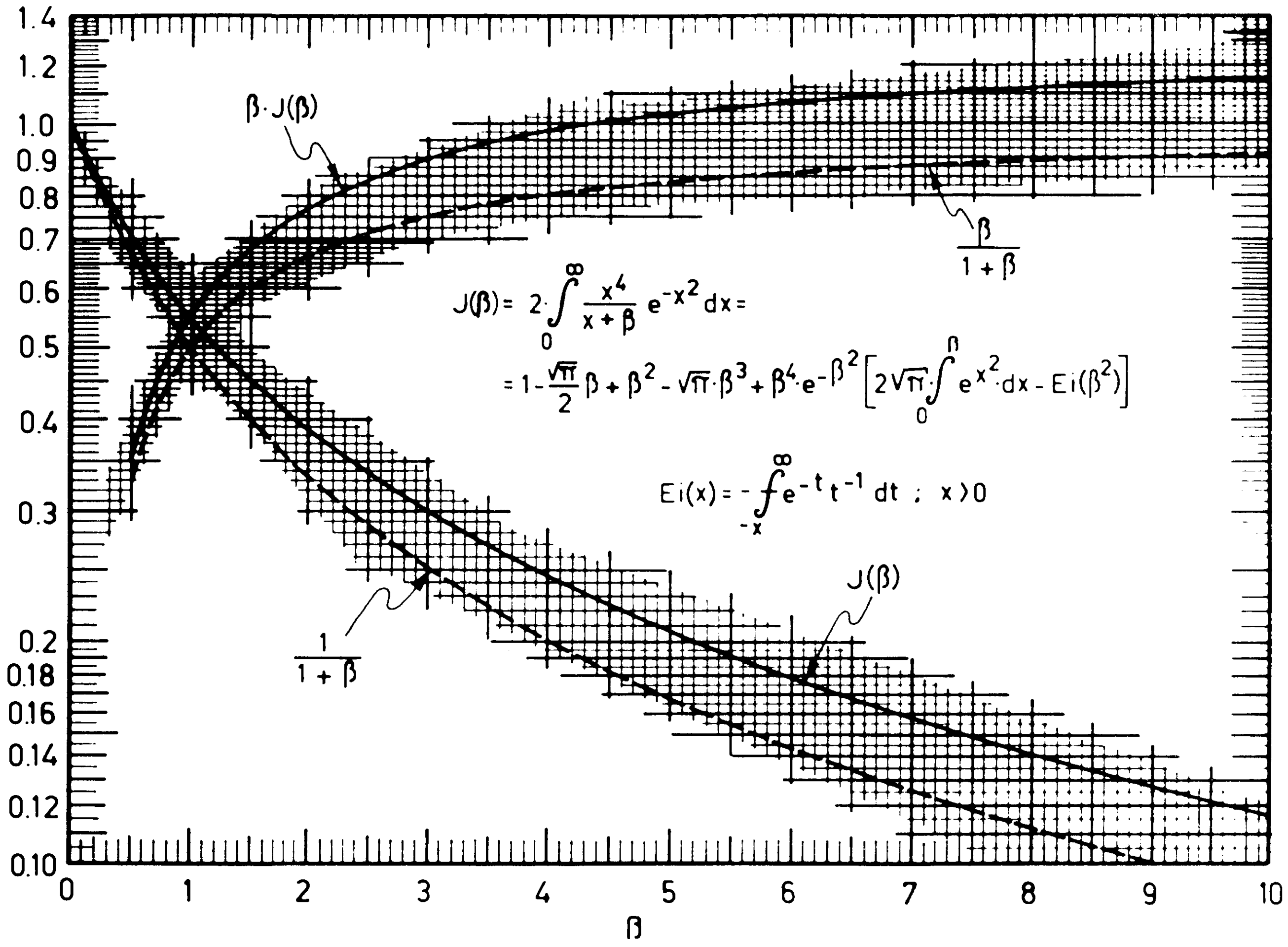

Fig. 2.2. Plots of the J (β) and β.J (β) functions calculated according to Eq.(2.35).

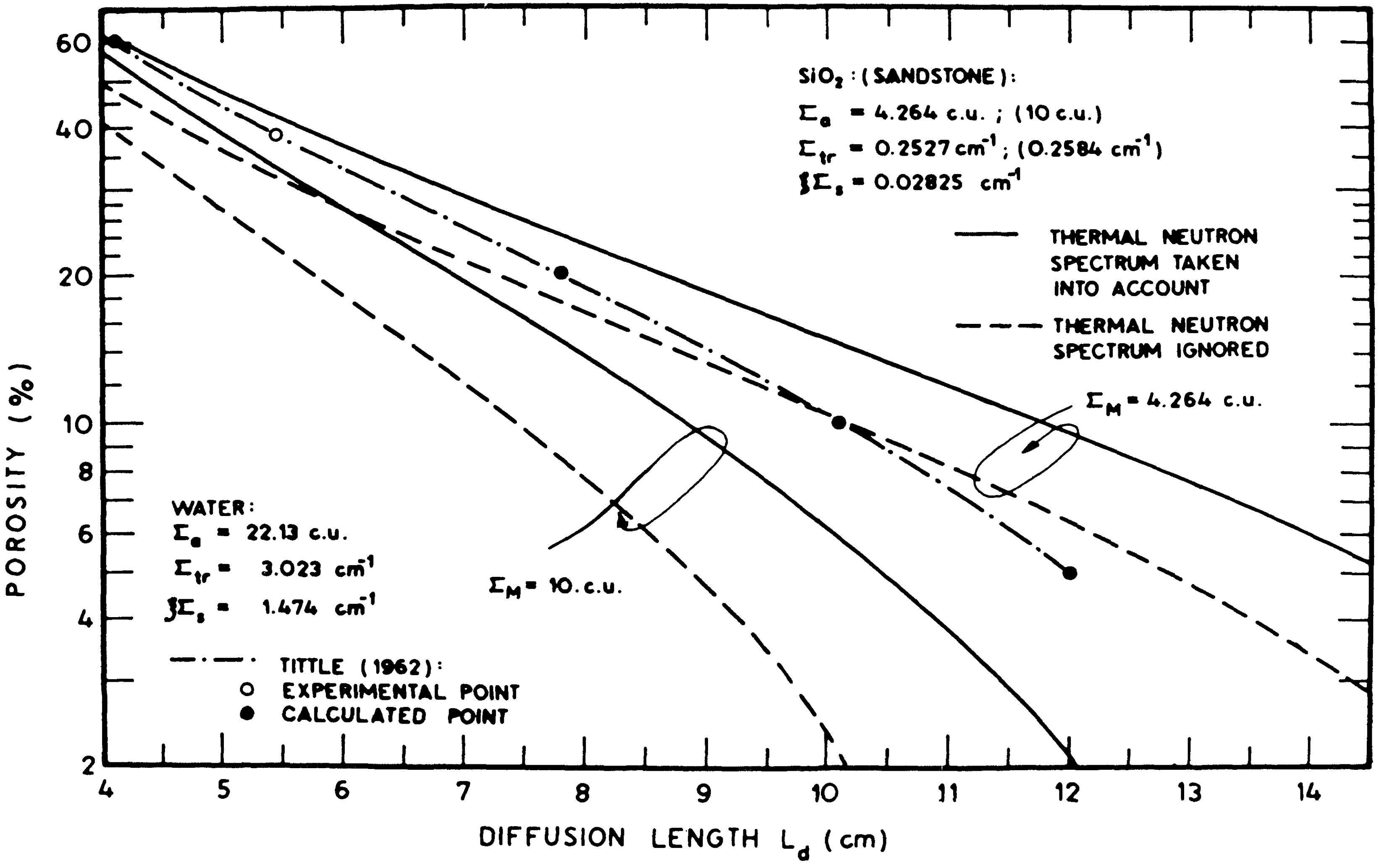

Fig. 2.3. Thermal neutron diffusion length, L_d, in SiO_2 and sandstone of different porosity saturated with fresh water. Calculations performed when the thermal neutron spectrum was taken into accoune or ignored, Tittle's data (1948) are presented for comparison.

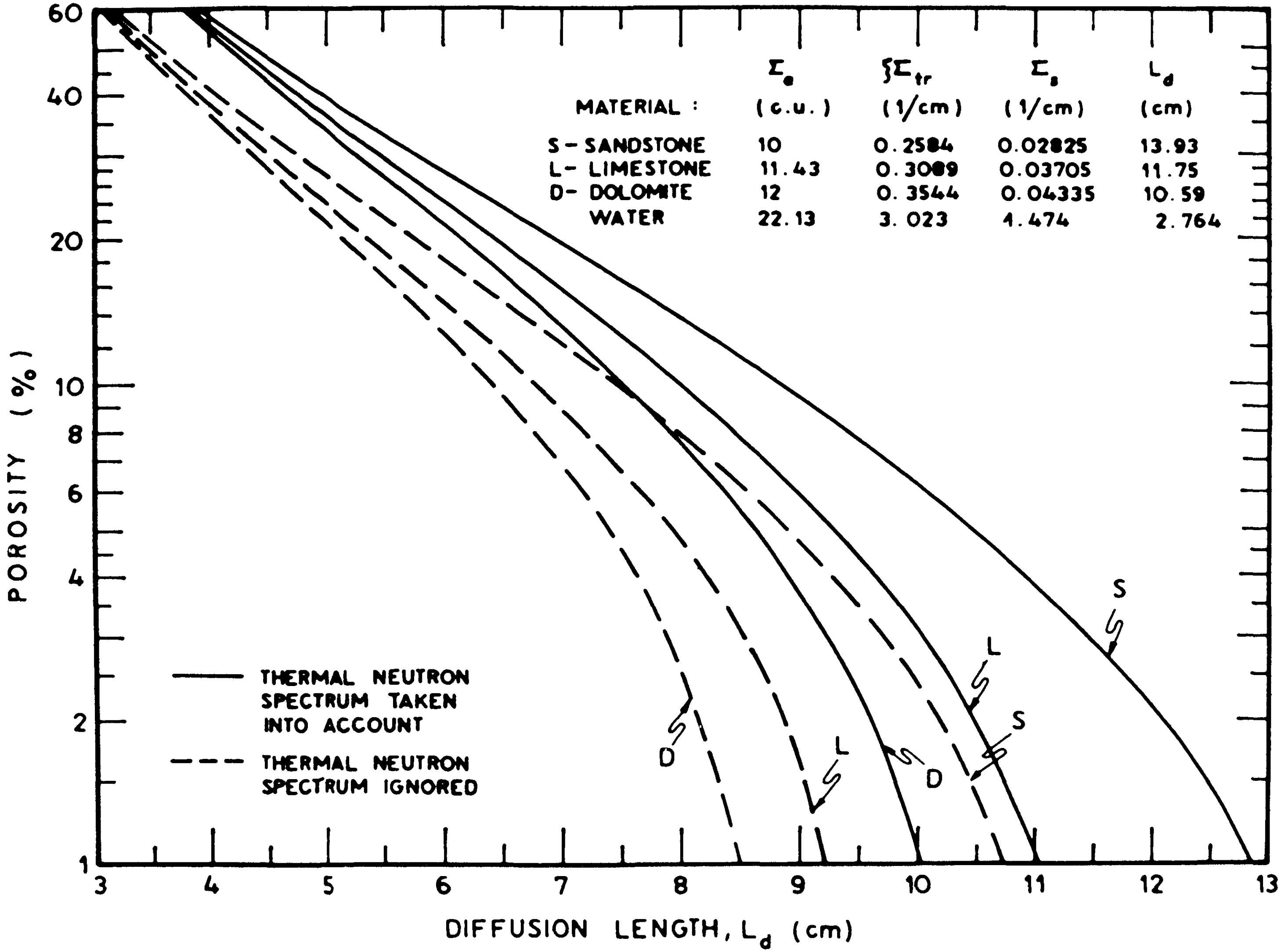

MATERIAL :	Σ_a (c.u.)	$\xi\Sigma_{tr}$ (1/cm)	Σ_s (1/cm)	L_d (cm)
S - SANDSTONE	10	0.2584	0.02825	13.93
L - LIMESTONE	11.43	0.3089	0.03705	11.75
D - DOLOMITE	12	0.3544	0.04335	10.59
WATER	22.13	3.023	4.474	2.764

Fig. 2.4. Thermal neutron diffusion length, L_d, in sandstone, limestone and dolomite of different porosity saturated with fresh water. Calculations performed when the thermal neutron spectrum was taken into account or ignored.

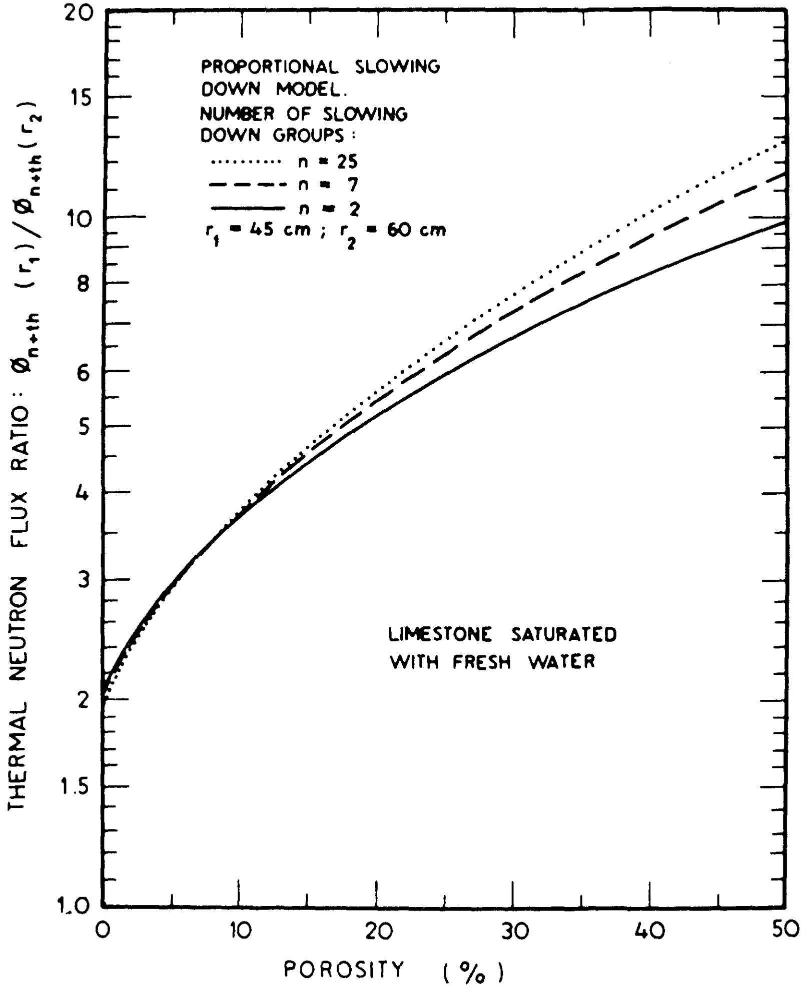

Fig. 2.5. Influence of the number of neutron slowing-down groups on the thermal neutron flux ratio in limestone saturated with fresh water. Calculations performed using the proportional slowing-down model. Thermal neutron spectrum was taken into account.

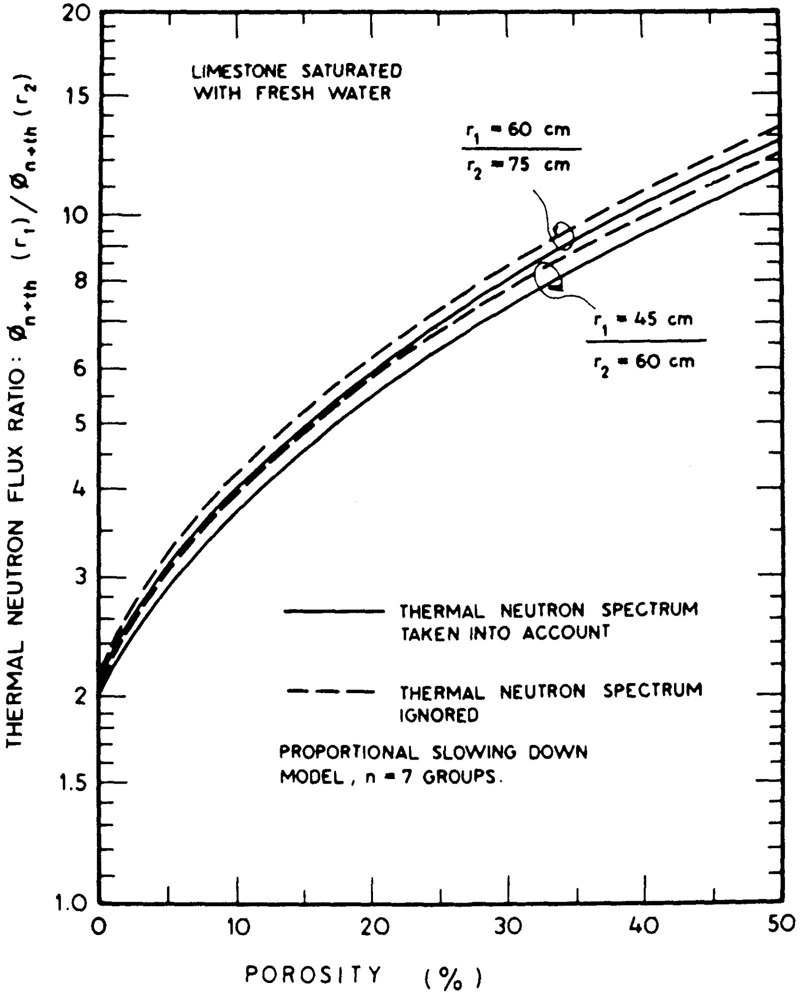

Fig. 2.6. Influence of the thermal neutron spectrum on the thermal neutron flux ratio in limestone saturated with fresh water. Calcultions performed using the proportional slowing-down model with seven slowing-down groups.

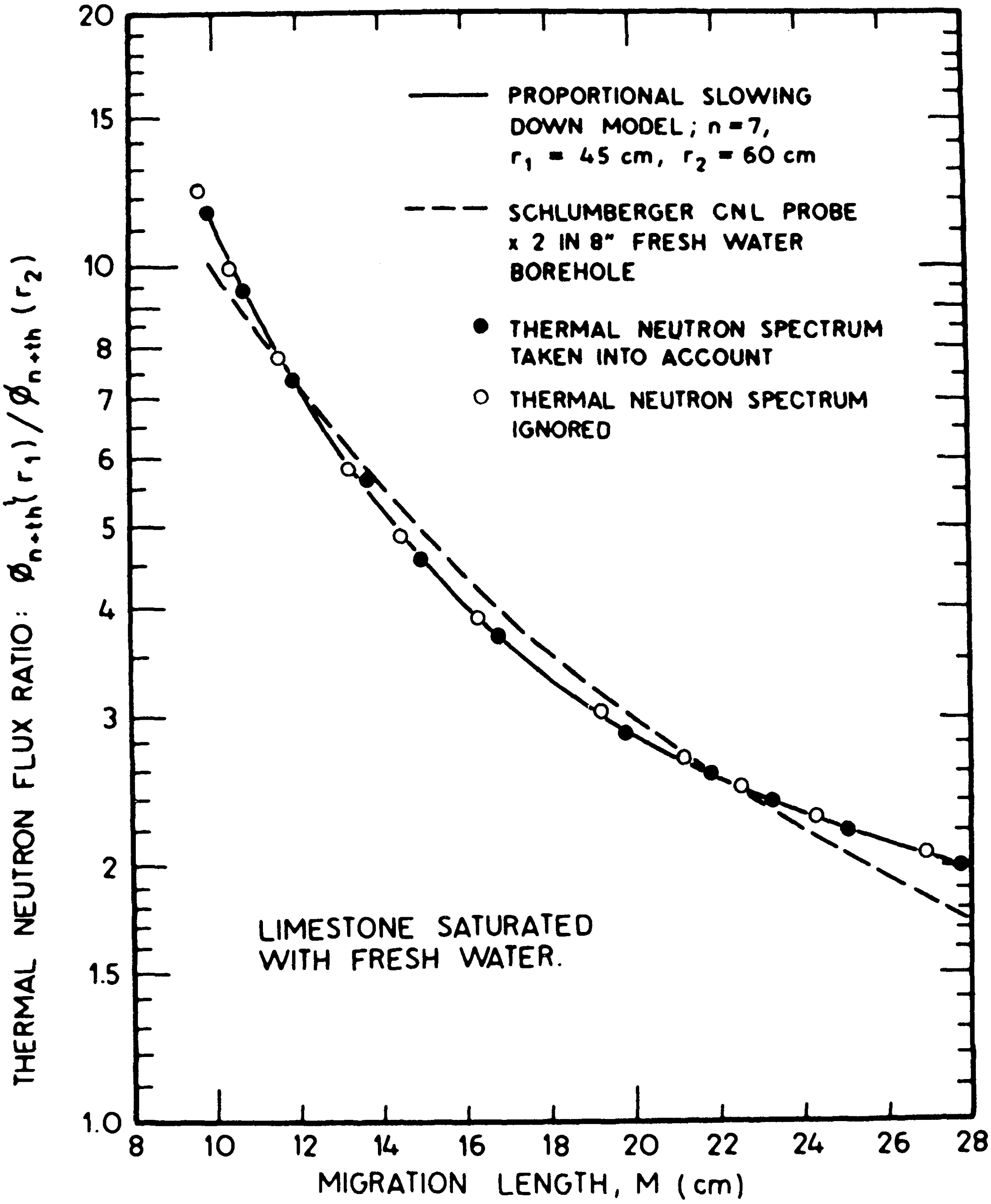

Fig. 2.7. Correspondence between thermal neutron flux ratio and migration length. For comparison the thermal neutron countrate ratio (multiplied by a factor of 2) of the CNL Schlumberger probe in a 8" fresh water filled borehole is shown. The rock medium is limestone saturated with fresh water in the porosity range between 0 and 50 per cent. The matrix absorption cross-section was assumed 11.43 c.u. for the calculation of diffusion lengths.

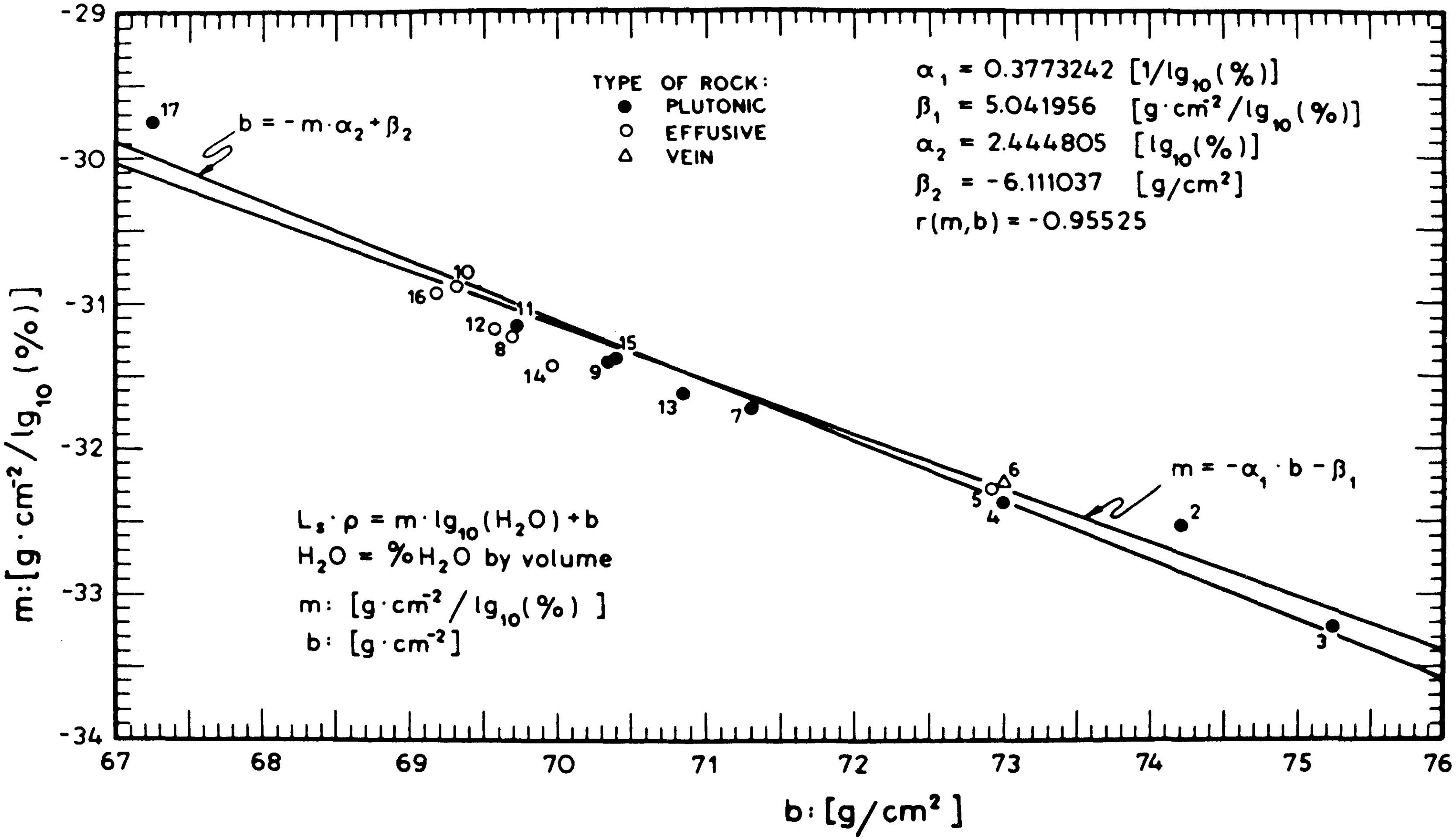

Fig. 3.1. Correlation between the m and b parameters (cf. Eq.(3.2)) for magmatic rocks. Numbers correspond to the rocks listed in Table 3.1. Two regression lines are drawn.

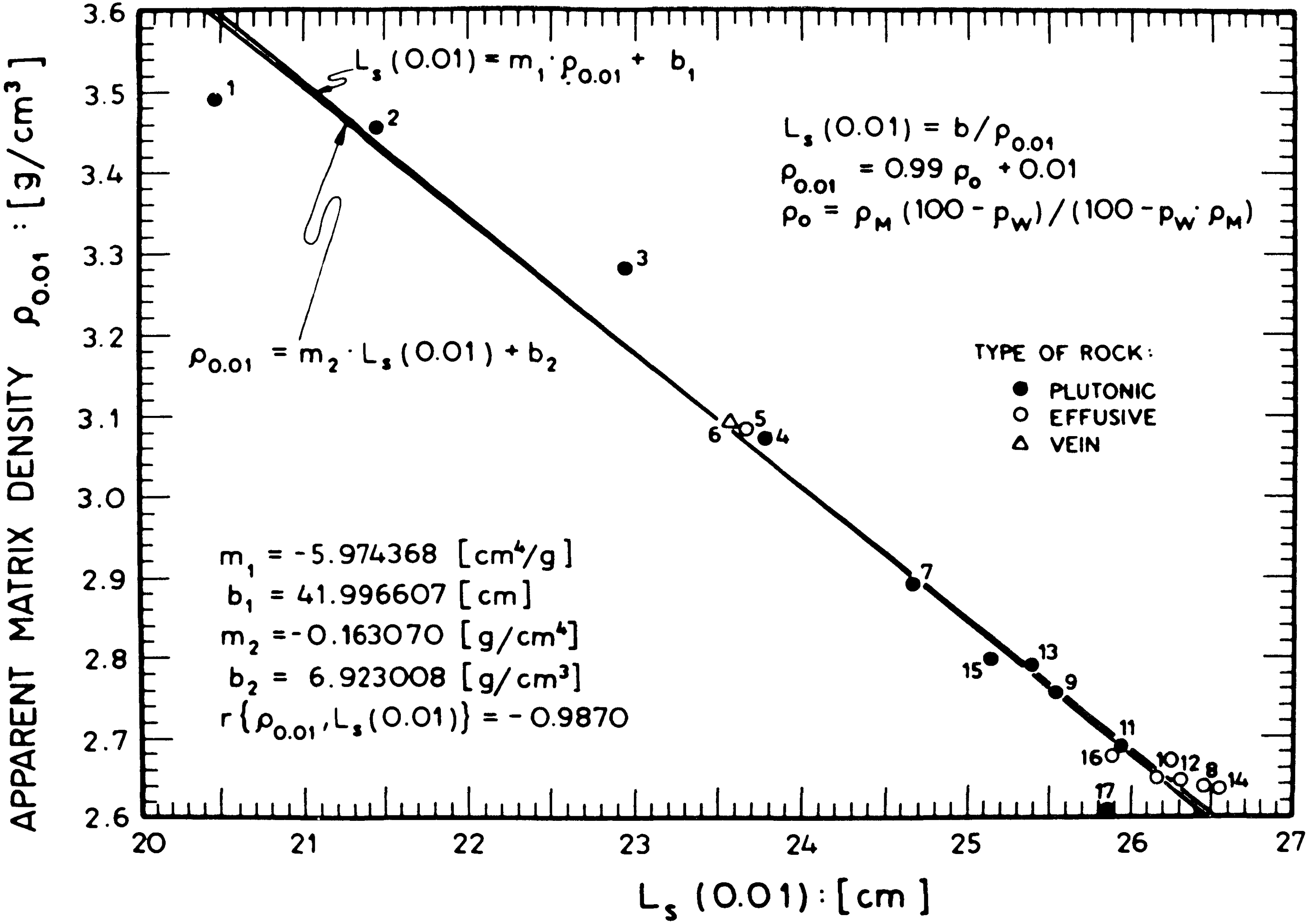

Fig. 3.2. Correlation between the slowing-down length $L_s(0.01)$ and apparent matrix density $\rho_{0.01}$ for magmatic rocks listed in Table 3.2. Apparent matrix density $\rho_{0.01}$ is calculated for one per cent water saturated porosity, when the rock matrix contains no water chemically bound.

Table 3.2

Elemental composition (weight per cent) of magmatic rocks due to Daly (1933)

Rock	Matrix density ρ_M (g/ccm)	Si %	Ti %	Al %	Fe %	Mg %	Ca %	Na %	K %	H %	O %
1. Dunite	3.28	18.96	0.01	0.46	6.31	28.00	0.50	0.07	0.03	0.32	45.34
2. Peridotite	3.23	21.14	0.38	3.06	9.85	13.86	5.37	0.85	0.47	0.35	44.67
3. Pyroxenite	3.23	22.00	0.58	3.38	11.32	7.34	11.49	0.61	0.41	0.11	42.76
4. Gabbro	3.0	22.63	0.58	9.50	6.86	4.55	7.89	1.90	0.74	0.16	45.19
5. Basalt	3.0	23.10	0.82	8.37	8.78	3.75	6.44	2.33	1.27	0.18	44.96
6. Diabase	3.0	23.70	0.87	8.15	8.77	3.51	6.42	2.29	0.81	0.21	45.27
7. Diorite	2.84	27.63	0.46	8.75	5.18	2.16	4.40	2.58	1.76	0.14	46.94
8. Andesite	2.60	27.96	0.46	9.20	4.78	1.67	4.16	2.67	1.70	0.14	47.26
9. Granodiorite	2.72	30.45	0.34	8.46	3.29	1.15	3.17	2.75	2.29	0.12	47.98
10. Dacite	2.6	30.75	0.34	8.62	3.15	0.85	2.48	2.95	2.22	0.17	48.47
11. Granite	2.67	32.89	0.24	7.68	2.49	0.53	1.43	2.59	3.42	0.09	48.64
12. Liparite	2.6	34.07	0.20	7.15	1.70	0.23	0.86	2.51	3.71	0.16	49.41
13. Syenite	2.75	28.24	0.40	8.65	4.49	1.51	3.09	2.96	3.74	0.13	46.79
14. Trachyt	2.60	28.43	0.23	9.41	3.89	0.68	2.22	3.30	4.78	0.14	46.92
15. Nepheline syenite	2.75	25.68	0.52	10.59	4.09	0.53	1.80	6.16	4.56	0.15	45.92
16. Phonolite	2.6	26.91	0.25	10.93	2.45	0.18	1.07	6.57	4.35	0.23	47.06
17. Urtite	2.6	21.34	0.00	14.71	2.96	0.12	1.24	12.07	3.09	0.05	44.42

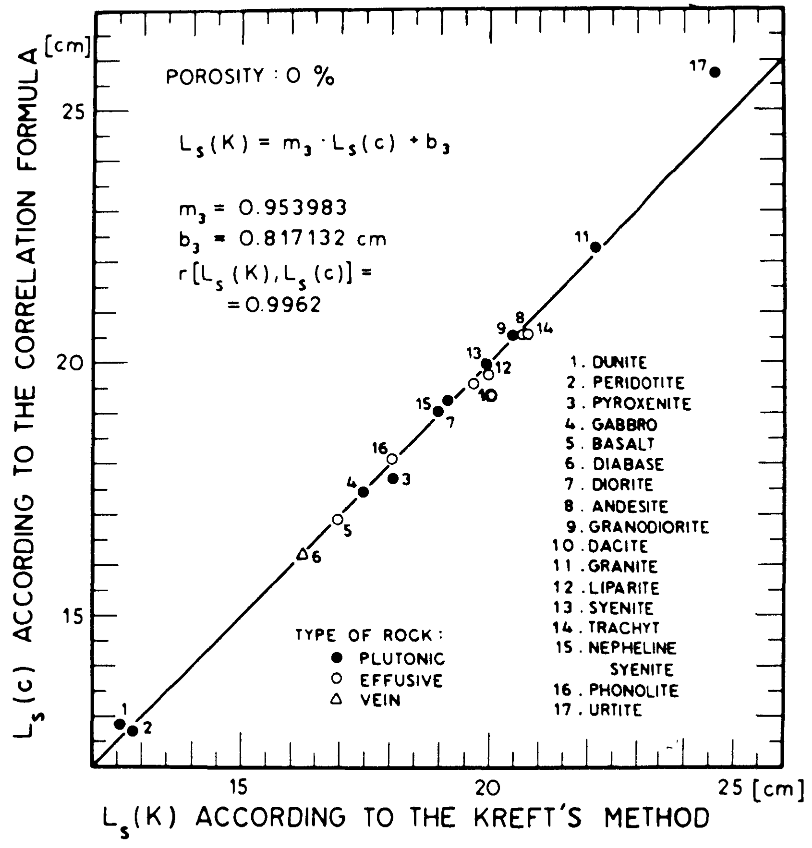

Fig. 3.3. Correlation between the L_s values calculated according to the correlation formula (Eq.(3.13)) and to the multigroup diffusion method due to Kreft (1974) for magmatic rocks listed in Table 3.2 for porosity 0 per cent.

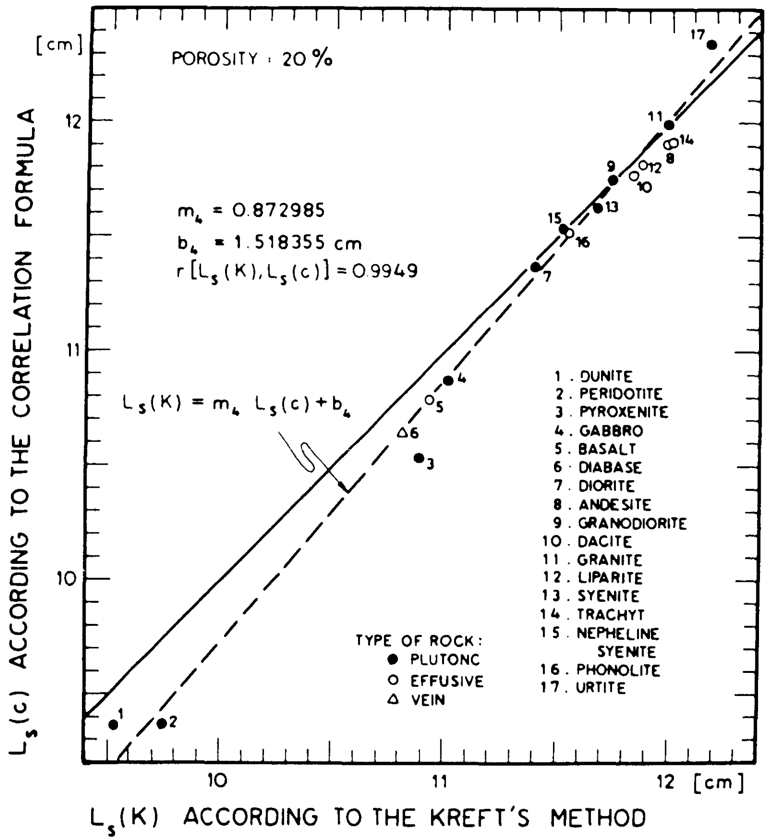

Fig. 3.4. Correlation between the L_s values calculated according to the correlation formula (Eq.(3.13)) and to the multigroup diffusion method due to Kreft (1974) for magmatic rocks listed in Table 3.2 for porosity 20 per cent saturated with water.

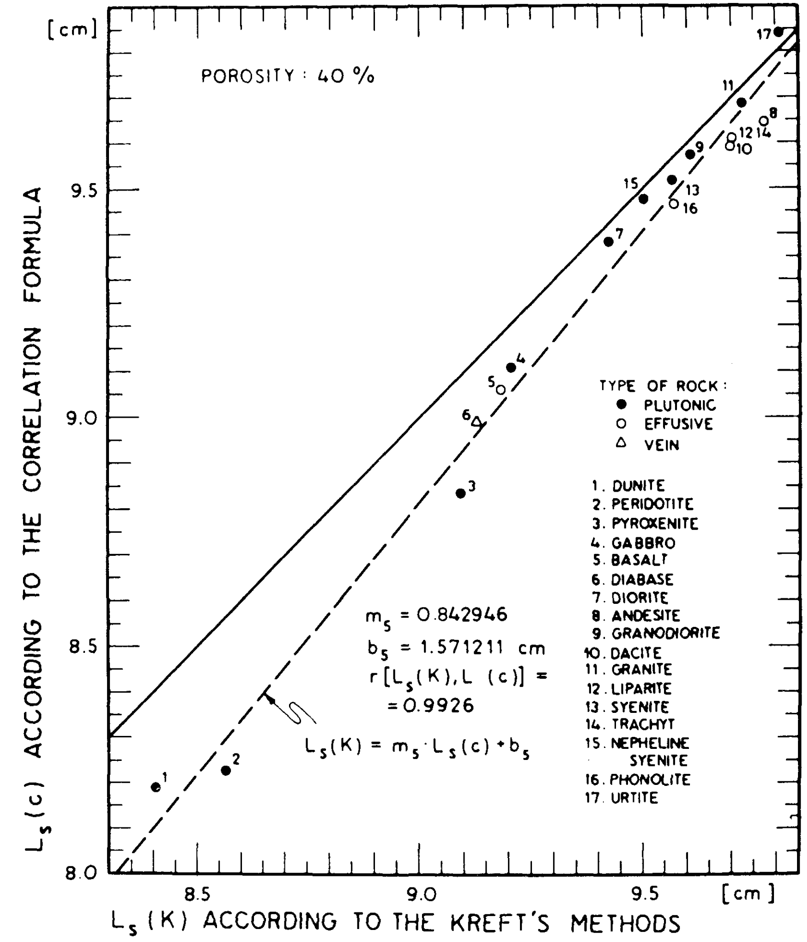

Fig. 3.5. Correlation between the L_s values calculated according to the correlation formula (Eq. (3.13)) and to the multigroup diffusion method due to Kreft (1974) for magmatic rocks listed in Table 3.2 for porosity 40 per cent saturated with water.

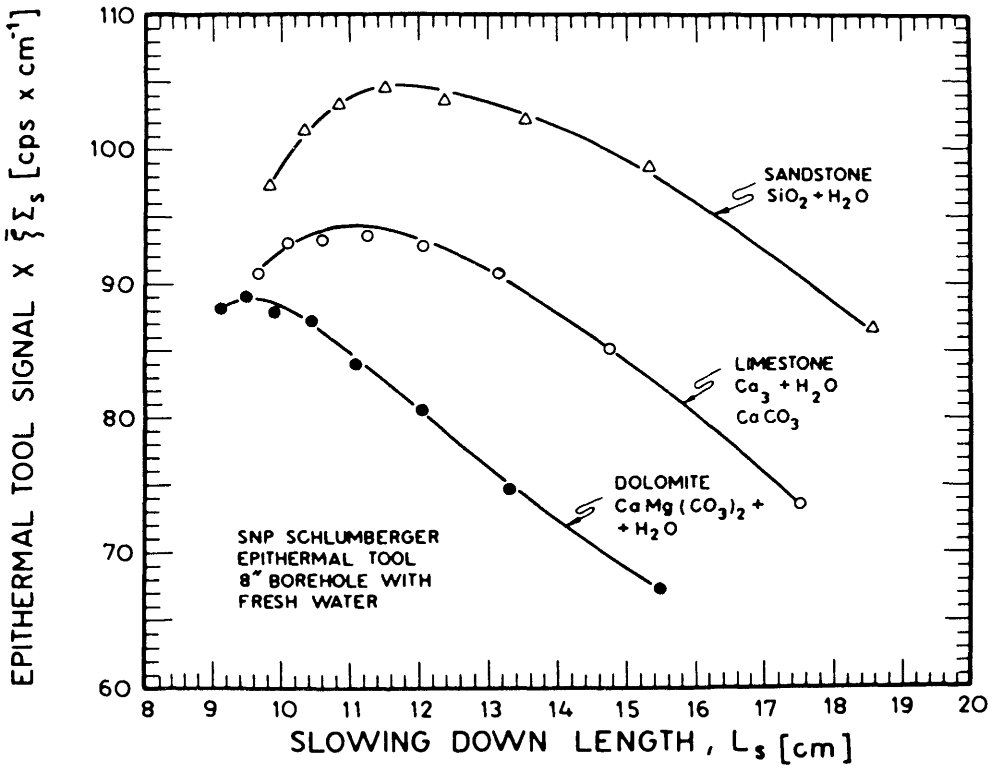

Fig. 4.1. Epithermal neutron tool signal (SNP Schlumberger tool in 8" borehole with fresh water) multiplied by the slowing-down cross-section for different porosities (saturated with fresh water) in sandstone, limestone and dolomite presented in function of the slowing-down length of the rock.

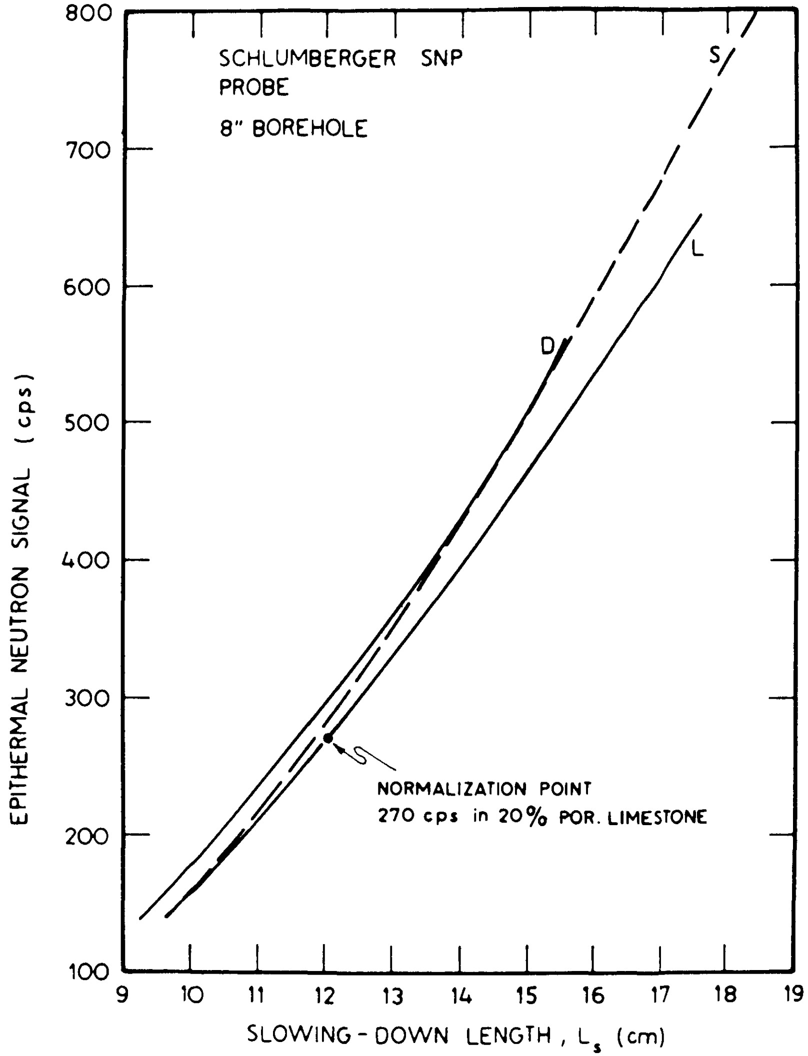

Fig. 4.2. Epithermal neutron signal of the SNP Schlumberger probe vs the slowing-down length calculated for SiO_2, $CaCO_3$ and $CaCO_3 \cdot MgCO_3$ of different porosities saturated with fresh water. S - sandstone, L - limestone, D- dolomite.

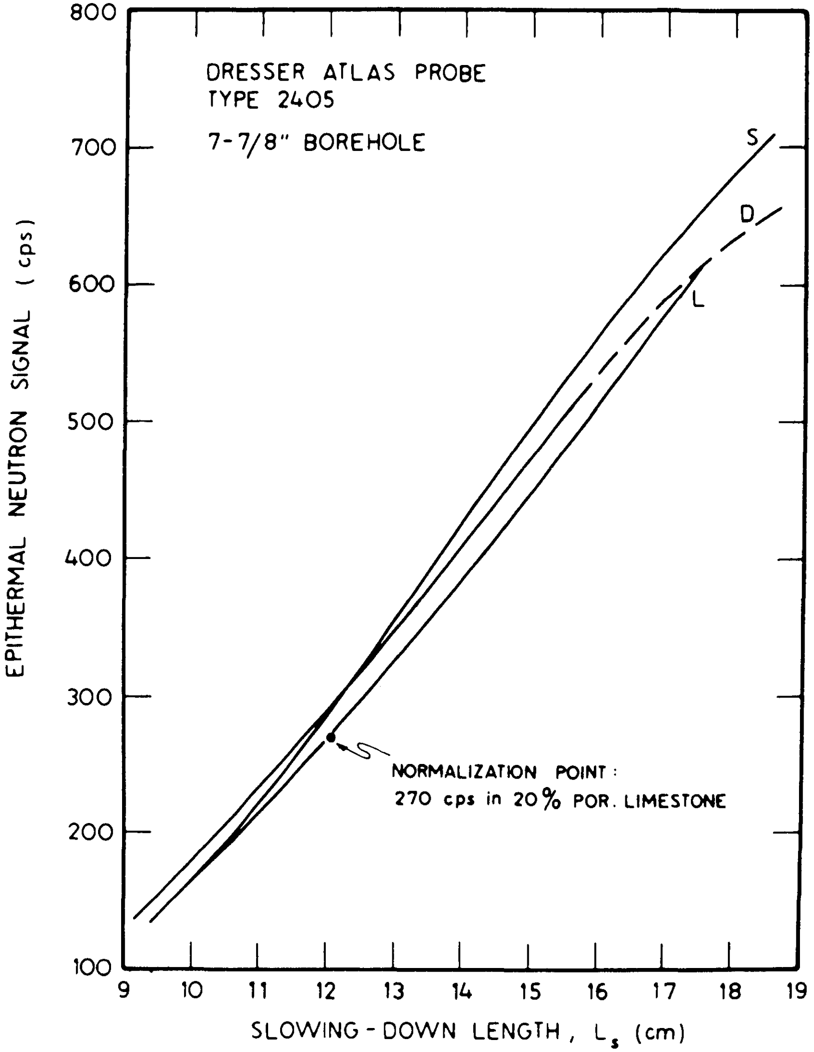

Fig. 4.3. Epithermal neutron signal of the Dresser Atlas probe type 2405 vs the slowing-down length calculated for SiO_2, $CaCO_3$ and $CaMg(CO_3)_2$ of different porosities saturated with fresh water. S - sandstone, L - limestone, D - dolomite. Curves are normalized to the same intensity as the Schlumberger probe (cf. Fig. 4.2) in limestone of 20 per cent porosity.

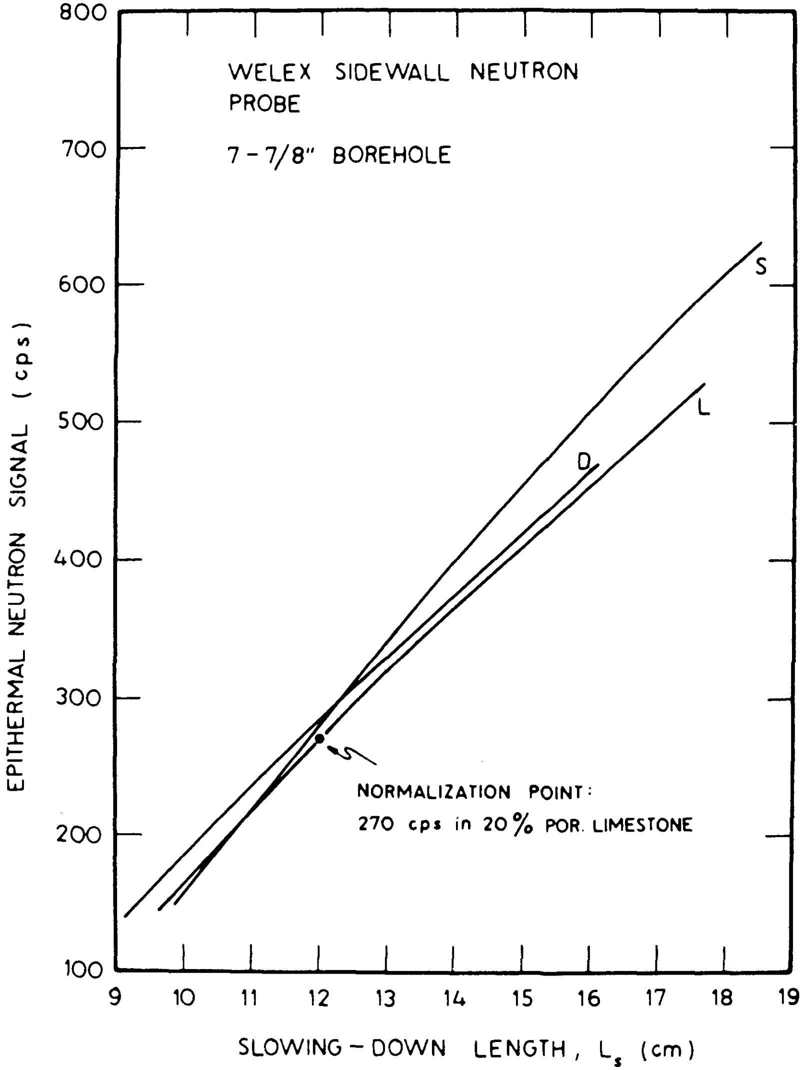

Fig. 4.4. Epithermal neutron signal of the Welex probe vs the slowing-down length calculated for SiO_2, $CaCO_3$ and $CaMg(CO_3)_2$ of different porosities saturated with fresh water. S - sandstone, L - limestone, D - dolomite. Curves are normalized to the same intensity as the Schlumberger probe (cf. Fig. 4.3) in limestone of 20 per cent porosity.

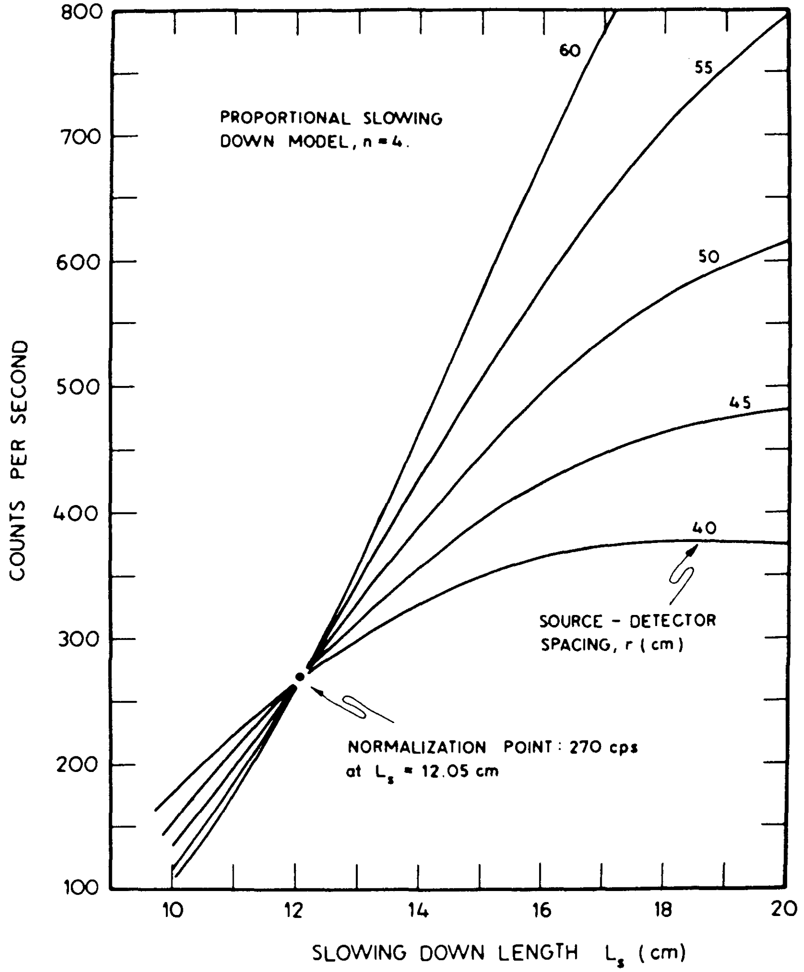

Fig. 4.5. Slowing-down density $\xi\Sigma_s.\emptyset_4(r)$ calculated for different source-detector spacings r in function of the slowing-down length L_s normalized to the Schlumberger SNP countrate (in 8" borehole) in 20 per cent porosity limestone saturated with fresh water. Four slowing-down groups in the proportional slowing-down model have been used.

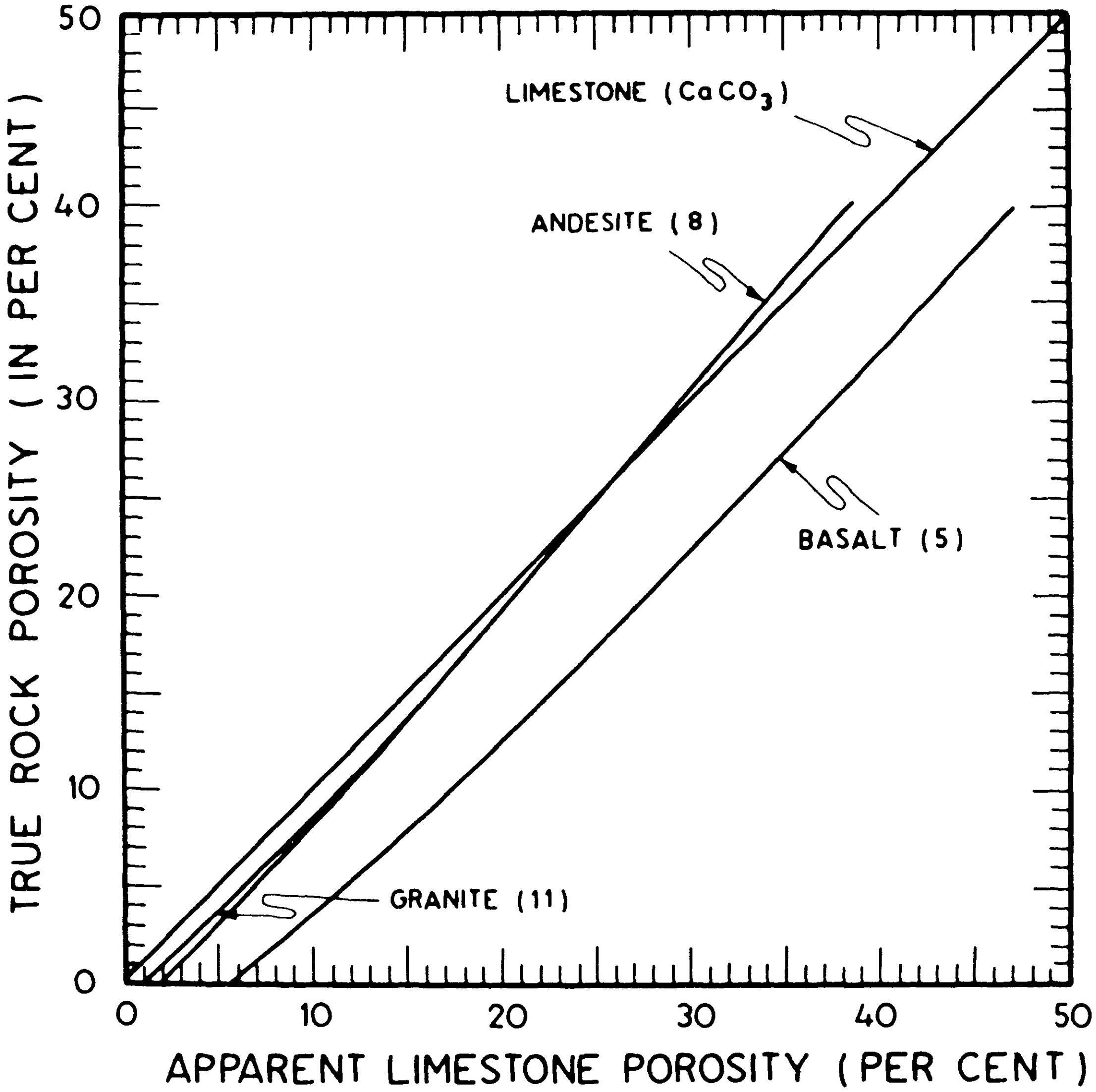

Fig. 4.6. Lithology effects for the epithermal neutron porosity tools calculated from the slowing-down, L_s, values. Numbers at magmatic rock names correspond to those in magmatic rock elemental composition Table 3.2. The corresponding water contents in rock matrix (in per cent by volume) and matrix densities (in g/cm^3) are: for basalt: 4.82, 3.0; for andesite: 3.25, 2.60; for granite: 2.15, 2.67; for limestone: 0, 2.72, respectively. The slowing-down lengths are calculated according to the Kreft's method.

RECENT PROGRESS IN FAST NEUTRON ACTIVATION CROSS SECTION DATA

W. Michaelis
GKSS Forschungszentrum Geesthacht
Institut für Physik
2054 Geesthacht
Federal Republic of Germany

Abstract

RECENT PROGRESS IN FAST NEUTRON ACTIVATION CROSS SECTION DATA

A brief review is given of some significant investigations performed during the past few years in the area of fast neutron activation cross sections that may be relevant for the use of nuclear techniques in the exploration of mineral resources, in process and quality control in industry as well as for general analytical purposes. Differential capture cross sections are considered for the natural elements or isotopes of Fe, Cu, Se, Y, Nb, Cd, In, Gd, W, Os and Au. Some of the data are compared with statistical model calculations. Experimental and evaluated average cross sections for capture and threshold reactions in the spontaneous fission neutron field of ^{252}Cf are reviewed taking into account the elements or isotopes of Mg, Al, Si, S, Ti, V, Mn, Fe, Co, Ni, Cu, Zn, Sr, Zr, Nb, Cd, In, Ba, Ta and Au. A summary of recent studies of differential cross sections for threshold reactions comprises data on Al, Si, S, Ti, Fe, Co, Ni, Cu, Zn, Zr, Nb, Ta, W and Au. Besides experimental investigations, evaluations and theoretical model calculations are considered. Cross sections at 14 MeV and in the region around this energy are reviewed for Na, Mg, Al, Cl, Ti, V, Cr, Mn, Fe, Co, Ni, Cu, Zn, Br, Sr, Zr, Nb, In, Er, Yb, Ta, W, Os, Ir, Au and Pb. Particular emphasis is laid on (n,p), (n,2n) and (n,α) reactions. (n,n') reactions are allowed for if the half-life of the metastable state excited permits elemental analyses by common experimental techniques.

INTRODUCTION

During the last decades nuclear techniques have found a broad application to the exploration of mineral resources by bore-hole logging and laboratory analysis of samples collected in the field, as well as to process and quality control in industry. Reviews of these techniques have been presented by several authors [1 - 7]. Nuclear methods using accelerator-type or isotopic neutron sources offer the advantage of high penetrability of the neutron and gamma radiation, and thus allow the assay of large sample volumes with accordingly representative analytical results. Since the availability of high-resolution solid-state detectors this feature is supplemented by a high degree of elemental sensitivity and specificity.

Because of its small size and its superior specific neutron emission, ^{252}Cf is the preferred isotopic source. The energy distribution of the neutrons results from the spontaneous fission spectrum. The neutron flux is steady and, therefore, does not require monitoring. Accelerator-type sources, in general, make use of the d-t-reaction producing neutrons with about 14 MeV energy. Two orders of magnitude lower fluxes are achieved with the d-d-reaction which delivers neutrons at about 3 MeV. Common to accelerator-type sources are the advantage that they can be turned off when not in use, and the drawback that flux monitoring is required. The additional disadvantage of damage to solid-state detectors is becoming less severe since the availability of high-purity germanium detectors which are more resistant to energetic neutron radiation than previous materials.

Precise and accurate nuclear data are an important prerequisite in practical applications of these neutron sources. Involved radiation transport computer codes are used, for instance, for calculating the tool response, in studying the influence of in situ realities such as varying porosity, moisture or inhomogeneities, for optimizing the source-detector configuration, or for estimating the contribution of interfering nuclear reactions. In general, all the relevant energy-dependent cross sections of the major and minor constituents of the medium to be investigated should be known to about 10 % or better. In many applications, this also applies to trace elements present in the sample.

Considerable effort has been devoted during the past thirty years to the treatment of neutron slowing down in complex media and the measurement of nuclear data required for interpreting reliably the analytical results. Nevertheless, there are still deficiencies, either because the demands as to accuracy increase, new applications emerge, new types of sources become available, interfering reactions have to be considered, or alternative reactions with improved elemental specificity are required.

The present paper briefly summarizes the progress achieved during the past few years in the field of fast neutron activation cross section data without claiming full completeness. The disposition of the subject is more or less arbitrary. The relative importance of the various data in each case depends on the task to be solved and the neutron source appropriate to it. Many of the investigations cited were performed for quite different reasons, for instance, in connection with fission and fusion reactor design or dosimetry applications. Fission product and actinide cross sections will be left out since they are not of direct relevance to this conference. Inelastic scattering will be considered only insofar as the isomeric states excited have sufficiently long half-lives to be utilized in common activation analytical techniques.

DIFFERENTIAL FAST NEUTRON CAPTURE CROSS SECTIONS

Fast neutron radiative capture may either contribute to the response of the analytical instrument, influence the shape of the neutron spectrum or interfere with other nuclear reactions that are used for the analysis. For instance, in 14 MeV activation analysis the capture process in manganese complicates the derivation of the absolute copper and nickel content in manganese nodules from the Mn/Fe ratio when realistic assemblies are considered [8].

Using the ^{3}H(p,n)^{3}He reaction with neutrons from a 3 MeV Van de Graaff accelerator, Herman and Marcinkowski [9] measured the activation capture cross sections of the isotopes ^{78}Se, ^{80}Se and ^{116}Cd for excitation of the metastable states ^{79m}Se (3.9 min), ^{81m}Se (57.3 min) and ^{117m}Cd (3.31 h), respectively, as well as of the isotopes ^{82}Se, ^{114}Cd, ^{116}Cd, ^{190}Os and ^{192}Os for population of the ground states in the product nuclei. The neutron energy ranged from 0.5 MeV to 1.3 MeV. Identification of the reaction products was achieved by detection of their characteristic gamma-rays. The results were compared with statistical model calculations. Fig. 1 summarizes the data obtained in this investigation.

A similar study was performed by Grenier and coauthors [10] who carried out capture cross section measurements for Y, Nb, Gd, W and Au, as well as for several isotopes among which ^{158}Gd, ^{160}Gd, ^{184}W and ^{186}W are of direct interest with respect to activation analysis. Neutrons in the energy range from 0.5 to 3.0 MeV were produced by the ^{7}Li(p,n)^{7}Be and ^{3}H(p,n)^{3}He reactions. The cross sections were determined by detection of the prompt capture gamma-rays using the integrated spectrum method [11] or by activation. The yttrium data agree well with values of Stupegia et al. [12] and Koroleva et al. [13]. The ENDF/B-IV evaluation is systematically too high. In the lower energy region the niobium cross section is in good agreement with data of Pönitz [14] and Macklin [15]. Above 1.2 MeV the results are slightly higher than previous values. Capture cross sections of natural gadolinium and tungsten as well as of the isotopes ^{160}Gd and ^{186}W are presented in Fig. 2. For most of the Gd and W isotopes the available data are still scarce and show some inconsistencies. Values reported by Komonov [16, 17] seem to be systematically too low. Considerable discrepancies also exist with the Devaney evaluation [18] for the tungsten isotopes. Statistical model calculations are, in general, consistent with the experimental data.

The results obtained by Grenier et al. on the capture cross section of gold which is also important as a standard agree quite well with measurements of Paulsen [19], Lindner [20] and Pönitz [21] up to about 2 MeV. Above this energy they are lower than previous data. Another study on this cross section [22], however, seems to favour the higher values. Measurements performed by Andersson, Bergqvist and Zorro are discussed in detail in a recent report of the Lund University [23]. Data of Chen Ying and coauthors [24] in the energy range below 1.5 MeV are in good agreement with values from the literature.

The integrated spectrum method [11] has also been used by Grenier, Joly and Voignier [25] to measure the absolute capture cross sections for natural copper and for the enriched isotopes ^{63}Cu and ^{65}Cu in the 0.5 to 3 MeV energy range. Excellent accordance was found with previously available data.

A recent evaluation of the ^{58}Fe(n,γ)^{59}Fe cross section up to 20 MeV may be found in Ref. [26]. Extensive measurements below 600 keV have been performed with the Oak Ridge linear accelerator neutron facility for many nuclei [27]. Data on the ^{115}In(n,γ)^{116m}In reaction are reported in Refs. [22, 23].

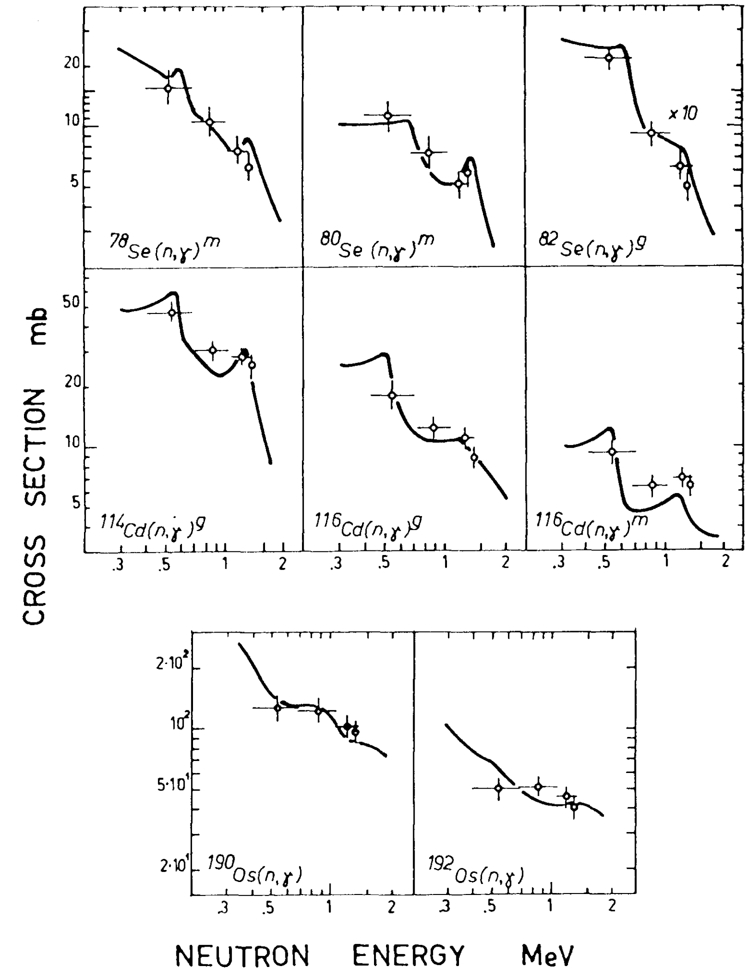

Fig. 1: Experimental capture cross sections in comparison with the predictions of the statistical model [9].

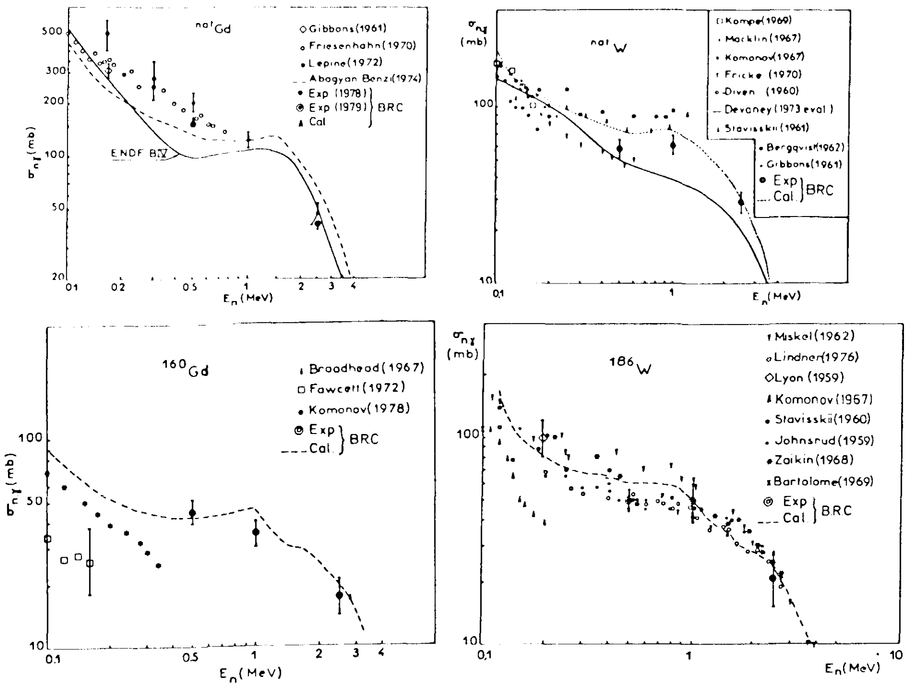

Fig. 2: Experimental and calculated capture cross sections for gadolinium and tungsten [10].

AVERAGE CROSS SECTIONS FOR ^{252}Cf NEUTRONS

Several cross section studies have been published not long ago on reactions in the spontaneous fission neutron field [28 - 32]. Dezsö and Csikai [28] used a scattering-free arrangement in the open air with a small Cf source and thin samples. The induced activities were measured relative to the ^{115}In(n,n')^{115m}In reaction. Fourteen (n,p), (n,γ), (n,n') and (n,γ) cross sections were determined. A similar study was performed by Benabdallah and coauthors [29] who also calculated the average values for various reactions using differential cross sections from the evaluated data files ENDF/B-IV and ENDF/B-V as well as results of Smith and Meadows [33]. A Maxwellian spectrum with a temperature of 1.42 MeV was assumed. Such calculations are of interest with respect to integral tests of the differential data. A comparison of the measured and calculated values shows that, in general, the agreement is quite good in view of the uncertainties in both the spectrum-averaged and the differential cross sections. Discrepancies, however, are observed in the cases of the ^{56}Fe(n,p), ^{138}Ba(n,γ) and ^{135}Ba(n,n') + ^{134}Ba(n,γ) reactions. Most probably, the explanation for the disagreement in the first case lies in a systematically too low value for the experimental average cross section in Ref. [29]. This is confirmed by a comparison with other published data (e.g. [28]). The experimental data on average cross sections of the Ba isotopes are still too scarce and inconsistent to allow definite conclusions in these cases.

Table I. Experimental and Evaluated ^{252}Cf Spectrum-Averaged Cross Sections in mb.

Reaction	$\langle\sigma\rangle_{exp}$ [28]	$\langle\sigma\rangle_{exp}$ [29]	$\langle\sigma\rangle_{exp}$ [30]	$\langle\sigma\rangle_{exp}$ [31, 32]	Other Experiments		$\langle\sigma\rangle_{eval}$ [31] [a]
					$\langle\sigma\rangle_{exp}$	Ref.	
^{24}Mg(n,p)^{24}Na	-	-	-	2.01 ± 0.06	1.94 ± 0.09	[34]	1.898 (4.2)
^{27}Al(n,p)^{27}Mg	4.84 ± 0.14	4.7 ± 0.4	-	4.80 ± 0.09	4.891 ± 0.179 4.90 ± 0.32 5.11 ± 0.43 5.04 ± 0.42 [b]	[34] [35] [36] [37, 38]	4.825 (3.2)
^{27}Al(n,α)^{24}Na	-	-	-	1.006 ± 0.022	-	-	1.004 (1.9)
^{28}Si(n,p)^{28}Al	7.12 ± 0.23	-	-	-	9.66 ± 0.55	[36]	-
^{32}S(n,p)^{32}P	68.4 ± 0.4	-	-	-	72.52 ± 2.96 72.4 ± 4.8	[34] [35]	71.20 (3.7)
^{46}Ti(n,p)^{46}Sc	13.6 ± 1.2	-	-	13.8 ± 0.3	13.8 ± 0.3 13.4 ± 1.1	[39] [36]	13.92 (2.1)
^{47}Ti(n,p)^{47}Sc	19.4 ± 0.1	-	-	-	18.9 ± 0.4 22.0 ± 0.9	[39] [36]	19.04 (2.0)
^{48}Ti(n,p)^{48}Sc	-	-	-	0.42 ± 0.01	-	-	0.4202 (2.2)
^{51}V (n,p)^{51}Ti	-	-	-	-	-	-	0.7092 (8.0)
^{55}Mn(n,2n)^{54}Mn	-	-	-	0.408 ± 0.009	0.58 ± 0.14	[37]	-
^{54}Fe(n,p)^{54}Mn	87.8 ± 0.9	-	89 ± 2	-	87.63 ± 4.36 87.0 ± 5.4 84.6 ± 2.0 92.5 ± 5.0	[34] [35] [39] [36]	85.58 (2.0)
^{56}Fe(n,p)^{56}Mn	1.40 ± 0.02	1.09 ± 0.07	-	1.450 ± 0.035	1.44 ± 0.07 1.43 ± 0.08 1.450 ± 0.035 1.45 ± 0.06	[34] [35] [39] [36]	1.446 (2.1)
^{59}Co(n,p)^{59}Fe	-	-	-	1.68 ± 0.04	1.96 ± 0.10	[37]	-
^{59}Co(n,2n)^{58}Co	-	-	-	0.406 ± 0.010	0.57 ± 0.06	[40]	-
^{59}Co(n,α)^{56}Mn	-	-	-	0.222 ± 0.004	0.218 ± 0.014 0.20 ± 0.01	[34] [37]	0.2165 (6.2)
^{58}Ni(n,p)^{58}Co	118.8 ± 0.4	95.0 ± 4.5	121 ± 2	-	118.5 ± 4.1 119 ± 6 118 ± 3 113.4 ± 4.8 118.8 ± 5.4 110.7 ± 4.8 [b]	[34] [35] [39] [36] [41] [37, 38]	115.0 (1.7)

[a] The brackets indicate the relative standard deviation in %.

[b] Renormalized in accordance with data from [29].

Table I. (continued)

Reaction	$\langle\sigma\rangle_{exp}$ [28]	$\langle\sigma\rangle_{exp}$ [29]	$\langle\sigma\rangle_{exp}$ [30]	$\langle\sigma\rangle_{exp}$ [31, 32]	Other Experiments		$\langle\sigma\rangle_{eval}$ [31] [a]
					$\langle\sigma\rangle_{exp}$	Ref.	
^{63}Cu(n,γ)^{64}Cu	-	-	-	10.39 ± 0.30	10.95 ± 0.51	[42]	-
^{63}Cu(n,2n)^{62}Cu	-	-	-	0.138 ± 0.007	0.30 ± 0.03	[40]	-
^{63}Cu(n,α)^{60}Co	-	-	-	0.671 ± 0.018	0.709 ± 0.017	[43]	0.7089 (2.3)
^{64}Zn(n,p)^{64}Cu	41.3 ± 2.9	36.2 ± 1.5	-	-	41.84 ± 1.75 41.7 ± 2.7 39.4 ± 1.0 46.4 ± 2.3	[34] [35] [39] [36]	39.81 (2.2)
^{68}Zn(n,γ)^{69m}Zn	-	1.85 ± 0.12	-	-	-	-	-
^{84}Sr(n,γ)^{85m}Sr	35.4 ± 2.3	-	-	-	-	-	-
^{86}Sr(n,γ)^{87m}Sr ^{87}Sr(n,n')^{87m}Sr }	-	130 ± 8	-	-	182 ± 22	[37, 38]	-
^{90}Zr(n,2n)^{89}Zr	-	-	-	0.221 ± 0.006	0.267 ± 0.015	[37]	-
^{93}Nb(n,α)^{90m}Y	0.028 ± 0.002	-	-	-	-	-	-
^{110}Cd(n,γ)^{111m}Cd ^{111}Cd(n,n')^{111m}Cd }	-	110.6 ± 4.0	-	-	204 ± 7	[37, 38]	-
^{113}In(n,n')^{113m}In	164.3 ± 1.8	168 ± 9	-	-	169.7 ± 8.1 170 ± 10 162.3 ± 4.1 [b] 178.3 ± 7.6	[34] [35] [33] [37]	160.8 (2.0)
^{115}In(n,γ)^{116m}In	-	115.6 ± 5.0	-	-	131.6 ± 5.7 123.8 ± 3.6 [b]	[37, 38] [33]	124.6 (2.6)
^{115}In(n,n')^{115m}In	-	196 ± 8	196 ± 4	-	198 ± 5 199.4 ± 10.5[b] 195 ± 5	[39] [37, 38] [33]	196.3 (2.0)
^{134}Ba(n,γ)^{135m}Ba ^{135}Ba(n,n')^{135m}Ba }	-	180.9 ± 11	-	-	255 ± 28	[37, 38]	-
^{138}Ba(n,γ)^{139}Ba	-	1.30 ± 0.26	-	-	3.8 ± 0.4	[37, 38]	-
^{181}Ta(n,γ)^{182}Ta	89.25 ± 1.07	-	-	-	119.9 ± 6.5 105.5 ± 6.1	[37] [42]	-
^{197}Au(n,γ)^{198}Au	77.0 ± 0.1	78 ± 3	-	-	76.2 ± 1.8 119.1 ± 5.2 79.9 ± 2.9	[33] [37] [42]	76.17 (2.0)
^{197}Au(n,2n)^{196}Au	-	-	-	5.50 ± 0.14	-	-	5.461 (2.2)

[a] The brackets indicate the relative standard deviation in %.

[b] Renormalized in accordance with data from [29].

Lamaze, McGarry and Schima [30] measured several integral reaction rates using the MnSO$_4$ bath technique for determining the emission rate of the Cf source. The authors performed careful uncertainty estimates, in particular to obtain scattering corrections.

Mannhart [31, 32] carried out extensive measurements with special emphasis on high-threshold reactions and also applied detailed integral testing to check the consistency of the experimental data with those calculated from ENDF/B-V cross sections. Various experimental and theoretical spectrum representations were considered. The NBS spectrum evaluation was found to yield better consistency than the Maxwellian and theoretical representations. Generalized least-squares techniques were used in the evaluation of a consistent set of integral data with regard to a complete covariance matrix.

Table I summarizes the experimental and evaluated cross sections reported in these studies. For comparison, the most recent previous data have also been included in the Table [34 - 43].

DIFFERENTIAL CROSS SECTIONS OF THRESHOLD REACTIONS

Fu, Hetrick and Perey [44] used previously available evaluations of cross sections and covariances as input for incorporating additional correlated data sets, particularly cross-section ratios, into the evaluation of the reactions ^{32}S(n,p), ^{56}Fe(n,p) and ^{65}Cu(n,2n). The cross sections of the input and output evaluations are shown in Fig. 3. Calculations of the neutron-induced cross sections on ^{54}Fe and ^{56}Fe have been performed by Arthur and Young [45] using the multistep preequilibrium Hauser-Feshbach model code GNASH [46]. Similar studies have been carried out by Arthur and Philis [47] on the (n,2n) reactions of the tungsten isotopes. The results of both investigations reproduce well most of the available experimental data. Schenter and coauthors [26] have applied a generalized least-squares adjustment procedure to evaluate the ^{54}Fe(n,p)^{54}Mn reaction for the ENDF/B-V file (Fig. 4). A priori curves were obtained using Hauser-Feshbach calculations from the HAUSER*5 code [48].

Calculations of ^{59}Co neutron cross sections between 3 and 50 MeV by Arthur, Young and Matthes [49] show good agreement with experimental data from the literature [50, 51] in the case of the (n,2n) reaction, as illustrated in Fig. 5. For the (n,p) reaction (Fig. 6) the theoretical cross section is somewhat lower than the experimental data at 14.6 MeV which cluster around values of approximately 50 - 60 mb. A very recent measurement by Bahal and Pepelnik at this energy, however, fits quite well with the calculated curve (cf. Table II). The theoretical result for the (n,α) reaction reasonably reproduces the general trend, exhibiting slightly higher values below and somewhat lower values above 12 MeV (Fig. 7).

Winkler, Smith and Meadows [52] investigated the previous discrepancy between differential and integral data for the ^{63}Cu(n,α)^{60}Co reaction. On the basis of a new measurement of the excitation function by activation with neutrons from the ^{7}Li(p,n)^{7}Be and D(d,n)^{3}He reactions and a reevaluation of the integral experimental data the inconsistencies have been eliminated.

The excitation function of the ^{61}Ni(n,p)^{61}Co reaction has been studied for the first time by Quaim, Wölfle and Stöcklin [53] in the energy range 6 to 15 MeV using the activation technique with a highly enriched sample.

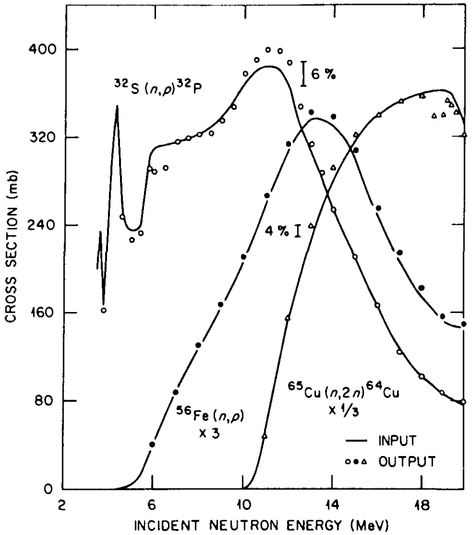

Fig. 3: Cross sections of input and output evaluations for $^{32}S(n,p)$, $^{56}Fe(n,p)$ and $^{65}Cu(n,2n)$ [44].

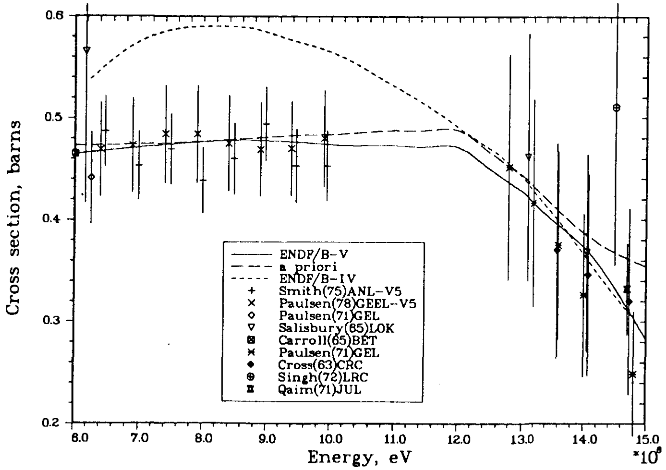

Fig. 4: $^{54}Fe(n,p)$ cross section evaluations and differential data. The a priori curve was calculated using Hauser*5 [26].

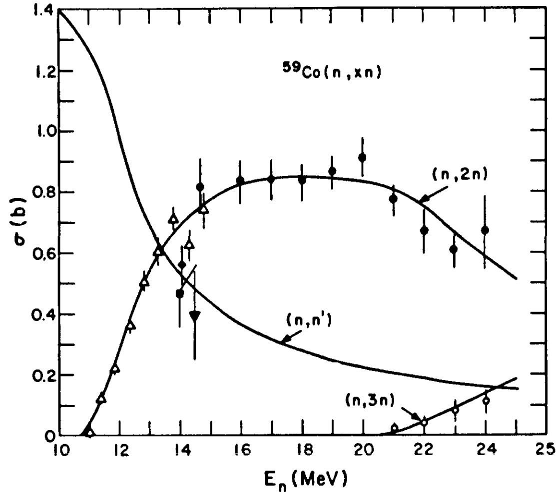

Fig. 5: Calculated and experimental $^{59}Co(n,xn)$ cross sections [50]. The open triangles and the closed circles for the (n,2n) reaction represent data from Refs. [51, 52].

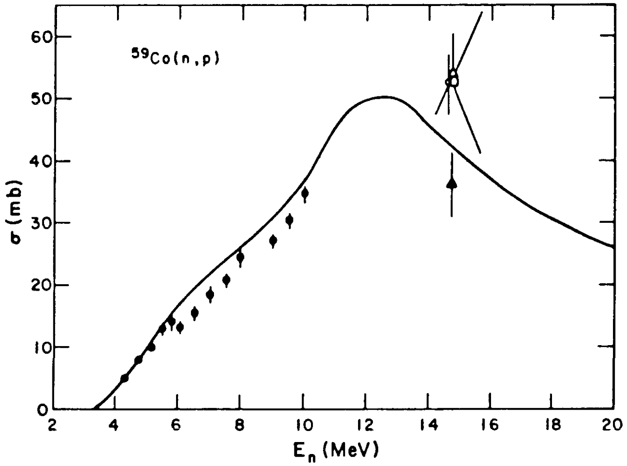

Fig. 6: Calculated and experimental values for the $^{59}Co(n,p)$ reaction [50].

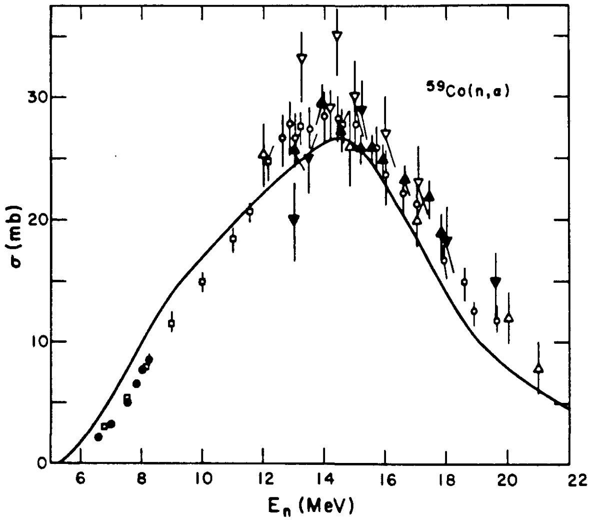

Fig. 7: Calculated and experimental values for the $^{59}Co(n,\alpha)$ reaction [50].

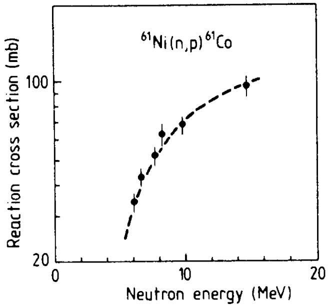

Fig. 8:
Excitation function of the $^{61}Ni(n,p)^{61}Co$ reaction [53].

Quasi-monoenergetic neutrons up to 10 MeV were produced in a gas target via the $D(d,n)^3He$ reaction with a deuteron beam from a compact cyclotron. Data at 14.7 ± 0.3 MeV were obtained by means of a $T(d,n)^4He$ neutron generator. The result is shown in Fig. 8.

Precise measurements of cross sections for the reactions $^{90}Zr(n,2n)^{89}Zr$ and $^{58}Ni(n,2n)^{57}Ni$ from threshold to 20 MeV were reported by Winkler et al. [54]. The $T(d,n)^4He$ reaction was used in connection with a 7 MV Van de Graaff accelerator and a Cockcroft-Walton neutron generator. The new cross section data were evaluated together with other experimental information from the literature to produce an improved set of group cross sections and their uncertainties. The excitation functions are displayed in Figs. 9 and 10. Detailed tables on the evaluated group cross sections may be found in the original paper [54].

Experimental data on the $^{58}Ni(n,2n)^{57}Ni$ reaction have also been published by Lu Hanlin et al. [55]. They agree quite well with the values given in Ref. [54]. The authors furthermore studied the excitation functions for the reactions $^{93}Nb(n,2n)^{92m}Nb$, $^{181}Ta(n,2n)^{180m}Ta$, and $^{197}Au(n,2n)^{196}Au$. The results are shown in Figs. 11 to 13. There is reasonable consistency with most of the previously available data for ^{93}Nb and ^{197}Au. Severe discrepancies

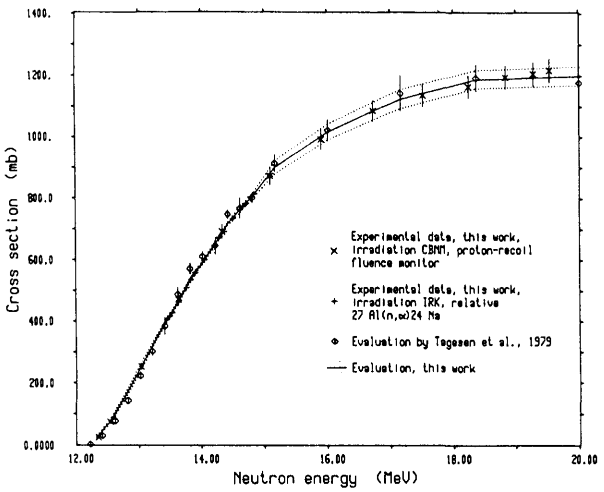

Fig. 9: Excitation function of the $^{90}Zr(n,2n)^{89}Zr$ reaction [54].

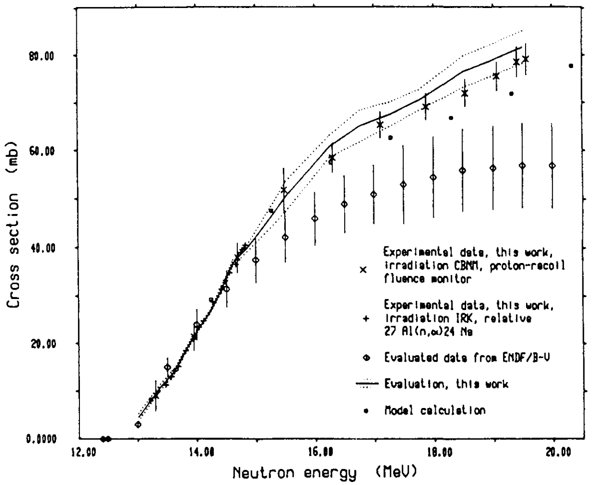

Fig. 10: Excitation function of the $^{58}Ni(n,2n)^{57}Ni$ reaction [54].

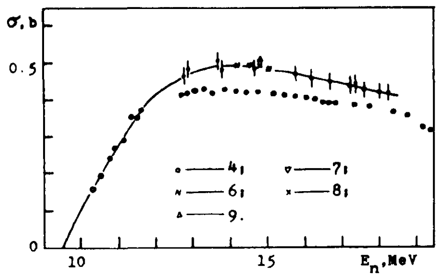

Fig. 11:
Cross section for the $^{93}Nb(n,2n)^{92m}Nb$ reaction. The closed circles with error bars represent data from Ref. [55]. Open circles are data given in Ref. [56].

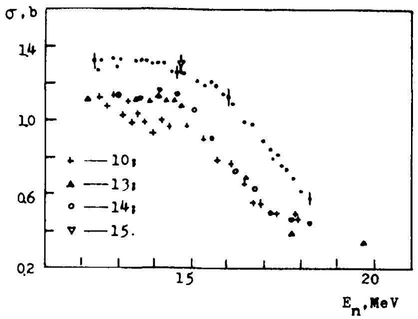

Fig. 12:
Cross section for the $^{181}Ta(n,2n)^{180m}Ta$ reaction. Data from Ref. [55] (closed circles) and previously available values.

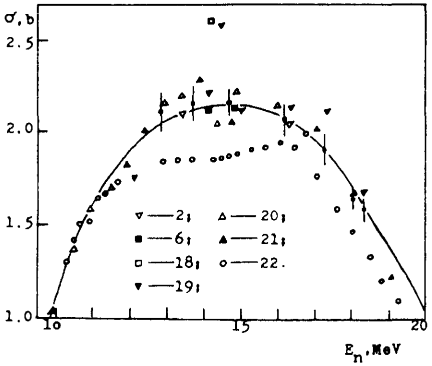

Fig. 13: Cross section for the $^{197}Au(n,2n)^{186}Au$ reaction. Comparison of data from Ref. [55] (closed circles with error bars) with previously available values. Open circles represent data from Ref. [57].

exist with the values of Paulsen and coauthors [56, 57] which are systematically lower above 12 MeV. As to the ^{181}Ta reaction, the situation is still unsatisfactory. The cross sections reported so far differ by factors of up to 3. Most probably, these discrepancies are due to the strong dependence of the results on details of the ^{180m}Ta decay scheme.

Hussain and Hunt [22] have performed absolute measurements of (n,p) cross sections in the energy range 2 to 4.5 MeV for ^{27}Al, ^{47}Ti, ^{58}Ni and ^{64}Zn by application of activation techniques. Neutrons were obtained from the $^{2}H(d,n)^{3}He$ reaction using a 2 MeV deuteron beam. The excitation functions of the $^{28}Si(n,p)$, $^{56}Fe(n,p)$, $^{64}Zn(n,2n)$ and $^{59}Co(n,\alpha)$ reactions above 13 MeV up to 20 MeV have very recently been studied by Jarjis [58]. The results are in excellent agreement with the latest values in the literature. Integral tests of the niobium cross sections are reported in Ref. [59]. Evaluations of cross sections on tungsten isotopes have been put under ENDF format [60].

CROSS SECTIONS FOR THRESHOLD REACTIONS IN THE ENERGY REGION AROUND 14 MEV

Five years ago, Csikai [61] presented a comprehensive review of the status of 14 MeV neutron cross section data. Since that time numerous additional investigations have appeared in the literature [62 - 75]. Most of the data were obtained by means of Cockcroft-Walton, Dynamitron and Van de Graaff accelerators or high-intense sealed neutron tubes. In general, use was made of standard reactions to eliminate the influence of the neutron flux. The preferred reactions are $^{27}Al(n,p)^{27}Mg$ and $^{27}Al(n,\alpha)^{24}Na$.

Marcinkowski [62] has measured and evaluated fast neutron cross sections for (n,2n) reactions on ^{23}Na, ^{58}Ni, ^{191}Ir and ^{193}Ir in the energy range 14 to 18 MeV. The results for ^{23}Na support earlier data of Menlove et al. [76] and Picard and Williamson [77], but at higher energies are more than a factor of 2 lower than those reported by Paulsen and Liskien [78]. The measured cross sections for the $^{58}Ni(n,2n)^{57}Ni$ reaction agree well with older data of Prestwood and Bayhurst [79] and also with recent values from Refs. [64, 70]. The data for the iridium isotopes are consistent with the literature.

Hyvönen-Dabek et al. [63] have measured 14.7 MeV (n,p), (n,α) and (n,2n) cross sections for isotopes of magnesium, chlorine and strontium. Some of the results are somewhat larger ($^{25}Mg(n,p)$; $^{86}Sr(n,p)$), others are lower ($^{26}Mg(n,\alpha)$; $^{37}Cl(n,p)$) than the mean values from the literature. By comparison with previous data the authors derived preferred values for each reaction.

Excitation functions of (n,p) reactions on titanium, iron and nickel isotopes have been studied by Viennot and coauthors [67] in the energy region 13.75 to 15 MeV. Quite good agreement is found with other recent data [68, 70] for the target nuclei ^{50}Ti, ^{54}Fe, ^{56}Fe, ^{57}Fe, ^{61}Ni and ^{62}Ni.

Extensive measurements of (n,p), (n,α) and (n,2n) cross sections for aluminium, titanium, nickel, copper, zirconium, niobium, tantalum and gold have been carried out by Csikai [64] between 13.5 and 14.8 MeV. The results were compared with the predictions of the Hauser-Feshbach model for aluminium and those of the Weisskopf model with T = 1.0 MeV and 1.4 MeV for other elements. Some calculated curves and measured data are shown in Fig. 14. There is excellent agreement between theory and experiment.

Jarjis [65] measured the $^{63}Cu(n,2n)^{62}Cu$ and $^{27}Al(n,p)^{27}Mg$ reaction cross sections for 12.9 to 15.9 MeV neutrons. The data on ^{63}Cu are well within those obtained by previous researchers, although the slope of the excitation function is slightly higher. The $^{27}Al(n,p)^{27}Mg$ cross section curve which was measured using the concentric ring technique with copper rings as flux monitors is systematically higher than that resulting from the data of Csikai [64], and also deviates from the values usually adopted for standardization purposes on the basis of the literature data (e.g. Ref. [67]). Unfortunately, the work of Chialdi et al. [66] who have studied several cross section ratios precludes any statement on this discrepancy since the authors failed to determine the ratios $^{63}Cu(n,2n)/^{27}Al(n,p)$ and $^{27}Al(n,\alpha)/^{27}Al(n,p)$ free from systematic errors.

The availability of a new high-intense 14 MeV neutron source, named KORONA, as developed by Fanger, Pepelnik and Michaelis [80 - 82], has stimulated a considerable effort to measure unknown and to redetermine uncertain or well-known, but strongly energy-dependent cross sections [68 - 71].

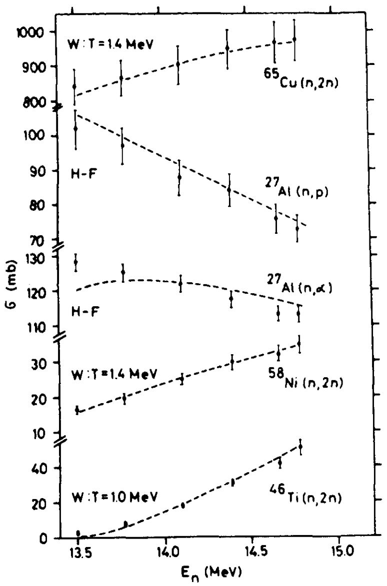

Fig. 14:
Measured and calculated (dashed curves) excitation functions [64]. W and H-F stand for the Weisskopf and the Hauser-Feshbach model.

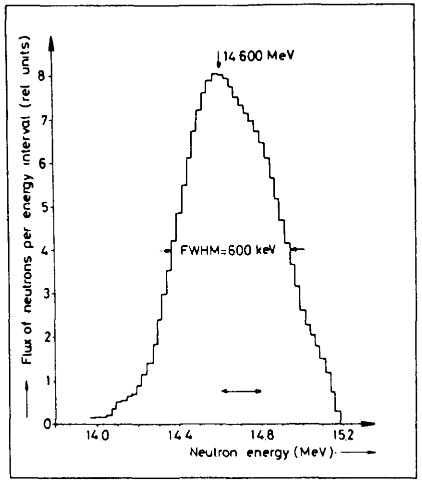

Fig. 15:
Calculated neutron spectrum for KORONA [83, 84] and experimentally determined average neutron energy using the Zr/U method.

The latter is motivated by the cylindrical acceleration structure that results in an effective neutron spectrum which differs from those of head-on targets. Bahal and Fanger [83, 84] have, therefore, performed a thorough theoretical study of the neutron spectrum. The contribution of neutrons scattered in the structure materials, the effects of scattering in the sample and the influence of the neutron spectrum on the average activation cross section were considered in detail. The most probable energy was found to be 14.6 MeV with a FWHM of 0.6 MeV (Fig. 15). Experimentally, the spectrum was investigated using two different techniques: (i) the activity-ratio method with Nb/Zr and Zr/U, and (ii) the reaction-threshold technique with 22 different samples [69]. The Zr/U method yielded an average energy of 14.7 ± 0.1 MeV (Fig. 15), whereas the other methods gave slightly lower values. A very recent study by Bahal and Fanger [85] using the Nb/Zr technique confirmed the Zr/U results so that there is strong evidence of a median at 14.7 MeV and a FWHM of 600 keV.

The new facility which has a source strength of up to $5 \cdot 10^{12}$ n s^{-1} allows improved elemental sensitivity and selectivity and has been applied with great success to the analysis of mineral samples [86]. The cross section measurements [68 - 71] have so far concentrated upon reactions with short-lived product nuclei which are of particular interest for many applications. In this connection (n,n') reactions also come to the fore. Where comparable cross section data are available, the agreement with other studies [64, 67]

Table II. Cross Sections for Threshold Reactions around 14 MeV Neutron Energy

Reaction	E$_n$ (MeV)	σ (mb)	Ref.
^{23}Na(n,2n)^{22}Na	15.5 ± 0.5	51.7 ± 4.2	[62]
	16.3 ± 0.3	57.7 ± 4.5	[62]
	16.6 ± 0.2	67.5 ± 4.4	[62]
^{24}Mg(n,p)^{24}Na	14.7 ± 0.2	187 ± 7	[63]
^{25}Mg(n,p)^{25}Na	14.7 ± 0.2	74 ± 9	[63]
^{26}Mg(n,α)^{23}Ne	14.7 ± 0.2	55 ± 6	[63]
^{27}Al(n,p)^{27}Mg	13.50 ± 0.02	102.0 ± 5.6	[64]
	13.77 ± 0.02	97.0 ± 5.3	[64]
	14.10 ± 0.01	88.0 ± 4.8	[64]
	14.39 ± 0.03	84.0 ± 4.6	[64]
	14.66 ± 0.04	76.0 ± 4.2	[64]
	14.78 ± 0.06	73.0 ± 4.0	[64]
^{27}Al(n,α)^{24}Na	13.50 ± 0.02	128.3 ± 2.6	[64]
	13.77 ± 0.02	125.3 ± 2.5	[64]
	14.10 ± 0.01	122.0	[64]
	14.39 ± 0.03	117.6 ± 2.4	[64]
	14.66 ± 0.04	113.2 ± 2.3	[64]
	14.78 ± 0.06	113.3 ± 2.3	[64]
^{37}Cl(n,p)^{37}S	14.7 ± 0.2	22 ± 3	[63]
^{35}Cl(n,2n)^{34m}Cl	14.7 ± 0.2	9.3 ± 1.5	[63]
^{46}Ti(n,p)^{46}Sc	13.77	310 ± 33	[67]
	13.93	297 ± 38	[67]
	14.11	310 ± 33	[67]
	14.30	306 ± 37	[67]
	14.47	242 ± 33	[67]
	14.73	306 ± 34	[67]
	14.83	275 ± 39	[67]
^{46}Ti(n,2n)^{45}Ti	13.50 ± 0.02	2.2 ± 0.2	[64]
	13.77 ± 0.02	7.5 ± 0.6	[64]
	14.10 ± 0.01	17.7 ± 1.3	[64]
	14.39 ± 0.03	30.9 ± 2.3	[64]
	14.66 ± 0.04	42.0 ± 3.2	[64]
	14.78 ± 0.06	50.2 ± 3.8	[64]
^{48}Ti(n,p)^{48}Sc	13.77	51 ± 3	[67]
	13.93	53 ± 3	[67]
	14.11	55 ± 3	[67]
	14.30	53 ± 3	[67]
	14.47	55 ± 3	[67]
	14.73	61 ± 3	[67]
	14.84	56 ± 3	[67]
^{50}Ti(n,p)^{50}Sc	13.77	8.4 ± 0.7	[67]
	13.93	8.6 ± 0.8	[67]
	14.11	10.3 ± 0.9	[67]
	14.30	9.8 ± 0.9	[67]
	14.47	9.8 ± 0.9	[67]
	14.73	11.7 ± 1.0	[67]
	14.84	12.6 ± 1.1	[67]
	14.7 ± 0.3^a	14.3 ± 2.1	[68]
^{51}V(n,p)^{51}Ti	14.7 ± 0.3^a	28.0 ± 1.5	[69]
^{50}Cr(n,2n)^{49}Cr	14.7 ± 0.3^a	27.2 ± 1.9	[70]
{ ^{52}Cr(n,p)^{52}V	14.7 ± 0.3^a }	85.7 ± 2.6	[70]
{ ^{53}Cr(n,np)^{52}V	14.7 ± 0.3^a }		
{ ^{52}Cr(n,2n)^{51}Cr	14.7 ± 0.3^a }	356 ± 24	[70]
{ ^{50}Cr(n,γ)^{51}Cr	14.7 ± 0.3^a }		
^{53}Cr(n,p)^{53}V	14.7 ± 0.3^a	47.2 ± 1.7	[70]
{ ^{54}Cr(n,α)^{51}Ti	14.7 ± 0.3^a }	12.6 ± 0.5	[70]
{ ^{53}Cr(n,^{3}He)^{51}Ti	14.7 ± 0.3^a }		
^{54}Cr(n,p)^{54}V	14.7 ± 0.3^a	16.4 ± 0.5	[70]
^{55}Mn(n,α)^{52}V	14.7 ± 0.3^a	23.3 ± 0.7	[70]
^{55}Mn(n,2n)^{54}Mn	14.7 ± 0.3^a	741 ± 22	[70]
^{54}Fe(n,p)^{54}Mn	13.77	411 ± 26	[67]
	14.11	433 ± 26	[67]
	14.47	366 ± 24	[67]
	14.73	346 ± 22	[67]
	14.83	314 ± 20	[67]
	14.7 ± 0.3^a	307 ± 9	[70]
^{54}Fe(n,2n)^{53}Fe	14.7 ± 0.3^a	7.9 ± 0.7	[70]
^{54}Fe(n,α)^{51}Cr	14.7 ± 0.3^a	88 ± 6	[70]
^{56}Fe(n,p)^{56}Mn	13.77	109 ± 7	[67]
	13.93	127 ± 8	[67]
	14.11	109 ± 7	[67]
	14.30	119 ± 7	[67]
	14.47	109 ± 7	[67]
	14.73	104 ± 6	[67]
	14.83	105 ± 6	[67]
{ ^{56}Fe(n,p)^{56}Mn	14.7 ± 0.3^a }	111.0 ± 5.5	[70]
{ ^{57}Fe(n,np)^{56}Mn	14.7 ± 0.3^a }		
^{57}Fe(n,p)^{57}Mn	13.77	96 ± 8	[67]
	13.93	96 ± 8	[67]
	14.11	90 ± 8	[67]
	14.30	93 ± 8	[67]
	14.47	83 ± 7	[67]
	14.73	89 ± 8	[67]
	14.83	92 ± 8	[67]
	14.7 ± 0.3^a	89 ± 5	[70]
^{58}Fe(n,p)^{58}Mn	14.7 ± 0.3^a	13.6 ± 0.7	[70]
^{59}Co(n,p)^{59}Fe	14.7 ± 0.3^a	46.5 ± 2.3	[70]
^{59}Co(n,2n)^{58}Co	14.7 ± 0.3^a	231 ± 10	[70]
^{59}Co(n,2n)^{58m}Co	14.7 ± 0.3^a	478 ± 24	[70]
^{59}Co(n,α)^{56}Mn	14.7 ± 0.3^a	30.2 ± 1.5	[70]
^{58}Ni(n,p)$^{58m+g}$Co	13.77	389 ± 14	[67]
	14.11	363 ± 13	[67]
	14.30	332 ± 12	[67]
	14.47	308 ± 11	[67]
	14.73	276 ± 10	[67]
	14.83	269 ± 9	[67]
^{58}Ni(n,p)^{58g}Co	14.7 ± 0.3^a	150.5 ± 6.0	[70]
^{58}Ni(n,p)^{58m}Co	14.7 ± 0.3^a	169 ± 10	[70]
^{58}Ni(n,np)^{57}Co	14.7 ± 0.3^a	586 ± 30	[70]
^{58}Ni(n,2n)^{57}Ni	14.02	19.9 ± 2.3	[62]
	16.42	53.4 ± 4.5	[62]
	17.42	63.0 ± 6.6	[62]
	17.85	66.6 ± 6.8	[62]
	13.50 ± 0.02	16.5 ± 1.0	[64]
	13.77 ± 0.02	19.2 ± 1.2	[64]
	14.10 ± 0.01	25.0 ± 1.5	[64]
	14.39 ± 0.03	29.4 ± 1.8	[64]
	14.66 ± 0.04	32.0 ± 1.9	[64]
	14.78 ± 0.06	34.8 ± 2.1	[64]
	14.7 ± 0.3^a	34.7 ± 1.7	[70]
^{60}Ni(n,p)^{60g}Co	14.7 ± 0.3^a	131 ± 4	[70]
^{60}Ni(n,p)^{60m}Co	13.77	40 ± 4	[67]
	14.11	33 ± 3	[67]
	14.47	39 ± 4	[67]
	14.73	29 ± 3	[67]
	14.83	28 ± 3	[67]

[a] The neutron spectrum has a median at 14.7 MeV with a FWHM of 600 keV (see text).

Table II. (continued)

Reaction	E_n (MeV)	σ (mb)	Ref.
^{61}Ni(n,p)^{61}Co	13.77	25 ± 5	[67]
	13.93	32 ± 6	[67]
	14.11	44 ± 8	[67]
	14.30	54 ± 10	[67]
	14.47	58 ± 10	[67]
	14.73	84 ± 15	[67]
	14.83	93 ± 15	[67]
{^{61}Ni(n,p)^{61}Co	14.7 ± 0.3[a]	84 ± 4	[70]
^{62}Ni(n,np)^{61}Co}	14.7 ± 0.3[a]		
^{62}Ni(n,p)^{62g}Co	13.77	20 ± 2	[67]
	14.11	17 ± 2	[67]
	14.47	20 ± 2	[67]
	14.73	16 ± 2	[67]
	14.83	22 ± 2	[67]
	14.7 ± 0.3[a]	24.8 ± 1.2	[70]
^{62}Ni(n,p)^{62m}Co	13.77	14 ± 2	[67]
	14.11	14 ± 2	[67]
	14.47	17 ± 2	[67]
	14.73	18 ± 2	[67]
	14.83	19 ± 2	[67]
	14.7 ± 0.3[a]	14.6 ± 0.9	[70]
^{64}Ni(n,np)^{63}Co	14.7 ± 0.3[a]	3.6 ± 0.7	[70]
^{64}Ni(n,α)^{61}Fe	14.7 ± 0.3[a]	3.7 ± 0.2	[70]
^{65}Cu(n,2n)^{64}Cu	13.50 ± 0.02	840 ± 50	[64]
	13.77 ± 0.02	862 ± 52	[64]
	14.10 ± 0.01	905 ± 54	[64]
	14.39 ± 0.03	955 ± 57	[64]
	14.66 ± 0.04	975 ± 59	[64]
	14.78 ± 0.06	980 ± 59	[64]
^{68}Zn(n,p)^{68g}Cu	14.7 ± 0.3[a]	5.0 ± 1.1	[71]
^{68}Zn(n,p)^{68m}Cu	14.7 ± 0.3[a]	3.6 ± 0.6	[71]
^{68}Zn(n,α)^{65}Ni	14.7 ± 0.3[a]	10.3 ± 1.8	[71]
^{79}Br(n,n')^{79m}Br	14.7 ± 0.3[a]	294 ± 16	[69]
^{86}Sr(n,p)^{86m}Rb	14.7	14 ± 2	[63]
^{86}Sr(n,2n)^{85m}Rb	14.7	244 ± 32	[63]
^{88}Sr(n,p)^{88}Rb	14.7	19 ± 3	[63]
^{88}Sr(n,2n)^{87m}Sr	14.7	289 ± 33	[63]
^{90}Zr(n,p)^{90m}Y	14.7 ± 0.3[a]	9.8 ± 1.7	[71]
^{90}Zr(n,2n)^{89g}Zr	13.50 ± 0.02	451	[64]
	13.77 ± 0.02	546	[64]
	14.10 ± 0.01	655 ± 20	[64]
	14.39 ± 0.03	743	[64]
	14.66 ± 0.04	819	[64]
	14.78 ± 0.06	852	[64]
^{90}Zr(n,2n)^{89m}Zr	14.7 ± 0.3[a]	75 ± 12	[71]
^{90}Zr(n,α)^{87m}Sr	14.7 ± 0.3[a]	3.2 ± 0.5	[71]
^{93}Nb(n,2n)^{92m}Nb	13.50 ± 0.02	453 ± 30	[64]
	13.77 ± 0.02	456 ± 30	[64]
	14.10 ± 0.01	461 ± 30	[64]
	14.39 ± 0.03	455 ± 30	[64]
	14.66 ± 0.04	458 ± 30	[64]
	14.78 ± 0.06	462 ± 30	[64]
^{167}Er(n,n')^{167m}Er	14.7 ± 0.3[a]	252 ± 18	[69]
^{168}Er(n,2n)^{167m}Er	14.7 ± 0.3[a]	581 ± 43	[69]
{^{167}Er(n,n')^{167m}Er	14.7 ± 0.3[a]	795 ± 59	[69]
^{168}Er(n,2n)^{167m}Er}	14.7 ± 0.3[a]		
^{174}Yb(n,p)^{174}Tm	14.7 ± 0.3[a]	3.0 ± 0.2	[69]
^{176}Yb(n,n')^{176m}Yb	14.7 ± 0.3[a]	19.7 ± 1.7	[69]
^{181}Ta(n,2n)^{180}Ta	13.50 ± 0.02	2210 ± 192	[64]
	13.77 ± 0.02	2167 ± 189	[64]
	14.10 ± 0.01	2148 ± 187	[64]
	14.39 ± 0.03	2163 ± 188	[64]
	14.66 ± 0.04	2154 ± 187	[64]
	14.78 ± 0.06	2131 ± 185	[64]
^{183}W(n,n')^{183m}W	14.7 ± 0.3[a]	127 ± 14	[69]
^{184}W(n,2n)^{183m}W	14.7 ± 0.3[a]	656 ± 74	[69]
{^{183}W(n,n')^{183m}W	14.7 ± 0.3[a]	715 ± 81	[69]
^{184}W(n,2n)^{183m}W}	14.7 ± 0.3[a]		
^{190}Os(n,n')^{190m}Os	14.7 ± 0.3[a]	14.0 ± 1.1	[69]
^{192}Os(n,n')^{192m}Os	14.7 ± 0.3[a]	2.6 ± 0.3	[69]
^{191}Ir(n,n')^{191m}Ir	14.7 ± 0.3[a]	221 ± 22	[69]
^{191}Ir(n,2n)$^{190g+m}$Ir	13.04 ± 0.38	2133 ± 136	[62]
	13.36 ± 0.24	2145 ± 133	[62]
	13.87 ± 0.34	2092 ± 138	[62]
	14.49 ± 0.34	2139 ± 139	[62]
	15.04 ± 0.28	2277 ± 176	[62]
	15.40 ± 0.24	2029 ± 141	[62]
	15.94 ± 0.46	2155 ± 137	[62]
	16.59 ± 0.11	1830 ± 111	[62]
	17.42 ± 0.44	1442 ± 93	[62]
	17.86 ± 0.08	1216 ± 97	[62]
^{191}Ir(n,2n)^{190m_2}Ir	13.04 ± 0.38	110.5 ± 9.5	[62]
	13.36 ± 0.24	117.9 ± 8.0	[62]
	13.87 ± 0.34	119.8 ± 7.8	[62]
	14.49 ± 0.34	134.1 ± 8.2	[62]
	15.04 ± 0.28	138.9 ± 9.1	[62]
	15.40 ± 0.24	141.0 ± 9.0	[62]
	15.94 ± 0.46	180.3 ± 12.9	[62]
	16.59 ± 0.11	175.5 ± 19.6	[62]
	17.42 ± 0.44	179.2 ± 18.7	[62]
	17.86 ± 0.08	163.2 ± 13.3	[62]
^{193}Ir(n,2n)$^{192g+m_1}$Ir	13.04 ± 0.38	2006 ± 232	[62]
	13.36 ± 0.24	1932 ± 121	[62]
	13.87 ± 0.34	1899 ± 115	[62]
	14.49 ± 0.34	1872 ± 115	[62]
	15.04 ± 0.28	1953 ± 148	[62]
	15.40 ± 0.24	1807 ± 122	[62]
	15.94 ± 0.46	1893 ± 219	[62]
	16.59 ± 0.11	1605 ± 141	[62]
	17.42 ± 0.44	1312 ± 115	[62]
	17.86 ± 0.08	1109 ± 138	[62]
^{197}Au(n,2n)^{196}Au	13.50 ± 0.02	2056 ± 140	[64]
	13.77 ± 0.02	2087 ± 142	[64]
	14.10 ± 0.01	2079 ± 141	[64]
	14.39 ± 0.03	2092 ± 142	[64]
	14.66 ± 0.04	2087 ± 142	[64]
	14.78 ± 0.06	2094 ± 142	[64]
{^{207}Pb(n,n')^{207m}Pb	14.7 ± 0.3[a]	1365 ± 68	[69]
^{208}Pb(n,2n)^{207m}Pb}	14.7 ± 0.3[a]		

[a] The neutron spectrum has a median at 14.7 MeV with a FWHM of 600 keV (see text).

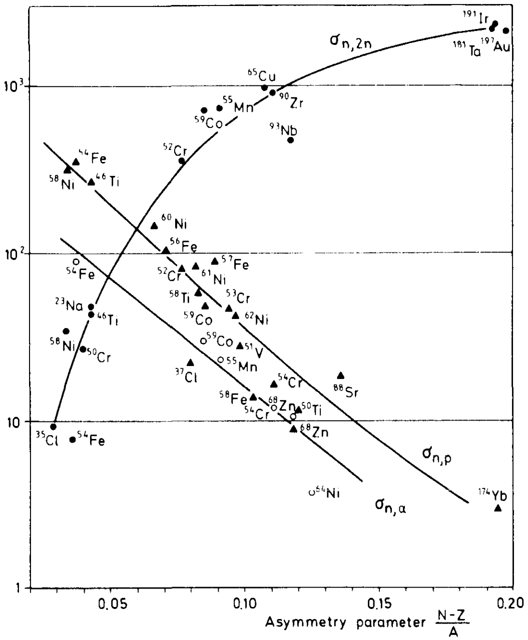

Fig. 16: Systematics of the (n,p) (A > 30), (n,α) and (n,2n) reaction cross sections from Table II at 14.7 MeV neutron energy.

is quite good. Deviations in the case of strongly energy-dependent reactions are not surprising. The data may also be compared with the differential cross sections reviewed in the preceding section. For instance, the results obtained for the (n,2n), (n,p) and (n,α) reactions on ^{59}Co [70] fit very well in the data shown in Figs. 5 to 7. The value for ^{61}Ni(n,p)^{61}Co is quite consistent with those from Ref. [67], but is somewhat below the excitation function presented in Fig. 8 [53].

Precision measurements of the cross section for ^{65}Cu(n,2n)^{64}Cu and various reactions of indium at 14 MeV have been completed by Winkler, Ryves and Ma Hongchang [72]. Data on helium production cross sections and (n,x) reactions induced by 30 MeV d(Be) break-up neutrons may be found in Refs. [73] and [75].

Table II summarizes the results of the recent investigations. The systematics of the data from this Table is presented in Fig. 16. It follows quite well the general trends established by previous authors [74].

REFERENCES

[1] R.L. Caldwell, W.R. Mills, W.L. Orr, L.S. Allen, Proc. Int. Symp. on Nuclear Techniques in Exploration, Extraction and Processing of Mineral Resources, IAEA, Vienna, 7 - 10 March 1977, p. 3

[2] C.G. Clayton, Proc. of the Vienna Conf. [1], p. 85

[3] C.G. Clayton, Proc. of the Vienna Conf. [1], p. 185

[4] J.S. Watt, Proc. of the Vienna Conf. [1], p. 569

[5] K.S. Quisenberry, in: J.L. Fowler, C.H. Johnson, C.D. Bowman (ed.), Proc. Int. Conf. on Nuclear Cross Sections for Technology, Knoxville, TN, October 22 - 26, 1979; NBS Special Publication 594, p. 599

[6] F.E. Senftle, Proc. of the Knoxville Conf. [5], p. 604

[7] W. Michaelis, Proc. of the Knoxville Conf. [5], p. 615; Report GKSS 79/E/52

[8] H.-U. Fanger, R. Pepelnik, G. Grondey, Report GKSS 77/E/50

[9] M. Herman, A. Marcinkowski, Proc. of the Knoxville Conf. [5], p. 307

[10] G. Grenier, J.P. Delaroche, S. Joly, Ch. Lagrange, J. Voignier, Proc. of the Knoxville Conf. [5], p. 323

[11] S. Joly, J. Voignier, G. Grenier, D. Drake, L. Nilsson, Nucl. Instr. and Methods 153 (1978) 493

[12] D.C. Stupegia et al., J. of Nucl. Energy 22 (1968) 267

[13] V.P. Koroleva et al., Conf. Internationale sur les données nucléaires, Paris (1966), p. 473

[14] W.P. Pönitz, Report ANL/NDM-8 (1974)

[15] R.L. Macklin, Nucl. Sci. and Eng. 59 (1976) 12

[16] V.N. Komonov et al., Conf. Kiev, 1977, Vol. 2, p. 206

[17] V.N. Komonov et al., Soviet J. of Nuclear Physics 4, no. 2 (1967) 204

[18] J.J. Devaney, Report LA 5221 (1973)

[19] A. Paulsen et al., Atomkernenergie 26 (1975) 80

[20] M. Lindner et al., Nucl. Sci. and Eng. 59 (1976) 381

[21] W.P. Pönitz, Nucl. Sci. and Eng. 57 (1975) 300

[22] D.J.S. Findlay (ed.): U.K. Nuclear Data Progress Report for the Period January - December 1982, UKNDC(83)P 109, p. 94

[23] P. Andersson, R. Zorro, I. Bergqvist, Nuclear Physics Report LUNDFD 6/(NFFR-3043)/1 - 26/(1982)

[24] Chen Ying, Jiang Songshen, Luo Dexing, Zhu Shengyun, Zhon Zuying in: K.H. Böckhoff (ed.), Proc. Int. Conf. Nuclear Data for Science and Technology, Antwerp, 6 - 10 September 1982, D. Reidel Publishing Company, Dordrecht, Holland

[25] G. Grenier, S. Joly, J. Voignier, Note CEA-N-2284 (1981) 67

[26] R.E. Schenter, F. Schmittroth, F.M. Mann, Proc. of the Knoxville Conf. [5], p. 68

[27] J.B. Garg, COO-2439-7 (1980)

[28] Z. Dezsö, J. Csikai, Proc. of the Antwerp Conf. [24], p. 418

[29] H. Benabdallah, G. Paic, J. Csikai, Proc. of the Antwerp Conf. [24], p. 421

[30] G.P. Lamaze, E.D. McGarry, F.J. Schima, Proc. of the Antwerp Conf. [24], p. 425

[31] W. Mannhart, Proc. of the Antwerp Conf. [24], p. 429

[32] W. Mannhart, W.G. Alberts, Nucl. Sci. and Eng. 69 (1979) 333

[33] D.L. Smith and J.W. Meadows, ANL/NDM-10 and ANL/NDM-14 (1977)

[34] K. Kobayashi, I. Kimura, W. Mannhart, J. Nucl. Sci. Techn. 19 (1982) 341

[35] K. Kobayashi, I. Kimura, Proc. Third ASTM-Euratom Symp. Reactor Dosimetry, Ispra, EUR-6813, Vol. II, p. 1004 (1980)

[36] Z. Dezsö, J. Csikai, Proc. VII. Symp. on Interactions of Fast Neutrons with Nuclei, Gaussig, 1977, p. 44

[37] Z. Dezsö, J. Csikai, Proc. IV. All Union Conf. Neutron Physics, Kiev, April 22-26, 1977, Vol. III, p. 32, Atomizdat, Moscow (1977)

[38] J. Csikai, Z. Dezsö, Ann. Nucl. En. 3 (1977) 527

[39] W.G. Alberts, E. Günther, M. Matzke, G. Rassl, Proc. First ASTM-EURATOM Symp. Reactor Dosimetry, Petten EUR 5667 e/f, Part I, 131 (1977)

[40] Z. Dezsö, J. Csikai, INDC(NDS)-103/M, p. 176 (1979)

[41] V. Spiegel, C.M. Eisenhauer, J.A. Grundl, G.C. Martin, Proc. Second ASTM-EURATOM Symp. Reactor Dosimetry, Palo Alto, NUREG/CP-0004, Vol. II, p. 959 (1978)

[42] L. Green, Nucl. Sci. and Eng. 58 (1975) 361

[43] G. Winkler, V. Spiegel, C.M. Eisenhauer, D.L. Smith, Nucl. Sci. and Eng. 78 (1981) 415

[44] C.Y. Fu, D.M. Hetrick, F.G. Perey, Proc. of the Knoxville Conf. [5], p. 63

[45] E.D. Arthur, P.G. Young, Proc. of the Knoxville Conf. [5], p. 72a

[46] P.G. Young, E.D. Arthur, "GNASH-A Preequilibrium Statistical Model Code for Calculation of Cross Sections and Spectra", LA-6947 (1977)

[47] E.D. Arthur, C.A. Philis, Proc. of the Knoxville Conf. [5], p. 333

[48] F.M. Mann, "Hauser*5, A Computer Code to Calculate Nuclear Cross Sections", HEDL TME 78 - 83, (October 1978)

[49] E.D. Arthur, P.G. Young, W.K. Matthes in: M.R. Bhat, S. Pearlstein (eds.), Symp. on Neutron Cross Sections from 10 to 50 MeV, Brookhaven National Lab., Upton, NY, May 12 - 14, 1980; BNL-NCS-51245, Vol. II, p. 751

[50] J. Frehaut, G. Mosinski in: Nuclear Cross Sections and Technology, NBS Special Publication, NBS 425, p. 855 (1975)

[51] L.R. Veeser, E.D. Arthur, P.G. Young, Phys. Rev. C16 (1977) 1791

[52] G. Winkler, D.L. Smith, J.W. Meadows, Proc. of the Knoxville Conf. [5], p. 199

[53] S.M. Quaim, R. Wölfle, G. Stöcklin, Proc. of the Antwerp Conf. [24], p. 356

[54] G. Winkler, A. Pavlik, H. Vonach, A. Paulsen, H. Liskien, Proc. of the Antwerp Conf. [24], p. 400

[55] Lu Hanlin, Huang Jianzhou, Fan Peiguo, Cui Yunfeng, Zhao Wenrong, Proc. of the Antwerp Conf. [24], p. 411

[56] A. Paulsen, H. Liskien, Nucleonik 7 (1965) 117

[57] A. Paulsen, H. Liskien, R. Widera, Atomkernenergie 26 (1975) 34

[58] D.J.S. Findlay (ed.): U.K. Nuclear Data Progress Report for the Period January - December 1982, UKNDC(83)P 109, p. 98

[59] D.T. Ingersoll. B.W. Wehring, Workshop on Theory and Application of Sensitivity and Uncertainty Analysis, Oak Ridge, TN, 22 - 24 August, 1978; CONF-780 858 - 5

[60] C.A. Philis, E.D. Arthur, P.G. Young, Note CEA-N-2284 (1981)

[61] J. Csikai, Proc. Advisory Group Meeting on Nuclear Data for Fusion Reactor Technology, IAEA, Vienna, 11 - 15 December 1978; IAEA-TECDOC-223, p. 199

[62] A. Marcinkowski, Proc. Advisory Group Meeting on Nuclear Data for Reactor Dosimetry, IAEA, Vienna, 13 - 17 November 1978; AG/160-5, p. 40

[63] M. Hyvönen-Dabek, M. Tarvainen, P. Holmberg, J. Radioanal. Chem. 46 (1978) 357

[64] J. Csikai, Proc. of the Antwerp Conf. 24 , p. 414

[65] R.A. Jarjis, J. Phys. G: Nucl. Phys., 4 No. 3 (1978) 445

[66] A. Chialdi, A. Ait Haddou, M. Viennot, G. Paić, Proc. of the Antwerp Conf. [24], p. 404

[67] M. Viennot, A. Ait Haddou, A. Chialdi, G. Paić, Proc. of the Antwerp Conf. [24], p. 406

[68] J.L. Barreira Filho, H.-U. Fanger, GKSS 81/E/53

[69] B. Anders, R. Pepelnik, H.-U. Fanger, Proc. of Antwerp Conf. [24], p.859

[70] B.M. Bahal, R. Pepelnik, GKSS (to be published)

[71] J.L. Barreira Filho, H.-U. Fanger, GKSS 82/E/8

[72] D.J.S. Findlay (ed.): U.K. Nuclear Data Progress Report for the Period January - December 1982, UKNDC(83)P 109, p. 85 and p. 86

[73] W. Wattecamps, H. Liskien, F. Arnotte, Proc. of the Antwerp Conf. [24], p. 156

[74] S.M. Quaim, R. Wölfle, G. Stöcklin , Proc. 5th All-Union Conf. on Neutron Physics, Kiev, 15 - 19 September, 1980, p. 215

[75] S.M. Quaim, S. Khatun, R. Wölfle in: M.R. Bhat, S. Pearlstein (eds.), Symp. on Neutron Cross Sections from 10 to 50 MeV, Brookhaven National Lab., Upton, NY, May 12 - 14, 1980, BNL-NCS-51245, Vol.II, p. 539

[76] H.O. Menlove, K.L. Coop, H.A. Grench, Phys. Rev. 163 (1967) 1308

[77] J.D. Picard, C.F. Williamson, Nucl. Phys. 63 (1965) 673

[78] A. Paulsen, H. Liskien, Nucl. Phys. 63 (1965) 393

[79] R.J. Prestwood, B.P. Bayhurst, Phys. Rev. 121 (1961) 1438

[80] H.-U. Fanger, R. Pepelnik, W. Michaelis, Proc. 4th Int. Conf. on Nuclear Methods in Environmental and Energy Research, Columbia, MO, April 14 - 17, 1980, CONF-800433, p. 195

[81] H.-U. Fanger, R. Pepelnik, W. Michaelis, J. Radioanal. Chem. 61 (1981) 147

[82] R. Pepelnik, H.-U. Fanger, W. Michaelis, B. Anders, J. Radioanal. Chem. 72 (1982) 393

[83] B.M. Bahal, H.-U. Fanger, GKSS 82/E/22

[84] B.M. Bahal, H.-U. Fanger, Nucl. Instr. and Meth. 211 (1983) 469

[85] B.M. Bahal, H.-U. Fanger, Nucl. Instr. and Meth. (in press)

[86] H.-U. Fanger, W. Michaelis, R. Pepelnik, GKSS Annual Report 1981, p. 28

NUCLEAR PETROPHYSIC AND INTERPRETATIONALLY-METROLOGICAL FOUNDATIONS OF BORE-HOLE RADIOMETRY

D.A. Kozhevnikov
Gubkins' Moscow oil-chemical and gas
Industry Institute, Moscow, U.S.S.R.

Abstract

A concise review is given of the principal results of investigations in nuclear petrophysics in the USSR. Generally examined modern state of neutron characteristics of rocks calculation and measurement methods.

The significance of nuclear petrophysics increases in connection with the complication of the problems to be solved, the growth of the exactness of measurements, the introduction of the algorithmical interpretation.

In nuclear-geophysical metrology and in the algorithmic solution of inverse problems some nuclear petrophysical characteristics take into account the properties of measuring instruments and have the meaning of metrological characteristics.

Introduction

The improvement of the nuclear geophysics methods is a scientific and technical problem of great importance for further development of oil and gas industry, the enlargement of mineral and energy resources and their recovery.

Modern oil-producing industry came to such a new stage when the meaning of the bor-hole radiometry became more important as the problems to be solved are more complicated. Among them are: exploration of oil-fields; control of exploitation, the necessity of studies of the complex lithology and structure reservoirs; deep and super-deep bore-holes sections investigations; off-shore wells logging; preparation and control of EOR projects.

For successfull solutions of the above-mentioned problems the following is necessary:

- to increase the amount of information transmitted from a down-hole tool by means of principally new telemetry systems;
- to improve the accuracy of measurements by means of metrological systems employment and powerful controlled radiation sources and down-hole tools with interference immunity applications;
- to apply new methods of difital processing, including filtering in frequency domain and methods of solution of incorrect inverse problems;
- to introduce new efficient methods and algorithms of interpretation.

All those problems cannot be solved on the empirical level. Theoretical investigations that are providing the development of nuclear geophysical methods can be subdivided into three interconnected fields.

(1) Calculation and analysis of different neutron and other nuclear-physical parameters of rocks in order to construct a physical models of the rocks aned to give foundations of the measurement methods and interpretation principles.

(2) The studies of the laws of neutron and γ-ray distributions in the rocks under the real borehole conditions of measurements with the purpose of creation the interpretational models and improvement of measuring equipment parameters, telemetry systems and metrological control devices;

(3) The creation of algorithms for quantative determination of nuclear physical characteristics of rocks, from the results of bore-hole measurements and their direct recalculation (or by means of combined processing) into the petrophysical characteristics or quantative content of the component in question.

Porosity, clay content, oil, gas and water saturation, chemical composition of the matrix of the rock, pressure and temperature influence on neutron methods readings not directly but through corresponding neutron parameters. Modern orientation of nuclear geophysics for direct measurements of neutron characteristics of the rocks puts forward the problem of selection of such a of a neutron characteristics of the rock, that is sufficient for the solution of direct and inverse problems.

The characteristics of the spatial-energy and temporal distribution are the following: slowing-down length (total age of neutrons) and fourth spatial moment, capture escape probability, slowing-down time and its dispersion, diffusion length and migration length, lifetime and diffusion coefficient of thermal neutrons. It is necessary to know all these parameters for petrophysical foundation of neutron methods employment, creation of algorithms of interpretation, improvement of characteristics of measuring devices, determination of correlation of interpretational parameters with the properties of the media that is studied.

While such physical properties of the rocks like specific resistance, density, permeability etc. can be measured directly on specimens, the neutron characteristics can be measured only in some exceptional cases [1,10-17].

Thus, the development of methods of calculation of these characteristics is very important, as well as the elaboration of experimental methods of nuclear petrophysical [1-3]. It requires the development of the theory of radiation transfer in the substance and accumulation, analysis and generalization of corresponding experimental information.

Parameters of neutron slowing-down in minerals and rocks

The accuracy of slowing-down parameters calculation (with taking into account absorption, inelastic scattering and angular anisotropy of elastic scattering) depends on the accuracy of the taking into consideration the non-asymptotic behaviour of Plachek function. To the increasement of the accuracy of the calculation of this function correspond the analogies of approximations of Vigner, Greuling-Gertzel and Weinberg-Wigner that were at first used for the solution of the stationary space homogeneous problem of slow neutron spectrum.

The requirements of accuracy are increasing with decreasement of the hydrogen content of the substance and with the increase of the number of spatial or temporal moment to be calculated. The Vigner-approximation increases the age of neutrons and significantly decreases the fourth spatial moment (being compared with Weinberg-Vigner approximation); the kinetics of the slowing-down process is described incorrectly. The energetical spectrum of the source and inelastic scattering have very insignificant influence upon the temporal destribution of neutrons.

The value of absorption section and its dependence from the energy influence on the amplitude of the pulse and in significantly lesser degree on the temporal decrease decrement.

The substances of different composition can be divided into three groups, the regularities of the slow neutrons distribution in which are different: (1) "light", (2) "resonance", (3) "heavy".

The first group consists of the medias of high hydrogen content. The neutron spectrum in such a medias have a shift into the area of greater energies with the increase the spacing (the length of the sonde), the spectral effect of the multienergy source reveals itself greatly; the pulse of slow neutron has and abrupt front, little dispersion and significant asymetry. The angular distribution transforms into isotropical with the decrease of the energy, and the age approximation can not be applied.

In the substances of the second group the energetical distribution of neutrons is determined by the resonance structure of the total section and besides the amplitude of the thin structure of the spectrum increases with the distance. According to the hydrogen content the regularities of spatialtemporal distribution are similar to those of the substances of the first or the third group.

The majority of the rocks are the substances with resonance slowing-down. The spectrum of neutrons is not characteristical because of the principal role of oxygen. By the energy E of 3-4 MeV there are reactions with charged particles emission and neutron absorption. The probability to avoid absorption while slowing-down decreases with the energy increase and to the greater degree when the hydrogene content of the substance decreases.

The principal process of slowing-down in the substances of the third group is the inelastic scattering. The spectrum with the increase of spacing have a shift into a lower energies area and its thin structure is slightly expressed, the pulse of the slow neutrons is symmetric and have significant dispersion. The generalized age-approximation (with taking into account the absorption and inelastic scattering) can be widely applied.

The rock-constitutioning minerals of different groups have their parameters of neutron slowing-down varying in a wide range even for one group. The content of chemically absorbed water (and groups OH^-) have principal role. There is a certain regularity in distribution of minerals according to their slowing-down parameters that reflects the above-mentioned classification of slowing-down substances. The minerals can be divided into three groups, independently of petrochemical type, that is: hydrogen-containing ($L \lesssim 20$ cm, $t_s \lesssim 20$ ms), oxygen-containing (without hydrogen, 20 cm $\lesssim L_s \lesssim$ 40 cm, 20 ms $\lesssim t_s \lesssim$ 55 ms) and those without hydrogen and oxygen ($L_s \gtrsim 40$ cm, $t_s \gtrsim 55$ ms).

In the absence of hydrogen the slowing-down properties of minerals are determined by the oxygene content. As oxygen is wide-spread its content in different minerals is close enough and the range of slowing-down parameters for the minerals of the second group is quite narrow. The minerals of the third group have the highest values of slowing-down parameters, that is waterless haloids, sulphides and their analogies, nuggets.

The influence of shell-structure of atom nucleus (magical and close to magical) upon the slowing-down parameters have been noticed.

While determination of porosity, oil and gas saturation with the neutron methods such a situation is common when the data for complex lithology rocks are processed on the basis of several interpretational relations for clean lithotypes such as limestone, dolomite or sandstone. It is possible to take into account complex lithological composition on the basis of phenomenon of postdiagenetical grouping of rocks with their neutron parameters (D.A. Kozhevnikov; B.Yu. Meltchuk that reveals itself in rapprochement of their neutron characteristics under the influence of different geological (hydrological, geochemical) processes.

For example, the computed dependencies of parameters vs. water-saturated porosity for (natural) sandstones and clean limestone often become close up to coincidence because of a large amount of Al_2O_3, the similarity of natural limestone and dolomite and the proximity of their parameters with the clean dolomite is caused by significant dolomitization of limestone.

The characteristics of neutron diffusion in minerals and rocks

The results of measurement of diffusion parameters of different media are unsatisfactorily described by the monoenergetical theory of diffusion at great absorption ($\Sigma_a/\Sigma_t > 0.1$), and for high temperatures (e.g. about 50°C for water) even at small absorption. Nowadays methods of computation of diffusion characteristics have been developed both for great absorption and for high temperatures (in connection with the studies of sections of deep and superdeep wells). An analysis of diffusion parameters of rocks and formation fluids dependancies vs. temperature have permitted to base the necessity and to develop the methods of taking into account the thermobarical environment of rocks for interpretation of measurements carried out in deep wells.

The rock-forming minerals can be divided into three groups according to the lenghts of diffusion. The first group consists of hydrogen-containing minerals with Li, B, Hg, Cl, Mn, Co and rare-earth elements that greatly absorb thermal neutrons. The waterless minerals, containing K, Ti, Cr, Fe, Cu, Mo, Ba constitute the second group; the third group consists of minerals containing the elements that are not included into the first and the third groups.

The taking into consideration the correlation of filtrating and containing properties of the rocks with the oil gas and water saturation, formation water mineralization, content of dissolved gas in oil and water, clay content and the composition of clay minerals, depth of occurence, thermobarical conditions and other factors is a conditio sine qua non for computation and application of neutron parameters of rocks in oil and gas geology.

It is possible to use directly the neutron characteristics on the basis of principle of physical equivalence of rocks and formation fluids (Yu. A. Gulin, I.L. Dvorkin et al., [2]).

This principle can be formulated in the following way: when the technical conditions of measurements are constant the results of measurements are the same for the rocks which are different in composition and petrophysical parameters (porosity, saturation, etc.) on the condition that their neutron parameters are the same. The principle of physical equivalence and the principle of similarity are mutually supplementary as a methods of experimental and theoretical investigations of the nuclear geophysics problems. As the amounts of interpretational dependencies and formation models are limited, the principle of physical equivalence (its particular case - the principle of L-equivalence) makes it possible to apply the interpretational relations obtained by mathematical and physical situations thus improving the accuracy of interpretation of well measurement data.

The solution of the totality of inverse problems of nuclear geophysics as a complex problem connected with the exploration and the exploitation of minerals correspond to the mutual points of the radiation transport theory, nuclear physics, geology, geochemistry, hydrology, petrophysics, oil and gas formation physics, electronics and metrology and thus cannot be obtained merely with theoretical methods without different additional information.

The best geological results can be achieved by combined application of neutron and γ-methods and other geophysical methods. The studies and employment of correlations between neutron and other petrophysical properties of the rocks, such as specific resistance, density, acoustic wave velocity, natural radioactivity are of special interest. These correlations are violated because of processes that are going in a nearborehole zone of formation, water invasion, occurence of the significant are concentration.

The degree of correlations violation is a quantative characteristic of rock in question. The application of such a characteristic in combined investigation of producing reservoirs by means of measurements in the open borehole and in the cased well permits to evaluate the reservoir properties of the formation - that is porosity, permeability; and also permits to determine the saturation of formations with fluids, to separate oil and gas-bearing parts of the section. It is possible to evaluate the degree of the exhaustion of producing formations, to delineate the location of contact of different types of formation fluids, to control the results of acid processing, to prepare the EOR projects and to evaluate their efficiency [9,2].

Nuclear petrophysics in metrology

For calibration and standartization of different well tools of (mono and multispaced) modifications of neutron methods imitators of porous bed (IPB) are used in the USSR. An IPB is a set of steel or polyethylene tubes of different diameters. A variation of porosity (or composition) of a bed is imitated by mean of alteration of the thickness of air-filled space between the centered in the tube measuring instrument and the wall of this tube, the latter is positioned in a water-filled capacity. In other word, the IPB can be considered to be an air-filled bor hole with variable diameter, surrounded with water; the source and the detector are positioned on the axis of the borehole [6].

For application of this method of calibration it is necessary to determine corresponding diameters of IPB for different types of measuring devices and different constructions of bore-holes, for different ranges of porosity variations and different lithology types, formation fluids and drilling muds. While investigations in offshore wells it is necessary to take into account the difference between sea and fresh water.

The importance of that problem have increased greatly in correspondence with technical requirement of well-radiometry methods that are solving the problems of quantative measurement of porosity and determination of the fluid type (an application of multispaced modifications, digital recording and algorithmic interpretation).

The results of measurement in thermal neutron logging (TNL) and neutron-γ-logging (NGL) methods are expressed in standard conventional units $J(z,r_o)$ that have a meaning of corresponding instruments readings in a calibration water-filled capacity; the interpretational relations are expressed in the same units.

The value of the interpretational parameters $J^*(z,r,r_o)$ of single-detector TNL tool in IPB is expressed as

$$J^*(z,r,r_o) = X^{-n} \exp\left[C(1-X^{-1})\right]; \quad C = Z\alpha(1); \qquad (1)$$

where $x=r/r_o$, r - radius of IPB, r_o - external radius of the tool; n have the values of 1 or 2 respectively for He-filled and scintillation counters, z - spacing of the sonde, $\alpha(1)$ - inverse length of migration for thermal neutron in system "tool-water" (fig. 1).

Non-monotonous variation of $J^*(x)$ have a simple physical explanation. The increasing part of the relation correspond to the decrease of efficient hydrogen content in IPB with the increase of the air-filled space. When the relative diameter is further increased, the readings start decreasing due to geometrical divergence of reverse diffused radiation flow as the emissing neutrons or γ-quanta surface is removed. Computed and experimental data are in good agreement for all the tools except for the case of small diameters (x 1,5) and when the thickness of metal walls of IPB is more than 4 mm.

The simplicity of the formula (1) is explained by the assumptions made for its theoretical inference (D.A. Kozhevnikov): the tool is considered to be a hollow cylinder, it is assumed that there is no intermediate medias between water and air. Actually the tool is a metal construction; air-filled hollow space where is the tool positioned is separated from the water with a steel pipe with walls from 2 to 9 mm thick.

Metal influence on fast neutrons as an inelastic scattering media that changes the high-energy part of the initial source spectrum into the area of lesser energies with corresponding accumulation of neutrons in a low energy part of a spectrum. That is the reason that the slowing-down length of neutrons getting into the water through metal is less than the slowing-down length of neutrons from the source placed into the water. Metal influence on thermal neutrons as an absorbent that decrease readings (being compared with computed ones) when the thickness of IPB walls increases, and it is the reason of radial depression of thermal neutrons field within and near the tool and IPB tube walls. This phenomenon display itself in reading decrease most significantly at small IPB diameters because of interferention of depressions, caused by both tool and IPB walls.

The length of diffusion of thermal neutrons and slowing-down length in the system "metal-water" is lesser than that in water. So the value of $\alpha(1)$ is greater than the inverse length of migration in water and depends on tool's construction (its "metal content") and on the thickness of IPB tube. In its turn the coefficient C is different for different tools even when the spacing is constant, thus every taype of tool is described with the individual relation J*(x) in the IPB with a given x.

The readings of a tool in a given IPB correspond to equivalent values of porosity K*n that can be expressed as:

$$Kn^*(X) = \left[1 - \frac{1 - 1/J^*(X)}{1 - 1/\varkappa} (1 - \mu^{\gamma})\right]^{1/\gamma} \qquad (2)$$

where $\varkappa = J(u)/J(M)$, u = min Kn; M = max Kn;

$\varkappa$ - is a differentiation coefficient of the tool for hydrogen content/M=1/.

The parameters γ depends on the tool's type, and on the diameter and construction of the borehole; and besides $\geqslant 1$ for TNL and $\leqslant 1$ for NGl (approximation given at the study [5] is a particular case of (2) when $\gamma = 1$).

The interpretational parameters of dual-spacing (multispacing) tools is a spatial decrement α. The value of α, measured in the IPB of a given diameter x, is:

$$\alpha(X) = (Z_2 - Z_1)^{-1} \ln[J(Z_1, r)/J(Z_2, r)] = -\frac{\partial}{\partial Z} \ln [J(Z, r)] = \frac{\alpha(1)}{X} \qquad (3)$$

Then, equivalent porosity is determined by a decreament as following:

$$Kn^*(X) = \left[1 - \frac{\alpha^{-1}(x) - \alpha^{-1}(1)}{\alpha^{-1}(\mu) - \alpha^{-1}(1)} (1 - \mu^{\gamma})\right]^{1/\gamma} ; \qquad (4)$$

Taking into account (3) we can obtain the relation in the evident form:

$$Kn^*(X) = \left[1 - \frac{(X-1)\ (1-\mu^{\gamma})}{\alpha(1)/\alpha(\mu) - 1}\right]^{1/\gamma} ; \qquad (5)$$

for the standard conditions: the type of formation-limestone, formation fluid-fresh water, no casing, borehole is filled with fresh water, borehole diameter is 190 mm, $\gamma = 0.028$ [7].

In nuclear-geophysical metrology and in the algorithmic solution of inverse problems some nuclear petrophysical characteristics take into account the properties of measuring instruments and have the meaning of metrological characteristics.

References:

I. Кожевников Д.А. Нейтронные характеристики горных пород и их использование в нефтегазопромысловой геологии. -М.: Недра, 1974.

2. Кожевников Д.А. Нейтронные характеристики горных пород и их использование в нефтегазопромысловой геологии. - 2-е изд., переработ. и доп.-М.: Недра, 1982. - 221 с.

3. Ядерная петрофизика как основа применения методов ядерной физики в геологии. - /И.Г.Берзина, С.А.Кантор, Д.А.Кожевников и др. - Тр./Моск. ин-т нефтехим. и газовой пром-сти, 1974, вып.III, с. 3-I5.

4. Влияние литологии горных пород на результаты оценки пористости по данным нейтрон-нейтронного каротажа. -/Б.К.Журавлев, Ф.Х. Еникеева, В.А.Велижанин, Ю.А.Гулин. - В сб. "Экспресс-информация ВИЭМС, сер. регионалън., развед. и промыслов. геофизика". М.: 1979, вып.4, с. 30-33.

5. Методика определения пористости по данным нейтронного каротажа. - /Э.Ю.Миколаевский, Т.И.Русинова, Э.А.Таратын и др. - В сб. "Прикладная геофизика", 1974, вып.76, с.173-180.

6. Состояние и перспективы развития метрологического обеспечения аппаратуры НК. - /В.М.Лобанков, Е.В.Семенов, В.И.Фоминых и др. - В сб. "Геофизич. аппаратура, вып.77. Недра, 1983, с.122-128.

7. Определение пористости по данным многозондового нейтронного каротажа по тепловым нейтронам. - /Н.Ф.Каргова, Э.Ю.Миколаевский, Э.А.Таратын. - В сб. "Экспресс-информация ВИЭМС, сер. региональн., развед. и промыслов. геофизика". М.: 1981, вып.6, с.26-32.

8. Козачок И.А., Ризник Я.-М.Е. Нейтронно-замедляющие характеристики пород-коллекторов на больших глубинах. Киев, "Наукова думка", 1977, 146 с.

9. Karus E.V., Shimelevich Yu.S. Nuclear Geophysics in Prospecting, Exploration and Development of Oil and Gas Fields.- Int. J. Appl. Radiat. Isot. Vol. 34, No.1, pp.95-117, 1983.

I0. Миллер В.В. Метод определения среднего времени жизни тепловых нейтронов по измерениям на небольших образцах вещества. Атомная энергия, 1967, т.22, вып.I, с.33-38.

II. Юрова Л.Н., Панкратенко Д.А. Определение коэффициента диффузии нейтронов в небольших количествах вещества с помощью импульсного нейтронного источника. Атомная энергия, 1975, вып.2, с.95.

I2. Czubek J.A. The Concept of Thermal Neutron Absorption Cross Section in Small Samples. Inst. Fizyki Jadrowej. Rap.No.1092/AP, Krakow, 1980, 36 p.

13. Czubek J.A. et al. Measurement of the Thermal Neutron Absorption Cross Section of Rock Samples. Int. J. Appl. Radiat. Isot. Vol. 34, No.1, pp. 143-151, 1983.

I4. Гума В.И., Миллер В.В., Шимелевич.Ю.С. Методы спектрометрии гамма-излучения захвата нейтронов для анализа горных пород. - В сб. "Доклады IУ Совещания по использованию новых ядерно-физических методов для решения научно-технических и народно-хозяйственных задач." ОИЯИ, Дубна, 1982, с.262-266.

I5. Вашакидзе Б.В., Горбатюк О.В., Гума В.И. и др. Применение прецизионной гамма-спектрометрии для исследования состава и нейтронных свойств образцов керна и сложнопостроенных коллекторов Зап. Сибири". - В сб. "Ядерная геофизика при поисках и разведке месторождений нефти и газа". М.: ВНИИЯГГ, 1981, с.78-83.

I6. Кантор С.А., Школьников А.С. Об уменьшении влияния нестабильности источников и индикаторов на результаты измерений отношения интенсивностей поля в двух точках пространства. - Тр./ВНИИЯГГ, вып.II. М.: Недра, 1972, с.34-37.

I7. Кантор С.А., Моисеев С.А., Школьников А.С.,Оценка влияния помех на результаты измерений ИННК с двумя источниками и двумя детекторами нейтронов. - В сб. "Скважинные ядерно-геофизические исследования на месторождениях нефти, газа и твердых полезных ископаемых". М.: ВНИИЯГГ, 1978.

I8. Медведев Ю.А., Степанов Б.М., Труханов Г.Я. Ядерно-физические константы взаимодействия нейтронов с элементами, входящими в состав атмосферы и земной коры. Справочник. М.: Энергоиздат, 1981. - 304 с.

19. Блюменцев А.М., Лухминский Б.Е., Мельчук Б.Ю., Панов И.В. Многогрупповая библиотека ядерных данных для ядерно-геофизических расчетов. /Версия Б-2/. М.: ВНИИЯГГ, 1976.

20. Погрешности расчетов защиты от излучений. - /В.В.Болятко, М.Ю.Вырский, А.И.Илюшкин и др. Под ред. В.П.Машковича. М.: Энергоиздат, 1983. - 176 с.

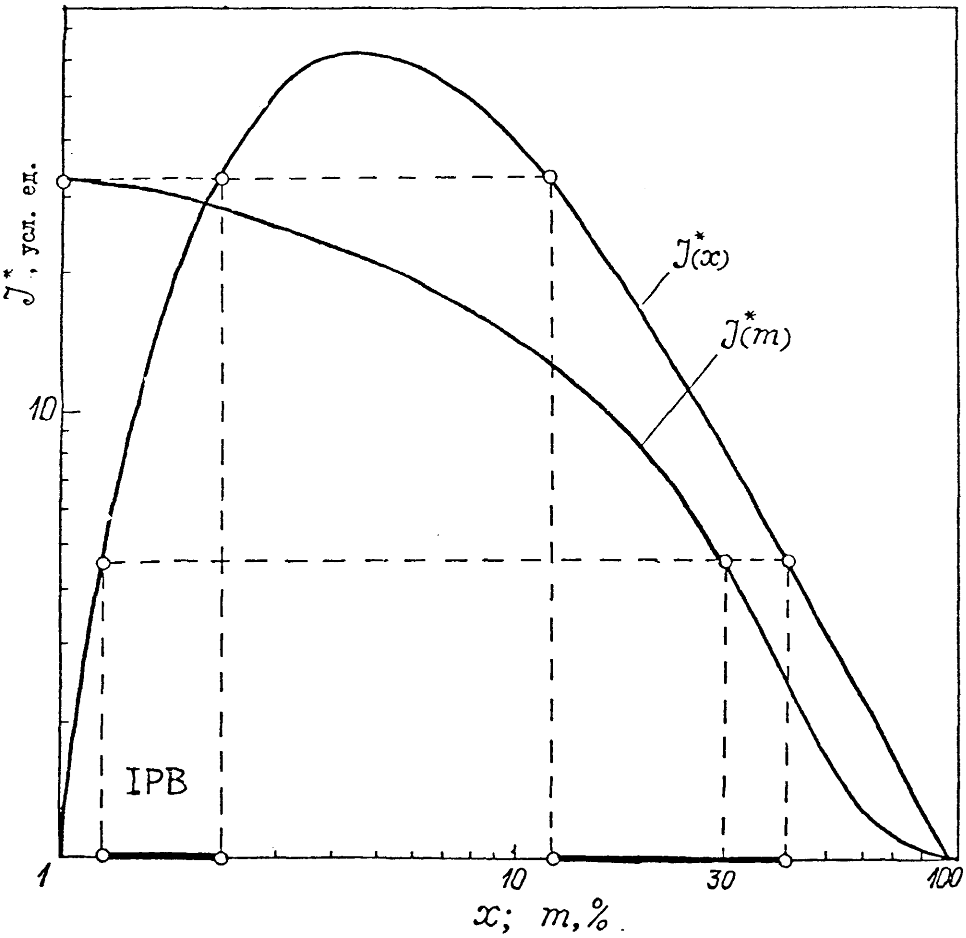

Интерпретационный параметр однозондового прибора как функция относительного диаметра ИПШ /в единицах диаметра скважинного прибора/ x и водонасыщенной пористости m.

ННМ-Т - 50, прибор ДРСТ - 3 - 90; пласт - известняк, скважина необсаженная диаметром 150 мм, в пласте и скважине - пресная вода.

fig.1

SENSITIVITY OF IN SITU BOREHOLE NEUTRON ACTIVATION FOR THE NOBLE ELEMENTS

F.E. Seftle, J.L. Mikesell, A.B. Tanner, and T.A. Lloyd
U.S. Geological Survey, Reston, VA 22092

Abstract

Calculations based on published nuclear data and on borehole measurements were used to estimate the minium detectable concentrations of the noble metals by means of delayed gamma-ray measurements from in-borehole activation by ^{252}Cf and 14-MeV neutron generator sources. Gamma rays from inelastic neutron scattering and thermal neutron capture should be less satisfactory. Decay-rate calculations assuming 1 disintegration/s of the radioactive decay nuclide and 10-minute irradiation of a 4-kg sample by a thermal-neutron fluence rate of 10^6 n/cm^2-s showed that Au, Ag, and possibly Rh should be detectable in their typical ore-grade concentrations; the technique is not sensitive enough for other noble metals. A method of calculation, based on a single borehole calibration standard, permits estimation of minimum detectable concentrations of noble and other elements. The method was tested with combinations of ^{252}Cf with planar and coaxial Ge detectors and of a 14-MeV borehole neutron generator with a coaxial Ge detector; only Au and Ag were found to be detectable in ores. For gamma rays of energy greater than about 75 keV, the coaxial detector yields greater signal-to-noise ratios than the planar detector. The neutron generator is a less efficient source for noble-metal exploration, because a greater fraction of its 14-MeV neutrons are slowed to epithermal- and thermal-neutron capture energies at a distance from the detector that is greater than the likely penetration range of the less-than-700 keV delayed gamma rays from the noble metals. More experimental study is needed of the neutron energy distributions resulting from fast-neutron irradiation of geologic materials in borehole geometry.

Introduction

Direct determination of the precious metals in ores by neutron activation and high resolution gamma-ray spectroscopy has been demonstrated to be a practical analytical technique in the laboratory.[1-4] For exploration purposes, however, it is advantageous to carry out the analyses in a borehole. Gamma-ray spectroscopic analyses in a borehole can be obtained with little delay, and the size of the sample is generally larger and statistically more meaningful than a chemical analysis obtained from a borehole core. This is particularly true of the precious metals, which are often inhomogeneously distributed.

Spectroscopy in the limited volume of a borehole is considerably more difficult than in the laboratory, requiring special tools and techniques. Because of the relatively low concentrations of the noble metals in most ores, careful consideration must be given to the types of reactions, the neutron sources, and the detector used. This paper discusses various alternatives for detecting the noble metals in a borehole, a calculation of the specific activities of the noble metals for practical irradiation and counting periods, and an experimental technique to determine the minimum elemental concentrations that are detectable using decay gamma-ray analysis. Decay gamma-ray measurement appears to be the most suitable method to study the precious metals. However, the most suitable neutron source and detector to use is not so evident, and tests were made to determine which is the most desirable.

Choice of Nuclear Reactions

There are four nuclear reactions to consider; (1) prompt capture gamma rays emitted immediately after neutron absorption, (2) gamma rays from radioactive decay following neutron capture, (3) prompt gamma rays from inelastic neutron scattering, and (4) prompt gamma rays following particle emission. For general borehole applications capture gamma rays and delayed gamma rays from radioactive decay are the most frequently measured. However, capture gamma rays prove useful only for relatively large targets, i.e., relatively high concentrations of the target element in the ore matrix. The most intense capture gamma rays for the precious metals occur between the x-ray region of the spectrum and 700 keV. In this part of the spectrum capture gamma rays suffer severe absorption and interference from Compton scattering events caused by high-energy capture gamma rays of other elements in the ore. Consequently, capture gamma-ray analysis is not the most desirable method for precious metal analysis.

Analyses by detection of gamma rays from inelastic fast neutron interactions and particle reactions are also impractical for essentially the same reasons. In addition, most of these reactions have low interaction cross sections. However, in a few cases, the cross section for inelastic neutron scattering is acceptably high, and if an isomeric state with a short half life is produced by either thermal capture or inelastic neutron scattering, the induced activity from radioactive decay may be detectable.

In a delayed gamma-ray spectrum there are no high-energy capture gamma rays which can be scattered and cause background interference at the low-energy (<700 keV) end of the spectrum. For this reason delayed gamma-ray spectra have a better signal-to-noise ratio. Thus, gamma rays from radioactive decay of isomeric states and decay gamma rays from normally produced radioactive nuclides give one the best opportunity to obtain the sensitivity required for in-situ borehole analysis of the noble metals. For these practical reasons, we limit our study of the precious metals to those nuclides which have moderately short half lives, large cross sections, and high photopeak intensities. As the most intense decay lines for all the precious metals are also less than 700 keV, this investigation is limited to the measurement of low-energy decay gamma rays.

Although delayed gamma-ray spectrometry at low energies has the advantage of producing less complicated spectra than high-energy capture gamma-ray spectra, it has the disavantage that, due to gamma-ray attenuation, a smaller sample is observed in the borehole than when high-energy capture gamma-rays are used. In spite of the smaller sample size, low-energy delayed gamma-ray measurement appears to be the most sensitive and practical approach to use to observe the precious metals in a borehole environment.

Neutron Sources and Gamma-Ray Detectors

Two types of neutron sources can be used: isotopic sources (usually californium-252) or neutron generators. The practical advantages and disadvantages of each have been outlined previously.[5,6] Relative to this problem the neutron energy distribution of each type of source is of importance. Some of the neutron inelastic scattering reactions considered have high threshold energies. The experiments described here were made with a ^{252}Cf neutron source and also with a borehole pulsed neutron generator.

In order to assure resolution of the photopeaks of the decay gamma-ray spectra, a high-resolution detector should be used. Normally, to obtain good photopeak efficiency, as well as high resolution, one would choose a coaxial germanium detector. However, at low energy the signal-to-noise ratio of a planar detector may exceed that of a coaxial detector, due to the reduced interaction and scattering of high-energy gamma rays in the detector. For this reason the efficiency and signal-to-noise ratio of each detector were determined and the appropriate detector was used to measure photopeaks in a given energy range. It is worth noting that when a planar detector can be used to advantage, there are additional benefits: Compton scattering is deemphasized in the planar detector, the resolution is somewhat better and only full-energy and double escape peaks are observed, which simplifies the spectrum. For these reasons both kinds of detector were used in these experiments.

Nuclear Data and Relative Detectability

To make an approximate assessment of the relative ease of detection of the precious metals, an initial comparison based on the calculated disintegration rates was made. The concentrations of most of the noble metals range from 1 ppm (parts per million) in sulfide ores to 0.001 ppm in igneous rocks.[4,7] Ideally, one would like to have an analytical sensitivity of a tenth of the lowest concentration, i.e., 0.0001 ppm. Considering gamma-ray energies of 50 to 700 keV, we estimate that in an 8-cm-diameter borehole, the maximum sample which can be practically observed is about 4 kg. Thus, a method must be capable of detecting about 0.4 μg in the irradiated sample. The total amount of a given noble metal in this 4-kg sample ranges from about 4 μg (3×10^{-5} oz/ton) in igneous rocks up to about 4000 μg (0.03 oz/ton) in sulfide ores. Gold and silver often are significantly more concentrated than the other noble metals. For calculation and comparison purposes, we will assume that the observed 4-kg sample contains 1000 μg (8×10^{-3} oz/ton) of each noble metal considered.

To obtain a rough idea of the ease of activation of the several noble metals, we have for simplicity assumed neutrons with a reactor energy distribution. Most of the basic nuclear data are taken from Erdtmann and Soyka[8] and from Erdtmann[9] and normalized to a neutron fluence rate of 10^6 n/cm^2-sec. Following Erdtmann, the ratio of the epithermal-to-thermal neutron fluence rate is set at 1:50, corresponding approximately to a reactor neutron distribution. The effects of neutron energy distributions that are to be expected from ^{252}Cf and from 14-MeV neutron generators are discussed below. The pertinent nuclear data and the specific activities of the more easily activated nuclides of the noble metals are shown in Table 1.

Considering the practical problems of borehole logging, such as attenuation and geometry, we arbitrarily assume as a worst case that 1 d/s is the threshold disintegration rate below which a nuclide will probably be undetected. Assuming 1000 μg of target nuclide, then, a lower limit of 10^{-3} d/s-μg appears to be a reasonable specific activity which a nuclide must have in order to be detected. Using these arbitrary criteria, the specific activities shown in the table are

Table 1 Nuclear data for noble metal nuclides having the highest specific activities*

Target Element, Nuclide, and Isotope Abundance	Daughter Nuclide	Half-Life $T_{1/2}$	Cross Section σ	Resonance Integral I	Best lines (keV) and Intensity (%)	Specific Activity (decays/sec per μg element) for irradiation time for	
						10 min	1 hour
Ruthenium All nuclides: - specific activity less than criterion value for irradiation of less than 1 hour							
Rhodium							
Rh-103/100 via (n,n'γ)	Rh-103m	56 m	-	533 mb$^{@20}$	39.5(0.6)	3.62x10^{-4}∇	1.63x10^{-3}
Rh-103/100	Rh-104m	4.35 m	11 b	610 b	51.4(57.), 77.6(2.5), 99.1(2.6), 555.8(0.18)	0.108	0.136
	Rh-104	42 s	139 b	1100 b	555.8(2)	1.08	1.08
Palladium							
Pd-108/26.71	Pd-109	13.46 h	12 b	250 b	88.1(5)	2.04x10^{-4}∇	1.2x10^{-3}
Silver							
Ag-107/51.83	Ag-108	2.41 m	35 b	87.2 b	433.9(0.47), 632.9(1.67), 511(0.56)	0.101	0.107
Ag-107/51.83 via (n,n'γ)	Ag-107m	44.3 s	-	530 mb #Δ^{18}	93.2(5)	1.55x10^{-3} #	1.55x10^{-3} #
Ag-109/48.17 via (n,n'γ)	Ag-109m	39.8 s			88(4)		
Ag-109/48.17	Ag-110	24.6 s	89 b	1112 b	657.7(4.5)	0.299	0.299
Rhenium							
Re-187/62.5	Re-188m	18.6 m	1.6 b	7.0 b	59.7(15), 61.1(28), 69.2(9.5), 106(10.5)	1.10x10^{-3}	3.14x10^{-3}
	Re-188	16.7 h	73 b	311 b	155(21), 478(1.3) 633(1.9)	1.13x10^{-3}	6.6x10^{-3}
Osmium All nuclides: - specific activity less than criterion value for irradiation of less than 1 hour							

Table 1 Nuclear data for noble metal nuclides having the highest specific activities*

Target Element, Nuclide, and Isotope Abundance	Daughter Nuclide	Half-Life $T_{1/2}$	Cross Section σ	Resonance Integral I	Best lines (keV) and Intensity (%)	Specific Activity (decays/sec per µg element) for irradiation time for	
						10 min	1 hour
Iridium							
Ir-191/37.4	Ir-192 m	1.4 m	300 b	1200 b	57(.005); 317(.008)	0.38	0.38
Ir-193/62.6	Ir-194	19.4 h	110 b	1368 b	328.5(13) 645(1.16)	1.62×10^{-3}	9.64×10^{-3}
Platinum	All nuclides: - specific activity less than criterion value for irradiation of less than 1 hour						
Gold							
Au-197/100	Au-198	2.69 d	98.8 b	1560 b	411.8(95.5)	7.11×10^{-4}	4.24×10^{-3}
Au-197/100 via (n,n'γ)	Au-197 m	7.2 s	-	1.398 bΔ[19]	279(72.5) 130(3.2)	4.27×10^{-3}	4.27×10^{-3}

---

* Based on $\phi_{th} = 10^6$, and $\phi_{epi} = 2\times10^4$ n/cm^2/sec (see ref. 9); if specific activity is less than 10^{-3} d/s-μg element, the reaction is not shown; (n,n'γ) reaction data from ref. 12, and gamma energies and intensities from ref. 8.

∇ Specific activity less than the criterion value for detection of "run-of-the-mill" ores (see text).

Average for both nuclides. Individual data not available.

Δ Cross section for 2.8 MeV neutrons.

@ Fast component of ^{252}Cf spectrum.

for those nuclides which undergo reactions yielding the highest specific activities. The longest practical irradiation time for most exploration applications is about 10-15 minutes, but the data for a 1-hour irradiation are included for comparison.

Also shown in the table are the specific activities of the metastable isomeric states of several precious-metal nuclides. While the specific activities are barely in the useful range, these excited states are formed by fast neutron activation, and may be useful in those situations where the thermal component of the neutron flux can be de-emphasized, e.g., in a dry borehole, or where a neutron generator is used.

The specific activities of ruthenium, osmium, and platinum even after a 1-hour irradiation are simply too low for practical detection in a borehole at normal concentration. Rh-104 has the highest specific activity, but because 98 percent of the decays are to the ground state by beta emission, the actual intensity of the 555.8-keV line is quite low. The gamma-ray activity is also high for the metastable state of iridium, Ir-192m, but because all the gamma rays have very low intensities, this nuclide would probably be difficult to detect. Rh-104m has a relatively high activity and may be detectable in some cases. Silver and gold ores frequently exceed the concentration range of the platinum group metals and may be detectable in many ores. While this assessment of the calculated activities gives an approximate solution of the problem, an experimental evaluation of the sensitivities is desirable.

Method of Estimation

An experimental method can be used to determine the approximate sensitivity of borehole delayed gamma-ray spectroscopy for the noble metals. To determine these practical limits of detection experimentally, one must be concerned with additional parameters such as the gamma-ray attenuation and intensity, neutron flux, and detector characteristics. In order to calibrate the spectrometer, large samples of quantitatively analyzed and relatively rich ores of the noble metals are usually required and these are difficult to obtain for each of the precious metals. However, by making some approximations, one can obtain a reasonable value of the lower limit of detection without such samples. These values can then be used to evaluate the practicality of using borehole gamma-ray spectroscopy for exploration of the noble metals.

If the counting rate of a photopeak of energy E, as measured by the detector, is C then at any time t during the measuring period defined by t_3-t_2 in Figure 1, one has

$$C = \frac{(\sigma + I/50)\,\phi\,MfLkgI_\gamma\varepsilon(1-e^{-\lambda t_1})e^{-\lambda(t_2-t_1)}e^{-\lambda(t-t_2)}}{A} \qquad (1)$$

where σ = isotopic thermal neutron capture cross section (barns)

I = resonance integral (barns)

ϕ = thermal neutron fluence rate (n/cm^2-sec)

M = mass of the sample (grams)

f = mass fraction of the parent isotope

L = Avogadro or Löschmidt's number

k = isotopic abundance of the parent isotope

g = geometrical factor

I_γ = gamma-ray intensity (gamma rays of energy E per 100 neutrons absorbed)

ε = detector counting efficiency

λ = decay constant of activation product

A = atomic weight

t_1 = irradiation time interval

t_2-t_1 = time lapse between irradiation and start of counting

t_3-t_2 = counting time interval

Equation 1 can be integrated to time t_3 to give the number of counts, N, in the photopeak. Thus

$$N = \frac{(\sigma + I/50)\ \phi\ MfLkgI_\gamma\varepsilon(e^{\lambda t_1}-1)(e^{-\lambda t_2}-e^{-\lambda t_3})}{A\ \lambda} \qquad (2)$$

Equation 2 may be simplified and rewritten in terms of the mass fraction as

$$f = \frac{N\ A\ \lambda}{(\sigma + I/50)\ kI_\gamma\varepsilon S\ H(t)} \cdot \frac{1}{\beta MgL} \qquad (3)$$

Where H(t) is the product of the exponential terms. As ϕ is proportional to the neutron source strength, one may write $\phi = \beta S$, where S is the neutron source mass in μg and β is the proportionality constant. Now consider two photopeaks from different elements in the same sample or position in the borehole and each appearing in a different spectrum but determined under identical experimental conditions, i.e. using the same detector and the same sonde and borehole geometries. The spectra may or may not have been taken with neutron sources of different intensities. Let one of the photopeaks be due to an element of unknown concentration and the other to an element of known concentration. If the photopeak energies are not greatly different, one can assume that the effective mass of the sample observed by the detector is about the same for each photopeak energy. One can then write

$$\frac{f_1}{f_2} = \frac{N_1\ A_1\ \lambda_1}{N_2\ A_2\ \lambda_2} \cdot \frac{(\sigma_2+I_2/50)\ k_2I_{\gamma_2}\ \varepsilon_2S_2\ H(t)_2}{(\sigma_1+I_1/50)\ k_1I_{\gamma_1}\ \varepsilon_1S_1\ H(t)_1} \qquad (4)$$

Equation 4 can thus be used to determine the concentration of the "unknown" element, f_1, because all the other parameters are known or can be determined. If we can accept less accuracy, we can further assume that the variation in borehole conditions for different boreholes will have less than an order of magnitude effect on the calculation of the concentration of the unknown element. Thus, if for a given borehole f_2 and N_2 are known, and if we establish the minimum photopeak area, N_1, required for positive peak energy identification of the unknown element, then the minimum detectable concentration of the unknown element can be estimated. This technique may be used to estimate sensitivities of the noble elements when no quantitative field information is known, assuming that the borehole conditions are similar.

Experimental Equipment

Experiments were made by means of a 125-μg ^{252}Cf source with both a planar and a coaxial germanium detector in a borehole spectrometer, and also by means of a D-T borehole neutron generator with the coaxial detector. The generator was pulsed at 100 s^{-1} with an output of about 3.7×10^5 neutrons for each 5-μs burst. The generator uses a Zetatron D-T accelerator tube and is similar to that described by Jensen et al.[10]

One of the borehole detectors had a 200-mm^2 planar, and the other a 40-cm^3 coaxial, high-purity germanium crystal. Although both detectors were equipped with a melting-propane cryostat,[11] liquid nitrogen was used for a cryogen. The tests were all made in the laboratory in a shallow dry borehole where venting nitrogen gas was not a problem. The thickness of the aluminum casing in the vicinity of the planar detector was reduced to 0.76 mm to reduce gamma-ray attenuation to a minimum. Other details of these spectrometers have been described previously.[11,12]

Five of the precious metals have their highest-intensity decay gamma ray at energies substantially less than 100 keV. At these energies it is important to reduce absorption as much as possible. The experiments were therefore made in a dry borehole to eliminate the water annulus. The water in the sample (estimated to be 5 to 10 percent) should be sufficient to moderate the neutrons from ^{252}Cf. In the case of the neutron generator, where the neutron energies and the slowing down lengths are considerably higher, a water-filled borehole would be advisable. However, gamma-ray absorption would again be a problem at low energies. To accomplish neutron moderation with minimum gamma-ray absorption in these experiments, a plastic sleeve that could be slipped over the target section of the generator was provided. The sleeve was 15 mm thick and 20 cm long. The thickness of the sleeve and the plastic borehole casing together gave a total thickness of 20 mm of moderator.

Other than the signal-to-noise and efficiency experiments described below, the experiments were performed in a borehole facility constructed below the laboratory floor. The facility consists of an 80-cm-diameter cylindrical well 3.92 m deep with concrete-finished sides and bottom (see Figure 2). Along the axis and extending 7.7 m below the bottom of the well is a 13-cm-diameter borehole. A steel casing was used in that part of the borehole below the bottom of the well. Acrylonitrile butadiene styrene plastic casing of 11.3-cm outer diameter and 6 mm thick was used to extend the metal casing from the bottom of the well to the surface (floor level). Annular drums of ore or concrete castings can be slipped over the plastic casing in order to change the ore environment around the upper part of the borehole. For these experiments, a standard sample of cast concrete containing analyzed amounts of aluminum, manganese and silver was prepared. The silver in the sample was in the form of finely ground dental filling alloy. The concrete cylindrical casting was 75.5 cm in diameter, 38 cm high, and had a 12.5-cm-diameter hole concentric with the axis. The casting weighed about 300 kg. Other concrete castings, made for unrelated experiments, were used to partially fill up the well as shown in Figure 2. The castings were lowered into the well so that the plastic casing was threaded through the central hole in the castings. The simulated borehole was filled with castings or annular barrels of sand as shown in the figure. The analysis of the standard casting is shown in Table 2.

Signal-to-Noise Ratio and Efficiency Determination

In order to determine the energy range in which each detector had the best signal-to-noise ratio, we compared spectra taken by means of the planar sonde and a coaxial Ge(Li) sonde, of about the same characteristics as the present coaxial one, in a uranium deposit. Both

TABLE 2

Chemical analysis and concentrations (in percent) calculated by equation 4 of Ag, Mn, and Al in the standard casting.

Element	Concentration (%)	
	Chemical	Calculated
Ag	0.43	-
Mn	0.013	0.017
Al	1.1	1.4

sondes were lowered 76 m in a borehole in southern Texas, USA[13] transecting a sandstone uranium ore. The resulting spectra were interpreted by stepping a correlation function through each spectrum. The correlation function was a normal distribution of the same width (2.35σ) as the expected full-width-at-half-maximum (FWHM) resolution of the detector at that channel in the spectrum at which the function was being applied. From each element of the distribution was subtracted a constant which made the sum of the elements equal zero. The scalar product of the channels spanned by 5 full-widths-at-half-maximum centered about a photopeak and the correlation function covering the same range was the "signal" for that photopeak and was proportional to its peak area. For the determination of the corresponding "noise", we summed the variances of the weighted channel contents and took the square root of that sum. The variance of each weighted channel contents was equal to the square of the weighting factor times the channel contents (or one, if the channel contents were zero). The ratio of the signal-to-noise of the coaxial to the planar detector at specific peak energies of the uranium decay products was greater than one at all energies above about 75 keV (see Figure 3). Thus, except for very low-energy gamma rays or for situations where the presence of nearby interfering photopeaks might dictate the use of a detector of the greatest resolution, the coaxial detector proved to be the more desirable detector.

To determine the efficiency of the two detectors, a relative method was used because efficiency ratios, rather than absolute values, are sufficient for equation 4. The photopeak areas of some uranium decay product gamma rays, measured in a similar borehole configuration, were divided by their respective absolute intensities and plotted as a function of energy for both detectors. The relative efficiency in counts per unit intensity follows the curves shown in Figure 4. As expected, the coaxial detector has a higher efficiency than the planar detector when measured under identical circumstances. The relative efficiency values used to calculate the minimum detectable limits were taken from these curves.

Noble Metal Sensitivities

Isotopic neutron source.

To determine the minimum detectable amounts of the noble metals, the silver concentration in the standard casting was used for the element of known concentration. The borehole sonde was lowered into the borehole until the ^{252}Cf neutron source was opposite the standard sample. Following the irradiation, the borehole sonde was lowered so that the detector was opposite the irradiated position in 6-8 seconds. The area under the 657.7-keV photopeak of ^{110}Ag in the standard sample (3270 counts) was used for the known value of N_2. This measurement was repeated twice for each of the experiments in which the ^{252}Cf source was used. The results of the two repetitions were not significantly different, and are not presented separately here.

The major problem in applying equation 4 to a borehole experiment is that it requires some knowledge of the ratio of the epithermal-to-thermal neutron fluence in the sample. We know of no experimental borehole determinations of this ratio in the literature. Fanger et al[14], Würz[15] and Sanders[16] have made calculations of the ratio using ^{252}Cf neutrons. Their results indicate values of about 1:2 to 1:4 compared with the value 1:50 for reactor neutrons used by Erdtmann[9]. As our standard sample was analyzed for three elements, we had an opportunity of obtaining indirectly an approximate value. Using one of the elements as the known element, and taking all the data from a single spectrum, we calculated the concentrations of the other two elements. When we used a ratio of 1:2 the values differed from the chemical determinations by more than an order of magnitude. However, when we used the 1:50 ratio, the calculated and chemically determined concentrations were in good agreement (Table 2). The estimated 5-10 percent water concentration in the concrete may supply sufficient moderation to increase the relative number of thermal neutrons. The agreement between the chemical analysis and the result of the calculations based on the epithermal-to-thermal ratio characteristic of reactors suggests that the neutron energy spectrum in the formation irradiated by ^{252}Cf neutrons is nearly that of a reactor. For the calculation of the sensitivities using a ^{252}Cf source we have therefore used a 1:50 ratio as a best choice.

From our experience it is felt that a photopeak having as low as 10 to 20 counts may often be sufficient to yield a good determination of the photopeak energy. It was deemed advisable to use a more conservative value of 50 counts to ensure positive peak area determination. Using this value for N_1 in equation 4, the chemically determined concentration value of 0.43 percent for silver (Table 2), and the experimentally determined value of silver photopeak area, N_2, the minimum detectable mass fraction of each of the noble-metal nuclides was calculated (Table 3). The calculations were all based on a 15-minute irradiation, t_1, a 10-second period to transfer the detector to the irradiated position, t_2-t_1, and a 15-minute counting time, t_3-t_2. These irradiation and counting time periods were selected as the maximum for a practical field operation.

Part A of Table 3 shows the estimates of the sensitivity for noble metals by means of delayed gamma rays in the 39- to 155-keV energy range, using the planar detector. Rh-104m and Re-188 have the lowest minimum detectable concentration and these are at best an order of magnitude greater than in most ores. The sensitivity is far too poor to detect the other low-energy emissions.

Part B of the table shows similar data for those noble metals yielding delayed gamma rays in the 155- to 658-keV energy range, using the coaxial detector. With the exception of gold and silver, which frequently occur in greater concentrations, the minimum detectable concentrations are significantly higher than the usual average abundance of these elements in ores. Some nuclides were calculated for both detectors because their photopeak energies are close to the crossover energy of the signal-to-noise ratio for the two detectors (Figure 2).

The minimum detectable limits for the noble metals could be enhanced by optimizing the irradiation, transfer, and counting times for each radionuclide, but in most cases the enhancement would not be sufficient without compromising the practicality of the geophysical technique. Optimization would be advantageous for very-short-half-life

TABLE 3

Minimum detectable concentrations of the noble metals using the highest intensity gamma ray (see Table 1) with the indicated detector and a 125-μg ^{252}Cf neutron source

Element	Product Nuclide	Minimum Detectable Concentration (ppm)
A - ^{252}Cf Neutron Source and Planar Detector		
Rhodium	Rh-104m	13
Palladium	Pd-109	9700
Silver	Ag-107m*	$3.3\text{x}10^{4}$
	Ag-109m*	$5.2\text{x}10^{4}$
Rhenium	Re-188m	760
	Re-188	11
Iridium	Ir-192m	$9.4\text{x}10^{3}$
	(via 57-keV gamma ray)	
B - ^{252}Cf Neutron Source and Coaxial Detector		
Rhodium	Rh-104	24
Silver	Ag-108	70
	Ag-110	69
Rhenium	Re-188	27
Iridium	Ir-192m	$2.6\text{x}10^{5}$
	(via 317-keV gamma ray)	
	Ir-194	66
Gold	Au-198	24
	Au-197m*	$1.3\text{x}10^{2}$

*Calculation based on cross section for 2.8-MeV neutrons nuclides but in essentially every case the saturation activity (see Table 1) is too low to be practical. One could use a higher neutron fluence rate, but 125 μg of ^{252}Cf is about as large a source as can be handled safely under field conditions. A considerably stronger neutron source of about 10^{10} low-energy neutrons per second is required to make in-situ borehole neutron activation a viable method for some of the platinum group metals. Gold and silver can be determined down to the concentration values stated in the table. It should be pointed out again that these data are based on a photopeak area of 50 counts. This is a conservative figure which may be reduced with some care. By optimizing as many conditions as possible one could reduce the minimum detectable limit as given in Table 3 by perhaps an order of magnitude.

Neutron generator neutron source

The above experiment was repeated with the neutron generator, the same Ag, Mn, and Al standard concrete casting, and the same irradiation and counting times. The spectral data were adjusted by multiplying the photopeak areas by the ratio of the neutron output of the 125-μg ^{252}Cf source to the neutron output of the neutron generator. The data thus adjusted were not consistent with the data from the ^{252}Cf experiments. For the same source output, the activation produced by the neutron generator was about eight times less than that produced by ^{252}Cf. To some extent this reduction was due to an insufficient concentration of neutron moderator (hydrogen). Addition of plastic sleeving about the target of the neutron generator improved results only slightly. A more important factor is the extreme range of the 14-MeV neutrons in the concrete matrix, for any reasonable water content (estimated here to be 5 to 10 percent). Because of the larger irradiated zone, the resulting activity is distributed over a larger volume of the matrix, from which only a small fraction of the delayed gamma rays can reach the detector before absorption. These results show that, for the same neutron output, the 14-MeV neutrons of a (D,T) neutron generator are less effective than the lower-energy neutrons of a ^{252}Cf source for thermal-neutron activation in a borehole by delayed gamma-ray analysis, particularly when low-energy gamma rays are measured. As was true for the ^{252}Cf experiment, one must know the epithermal-to-thermal neutron ratio. Monte Carlo calculations[16] on typical geologic samples show that for 14-MeV neutrons the epithermal-to-thermal neutron ratio is close to 1:2. We tried to verify this ratio by using it and silver as the known element to estimate the concentrations of manganese in the standard casting, but obtained a result that was much too large.

The ratio of the photopeak area for manganese (847 keV) to that for silver (657.7 keV) was *18 times greater using 14-MeV neutrons* than using ^{252}Cf neutrons. Very likely this was due to the strong resonances in the manganese cross section in the neutron energy range from 200 eV to 100 keV. The response of manganese is very sensitive to the shape of the neutron energy distribution in this energy range, and the distribution produced by the 14-MeV neutrons is likely to differ significantly[16] from the 1/E reactor spectrum assumed in tabulated values of the resonance integral, or from the distribution of ^{252}Cf neutrons in the formation as inferred above. None of the noble metals have strong resonances in the high-energy epithermal region that would cause their sensitivities to be badly underestimated by using silver as the known element in the calculations above, if the ratio of epithermal to thermal neutrons is adequately known. We were consequently unable to determine the correct epithermal-to-thermal ratio to use for neutrons from the neutron generator. In the absence of an experimentally determined ratio, we have assumed the ratio obtained by Monte Carlo calculations for estimation of the minimum detectable concentrations of the noble metals using activation by means of the neutron generator (Table 4).

Other Elements

The above method can also be applied to the non-noble elements to determine the minimum detectable limits by borehole neutron activation. The only known published experimental elemental sensitivities for in situ neutron activation are those determined by Moxham et al.[17] for several elements in a river-bottom mud. They measured the photopeak area for a gamma ray of each element, and using the known concentrations calculated a minimum detectable concentration. Using our method and correcting for the size of the ^{252}Cf neutron source we have calculated the minimum detectable amounts of the same elements for the gamma-ray photopeaks experimentally measured by Moxham et al. The results are compared in Table 5. Considering that the geometry of the marine experiment was somewhat different from our borehole geometry, the agreement is

TABLE 4

Minimum detectable concentrations of the noble metals using the highest intensity gamma ray (see Table 1), a coaxial detector, and a neutron generator (flux normalized to 125-μg ^{252}Cf)

Element	Product Nuclide	Minimum Detectable Concentration (ppm)
A - Dry Borehole with No Moderator		
Rhodium	Rh-104	$1.1\text{x}10^{3}$
Silver	Ag-108	$6.6\text{x}10^{3}$
	Ag-110	$2.4\text{x}10^{3}$
Rhenium	Re-188	$2.6\text{x}10^{3}$
Iridium	Ir-192m (via 317-keV gamma ray)	$3.8\text{x}10^{5}$
	Ir-194	$2.3\text{x}10^{3}$
Gold	Au-198	698
	Au-197m	$2.7\text{x}10^{5}$
B - Dry Borehole with Moderator		
Rhodium	Rh-104	670
Silver	Ag-108	$3.8\text{x}10^{3}$
	Ag-110	$1.4\text{x}10^{3}$
Rhenium	Re-188	$1.5\text{x}10^{3}$
Iridium	Ir-192m (via 317-keV gamma ray)	$2.5\text{x}10^{5}$
	Ir-194	$1.3\text{x}10^{3}$
Gold	Au-198	408
	Au-197m*	$1.5\text{x}10^{5}$

* Calculation based on cross section for 2.8-MeV neutrons

Table 5 - Comparison of the calculated minimum detectable concentrations of several elements with the experimental determinations of Moxham et al.[17]

Photopeak	Element	Minimum Detectable Concentrations (%)	
Energy (keV)		(Moxham et al.)	This work
847	Mn	0.001	0.0003
1014	Mg	0.19	0.11
1039	Cu	0.02	0.015
1434	V	0.003	0.0002
1507	In	<0.001	0.0006
1779	Al	0.09	0.004
2754	Na	0.02	0.05

relatively good. Our values are lower than theirs for Mn, V, and Al. It is not clear why this should be the case for these three elements. When we use the method of Moxham et al. on the aluminum and manganese photopeak areas measured in our standard casting we obtain minimum detectable values which are in better agreement with those calculated by our method of estimation, suggesting a possible error in their measurement for these three elements. Thus, our technique appears to be a valid way to estimate the minimum detectable quantity of any element which can be activated and measured by means of borehole gamma-ray spectroscopy.

Field Application

If the photopeak of a trace or minor element is large enough for positive identification, then equation 4 can be used to estimate the concentration of the element. Consider the borehole transecting a lithologic unit in which the spectrum was taken. If one knows the rock type, then generally the concentration of the major elements can be estimated to within 30 to 40 percent error and often more precisely. If one of these elements can be activated, its associated decay peak then becomes the standard by which the concentration of a trace element can be estimated. The technique is thus one of using the approximate concentration of a major element to estimate the amount of a trace element. The accuracy of course depends on the accuracy of the estimation of the concentration of the major element, but generally this is sufficient for useful field information.

For example, suppose a spectrum were taken in granite, and that the aluminum photopeak was prominent. The aluminum concentration in granites ranges from about 5 to 11 percent. If one assumed an 8-percent concentration of aluminum as a standard, the concentrations of elements associated with the other photopeaks in the spectrum could be estimated from equation 4. Thus, a minor photopeak at 1434 keV corresponding to vanadium could be used to estimate the vanadium concentration. The error associated with the estimation of the alumimum concentration would be reflected in the estimation of the vanadium concentration, but because of the low concentration of vanadium, the error of the estimate would be acceptable for most field investigations.

Conclusions

The minimum amounts of the noble metals detectable by in-situ borehole neutron activation have been estimated by comparison of their neutron activation characteristics with those of an element of known concentration. Assuming similar borehole conditions, and a minimum photopeak area for positive energy determination, the sensitivity of borehole analysis of the precious metals has been estimated. The results, determined with a ^{252}Cf neutron source and with a 14-MeV neutron generator, indicate that for the present state of the art, gold and silver are the only noble metals that are amenable to in-situ measurement.

The method can also be used to determine the minimum detectable quantities of any other elements. In addition, under some field conditions the technique can be useful to estimate trace or minor concentrations of those elements which have photopeaks that can be positively identified.

Comparison tests between a ^{252}Cf neutron source and a 14-MeV neutron generator indicate that at the same neutron output, the generator is not as efficient as ^{252}Cf for conducting thermal-neutron activation in a borehole. The greater efficiency of the ^{252}Cf neutron source is due to the greater moderation and capture of the neutrons while they are still within gamma-ray penetration range of the borehole.

This study points out the need for experimental determination of the neutron energy distributions resulting from fast-neutron irradiation of geologic materials in borehole geometry and for compilations of a quantity analogous to the resonance integral but appropriate for fast-neutron irradiation.

Acknowledgements

The authors are grateful to Drs. Jim O'Brient and George Salaita of Chevron Oil Company for supplying precious metal ore samples and also for their helpful discussions during the investigations. Special thanks are due to Drs. Franklin B. Woodbury and Paul B. Needham of the U. S. Bureau of Mines, which supported this work in part. We also wish to thank our colleagues Gene Alban, Asghar Ghias, and Peter Intsiful for helping with the experimental work.

References

1. Turkstra, J., Pretorius, P. J., and DeWet, W. J., (1970) Non-destructive determination of platinum metals in ores, matte, and lead assay leads by reactor activation analysis and high-resolution gamma-spectrometry, Anal. Chem. 42, 835-841.

2. DeWet, W. J., Turkstra, J., and Toerien, F.V.S. (1970) Direct determination of the noble metals by activation analysis utilizing high-resolution gamma-spectrometry, in Activation Analysis in Geochemistry and Cosmochemistry, Brunfelt, A. O., ed., Proc. NATO Advanced Study Inst., p. 371-379 (Pub. 1971).

3. Gijbels, R. (1971) Determination of noble metals by neutron-activation analysis, Talanta, 18, 587-601.

4. Parry, S. (1982) Neutron activation analysis for the noble metals in geological sample, Anal. Proc. (London), 19, p. 90-93.

5. Senftle, F. E. (1980) Application of gamma-ray spectral analysis to subsurface mineral exploration, Chapter VIII, in Short Course in Neutron Activation Analysis in the Geosciences, Muecke, G. K., ed., Mineral. Assoc. of Canada, Halifax, Canada, p. 211-254.

6. Senftle, F. E., Mikesell, J. L., Tanner, A. B., Evans, L., Trombka, J., Jensen, D., Stephenson, W., and Hoover, R. (1983) Time-dependent neutron excitation spectra applied to well logging, Trans. Amer. Nucl. Soc. 44, p. 201-203; and Nucl. Inst. and Methods, 1984 (in press).

7. Wedepohl, K. H., ed. (1974) Handbook of Geochemistry, Springer-Verlag, Berlin.

References (cont)

8. Erdtmann, G., and Soyka, W. (1974) Die Gamma-Linien der Radionuklide, Band 1., Zentralbibliothek der Kernforschungsanlage Jülich GmbH, Jülich, West Germany, 261 pp.

9. Erdtmann, G. (1976) Neutron Activation Tables, Kernchemie in Einzeldarstellungen, Vol. 6, Verlag Chemie, New York.

10. Jensen, D. H., Humphreys, D. R., Stephensen, W. A., Weinlein, J. H. and Bivens, H. M. (1981) Pulsed neutron gamma ray logging for minerals associated with uranium, IEEE Trans. Nucl. Sci., NS-28, p. 1685-1690.

11. Tanner, A. B., Moxham, R. M., Senftle, F. E., and Baicker, J. A. (1972), A borehole sonde using a ^{252}Cf source and a Ge(Li) detector cooled by a melting cryogen, Nucl. Instr. and Methods 100, p. 1-7.

12. Senftle, F. E., Moxham, R. M., Tanner, A. B., Boynton, G. R. Philbin, P. W. and Baicker, J. A. (1976) Intrinsic germanium detector used in borehole sonde for uranium exploration, Nucl. Instr. and Methods 138, p. 371-380.

13. Tanner, A. B., Moxham, R. M., and Senftle, F. E. (1977) Assay for uranium and determination of disequilibrium by means of in situ high resolution gamma-ray spectrometry, U. S. Geol. Survey Open-File Report 77-571, 21 p.

14. Fanger, U., Lubecki, A., Pepelnik, R., and Würz, H. (1973) Borehole analysis by means of (n, γ)- and XRF-technique demonstrated in a **scheelite deposit near Mittersill, PACT-Bericht No. 37, Gesell.** für Kernforschung mbH, Karlsruhe, Federal Republic of Germany, 80 p.

References (cont)

15. Würz, H., and Buth, L. (1973) Theoretische and experimentelle Untersuchungen zur Lagerstättenprospektion mit Hilfe von neutroneninduzierter Gammastrahlung, Rept. KFK 1771, Gesell. für Kernforschung mbH, Karlsruhe, Federal Republic of Germany, 62 p.

16. Sanders, L. G. (1983) The application of Monte Carlo computations to formation analysis by neutron interactions, in Nuclear Geophysics, Clayton, C.G., ed., Pergamon Press, New York, p. 173-198.

17. Moxham, R. M., Tanner, A. B. and Senftle, F. E., 1976, In situ neutron activation analysis of bottom sediments, Anacostia River, Washington, D. C. Marine Tech. Soc, Jour. 11, p. 14-21.

18. Broadhead, K. G., and Shanks, D. E. (1967) The application of 2.8 MeV (D,d) neutrons to activation analysis, Int. J. App. Rad. and Isotopes 18, p. 279-283.

19. Özek, F., Özyol, H. and Ortaovali, A. Z. (1979) Formation cross-sections of the short-lived isomer Au-197m for 3 and 14.1 MeV neutrons, Radiochem. Radioanal. Letters 41/1, p. 87-94.

20. Buczkó, M., Bődy, Z. T., Csikai, J., Dezső, S., Juhász, S., Al-Mundheri, H. M., Pető, G. and Varnagy, M. (1976) Average cross sections for ^{252}Cf neutron spectrum, in Proceedings of the Paris Symposium on Californium-252 Utilization, NTIS Rept. CONF-760436, p. IV-19-IV-36.

Figure Captions

1 - Relation of the counting rate with the times t_1, t_2, and t_3.

2 - Sketch showing borehole facility and placement of the casting.

3 - Ratio of the signal-to-noise of the coaxial to the planar detectors.

4 - Relative efficiency of the planar and coaxial detectors with energy determined in a borehole transecting a uranium deposit.

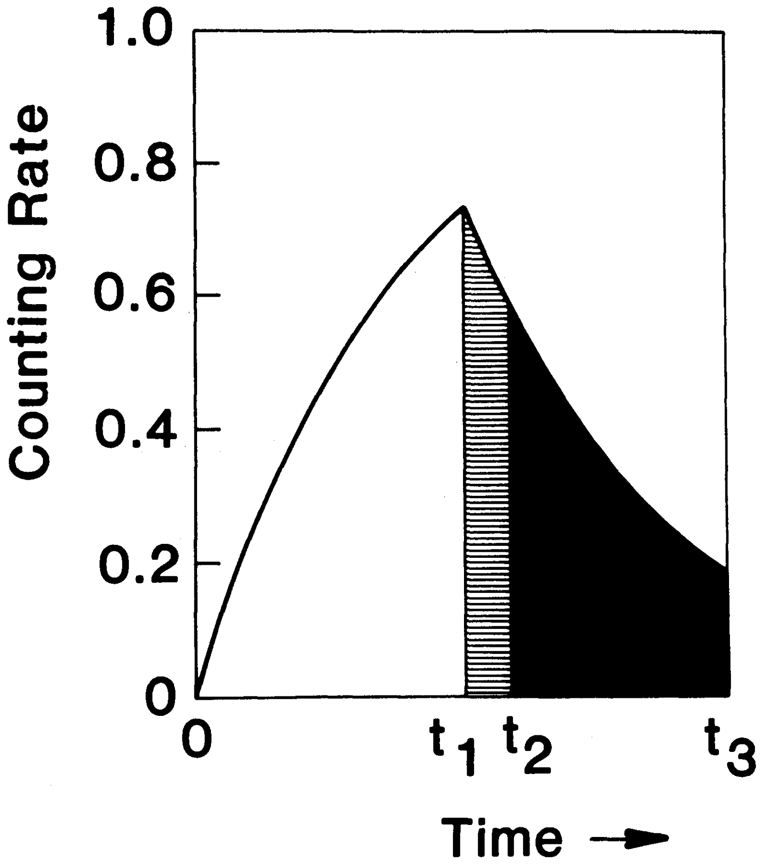
1.0
0.8
0.6
0.4
0.2
0
Counting Rate
0
t_1
t_2
t_3
Time →

FIG. 1.

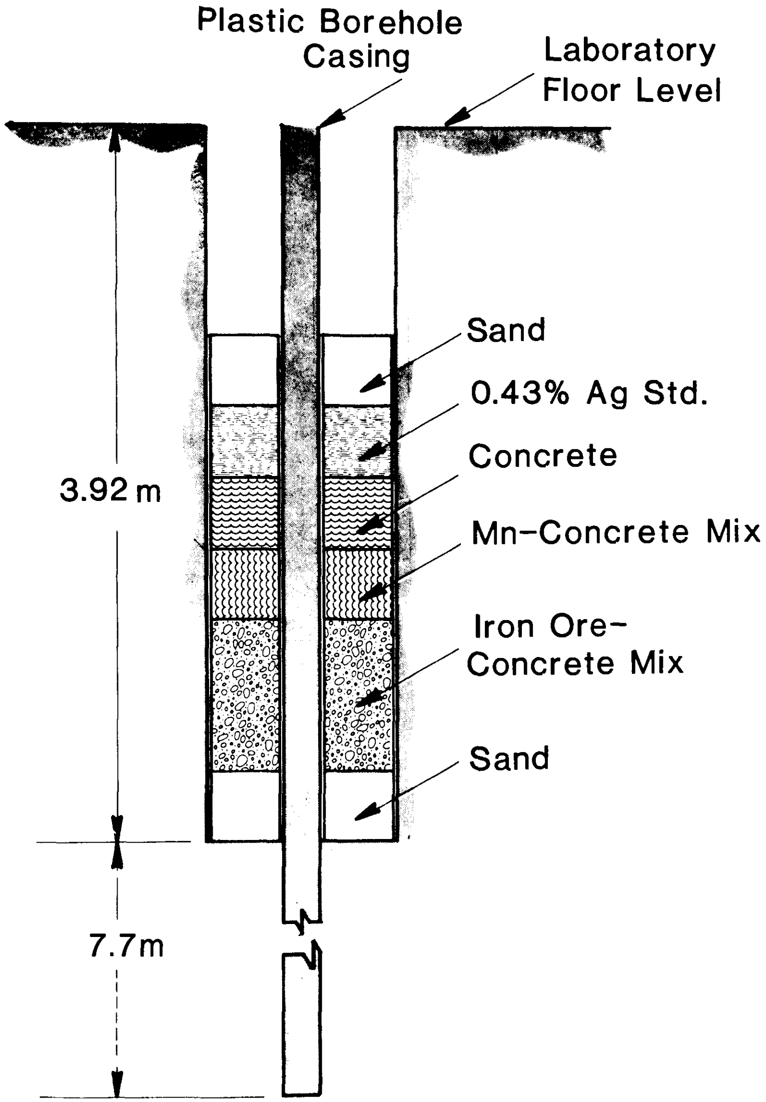
Plastic Borehole Casing
Laboratory Floor Level
Sand
0.43% Ag Std.
Concrete
Mn–Concrete Mix
Iron Ore–Concrete Mix
Sand
3.92 m
7.7m

FIG. 2.

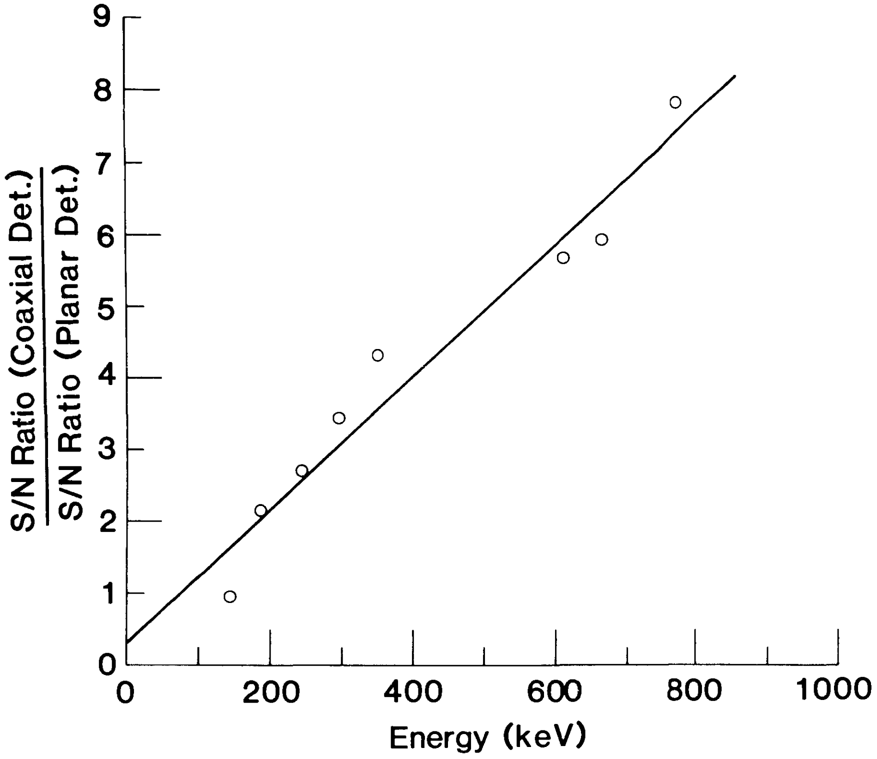
S/N Ratio (Coaxial Det.)
S/N Ratio (Planar Det.)
0
1
2
3
4
5
6
7
8
9
0
200
400
600
800
1000
Energy (keV)

FIG. 3.

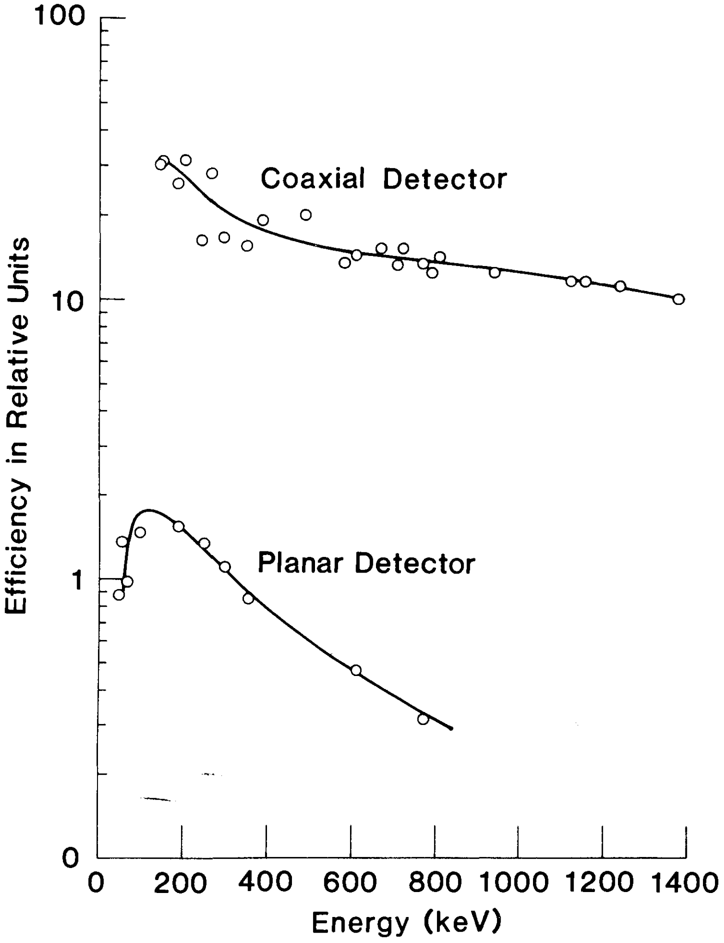
Efficiency in Relative Units
100
10
1
0
Coaxial Detector
Planar Detector
0
200
400
600
800
1000
1200
1400
Energy (keV)

FIG. 4.

CONTRIBUTED PAPERS

DETERMINATION OF ROCK PROPERTIES IN A METAMORPHIC/IGNEOUS FORMATION BY INTEGRATED FORMATION EVALUATION

R. C. A. Peveraro
Britoil plc
150 St. Vincent Street
Glasgow, G2 5LJ
Scotland, U.K.

ABSTRACT

A series of target horizons in Pre-Cambrian rocks was penetrated, and an exhaustive program of data acquisition was conducted. Apart from a comprehensive suite of wireline logs, the formation was extensively cored, and drill stem tested.

Rock formations were identified lithologically and mineralogically by careful core description, and emission and mass spectroscopy was performed on a number of selected and preserved samples for element identification.

Whole core analysis was performed on selected and preserved core samples to determine porosities, permeabilities, grain densities, and wherever possible, capillary pressures.

A "conventional" log analysis was then performed, that is using tool responses in the "conventional" lithologies as far as possible. Results obtained were in some instances acceptable, although a substantial number of descrepancies came to light, which were in stark contrast with the known facts.

It was then decided to attempt to explain these discrepancies in the light of anomalous tool responses, and the necessity to obtain a different set of calibration parameters and tool responses was identified. This was particularly apparent for the formation density and compensated neutron porosity tools.

On the basis of the rock analyses, tool responses were calibrated accordingly, and log analysis results were produced, using an integrated tool response approach, corresponding to the lithologies and elements identified as particularly relevant. Particular care was taken to include the effects of the existing fracture network, and of the presence of heavily mineralized zones (pyrite, etc.).

The results of drill stem tests were finally interpreted in the light of the petrophysical and geological environment obtained.

The sequence of data acquisition and the process of calibration and interpretation are presented, and the results are shown and discussed.

INTRODUCTION

Despite previous work on the subject (ref. 1, 2) there is, unfortunately, still a noticeable shortage of published documentation on both the necessary parameters and methodology for the geophysical interpretation of igneous and metamorphic rocks. The first problem in the interpretation is that of defining the necessary parameters to accurately describe the rock matrix. Various sources exist, but these are mostly confined to laboratory measurements on downhole samples from a specific area, and as yet these parameters have not been universally defined as they have been for sedimentary structures. The second problem is one of defining a suitable model for the interpretation, as the classical models which are well suited to sedimentary lithologies at best may be unsuited to igneous/metamorphic rocks and at worst may be totally unusable.

This paper describes the sequence of events undertaken in the geophysical interpretation of a Pre-Cambrian igneous/metamorphic sequence. The interpretation model to be used had to be capable of handling the often complex mixture of "unusual" non sedimentary components which constitute the matrix of metamorphic rocks, and the log responses associated with these minerals. In particular, the responses of the radioactive source porosity tools are usually affected, but in the case of accessory minerals such as Pyrite even resistivity logging devices can be affected. The model chosen for this study was that developed by Peveraro and Cable (ref. 3) in which the result is achieved by solving a matrix of simultaneous equations, each equation describing the response of a given logging device to the volume proportions of the constituents of the rock matrix. This method suited the particular structure under study in that it was capable of simultaneously making use of whatever logs were available, and also allowed the matrix to be described in terms of several components, each with their own specific log responses. In addition, the error computation built into the model allowed the refinement of the parameters chosen.

DATA ACQUISITION SEQUENCE

The Pre-Cambrian sequence under study was penetrated at a depth of 4150' and the formation was cored/drilled to a total depth of 4595'. Both sample and solvent fluorescence were recorded from 4200' - 4250' and from 4415' - 4595', with occasional traces of methane recorded, and traces of methane recorded as trip gas when changing from drilling bit to core barrel and vice versa. On reaching total depth the following wireline logs were run:

COMPENSATED DENSITY/COMPENSATED NEUTRON/GAMMA RAY.
INDUCTION ELECTRICAL LOG/SPONTANEOUS POTENTIAL.
ACOUSTIC TRAVEL TIME/VARIABLE DENSITY.
FRACTURE IDENTIFICATION LOG.
DUAL LATEROLOG/MICRO LATEROLOG.
MINILOG (MICRO INVERSE/MICRO NORMAL).
NATURAL GAMMA RAY SPECTROMETRY LOG.
FORMATION TESTER.

Two open hole drill stem tests were conducted. In Drill Stem Test #1 the entire interval from the 9 and 5/8" casing shoe at 4021' - 4595'. For Drill Stem Test #2 the open hole interval was plugged back to 4300' and the interval from 4021' - 4300' was tested.

Full diameter core samples were selected at various intervals throughout the section for conventional analysis. These were first cleaned in hot refluxing solvents and thoroughly dried at 60°C. Two horizontal air permeabilities were than measured, a maximum, and another at 90° to the maximum, together with a vertical air permeability, helium injection porosity and grain density.

Another seven samples were sent for a more detailed analysis, in an attempt to better define the geological history and mineral composition of the interval. These samples were analysed by x-ray diffraction to help define mineralogy, and thin section samples were cut and were examined using Scanning Electron Microscopy.

Initially, when examining the logs from this well it was thought that the porosities recorded by the neutron tool were anomalously high, and with this in mind three samples were selected in zones corresponding to high neutron readings and an elemental analysis was performed on these samples using atomic absorption and spark source spectrometric analysis methods.

INITIAL INTERPRETATION

With the well logs and the wellsite core and cuttings as the only data available, a preliminary petrophysical interpretation was attempted. The wellsite geological information indicated the entire metamorphic sequence from 4150' RKB to a total depth of 4590' RKB consisted of Lewisian basement gneiss, the result of high grade regional metamorphism caused by an igneous intrusion. The structure also appeared to have been hydrothermally altered as witnessed by the presence of various lower grade minerals such as Pyrite and Chlorite. The gneiss was described as predominantly metaquartzite, minor plagioclase with weathered feldspar, Kaolinite, Chlorite and Pyrite present in varying degrees. A composite plot of the neutron, density, sonic, and laterolog resistivity over the interval is shown as Figs. 1, 2. Initially, the logs were examined with a view to identifying the most likely zones of fracturing. These were identified as follows:

- "cycle skipping" on the sonic transit time.
- separation of the shallow and deep laterolog resistivity curves.
- "Chevron" patterns and compressional-shear wave interference on the open hole variable density log.
- curve separation on the fracture identification log.

The most probable fractured zones were identified as being from 4180' - 4240' RKB and 4460' - 4530' RKB. In an attempt to establish a relationship between apparent porosity and resistivity the conventional crossplots of Δt, ρb and ØN vs $1/\sqrt{Rt}$ were made and these are enclosed as Figs. 3, 4, 5. Rt was taken from the dual laterolog as the induction curve was often saturated.

The next task was that of defining the matrix parameters. Several "anomalies" were discovered in this area in trying to treat the section as one would treat a normal sedimentary section. The conventional litho-porosity crossplots between ρb, ØN and ΔT were made but these did not provide any clear indications that there was a predominant matrix component, let alone define its parameters. Previous work on defining matrix logging parameters in metamorphic sections sometimes has stated that the matrix parameters of metamorphosed rocks are not dissimilar to their sedimentary counterparts. This may be the case, but in this particular study the rock matrix itself appears to vary considerably, thus producing the scatter seen on crossplots. One persistent feature which can be seen in various intervals throughout the section is that in the zones of lowest natural radioactivity, on the limestone compatibly scaled density/neutron log the neutron porosity may be up to twice that of the indicated density porosity. This could be due to the presence of heavy accessory minerals affecting the density log, or the presence of a clay such as chlorite which has low gamma radiation and would seriously affect the neutron log values, or indeed the presence of an element which was a strong neutron absorber. It was soon obvious that to attempt to treat the section using normal sedimentary models would require very simplistic assumptions. To treat the interval using a complex mineral model which allowed only the options of the normal sedimentary minerals of sandstone, limestone and dolomite would only further enhance the uncertainties, so in order to produce an initial interpretation it was decided to employ a single mineral model with a single clay component, and to assume "average" apparent matrix parameters and "average" apparent clay parameters. The crossplots (Figs. 3, 4, 5) used to determine Rw all showed a reasonably clear trend towards matrix points and these values were used, ØN = 0, ρb = 2.7, and ΔT = 50. The "average" clay parameters were chosen from the lithoporosity crossplots (Figs. 6, 7, 8) which have the Z-variable as of gamma ray. These were chosen as $\rho b_{sh} = 2.58$, $\Delta t_{sh} = 55.0$, and $\emptyset N_{sh} = 0$. It can then be seen immediately that having chosen these "average" shale parameters their values are

sufficiently close to the chosen matrix parameters that there would be little or no resolution in the computation of the clay volume fraction using either density, neutron or sonic logs.
As the spontaneous potential was very "slow" in character, the gamma ray was used to compute the volume of clay using minimum and maximum values of 25 API and 145 API respectively. Using this computed V_{CL} and the clay and matrix parameters chosen above the initial interpretation was carried out using a neutron/density crossplot porosity and an Rw of 0.09Ωm at a bottom hole temperature of 125°F derived from the crossplots of Fig. 3, 4, 5. The resultant output plot is shown as Fig. 9.

CORE ANALYSIS RESULTS

In any interpretation in this sort of structure, core analysis is invaluable as a guide to the minerals which constitute the rock matrix, and core derived porosity and grain density measurements are also useful in that they can be used to ensure that the model chosen for the interpretation of the well logs is valid and produces coherent results. The first results to be received and examined were the conventional measurements performed on the full diameter samples. These are tabulated overleaf as Table 1.

The necessary core slips have been accounted for using the core gamma log and the quoted depths are log depths.

It can be seen immediately that in the two highly fractured zones there is a development of porosity and the values found in the initial interpretation are reasonable, although consistently slightly high.

TABLE 1 - Core Analysis Results

Log Depth	Perm. to Air (MD) Horizntl	90°	Vertical	Ø Helium	Grain Den.
4172.0	24.00	12.00	0.66	4.5	2.70
4172.7	23.00	20.00	9.90	9.5	2.69
4174.0	1170.00	1140.00	27.00	9.7	2.75
4175.7	19.00	19.00	16.00	11.0	2.69
4176.6	57.00	48.00	68.00	11.0	2.71
4221.7	0.29	0.25	0.44	22.1	2.74
4222.7	2.00	0.45	0.99	22.2	2.85
4224.3	0.56	0.30	0.51	19.7	2.80
4225.7	0.66	0.39	0.47	19.4	2.90
4227.0	0.34	0.21	0.27	13.3	2.74
4228.7	0.11	0.08	0.07	9.2	2.76
4268.0	<0.01	<0.01	<0.01	0.5	2.72
4269.0	0.01	<0.01	<0.01	0.9	2.75
4271.0	0.10	0.04	<0.01	1.0	2.73
4272.0	<0.01	<0.01	<0.01	0.8	2.72
4273.4	<0.01	<0.01	<0.01	1.6	2.76
4276.7	0.07	0.01	0.08	1.4	3.02
4291.5	0.01	0.05	<0.01	0.0	2.76
4293.6	0.06	<0.01	0.05	2.1	2.85
4449.1	1.90	0.33	0.08	3.0	2.89
4450.2	0.03	0.12	0.09	2.7	2.91
4453.0	1.40	0.01	<0.01	1.9	2.86
4455.0	<0.01	0.06	0.01	2.5	2.86
4457.0	<0.01	<0.01	<0.01	0.9	2.72
4458.0	0.74	0.22	<0.01	3.3	2.76
4460.0	<0.01	<0.01	<0.01	0.2	2.72
4462.0	<0.01	0.17	<0.01	6.3	2.81
4512.0	0.01	0.03	<0.01	11.9	2.74
4514.0	<0.01	0.03	<0.01	15.4	2.83
4515.0	1.30	5.40	0.11	13.9	2.80
4516.0	<0.01	0.05	<0.01	7.0	2.72
4519.0	5.70	21.0	1.60	4.3	2.71
4522.0	<0.01	0.07	<0.01	7.2	2.76

This is in disagreement with the fact that the "average" grain density of 2.70 g/cc which was used is significantly lower than the average of the grain densities measured by core analysis which is 2.78 g/cc. If the initial interpretation were redone with the grain density of 2.78 g/cc seen from cores the resultant discrepancy in porosity would be even greater.

The results of the x-ray diffraction and scanning electron microscope work are too voluminous to be individually assessed within the scope of this paper. A summary of the analysis concluded that the sequence had been hydrothermally altered to varying degrees, the most intensely altered zones coinciding with the areas previously identified as being heavily fractured. The feldspars in these sections had been altered to clay which seemed to be mainly kaolinite, indicating that the pH of the percolating was acidic as kaolinite had been formed in preference to illite. It was also thought that the interval composed of a suite of rocks which had undergone contact metamorphism perhaps with the introduction of a nearby igneous intrusion. The samples from the heavily fractured zones which appeared brecciated due to hydrothermal alteration would have been spatially closer to the intrusion while the interval between the fractured zones was further away and hence only affected by the heat and associated fluids at fairly low pressure.

A summary of the x-ray diffraction analysis of mineralogy is tabulated below as Fig. 10.

DEPTH	4175	4223	4294	4450	4460	4514	4519
QUARTZ	42	30	7	27	19	12	46
PLAGIOCLASE	22	10	20	25	42	26	25
K-FELDSPAR	13	7	17	8	9	17	10
KAOLINITE	6	20	-	-	3	13	-
SIDERITE	2	10	5	5	5	19	2
MICA	5	-	17	2	-	3	3
CALCITE	2	2	16	1	3	5	2
TREMOLITE	-	-	6	12	2	4	-
RUTILE	-	3	2	Tr	1	2	2
PYRITE	8	Tr	2	-	4	Tr	2
ILLMENITE	-	Tr	2	2	2	2	2
HAEMATITE	-	Tr	Tr	Tr	5	Tr	Tr
DOLOMITE	-	Tr	-	-	Tr	Tr	3
TALC	-	-	4	11	1	-	-
HORNBLENDE	-	-	2	3	-	-	-
OTHERS	-	-	-	-	-	-	4

Fig. 10. Volume % mineralogical split by x-ray diffraction.
Tr = trace.

The results of the elemental analysis carried out are tabulated in the appendix as Fig. 11. For each element listed the elemental macroscopic thermal neutron absorption cross section was calculated using the relationship

$$\Sigma_i = \frac{\sigma_i \, N_A}{A_i} \rho_{ma} \, C_i \ (m^{-1}).$$

where

σ_i = elemental microscopic absorption cross section.

N_A = Avogadro's number.

A_i = atomic weight.

ρ_{ma} = matrix density of sample.

C_i = weight concentration of the element.

The list of cross sections obtained for the elements in the three samples is shown as Fig. 12, and the value for the elements were taken from ref. 9. It can be seen that the only elements of any significance to the rock cross section are those with contributions of 0.01 m^{-1} or greater, i.e. K, Ca, Fe, Si, Al, Sm, Eu, Gd and of these the elements showing significant differences among the samples are Fe, Gd and K in order of importance. The total material cross sections for each of the three samples were found by summing the individual elemental contributions. The results are shown in Table 2, together with the results of core analysis and the corresponding wireline log readings.

TABLE 2

Sample No.	1	2	3
Log Depth (ft)	4243.0	4292.5	4450.0
He Porosity $Ø_{He}$ (%)	?	~0	~3.00
Grain Density ρg (g/cc)	?	2.80	2.90
Log Bulk Density ρ_B (g/cc)	2.59	2.67	2.70
Neutron Porosity $Ø_N$ (%)	6.00	21.00	18.00
Macroscopic Cross Section $\Sigma(m^{-1})$	0.778	1.41	1.83

In calculating the cross sections two limitations must be borne in mind: the total concentration of elements does not add up to 100%. Presumably this is because of the inability of the analysis techniques used to detect elements such as oxygen which must be present in considerable amounts. However, the absorption cross section of oxygen is so low (0.0002 barns) that it will not significantly contribute to the macroscopic cross section. Similarly, significant thermal neutron absorbers such as boron and chlorine have not been evaluated because of difficulties in the experimental techniques.

Referring to Table 2, the large differences between cross sections will undoubtedly lead to differences in the neutron log response in the different materials. An estimate of the degree to which the log response of a neutron tool of the type used can be affected is obtained from Fig. 15, showing simulated count-rate ratio sensitivity with cross section, obtained from Monte Carlo simulation runs (ref. 6). In turn, Fig. 16 shows the relationship between count-rate ratio changes and porosity (ref. 10), and it can be seen that for Sample 1 the tool response would be reduced by approximately 0.97, which is insignificant in this context. For Samples 2 and 3, cross sections as calculated could cause a reduction of 0.72, causing the tool to read erroneously high by as much as 8 limestone porosity units. This agrees, on a qualitative basis at least, with the present knowledge of lithology of the well. Sample #1 is from one of the less fractured and altered zones which has not been heavily mineralized. On the other hand, Samples #2 and #3 are both from zones which x-ray diffraction and Scanning Electron Microscope work have confirmed to be of a very complex nature. It was not felt to be within the scope of the work encompassed in this paper to quantify the correction required to the neutron log with only 3 data points, and this part of the work for the time being remains only as an observation.

FINAL INTERPRETATION

In the light of the information received from core analysis it was decided to re-interpret the interval using a more sophisticated model, thereby hopefully eliminating most, if not all, of the uncertainties attached to the initial interpretation which was done by conventional methods. In summary these inconsistencies were:

(i) The matrix density used was 0.8 g/cc lighter than that indicated by core analysis, yet porosities derived from log analysis were of the same order.

(ii) In the region 4198' - 4210' a severe reduction in the porosity is calculated because of the high "clay" content indicated by the gamma ray, whereas all three porosity logs show no significant reduction in porosity.

(iii) The single mineral model used quartz and plagioclase in the matrix. Potassium feldspars could be identified by the gamma ray, being treated as a "clay" in the model, but this makes no allowance for the effect of kaolinite and accessory low grade minerals on the log response.

Full explanations of the workings of the final model used can be found in ref. 1, but in principle it operates on a system of simultaneous equations with each equation representing the response of a single logging tool. For the case of the density log,

$$\rho_b = 2.66\ V_{QUARTZ} + 2.52\ V_{FELDSPAR} + 4.99\ V_{PYRITE} + \ldots\ldots.$$

where V in each case is the volume of that component present in the unit volume. Water and hydrocarbons are similarly treated as being another constituent of the unit volume. Similar linear equations can be expressed for the gamma ray, neutron and sonic tools. In the case of resistivity measurements, a problem arises in that resistivity is obviously not linearly additive, but good success has been obtained in the past (ref. 3) by using the square root of conductivity as being linearly additive. Thus the principal tasks facing the log analyst are the choice of components to be input to the model and the log response coefficients for each component. The eventual model chosen contained 5 minerals, water and hydrocarbon. This meant that by using 5 input logs plus the unit volume equation, $\Sigma V_i = 1$, we have 6 equations in 7 unknowns and are thus under-determined, although the relatively independent nature of the equations will still ensure a satisfactory solution. This choice is by necessity a compromise between having sufficient components to accurately describe the matrix, whilst being still able to achieve a coherent mathematical solution. The table of coefficients used is shown as Fig. 14.

Component / Log Response	MIN. #1	MIN. #2	MIN. #3	MIN. #4	MIN. #5	OIL	WATER
ΔT	54	55	69	48	50	238	189
ρb	2.66	2.55	2.41	4.99	2.76	0.85	1.05
$\emptyset_N$	-3	-3	37	4	52	100	105
GR	20	250	20	0	0	0	0
$1/\sqrt{R_t}$	9.1×10^{-7}	9.1×10^{-7}	0.47	0.10	1.7×10^{-4}	0.7×10^{-7}	2.83

where MINERAL #1 = QUARTZ/PLAGIOCLASE
MINERAL #2 = POTASSIUM FELDSPAR
MINERAL #3 = KAOLINITE
MINERAL #4 = METALLIC MINERALS
MINERAL #5 = ACCESSORY MINERALS

Quartz and plagioclase have been combined as their densities are close and all other logging tool responses are more or less identical. Mineral #4 is a "composite" of the iron and titanium ore minerals characterized by their exceptionally high density, low neutron response, and high conductivity. Mineral #5 is a composite of the remaining accessory minerals typified by their high neutron response. This model is still less than perfect but the "averaging" applied to the coefficients of minerals #4 and #5 is not very severe as for both groups the logging tool characteristics are reasonably consistent. Another benefit is that whatever errors have been introduced by these assumptions are being generated only a volume percentage typically of the order of 10% as opposed to the conventional model where greater assumptions were made on the complete matrix. Ironically, the only two minerals which are ignored in this model are the two "conventional" sedimentary minerals of calcite and dolomite. However, with the exception of the sample at 4294' these have only been recorded as being very small percentages by volume of the rock matrix. In small sections of the heavily fractured zones the ΔT curve was edited out of the calculation where it was obviously cycle skipping. The results of the interpretation are shown as a plot, Fig. 13, in the appendix.

WELL TESTING

As the initial interpretation available at the completion of drilling contained many uncertainties as to the nature of the porosity and also the proportions of the pore fluids, it was decided that the interval warranted testing. Because of the mud losses encountered while drilling it was also a possibility, albeit a slim one, that the invasion into the heavily fractured zones may have been excessive and thus log derived hydrocarbon saturations were pessimistic. Although the zone did not appear particularly promising, it also had to be borne in mind that similar basement structures in the area had produced small quantities of hydrocarbons when tested.

To ensure that the potentially fractured zones were not plugged by the invasion of cement, as could occur if the zone was cased off, it was decided to test the section barefoot. Drill stem test #1 was conducted with a full air cushion in the test string, to give the maximum possible differential pressure into the wellbore at the beginning of the test. The well was allowed to flow until the hydrostatic pressure of the produced fluids caused the well to kill itself. Interpretation of the initial build up implied flow from the fractures only, with no contribution from the matrix. The indicated increase in bottom hole pressure indicated an influx of fluid of 10.5 ppg (1.26 g/cc), at a rate of 1200 BPD. In an attempt to recover more fluid than had been lost while drilling, to allow the original pore fluids to be produced, the following procedure was followed. The produced fluids were reverse circulated out and the test string circulated to diesel. The well was then allowed to flow until again the hydrostatic pressure of the produced fluids killed the flow. This cycle of displacing the produced fluids to diesel was repeated several times.

Following the disappointing results of drill stem test #1, one remaining possibility was that the produced water came from the lower fractured zone and the upper fractured zone could be capable of producing hydrocarbons if allowed to flow on its own. With this in mind a cement plug was set from T.D. at 4585' to 4300' to test the upper fractured zone on its own. The same test procedure was followed as for DST #1 with the exception that the test string was diesel filled instead of air filled for the initial flow period. The cycle of displacing the produced fluids with diesel was carried out as before. From flow period #7 until flow period #13 the density of the produced fluid was 8.6 - 8.7 ppg (1.03 - 1.04 g/cc), strongly indicating the influx was formation water rather than mud filtrate. At that point DST #2 was terminated.

CONCLUSIONS

The conclusions to be drawn from this exercise are two-fold. Firstly, the success, or lack of it, in determining an interpretation method capable of giving acceptable results in a metamorphic rock sequence, and secondly, the broader implications of the inherent uncertainties in any examination of a non-sedimentary environment using data acquisition methods primarily designed for conventional sedimentary structures. On the first count it is felt that the final interpretation is an order of magnitude better than conventional methods in terms of the uncertainties involved. The correlation with core derived porosities and grain densities is good. The breakdown of the rock matrix into its components correlates well with the mineralogy obtained by x-ray diffraction, on a semi-quantitative basis. In a general view of the section, there is consistency with the geological model in that the largest proportions of the accessory minerals are found in the two highly altered zones. One notable exception is in the region c. 4290' where the model was obviously incapable of handling the large amounts of talc and mica reported. In the light of the final interpretation, the results of the drill stem testing are perfectly acceptable. The two main fracture zones both have high water saturations, and the only encouraging oil saturations are calculated in zones such as that mentioned above c. 4290' and these are most likely erroneous. In summary, it is felt that this approach is one which will give reasonably good results in non-sedimentary environments universally, with the provision that analysis of cores or cuttings is available to define mineralogy.

On the broader issue of data acquisition in non-sedimentary structures, all the limitations of conventional logging tools are highlighted. Direction of fractured zones, and in some way quantifying the degree of fracturing, is still more of an art than a science. Development of existing borehole viewers or of an acoustic device working on a micro-scale rather than a macro scale may help in this respect. The validity of the Wylie time average equation is being questioned in sedimentary structures, and the relationship between acoustic travel time and "porosity", of whatever nature, is even less well defined in fractured formations. Typically, neutron porosity devices in this type of structure are working in their range of least performance, i.e. very low porosities. Extensive analysis of core samples by x-ray diffraction, mass spectrometry and other methods can provide the required accurate description of the rock composition on a discrete sample basis. To do this with a high degree of confidence on a continuous interval basis will require further development of our knowledge of the response of existing logging devices, or indeed perhaps the design of new logging devices.

ACKNOWLEDGEMENTS

The author would like to offer his thanks to Britoil plc for access to the necessary information and permission to publish this paper, and also to Dr. J. Hook for his investigating of neutron absorption cross sections, to D. J. Blackwood for his extensive help in the computations, and to his colleagues in Petrophysics for numerous helpful discussions.

REFERENCES

1. Daniels, J.J., J.H. Scott and G. Olhoeft: Interpreting Precambrian Metamorphic Geology from Geophysical Well Logs. SPWLA 22nd Annual Logging Symposium Transactions, 1981, Vol. 1, Paper T.

2. Scott Keys, W.: Borehole Geophysics in Igneous and Metamorphic Rocks. The Log Analyst, July-August 1979, 14-28.

3. Peveraro, R.C.A. and H.W. Cable: Determination of Rock Properties by Quantitative Processing of Geophysical Borehole Logs. 1982 European Petroleum Conference Proceeding (EUROPEC), Paper EUR273.

4. Carmichael, R.S. (Editor): Handbook of Physical Properties of Rocks. CRC Press, 1982.

5. Edmundson, H. and L.L. Raymer: Radioactive Logging Parameters for Common Minerals. The Log Analyst, September-October 1979, 38-47.

6. Mining Instrumentation and Advisory Service, Atomic Energy Research Establishment: Report No. 12. Harwell, 1982.

7. Dresser Atlas Log Interpretation Charts. Dresser Industries, Inc., 1979.

8. Formation Evaluation Data Handbook. Gearhart Industries, Inc., 1982.

9. Mughabghab, S.F. and D.I. Garber:
Neutron Cross Sections, BNL 325.
National Neutron Cross Section Center,
Brookhaven National Laboratory, 1973.

10. Neutron Logs.
Dresser Atlas, Dresser Industries, Inc., 1980.

Figure 1. Density, Neutron and Sonic Logs

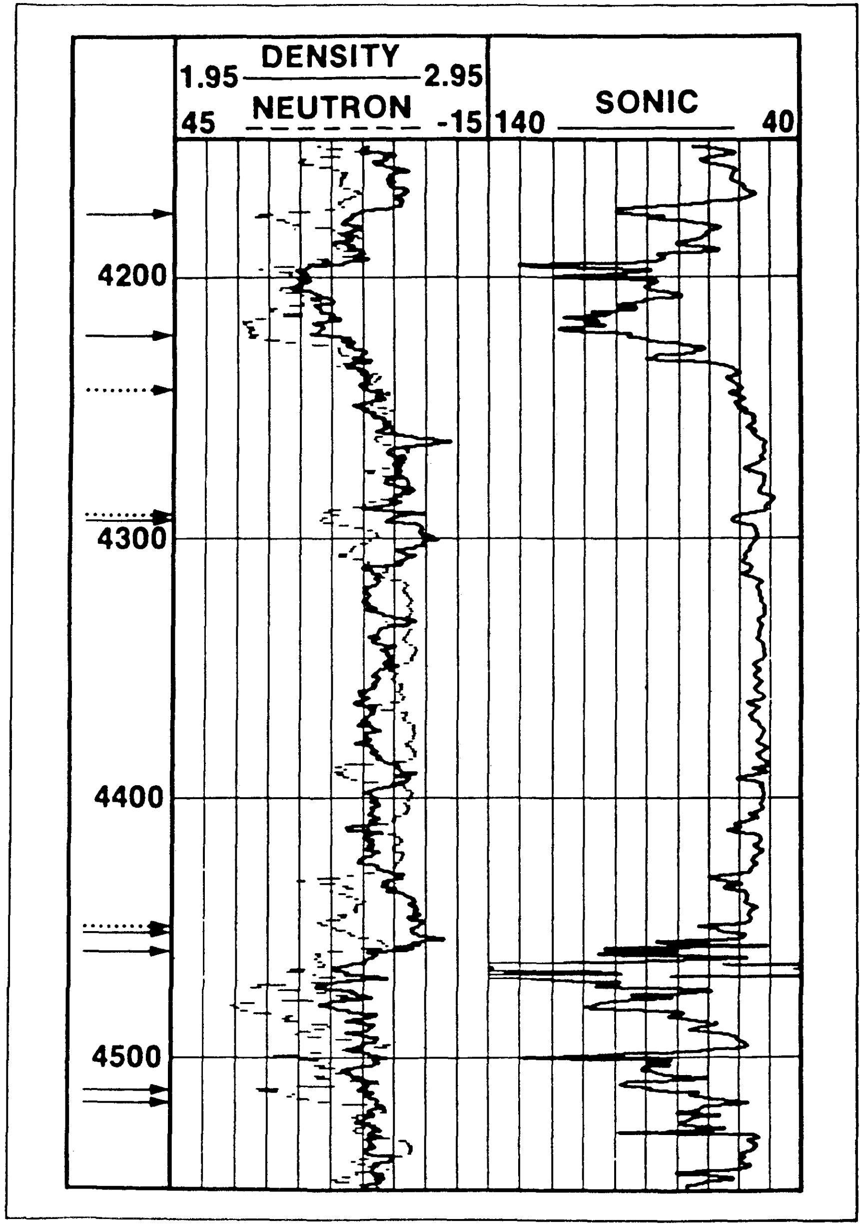

Figure 2. SP, Gamma Ray and Dual Laterolog

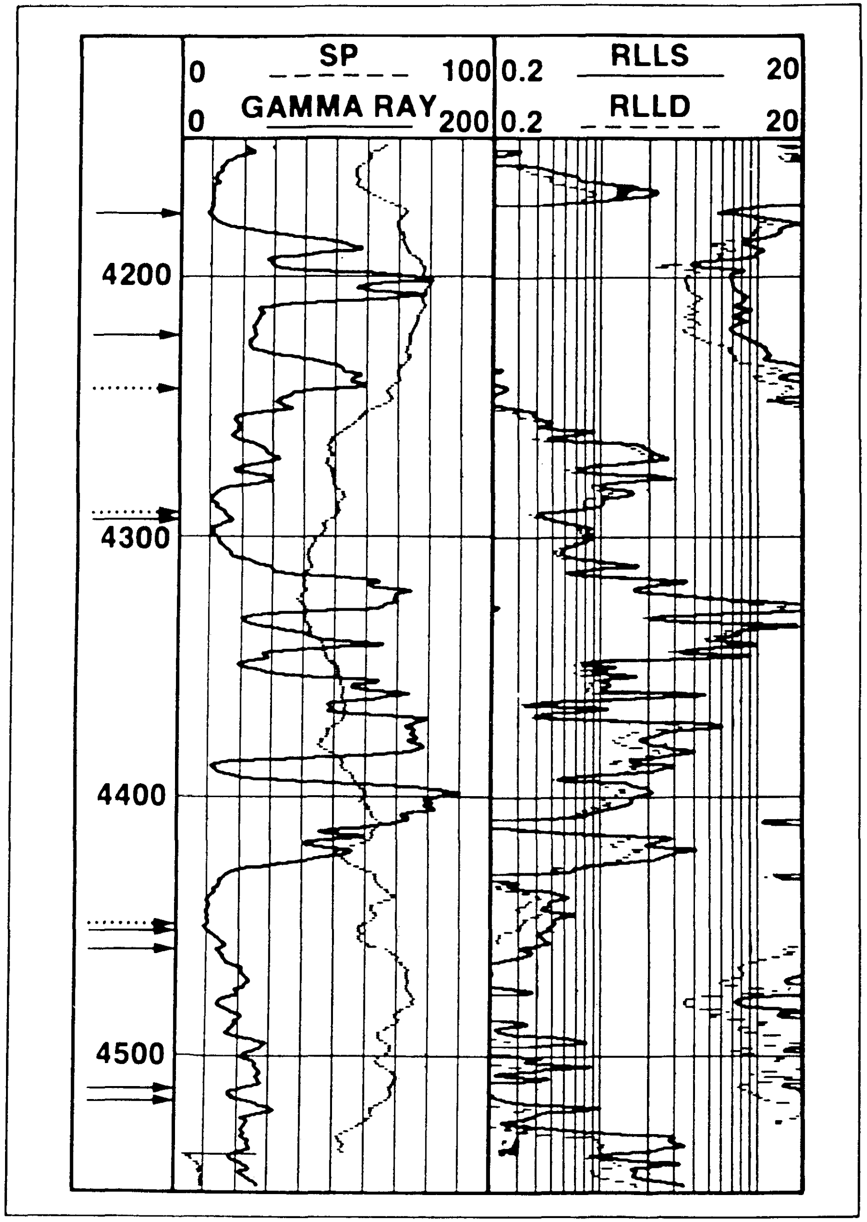

Figure 3.

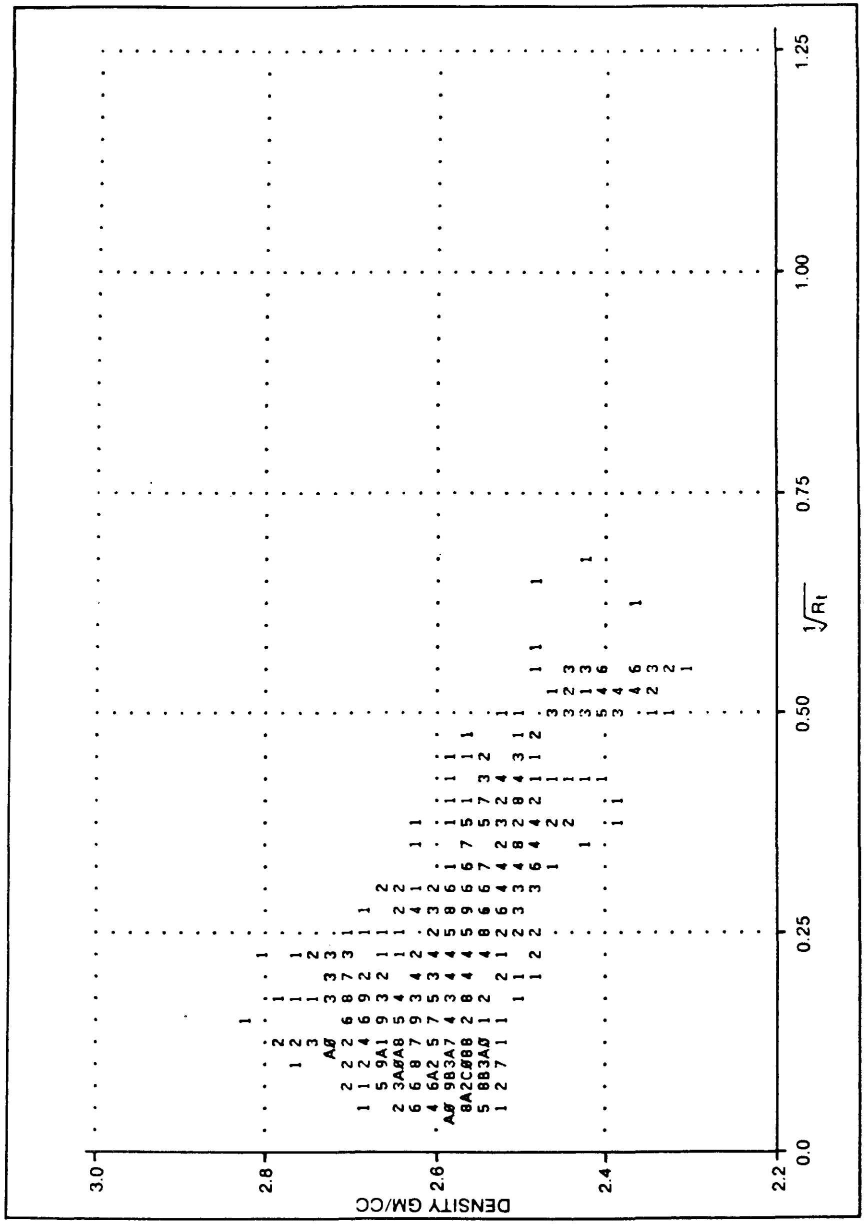

Figure 4.

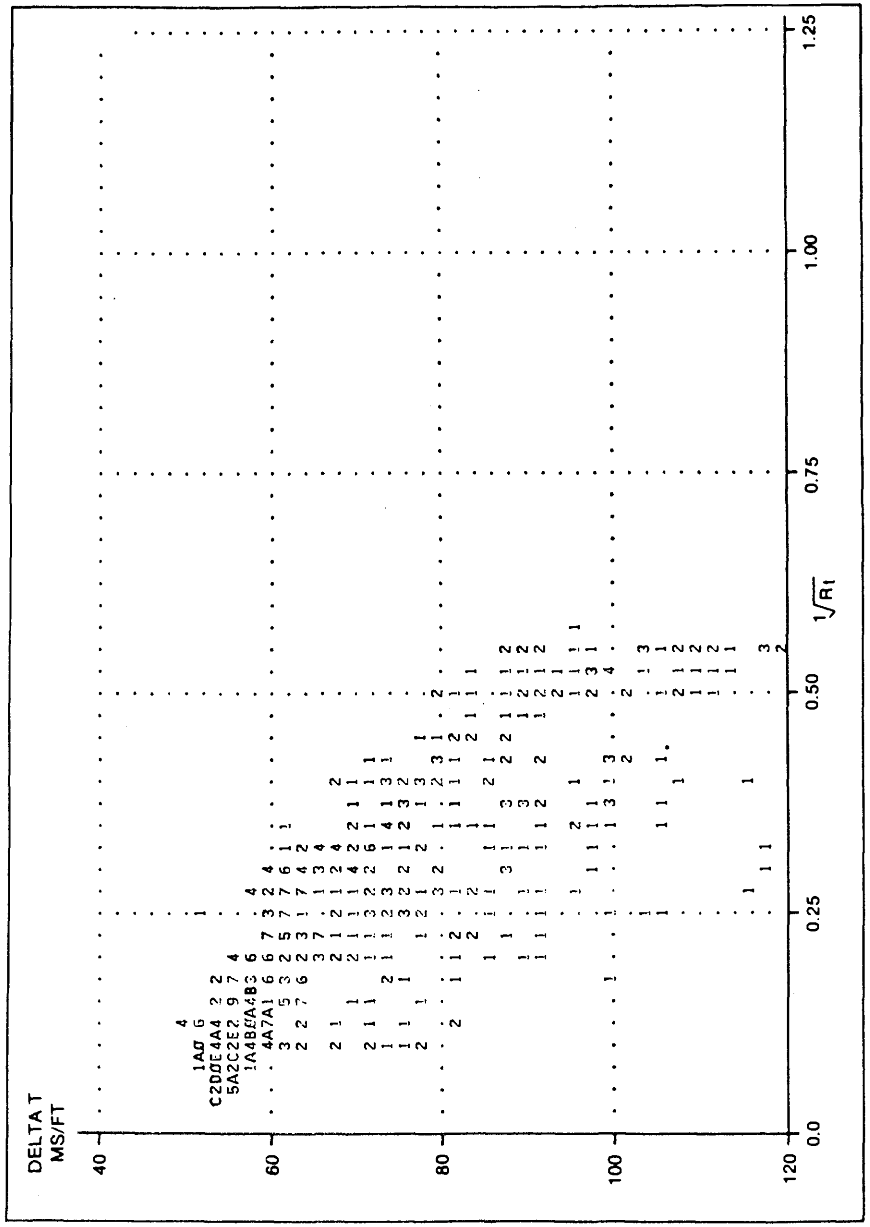

Figure 5.

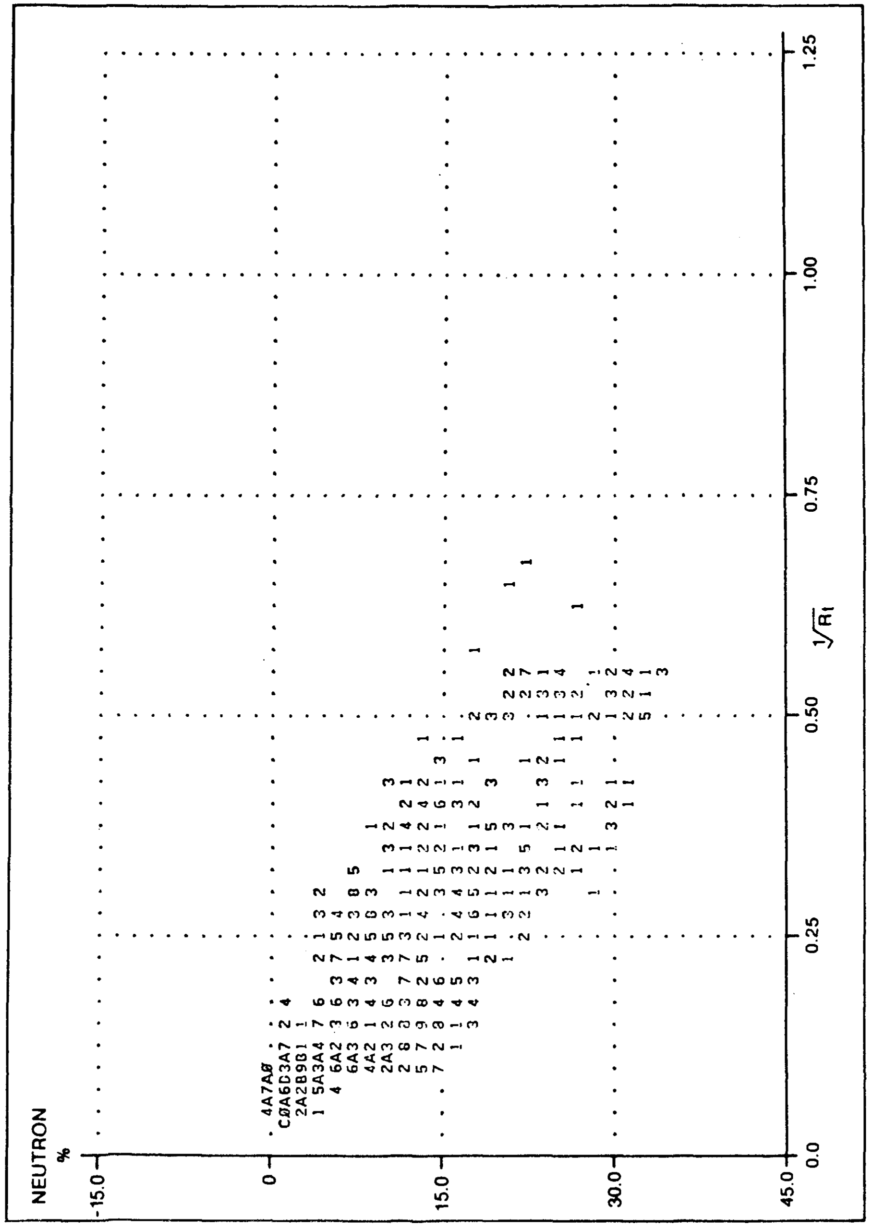

Figure 6.

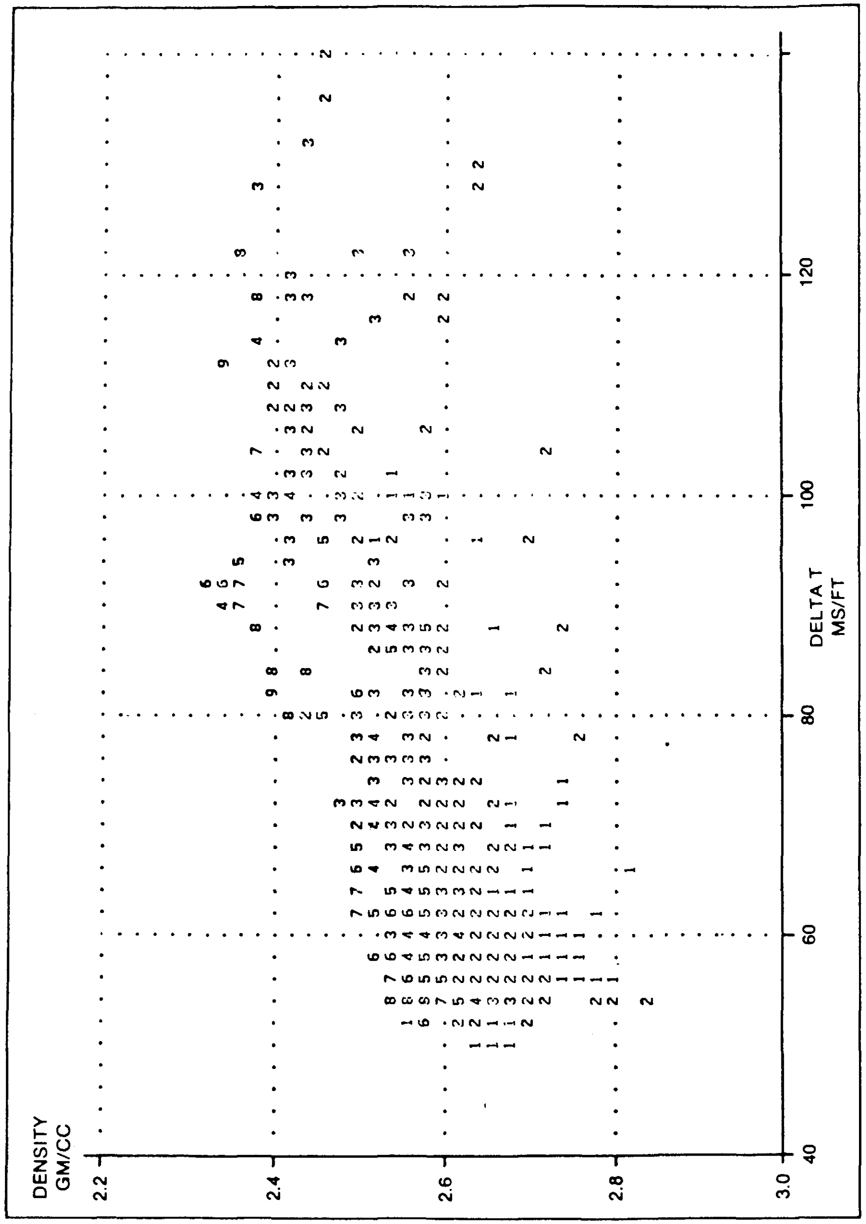

Figure 7.

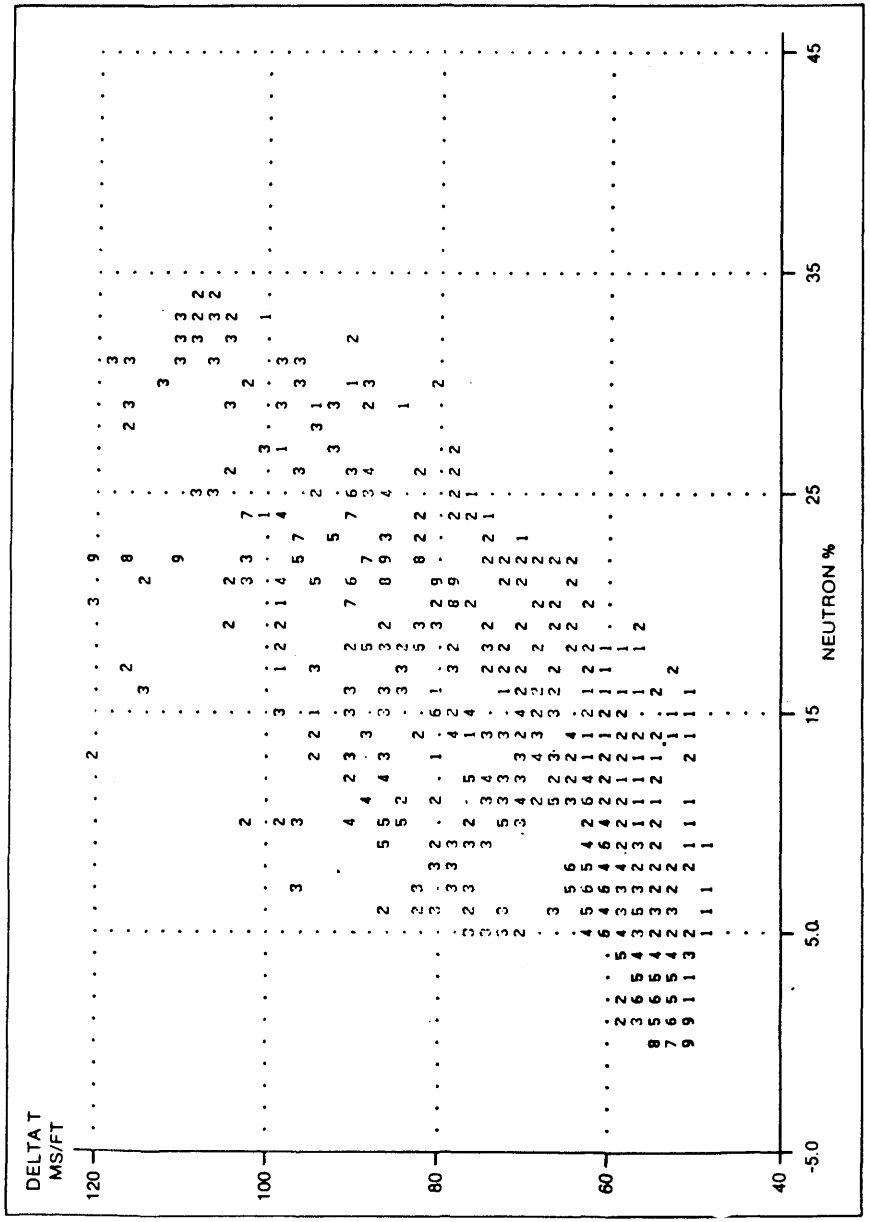

Figure 8.

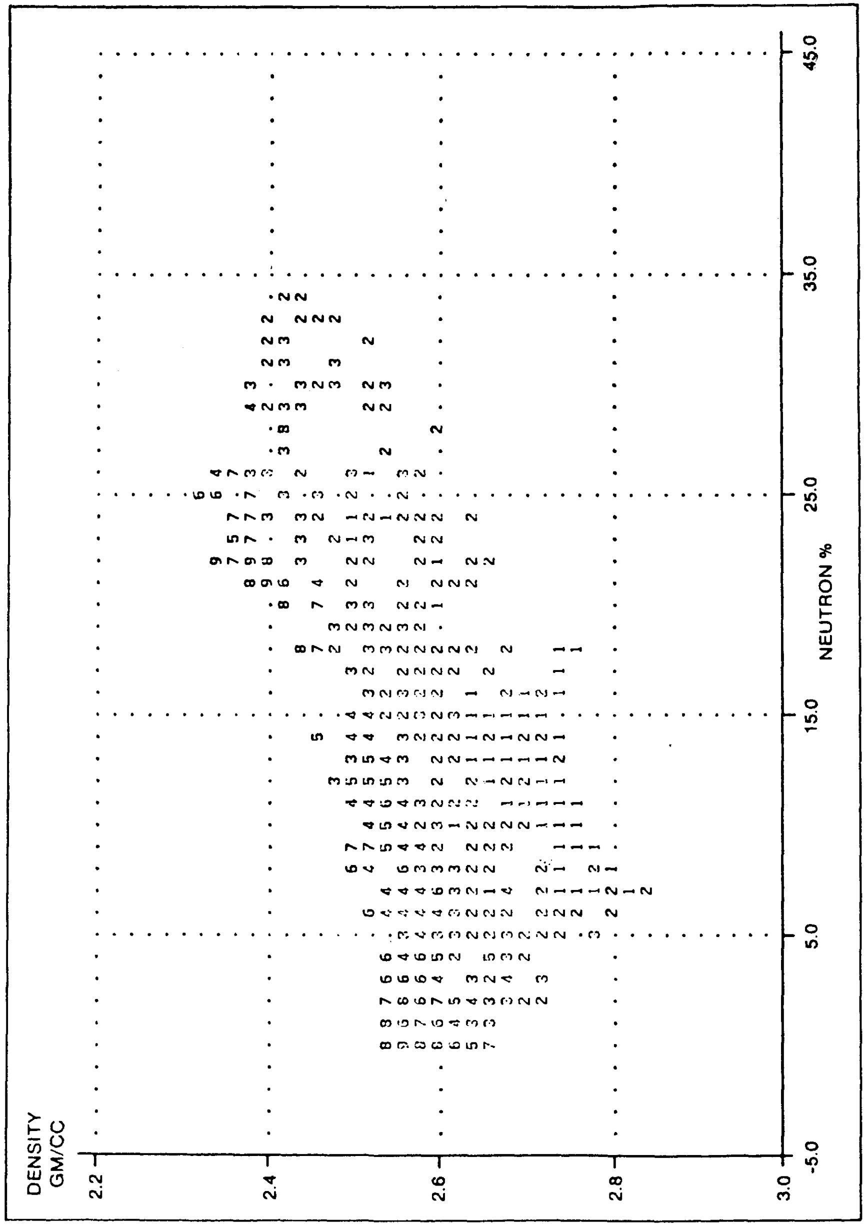

Figure 9.

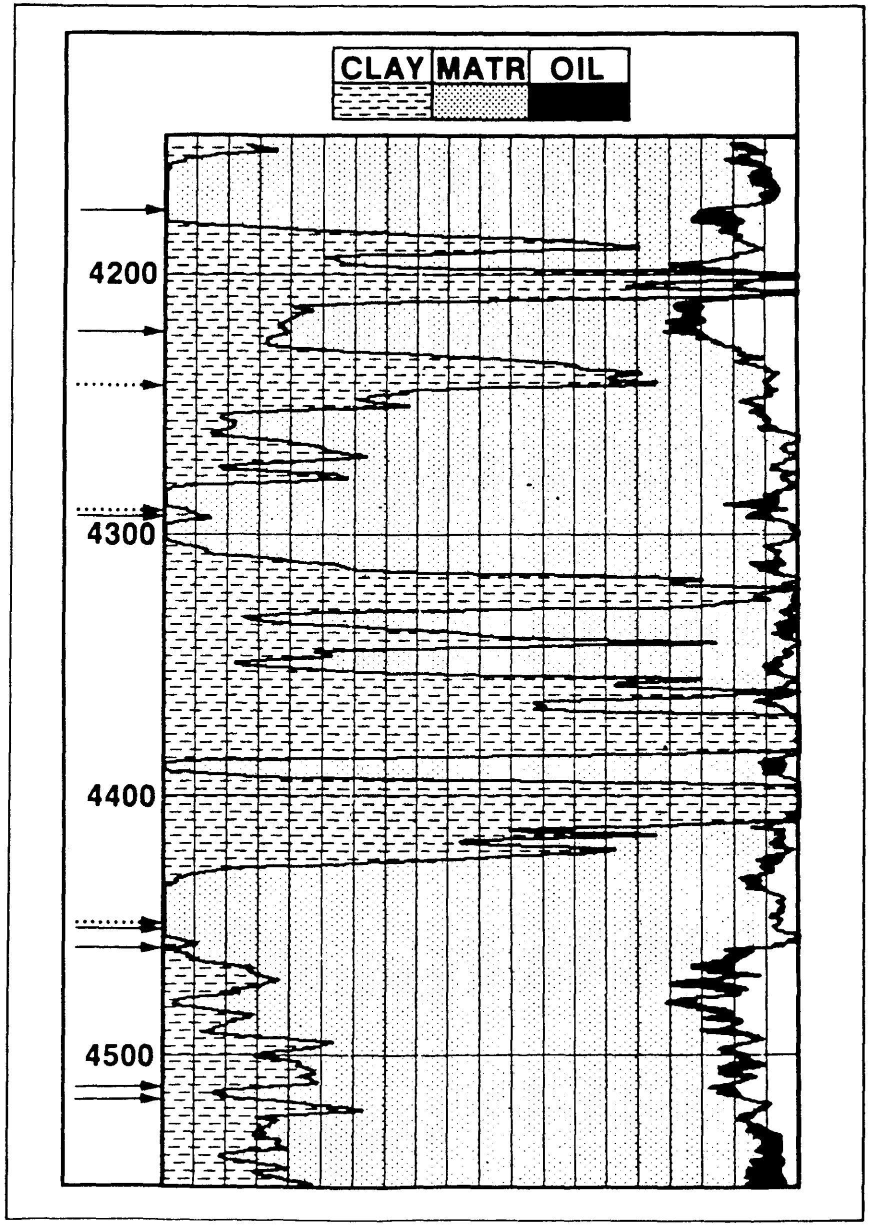

Figure 11a. Elemental Composition

	Composition (ppm)		
Element	4243ft	4292ft	4450ft
K	19900.0	5600.0	3900.0
Ca	14000.0	35700.0	16700.0
Fe	15220.0	52820.0	125200.0
Si	218900.0	179500.0	174400.0
Al	56400.0	77300.0	59900.0
Ag	1.0	0.9	0.7
Sn	1.4	1.8	5.0
I	1.1	1.0	0.6
Cs	0.9	2.6	5.9
La	150.0	13.0	11.0
Ce	200.0	24.0	33.0
Pr	25.0	12.0	10.0
Nd	86.0	70.0	28.0
Sm	18.0	16.0	12.0
Eu	3.0	3.6	4.3
Gd	2.4	8.3	6.4
Tb	0.5	1.2	1.4
Dy	2.3	6.2	16.0
Ho	0.6	0.9	1.8
Er	2.3	4.5	4.6
Tm	0.9	0.5	0.8
Yb	7.5	4.4	6.9
Lu	0.3	0.4	0.7
Hf	3.8	5.1	2.4
Ba	1500.0	1000.0	200.0
Be	10.0	10.0	10.0
Bi	30.0	30.0	30.0
Co	3.0	20.0	20.0
Cr	8.0	25.0	1.0
Cu	3.0	60.0	25.0
Ga	20.0	20.0	25.0
Mn	250.0	600.0	600.0
Mo	1.0	1.0	1.0
Ni	10.0	40.0	40.0
Pb	80.0	4.0	10.0
Sn	3.0	3.0	3.0
Sr	300.0	1000.0	300.0
V	8.0	60.0	150.0
Y	10.0	30.0	15.0
Zr	250.0	200.0	300.0

Figure 11b. Rock composition by element.

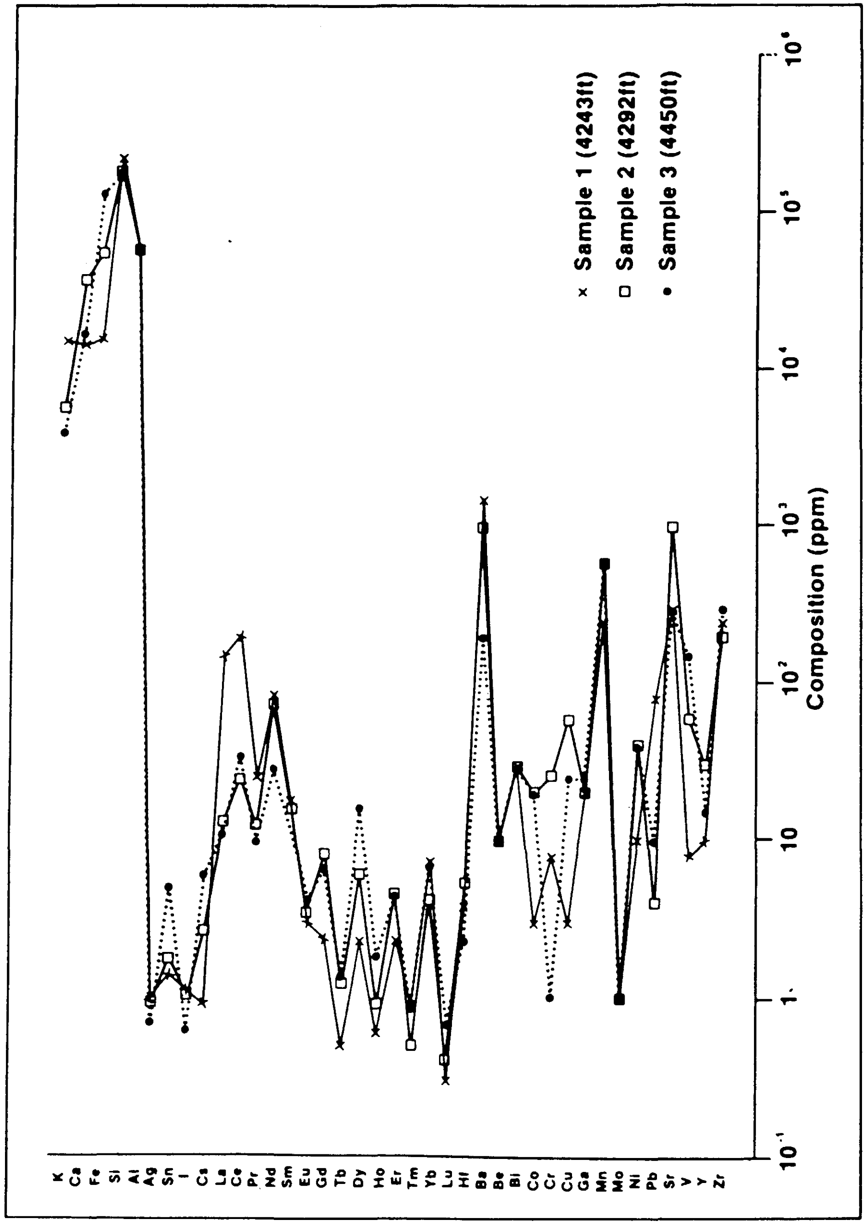

Figure 12a. Elemental Macroscopic cross-section.

Element	σi	Elemental Macroscopic Cross Section (m^{-1})		
	(10^{-28} m^2)	4243ft	4292ft	4450ft
K	2.1	0.123	0.051	0.037
Ca	0.43	0.023	0.065	0.031
Fe	2.55	0.107	0.407	0.988
Si	0.16	0.191	0.172	0.174
A1	0.23	0.074	0.111	0.089
Ag	63.6	2.080 x 10^{-4}	2.050 x 10^{-4}	1.650 x 10^{-4}
Sn	0.63	0.011 x 10^{-4}	0.016 x 10^{-4}	0.046 x 10^{-4}
I	6.2	0.083 x 10^{-4}	0.082 x 10^{-4}	0.051 x 10^{-4}
Cs	29.0	0.301 x 10^{-4}	0.957 x 10^{-4}	2.250 x 10^{-4}
La	9.0	14.900 x 10^{-4}	1.420 x 10^{-4}	1.240 x 10^{-4}
Ce	0.63	3.720 x 10^{-4}	0.490 x 10^{-4}	0.700 x 10^{-4}
Pr	11.5	3.130 x 10^{-4}	1.650 x 10^{-4}	1.430 x 10^{-4}
Nd	50.5	46.300 x 10^{-4}	41.300 x 10^{-4}	17.100 x 10^{-4}
Sm	5800.0	0.107	0.104	0.081
Eu	4600.0	0.014	0.018	0.023
Gd	49000.0	0.115 x 10^{-4}	0.436	0.348
Tb	25.5	0.120 x 10^{-4}	0.320 x 10^{-4}	0.390 x 10^{-4}
Dy	930.0	20.200 x 10^{-4}	59.800 x 10^{-4}	0.016
Ho	66.0	0.370 x 10^{-4}	0.610 x 10^{-4}	1.260 x 10^{-4}
Er	162.0	3.420 x 10^{-4}	7.360 x 10^{-4}	7.790 x 10^{-4}
Tm	103.0	0.840 x 10^{-4}	0.510 x 10^{-4}	0.860 x 10^{-4}
Yb	36.6	2.440 x 10^{-4}	1.570 x 10^{-4}	2.550 x 10^{-4}
Lu	77.0	0.200 x 10^{-4}	0.300 x 10^{-4}	0.540 x 10^{-4}
Hf	102.0	3.340 x 10^{-4}	4.910 x 10^{-4}	2.400 x 10^{-4}
Ba	1.2	20.100 x 10^{-4}	14.700 x 10^{-4}	3.050 x 10^{-4}
Be	0.0092	0.020 x 10^{-4}	0.020 x 10^{-4}	0.020 x 10^{-4}
Bi	0.033	0.010 x 10^{-4}	0.010 x 10^{-4}	0.010 x 10^{-4}
Co	37.2	2.900 x 10^{-4}	21.300 x 10^{-4}	22.100 x 10^{-4}
Cr	3.1	0.750 x 10^{-4}	2.510 x 10^{-4}	0.100 x 10^{-4}
Cu	3.8	0.280 x 10^{-4}	6.050 x 10^{-4}	2.610 x 10^{-4}
Ga	2.9	1.280 x 10^{-4}	1.400 x 10^{-4}	1.820 x 10^{-4}
Mn	13.3	93.000 x 10^{-4}	0.025	0.025
Mo	2.65	0.040 x 10^{-4}	0.040 x 10^{-4}	0.040 x 10^{-4}
Ni	4.43	1.160 x 10^{-4}	5.090 x 10^{-4}	5.270 x 10^{-4}
Pb	0.17	0.100 x 10^{-4}	0.005 x 10^{-4}	0.010 x 10^{-4}
Sr	1.21	6.360 x 10^{-4}	23.300 x 10^{-4}	7.230 x 10^{-4}
V	5.04	1.220 x 10^{-4}	10.000 x 10^{-4}	25.900 x 10^{-4}
Y	1.28	0.220 x 10^{-4}	0.730 x 10^{-4}	0.380 x 10^{-4}
Zr	0.18	0.760 x 10^{-4}	0.670 x 10^{-4}	1.030 x 10^{-4}

Figure 12b. Macroscopic Absorption cross-section for the Rock Samples, by Element

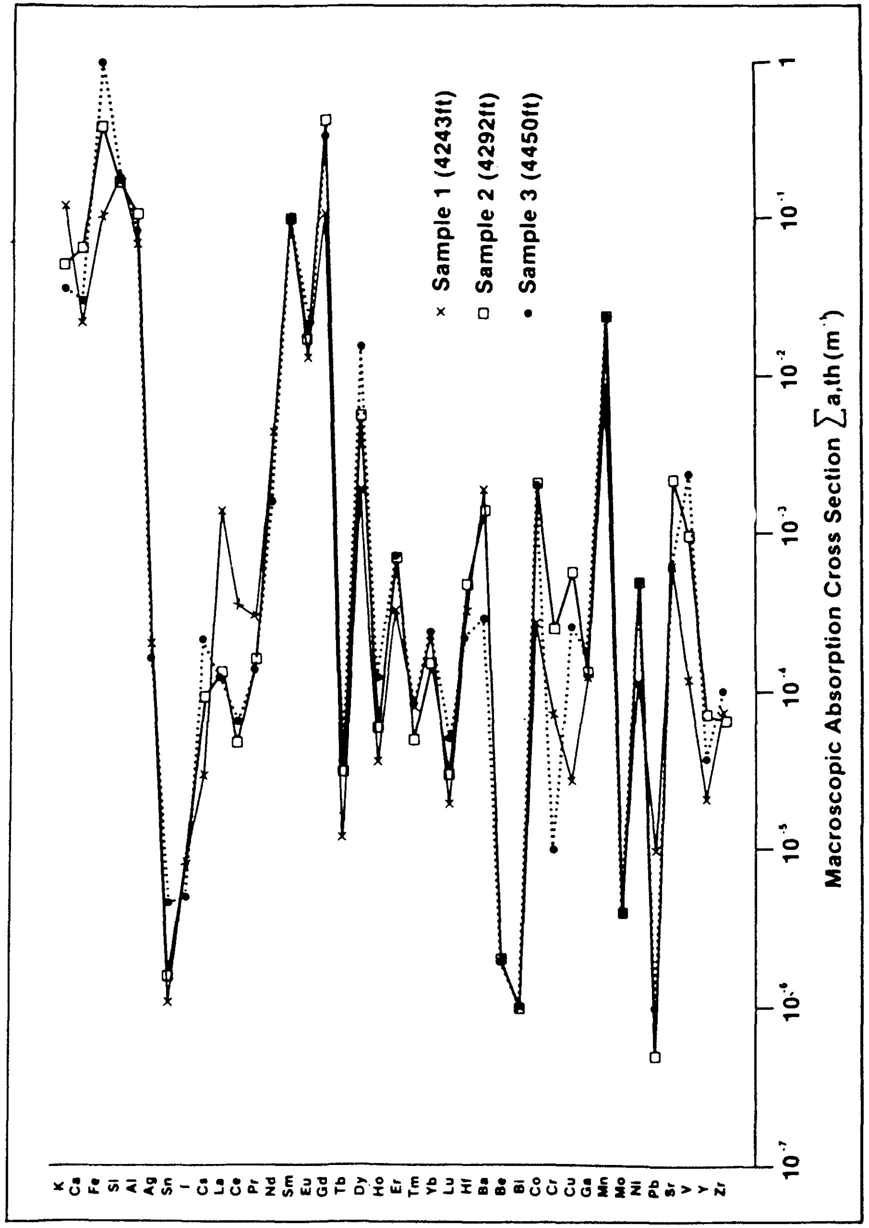

Figure 13.

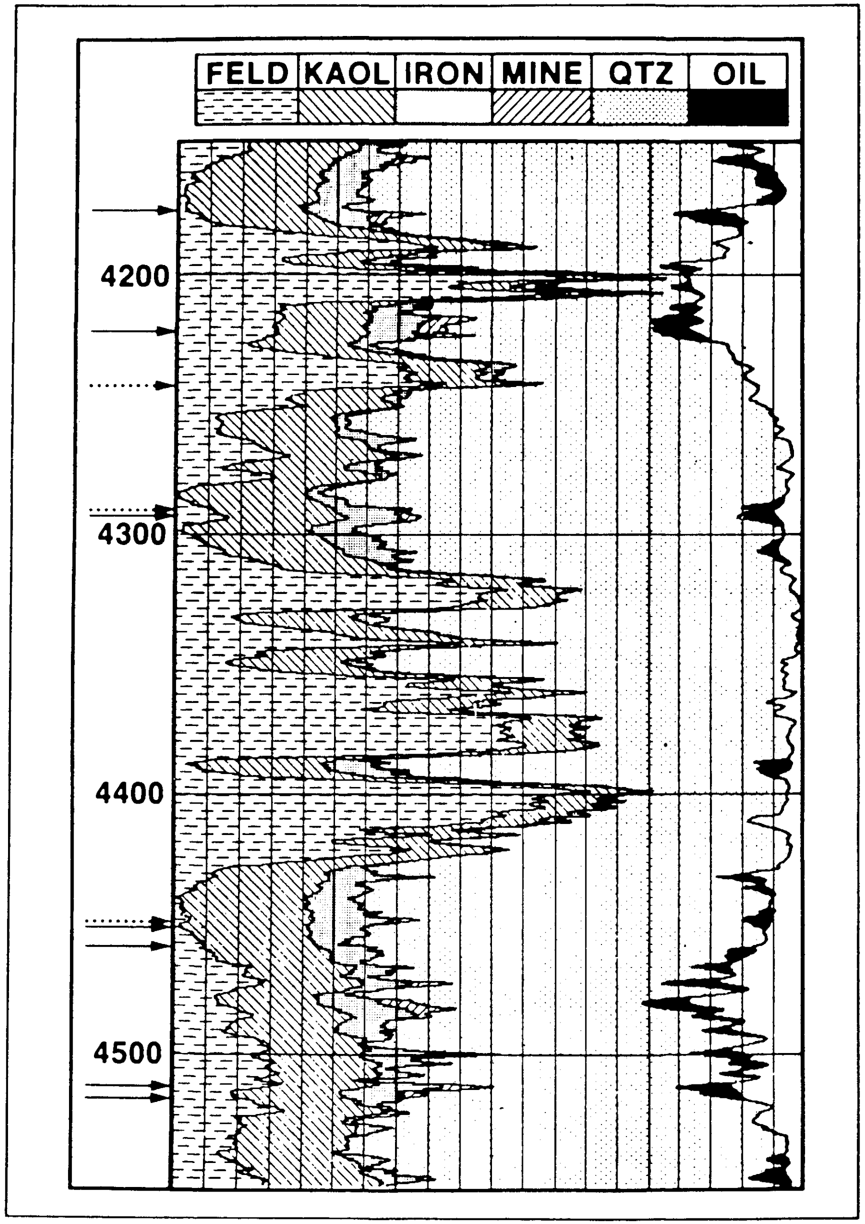

Figure 15. Monte Carlo values of tool response for increasing values of formation thermal neutron absorption.

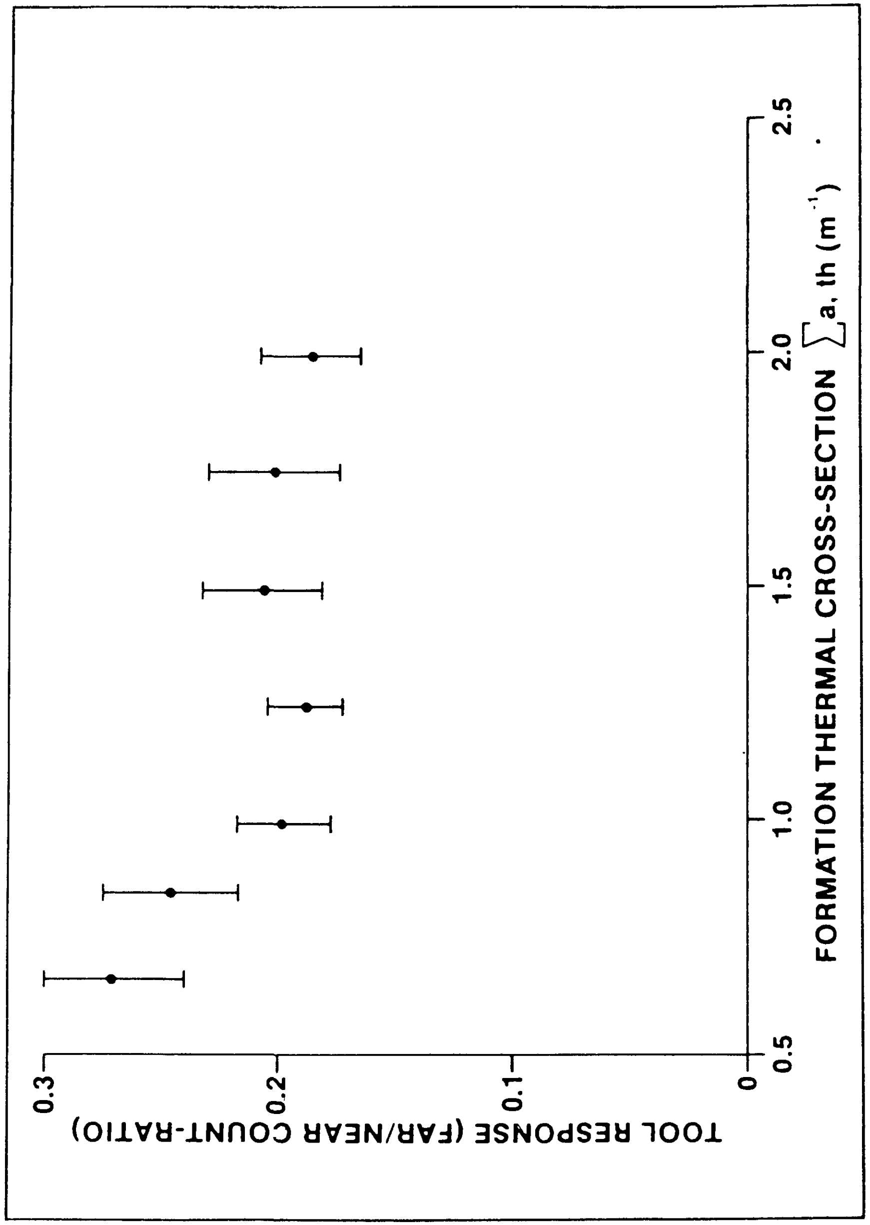

Figure 16. Tool Response.

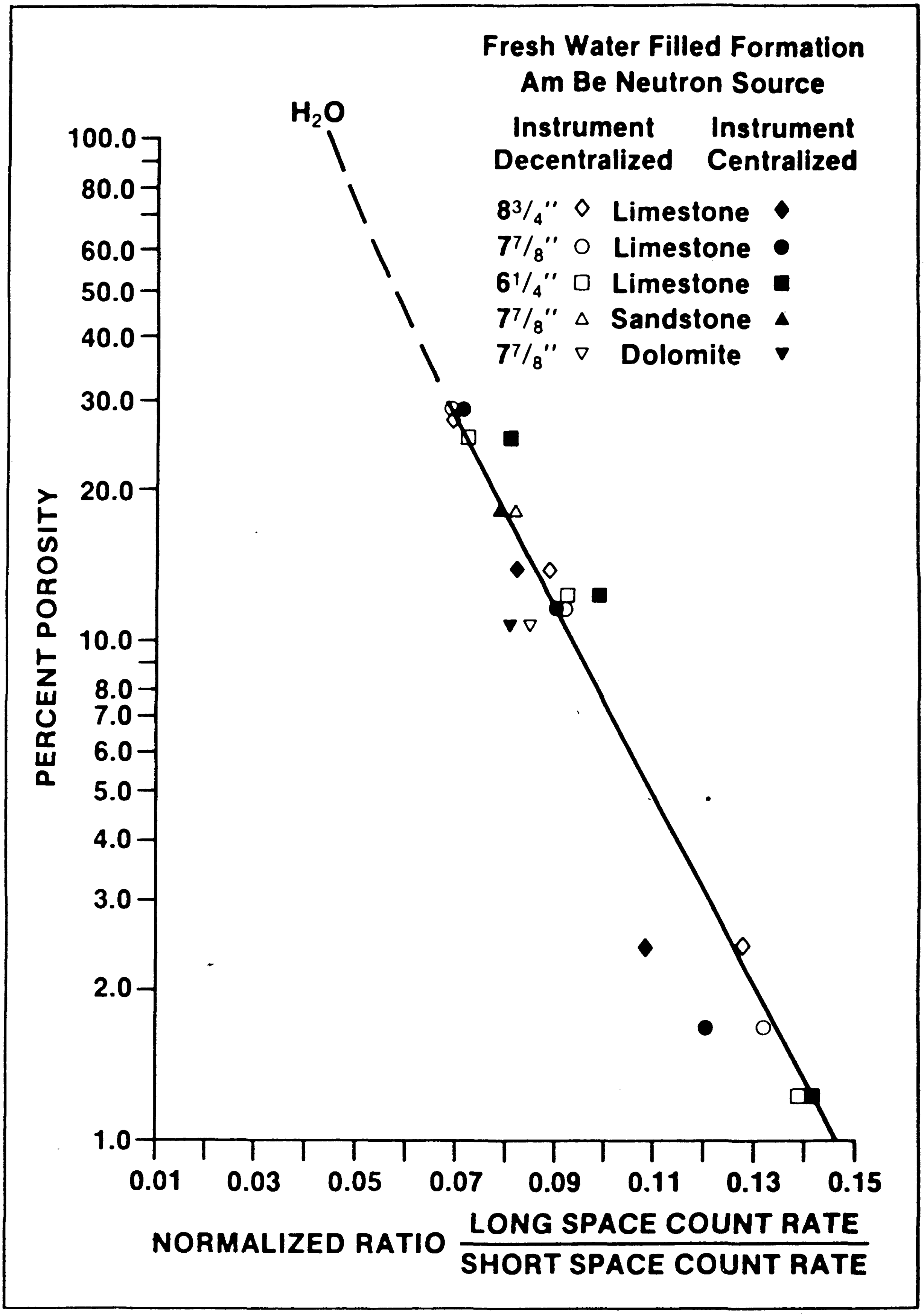

SILICON AND ALUMINIUM DETERMINATION IN GEOLOGICAL SAMPLES BY 14 MEV NEUTRON ACTIVATION BASED ON SIMPLE EQUIPMENT

F. Divós, G. Kontra and G. Petö

Institute for Experimental Physics, Kossuth University, Debrecen
Hungary

Abstract

An internal comparator method was developed to determine silicon and aluminium contents in geological samples by 14 MeV neutron activation. This method is particularly suitable for modestly equiped developing neutron generator laboratories. In the present work vanadium was chosen as the comparator element mixed into the powdered samples. The reproducibility of this method was good despite the cylindrical tubes of pneumatic transfer system in which the sample positioning at the irradiations and detection positions is random. The standard samples were prepared from pure chemical compounds. Using this method international rock standards were analysed. The results obtained agreed within 2% with those obtained by other methods. The detection limits for the present method have been determined under realistic background conditions. These are 2.4 mg for Al and 0.3 mg for Si at a neutron flux of 10^8 $cm^{-2}s^{-1}$ for 5 min irradiation time, 5 min measuring time using a 20 cm^3 Ge/Li/detector and allowing ± 10% statistical error. These limits of detection are higher than the published values based on theoretical calculations only.

A catalogue of 14 MeV neutron produced gamma spectra of possible comparator elements would be useful to extend the internal comparator method for determination of other elements.

Silicon and Aluminium Determination in Geological Samples by 14 MeV Neutron Activation Based on Simple Equipment

F.Divós, G.Kontra and G.Pető

Institute for Experimental Physics, Kossuth University,
Debrecen, Hungary

Extended summary

The modestly equiped neutron generator laboratories usually have a cylindrical pneumatic rabbit system connected to a neutron generator with a yield of about 10^9 n/s and a detector system with moderate efficiency and resolution. At such conditions the possibilities of 14 MeV neutron activation analysis rather limited. Selecting the most suitable method to the experimental conditions one can overcome some of difficulties. To avoid the disturbing effect of the cylindrical tube of pneumatic transfer system in which the sample positioning at the irradiations and detection position is random, the internal comparator method was tested in the present work at the above conditions.

As a comparator element, i.e. as an internal neutron flux monitor, vanadium was mixed into the powdered rock samples. The standard samples were prepared from pure chemical compounds. The nuclear reactions used for Al and Si determination as well as the interfering reactions are listed in Table 1. Using this method international rock standars provided by Roland Eötvös Geophysical Institute were analysed. The obtained results are indicated in Table 2. with the reference values. The accurancy and reproducibility of this method was good despite the cylindrical transfer system.

Several rock samples were analysed to investigate the role of background and different corrections. The Si correction for Al was the most considerable value while the Al correction for Si has been found less important and P correction for Si was negligible. The results are listed in Table 3. The oxygen content of these rocks are also indicated from a previous measurement /2/.

The detection limits /1/ for the present method have been determined under realistic background conditions averaging the backgrounds obtained experimentally with the ten different rock samples. The results are 2.4 mg for Al and 0.3 mg for Si at a neutron flux of 10^8 $cm^{-2}s^{-1}$ for 5 min irradiation time, 5 min measuring time using a 20 cm^3 Ge/Li/ detector. These detection limits are higher then the published /1/ values based on theoretical calculations neglecting the role of the matrix.

According to the present results the internal comparator method can be applied at relativelly poor experimental conditions with reasonable accurancy but the sample preparation is more complicated comparing to the methods based on more advanced experimental technique.

A catalogue of 14 MeV neutron produced activation gamma spectra for the possible comparator elements measured at fixed irradiation and detection conditions would help to select comparator elements to extend the method for determination of other elements. Similar work /3/ has already been done by a 3"x3" NaI/Tl/ detector. It worth to revise this using recent data obtained by high resolution Ge/Li/ detector as well as HP germanium detector in the low gamma energy region.

The authors are indebted to Prof.J.Csikai for his valuable comments and interest in this work.

REFERENCES

1./ S.S.Nargolwalla and E.P. Przybylowicz: Activation analysis with Neutron Generators, J.Wiley and Sons, New York, 1973

2./ S.Szegedi and F.Divós: Determination of Oxygen in Rock Samples by Fast Neutron Actyvation, to be published in J. of Radioanal. Chem.1983.

3./ M.Cuypers and J.Cuypers: Gamma Ray Spectra and Sensitivities for 14 MeV Activation Analysis, Texas A/M University 1966.

TABLE 1. Nuclear reactions used for Al and Si determination as well as the interfering reactions

Reactions	Isotopic abundances	Cross Section /mb/	$T_{1/2}$ /s/	E_γ /keV/	I_γ /%/
$^{27}Al/n,p/^{27}Mg$	100	75	568	844	73
$^{56}Fe/n,p/^{56}Mn$	91.68	103	9284	847	99
$^{59}Co/n,\alpha/^{56}Mn$	100	39.1	9284	847	99
$^{30}Si/n,\alpha/^{27}Mg$	3.05	45.9	568	847	73
$^{28}Si/n,p/^{28}Al$	92.27	235	139	1779	100
$^{27}Al/n,\gamma/^{28}Al$	100	0.5	139	1779	100
$^{31}P/n,\alpha/^{28}Al$	100	150	139	1779	100

TABLE 2. Al_2O_3 and SiO_2 contents of standard rock samples

No of the sample	Al_2O_3 /w%/ present measurement	Al_2O_3 /w%/ reference value	SiO_2 /w%/ present measurement	SiO_2 /w%/ reference value
Bauxit-20076	56.2 ± 1.9	54.2	7.3 ± 0.3	7.5
Disten-20077	60.2 ± 1.9	59.0	35.4 ± 1.2	36.3
Bauxit-20507	51.0 ± 1.5	49.0	13.2 ± 0.31	13.1

TABLE 3. Aluminium, silicon and oxygen /2/ concentrations in different rock samples

SAMPLE	m of Al uncorrected /mg/	m of Si uncorrected /mg/	Si correction for Al /mg/	Al correction for Si /mg/	Al conc. /w%/	Si conc. /w%/	O conc. /w%/
Copper ore	118.3	296.9	- 4.9	- 0.25	5.46±0.52	14.24±0.36	32.57±0.61
Carbonatic manganese	33.6	234.9	- 2.2	- 0.07	1.29±0.13	9.66±0.37	42.52±0.75
Phonolite	181.0	512.8	- 8.4	- 0.38	8.91±0.92	26.45±0.65	48.69±0.96
Bauxite	477.1	23.0	- 0.4	- 1.06	31.09±0.94	1.43±0.11	50.99±0.96
Dolomite	4.1	4.6	- 0.1	- 0.01	0.23±0.13	0.27±0.05	50.77±0.93
"Lajta" limestone	<1.4	12.5	- 0.2	-	<0.08	0.79±0.09	48.19±0.93
Muscovite gneisse	142.0	599.0	- 9.9	- 0.29	6.68±0.68	30.25±0.61	48.86±0.89
Granite	179.4	547.3	- 9.0	- 0.38	9.06±0.08	29.07±0.61	48.06±0.93
Florencitic rock	429.6	283.6	- 4.7	- 0.94	20.58±0.77	13.69±0.34	47.56±0.92
Basalt	125.8	337.7	- 5.6	- 0.26	6.62±0.67	18.70±0.47	48.08±0.91

MEASUREMENTS AND CALCULATIONS OF NEUTRON SPECTRA IN INFINITE MEDIA

S. ANTKIW, C. CASE, P. ALBATS

ABSTRACT

Measurements and calculations of the spatial dependence of neutron spectra in simulated infinite 0 p.u. sandstone, limestone and dolomite media will be shown. A 14 Mev neutron generator source and an organic scintillator detector, which is sensitive to Mev neutrons, were used in the measurements. Basically, 1-ft cubes were offset to form 3-in. square measuring ports to allow detection at 1, 2 and 3 feet from the source. Mathematical modeling was used to identify the characteristic features of the neutron spectra. It is intended that such experimental to calculational comparisons will test the high energy cross sections used in the modeling calculations.

SCHLUMBERGER-DOLL RESEARCH
RIDGEFIELD, CONNECTICUT 06877

MEASUREMENTS AND CALCULATIONS OF NEUTRON SPECTRA IN INFINITE MEDIA

S. ANTKIW, C. CASE, P. ALBATS

INTRODUCTION

A number of studies of the transport of 14 MeV neutrons from the (D,T) reaction have been reported for materials of interest in fission and fusion reactor technology, medicine and shielding. Measurements and calculations of the spatial variation of the energy dependent high energy neutron flux have been reported for individual elements including carbon, oxygen and iron as well as for air, water, concrete and others.[1-6] In addition to describing the characteristics of the measured flux, this work has demonstrated the ability of different calculational techniques to predict the measured spectra and the effects that uncertainties in cross sections have on them.

In this report, we describe the spatial and energy dependence of the neutron flux at distances of one to three feet from a 14 MeV source in several simulated infinite media of interest in geological applications. Measurements have been made in dolomite, sandstone, limestone and water media whose extended size (~ 8x6x5 ft.) makes them effectively infinite media.

The high energy (2-14 MeV) proton recoil spectra are measured with a liquid scintillator with pulse shape discrimination to remove gamma ray background. A derivative method unfolding code (FLYSPEC) is used to obtain the neutron flux from the proton recoil distributions.[7,8] Monte Carlo calculations using MCNP with ENDF/B-V cross sections have been made in infinite media, as well as selected cases of the experimental geometry, and comparisons are made with measured data. The contribution of the major physical processes to the character of the neutron flux has also been calculationally determined. These results provide insight into the mechanism of neutron transport and add to the understanding of presently used logging techniques.

EXPERIMENTAL ARRANGEMENT AND METHOD

Simulated infinite media were constructed of one foot cubes of dolomite and sandstone offset to make 3x3 inch ports as shown in Fig.1. Placement was made to minimize the size of spaces between blocks during assembly and measurements were made during disassembly to determine if spaces had developed. The bottom layer for both formations was limestone.

A different configuration was used for the limestone medium where 12x12x3 inch pieces were placed between each row of blocks (Fig.1), which made the interfaces perpendicular to the line between ports. This more satisfactory geometry was not possible with the dolomite and sandstone since the 3 inch slabs were not available for them. The water was contained in a tank 5x8x5 ft. (LxWxH) with aluminum tubes 3 inch in diameter (0.028 inch wall thickness) suspended from and secured to a rail on top of the tank to contain the accelerator neutron source and detector.

The accelerator and detector were positioned as shown in Fig.1 to be midway between the floor and the top of each medium. All ports not used for the accelerator or detector were filled with material identical to the blocks during measurements. The (D,T) accelerator voltage was 60-75 kV which made the neutron energy toward the detector at 90 degrees 14.05 MeV. A source neutron monitor, insensitive to gamma rays, was positioned in the vicinity of the accelerator and its output was used to normalize all data to equal source neutrons.

Proton recoil spectra were recorded with a Bicron BC501 Model MAB1 liquid scintillator (2x2 inch) whose pulse shape discrimination properties are similar to NE213, coupled to an RCA8850 photomultiplier. Standard ORTEC electronics modules were used for both the dynode signal (113 preamp, 572 amplifier) as well as for pulse shape discrimination using the anode signal (113 preamp, 460A amplifier, 552 pulse shape analyzer and 467 time-to-pulse height converter). Dynode pulses were sent through a linear gate and a Tracor-Northern analog-to-digital converter and multi-channel analyzer. Triggering of the upper level of the TPHC single channel analyzer (SCA) opened the gate for storage of neutron induced pulses in 256 channels of memory, and the SCA window output routed the gamma ray pulses to a separate group of memory. This allowed monitoring the gain of the system to assure that there was no drift during the typical one hour run, and that addition of as many as six runs to have the required counts in the spectrum, would not degrade the data. Compton edge electrons from the .51 and 1.26 MeV gamma rays emitted by Sodium 22 were used to calibrate the system gain. The measured feedthrough of the gamma ray spectrum into the neutron spectrum was .4% and was subtracted out before unfolding. The sum of the neutron and gamma ray pulses at the pulse shape analyzer (2-14 MeV) was maintained at 4000 per second.

Unfolding of the proton recoil spectra to obtain the energy dependent flux was performed with the FLYSPEC code,[7] which is a derivative method suitable for use with small computers, whose performance compares favorably with more elaborate inversion methods.[10] Error estimates shown on the curves are generated by the unfolding code and are based on Poisson statistics. Accumulation times were long enough to limit the error to several percent at the two closest spacings except in the 9.5 to 10.5 MeV region where they are larger because of the behavior of the algorithm used in the unfolding procedure. At the long spacing the errors are near 10% in the 14 MeV region.

MEASURED AND UNFOLDED SPECTRA

A typical neutron and gamma ray distribution is shown in Fig.2. Neutrons whose energy is 14 MeV are at channel 210 and, because of the nonlinear output for protons, channel 10 is at 2 MeV. Unfolding the neutron spectrum measured in dolomite results in the spectra shown in Fig. 3, for transmission through 9.5, 22 and 35 inches. As expected, the flux at 14 MeV decreases faster with spacing than the flux at lower energies. At the longest spacing there is little evidence of a 14 MeV peak but the character of the low energy region of the spectrum is not severely altered. The rapid rise below 3.5 MeV is the result of the changing oxygen cross section with the large anti-resonance at 2.35 MeV. Neutrons interacting inelastically with oxygen (1st excited state at 6.1 MeV) before being detected, produce the shoulder at 8 MeV. A similar shoulder at 10 MeV is partly a result of inelastic scattering in the carbon of the detector and is emphasized in dolomite and limestone. Elastically scattered neutrons in carbon as well as other elements contribute to the increasing flux between 10 and 14 MeV. Although these are the physical effects contributing to the spectra in the 10 to 14 MeV region, there is additional uncertainty because of the incomplete treatment of carbon interactions in the unfolding code.

A linear plot of the spectra measured at 9.5 inches in dolomite and sandstone, normalized at the peak, is shown in Fig.4. The most significant difference is in the region of 8.5 to 11 MeV where the presence of carbon in dolomite increases the flux.

Measurements in a simulated infinite water medium were also made since it is a simple geometry and has only two elements, with the cross sections for hydrogen being well known. Curves of the energy dependent flux at 12, 24 and 36 inches are shown in Fig. 5. The most striking difference between these curves and those from the solid media is the persistence of the 14 MeV peak at the greatest distance and the more gradual rise of the flux for energies below 10 MeV.

In addition to the spectral character of the flux discussed, it is also interesting to compare the spatial dependence of the integrated flux greater than 10.5 MeV with that expected on the basis of total macroscopic cross sections and calculations. This is discussed in the next section dealing with Monte Carlo calculations.

CALCULATIONAL METHOD

The calculational results presented here were generated using the Monte Carlo code MCNP developed at the Los Alamos National Laboratory. MCNP is a general purpose, continuous-energy, generalized geometry, time dependent, coupled neutron-photon Monte Carlo transport code. The code uses pointwise cross section data on energy grids that are tailored to reproduce the salient features of each isotope to within a few percent of the original cross section data values. A detailed description of the code is given in Reference [11].

In addition to benchmarking the models against the experimental results, calculations were also run under truly infinite media conditions at a series of identical source-to-detector distances. This allowed direct spectrum-to-spectrum comparisons to be made for the four materials studied (0 pu limestone, sandstone, dolomite, and water). This was not strictly possible with the experimental results because of the different source-to-detector distances used.

BENCHMARK CALCULATIONS

Two approaches to benchmarking were taken. The first dealt with a spectrum-to-spectrum comparison between experiment and calculation and the second dealt with an integral flux comparison at high energy. An example of a spectrum-to-spectrum comparison is given in Fig. 6. It shows a comparison between calculation and experiment at three different source-to-detector distances in water; 12, 24 and 36 inches. The calculations were done in spherical geometry with a 14.05 MeV isotropic source. The source was centered in a two inch radius vacuous sphere to simulate the fact that, in the experiment, both the source and detector were contained within three inch diameter aluminum tubes and therefore the true amount of water separating source and detector was somewhat less than 12, 24 or 36 inches. Calculations performed without the vacuous sphere showed that the only difference was the absolute magnitude of the peak value. The relative positioning of the three spectra, with respect to one another, remained the same and as can be seen in Fig. 6, are very close to the experimental results.

It should be noted that the calculated results shown in Fig. 6 are the product of the MCNP flux estimates times a resolution function which simulates the broadening effect of the detector's resolution. The resolution function used began at 7% FWHM at 14 MeV and increased with decreasing energy based on a $1/\sqrt{E}$ relationship. (This resolution comes from measurements of 14 MeV and 2.5 MeV sources at SDR and is substantiated by data from other laboratories, Reference [9].) In addition, a normalization factor was applied to the 12 inch calculated water spectrum to bring the 14 MeV peak value into agreement with the experiment. The same normalization factor was then applied to the 24 and 36 inch calculated data. It can be seen that the experimental and calculational results are in basic agreement as a function of distance and energy. However, at present we do not fully understand the reasons for the discrepancy near 10 MeV at the close spacing. We will investigate this in more detail through measurements using a small 3/4 by 3/4 inch detector to determine the effect of carbon scattering within the detector itself. Calculations will be used to check the effects of the energy/angle treatment of the scattering from oxygen. There is also some deviation between the two sets of curves below 3 MeV in which the experimental data rises at a faster rate. This rise, as will be seen later, is probably due to the influence of oxygen inelastic reactions. The reason for the calculation to experiment difference below 3 MeV is also not presently understood.

Another spectrum-to-spectrum comparison is shown in Fig. 7. This comparison is for 0 pu dolomite at the first source-to-detector spacing performed in the experiments, approximately 9 inches. In this case, the experimental geometry was faithfully reproduced in the model. The calculated curve has been normalized to match the experimental peak at 14 MeV and has been smoothed with a 6% FWHM resolution broadening function similar to the one described above. Though the two curves do not match explicitly over the total energy range shown, the general trends of a large peak in the 14 MeV region, a rapid flux decrease to 12 MeV and then a gradual increase in flux below 8 MeV are in agreement. The disagreement in the region between 9.5 and 11.5 MeV is similar to that discussed above in the water comparisons.

Looking at the details of the two spectra, we observe that the measured shoulder between 12 and 13 MeV is only marginally present in the calculated data. In addition, there appears to be approximately 1 MeV difference between the location of a peak near 7 MeV (the calculation peaks at 6.5 and the experiment peaks near 7.5 MeV). The peaks at 4.2 and 5 MeV are, on the other hand, in good agreement with one another. The discrepancies may be the result of either cross section deficiencies or uncertainties introduced through the unfolding of the experimental data.

The second approach at benchmarking dealt with integrating the flux for both calculation and experiment above 10.5 MeV and plotting the results as a function of distance. Both the experimental and calculational results have been plotted at a distance equal to a center-of-source to center-of-detector distance. This is explicitly correct for the infinite media calculations and approximately correct for the experimental values. (It is only approximate for the experiments because both the source and detector were encapsulated in three-inch diameter aluminum tubes and therefore the true amount of material between the two, on a straight line basis, is less than the center-of-source to center-of-detector distance.) Fig. 8 shows the integrated flux values for water and sandstone. Note that the sandstone flux values have been reduced by a factor of 10 for clarity of presentation. A single normalization factor has been used for the calculated points. The factor was chosen so that the calculated water point at 12 inches would match the value obtained experimentally. As might have been expected from Fig. 6, the match between calculated water and experiment is excellent. A comparison of the sandstone calculated and experimental points reveals that even though the absolute magnitudes do not agree exactly (remember that the sandstone calculated points have been normalized by the 12 inch water normalization factor), the rates of flux falloff for the two curves are very close. Fitting an exponential to the data beyond 20 inches yields coefficients of .115, .113, .125 and .102 inverse centimeters for the calculated limestone, sandstone, dolomite and water fluxes, respectively. The corresponding coefficients for the measured data are .115, .108, .119 and .101 inverse centimeters. The values for water are in agreement with the total macroscopic cross section for water. The values for the three 0 pu matricies are lower than their corresponding macroscopic values.

INFINITE MEDIA CALCULATIONS

Figs. 9-12 display the results of a series of infinite media MCNP calculations in spherical geometry. A gaussian shaped source, with a 3.4% FWHM profile centered at 14.05 MeV and isotropic emmission, was placed at the center of a solid sphere. Fluxes were then estimated in spherical shells centered at 6, 12, 24, and 36 inches away from the source center. The results shown have not been resolution broaded. The intent of these calculations was to allow direct matrix-to-matrix comparisons as a function of energy and source-to-detector spacing.

UNDERSTANDING SPECTRAL CHARACTER

A first step at understanding the shape of the family of flux profiles shown in Figs. 9-12 can be made by overlaying macroscopic cross section curves on top of the matrix profiles. For example, Fig. 13 shows the 24 inch profile for 0 pu limestone from Fig. 9 superimposed on top of three macroscopic cross section profiles representing total cross section, total scattering cross section and absorption cross section for 0 pu limestone. (The macroscopic cross section values were calculated from a multigroup cross section data library and are not the cross sections used in the modeling.) There are obvious energy regions, such as the oxygen anti-resonance region centered near 2 MeV that play a dominant part in defining the spectral shape in that energy region. In fact, even the small flux perturbations between 3 and 6 MeV are seen to be strongly correlated with the total cross section fluctuations. It is interesting to note that most of the macroscopic cross section character is due to oxygen and carbon.

Another approach was also taken to increase our understanding of the physical processes which produce the spectral character of the neutron fluxs. Because the Monte Carlo technique of solving a particle transport problem is to simulate actual neutron histories, it is possible to keep track of the different kinds of interactions a neutron experiences from the time it leaves the source until the time it is detected. An analysis of these "successful" histories yields information about the relative importance of the different interactions. Fig. 14 shows a decomposition of a scaled infinite medium 0 pu limestone calculated flux at 24 inches into five different flux profiles. The profile labeled elastic represents the sum of all neutron histories in which the only kind of interaction the neutron experienced was elastic scattering. The profiles labeled inelastic calcium, carbon and oxygen represent a sum of those histories in which the neutron experienced at least one inelastic calcium, carbon or oxygen event, respectively. Those neutron histories which contained inelastic events with more than one element were placed in the "other" category. Of course, because almost all neutron histories are the result of multiple interactions, even the so-called inelastic flux profiles are the result of some elastic scattering events as well.

Three general observations can be made regarding Fig. 14. The first is that above 10 MeV, the total flux is almost completely due to elastic scattering (other edits have shown that it is elastic scattering with oxygen that dominates this high energy process). The second observation is the fact that the rise in the total flux below 8 MeV is basically due to those neutron histories which experience inelastic oxygen reactions. And finally, it is seen that the other inelastic profiles play only a secondary role to oxygen in defining the total flux profile. These observations, and the fact that the oxygen atomic number densities among the three 0 pu formations do not differ by more than 15% from one to another, explains the similarity of the general character of the flux profiles shown in Figs. 9-11.

Another example of this kind of analysis is shown in Fig. 15 for water. The profile breakdown is similar (i.e., elastic and inelastic) with the exception that there are two elastic profiles; one for hydrogen and one for oxygen. The curve labelled "hydrogen dominated" refers to the fact that greater than half of the energy loss required to reach the detection energy was the result of elastic scatterings with hydrogen. A similar definition is true for the "oxygen dominated" elastic curve. These results show that almost all of the water profile is mainly due to elastic scattering and that below 12 MeV, hydrogen is the most influencial element. One therefore does not see the large flux at 2.4 MeV caused by the oxygen anti-resonance as in the 0 pu matricies.

SUMMARY and CONCLUSIONS

The spatial variation of the energy dependent neutron flux in limestone, sandstone, dolomite and water has been measured and calculated using the Monte Carlo technique. Major features of the flux profiles from the two methods are in good agreement and the physical processes responsible for them have been identified through calculations.

Calculated and measured neutron flux integrated above 10.5 MeV decreases with distance with an implied total cross section that agrees for limestone, differs by 1% in water, and 5% in sandstone and dolomite.

These initial results are encouraging and work will continue toward improved agreement between measured and calculated flux. We are now looking at the flux sensitivity to different cross sections and from this work we will be able to point out areas where more accurate cross section determination is warranted.

REFERENCES

[1] Stelts, M.L., Anderson, J.D., Hansen, L.F., Plechaty, E.F. and Wong, C.: *Nuc. Sci. Eng.*, 46, 53-60 (1971).

[2] Hansen, L.F., Anderson, J.D., Goldberg, E., Plechaty, E.F., Stelts, M.L. and Wong, C.: *Nuc. Sci. Eng.*, 35, 227-239 (1969).

[3] Cramer, S.N. and Oblow, E.M.: *Nuc. Sci. Eng.*, 58, 33-53 (1975).

[4] Tsechanski, A., Segev, M. and Shani, G.: *Nuc. Sci. Eng.*, 84, 226-233 (1983).

[5] Hansen, L.F., Anderson, J.D., Brown, P.S., Howerton, B.J., Kammerdiencv, J.L., Logan, C.M., Plechaty, E.F. and Wong, C.: *Nuc. Sci. Eng.*, 51, 278-295 (1973).

[6] Santoro, R.T., Barnes, J.M., Alsmiller, R.G., Jr. and Soran, P.D.: *Nuc. Sci. Eng.*, 84, 260-270 (1973).

[7] Slaughter, D. and Strout, R., II: NIM, 198, 349-355 (1982).

[8] Slaughter, D.R., Rueppel, D.W., Fuess, D.A.: UCRL -52415 (1978).

[9] Slaughter, D.R.: IEEE Trans. Nuc. Sci., NS26 (1), 802 (1979).

[10] Miller, W.H. and Meyer, W.: NIM 205, 185-195 (1983).

[11] MCNP - A General Purpose Monte Carlo Code for Neutron and Photon Transport, LA-7396-M (rev.) Version 2B, Los Alamos National Laboratory (1981).

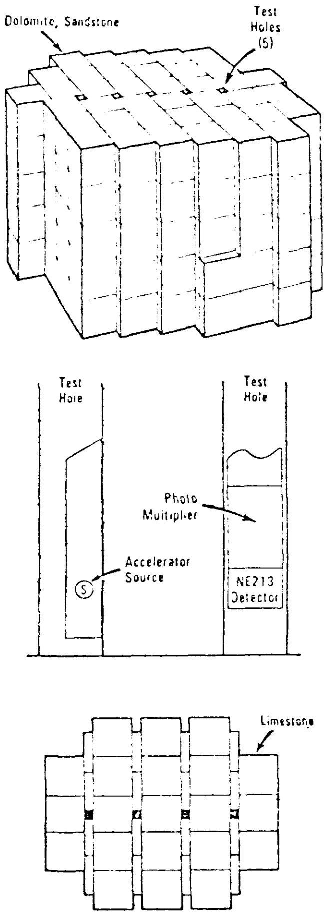

Figure 1

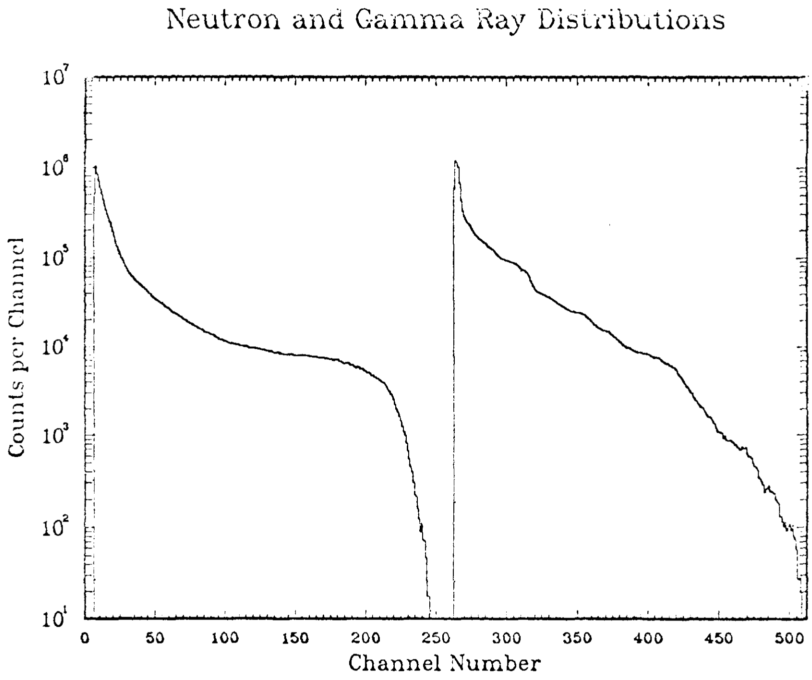

Figure 2

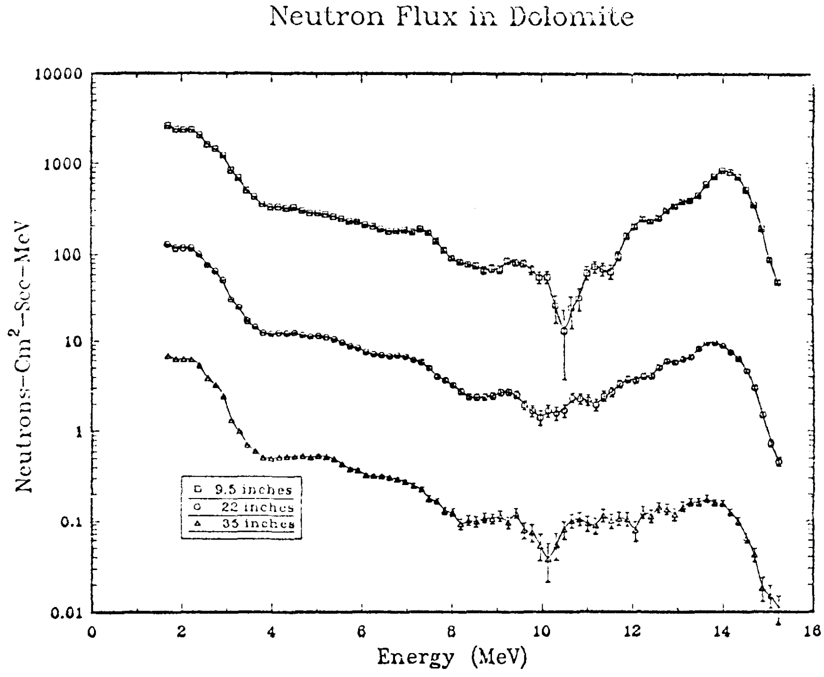

Figure 3

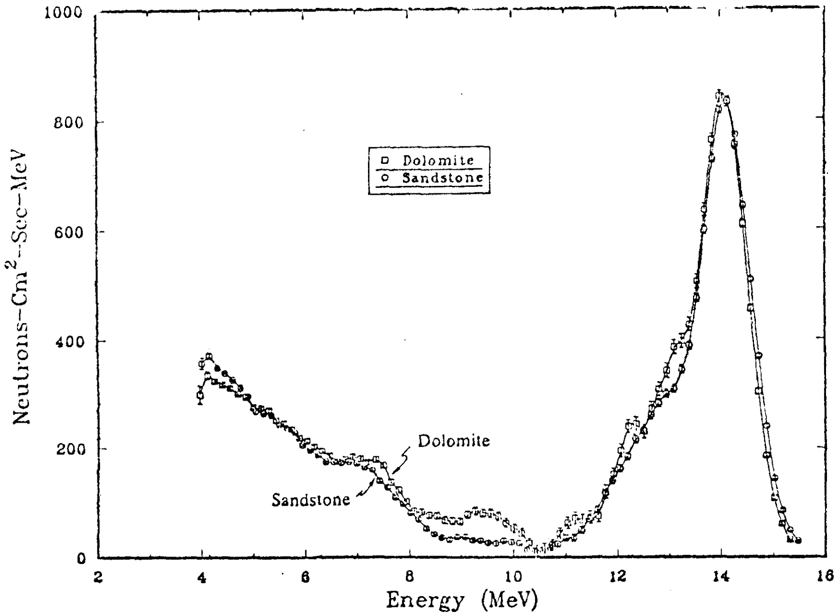
Dolomite and Sandstone Comparison

Figure 4

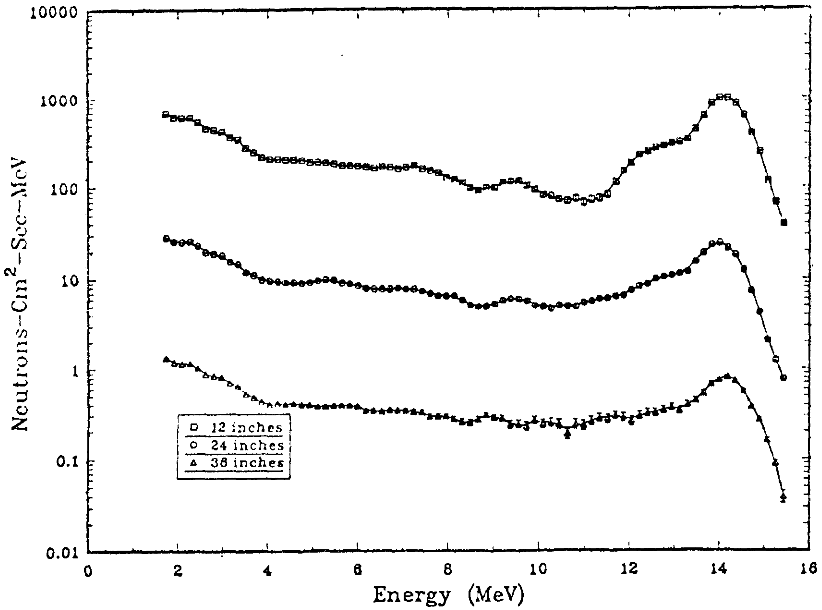
Neutron Flux in Water

Figure 5

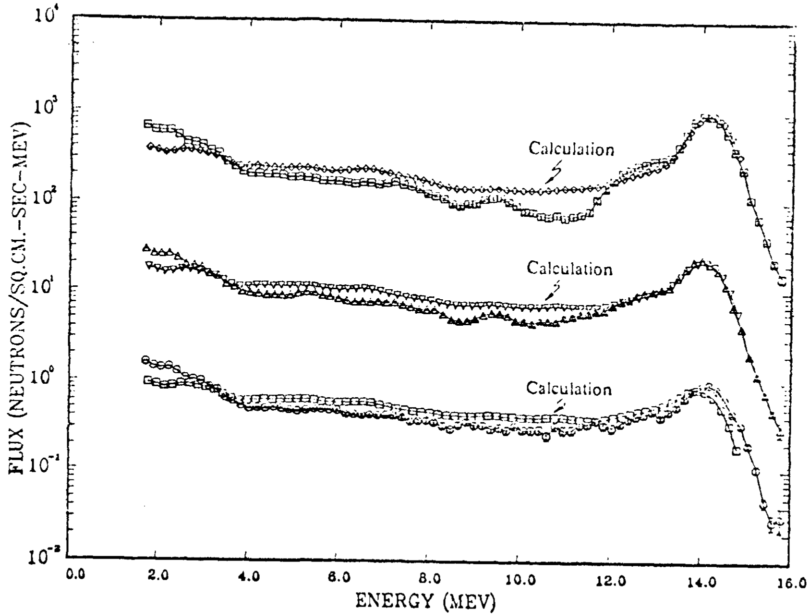
WATER / CALCULATION VS EXPERIMENT AT 12,24,36 INCHES

Figure 6

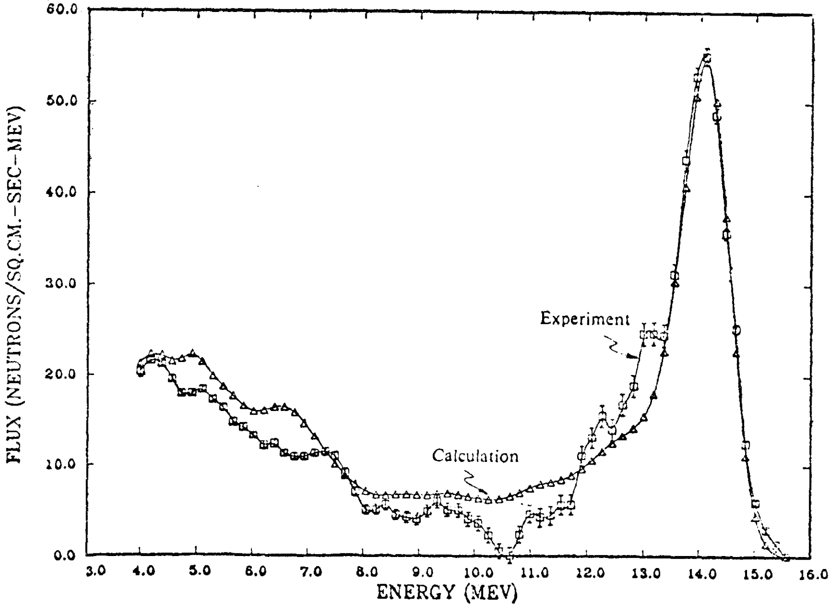
0 PU DOLOMITE / CALCULATION VS EXPERIMENT AT 9.4 INCHES

Figure 7

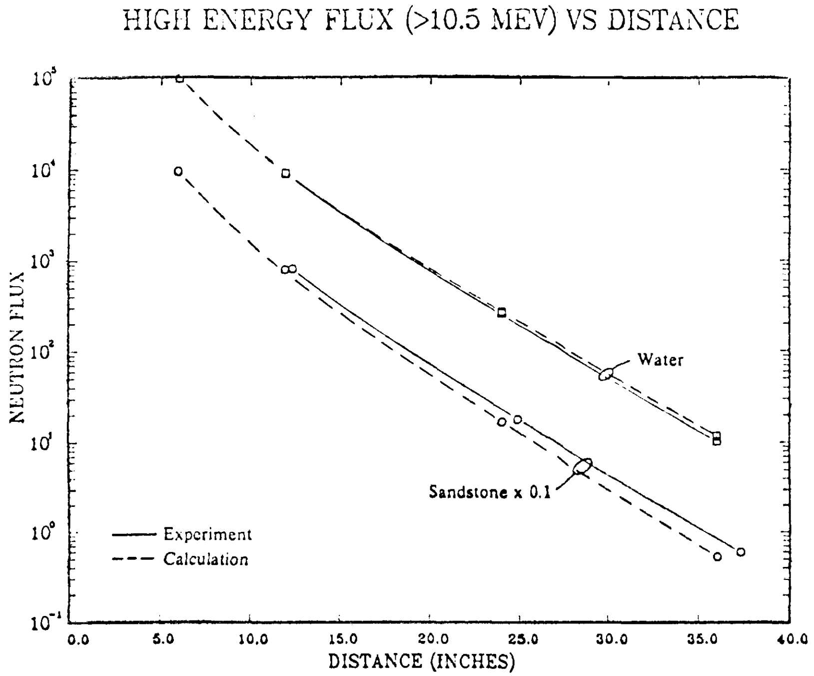
HIGH ENERGY FLUX (>10.5 MEV) VS DISTANCE

Figure 8

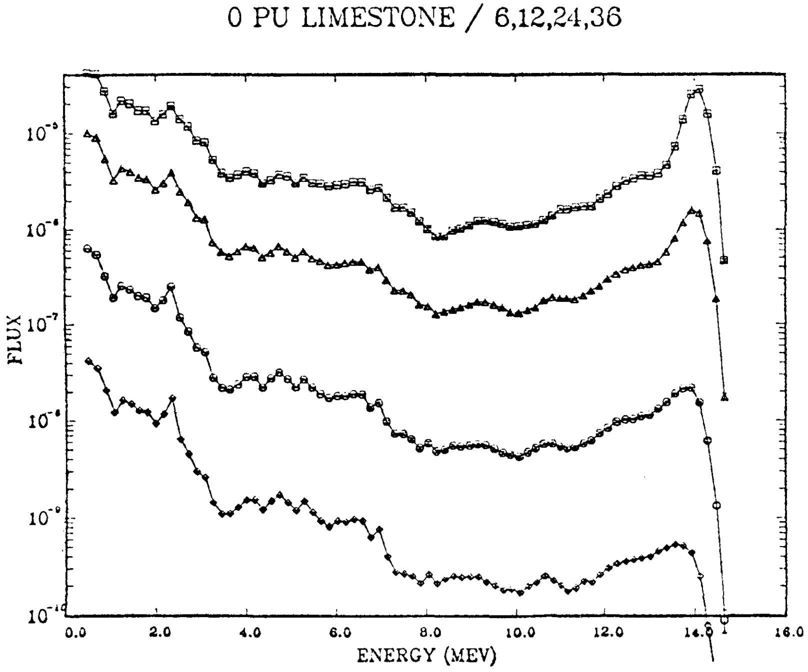
0 PU LIMESTONE / 6,12,24,36

Figure 9

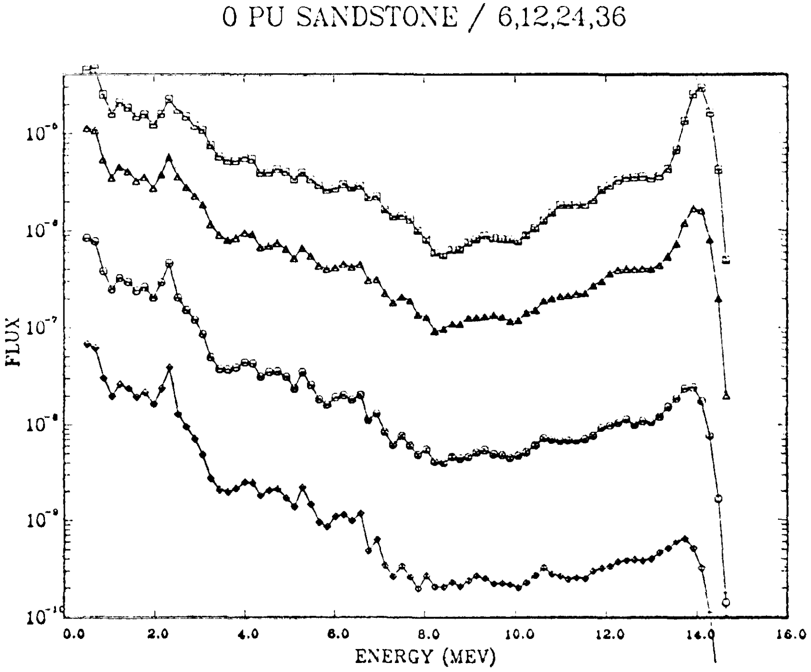
0 PU SANDSTONE / 6,12,24,36

Figure 10

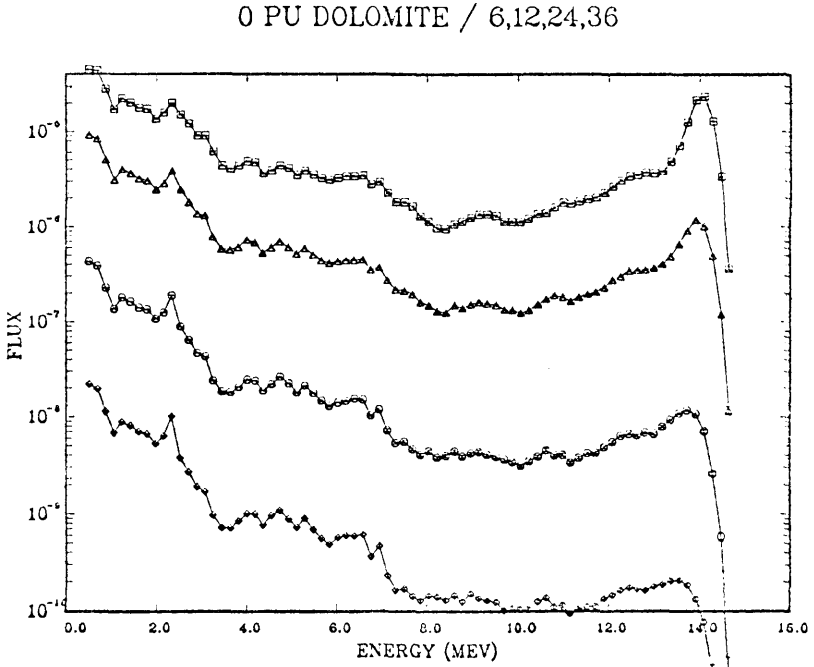
0 PU DOLOMITE / 6,12,24,36

Figure 11

WATER / 6,12,24,36

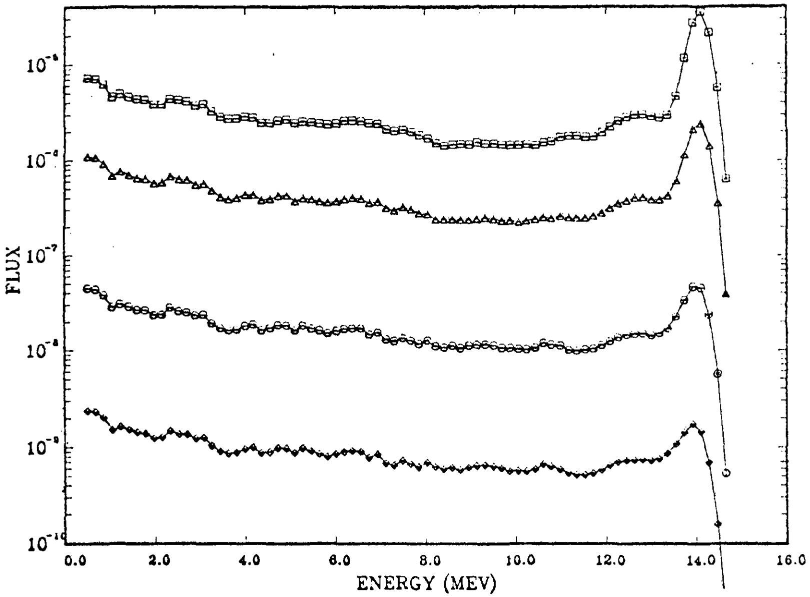

Figure 12

0 PU LIMESTONE AT 24 INCHES

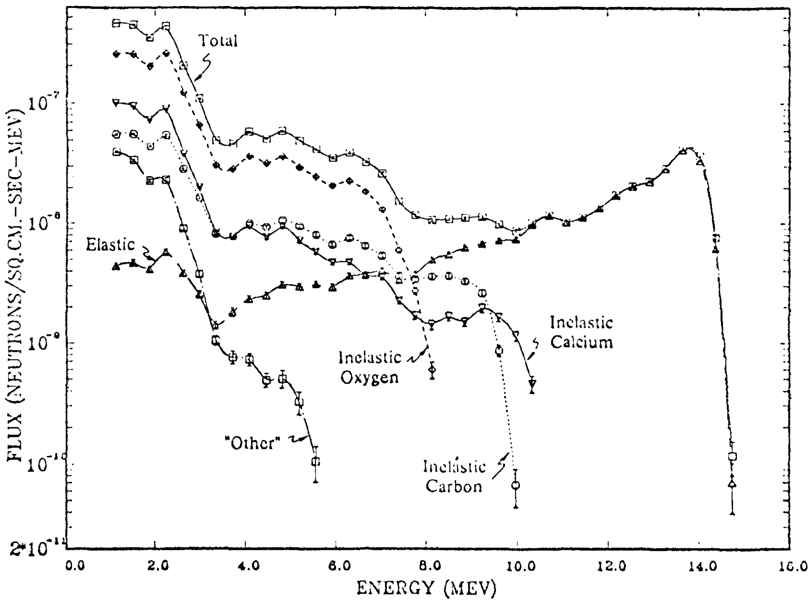

Figure 14

0 PU LIMESTONE AT 24 INCHES

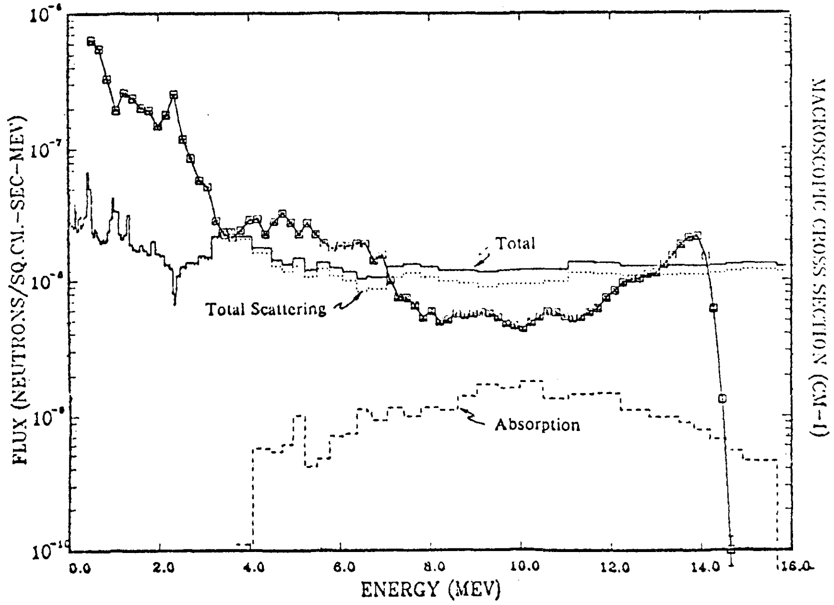

Figure 13

WATER AT 24 INCHES

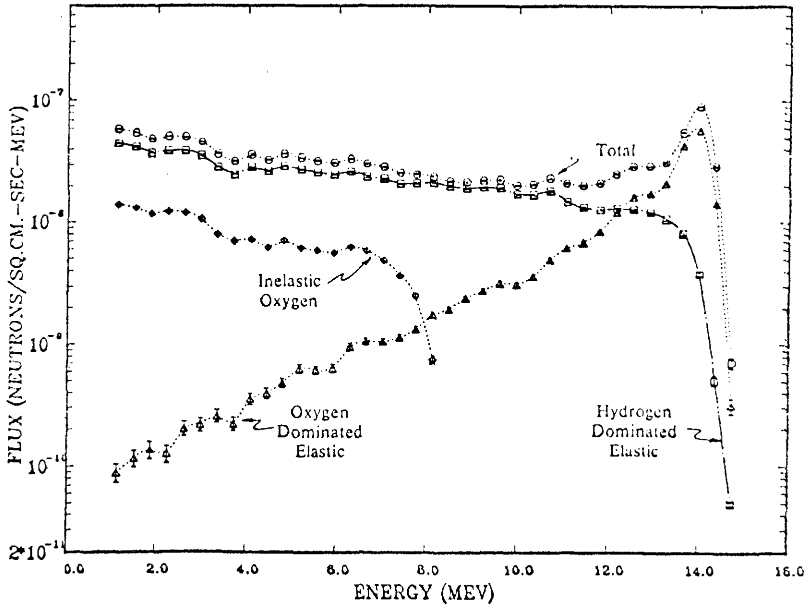

Figure 15

APPLICATION OF THE PULSED NEUTRON - NEUTRON METHOD FOR THE DETERMINATION OF OIL - WATER CONTACTS IN A BORE HOLE

Vo Dac Bang, Nguyen Phuc, Tran Dai Nghiep, Pham Duy Hien
Institute of Physics, Hanoi

Abstract: The experience of using the pulsed neutron - neutron method (PNNM) for determination of oil - water contacts is presented. The neutron diffusion constants were measured for different geological bore-hole layers. The correlation of the neutron life-time and geological characteristics is discussed. The convenience and disadvantages of pulsed neutron - neutron method, as well as the technical characteristics of apparatus needed for a developing country such as Vietnam are formulated.

The pulsed neutron method widely used in reactor physics for the determination of neutron parameters of multiplying and non-multiplying systems (see, e.g., [1]) has been used for investigation of an oil - gas bore hole [2,3,4]. Here were present some results of the application of the PNNM in Vietnam for the determinationof oil - water contacts.

Experiments and Results

A well - logging neutron generator type IGN-4 was used in the experiment. The point - measured method was chosen to obtain reliable results. The experiments were performed at depths larger than 1000 m. The measuring time at each point was 5 min. The neutron densities were measured after a delay time ranging from 600 to 1200 μs at each point (the channel width is 150 μs). Measurement data for one of the deposits are shown in Fig.1.

It is worthwhile to note that in the case of an oil layer the count rates increase appreciably and the delay time effect is large. In the case where the total counts in the oil and water layer differ by a factor of 1, the counts at the 600 μs delay time - by a factor of 1,5, 750 μs - 4, 900 μs - 6, 1050 μs-nearly 10. The oil-water boundary determined by the PNNM is in agreement with other methods.

The neutron life-times were determined for different bore holes layers. The results are shown in Table 1.

Table 1.

The neutron lifetimes for different layers

Layers	Proposed for calculation of the chemical composition	Calculated lifetime, μs	Experimental lifetime, μs
Water	100% SiO_2	500	340 ± 30
	95% SiO_2; 3% Al_2O_3; 2% Fe_2O_3	560	
Oil	100% SiO_2	585	590 ± 50
	95% SiO_2; 3% Al_2O_3; 2% Fe_2O_3	670	
Clay with 40% H_2O	65% SiO_2; 20% Al_2O_3; 10% $CaCO_3$; 5% Fe_2O_3	175	160 ± 20

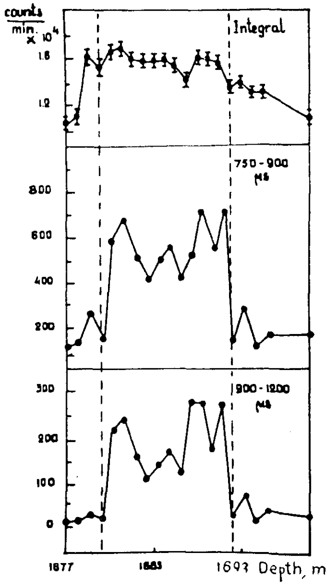

Fig. 1: Dependence of neutron counts on the borehole depth at different delay time:
--- The oil-water boundary determined by the electrical method

The last value of the calculated lifetime is in agreement with the experimental one. For the oil layer, the sand with 100% SiO_2 gives a calculated result which agrees with the experimental one better than the sand with 95% SiO_2; 3% Al_2O_3; and 2% Fe_2O_3. Under our conditions with the salt content of 30 g/l and porosity about 17 per cent, the value of life time 340 μs was not expected for the water layer. Perhaps, some strongly neutron absorbing elements are present here. The calculation data were taken from Table 2.

Table 2.

Some characteristics of the media of interest.

Media	Chemical composition	Density, g/cm^3	Neutron lifetime, μs
Sand	100% SiO_2	2.75	1033
Sand	95%SiO_2;3%Al_2O_3;2%Fe_2O_3	1.8	1415
Oil	86%C; 14%H	0.875	188
NaCl		2.15	6.3
H_2O		1	207
Clay with 40% H_2O	65%SiO_2;20%Al_2O_3;10%$CaCO_3$ 5%Fe_2O_3	2.28	175

Discussion

The experimental results have a fairly high degree of reliability. The oil-water boundaries determined were consistent with those determined by electrical and sampling methods. As the yield of the neutron logging generator was comparatively small. the point measurement method was chosen to reach the expected results, although that is a very time-consuming method.

Besides the high neutron yield, portable neutron generators working reliably under any tropic conditions are needed for developing countries such as ours. We feel a lack of nuclear data for the interpretation of the experimental results. We shall be very grateful for any support from IAEA in obtaining modern nuclear data for bore-hole and bulk-media assay.

References

1. Vo Dac Bang, Doctor's Thesis, Institute of Physics of the Academy of Sciences of the USSR, 1972.
2. Flerov G.N.et al. Proc. of the Symp. on the use of radioactive isotopes in national economy (in Russian), Gostoptechizdat, Riga, 1961
3. Portable Neutron Generators in Nuclear Geophysics (in Russian) Gosatomizdat, Moscow, 1962
4. Caldwell R.L. Proc. of the Int. Symp. on Nuclear Technique and Mineral Resources, Vienna, May 1969, p.937.

THERMAL NEUTRON ABSORPTION CROSS-SECTION MEASURED ON ROCK SAMPLES AND BRINES IN THE INSTITUTE OF NUCLEAR PHYSICS

POMIARY PRZEKROJU CZYNNEGO ABSORPCJI NEUTRONÓW TERMICZNYCH PRÓBEK SKALNYCH I WÓD ZŁOŻOWYCH PRZEPROWADZONE W INSTYTUCIE FIZYKI JĄDROWEJ

Измерения сечения захвата тепловых нейтронов на образцах горных пород и флюидов проведенные в Институте Ядерной Физики

J.A. Czubek, K. Drozdowicz, E. Krynicka-Drozdowicz
A. Igielski, U. Woźnicka

Institute of Nuclear Physics

Working paper prepared for the IAEA Consultants' Meeting on Nuclear Data for Borehole and Bulk-media Assay Using Nuclear Techniques, Krakow, Poland, 14-18 November, 1983.

ABSTRACT

A knowledge of the true absorption cross-section of thermal neutrons for different rocks and brines is an important factor in the quantitative interpretation of the neutron lifetime logs. This parameter is also indispensable in the theoretical or semi-theoretical establishment of the porosity calibration curves based on the detection of thermal neutrons. The absorption cross-section is directly related to the elemental composition of investigated materials. Geological materials, however, contain very often some admixtures of highly absorbing isotopes in quantities which are still too low to be detected in the usual elemental analysis (like boron, rare earths, etc.). The only way to know that cross-section is to measure it on geological samples. Due to the particular features of rock material (heterogeneities, impossibility to reproduce the sample of exactly the same composition and bulk density and with different dimensions, etc.) this is not an easy task using the experimental methods known so far. A new approach to this problem is presented in the paper.

In consecutive measurements the rock sample (having a fixed and well known shape - in our case it is a sphere or a cylinder and the sample is powdered or liquid) is enveloped in shells of a Plexiglass moderator (the neutron parameters of which are known) of variable thickness and irradiated with the pulsed beam of fast neutrons. The die-away rate of thermal neutrons escaping from the whole system is measured. The absorption cross-section of the sample is found as the intersection of the experimental curve (i.e. die-away rate vs thickness of the moderator) with the theoretical one. The theoretical curve is calculated for a given moderator under the assumption of a constant value of the neutron flux inside the sample. This method is independent of the value of the transport cross-section of the sample.

The method has been checked on artificial materials with a well known elemental composition (liquid or solid) and on the natural brines and rock samples (basalts and dolomite). A spe-

cial method of calculation of the variance of the measurement has been established. It is based on the multiple computer simulations of all experimental data used in the computation. This approach makes possible to discuss the contribution of the variance of the measurement of the absorption cross-section of geological sample. The one standard deviation of our methods is of the order of 1 up to 3 capture units (1 c.u. = 10^{-3} cm^{-1}). The volume of the sample needed here is of the order of 500ccm.

Streszczenie

Znajomość przekroju czynnego absorpcji neutronów termicznych dla skał i wód złożowych jest niezbędna przy interpretacji profilowania czasu życia neutronów w odwiercie, jak również przy teoretycznym lub półteoretycznym kalibrowaniu sond neutronowych do pomiaru porowatości skał. Wartość przekroju czynnego absorpcji jest funkcją składu chemicznego badanego ośrodka. Jednakże bardzo często materiały geologiczne zawierają niewielkie domieszki silnie absorbujących pierwiastków, takich jak bor czy lantanowce, w ilościach niewykrywalnych w rutynowej analizie chemicznej. Jedyną metodą wyznaczania przekroju czynnego absorpcji jest wtedy jego pomiar laboratoryjny na próbkach geologicznych. Uwzględniając specyficzne właściwości materiałów skalnych (niejednorodność, niepowtarzalność próbki o dokładnie tym samym składzie chemicznym, zmiany ciężaru nasypowego z granulacją itp.) niełatwo jest dostosować którąkolwiek ze znanych dotychczas metod do pomiaru przekroju czynnego absorpcji dla próbek geologicznych. W prezentowanej pracy przedstawiono nowe podejście do tego typu pomiaru.

W kolejnych pomiarach próbka (o znanym kształcie i rozmiarach - naszym przypadku kula lub walec; próbka może być rozdrobnionym materiałem skalnym lub cieczą) jest otaczana coraz grubszą warstwą moderatora z pleksiglasu (o znanych rozmiarach i parametrach neutronowych) i naświetlana impulsowym strumieniem szybkich neutronów. Wykonuje się pomiar stałej zaniku strumienia neutronów termicznych powstającego w układzie próbka - moderator. Przekrój czynny absorpcji próbki jest wyznaczany jako punkt przecięcia krzywej eksperymentalnej (tzn. zależności stałej zaniku od grubości moderatora) z pewną krzywą teoretyczną. Krzywa teoretyczna jest obliczana dla danego moderatora jako rozwiązanie niestacjonarnego równania dyfuzji neutronów termicznych w układzie próbka - moderator przy założeniu, że strumień neutronów termicznych wewnątrz próbki ma wartość stałą w przestrzeni. Metoda jest niezależna od przekroju czynnego transportu próbki.

Metoda została sprawdzona na roztworach kwasu borowego cz.d.a. oraz na tlenku krzemu cz.d.a. rozdrobnionym do jednorodnej granulacji. Wykonano szereg pomiarów dla próbek geologicznych (wody złożowe, próbki skalne bazaltowe i dolomitowe).

Została opracowana metoda znajdowania końcowego błędu pomiaru, wynikającego z błędu wyznaczenia punktu przecięcia dwóch krzywych charakteryzujących się pewną nieoznaczonością statystyczną (metoda oparta jest na komputerowej symulacji odchyłek tych krzywych). Wartość jednego odchylenia standardowego odpowiada wartości 1 - 3 c.u. (1 c.u. = 10^{-3} cm^{-1}) przekroju czynnego absorpcji. Wielkość próbki potrzebna do pomiaru jest rzędu 500 cm^3.

Резюме

Знание сечения поглощения тепловых нейтронов горных пород и флюидов является очень важным для интерпретации каротажа времени жизни нейтронов и тоже для теоретической или пол-теоретической калибровки нейтронных зонд для измерений пористости горных пород. Сечение поглощения тепловых нейтронов прямо функцией химического состава данной среды. Очень часто в геологических средах находятся небольшие включения очень сильно поглощающих элементов, таких как бор или лантаноиды, которые уходят химической анализе. Самый лучший путь для определения сечения поглощения это измерить этот параметр на геологических образцах. Учитивая особные свойства горных пород (неоднородность,неповторимость образца о таком же самым химическим составе, вариатность насыпного веса с грануляцией и тому подобные) нелегко было приспособить какий - то известный метод для измерения сечения поглощения геологических сред. В работе представлен новый подход к этому делу.

В очередных измерениях образец (имеющий известную форму и размеры-у нас это может быть шар или цилиндр, образец может быть измельченной горной породой или жидкостью) обводится все толстшим слоем внешнего модератора сделаного из плексигласа (об известных размерах и нейтронных параметрах) и облучается импульсным потоком быстрых нейтронов. Измеряется постоянная затухания тепловых нейтронов в системе образец - модератор. Сечение поглощения образца определается как точка пересечения экспериментальной кривой (т.е. зависимости постоянной затухания от размеров модератора) с некоторой теоретической кривой. Эта крива вычисляется как решение нестационарного уравнения диффузии тепловых нейтронов в системе образей - модератор при основании неизменного в пространстве потока нейтронов во внутри образца. Метод является независимым от сечения транспорта образца.

Метод был испытан на водных растворах борной кислоты H_3BO_3 (чистой для анализа) и на окиси кремния SiO_2 (чистого для анализа) измельчённой однородно. Были проведены измерения для геологических образцов (пластовые воды, горные породы: базальты и доломиты).

Произведено метод вычисления конечной погрешности измерения, которая возникает с погрешности точки пересечения двух кривых характеризующихся какой - то статистической погрешностью (метод опирается на моделировании отключений кривых с помощью вычислительной машины). Одно стандартное отклонение нашего измерения соответствует значению I ÷ 3 единиц захвата (I е.з. = = IO^{-3} см$^{-I}$) сечения поглощения.Объём образца должен быть около 500 см^3.

1. INTRODUCTION

The absorption cross-section, Σ_a, for thermal neutrons in geological formations becomes now an important parameter in the interpretation of many neutron logs based on the detection of thermal neutron flux in boreholes. The absorption cross-section is directly related to the elemental composition of rocks. Geological materials, however, very often contain some highly absorbing trace elements in quantities that are still too low to be detected in the routine elemental analysis.

When one takes the absorption cross-section of all elements of the periodic table, their contributions to the macroscopic absorption cross-section of rock are given through the $N_A\sigma_a^i/A_i$ value (N_A - Avogadro's number, σ_a^i - microscopic absorption cross-section of the i-th element having the atomic mass A_i). This situation is depicted in Fig.1. It is cleary visible that even very small admixtures of such elements as gadolinium, samarium, cadmium, europium or boron in the rock matrix can considerably increase the Σ_a value of the rock. When one takes into account, for example, the average elemental composition of the Earth Crust its mass absorption coefficient Σ_a/ϱ (where ϱ is the rock density) can be presented in the way given in Table 1. To gain a better knowledge of the problem we have taken the average elemental composition of the Earth Crust given by Fersman and that by Taylor (Rösler and Lange, 1972). From the table it is well visible that the ten (or eleven) principal elements making up more than 99 per cent of the total mass contribute in

Table 1. Contribution of major and trace elements to the mass absorption cross-section of the Earth Crust.

	σ_a [barn]	p Abundance according to:		$p\Sigma_a/\varrho$ according to:	
		Taylor [%]	Fersman [%]	Taylor [$10^{-3}cm^2/g$]	Fersman [$10^{-3}cm^2/g$]
O	0.00027	46.4	49.13	0.0047	0.0050
Si	0.16	28.15	26.00	0.9657	0.8920
Al	0.230	8.23	7.45	0.4225	0.3824
Fe	2.55	5.63	4.20	1.5481	1.1549
Ca	0.43	4.15	3.25	0.2681	0.2100
Na	0.530	2.36	2.40	0.3276	0.3332
K	2.10	2.09	2.35	0.6759	1.0932
Mg	0.063	2.33	2.35	0.0363	0.0367
H	0.332	-	1.00	-	1.9836
Ti	6.1	0.57	0.61	0.4371	0.4678
C	0.0034	0.02	0.35	0.0000	0.0006
Total		99.93	99.03	4.6560	6.5594
		[ppm]	[ppm]		
Li	70.7	20	50	0.1227	0.3068
B	759	10	50	0.4228	2.1139
Cl	33.2	130	2000	0.0733	1.1279
Mn	13.3	950	1000	0.1385	0.1458
Cd	2450	0.2	5	0.0026	0.0656
Sm	5800	6	7	0.1394	0.1626
Eu	4000	1.2	0.2	0.0219	0.0036
Gd	49000	5.4	7.5	1.0133	1.4074
Dy	930	3	7.5	0.0103	0.0258
Total		1125.8	3127.2	1.9448	5.3594
	Σ_a/ϱ [10^{-3} cm^2/g]			6.6008	11.9188

the Σ_a/ϱ value in 55 (Fersman) or 70.5 (Taylor) per cent, whereas the rest is given by the contribution of the nine elements which give 0.11 (Taylor) or 0.3 (Fersman) per cent of the total mass. For a particular rock the contribution of the trace elements in the absorption cross-section can be variable in a broad range, and this contribution is different for different types of lithology.

In the well logging practice the absorption cross-section of rocks is needed for several purposes. Pulsed neutron methods, for example, are mainly used to determine the neutron lifetime

$$\tau = \frac{1}{v\Sigma_a} \qquad (1)$$

of geological formations. This parameter describing the time behaviour of the neutron die-away curve in a formation is closely related to the absorption cross-section Σ_a of thermal neutrons in the formation through the thermal neutron velocity v. The Σ_a parameter is a linear combination of all rock compounds. For example in oil wells:

$$\Sigma_a = (1 - \phi - V_{sh})\Sigma_{ma} + V_{sh}\Sigma_{sh} + \phi\,(1 - S_w)\Sigma_{hc} + \phi\, S_w\Sigma_w, \qquad (2)$$

where ϕ is the porosity, V_{sh} is the shale content by volume and S_w is the water saturation of the pore space; Σ_{ma}, Σ_{sh}, Σ_{hc} and Σ_w are the absorption cross-sections of the rock matrix, shale, hydrocarbons and brine, respectively. All these absorption cross-sections have to be known for any quantitative interpretation of the neutron lifetime log .

Another reason of interest in the absorption cross-section of rocks is the problem of the calibration curves. Any quantitative application of the neutron method in well logging which is based on the detection of thermal neutrons (porosity logs, activation logs, etc.) needs the calibration curves, where the thermal neutron signal of the borehole tool is related to a given geological parameter (porosity, metal content, etc.). The shape of the calibration curves also depends, however, on the fast and thermal neutron parameters of rocks. All these parameters, except the macroscopic absorption cross-section for thermal neutrons (and the parameters related to it as the diffusion length, for example) can be calculated starting from the knowledge of the elemental composition of the rock in its principal constituents. Hence, when there is a problem of the transform of the calibration curve for a given tool known from a given lithology to another one, the knowledge of the neutron parameters for both lithologies becomes crucial. This is specially important when one wants to obtain the porosity calibration curves in magmatic rocks, starting from the knowledge of the curves in sedimentary rocks (no one real calibration facility for magmatic rocks exists).

Finally, the last but not least reason for our interest in the absorption cross-section of rocks is that it is also a geochemical parameter, which is very sensitive to the presence of absorbing trace elements and can be used for rock classification.

The only way to know the absorption cross-section of rock is to measure it on a geological sample. Due to particular features of the rock material (heterogeneities, impossibility to reproduce the sample of exactly the same elemental composition and bulk density but having variable geometrical dimensions, etc.) this is not an easy task, with the experimental methods known so far.

So far there have been three methods for the measurement of the absorption cross-section of rock samples: the one proposed by Antonov et al. (1966), another invented by Allen and Mills (1975) and that reported by Harris and Mc Daniel (1982). The first one requires a special calibration curve for which the value of the transport cross-section, Σ_{tr}, has to be known for the (unknown) sample. The two other methods require the knowledge of the elemental composition of the sample just to make the calculation of the Σ_{tr} value possible. The last method (as well as the one used by Carre (1968) which was more classic one) requires, in addition, the nuclear reactor with special equipment to perform the measurement. What we are presenting here is still another method free of those limitations. The research on this new method has been done in our laboratory since 1970 and its fundamental principles are published elsewhere (Czubek 1981, Woźnicka 1981, Drozdowicz 1981, Drozdowicz and Woźnicka 1983). In this paper we are going a very short description of the method and a full list of all our assays performed so far on geological materials.

2. PRINCIPLES

2.1. OUTLINE OF THE METHOD

Let the rock sample (for the sake of simplicity we assume a spherical shape for the sample) be characterized by the radius R_1 (known), absorption cross-section Σ_{a1} (unknown) and transport cross-section Σ_{tr1} (unknown). We envelope the sample in the shell of a moderator having external radius R_2 (known), absorption cross-section Σ_{a2} (known) and transport cross-section Σ_{tr2} (known). The whole system is irradiated by an instant beam of fast neutrons. Fast neutrons are slowed down in the whole sample- moderator system. Thermal neutrons appearing in such a bounded system decay in time. Mathematically this decaying thermal neutron flux (integrated over all thermal neutron energies) is given as a set of the eigenfunctions being the solution of the problem, each n-th eigenfunction characterized by its own decay constant λ_n being the eigenvalue of the problem $(n = 0,1,2,\dots)$. In other words the thermal neutron flux is given as a sum of decaying modes. The relative abundance of each mode and its decay constant λ_n depends upon the geometrical dimensions of the system.

Let us consider the fundamental mode (described by $\lambda \equiv \lambda_0$) only. The space distribution of this fundamental mode at some instant t depends upon the geometrical and neutron parameters of the system. Some typical situations are presented in Fig.2 for different thicknesses $(R_2 - R_1)$ of the moderating shell. The moderating shell having the neutron lifetime

$$\tau_2 = \frac{1}{v\Sigma_{a2}} \tag{3}$$

longer than that of the sample can be considered as a supplying source of thermal neutrons, because the thermal neutrons in the sample die more quickly $(\Sigma_{a1} > \Sigma_{a2})$. In the case of (a) in Fig.2 the thickness $(R_2 - R_1)$ of the moderator is too small and the whole thermal neutron population escapes outside. In the case of (c) the moderating shell is very thick and there is a net inflow of thermal neutrons from the moderator towards the sample, where they are absorbed giving a characteristic "hole" in the neutron flux. Finally the thickness $(R_2 - R_1)$ of the moderating shell is such that it gives an equilibrium between the die-away rate of thermal neutrons in the sample and the thermal neutron inflow towards the sample. This results in the constant (in space) value of the thermal neutron flux inside the sample, which is depicted in Fig.2(b).

Let zero order space eigenvalues for the sample and for the moderating shell be B^2_{d1} and B^2_{d2}, respectively. They are connected with the fundamental mode decay constant λ (Czubek 1981) by equations:

$$B^2_{d1} = 3(\lambda/v - \Sigma_{a1})(\Sigma_{tr1} + \Sigma_{a1} - \lambda/v) \tag{4a}$$

$$B^2_{d2} = 3(\lambda/v - \Sigma_{a2})(\Sigma_{tr2} + \Sigma_{a2} - \lambda/v)\ . \tag{4b}$$

On the other hand the constant (in space) value of the flux inside the sample implies the zero value of the sample eigenvalue, i.e.

$$B^2_{d1} = 0 \tag{5a}$$

which in turn requires [cf. equation(4a)]

$$\lambda / v = \Sigma_{a1} . \tag{5b}$$

Unfortunately we do not know in advance what moderator shell thickness $(R_2 - R_1)$ this condition has fulfilled. We can only measure the λ value obtained for different values of $(R_2 - R_1)$, or simply R_2 when R_1 is constant, knowing that somewhere, within the range of λ thus obtained, there probably is the corresponding one to the condition given by equation (5b). To localize this value, however, one should for example, solve the theoretical problem of the thermal neutron flux calculation for a given sample-moderator system assuming the condition given by equation (5a) in the solution. This solution gives some values of λ^* as a function of the R_1, R_2, Σ_{a2} and Σ_{tr2} values [and independent of the Σ_{a1} and Σ_{tr1} values according to equation (4)]. These λ^* values are , in general, not true except for that one particular R_2 value (when R_1, Σ_{a2} and Σ_{tr2} are fixed) for which the condition given by equation (5b) is really fulfilled. This particular λ^* value is localized, simply speaking, at the intersection of the relationship $\lambda = f_1(R_2)$ experimentally known with the theoretically known function $\lambda^* = f_2(R_2)$, as it is shown in Fig.3.

2.2. SOLUTION FOR THE SPHERICAL AND CYLINDRICAL GEOMETRIES OF THE EXPERIMENT

For the spherical geometry of the experiment (i.e. where the sample and the outer moderator are concentric spheres) the λ values are obtained (Czubek 1981) from the equation:

$$D_{d1} \sqrt{B^2_{d1}} \,\mathrm{cotan}(R_1 \sqrt{B^2_{d2}} + D_{d2} \sqrt{B^2_{d2}} \,\mathrm{cotan}[(R_2 - R_1) \sqrt{B^2_{d2}}]$$

$$= \frac{D_{d1} - D_{d2}}{R_1} \quad , \tag{6}$$

where B^2_{d1} and B^2_{d2} are given in equation (4) and

$$D_{dj} = \frac{1}{3(\Sigma_{trj} + \Sigma_{aj} - \lambda/v)} \quad , \quad j = 1 \text{ or } 2 \ , \tag{7}$$

are the so-called dynamic diffusion coefficients. In the R_2 value the dynamic extrapolated distance d_d of the moderating material is included, i.e.

$$R_2 = R_{2g} + d_d \ , \tag{8}$$

where R_{2g} is the geometric radius of the moderator.

When the value $B^2_{d1} = 0$ is introduced into equation (6), equation (9) for the λ^* value is obtained:

$$R_1 B^*_{d2} = -\tan[(R_2 - R_1) B^*_{d2}] \ , \tag{9}$$

where

$$B^{*2}_{d2} = 3\,(\lambda^*/v - \Sigma_{a2})(\Sigma_{tr2} + \Sigma_{a2} - \lambda^*/v)\ . \tag{10}$$

The problem for the cylindrical geometry of the experiment (where the cylindrical sample is surrounded by the cylindrical outer moderator) has been solved by Woźnicka(1981). The dependence of the theoretical decay constant $\lambda^*(H_2,R_2)$ upon the external dimensions (H_2 being the height and R_2 being the radius) of the outer moderator cannot be obtained in this case in the form of one final equation. The best method to find the theoretical curve is to use the perturbation method for the neutron flux calculation. Then the formula for the n-th order approximation value of the dynamic material buckling of the outer medium is:

$$(B^{*(n)}_{d2})^2 = (\alpha^{*(n)})^2 + (W^{*(n)})^2\ , \tag{11}$$

where

$$(\alpha^{*(n)})^2 = \alpha_e^2\, K^{(n)}\ , \tag{12}$$

$$(W^{*(n)})^2 = W_e^2\, K^{(n)}\ , \tag{13}$$

and α_e^2 and W_e^2 are the eigenvalues of the diffusion equation for the homogeneous cylinder. They are equal to

$$\alpha_e = \frac{\pi}{H_2}\ , \tag{14}$$

$$W_e = \frac{j_o}{R_2} \tag{15}$$

[$j_o \approx 2.405$ is the first zero of the Bessel function of the first kind of the order zero $J_o(x)$]. The extrapolated radius R_2 is given as in equation (8) and the height H_2 is equal to:

$$H_2 = H_{2g} + 2d\ , \tag{16}$$

where H_{2g} is the geometric height of the outer moderator. The term $K^{(n)}$ is defined as:

$$K^{(n)} = 1 + \frac{\int_{V_1} \varphi(z,\varrho)\ \varphi_1^{*(n)}(z,\varrho)\ dV}{\int_{V_2} \varphi(z,\varrho)\ \varphi_2^{*(n)}(z,\varrho)\ dV}\ , \tag{17}$$

where $\varphi(z,\varrho)$ is the thermal neutron flux in the homogeneous cylindrical system and $\varphi_j^{*(n)}(z,\varrho)$ is the n-th order approximation of the perturbed flux in the j-th part of the volume of the two-region cylindrical system ($j = 1,2$). The substitution of the dynamic material buckling B^{*2}_{d2} [given in equation (10)] and of the formulae for the fluxes φ, $\varphi_1^{*(n)}$ and $\varphi_2^{*(n)}$ [obtained by Woźnicka (1981)] into equation (11) determines the n-th order approximation of $\lambda^{*(n)}$ for the theoretical decay constant λ^*.

All formulae discussed so far have been obtained in the one velocity approximation (i.e. for the constant value of the neutron velocity v). In the real experiment, however, the whole spectrum $\phi(v)$ of the thermal neutron flux is observed. We have assumed that the $\phi(v)$ spectrum follows the Maxwellian distribution $\tilde{M}(v)$ given for some effective velocity v_{oc} in a given material, thus:

$$\phi(v)\ dv \equiv \tilde{M}(v)\ dv$$

$$= 2\ (v/v_{oc})^3 \exp[-(v/v_{oc})^2]\ d(v/v_{oc}) \quad . \qquad (18)$$

Assuming the hydrogeneous moderator, by the consistent application of the spectrum averaged neutron parameters (Drozdowicz 1981) one arrives at the notion of the spectrum averaged dynamic material buckling $\tilde{B}^{*2}_{d2}$ value and dynamic diffusion coefficient $\overline{D^{*}_{d2}}$ value:

$$\tilde{B}^{*2}_{d2} = \frac{4\ (\frac{\lambda^*}{v_{oc2}} + \Sigma_{a2})(\Sigma_{tr2} + \Sigma_{a2} - \frac{\lambda^*}{v_{oc2}})}{1 + \sqrt{1 - 16\frac{C_2}{v_{oc2}}(\frac{\lambda^*}{v_{oc2}} - \Sigma_{a2})(\Sigma_{tr2} + \Sigma_{a2} - \frac{\lambda^*}{v_{oc2}})^2}} \qquad (19a)$$

$$= \frac{4\ (\frac{\lambda^*}{v_{oc2}} + \frac{\overline{v\Sigma_{a2}}}{v_{oc2}})(\frac{v_{oc2}}{2D_{o2}} - \frac{\lambda^*}{v_{oc2}})}{1 + \sqrt{1 - 16\frac{C_2}{v_{oc2}}(\frac{\lambda^*}{v_{oc2}} - \frac{v\Sigma_{a2}}{v_{oc2}})(\frac{v_{oc2}}{2D_{o2}} - \frac{\lambda^*}{v_{oc2}})^2}} \qquad (19b)$$

and

$$\overline{D^{*}_{d2}} = \frac{\sqrt{\pi}}{4(\Sigma_{tr2} + \Sigma_{a2} - \frac{\lambda^*}{v_{oc2}})} \qquad (20a)$$

$$= \frac{\sqrt{\pi}}{4(\frac{v_{oc2}}{2D_{o2}} - \frac{\lambda^*}{v_{oc2}})} \quad . \qquad (20b)$$

The effective neutron velocity v_{oc2} is assumed, according to Williams (1966), to be equal to that for the homogeneous bounded medium:

$$v_{oc2} = v_o\ (1 - \frac{C_2}{D_{o2}}\ \tilde{B}^{*2}_{d2}) \quad . \qquad (21)$$

Here we introduce the dynamic material buckling $\tilde{B}^{*2}_{d2}$ instead of the geometrical buckling as was the case in the original work of Williams. The v_o is the neutron velocity corresponding to the moderator temperature $T(^oK)$:

$$v_o = 2198 \sqrt{\frac{T}{293.15}} \quad [m\ s^{-1}] \quad , \qquad (22)$$

C_2 is the diffusion cooling coefficient for the moderator and D_{o2} is its diffusion coefficient as they have been obtained in the experiment. The $\overline{v\Sigma_{a2}}$ value is also the direct, experimentally obtained value, thus equations (19b) and (20b) give the $\tilde{B}^{*2}_{d2}$ and $\overline{D^{*}_{d2}}$ parameters in terms of the experimentally observable values (Drozdowicz et al. 1980), whereas equations (19a) and (20a) give the same parameters in terms of the tabulated cross-sections. Here the Σ_{a2} and Σ_{tr2} cross-sections are velocity dependent, and they have to be taken for the neutron velocity equal to v_{oc2}.

Now, the $\tilde{B}^{*2}_{d2}$ values from equation (19) are used in equation (9) or (11) to obtain the dependence of λ^* vs $\hat{R}_{2g}$ where $\hat{R}_{2g}$ denotes the geometric external size of the outer moderator [i.e. $\hat{R}_{2g} = R_{2g}$ for the spherical geometry and $\hat{R}_{2g}=(H_{2g},R_{2g})$ for the cylindrical one]. The extrapolated dimensions are obtained according to equations (8) and (16) with

$$d_d = 2.28\,\overline{D^*_{d2}}\ , \tag{23}$$

where the coefficient 2.28 is taken according to the results obtained for hydrogeneous media by Nelkin (1960) and Williams (1964).

The theoretical curve for the spherical geometry is easily obtained from equation (9) and for the cylindrical geometry it is calculated by the method of the perturbation calculation (Drozdowicz and Woźnicka 1983, Drozdowicz and Woźnicka 1982).

Now, with the relationship λ^* vs $\hat{R}_{2g}$ settled, the relation λ vs $\hat{R}_{2g}$ known experimentally gives, at the intersection of both curves (cf. Fig.3), the value:

$$\lambda = \lambda^* = \overline{v\Sigma_{a1}} \tag{24a}$$

just sought which is the reciprocal of the neutron lifetime for the sample. The absorption cross-section $\Sigma_{a1}(v_o)$ valid for some thermal neutron velocity v_o (for example $v_o = 2200\ \mathrm{ms}^{-1}$) is simply

$$\Sigma_{a1}(v_o) = \frac{\overline{v\Sigma_{a1}}}{v_o}\ . \tag{24b}$$

The disadvantage of this method of measurement consist in the imposed condition that

$$\Sigma_{a1} > \Sigma_{a2} \tag{25}$$

which for the hydrogeneous moderators limits the accessible range of the Σ_{a1} parameter to rather high values, higher than the ones interesting for the study of ordinary sedimentary rocks. For brines, however, this method is quite adequate. To measure the Σ_{ma} values of the rock matrix one can use another form of equation (2) written for $V_{sh} = 0$ and $S_w = 1$:

$$\Sigma_{ma} = \frac{\Sigma_{a1} - \phi\Sigma_w}{1 - \phi} \tag{26}$$

which means, from the experimental point of view, that the rock crushed matrix material has to be "poisoned" by some highly absorbing fluid introduced into the pore space ϕ. The absorption cross-section Σ_w of this highly absorbing fluid, as well as the porosity ϕ value, have to be known accurately. By measuring the Σ_{a1} value for such a composite sample the Σ_{ma} value can be obtained from equation (26). The accuracy of such measurement is lower in this case, of course, than in the case of the "pure" sample. This problem will be discussed later in the paper. Another possibility for the measurement of the Σ_{ma} value is to use nuclear graphite as the moderator. We are not going to discuss this problem.

3. EXPERIMENTAL SET-UP

The experiment was carried out in spherical and cylindrical geometries with a Plexiglass moderator. The scheme of this sample-moderator system is given in Fig.4. The external surface of the moderator was lined with a 2 mm cadmium shell to fix the thermal neutron boundary conditions well. The whole system was irradiated by a pulsed beam of 14 MeV neutrons from the (D,T) reaction and the thermal neutron flux was measured by a bell shaped ^{3}He detector situated at an opening in the cadmium sheet.

The Plexiglass moderator (i.e. the methyl-polymethacrylate resin $(C_5H_8O_2)_n$) had the density (1.180 ± 0.08) g/cm^3 and its thermal neutron parameters measured by Drozdowicz et al. (1980) are presented in Table 2.

Table 2. Thermal neutron parameters for Plexiglass.

t = 19.5 °C

Parameter	$\overline{v\Sigma_{a2}}$ $[s^{-1}]$	D_{o2} $[cm^2s^{-1}]$	C_2 $[cm^4s^{-1}]$
Value	4 120	36 882	7 149
Standard deviation	30	314	615

The width of the fast neutron burst was 100 μs and the burst repetition time was adjustable from 0.6 ms up to 2.4 ms. The thermal neutron die-away curve was measured for each value of R_{2g} of the moderating envelope of the sample by the electronic system which is schematically presented in Fig.5. The system consists of a chain of electronic devices for measured pulses (i.e. detector, preamplifier, amplifier, discriminator) and for start pulses, multichannel time analyser, control unit, paper tape puncher and other auxiliary electronic units. The main purpose of the system is to register the thermal neutron die-away curve in the multichannel time analyser (256 channels, channel width - 1 μs, 2 μs or 5 μs) and to punch the registered data on a paper tape. The data are punched in the Fortran 1900 code.

The measurement should be done in well known and fixed conditions. The most important are: the fixed average neutron flux, proper counting statistics, and a stable temperature of the sample. The control unit delivers the start pulses to the analyser when all conditions required are fulfilled.

4. DATA TREATMENT AND ACCURACY OF MEASUREMENT

The decay constant λ of the fundamental mode of the thermal neutron flux is separated from the measured die-away curve by means of the computer program (Drozdowicz and Krynicka-Drozdowicz 1979). It is based on Cornell's (1956) method of analysis of the curves being the sum of the exponentials and the background. The program takes into account the analyser dead time and traces the behaviour of the fundamental decay constant λ as a function of the delay time from the end of the fast neutron burst to the beginning of the analysis.

The dependence of the experimental decay constant λ upon the value of $1/\hat{R}^2_{2g}$ is the experimental curve. For further data treatment one takes the experimental points λ_i as a function of $1/\hat{R}^2_{2gi}$ which follow a straight line. The parameters of the straight line are fitted with the least square method.

The theoretical curve λ^* is calculated also as a function of $1/\hat{R}^2_{2g}$, as described in the previous paragraph.

The value $\overline{v\Sigma_{a1}}$ of the intersection point of the experimental $\lambda(\hat{R}_{2g})$ and theoretical $\lambda^*(\hat{R}_{2g})$ curves is obtained, independent of the geometry, as the solution of the equation (24a) by means of the Newton's method (Korn and Korn 1968).

The problem appears how to estimate the accuracy of the determination of the $\overline{v\Sigma_{a1}}$ value. Each measurement point $\lambda_i(\hat{R}_{2gi})$ is known with a standard deviation $\sigma(\lambda_i)$, which affects a statistical uncertainty of the experimental curve $\lambda(\hat{R}_{2g})$. The theoretical curve $\lambda^*(\hat{R}_{2g})$ is computed for a given external moderator, using its thermal neutron parameters $\overline{v\Sigma_{a2}}$, D_{o2}, C_2, which are known with some statistical accuracy. Thus, the theoretical curve $\lambda^*(\hat{R}_{2g})$ is also statistically uncertain. A method of estimating the standard deviation of the intersection point of two curves characterized by some statistical ucertainties (Krynicka-Drozdowicz 1983) is used to estimate the accuracy of the thermal neutron macroscopic absorption cross-section measurement. The method is based on a computer simulation of deviations of the curves.

The parameters of the k-th simulated experimental curve $\lambda_k(\hat{R}_{2g})$ are calculated by the fit of the k-th set of the experimental points $\{\lambda_i(\hat{R}_{2gi})\}_k$ obtained from the computer simulation as follows:

$$\{\lambda_i\}_k = \{\lambda_i + G^{\lambda}_{ik}\cdot\sigma(\lambda_i)\}\ . \tag{27}$$

Here G^{λ}_{ik} is the random number from the normal distribution with the mean equal to 0 and the standard deviation equal to 1.

The theoretical curve $\lambda^*_k(\hat{R}_{2g})$ in the k-th simulations is calculated basing on the new values of the thermal neutron parameters of the outer moderator. They are obtained as:

$$\overline{v\Sigma_{a2,k}} = \overline{v\Sigma_{a2}} + G^{\Sigma}_{k}\cdot\sigma(\overline{v\Sigma_{a2}}) \tag{28}$$

$$D_{o2,k} = D_{o2} + G^{D}_{k}\cdot\sigma(D_{o2}) \tag{29}$$

$$C_{2,k} = C_2 + G^{C}_{k}\cdot\sigma(C_2)\quad , \tag{30}$$

where G^{Σ}_k, G^{D}_k, G^{C}_k are the random numbers generated independently for each neutron parameter (from the normal distribution as mentioned above).

Equation (24a) is solved for each k-th pair of the simulated curves $\lambda_k(\hat{R}_{2g})$, $\lambda^*(\hat{R}_{2g})$ giving the set of the values $\{\overline{v\Sigma_{a1,k}}\}$. The standard deviaton $\sigma_A(\overline{v\Sigma_{a1}})$ of the intersection point $\overline{v\Sigma_{a1}}$ for the absolute measurement is estimated from this set as:

$$\sigma^2_A(\overline{v\Sigma_{a1}}) = \frac{1}{K-1}\sum_{k=1}^{K}[\overline{v\Sigma_{a1,k}} - e(\overline{v\Sigma_{a1}})]^2\ , \tag{31}$$

where

$$e(\overline{v\Sigma_{a1}}) = \frac{1}{K}\sum_{k=1}^{K}\overline{v\Sigma_{a1,k}} \tag{32}$$

and K is the number of the simulations.

In all the measurements the same sets of Plexiglass moderators were used. The part of the standard deviation caused by the uncertainty in the knowledge of the thermal neutron parameters of the moderator can be recognized as a source of a possible systematic error. Then the standard deviation $\sigma_R(\overline{v\Sigma_{a1}})$ for the relative measurement (following from the standard deviations of the experimental points only) is sufficient for an intercomparison of the results obtained for different samples. Thus, the standard deviation for the relative measurement is computed on the assumption that the theoretical curve $\lambda^*(\hat{R}_{2g})$ is exactly known.

The value of the intersection angle α^o between the experimental $\lambda(\hat{R}_{2g})$ and theoretical $\lambda^*(\hat{R}_{2g})$ curves is very important for the accuracy of $\overline{v\Sigma_{a1}}$ determination. An example for the spherical geometry of the general behaviour of the intersection angle α^o for different experimental conditions for $\Sigma_{tr2} = 2.3\ \mathrm{cm}^{-1}$ (which is roughly valid for the Plexiglass moderator) is given in Fig.6. From the figure it is clear that for small $(\Sigma_{a1} - \Sigma_{a2})$ values the bigger sample is even more convenient.

Knowing the accuracy of our measurement one can try to find the accuracy of the Σ_{ma} determination for the "poisoning" method [cf. equation (26)]. One has from equation (26) the variance $\sigma^2(\Sigma_{ma})$:

$$\sigma^2(\Sigma_{ma}) = \frac{\sigma^2(\phi)}{(1-\phi)^4}(\Sigma_w - \Sigma_{a1})^2 + \frac{\sigma^2(\Sigma_{a1}) + \phi^2\sigma^2(\Sigma_w)}{(1-\phi)^2} \qquad (33a)$$

$$= \frac{(\Sigma_w - \Sigma_{ma})^2\,\sigma^2(\phi) + \phi^2\,\sigma^2(\Sigma_w) + \sigma^2(\Sigma_{a1})}{(1-\phi)^2} \qquad (33b)$$

valid for $\Sigma_w > \Sigma_{a2}$.

5. EXPERIMENTAL RESULTS

We have checked the new method of absorption cross-section measurement for the spherical and cylindrical geometries on liquid samples of well known chemical compositions. The very good agreement between the theoretical principles of the method and experimental results has been obtained when the influence of the thermal neutron spectrum has been taken into account (the details are reported by Drozdowicz (1981) and by Drozdowicz and Woźnicka (1983)). This situation is presented in Fig.7.

To check the usefulness of the "poisoning" method we have performed another experiment with SiO_2, pure for the chemical analysis, saturated with boric acid solution. The experiment performed in extremely adverse conditions (a very low value of the absorption cross-section for the SiO_2 matrix $\Sigma_{ma} = 3.7$ c.u.) has defined the lowest limit of the measurable value of Σ_{ma} when Plexiglass moderator is used (Czubek et al. 1981).

Several measurements for geological samples (mineralized waters and rock matrices) were performed. Some values of the absorption cross-section obtained experimentally were compared with the calculated ones according to the chemical assay for the samples.

5.1. MINERALIZED WATERS

We have collected 15 samples (marked P1 ÷ P15) of mineralized waters from different geological regions of Poland (see map in Fig.8). The chemical analysis for major elements has been performed for all samples in the Laboratory of Balneochemistry at the Balneoprojekt in Warsaw, Poland. The analysis for sample P1 is listed in Table 3. The content of rare earths elements was also checked (none have been found at the levels given in Table 4) for this sample. The absorption cross-section $\Sigma_{a1\ calc}$ has been calculated according to the elemental composition of each sample using the data of Mughabghab and Garber (1973) and the results are listed in Tables 5 and 6.

The absorption cross-section Σ_{a1} was measured for samples P1 and P6. The results are presented in Table 5. The agreement between the measured values of Σ_{a1} and those calculated according to the chemical composition $\Sigma_{a1\ calc}$ is very good for sample P6. It is not so good for sample P1, probably because the knowledge of its elemental composition is not perfect.

The simplified experimental procedure was applied for the samples P2 ÷ P5 and P7 ÷ P15 and it was performed to find out the samples containing highly absorbing elements omitted in the chemical analysis.

Table 3. Elemental composition of sample P1.

Element	Concentration [µg/ml]	Element	Concentration [µg/ml]
Na^+	29,000	Mn^+	2.15
K^+	275	Cl^-	67,006.2
NH_4^+	62	Br^-	333.0
Ca^{2+}	8258.1	I^-	14.77
Mg^{2+}	2406.4	SO_4^{2-}	25.0
Ba^{2+}	42	HCO_3^-	226.42
Sr^{2+}	400	H_2SiO_3	9.10
Fe^{2+}	45.77	HBO_2	40.53
Total solid compounds: 108146.44 µg/ml			

The fundamental decay constant λ was measured for each sample in the spherical geometry for several values of the external radius of the moderator. Next, the fundamental decay constant λ_{calc} was calculated from equation (6) as a function of the radius of the external moderator, using the calculated (from chemical composition) neutrons parameters for the samples. The measured and calculated values λ and λ_{calc} were compared (cf. Table 6). They are equal to each other or the measured values are lower than the calculated ones. The latter case could occur, because for calculating λ_{calc} the elemental composition of the water samples taken was that of the upper limit of the trace element contents, and/or because the dimensions of the measured system could be larger than had been assumed (due to

Table 4. Rare earths in sample P1. Analysis has been carried out at the Department of Analytical Chemistry of the Institute of Nuclear Research in Warsaw, Poland.

Oxide	Content found below [μg/ml]	Oxide	Content found below [μg/ml]
Y_2O_3	2.5×10^{-4}	Tb_4O_7	1.0×10^{-3}
Gd_2O_3	2.5×10^{-4}	Sm_2O_3	1.0×10^{-3}
Er_2O_3	2.5×10^{-4}	La_2O_3	1.0×10^{-3}
Dy_2O_3	2.5×10^{-4}	Ho_2O_3	1.0×10^{-3}
Eu_2O_3	2.5×10^{-4}	Nd_2O_3	2.5×10^{-3}
CeO_2	1.0×10^{-3}	Pr_6O_{11}	2.5×10^{-3}
Lu_2O_3	1.0×10^{-3}		

inaccuracy of the fit of the cadmium sheet to the external surface of the Plexiglass sphere).

All the same, our measurements have shown that no sample did contain any highly absorbing elements undetected in chemical analysis.

A detailed description of those measurements on the mineralized waters and all the informations about their geological parameters are presented by Drozdowicz et al. (1983).

Table 5. Final results of the absorption cross-section measurements on the liquid samples.

t = 19.5 °C

Sample No	Density of sample ϱ $\sigma(\varrho)$	Run No	Absorption cross-section Measured $\Sigma_{a1}(v_o)$ $\sigma_A(\Sigma_{a1})$ $\sigma_R(\Sigma_{a1})$	Absorption cross-section Calculated $\Sigma_{a1\ calc}(v_o)$
	[g/cm^3]		[c.u.]	[c.u.]
P1 Jaworze IG-1	1.075 ?	1	55.81 0.99 0.59	60.16
		2	55.60 1.24 0.39	
P6 Ciechocinek XVI	1.0430 0.0005	1	44.10 1.19 0.62	44.8

Table 6. Fundamental decay constant for liquid samples P2 ÷ P5 and P7 ÷ P15.

$t = 19.5\ ^{o}C$	Specific gravity ϱ $\sigma(\varrho)$	Absorption cross-section (calculated) $\Sigma_{a1\ calc}(v_o)$	Radius of the sample R_1	Radius of the moderator R_{2g}	Number of runs	Fundamental decay constant	
Sample No						Measured *) $\bar{\lambda}$ $\sigma(\bar{\lambda})$	Calculated λ_{calc}
	[g/cm^3]	[c.u.]	[cm]	[cm]		[s^{-1}]	[s^{-1}]
1	2	3	4	5	6	7	8
P2 Edward II	1.0215 0.0005	33.6	5.03	11.5	3	7 274 26	7 672
				10.5	1	8 097 41	8 425
				9.5	2	9 413 24	9 414
P3 Kołobrzeg B1	1.0355 0.0005	41.3	4.01	11.5	2	7 194 43	7 413
				10.5	2	7 854 32	8 110
				9.5	2	8 962 28	9 042

1	2	3	4	5	6	7	8
				8.5	5	10 296 26	10 315
P4 Kołobrzeg 16A	0.9995 0.0005	22.7	5.03	8.5	1	9 187 70	9 286
P5 Ciechocinek XIV	1.0270 0.0005	37.2	5.03	13.5	2	6 551 53	6 725
				12.5	2	6 775 44	7 204
				11.5	2	7 461 44	7 819
				10.5	4	8 278 37	8 621
				9.5	3	9 437 27	9 678
P7 Ciechocinek 18	1.0460 0.0005	46.4	5.03	7.5	3	14 132 59	14 293
P8 Warszawa IG-1	1.0440 0.0005	45.1	4.01	9.5	2	9 103 50	9 279
				8.5	2	10 451 46	10 648

1	2	3	4	5	6	7	8
				7.5	1	12 447 42	12 572
P9 Zuber I	1.0150 0.0005	22.8	4.01	7.5	3	10 290 55	10 426
P10 Zuber III	1.0170 0.0005	23.1	4.01	7.5	2	10 393 48	10 459
P11 Piwniczanka II	0.9995 0.0005	22.2	4.01	5.5	1	14 954 75	15 164
P12 Zakopane IG-1	0.9990 0.0005	22.2	4.01	5.5	1	14 962 47	15 164
P13 Bańska IG-1	1.0004 ?	22.8	5.03	6.0	1	13 662 75	13 831
P14 Bańska IG-1	0.9995 0.0005	22.5	5.03	7.5	2	10 652 58	10 670
P15 Bańska IG-1	1.0005 ?	22.9	5.03	6.0	1	13 580 33	13 852

*) averaged over the number of runs.

5.2. SOLID SAMPLES

Some measurements for crushed rocks have been performed in order to get the absorption cross-section Σ_{ma} of the rock matrix. The intersection of the theoretical and experimental curves, which determines the thermal neutron absorption cross-section of the sample $v\Sigma_{a1}$, can be obtained when the condition (25) is fulfilled.

The H_3BO_3-saturation method was used in this case. The crushed rock was saturated by some highly absorbing fluid. The 1.0, 1.5 or 2.0 per cent water solutions of boric acid (H_3BO_3) were used here. The absorption cross- section of the "poisoned" sample fulfilles the condition (25) and the absorption cross-section of the rock matrix Σ_{ma} can be obtained from equation (26). High precision in the porosity determination needed here requires very careful filling of the sample vessel. Still, when the saturation is made under normal atmospheric pressure some errors occur. They are due to small amounts of the air which always remain in the sample. In our treatment of data we have taken these errors into account (equation (33)). A special equipment for saturating under a low pressure the crushed solid samples is being constructed for future measurements.

The measurements for one core sample of dolomite and for seven samples taken from different basalt quarries in Poland have been performed. We have taken the dolomite core sample (marked S1) from the Tokarnia IG-1 borehole situated about 60 km south of Cracow in the Carpatian Mountains. It is a pelitic limestone and dolomite series of Middle and Upper Jurassic age in the Magura nappe, Siary Subunit situated in the Basement of the Outer Carpatian Flysch at the depth of $3450 \div 3470$ m. The basalt samples marked S4, S8, S9 are of the Miocene age from the Lower Silesia and the other marked S3, S7, S10, are of the Permian age, taken from the Carpatian Foreland 30 km West of Cracow (see map in Fig.9).

The granulation of the crushed samples was $0.6 \div 0.75$ mm. The results of the determination of the $\overline{v\Sigma_{a1}}$ values for the "poisoned" samples together with the $\Sigma_{ma}(v_o)$ values obtained for these basalts are presented in Table 7. The relatively high standard deviations of the final results $\Sigma_{ma}(v_o)$ were obtained due to high standard deviations of the $\overline{v\Sigma_{a1}}$ values, probably caused by some apparatus errors (during registration of the die-away curves). An example of the plot of the theoretical curve λ^* with the experimental values of the decay constant λ are shown for dolomite in Fig.10, in function of $1/R_{2g}^2$, where R_{2g} is the outer radius of the Plexiglass spherical moderator.

A chemical assay for the dolomite sample has been performed for the major elements and the result is: moisture - 0.09 %; roasting loses - 45.42 %; SiO_2 - 2.62 %; Fe_2O_3 - 0.33 %; Al_2O_3 - 0.46 %; CaO - 34.37 %; MgO - 16.35 %; MnO - 0.05 %; BaO - 0.04 %; total - 99.64 %. The value of $\Sigma_{ma\ calc}(v_o)$ can be calculated for this dolomite according to its elemental composition (Mughabghab and Garber (1973) data of microscopic absorption cross-section were used). The value of the calculated absorption cross-section (see Table 7) was too low, because the

Table 7. Final results of the absorption cross-section measurements for the solid samples.

Sample	Specific gravity	Absorption cross-section of poisoned sample	Absorption cross-section of the rock matrix	
No and name	ϱ $\sigma(\varrho)$	$\overline{v\Sigma_{a1}}$ $\sigma_A(\overline{v\Sigma_{a1}})$ $\sigma_R(\overline{v\Sigma_{a1}})$	$\Sigma_{ma}(v_o)$ $\sigma_A(\Sigma_{ma})$ $\sigma_R(\Sigma_{ma})$	$\Sigma_{ma}(v_o)/\varrho$ $\sigma_A(\Sigma_{ma}/\varrho)$ $\sigma_R(\Sigma_{ma}/\varrho)$
	[g/cm^3]	[s^{-1}]	[c.u.]	[c.u./(g cm^{-3})]
S1 Tokarnia IG-1	2.73 0.01	13 795 306 100	10.5 *) 2.8 1.5	3.83 1.02 0.55
		10 227 232 108	10.4 *) 2.5 1.9	3.83 0.92 0.70
S3 Rudno I	2.69 0.01	18 161 481 282	16.8 4.4 2.9	6.26 1.62 1.09
S4 Księginki	2.98 0.01	15 028 513 231	23.6 4.1 2.1	7.92 1.39 0.70
S7 Tenczynek	2.68 0.01	18 373 324 150	20.9 3.1 2.1	7.78 1.15 0.77
S8 Wieża	2.98 0.01	15 027 643 258	20.2 5.2 2.3	6.77 1.74 0.77
S9 Józef	3.02 0.01	19 226 445 293	22.5 4.0 3.0	7.45 1.34 0.99
S10 Zamek	2.72 0.01	14 985 506 240	14.8 4.4 2.3	5.44 1.62 0.85

*) The absorption cross-secton calculated for this sample according to the chemical composition is:

$$\Sigma_{ma\,calc}(v_o) = 5.6 \text{ c.u.}$$

elemental analysis was incomplete (e.g. elements of the rare earths have not been analysed at all).

Our results of Σ_{ma}/ϱ obtained for basalts are presented in Fig. 11 together with the experimental data obtained by Allen and Mills (1975) for other magmatic rocks. For comparison the Σ_{ma}/ϱ values computed for the average elemental composition of 17 different magmatic rocks (according to the averaged data reported by Daly, 1933) are also plotted in Fig. 11. The elemental composition of our basalt samples was unknown, so these results are plotted on the abscissa corresponding to the average range of the SiO_2 content for basalts. The experimental Σ_{ma}/ϱ values are always much higher than the calculated ones (according to the chemical assay), sometimes by a factor of 2. Furthermore, the dispersion of experimental Σ_{ma}/ϱ values for the same kind of magmatic rock is higher than the accuracy of measurement, which suggests that the traces of highly absorbing elements in these rocks are variable.

6. FINAL REMARKS

We have checked the utility of the new method of measurement of the absorption cross-section for thermal neutrons on small samples. The advantage of this method is the independence of the final results upon the transport cross-section of the sample and the fact that only one sample having some well defined geometrical form is needed here. One standard deviation of the absolute measurement for liquid samples did never exceed 1.24 c.u. in our measuremennts, whereas for solid samples it was 5.2 c.u.. For the relative measurements it was 0.62 c.u. and 3.0 c.u., respectively. A higher standard deviation observed for solid samples is due to the "poisoning" method of measurement for which the two independent absorption cross-section measurements (one for sample saturated with poisoning liquid, the other for the liquid itself) have to be carried out. Such procedure is common for all methods of measurement of weakly absorbing samples and we have studied this problem carefully. Moreover, the high standard deviation values (up to 5.2 c.u.) were observed for basalt samples only, when we had some doubts concerning good operation of our equipment. An inaccuracy of determination of porosity is another source of errors in the absorption cross-section measurement for solid samples.

The factors mentioned above, which influence the final accuracy of measurement, do not seem to have been considered with sufficient attention by other experimenters using the poisoning method. Such an attitude leads to estimating lower statistical errors than really occured in their essays. We suspect that the errors reported by them are close to our errors for the relative measurement.

REFERENCES

Allen L.S. and Mills W.R.Jr. (1975): Measurement of the thermal neutron absorption cross-section of rock samples by a pulsed source method. The Log Analyst, 16, 10÷13.

Antonov A.V., Granatkin B.V., Merkulev A.Yu., Miller V.V. and Shimelevich Yu.S. (1966): pp 139÷150 in "Radioisotope Instrument in Industry and Geophysics", vol.2, IAEA, Vienna.

Burda J., Igielski A. and Kowalik W. (1982): Electronic instrumentation system for pulsed neutron measurements. INP Report No 1182/E.

Carre J.C. (1968): Mesure de la section de capture thermique des matherieux utilises pour la fabrication des betons. CEA CEN Fontenay aux Roses, DEP SEPP-GEP, Note MIN, Octobre 1968.

Cornell R.G. (1956): A new estimation procedure for linear combination of exponentials. ORNL Report No 2120.

Czubek J.A. (1981): A method for measurement of thermal neutron absorption cross-section in small samples. J.Phys.D: Appl. Phys. 14, 1167÷1182.

Czubek J.A., Drozdowicz K., Igielski A., Krynicka-Drozdowicz E., Sobczyński Z. and Woźnicka U. (1981): Thermal neutron absorption cross-section for small samples: experiments in spherical geometry. J.Phys.D: Appl. Phys. 14, 977÷984.

Daly R.A. (1933): Igneous rocks and the depths of the Earth. McGraw-Hill Book Company, New York.

Drozdowicz K. (1981): Energy corrections in pulsed neutron measurements. J.Phys.D: Appl.Phys. 14, 793÷804.

Drozdowicz K. and Krynicka-Drozdowicz E. (1979): Fit of experimental points to the sum of two (or one) exponentials with background. Part II. INP Report No 1044/PM.

Drozdowicz K., Igielski A., Krynicka-Drozdowicz E., Sobczyński Z. and Woźnicka U. (1980): Thermal neutron diffusion parameters for Plexiglass. Nucl.Instrum.Methods 178, 513÷516.

Drozdowicz K. and Woźnicka U. (1982): A solution of the thermal neutron diffusion equation for a two-region cylindrical system. Program for ODRA-1305 computer. INP Report No 1180/PM.

Drozdowicz K. and Woźnicka U. (1983): Energy corrections in pulsed neutron measurements for cylindrical geometry. J.Phys. D: Appl.Phys. 16, 245÷254.

Drozdowicz K., Igielski A., Krynicka-Drozdowicz E. and Woźnicka U.(1983): Thermal neutron absorption cross-section for mineralized waters. INP Report No 1224/AP.

Harris J.M. and Mc Daniel P.J. (1982): Small sample thermal neutron cross-section determination from reactivity measurements. SPWLA 23-rd Ann.Logg.Symp.Trans., Paper HH, July 6÷9, 1982, Corpus Christi, Texas.

Korn G.A. and Korn T.M. (1968): Mathematical Handbook for Scientists and Engineers. McGraw-Hill Book Company, New York.

Krynicka-Drozdowicz E. (1983): Standard deviation of the intersection point for two stasistically uncertain curves. INP Report No 1212/PM.

Mughabghab S.F. and Garber D.I. (1973): Neutron Cross-sections, Vol.1: Resonance Parameters. BNL Report No 325.

Nelkin M. (1960): Milne's problem for a velocity-dependent mean free path. Nucl.Sci.Eng. 7, 552÷553.

Rösler H.J. and Lange H. (1972): Geochemical Tables. Edition Leipzig.

Williams M.M.R. (1964): The energy-dependent Milne problem with a simple scattering kernel. Nucl.Sci.Eng. 18, 260÷270.

Williams M.M.R. (1966): "The Slowing Down and Thermalization of Neutrons". North-Holland, Amsterdam. p.238.

Woźnicka U. (1981): Solution of the thermal neutron diffusion equation for a two-region system by perturbation calculation. J.Phys.D: Appl.Phys. 14, 1167÷1182.

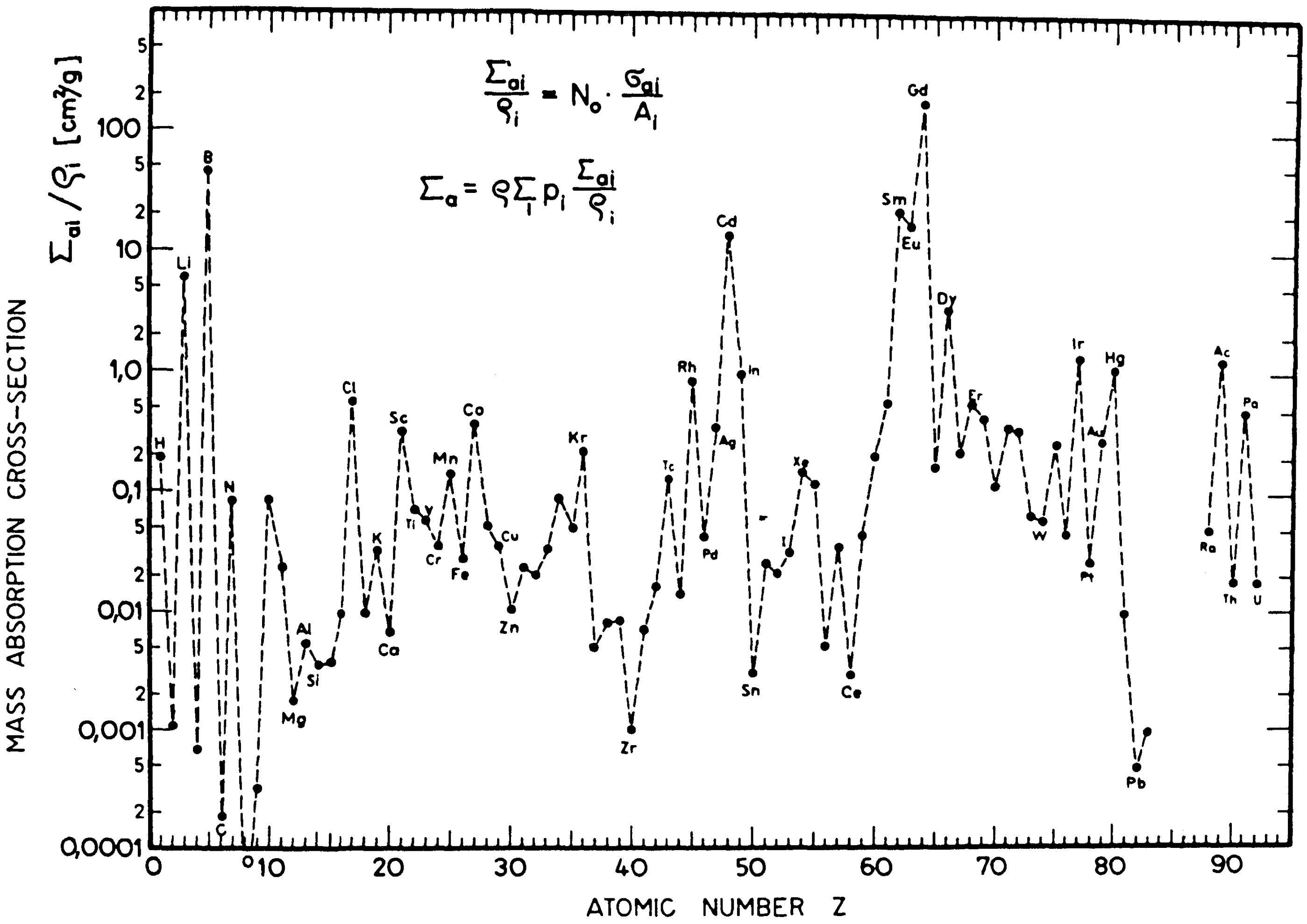

Fig.1. The absorption cross-section Σ_{ai}/ϱ_i of all elements of the periodic table.

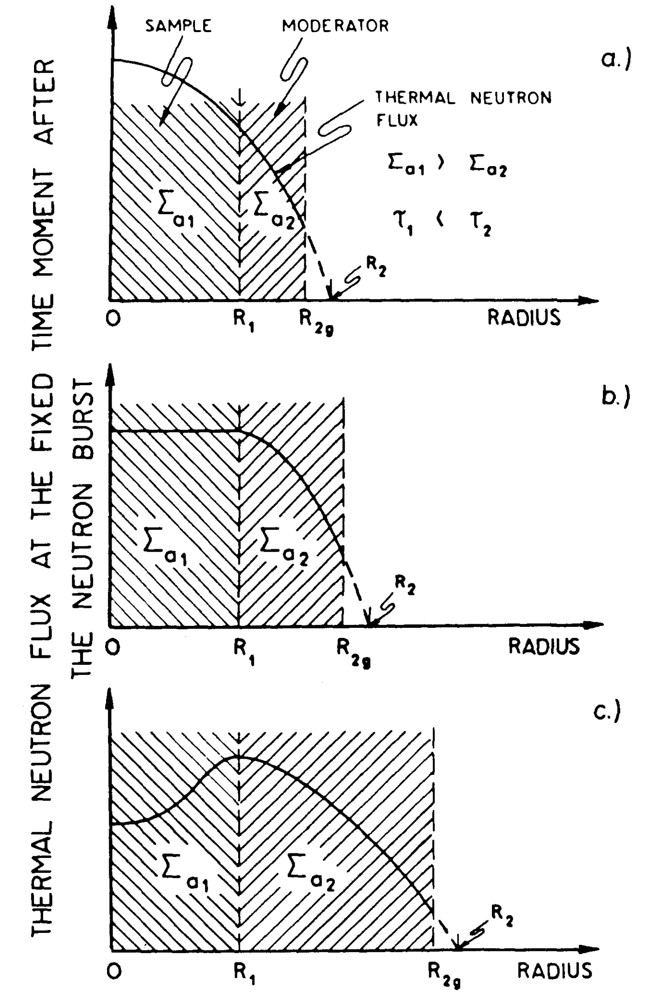

Fig.2. Schematic view of the space distribution of the thermal neutron flux inside the sample-moderator system for some fixed time moment after the fast neutron burst.

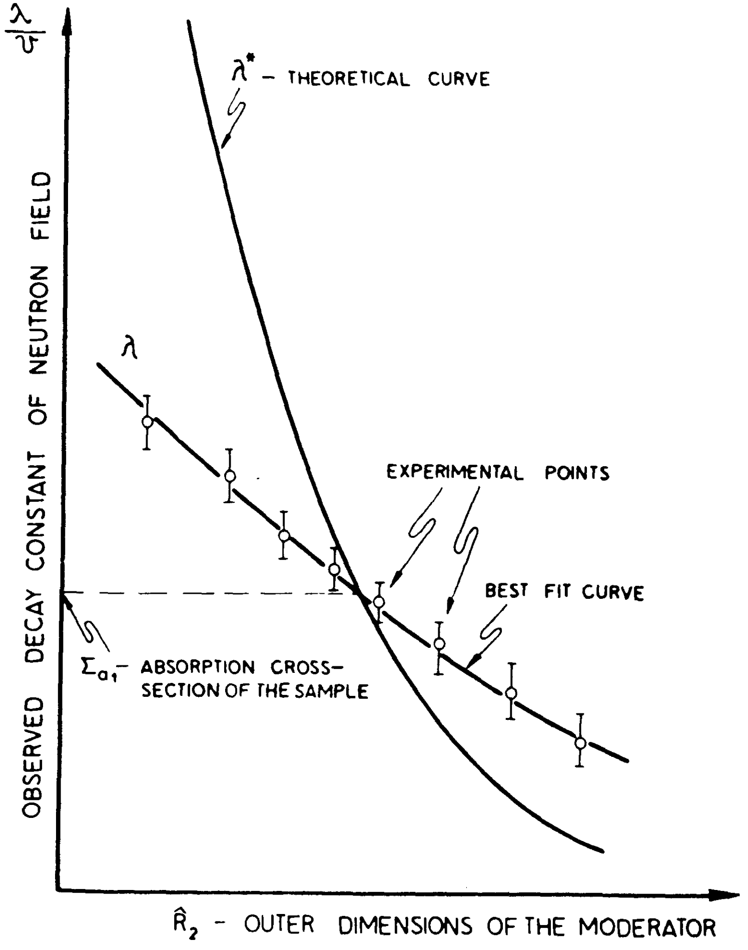

Fig.3. Mutual positions of the experimental λ and theoretical λ^* curves as a function of the dimensions $\hat{R}_2$ of the moderator.

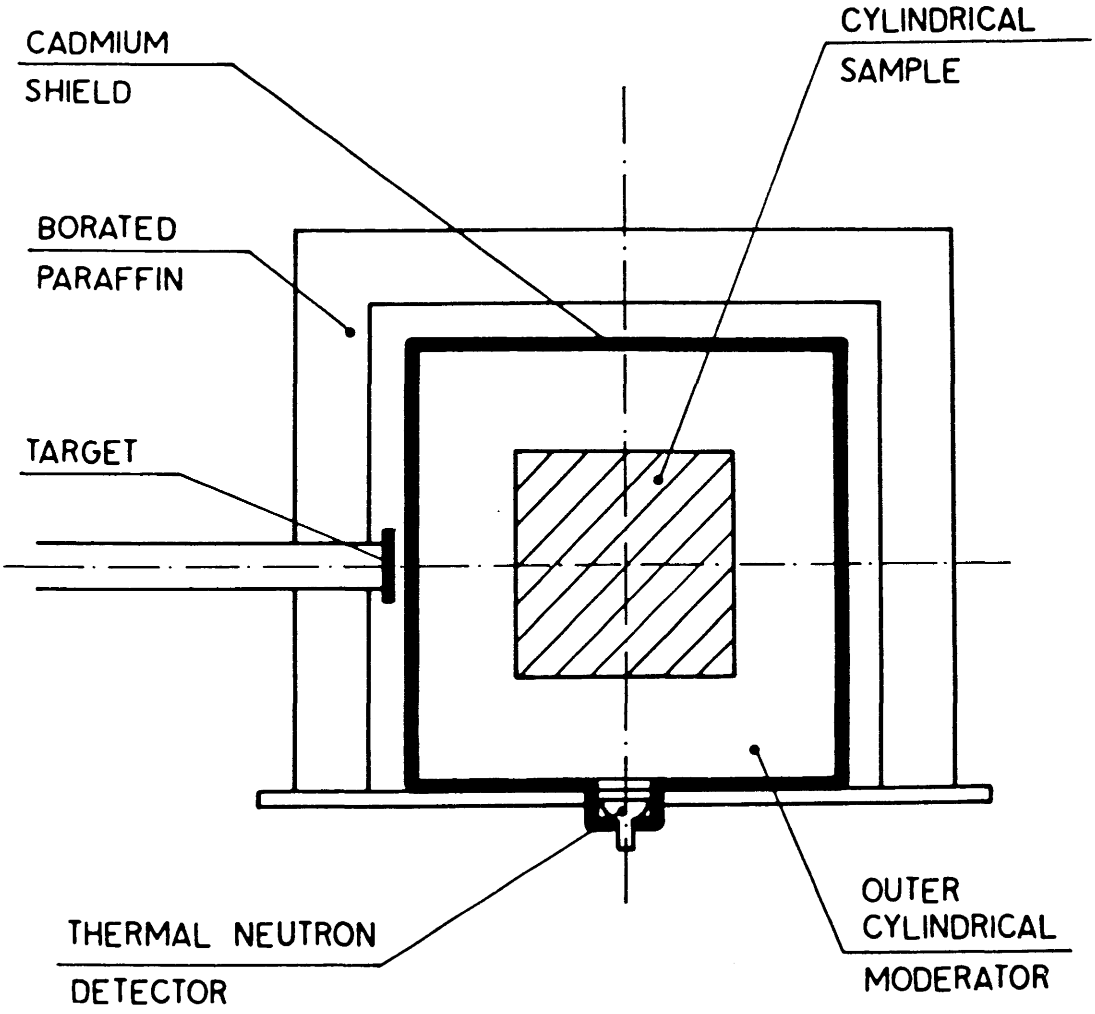

Fig.4. Cylindrical measurement geometry realized in the experiment.

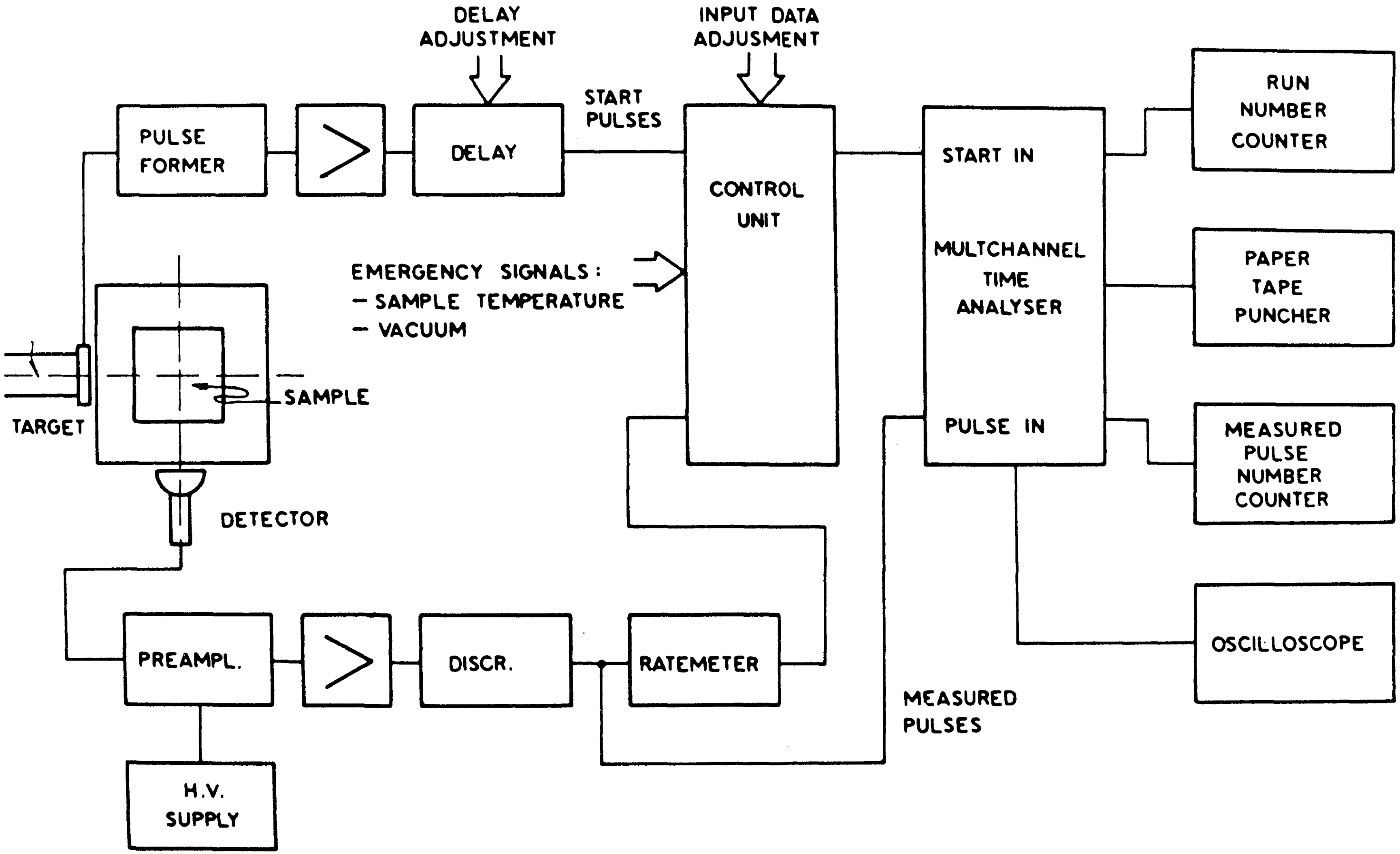

Fig.5. Instrumentation system used in the experiment
(Burda et al. 1982).

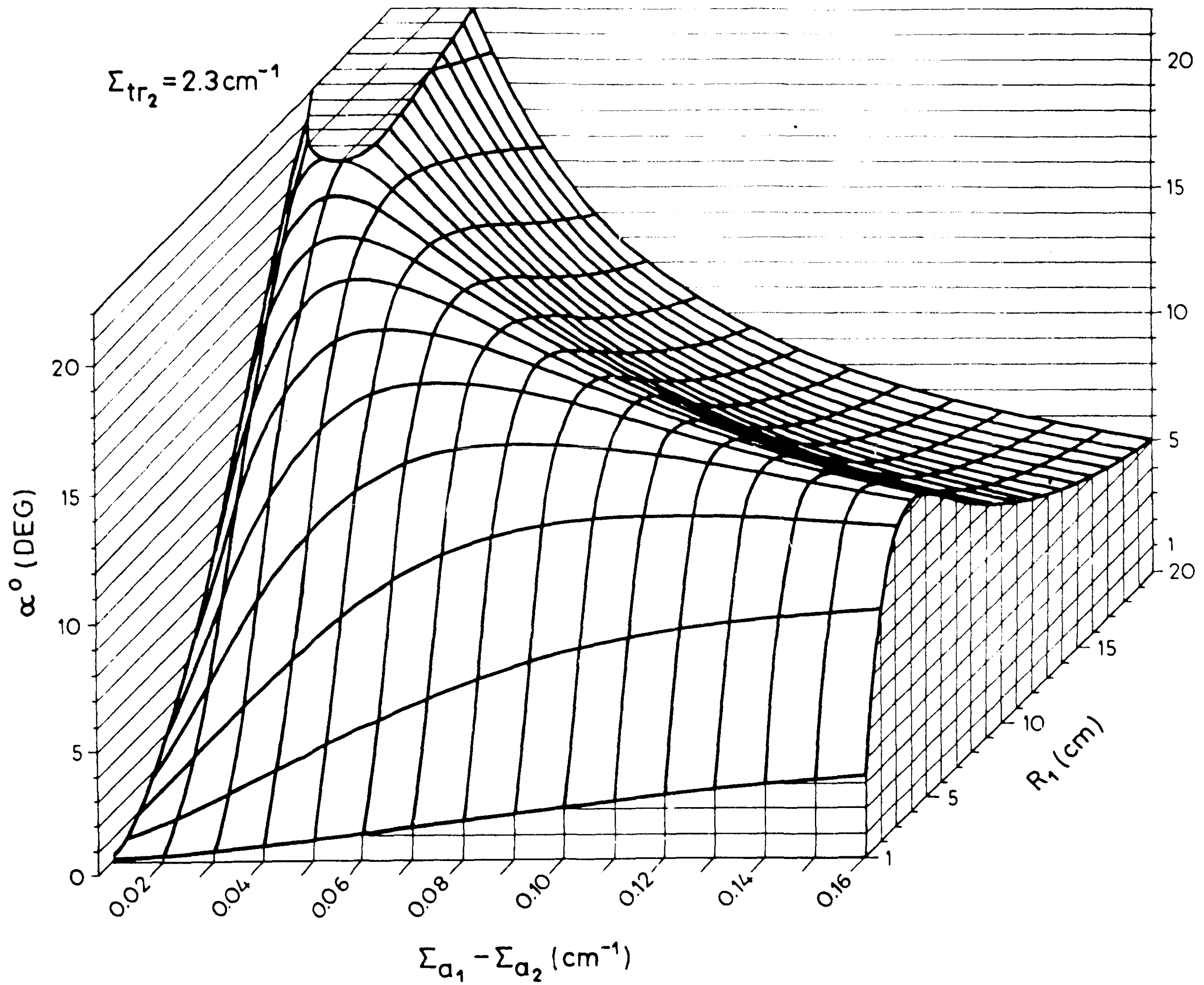

Fig.6. Intersection α^o values in function of the radius R_1 of the spherical sample and of the absorption cross-section $(\Sigma_{a1}-\Sigma_{a2})$ and for the constant value of the moderator transport cross-section Σ_{tr2} = 2.3 cm^{-1} (Czubek 1981).

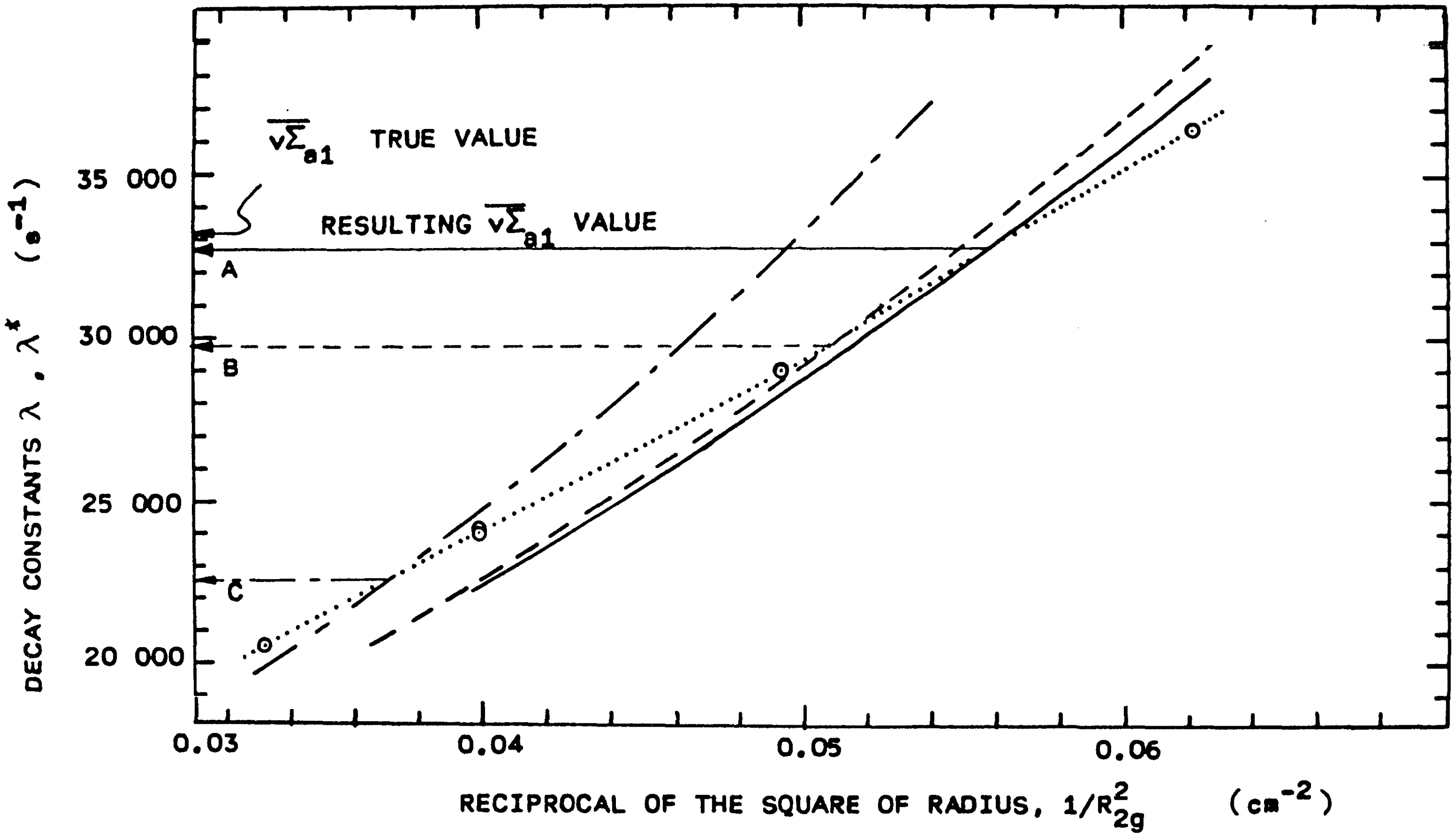

Fig. 7. Positions of the intersection point between the theoretical curve and measured one. Outer moderator: Plexiglass. Theoretical λ^* curves are calculated for the assumptions: A - correct solution according to equations (19b) and (21). B - velocity v_{oc} was assumed to be equal to v_o. C - diffusion cooling coefficient was neglected (i.e. C_2=0). The standard deviation due to the counting statistics for each experimental point is smaller than the size of the point in the figure (Czubek et al. 1981).

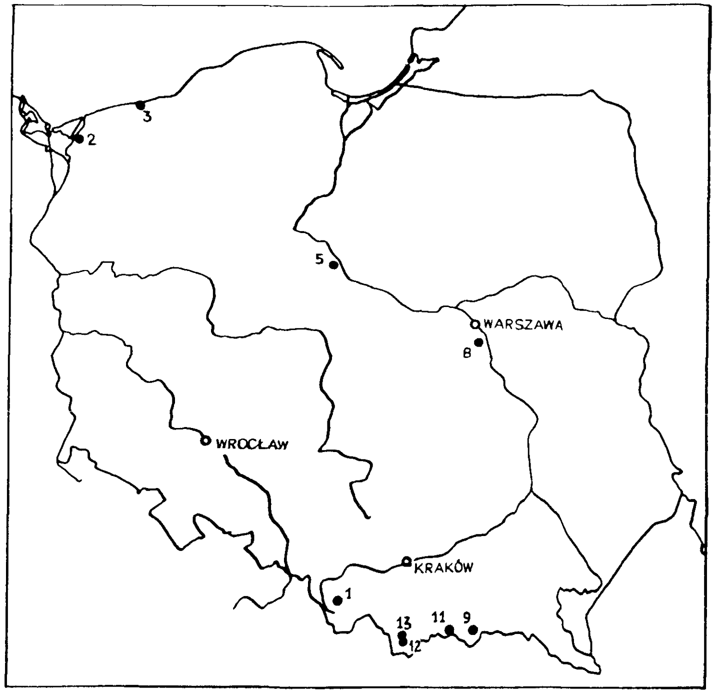

1.JAWORZE IG-1: P1
2.KAMIEŃ POMORSKI EDWARD II: P2
3.KOŁOBRZEG B-1: P3
16-A: P4
5.CIECHOCINEK TERMA XIV: P5
TERMA XVI: P6
TERMA XVIII: P7
8.KONSTANCIN WARSZAWA IG-1: P8
9.KRYNICA ZUBER 1: P9
ZUBER 3: P10
11.PIWNICZNA PIWNICZANKA II: P11
12.ZAKOPANE IG-1: P12
13.BIAŁY DUNAJEC
BAŃSKA IG-1: P13,P14,P15

Fig.8. Collection sites of mineralized waters.

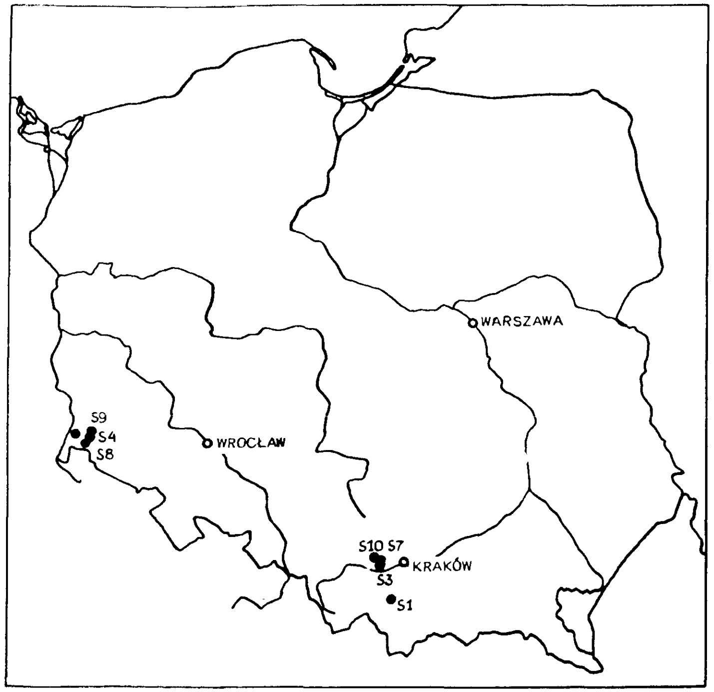

S1.	TOKARNIA IG-1	DOLOMITE	JURASSIC AGE
S3.	RUDNO I	BASALT	PERMIAN AGE
S4.	KSIĘGINKI	BASALT	MIOCENE AGE
S7.	TENCZYNEK	BASALT	PERMIAN AGE
S8.	WIEŻA	BASALT	MIOCENE AGE
S9.	JÓZEF	BASALT	MIOCENE AGE
S10.	ZAMEK	BASALT	PERMIAN AGE

Fig.9. Collection sites of solid samples.

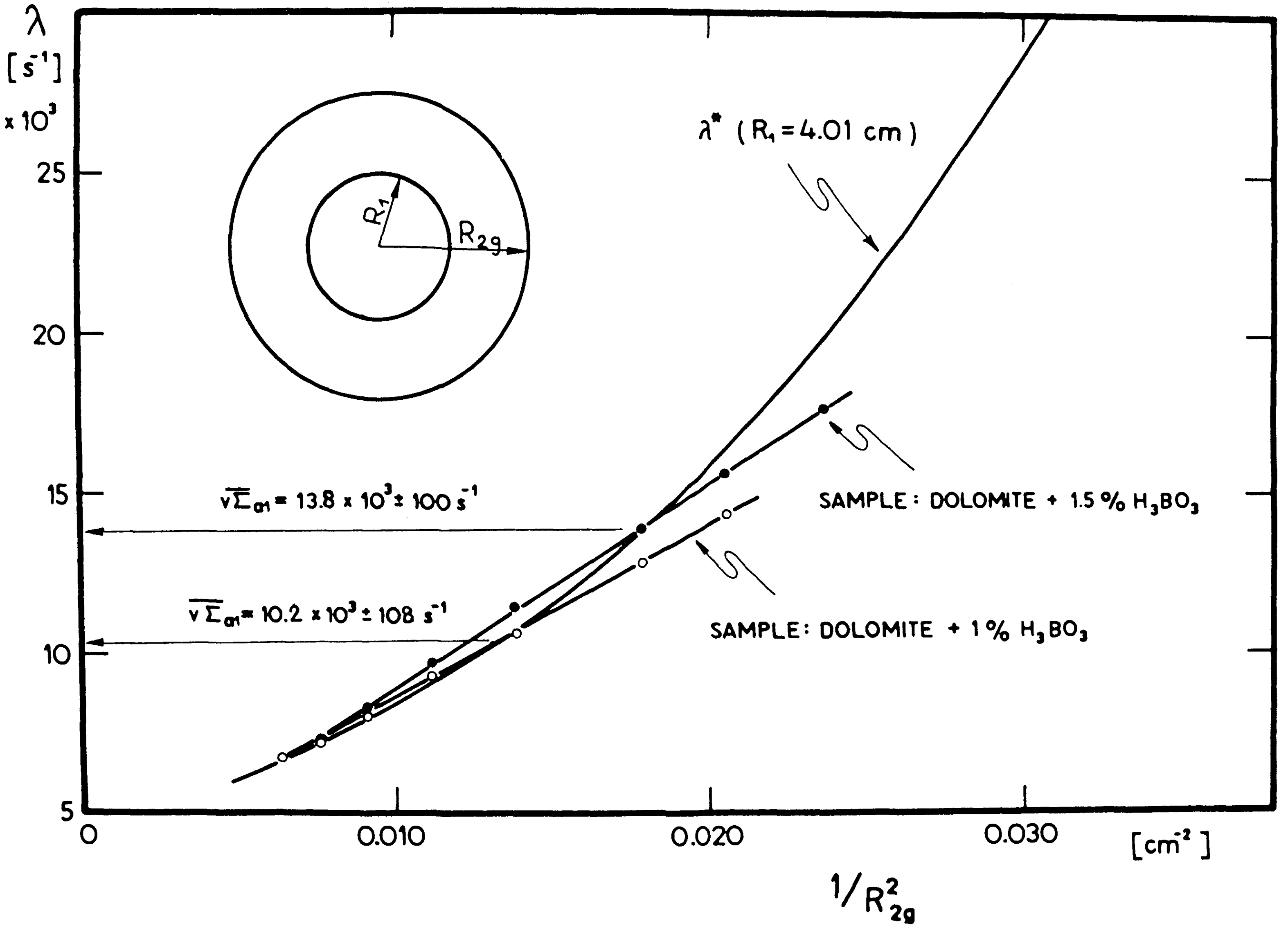

Fig.10. Determination of the $\overline{v\Sigma}_{a1}$ value for the dolomite sample for two solutions of boric acid. The standard deviation of each experimental point - see remark under Fig. 7.

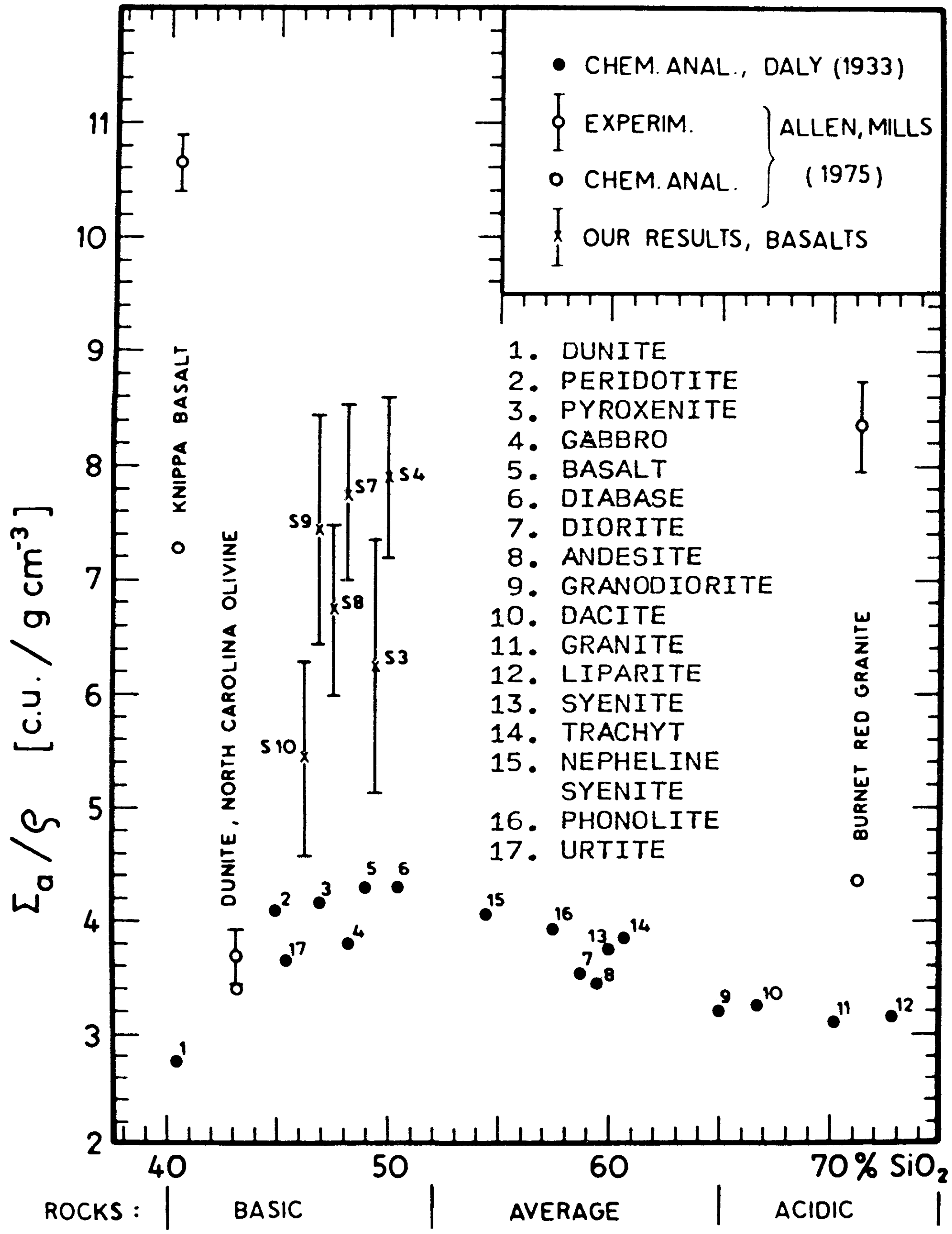

Fig.11. Thermal neutron mass absorption cross-section for igneous rocks.

CALCULATION OF NEUTRON SPECTRA AND MODERATION CHARACTERISTICS OF ROCKS - AN ARITHMETIC APPROACH

K. Morstin & A. Kreft
Institute of Physics and Nuclear Techniques AGH, Krakow, Poland

ABSTRACT

An efficient method of calculating the slowing down length, probability of non-capture during slowing down and fast neutron spectrum based on the multigroup cross section data is presented. The computational procedure takes into account the elastic scattering, the inelastic scattering and the neutron absorption during slowing down and applies for rocks and soils of any chemical composition and for any neutron sources of energies up to 15 MeV. The method has been employed for the water saturated sandstone, limestone, dolomite and some other media for different neutron sources. A comparison between the calculated slowing down length values and the available experimental data is done. The dependences of slowing down parameters on the neutron energy and chemical composition of rocks and soils have been investigated.

CALCULATION OF NEUTRON SPECTRA AND MODERATION CHARACTERISTICS OF ROCKS - AN ARITHMETIC APPROACH

K. Morstin & A. Kreft
Institute of Physics and Nuclear Techniques AGH, Krakow, Poland

Introduction

Calculation of neutron transport through extended media is at present a routine but expensive and time consuming task. Although some standard radiation-shielding transport codes, such as ANISN, DOT, MORSE, etc., are now widely distributed, most nuclear geophysics research groups (particularly in developing countries) can hardly operate them due to the lack of large computers and required skills. Moreover, there are still some difficulties with access to up-to-date nuclear data files.

However, for many practical problems of nuclear geophysics, knowledge of space and time integrated neutron spectra and some related integral parameters, describing the slowing-down process in the whole investigated medium, is sufficient. A simplified arithmetic approach may be easily applied for this purpose, provided the medium is large enough to neglect the outer leakage, which is certainly the case in all nuclear well-logging questions. The only input data required are: the source spectrum, the elemental composition of the medium, and some multigroup P_o (but transport-corrected) cross-section set.

Integrated spectra

The probability that a neutron originating in the group "1" will appear in the group "i" can be determined from the simple recurrence procedure/1/:

$$R_{1,i} = \sum_{j=1}^{i-1} \frac{\Sigma_s(j,i)}{\Sigma_{r,j}} R_{1,j} \ , \quad R_{1,1} \equiv 1 \ ,$$

where $\Sigma_{r,j}$ stand for macroscopic removal (outscatter + absorption) cross-sections, whereas $\Sigma_s(j,i)$ are the elements of the inter-group transfer matrix. The integrated neutron spectrum can be now evaluated as

$$\Phi_i \cdot \Delta E_i = \frac{Q_1 \cdot R_{1,i}}{\Sigma_{r,i}} \ ,$$

where Q_1 and ΔE_i denote the source spectrum (normalized group fractions) and group widths, respectively. It is sometimes more convenient to display spectra in the lethargy scale ($\phi(u)=E\cdot\Phi(E)$), as it is done in Fig. 1 which presents the neutron spectra calculated for dry sandstone and for different sources, with the use of the old ABBN data set /2/ (after some updating, modifications and extension up to 15 MeV /3/$^{x)}$).

The same algorithm may be also applied for determining scattered spectra of neutron-induced prompt gamma radiation, provided the appropriate photon cross-sections are coupled with neutron data in a common group scheme. According to our experience, however, the large uncertainties and gaps in accessible gamma-ray production data files create drastic problems in coupling procedures, and consequently result in significant inaccuracies of calculated spectra, even though the photon interaction data are properly evaluated.

Slowing-down parameters

The probability that a neutron appearing in the group "i" will reach the group "n" can be also determined in a recurrent way, that is /1/

$$X_{i,n} = \frac{1}{\Sigma_{r,i}} \sum_{j=i+1}^{n} \Sigma_s(i,j)\cdot X_{j,n} \ , \quad X_{n,n} \equiv 1 \ .$$

Thus, the probability that neutrons from a given source will avoid absorption when slowing-down is obviously given as

$$P = \sum_{1} Q_1 \cdot X_{1,N} \ ,$$

where N is the total number of neutron groups. In Fig. 2 the

---

x) Most of the results presented in this communication were obtained with these data called further on as ABBNM.

non-capture probabilities for D-T neutrons are plotted vs. water-saturated porosity of some typical rock media, i.e. sandstone (SiO_2), limestone ($CaCO_3$), and dolomite ($CaCO_3.MgCO_3$).

Also the parameters characterizing the space and time evolution of a neutron field during the slowing-down process can be now evaluated. The slowing-down length L_s, which is a measure of the second spatial moment of moderated neutrons, is given by the relation

$$L_s^2 = \sum_l Q_l \cdot \sum_i \frac{1}{3\Sigma_{tr,i} \cdot \Sigma_{r,i}} \cdot \frac{R_{l,i} \cdot X_{i,n}}{P} ,$$

where $\Sigma_{tr,i}$ are macroscopic transport cross-sections. Similarly, the slowing-down time

$$t_s = \sum_l Q_l \cdot \sum_i \frac{1}{\Sigma_{r,i} \cdot \bar{v}_i} \cdot \frac{R_{l,i} \cdot X_{i,n}}{P} ,$$

where $\bar{v}_i$ are group-mean values of neutron velocity. The resulting values of L_s and t_s for D-T neutrons slowed-down to 0.215 eV in water-saturated rocks are presented in Fig.3 (the values for dense media are marked at the ordinate axes).

The values of L_s^2, calculated to 1.46 eV for some typical neutron spectra, are compared in Table 1 with available experimental values of the neutron age at this energy. In most cases the agreement is fairly good. The most pronounced discrepancy (∿25 %) occurs for $CaCO_3$. It does not necessarily derive from inaccuracies in cross-sections and/or computational procedure - TITTMAN's /10/ experimental value is the only one avaible for this substance. For graphite there are also given the results of calculations with another multigroup data set, processed into the ABBNM group structure (27 groups from 15 MeV down to the thermal energy range) from ENDF/B-IV library /16/ with the use of the XLACS code /17/. In no case they deviate more than by 10 % from the ABBNM results.

Table 1. Comparison between measured and calculated neutron ages to 1.46 eV

Source	Medium	Experiment		Present calculations x)
		$\tau = L_s^2$ [cm^2]	Ref.	L_s^2 [cm^2]
^{235}U	H_2O	27.68 ± 0.10 26.60 ± 0.30 27.82 ± 0.66	4 5 6	25.5
	graphite 1.6 g/cm^3	307.8 ± 1.9	7	295.6 282.8 xx)
Ra-Be	H_2O	54.4 ± 2.1	8	53.3
	graphite 1.6 g/cm^3	∿380	9	384 368 xx)
	SiO_2 1.61 g/cm^3	1906 ± 90 xxx)	10	2079
	$CaCO_3$ 2.72 g/cm^3	461 ± 23 xxx)	10	580
	dolomite	361	11	414
Pu-Be	H_2O	52.8 ± 2.5	12	55.8
	graphite 1.6 g/cm^3	∿416	9	385 370 xx)
Po-Be	H_2O	55.4 ± 1.7 57.9 ± 1.7 57.3 ± 2.0 57.4 ± 2.5	13 13 12 14	56.9
D-T	H_2O	150 ± 6	15	145.5
	graphite 1.6 g/cm^3	∿500	9	468 509 xx)

x) Performed with ABBNM unless marked otherwise. Results slightly differ from those obtained with original ABBN data /1/

xx) Achieved with data derived from ENDF/B-IV

xxx) Age to 1.6 eV

Influence of a borehole

Well-logging probes are always located in a borehole which intersects inverstigated rock formations and is usually filled with some water-based drilling fluid. This significantly influences detector response and must not be neglected in calibration and interpretation procedures. The borehole-disturbed distributions of registered radiation may, however, be characterized by some effective parameters, related to properties of both outer and inner media.

In order to evaluate such effective neutron slowing-down parameters one has to account for the probability $P_H(E)$ that neutrons emitted in the borehole may subsequently collide there before being "homogenized" (i.e. before leaving the hole with energy E and some chance to return). This concerns all macroscopic cross-sections involved, i.e.

$$\Sigma_{eff} = \Sigma_H(E)\cdot P_H(E) + \Sigma(E)\cdot(1-P_H(E)) ,$$

where $\Sigma_H(E)$ denotes any macroscopic cross-sections of the inner medium. By introducing these effective cross-sections into the algorithms previously described, one can readily obtain the effective neutron spectra and evaluate the effective values of L_s and t_s . But how to estimate the group values of the probability P_H?

As it has been already derived /3/, the probability that neutrons will not leave the strong moderator while scattering within the group "j" is well approximated by

$$p_j = \frac{\pi_j}{\bar{n}_j}\,\frac{1-\pi_j^{\bar{n}_j}}{1-\pi_j} ,$$

where $\bar{n}_j \approx \Sigma_{tot,j}/\Sigma_{r,j}$ is a mean number of non-capture collisions in the group "j", while π_j denotes the group-averaged value of the collision probability in a finite medium. The latter can be estimated /18/ from the formula

$$\pi_j = \frac{4\,(V/S)\,\Sigma_{s,j}}{1+4\,(V/S)\,\Sigma_{s,j}} ,$$

where (V/S) stands for an effective linear dimension of a finite medium (e.g. the half-radius for an axially infinite cylinder). Hence, the probability that a neutron born in the group "1" will appear in the group "i",selectively due to collisions within the source heterogeneity, can be determined from the recurrence procedure /3/:

$$T_{1,i} = \sum_{j=1}^{i-1} p_j \frac{\Sigma_s(j,i)}{\Sigma_{r,j}}\, T_{1,j} , \qquad T_{1,1} = 1 ,$$

and finally,

$$P_{H,i} = \frac{\sum_l Q_l\cdot T_{l,i}}{\sum_l Q_l\cdot R_{l,i}}\, p_i .$$

The effective L_s values calculated in this manner for sandstone of varying porosity are displayed in Fig. 4 vs. the radius of the borehole filled with fresh water. Similar in shape results were obtained for the effective slowing-down length in limestone and dolomite, as well as for the slowing-down time (see Fig. 5). Such strong interrelations with borehole properties are in accordance with the results of CZUBEK's calculations /19/ which were performed in a completely different manner. It has to be emphasized, however, that since most of the introduced approximations assume strong moderation abilities of the inner medium, the proposed algorithm must not be applied for the case of an empty hole.

Summary

The presented method of calculating the neutron spectra and slowing-down parameters of extended media allows for all fundamental fenomena of neutron transport, i.e. both elastic and inelastic scattering, absorption and multiplication, fission, etc. Associated production of gamma-rays and their subsequent interactions can also be taken into account. In spite of this, connected efforts, computer time and costs are negligible when compared with those of regular radiation transport calculations. With some moderately extended cross-section file (as e.g. those applied here: 27 groups, 15 elements) such an arithmetic approach can be realized with a 16 kB-memory personal computer. Its applicability has been proved by comparison of computed L_s^2 values with experimental data for water, graphite and some typical rock-forming substances. The method was originally developed for geophysical purposes, where angular distributions of scattered radiations are usually not of primary importance. But why not to try it also in some other areas of neutron applications?

The reasonable accordance of achieved results with both experiment and ENDF/B-IV-based calculations may also be interpreted that easy-to-handle but not extremely up-to-date cross-section library, commonly known as ABBN, is still adequate at least for typical well-logging problems.

Calculations of the effective characteristics of neutron fields disturbed by a presence of a water-filled source heterogeneity resulted in strong dependences on its dimensions. It may be concluded then, that macroscopic slowing-down parameters of rocks, which by definition refer to infinite media rather than to a borehole-formation system or laboratory set-up, can hardly be determined by experimental methods of nuclear geophysics.

On the other hand, however, experimentally verified calculations, making use of microscopic cross-sectional data, should not be considered as pure theory but rather as processing of experimental information collected in perfect (hopefully) laboratory conditions.

Acknowledgements

We are indebted to Prof. J.A.Czubek for many helpful (although controversial) discussions, and to the Nuclear Data Section IAEA for supplying us with the ENDF/B-IV library, which enabled positive verification of our former work.

References

1. A.KREFT, Nukleonika 18, 615(1973) & 19, 145(1974)
2. L.P.ABAGYAN, N.O.BAZAZYANTS, I.I.BONDARENKO, M.N.NIKOLAEV: Group Constants for Nuclear Reactor Calculations, Atomizdat, Moscow 1964 (in Russian)
3. K.MORSTIN: Solution of a Non-Stationary Neutron Transport Problem in the Aspect of Pulse Neutron Logging, Ph.D. thesis, Univ. of Mining & Metallurgy, Cracow 1978 (in Polish)
4. R.C.DOERNER et al., Nucl.Sci.Eng. 9, 221(1961)
5. R.K. PASCHALL, Nucl.Sci.Eng. 26, 73(1966)
6. J.P.SPENCER, T.G.WILLIAMSON, Nucl.Sci.Eng. 27, 568(1967)
7. R.C.CAMPBELL et al., Nucl.Sci.Eng. 20, 445(1964)
8. V.P.DUGGAL, Proc.Int.Conf. Peaceful Uses of Atomic Energy, vol.13, p.85, 1958
9. K.H.BECKURTS, K.WIRTZ: Neutron Physics, Springer Verlag, Berlin 1964
10. J.TITTMAN, J.Appl.Phys. 26, 394(1955)
11. H.SHERMAN (Schlumberger-Doll Research Center, Ridgefield, Conn.), private communication
12. F.A.VALENTE, R.E.SULLIVAN, Nucl.Sci.Eng. 6, 162(1959)
13. L.GREEN, Nucl.Sci.Eng. 37, 232(1969)
14. M.A.J.RATHUR, P.J.GRANT, Brit.J.Appl.Phys. 15, 93(1964)
15. R.S.CASWELL et al., Nucl.Sci.Eng. 2, 143(1957)
16. D.GARBER et al., ENDF-102, BNL-NCS-50496, Upton, NY, 1975
17. N.M.GREENE et al., ORNL-TM-3646, Oak Ridge, Tenn., 1972
18. E.T.JÓZEFOWICZ, Rep.INR, 1482/IXA/PR/B, Warsaw 1973 (in Polish)
19. J.A.CZUBEK (Inst. of Nucl.Phys., Cracow, Poland), private communication (in Polish)

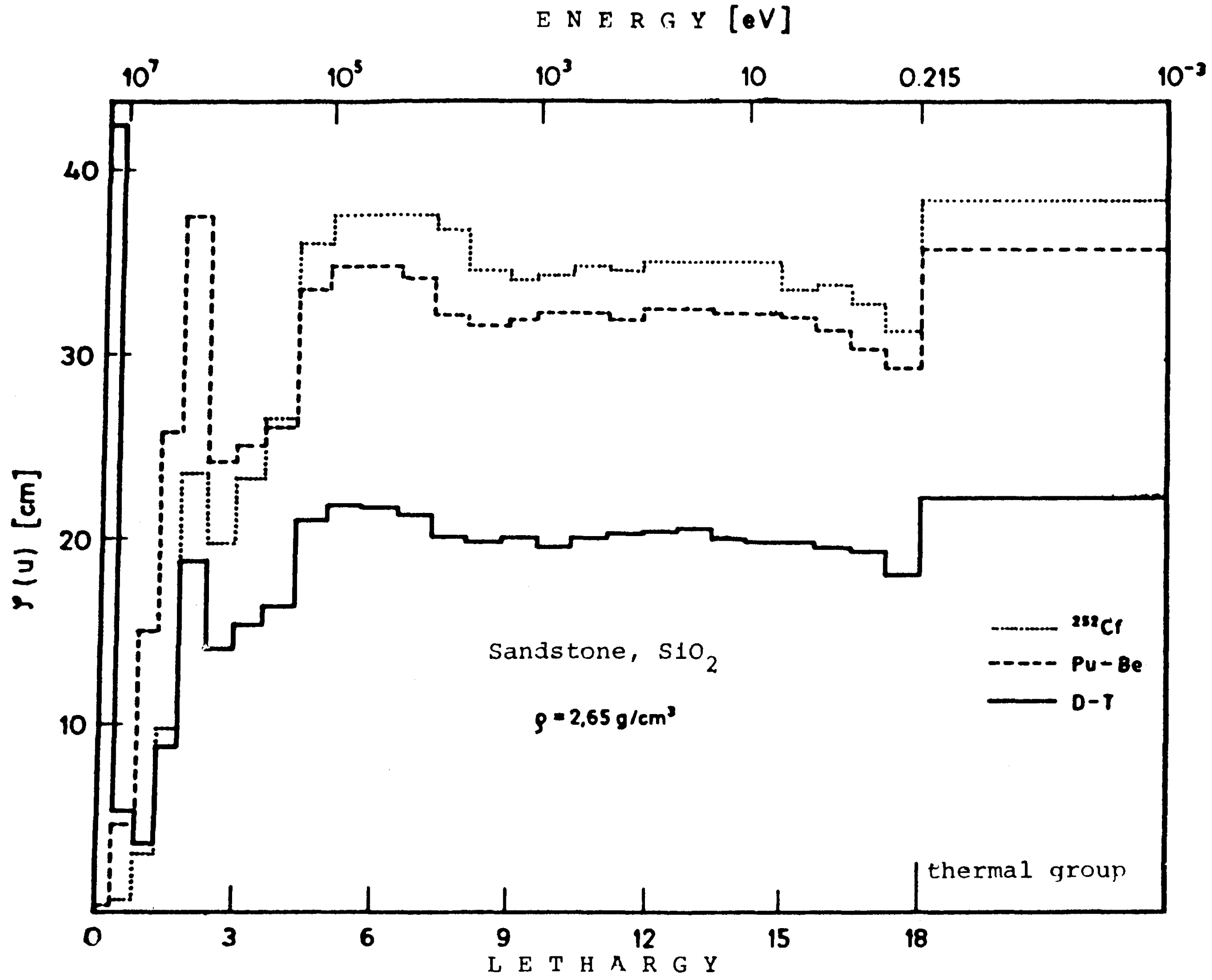

Fig.1. Neutron spectra in dry sandstone (SiO_2) calculated with the ABBNM data

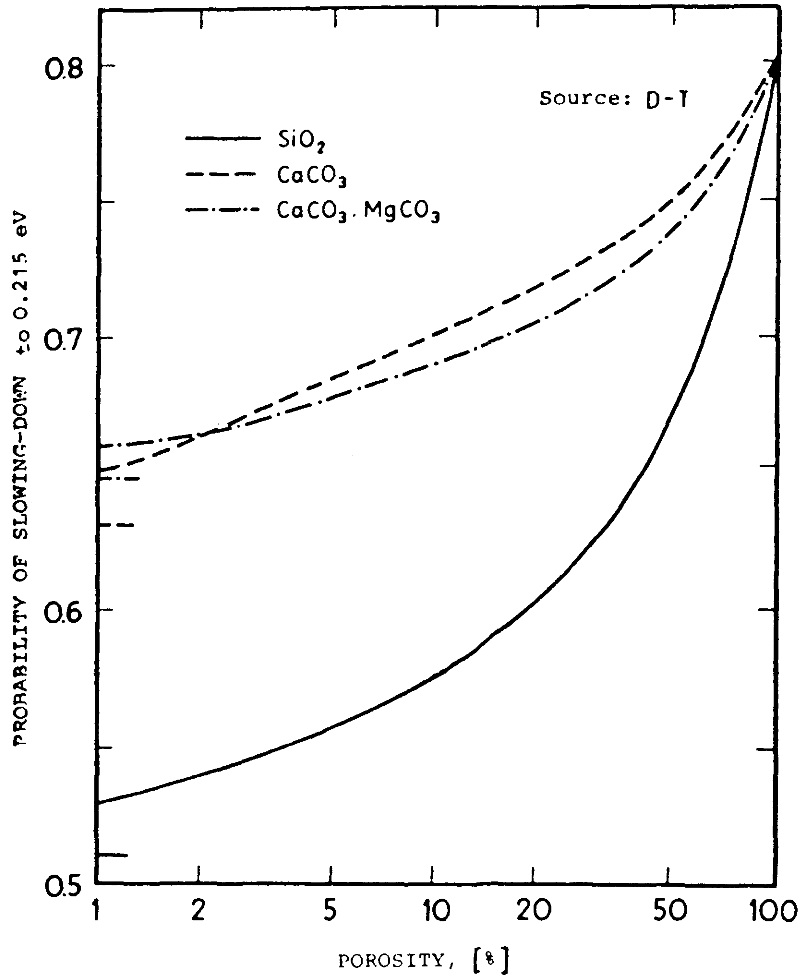

Fig.2. Non-capture probability of D-T neutrons slowed-down to 0.215 eV in some typical rock media saturated with water. Calculation with the ABBNM data

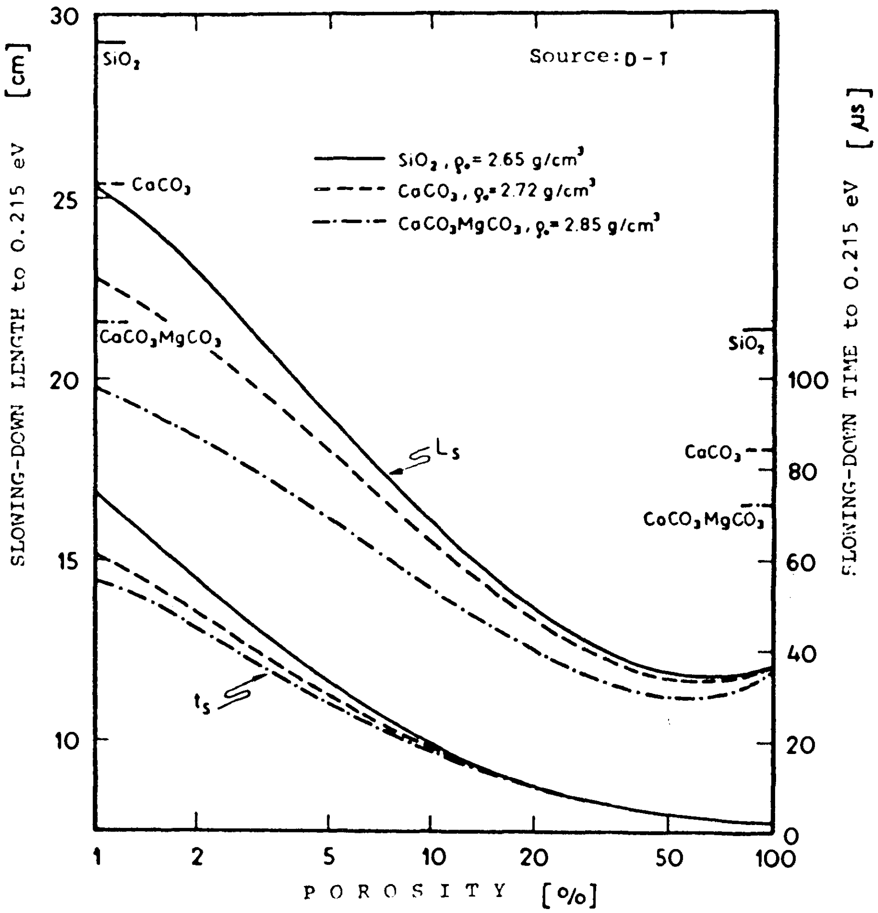

Fig.3. Slowing-down length and slowing-down time (to 0.215 eV) of D-T neutrons in some typical rock media saturated with water. Calculation with the ABBNM data

At the ordinate axes are marked the values for dense dry media

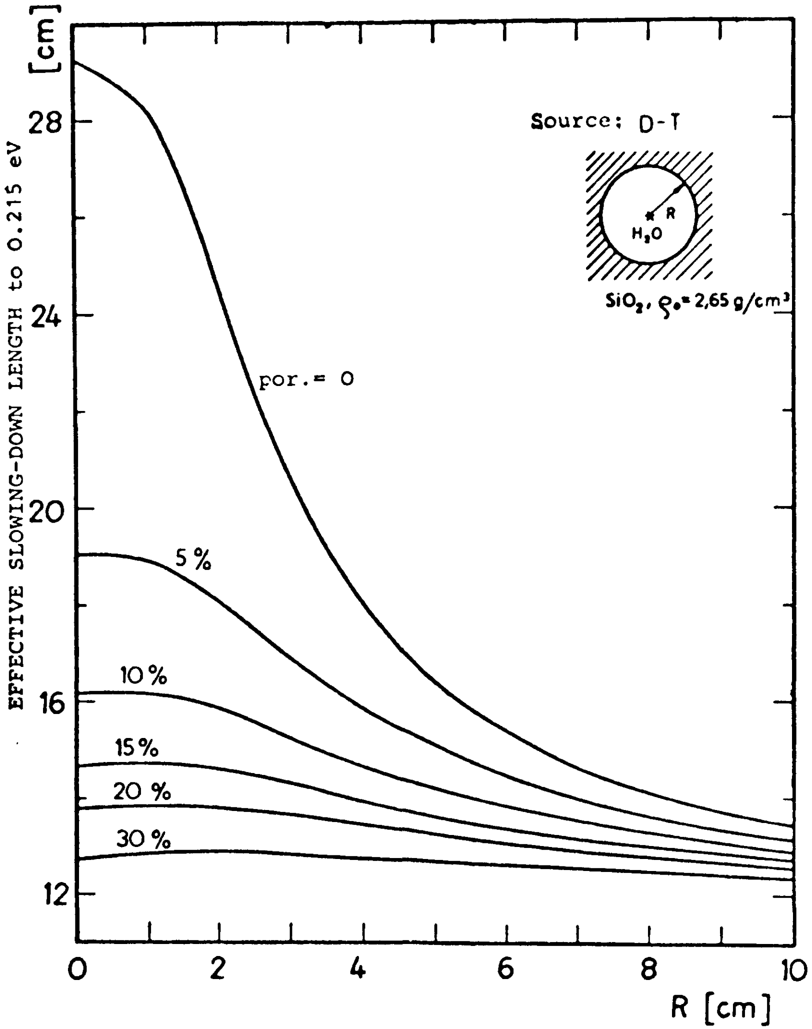

Fig.4. Effective slowing-down length (to 0.215 eV) of D-T neutrons in water-saturated sandstone (SiO_2) intersected by a cylindrical hole filled with water. Calculation with the ABBNM data

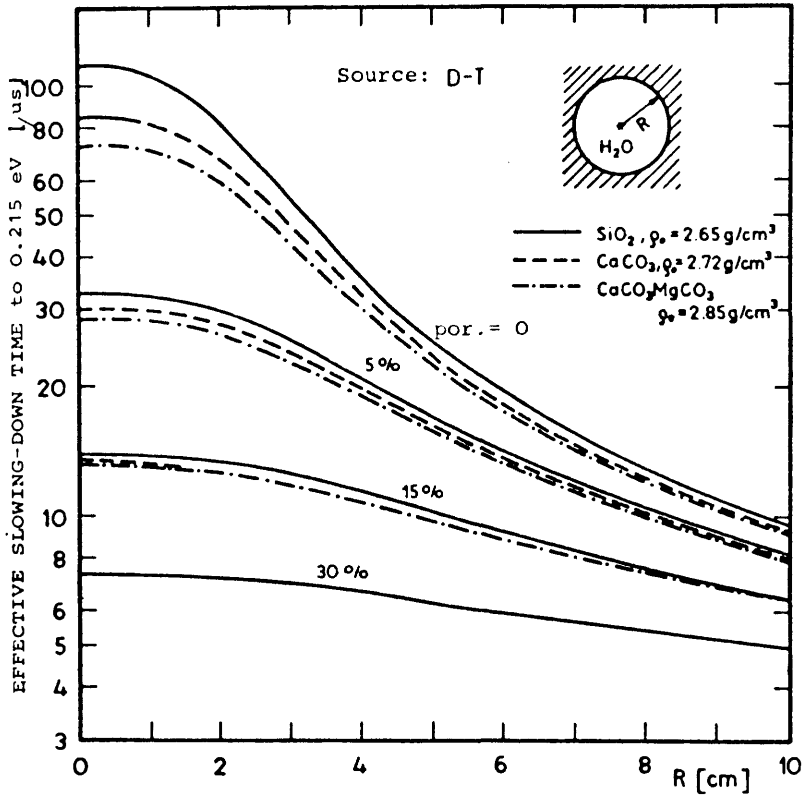

Fig.5. Effective slowing-down time (to 0.215 eV) of D-T neutrons in some typical rock media saturated with water and intersected by a cylindrical hole. Calculation with the ABBNM data

GAMMA-RAY SPECTROMETRY APPLIED TO DOWN-HOLE LOGGING

by

Patrice DUMESNIL - Krzysztof UMIASTOWSKI

Centre d'Etudes Nucléaires de Saclay
IRDI/DEIN
F-91190 Gif-sur-Yvette

SUMMARY

Gamma-ray spectrometry permits to improve the accuracy of natural gamma, gamma-gamma and neutron-gamma geophysical measurements. The probe developed at Centre d'Etudes Nucléaires de Saclay allows donw-hole gamma-ray spectrometry. Among others, this probe can be applied to the uranium content determination by selective natural gamma method, down-hole determination of the ash content in the coal by gamma-gamma selective method and elemental analysis by neutron-gamma method.

For the calibration and an exact interpretation of the measurements it is important to know the gamma-ray and neutron characteristics of the different kinds of rocks considered as probabilistic variables.

- DIAGRAPHIES UTILISANT LA SPECTROMETRIE GAMMA -

RESUME

La spectrométrie gamma permet d'accroître la pécision des mesures portant sur les rayonnements naturel, diffusé (gamma-gamma) ou artificiel (n-gamma).

Une sonde a été développée au Centre d'Etudes Nucléaires de Saclay pour permettre l'exécution de la spectrométrie gamma en forage. Elle peut être utilisée notamment pour la détermination de la teneur en uranium des minerais par la méthode gamma naturel sélectif, la mesure de la teneur en cendre des charbons par la méthode gamma-gamma sélective et pour l'analyse élémentaire par activation neutronique.

Pour effectuer l'étalonnage et l'interprétation de ces diagraphies, il est très utile de connaître sous forme statistique les paramètres photoniques et neutroniques des roches concernées.

GAMMA-RAY SPECTROMETRY APPLIED TO DOWN-HOLE LOGGING

1. - INTRODUCTION

The need for more accurate measurements in geophysics has resulted in an application of the methods based on gamma-ray spectrometry. These spectrometric methods are used as well for natural gamma radiation as for gamma-gamma and neutron-gamma measurements.

For down-hole gamma ray spectrometric logging a spectrometric probe is needed. There are two possibilities to perform the gamma spectral log:

- the first one, more conventional and widely applied, consists in transmitting an amplified analog pulse through the logging cable to the pulse-height analyser on the surface;

- in the second case the pulse amplitude is converted in the probe into binary number and the latter is transmitted by a cable in digital form.

In the first case the pulse shape modification during transmission through the cable is the source of the additional errors. For the standard logging cable these errors could be important. Digital transmission between the probe, and surface unit, suppreses the errors introduced by the logging cable.

2. - EQUIPMENT DESCRIPTION

The spectrometric gamma tool developed at Centre d'Etudes Nucléaires de Saclay performs the pulse height digital coding down-hole inside the probe.

The probe has an external diameter of 33.7 mm and a length of 1.90 m. It contains four main subsets: conversion, transmission and control logic, and power supply. The description of these subsets will be given hereafter.

Detection subset - It consists in a NaI (Tl) 21 mm by 46 mm crystal, a photomultiplier (a XP 1910 type of RTC), a regulated high voltage supply and a pulse amplifier. The design of this subset is rather conventional. At the output the amplitude of the electric pulses is proportional to the energy of the incident gamma radiation.

A/D conversion subset - It contains a sample and hold amplifier, a peak detector, and the analog to digital converter (ADC) delivering the binary coded pulse height measure.

Transmission and control unit. It controls and synchronises the operations of the sample and hold amplifier, AD converter and transmission circuits. The binary signal is transmitted on two wires in a differential mode.

The surface equipment used for the tests of the probe consists in a specific interface adapter, the memory block of the SILENA selector, and a HP 85 computer. The spectres can be treated on line or recorded on magnetic cartridges.

3. - APPLICATIONS OF THE SPECTRAL GAMMA-RAY PROBE

The gamma-ray spectrometric down-hole probe gives accurate results in different field of nuclear logging. These are:

- natural gamma-ray spectrometry for uranium content determination by selectve gamma logging proposed by Czubek (1),

- gamma-gamma spectrometric measurements to determine the heavy elements content, coal ash content or for lithology determination,

- neutron activation down-hole analyses to determine specific elements content.

There does not exist any standard facility for the calibration of the probes for different tests as mentioned below. In many cases the only calibration method is to compare the measurements performed in the holes with the results of core samples analysis.

To interpret the results of natural gamma or gamma-gamma spectrometric measurements correctly it is important to know the gamma ray attenuation coefficient and the build-up factor as a function of energy. The chemical composition of the different kinds of rock is not constant, but can be considered as a multidimensional random variables, thus the attenuation coefficient and build up factor are also the random variables.

The random variable is characterized by the probability distribution function or less precisely can be approximated by first two moments of this function i.e. the mean value and the standard deviation.

The computation of the attenuation coefficient starting from the microscopic cross-sections for different elements needs the exact knowledge of the chemical composition of the rock of interest.

There are two possibilities: either to determine the probabilistic parameters of the chemical composition for the different kinds of rocks and next to compute the macroscopic parameters on the basis of microscopic cross-sections for each element, or to determine the probabilistic distribution of the macroscopic parameters for different kind of the rock directly. It is not clear which approach is best.

In the case of the determination of the neutron parameters of the rock (i.e. thermalisation length, diffusion coefficient, and macroscopic absorption cross-section) a little change of the trace elements content can result in a significant variation of these parameters, thus in this case the determination of the chemical composition of the rock is much more important.

CONCLUSIONS

Down-hole gamma-ray spectrometry to deal with the natural gamma, gamma-gamma and neutron-gamma logging gives much more precise results, than the standard measurements. Spectrometric measurements also permits to determine the properties of the rock which cannot be determined otherwise.

For an exact interpretation of the measurements and the determination of the precision of the results obtained it is important to know the gamma and neutron caracteristics of the rock considered as probabilistic variable.

Lithological Analysis of Volcanic Rock by Using the Differential Gamma Ray Log.

Toshinobu Itoh

Susumu Kato

Department of Exploration.
Japan Petroleum Exploration Corp.
17-22, 2 Chome, Akasaka, Minato-ku,
Tokyo, Japan

Abstract;

At the giant oil and gas field in northern part of Japan, the most of reservoir rocks consist mainly of a volcanic complex, and the hydrocarbon productivity of formation is strongly affected by a degree of alteration of rock matrix and existing values of clay minerals in the formation.

The acidic and basic rock can be discriminated by the use of a differential gamma ray analysis. The degree of alteration of basic rock can also be discriminated by means of 40K gamma ray value and the formation resistivity crossplot.

The lava flow direction of underground formation may be estimated by this crossplot method with a correlation of several number of welds at the specific oil and gas field.

I. Introduction.

The giant oil and gas fields in northern part of Japan produce hydrocarbons from the reservoir of volcanic rock. The log interpretation of such volcanic formation is usually very difficult because of the complexity of rock matrix, the strong change of horizontal permeability and the horizontal discontinuity of water level etc., and any standard method used like in the intergranular formation has not been realized for the volcanic formation yet.

A hydrocarbon productivity of volcanic rock is strongly affected by a degree of alteration of the rock, because the fluid path or fractured path at the altered zone is usually plugged by clay minerals of low permeability. Therefore, the estimation of clay contents in the rock has an important meanings at the log interpretation.

II. Discrimination of acidic rock and basic rock.

Fig. 1 is an aerial location of wells at Yurihara oil and gas field, Akita Prefecture, Japan, and the hydrocarbon productivity at volcanic formation is increasing with a direction from Kita Yurihara AK-1 to north-east, Higashi-Yurihara AK-1 and SK-8D.

Fig. 1

Fig. 2 is a composite log of Yurihara SK-8D, and from left to right of the figure,1) a legend of lithology, 2) a texture in groundmass observed from rock thin sections, 3) a total gamma ray curve, 4) a lithology from cuttings, 5) a resistivity curve from ILD, 6) a curve of POTA (%), 7) a curve of URAN (ppm) and 8) a curve of THOR (ppm) are listed.

Fig. 2

Five sections marked at the depth column were put into the production test, and the tests of No. 5, No. 3, No. 2 and No. 1a produced a considerable volume of oil and gas. The reservoir rock at the test zones of No. 3, No. 2 and No. 1a mainly consists of a basaltic lava corresponding to the interglanular or intersertial texture. The volcanic rocks at the test zones of No. 1 and No. 4 show a relatively fine texture and corresponding to the relatively high gamma ray level and low formation resistivity. The rocks having a relatively high resistivity and low gamma ray level are mostly corresponding to the ophitic or subophitic texture.

Fig. 3 is a figure of differential gamma ray crossplots, the left side is a Th-U crossplot and the right side is a Th-K crossplot. According to this figure, it is recognized that the basic rock can be separated from the acidic rocks and mudstone on those crossplots, moreover, with the Th-K crossplot, a muddy tuff, a pumice tuff and mudstone are also clearly be defined. However, it is very difficult to discriminate the basalt whether the rock is altered or not by those crossplots.

Fig. 3

Fig. 4 is crossplots of GR-ILD resistivity, and the left side is GR-ILD crossplots and the right side is K-ILD crossplots respectively. The both crossplots were separated by two groups on the depth, the one is from 2014^m to 2165^m and the other is from 2165^m to 2425^m, because of the change of base line at GR log. Although the pattern of crossplots at individual depth's group are quite different, the discrimination between an altered basalt and a none altered basalt has been clearly achieved on those crossplots.

Fig. 4

At the K-ILD corssplot for the depth of $2014\text{-}2165^m$, two groups of crossplot point which are circulated by the dots line are pointed out. The points concentrated at the low resistivity and high K level are mostly corresponding to the one pointed out by the GR-ILD crossplot. However, points distributed between the resistivity of 12 to 17 ohms and the K concentration of 3 to 4.5 % are mainly corresponding to the volcanic tuff at the depth of $1955 - 2020^m$, $2060 - 2070^m$ and $2108 - 2121^m$.

Phto. 1 is photo-samples of rock thin section, and the upper is the one taken at the depth of 2050^m and the lithology of cuttings shows the basalt, and the lower is the one taken at the altered basalt. According to this photograph, it is understood that the basalt shows a clear texture and fractured fluid paths, however, the altered basalt shows many fractured paths which were plugged by clay minerals.

Photo. 1

III. Estimation of lava flow direction.

As mentioned at Section II, the degree of alteration of the rock has some relationship with the formation resistivity and the gamma ray level. Fig. 5 is an ideal model of the relation between GR level, resistivity of formation and the alteration of rock matrix.

Fig. 5

Since a front terminal of lava flow will be more altered than the core of lava generally, the iso-resistivity counter map of underground formations based on the model shown at Fig. 5 may indicates the lava flow direction at the stage of lava flow.

Fig. 6 is a correlation map of the wells based on GR log and Induction resistivity log at Yurihara field. According to the lithological analysis of each wells, it was cleared that the lava flow stage on this area may be separated by three blocks as Unit 1, Unit 2 and the other rocks.

<u>Fig. 6</u>

Fig. 7 is an iso-resistivity contour maps for each lava units. The resistivity values shown at the figure are taken as a average of Induction resistivity reading at each units. This figure shows that the average formation resistivity decreases gradually from the right side to the left side. As basing on the rule shown at Fig. 5, the lava flow direction at both units may be determined as from the north-east to the south-west direction as shown in the figure. Therefore, the higher hydrocarbon productive reservoir might be expected at the east side of Higashi Yurihara AK-1 and 8D.

<u>Fig. 7</u>

IV. Conclusion.

Over five giant oil and gas fields have been developed at northern part of Japan in 1970 age. However, the standard log interpretation method has not still been established because of the complexity of rock matrix, the strong change of horizontal permeability and the horizontal discontinuity of water level.

The method discribed on this paper may help of the prediction of horizontal extention of the permeable formation.

<u>Reference;</u>

1) Kerherve, J. (1977) ; An Introduction to Volcanic Reservoirs and to Their Evaluation from Wireline Electrical Measurements. Notes for Seminar, Tokyo.

2) Khatchikian, A (1982) ; Log Evaluation of Oil-bearing Igneous Rocks., SPWLA 23rd Annual Logging Symposium Transactions.

3) Schlumberger (1982) ; Natural Gamma Ray Spectrometrt, Essentials of NGS. Interpretation.

4) Fertl, W. H. (1979) ; Gamma Ray Spectral Data Assists in Complex Formation Evaluation. The Log Analyst, Vol. 20, No. 5.

5) Makiyama, Y., Aramaki, Y., Nakamura, K. (1979) ; Volcano, Iwanami Geoscience Series. 7.

6) Toki, A., Kushiro, Y. (1975) ; Petrology II, Kyoritsu Shuppan.

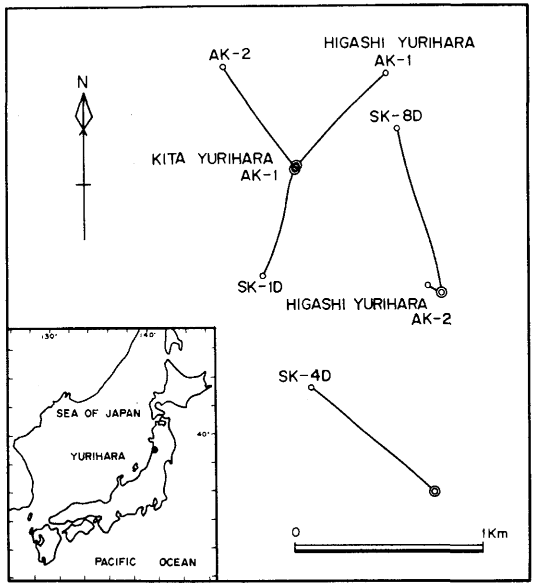

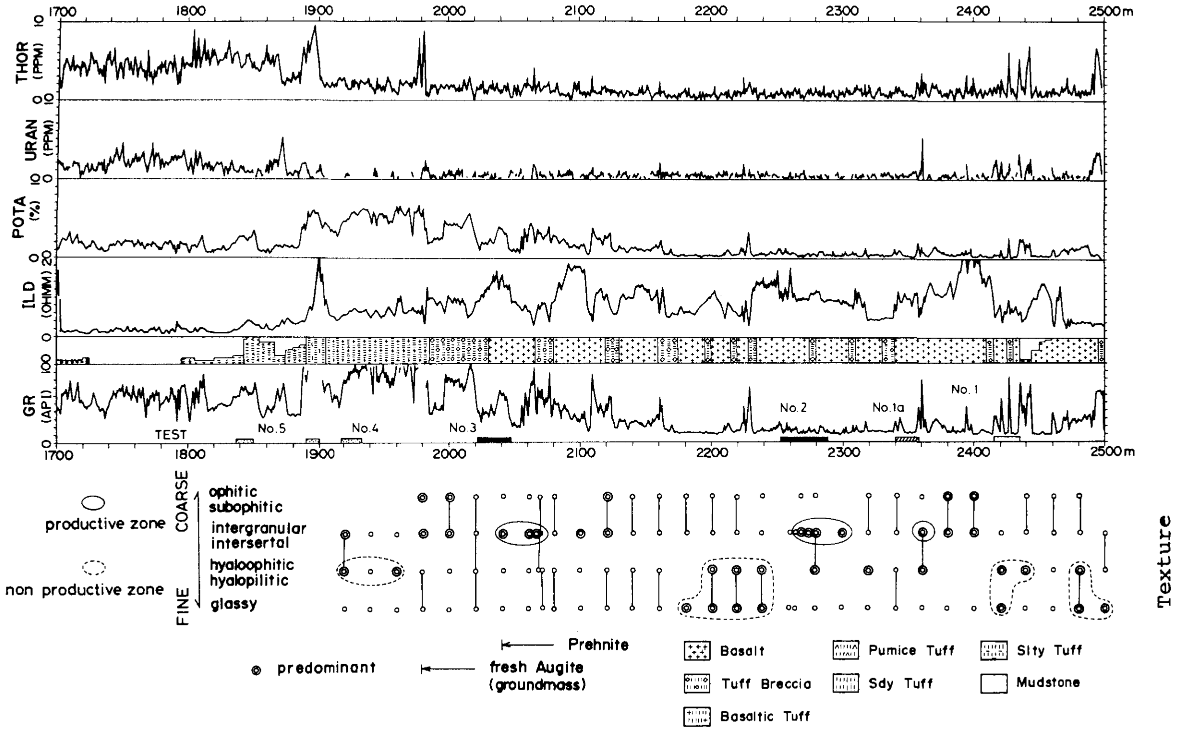

Fig. 1, Areal location of wells at Yurihara oil and gas field.

Fig. 2, Composit log of Yurihara SK - 8D.

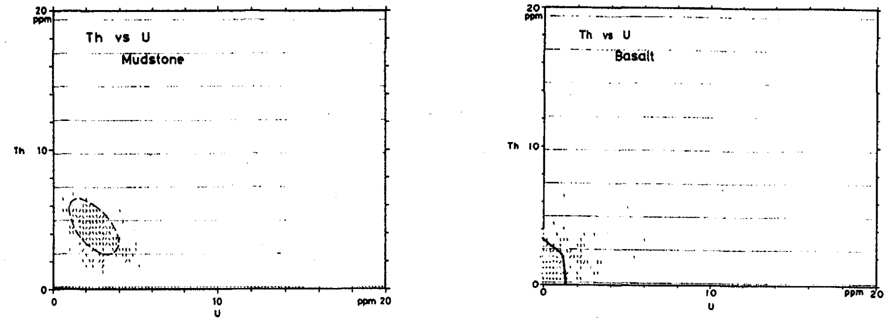

a) Mudstone

d) Basalt

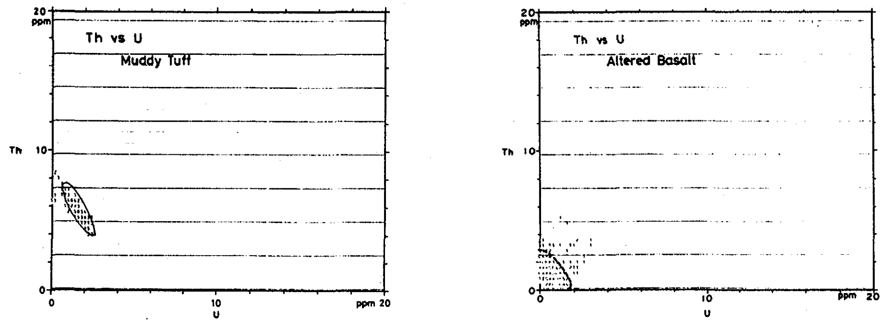

b) Muddy Tuff

e) Altered Basalt

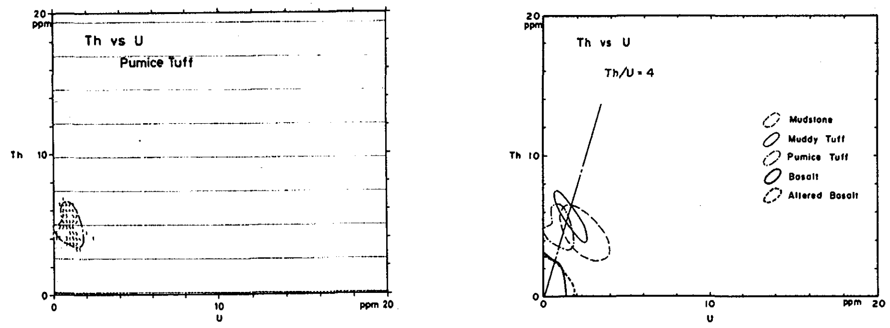

c) Pumice Tuff

f) Overlayed of points

Fig. 3-a, Th - U crossplots of Yurihara SK - 8D
(Left side)

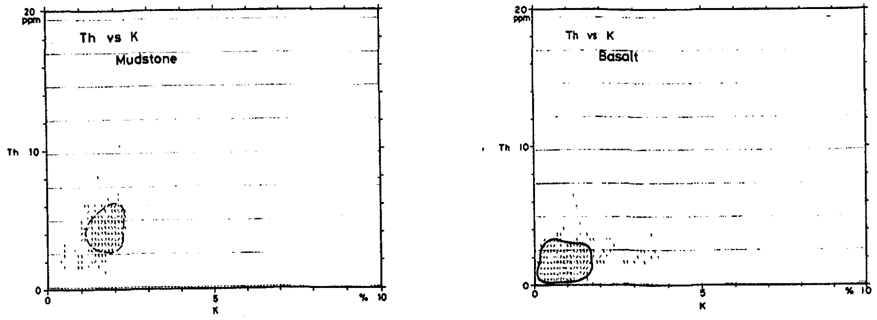

a) Mudstone

d) Basalt

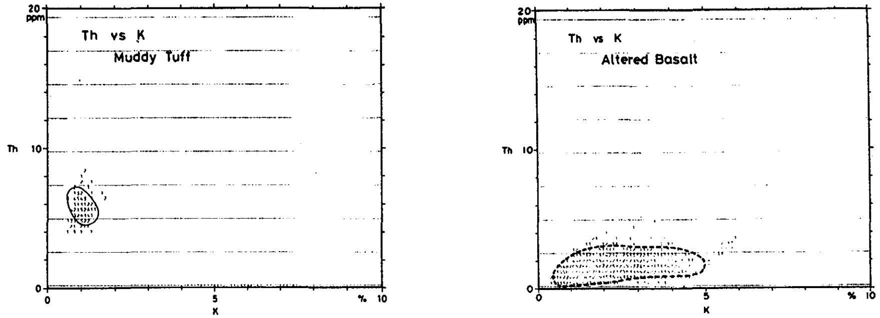

b) Muddy Tuff

e) Altered Basalt

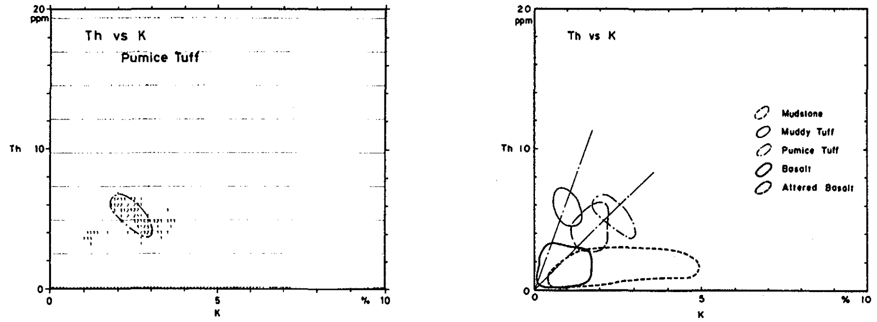

c) Pumice Tuff

f) Overelayed of points

Fig. 3-b, Th - K crossplots of Yurihara SK - 8D.
(Right side)

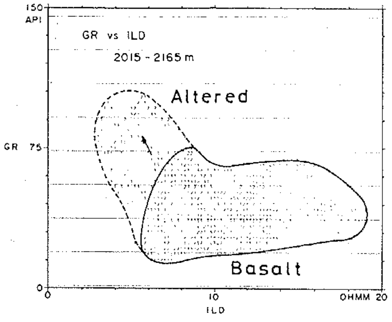

a) 2015 - 2165^m

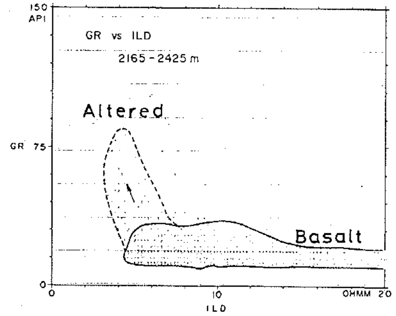

b) 2165 - 2425^m

1) GR - ILD resistivity

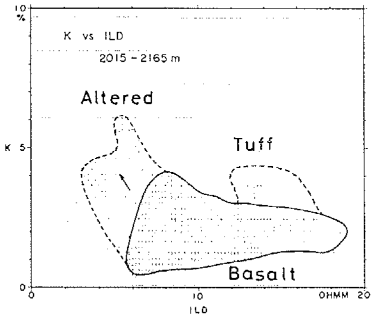

a) 2015 - 2165^m

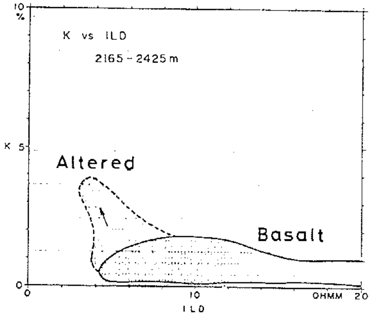

b) 2165 - 2425^m

2) K - ILD resistivity

Fig. 4, GR - ILD and K - ILD crossplot
of Yurihara SK - 8D.

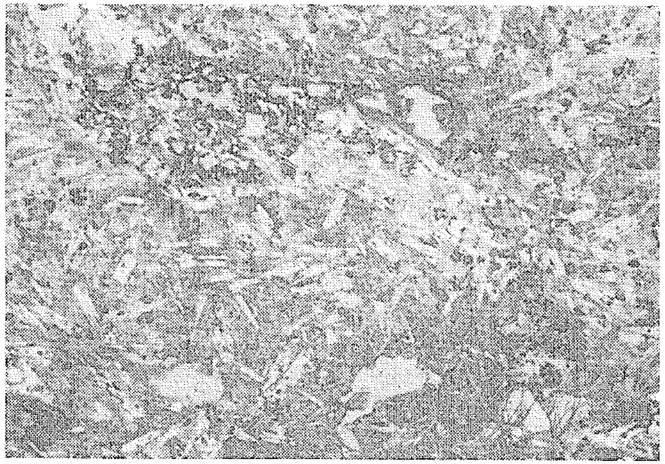

a) Basalt

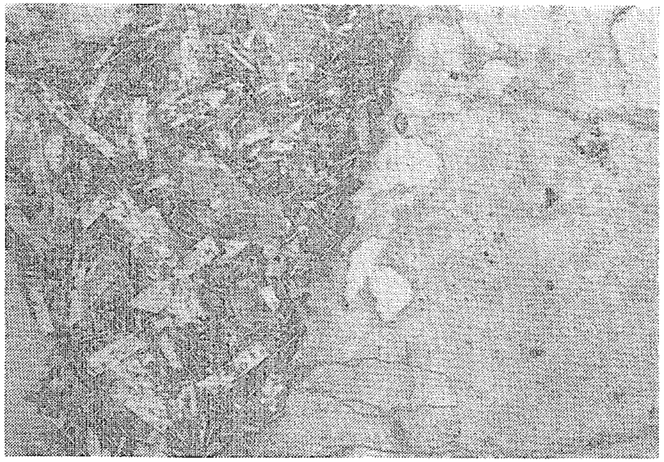

b) Altered Basalt

Photo. 1, Photograph of Rock Thin Section.

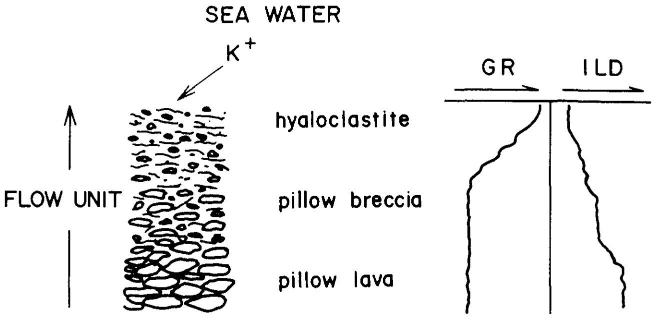

Fig. 5 THe ideal model of the relation between GR level, ILD resistivity and the degree of alteration of rock matrix.

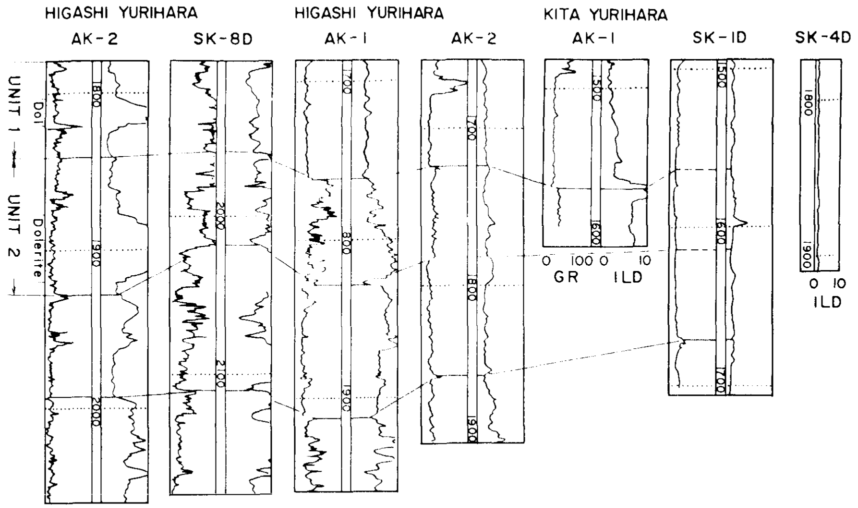

Fig. 6, Well co-relation by the use of GR log and Induction resistivity.

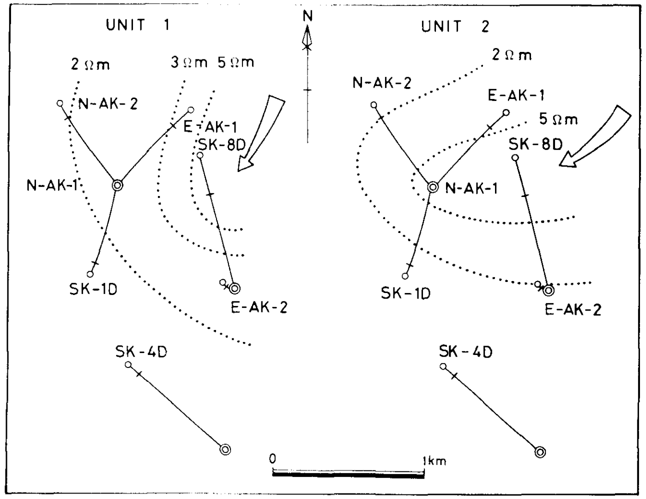

Fig. 7 Iso-resistivity counter map and lava flow direction at Unit 1 and Unit 2 on Yurihara oil field.

SOME COMMENTS ON FORMATION DENSITY MEASUREMENT BY GAMMA-RAY INTERACTIONS BASED ON OBSERVATIONS FROM MONTE CARLO CALCULATIONS

C.G. Clayton
L.G. Sanders
B.W. Thom

Nuclear Physics Division, AERE-Harwell,
Didcot, Oxon, U.K.

and

P.B. Kemshell

Reactor Physics Division, AEE-Winfrith,
Winfrith, Dorset, U.K.

ABSTRACT

The measurement of bulk density by the (γ-γ) scattering technique is well established and accuracy has been investigated experimentally and theoretically by several authors, especially with relation to the change in energy of the source γ-rays by the material interrogated and to the detector energy response. However, measurement accuracy also depends directly on the effective (Z/A) for the material and this may vary significantly, especially between different types of coal and shale.

By means of Monte Carlo calculations, the present paper examines the effect of hydrogen variations on γ-ray flux for several model coals for a point source, infinite sphere configuration and for a simple borehole probe arrangement. Within the limits of these models it is concluded that the flux variations can be significant, but that results lie within predictions of the Principle of Similitude assuming γ-electron interactions only.

1. INTRODUCTION

The gamma-gamma scattering technique is the basis of a well established method for measuring the bulk density of rocks and ores during borehole logging in minerals exploration and mining. The method is based on a radioisotope γ-ray source, such as ^{137}Cs (662 keV) or ^{60}Co (1173 keV and 1332 keV) and a scintillation detector, the source and detector being separated by a heavy metal shield so as to restrict γ-rays from the source reaching the detector directly. The output from the scintillation detector is normally arrranged to be above some energy threshold (approx. 100 keV to 200 keV) which attempts to ensure that Compton scattered γ-rays only are displayed.

Determination of the bulk density ρ_b of the rocks is based on the relation,

$$\rho_e = \rho_b N_{A} \Sigma_i w_i \left[\frac{Z_i}{A_i}\right] \qquad (1)$$

where ρ_e is the electron density, N_A is Avogadro's Number and w_i is the weight fraction of the i th element of mass number A and atomic number Z. Since Compton processes imply γ-ray, electron interactions only, then, if the detector responds only to Compton scattered γ-rays the output is directly related to electron density and ρ_b can be derived, provided $\Sigma_i w_i [Z_i/A_i]$ is constant.

The validity of the (γ-γ) method for a range of operational situations, particularly relating to lithological variations and their effect on the competition between photo-electric and Compton processes, has been well examined, especially by Czubek(1,2).

However it is important to recognise that although $\Sigma_i w_i [Z_i/A_i]$ is relatively constant for many rock types, it is not invariant and imposes a limit on the ultimate accuracy of the method. Values of [Z/A] for a number of elements are given in Table 1. As is clear the most significant changes in matrix [Z/A] values would generally arise from variations in the hydrogen content.

Significant natural variations in [Z/A] occur in coal. Anthracite typically contains about 2 wt.% hydrogen and in some brown coals hydrogen concentrations may approach about 12 wt.%. In specific types of coal deposit, such as bituminous coals, variations in hydrogen content are largest when the coal seams are interrupted by mineralised strata. The mean value of hydrogen content occurs when banding is severe and the band thickness is small (e.g. 1 mm), the limits of the range being associated with the particular hydrogen contents of the combustible material and the mineral matter. Mineralisation of this type imposes a limit on the accuracy of the (γ-γ) method which appears at present to be outside a simple calibration procedure.

To isolate the magnitude of possible errors from variations in [Z/A] we have carried out a series of Monte Carlo computations with particular reference to borehole logging during coal exploration. Initially, a simple geometrical system (point source, infinite sphere) and simple materials have been examined in order to derive diagnostic information. The programme has so far been extended to include an elementary borehole and it is our intention to proceed to examine the response of operational equipment in realistic situations.

2. MONTE CARLO RESULTS FOR A POINT SOURCE AND INFINITE SPHERE

The Monte Carlo computations were carried out using the McBEND Code(3), with spatial scoring regions and energy groups according to Table 2. A typical number of source particles was 25,000.

2.1 Carbon

Figure 1 gives the variation in the total number of γ-rays in the range from 100 keV to source energy with radius for a point mono-energetic source (660 keV, ^{241}Am) in carbon, carbon containing 0.2 wt.% Zr and carbon containing 20 wt.% H, all three materials being normalised to the same density. Zirconium was included to simulate the effects of medium-Z elements (Z_{zr} = 40, K_{ab} = 17.998 keV) and the effect is seen to be virtually zero over this energy range. The change in γ-ray intensity with 20 wt.% H content is clearly seen.

Figure 2 displays the change in intensity relative to pure carbon; at 35 cm radius the intensity being reduced to about 65% compared to the intensity at 5 cm.

Figures 3 and 4 refer to the same materials for an energy group from 90-100 keV. The intensity curve (Fig. 3) displays a definite cross-over at about 15 cm and photo-electric effects from Zr are becoming evident. The total range of the hydrogen effect is seen from Fig. 4 to be about 100%.

Figures 5 and 6 indicate the variations in γ-ray energy spectra in four spatial zones for pure carbon and carbon with 20 wt.% hydrogen. These curves are similar in form to the differential energy curves derived by Goldstein and Wilkins(4). Several comments can be made. For the spatial zone between 2 and 4 cm, in which there is a strong component of source γ-rays, the maximum in the γ-ray flux at 184 keV corresponds to the energy of the backscatter peak for a source energy of 660 keV.

The sharp reduction in amplitude of the curves at low energies corresponds to the dominance of the photoelectric cross-section at these energies. The differential increase in slope of the curves at the higher energies is consistent with an increase in the lower energy component of the γ-rays with increase in distance from the source. Very similar curves are displayed in Fig. 6 which relates to carbon +20 wt.% H.

The Principle of Similitude(1) has been applied to the data for carbon and to the carbon +20 wt.% H and carbon +0.2 wt.% Zr mixtures and the results are plotted in Figs. 7 and 8. It is clear that the measurement is sensitive solely to electron density from source energy to the low energy region where photo-electric competition becomes severe. The change in direction of the curves in Figs. 7 and 8 at low energies is due to the relative photo-electric absorption coefficients of the two materials in the two cases studied.

By the Principle of Similitude it can be shown that, for a point γ-ray source in different materials, and assuming Compton interactions only,

$$r^2 I_\gamma = r'^2 I'_\gamma = r''^2 I''_\gamma = - - - -$$

where r, r', r" are the selected radii in the various materials and I_γ, I'_γ, I''_γ are the corresponding γ-ray intensities.

Correspondingly, if ρ_e, ρ'_e, ρ''_e are the electron densities at r, r', r"

$$\rho_e r = \rho'_e r' = \rho''_e r'' = - - - -$$

Thus, independent of material composition for each value of $\rho_e r$ there should be a constant value of $r^2 I_\gamma$.

Figure 9 has been constructed to demonstrate this feature for carbon and carbon +20 wt.% H. Since fixed values of r were taken, corresponding points do not overlap but all points lie on a continuous curve, as expected.

2.2 Coal

Similar data to that exhibited in Figs. 1 to 4 for pure carbon and carbon with additives are presented in Figs. 10 to 13 for three model coals which have hydrogen contents of zero, 5.36 wt.% and 20.0 wt.%, the concentrations of the other elements being proportionally adjusted to give the same bulk density of 1.4183 g/cm^3 for each coal. The elemental concentrations of these coals are given in Table 3.

The absolute variation in γ-ray intensity with radius is shown in Fig. 10 for γ-ray energies in the range 100 keV to 660 keV and it can be seen that there is a significant reduction in γ-ray intensity as the hydrogen content is increased. The relative responses which are displayed in Fig. 11 show the magnitude of the large hydrogen effect.

The data presented in Figs. 12 and 13 are similar to those in Figs. 10 and 11 except that a narrower energy band from 90 keV to 100 keV is selected. The relative responses in this lower energy range are quite different. In Fig. 13 the cross-over between zero hydrogen and 20 wt.% hydrogen is moved from 7 cm radius to 15 cm radius whilst at 5 wt.% hydrogen the change in γ-ray flux relative to hydrogen increases and passes through a maximum before decreasing to fractional values.

Figures 14 and 15 contrast the relative energy distribution for a coal with zero hydrogen to one with 20 wt.% H over a series of radial zones. The shapes of the curves are very similar and the backscatter peak close to the source is still evident, but weaker than with pure carbon. In general, the effect of increasing hydrogen concentration is to increase the γ-ray intensity per unit energy interval, as might be expected from the higher electron density. The greatest relative effect occurs at the larger radii.

The relatively high value of unscattered source γ-rays is worth noting.

3. MONTE CARLO RESULTS WITH AN ELEMENTARY BOREHOLE

The configuration adopted to gain an understanding of the primary effects of introducing a borehole into the formation is shown in Fig. 16. In this programme the γ-ray source energy is 1.25 MeV to simulate a ^{60}Co γ-ray source.

In all cases considered so far the borehole was empty, apart from the black absorber shown in Fig. 16. This was introduced to simulate a simple source-detector shield in as much as it prevents direct access of source γ-rays to the scoring regions.

The extremes of the response of a borehole probe for a bituminous coal are considered to occur when the probe is adjacent to a near-mineral-free coal and when it is adjacent to a shale formation. The mean response would then result from a highly banded formation, for example, in which coal and shale thicknesses are very small compared to the distance between source and detector in the probe. The elemental concentrations of the model (pure) coal and the model shale used in the present computations are given in Table 4. The fact that the composition of this 'coal' is different from that of Table 3 is purely fortuitous as it was simply derived from a different data set of analyses of natural coals.

Figure 17 displays the γ-ray flux distribution along the borehole axis when the formation comprised various mixtures of coal and shale. It is clear that there is a strong reduction in γ-ray flux with increasing shale content.

The data from Fig. 17 was used to derive Fig. 18 which shows how the γ-ray intensity falls off with increasing formation density at two selected distances up the borehole. Clearly there is higher sensitivity of γ-ray flux to formation density as the distance from the source is increased.

For the assumed coal and shale compositions the constituent-weighted $[Z/A]$ values are 0.527 and 0.497 respectively. It follows that the ratio of the coal/shale electron number densities, at the same bulk density, is 1.061. Thus, a density tool calibrated with a range of similar coals exhibits an error, due to this electron density difference, between a negligibly-small value and 6% as the shale content varies from zero to 100%. This point has been demonstrated with Monte Carlo runs on the coal with its density increased to that of the shale.

The effect of varying the formation close to the borehole was examined by comparing a formation of pure water with a shale formation and with a shale formation including an annular thickness of 5 cm of water. The results are displayed in Fig. 19.

It is evident that the γ-ray flux distribution with a 5 cm annular water zone is much closer to the flux distribution corresponding to a water formation than to that observed with shale alone. The relatively weak penetration into the formation is thus apparent.

Taking into account the bulk densities and weighted $[Z/A]$ values for water and coal, the ratio of the electron number densities (water/coal) is found to be 1.206. Then, according to the Principle of Similitude, the γ-ray flux for the coal formation 40 cm distant from the source may be compared with that for the water at 48.24 cm. The computed value for the former is 1.692×10^{-5} γ-rays/cm^2 per source photon while the value read from the curve for the latter is 1.16×10^{-5}. On multiplying the water value by the square of the electron number densities (1.206^2) the result is 1.687×10^{-5}. This close correspondence with the coal value suggests a very small "borehole effect" for the slim, empty borehole.

4. CONCLUSIONS

1. A programme has been started to use Monte Carlo computations to give detailed information on the accuracy of the (γ-γ) scattering technique for measuring the bulk density in rock formations of varying composition.

2. Initially the variations in γ-ray space, energy distributions have been examined for a point mono-energetic source in an infinitive medium and in addition, the effect of an elementary borehole has been observed. Materials considered so far relate to coal and shale formations.

3. The viability of the (γ-γ) technique relies on the choice of interrogating γ-ray energies which refer solely to electron (Compton) interactions and to a constant $[Z/A]$.

4. The Principle of Similitude has been shown to be a useful tool in the current studies to establish those regions in which photo-electric processes begin to compete with Compton interactions.

5. The effect of variations in $[Z/A]$ are likely to be significant during borehole logging in coal and the importance of this in realistic geometrical configurations (which are well suited to Monte Carlo studies) is presently being investigated.

REFERENCES

(1) CZUBEK, J.A. Physical possibilities of gamma-gamma logging. Radioisotope Instruments in Industry and Geophysics, 2, 249 (IAEA, Vienna, 1966).

(2) CZUBEK, J.A. Advances in gamma-gamma logging. Int. J. Appld. Radn. and Isotopes, 34, 153 (1983).

(3) BENDALL, D.E. and BRISSENDEN, R.J. McBEND Programme Users Guide, COSMOS Ref. set Doc/147 (1980).

(4) GOLDSTEIN, H. and WILKINS, J.E. Calculations of the penetrations of gamma-rays. USAEC Report NYO-3075 (1954).

Table 1. Values of [Z,A] for elements commonly found in combustible and mineral components of coal.

Element	Z	A	Z/A	A/Z
O	8	15.999	0.5000	1.999
Si	14	28.086	0.4985	2.006
Al	13	26.981	0.4818	2.075
Fe	26	55.847	0.4656	2.148
Ca	20	40.080	0.4990	2.004
Na	11	22.990	0.4785	2.090
K	19	39.102	0.4859	2.058
Mg	12	24.312	0.4936	2.026
Ti	22	47.900	0.4593	2.177
P	15	30.974	0.4843	2.065
Mn	25	54.938	0.4551	2.197
S	16	32.064	0.4990	2.004
Cl	17	35.453	0.4795	2.085
C	6	12.011	0.4995	2.002
H	1	1.008	0.9921	1.008
O	8	15.999	0.5000	1.999
N	7	14.007	0.4998	2.001

Table 2. Spatial zones and gamma-ray energy scoring regions for a point source, infinite sphere configuration.

Typical number of source particles: 25,000.

Spatial zones at radii (cm) of:

2, 4, 6, 8, 10, 12, 14, 16,
18, 20, 25, 30, 35, 40, 45, 50.

Energy group boundaries (keV) at:

10, 15, 20, 30, 40, 45, 50, 60,
70, 80, 90, 100, 150, 200, 250, 300,
350, 400, 450, 500, 550, 600, 650, 700.

Energy responses (keV):

700 - 600
600 - 400
400 - 200
200 - 100
100 - 50
50 - 10

Table 3. Elemental concentrations (wt.%) of the model coals used in the point source, infinite sphere calculations.

Element		Model bituminous coal wt.%	Zero hydrogen coal wt.%	20 wt.% hydrogen coal wt.%
Model combustible component	C	63.20	66.78	53.42
	H	5.36	0	20.00
	O	24.61	26.01	20.18
	N	1.20	1.27	1.01
Model mineral component	Si	2.50	2.64	2.11
	Al	1.87	1.98	1.58
	Fe	1.25	1.32	1.06

The values of elemental concentration for the coals with zero hydrogen and 20 wt.% hydrogen are derived from the corresponding elemental concentrations of the model bituminous coal by proportional adjustment to give the same bulk density of 1.4183 g/cm^3 for each coal.

Table 4. Elemental concentrations of the model. Coal and shale used in the borehole configuration computations.

	Element	Concentration wt.%
COAL (ρ = 1.27 g/cm^3)	C	84.18
	H	5.60
	O	8.75
	N	1.47
SHALE (ρ = 2.55 g/cm^3)	O	49.90
	Si	27.53
	Al	8.79
	Fe	4.82
	Ca	1.57
	Na	1.19
	K	2.99
	Mg	1.60
	Ti	0.47
	P	0.07
	Mn	0.07
	C	0.72
	H	0.28

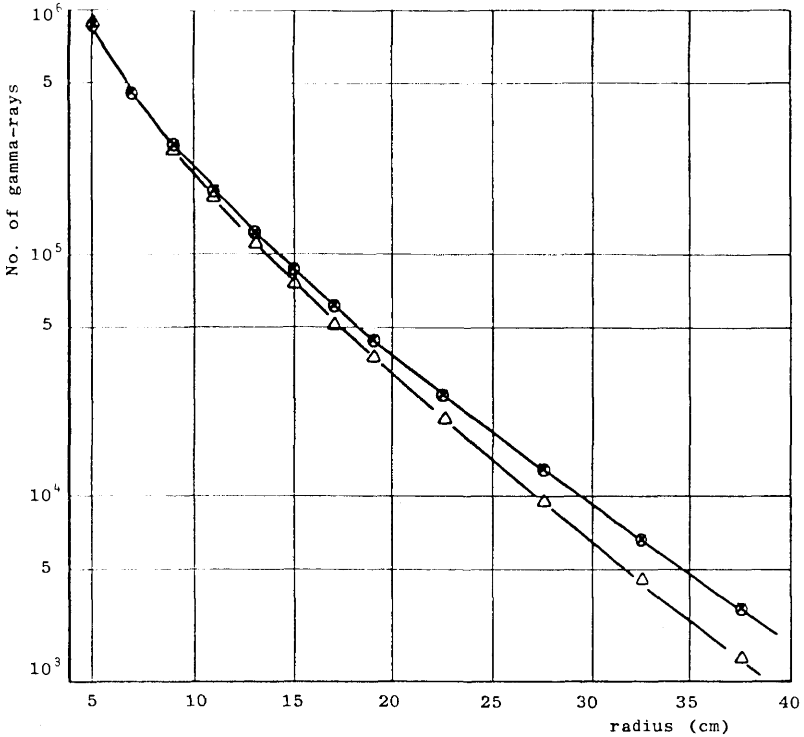

FIG. 1. Variation of gamma-ray intensity with radius.

Gamma-ray energy range from 90 keV to 100 keV

x - pure carbon

0 - carbon + 0.2 wt.% zirconium

Δ - carbon + 20 wt.% hydrogen.

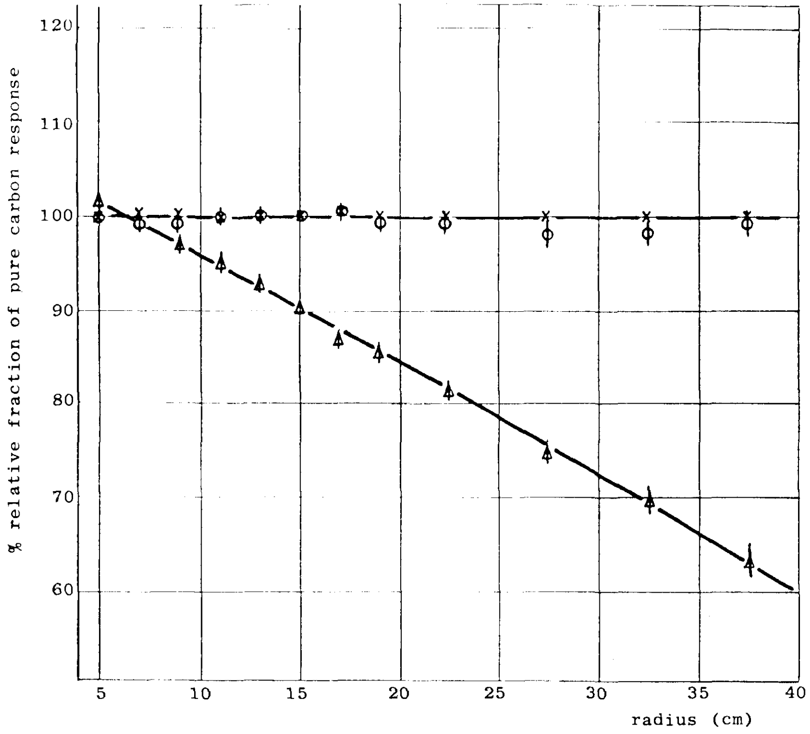

FIG. 2. Variation of gamma-ray intensity with radius relative to gamma-ray intensity in carbon.

Gamma-ray energy range from 100 keV to 660 keV

x - pure carbon

0 - carbon + 0.2 wt.% zirconium

Δ - carbon + 20 wt.% hydrogen.

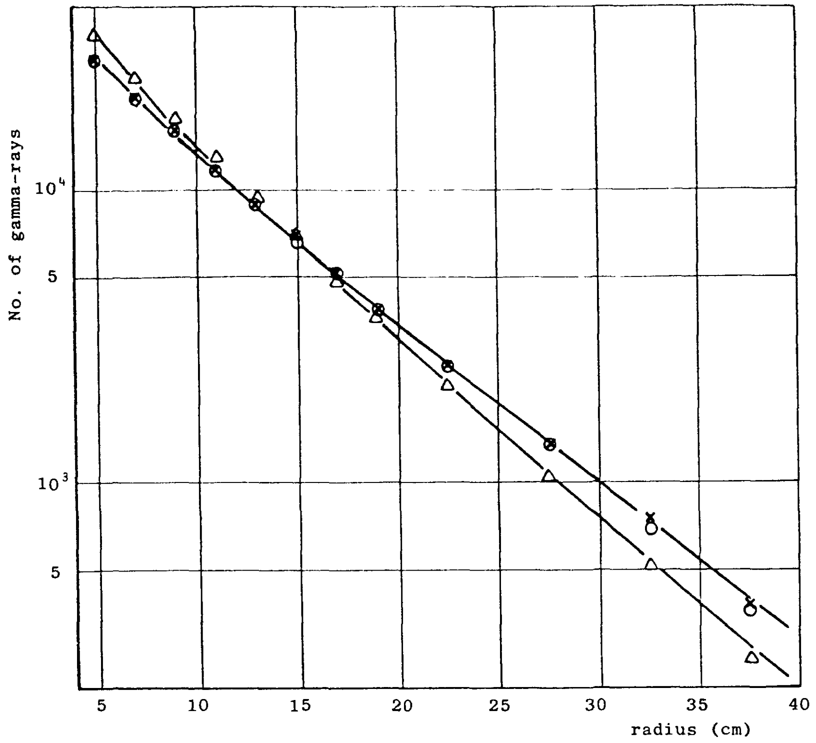

FIG. 3. Variation of gamma-ray intensity with radius.

Gamma-ray energy range from 90 keV to 100 keV

x - pure carbon

0 - carbon + 0.2 wt.% zirconium

Δ - carbon + 20 wt.% hydrogen.

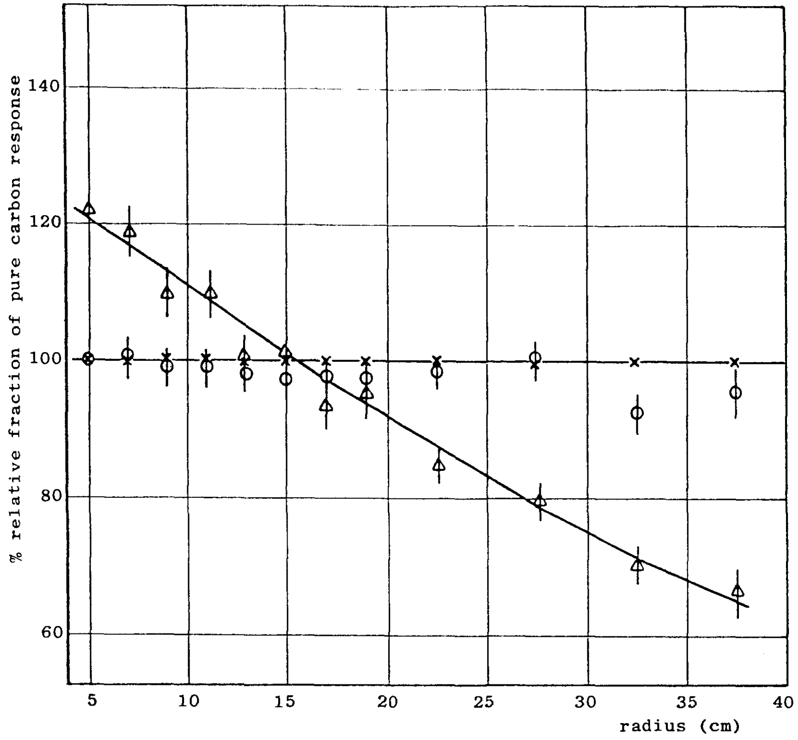

FIG. 4. Variation of gamma-ray intensity with radius relative to gamma-ray intensity in carbon.

Gamma-ray energy range from 90 keV to 100 keV

x - pure carbon

0 - carbon + 0.2 wt.% zirconium

Δ - carbon + 20 wt.% hydrogen.

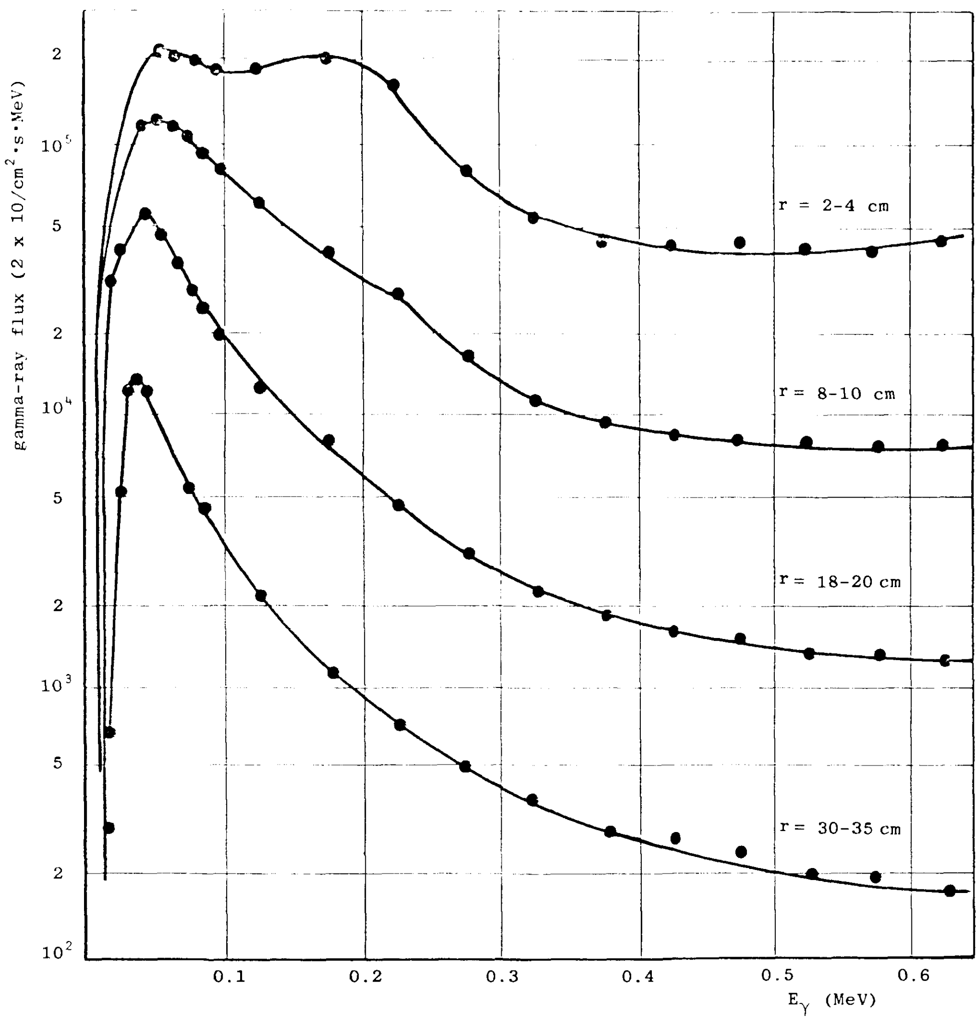

FIG. 5. Variation of gamma-ray flux with energy in selected radial zones for a point mono-energetic source (600 keV) in carbon (density 1.4183 g/cm^3).

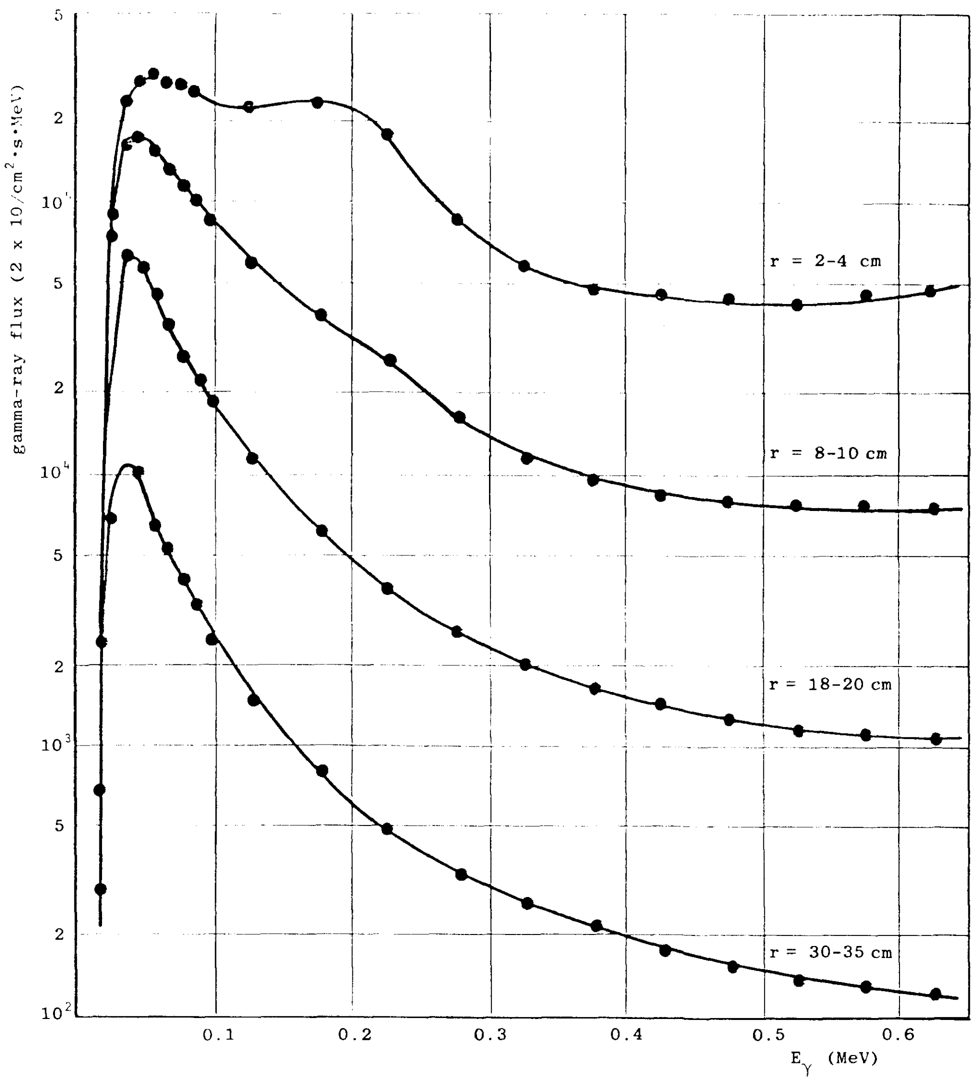

FIG. 6. Variation of gamma-ray flux with energy in selected radial zones for a point mono-energetic source (660 keV) in carbon +20 wt.% hydrogen (density 1.4183 g/cm^3).

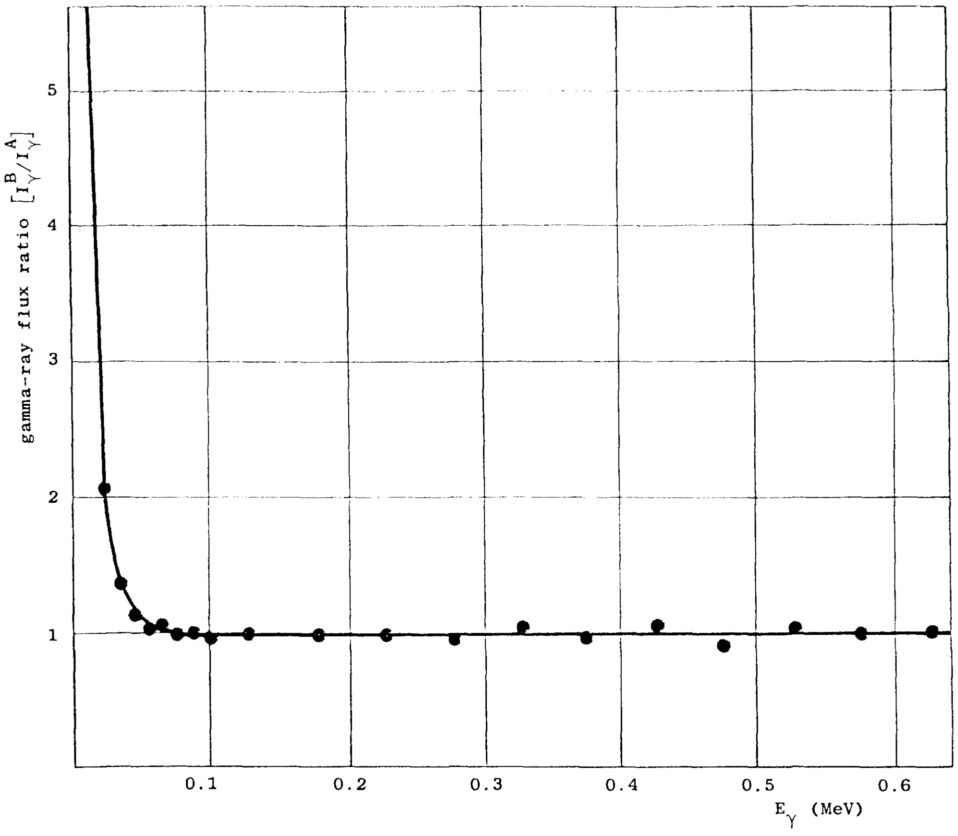

FIG. 7. Application of the Principle of Similitude to demonstrate the region of influence of photo-electric absorption.

Material A: carbon

Material B: carbon + 20 wt.% hydrogen

Electron density ratio: [B/A] = 1.197.

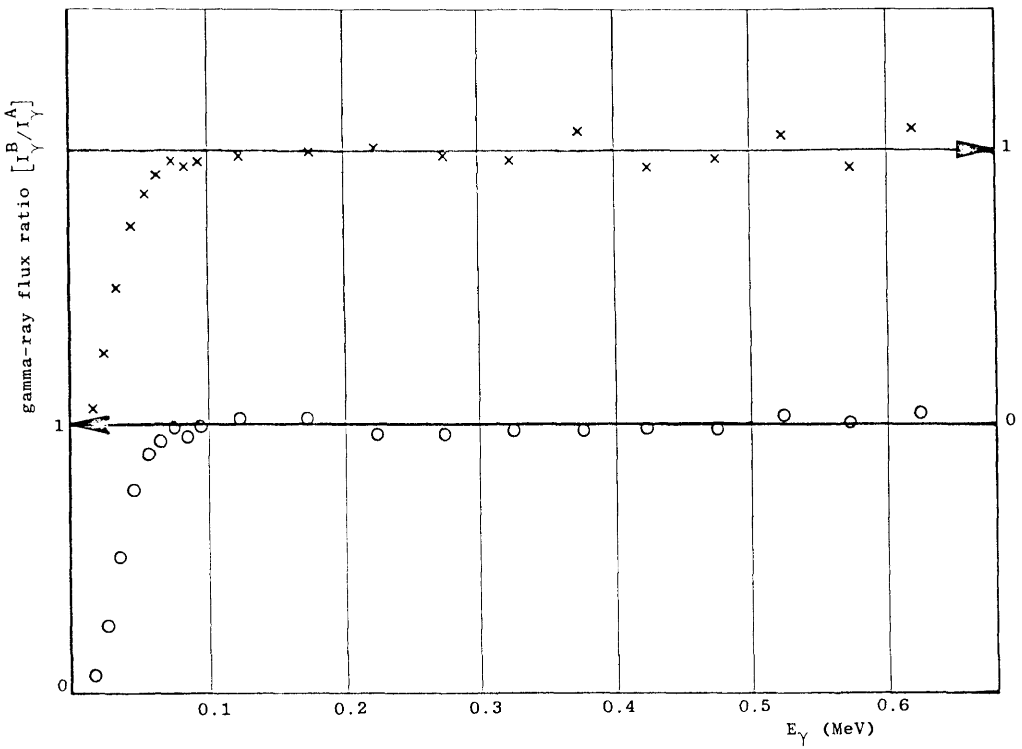

FIG. 8. Application of the Principle of Similitude to demonstrate the region of influence of photo-electric absorption.

Material A: carbon

Material B: carbon + 0.20 wt.% zirconium

Electron density ratio: [B/A] = 0.99976.

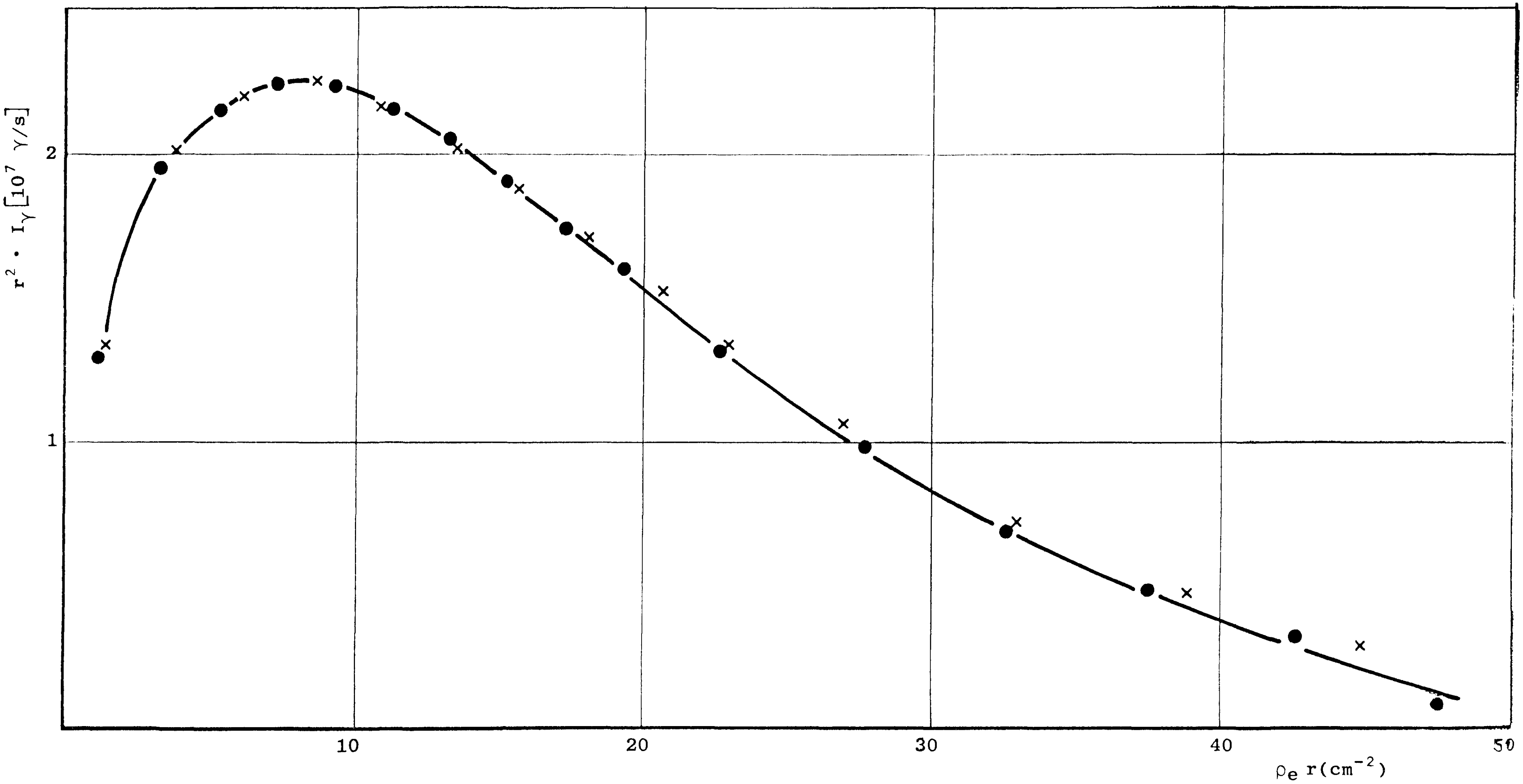

FIG. 9. Absolute relationship between gamma-ray flux and distance from a point source (E_γ = 660 keV) in an infinite medium of any composition assuming only Compton interactions.

● - carbon, ρ_e normalised to unity

x - carbon + 20 wt.% hydrogen ($\rho_e = 1.197$)

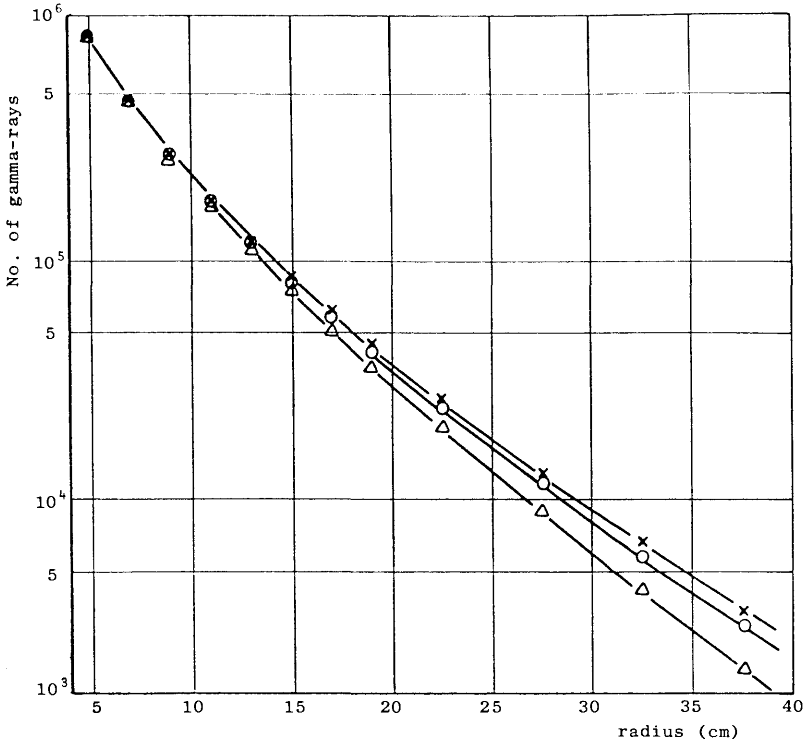

FIG. 10. Variation of gamma-ray intensity with radius for the model coal.

Gamma-ray energy range from 100 keV to 660 keV

x - no hydrogen

0 - 5.36 wt.% hydrogen

Δ - 20 wt.% hydrogen.

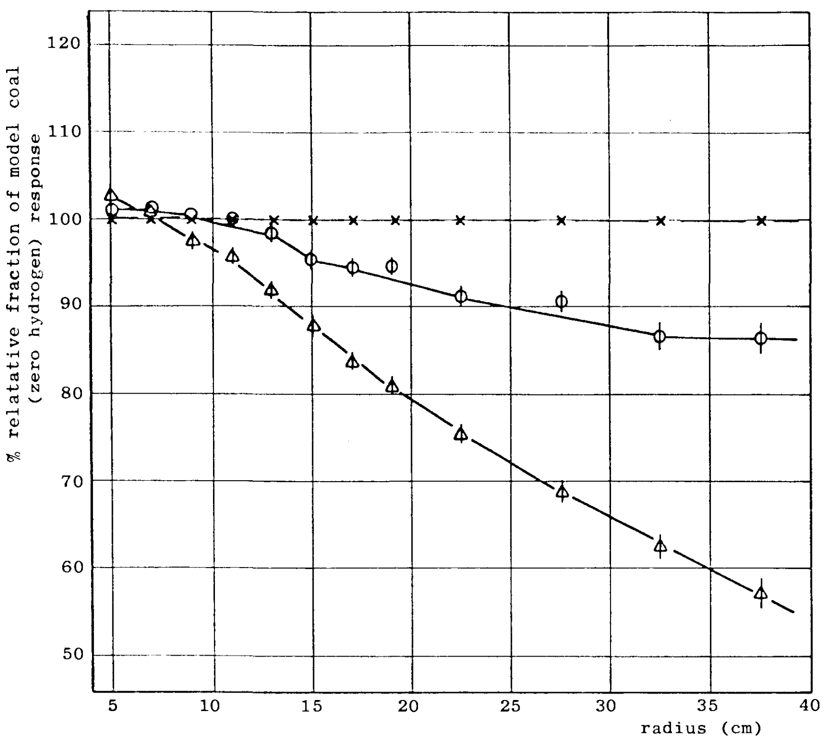

FIG. 11. Variation of gamma-ray intensity with radius relative to the model coal with zero hydrogen content.

Gamma-ray energy range from 100 keV to 660 keV

x - no hydrogen

0 - 5.36 wt.% hydrogen

Δ - 20 wt.% hydrogen.

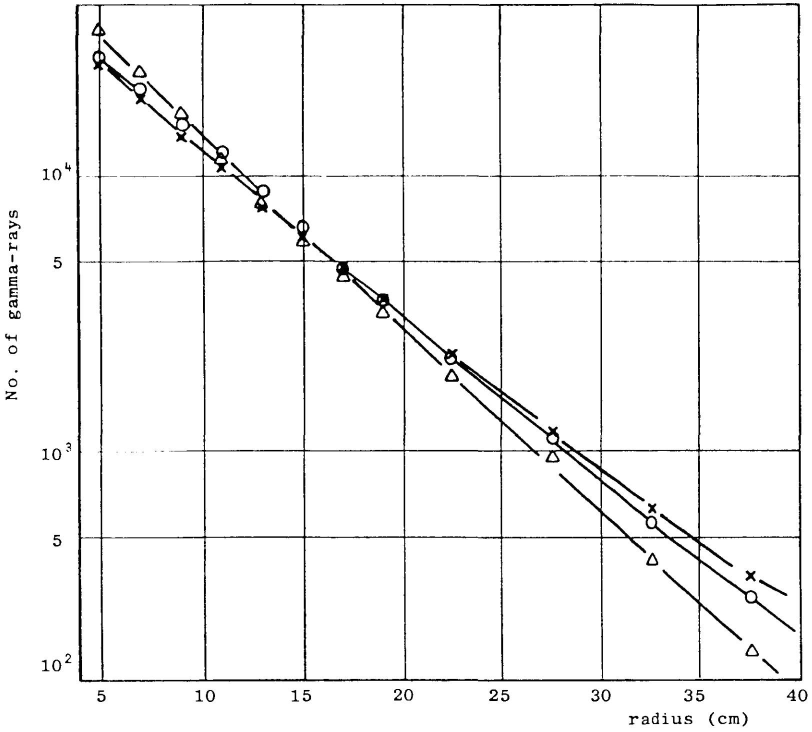

FIG. 12. Variation of gamma-ray intensity with radius for the model coal.

Gamma-ray energy range from 90 keV to 100 keV

x - no hydrogen

0 - 5.36 wt.% hydrogen

Δ - 20 wt.% hydrogen.

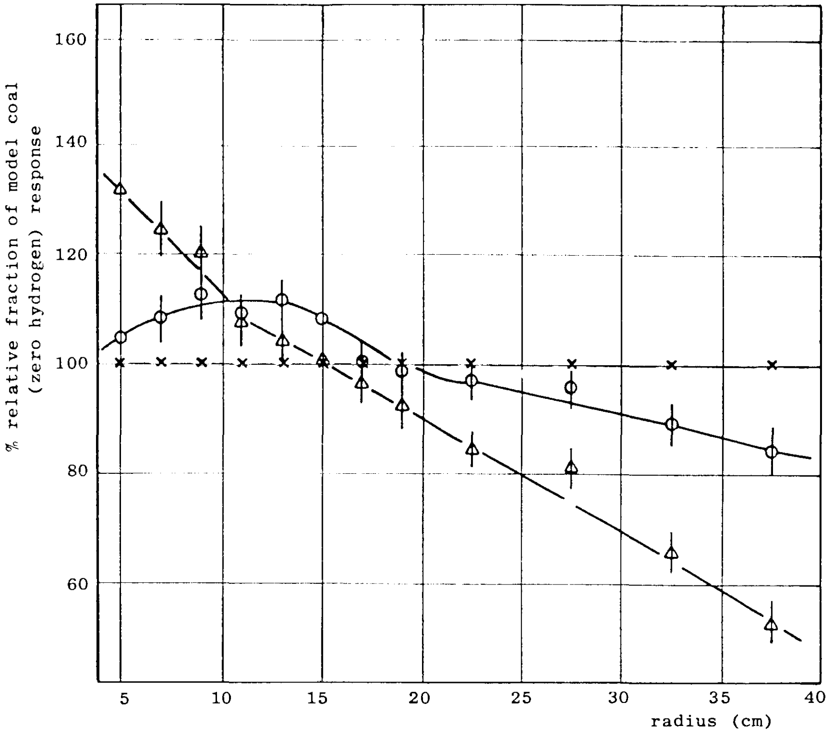

FIG. 13. Variation of gamma-ray intensity with radius relative to the model coal with zero hydrogen content.

Gamma-ray energy range from 90 keV to 100 keV.

x - no hydrogen

0 - 5.36 wt.% hydrogen

Δ - 20 wt.% hydrogen.

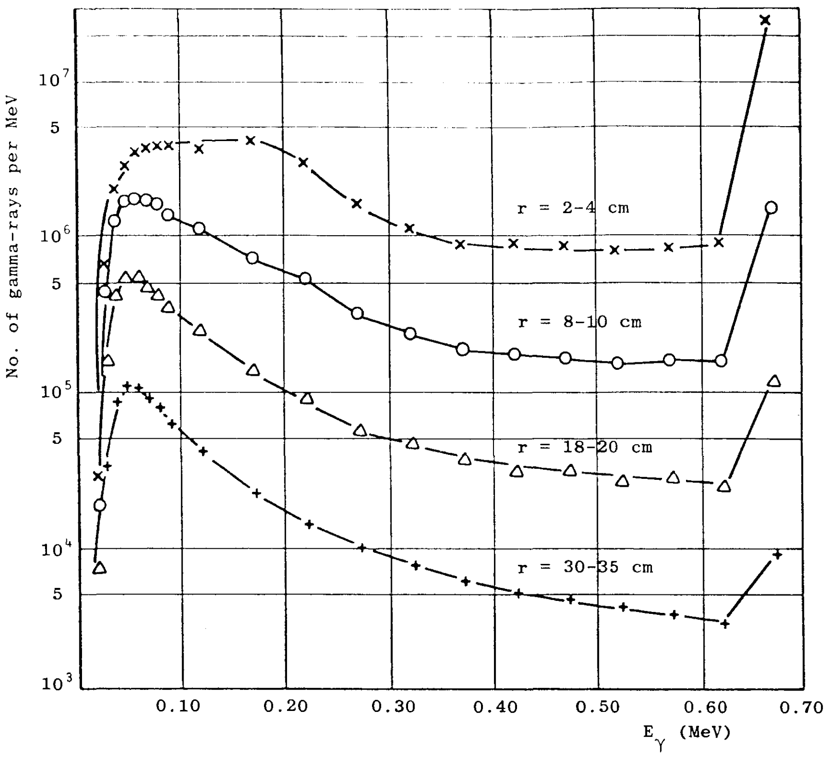

FIG. 14. Relative energy distribution of γ-rays with radius for the coal with zero hydrogen content.

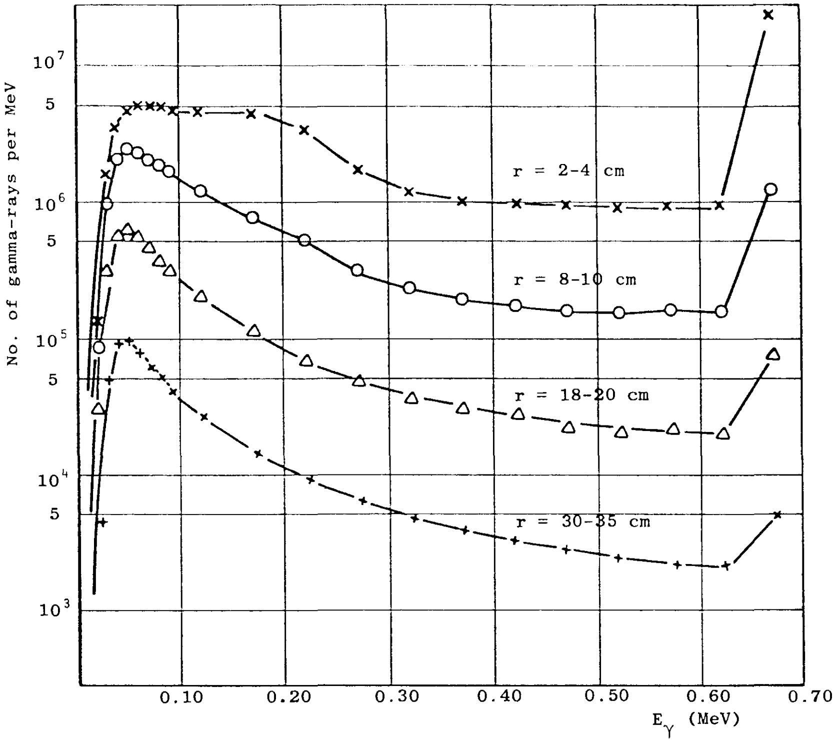

FIG. 15. Relative energy distribution of γ-rays with radius for the coal containing 20 wt.% hydrogen.

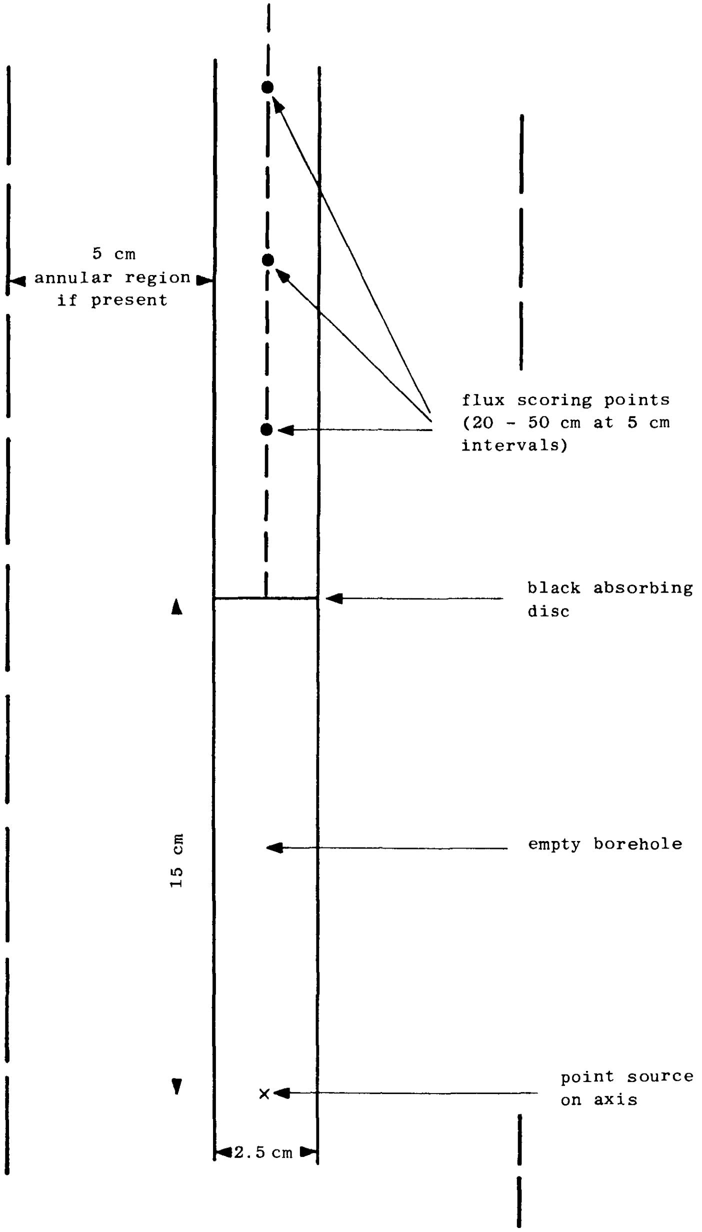

FIG. 16. First borehole configuration

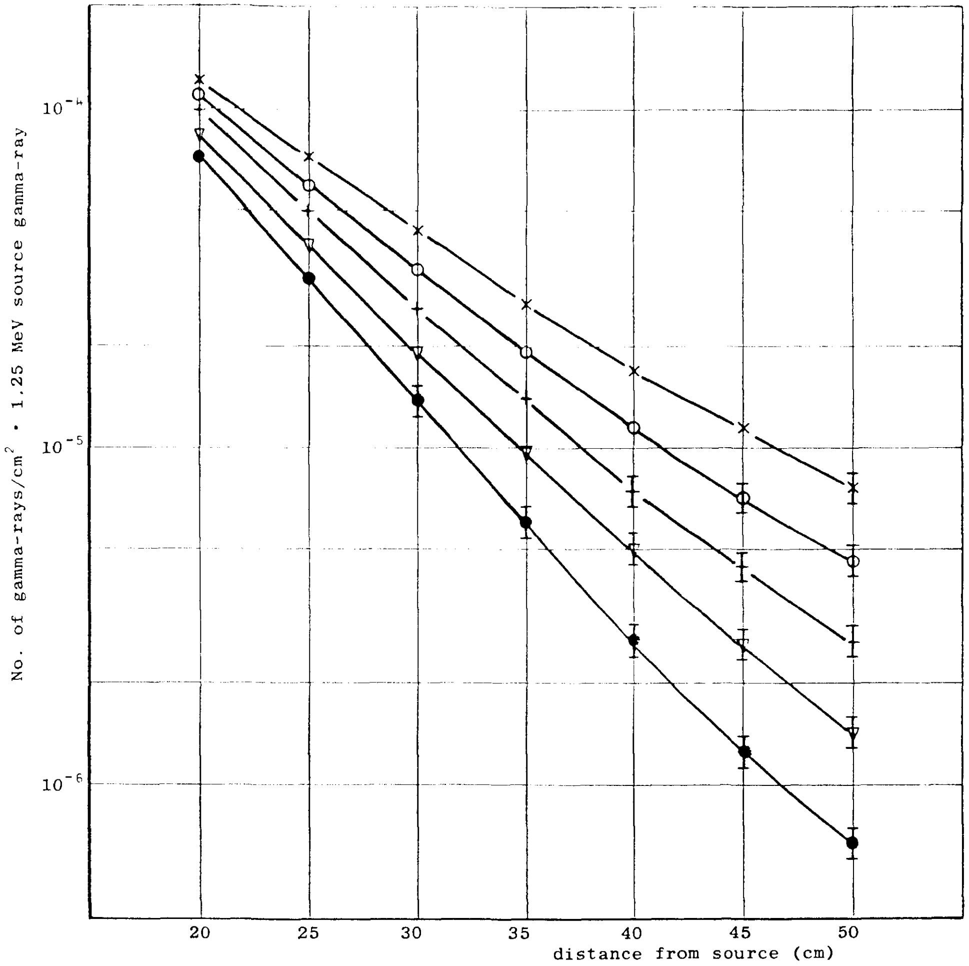

FIG. 17. Gamma-ray flux distribution above 200 keV in empty borehole of 2.54 cm diameter.

x - coal

0 - 75% coal, 25% shale

+ - 50% coal, 50% shale

∇ - 25% coal, 75% shale

● - shale.

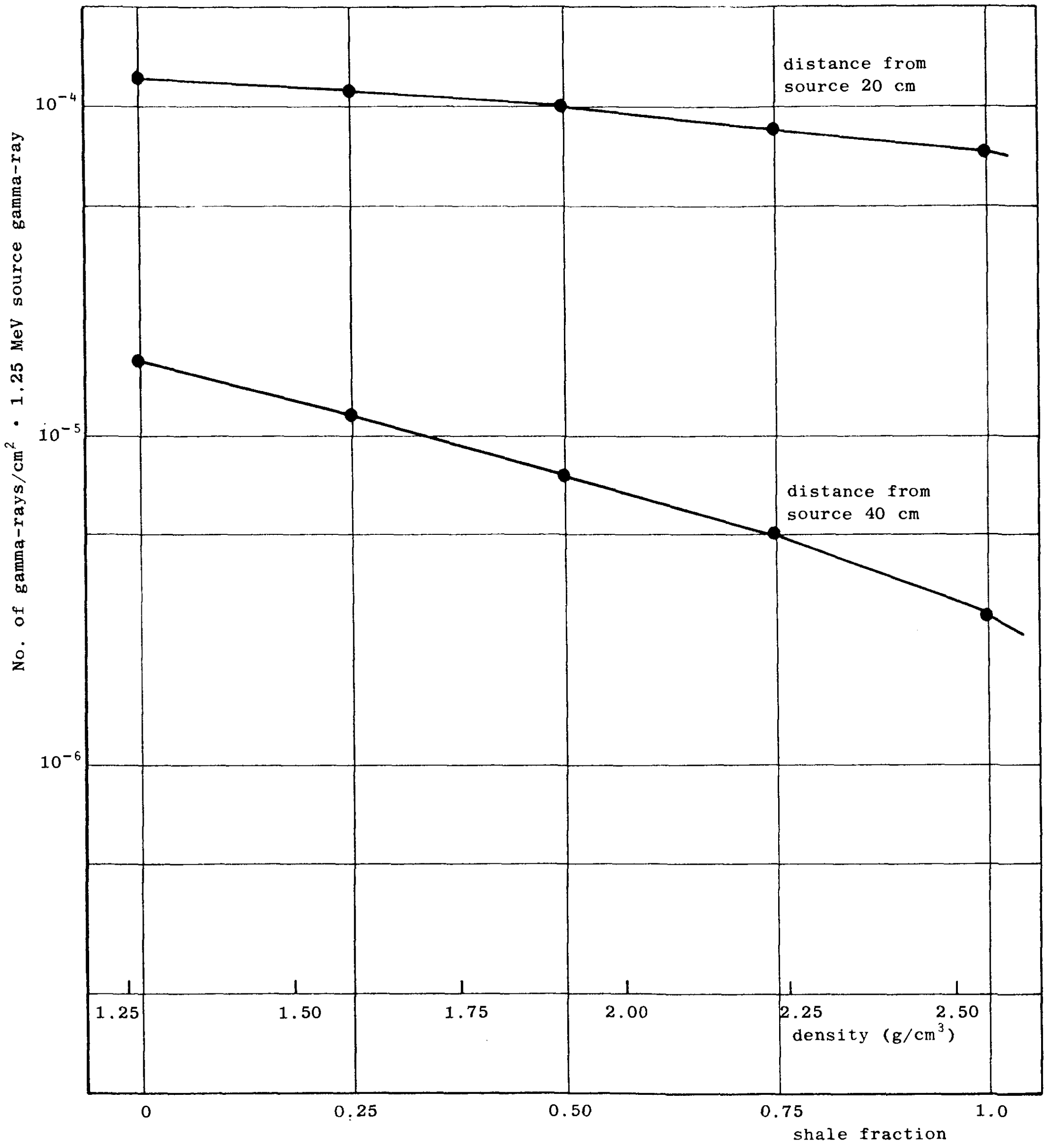

FIG. 18. Gamma-ray flux above 200 keV for a range of coal/shale mixtures (empty borehole, 2.54 cm diameter).

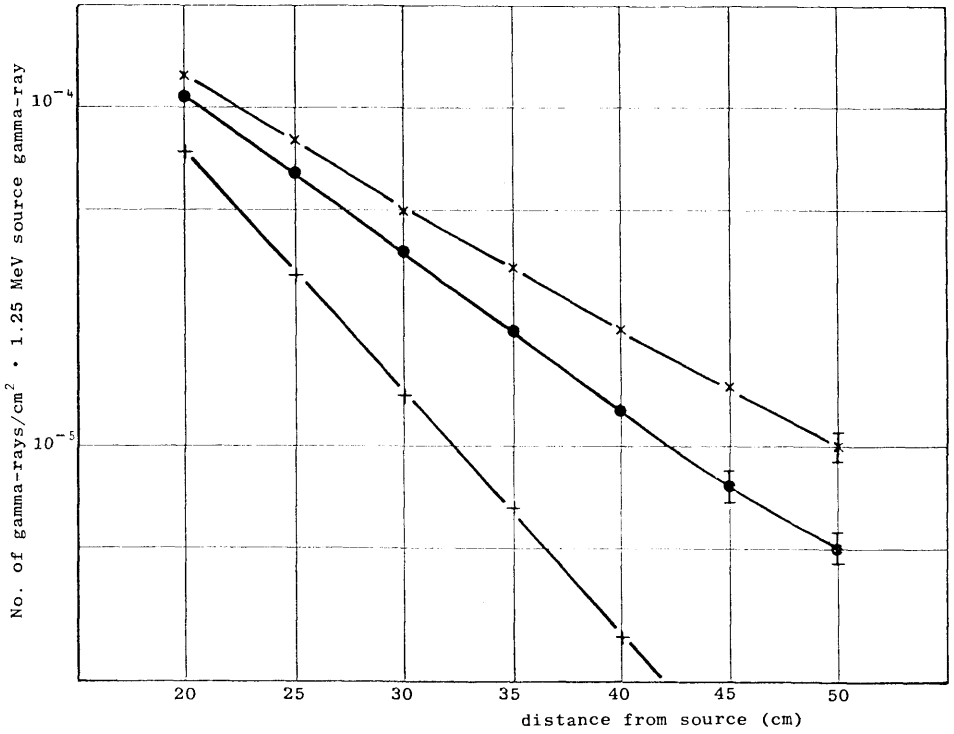

FIG. 19. Gamma-ray flux distribution above 200 keV in empty borehole of 2.54 cm diameter.

x - water as formation

● - 5 cm thick water annulus surrounding borehole, shale formation

\+ - shale formation.

AIRBORNE GAMMA SPECTROMETRY, EVALUATIONS AND CALIBRATION

I. Wendt

Bundesanstalt für Geowissenschaften u. Rohstoffe
Post fach 510153, D-3000 Hannover 51
Federal Republic of Germany

Abstract

The airborne geophysical system of the BGR (German Geological Survey) consists of a helicopter equipped with an electromagnetic system with two transmittors and two receivers, a proton resonance magnetometer and a 16 L NaJ-crystal with four channel recording. All these data together with navigation data and flight altitude above ground are recorded each second on a nine track magnetic tape for further data evaluation.

Different corrections have to be applied to the rough data such as

- smoothing by means of a digital filter to reduce statistical noise
- altitutde correction
- Compton-correction
- drift correction (cross-profile evaluation)

Then the corrected measuring data are combined with the navigation data in order to be able to produce iso-line maps.

The final results are presented as:

- line plots for U, Th, and K (and EM-data and magnetometer data)
- actual flight line plots
- iso-line maps for U, Th, and K
- iso-line maps for conductivity
- depth of conducting layer
- magnetometry maps

The procedures of correction and evaluation of the above mentioned data as well as the calibration of the NaJ-detector in terms of ppm U, Th, and % K are discussed in the paper.

Airborne Radiometrie: Data evaluation and calibration

I. Wendt, K.-P. Sengpiel, H. Lenz

1. Introduction

Airborne -spectrometric measurements of the gamma-radiation are carried out by fixed wing planes as well as by helicopters. For more detailed prospection helicopters are used because of their ability to fly at very low altitude and to keep a constant height above ground (contour flying). Large NaJ crystals are used (16 l in our case) to obtain sufficiently high count rates i.e. to get a sufficiently low statistical counting error even for short counting times like 1 sec. There are two possibilities to record the relevant spectrometric data: multichannel and four channel recording. Usually in case of multichannel counting a reduction to 3 channels by integration over selected energy-ranges is carried out after each counting period while the complete spectrum is used to calibrate the energy scale.

In this paper we will discuss predominantly the four channel method.

2. Description of the BGR equipment

Since the airborne prospection equipment of the BGR is a combination of three geophysical systems (fig. 1) a rather big helicopter is required (Sykorsky S 58 ET). The system consists of an electromagnetic system (Dighem-II) with a "bird" of 10 m length and 0.5 m in diameter which is towed about 30 m below the aircraft, a proton precession magnetometer with a sensor about 15 m below the helicopter and a Geometrics DiGRS-3001 spectrometer with a 16 l NaJ-crystal gamma-ray detector placed in the rear part of the helicopter (fig. 1).

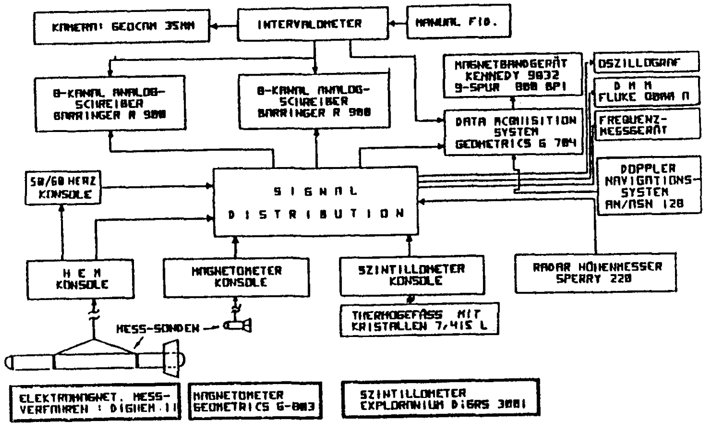

Fig. 1 SIGNAL FLOW OF THE HELICOPTER BORNE GEOPHYSICAL SYSTEM

Auxiliary instruments are necessary like radar doppler (Singer-Kearfott) for navigation and actual flight track-recovery, a radar altimeter, and data storage on analogue recorders and on 9 track magnetic tape recorder.

Fig. 1 shows the signal flow within the helicopter measuring system.

3. Data collection

3.1. Gamma radiation from natural sources

The gamma radiation emitted from the ground has three sources:

1) U + daugther products (^{214}Bi)
2) Th + daugther products (^{208}TI)
3) K (^{40}K)

Th and U and their daugther isotopes emit photons at several gamma energies. The primary gamma energy is partially reduced by Compton scattering which can occur in the source (soil) itself, in the air between source and detector and in the crystal. Therefore a single gamma energy (like ^{40}K) produces a photo peak (fig. 2) and a Compton continuum of lower energies. The spectra of U and Th are produced by several different photo peaks and their Compton continua, i.e. the measured spectrum at a certain altitude above ground is a linear combination of the three spectra shown in fig. 2. These spectra are slightly modified by Compton scattering in the air.

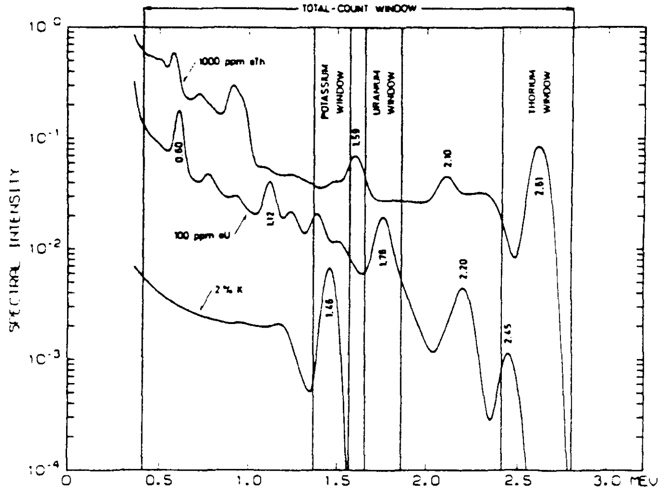

FIG. 2 : Thorium, uranium, and potassium gamma-ray spectra obtained at ground level with a 76 X 76 mm sodium-iodide scintillator,(IAEA,1979)

Some predominant peaks of these spectra are used to separate the contribution of the three sources of the total gamma spectrum. As can be seen from fig. 2 a photopeak at 2.61 MeV energy is characteristic for Th, at 1.76 MeV for U and at 1.46 MeV for K. Therefore three count rates from energy-windows centered at these energies are recorded in periods of usually 0.5, 1.0 or 2.0 seconds. In case of four channel recording it is very important that the overall gain remains constant at least during one flight. In case of multichannel recording of the total gamma spectrum the integration of the energy windows can be performed in relation to the peak center even if the peak itself has slightly shifted because of gain variation.

4. Data processing

4.1. Filtering of rough data

The counting rates Ni of the three channels have an uncertaincy of ± $\sqrt{N_i}$ due to the statistical behavior of the radioactive disintegration, i.e. the ideal data which could be obtained by measuring at each point along the flight line for an infinite time is superimposed by a statistical noise. Thus small anomalies may not be distinguished from accidental noise peaks. A smoothing procedure can improve the evaluability of the data (Tammenmaa et al. 1976).

As is well known the radiation measured at flight altitude h would yield a smooth curve even for abrupt changes of the radioelement concentration in the ground (see fig. 4 for the point source). This curve is superimposed by a statistical noise due to the statistical nature of the disintegration processes of the radioelements. The noise can be reduced by digital filtering. The filters should virtually not affect the above mentioned signal curve.

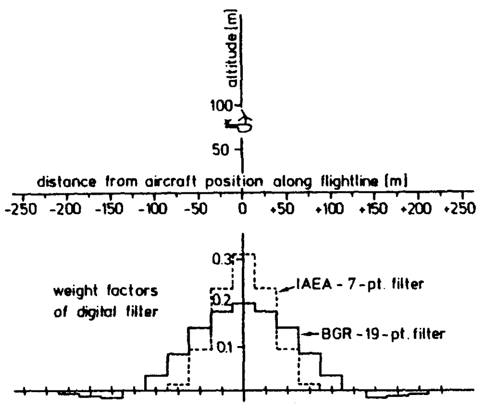

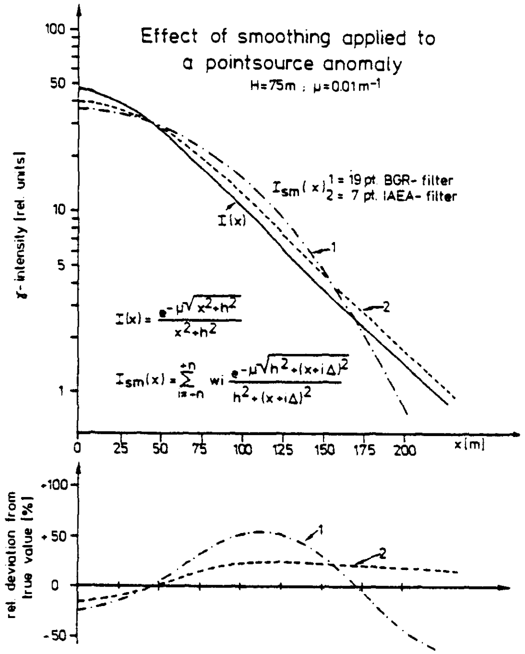

Fig. 3 Filterfactor of BGR and IAEA digital filter

Fig. 4 Comparison of exact point source anomaly and 'smoothed' anomalies

The smoothed counting rate N_i is obtained as

(1) $$\overline{N}_i = \sum_{k=-n}^{+n} w_k N_{i+k} \; ; \quad \sum_{-n}^{+n} w_k = 1$$

where w_k are weight factors. We apply a 19 point-digital filter with the following weight factors (Sengpiel 1981)

w_0 = + 0.2 ; $w_{\pm 1}$ = + 0.1840; $w_{\pm 2}$ = 0.1416
$w_{\pm 3}$ = + 0.0866; $w_{\pm 4}$ = + 0.0354; $w_{\pm 5}$ = 0.0
$w_{\pm 6}$ = - 0.0157; $w_{\pm 7}$ = - 0.0159; $w_{\pm 8}$ = 0.0088
$w_{\pm 9}$ = - 0.00714

flying at an altitude of 75 m with a mean speed of 25 m/sec (fig. 3). The filter was designed using the filter theory of Hamming (1977). The filter function in the frequency domain is represented in fig. 5.

A filter should reduce the statistical noise as much as possible but it should influence the sharpest possible real anomaly as little as possible.

Our filter reduces the statistical noise σN_i to

$$\sigma \overline{N}_i = \sqrt{\sum_{-n}^{n} w_k^2 \sigma N_{i+k}^2} = 0.41\ \sigma N_i$$

while the 7 point IAEA-filter has a factor of 0.47. The anomaly with the narrowest half width would be produced by a point source at the surface of the ground.

Fig. 4 shows the theoretical anomaly of a point source recorded at an altitude of 75 m in comparison to the smoothed curve after passing the data through the above mentioned filter. The ideal curve is given by

(2) $$I(x) = k \frac{\exp(-\mu \sqrt{x^2 + h^2})}{x^2 + h^2}$$

while the smoothed curve is given by

(3) $$I(x) = k \sum_{i=-n}^{+n} w_i \frac{\exp(-\mu \sqrt{(x + i\Delta)^2 + h^2})}{(x + i\Delta)^2 + h^2}$$

The examples of Fig. 4 show that the anomaly of a point source is somewhat changed by the filtering process. Geological bodies will produce broader anomalies which will be even less affected by filtering (see fig. 8). The noise reduction of the 19-point filter is also represented in fig. 8.

The normalized amplitude spectrum of the anomaly of a point source which is crossed at a height of 75 m is drawn in fig. 5, together with the transfer function of the filter (filter function), and the filtered amplitude spectrum. The "frequency" f is based on a sampling distance = 25 m. L is the corresponding spectral wavelength.

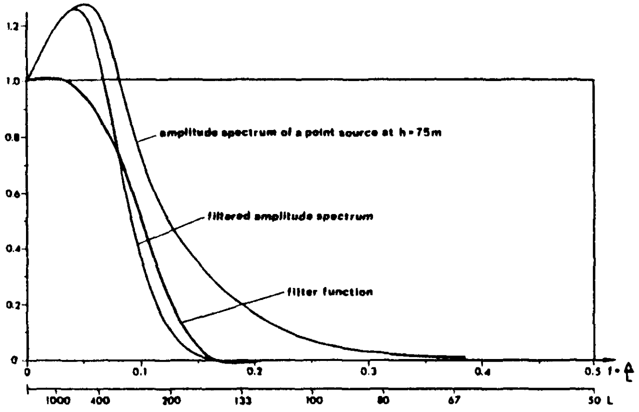

Fig. 5 Filterfunction of 19 point digitalfilter and amplitude spectrum of a point source

4.2. Background correction

The "background" is the radiation recorded with no radioactive material at the ground. It can be measured above sufficiently large water areas. It consists of the constant radiation of the materials of the helicopter and its components and of the cosmic radiation which depends on the altitude above sea level.

Since there is a linear relationship between the count rate for gamma energies > 3 MeV and the cosmic radiation background component in the three energy-windows, a background subtraction can be applied easily.

4.3. Compton correction

As can be seen from fig. 2 the Th-gamma radiation also contributes to the count rates in the U- and K-window and the U-radiation to the K-window (also to a slight extend to the Th-window). In order to obtain the net count rates of each of the three sources of gamma radiation, certain fractions of the other two count rates have to be subtracted from each gross window count rate N, namely

$$
(4) \qquad \begin{aligned} Th &= N_{Th} \\ U &= N_u - \alpha(h)\ Th \\ K &= N_K - \beta(h)\ Th - \gamma(h) \cdot U \end{aligned}
$$

The "stripping" ratios α, β, γ depend - among others - on the altitude h above ground as has been shown by Grasty (1975).

A simple approximation of the height dependency of the stripping ratios is given by the following formulas (IAEA, 1979):

$$
\begin{aligned} \Delta\alpha &= 0.0004\ h + 0.01 \\ \Delta\beta &= 0.0004\ h + 0.01 \\ \Delta\gamma &= 0.0005\ h + 0.01 \end{aligned}
$$

These values have to be added to the constant part of the stripping ratios (due to Compton scattering in the ground and in the crystal). For our system (16.8 l detector) the following values apply:

$$
\begin{aligned} \alpha &= 0.27 \\ \beta &= 0.41 \\ \gamma &= 0.89 \end{aligned}
$$

4.4. Reduction to constant altitude above ground

The ratio of the gamma intensity at height h to the intensity at ground level measured by a spherical detector above an infinite halfspace of homogeneous radioactivity is given approximately by

$$(5) \qquad I(h) = E_2(\mu h) = \int_1^\infty \frac{\exp(\mu h x)}{x^2}\, dx$$

or according to Grasty (1975)

$$(6) \qquad I(h) = (E_2\ (\mu h) + k\ \exp\ (\mu h))\ (1 + k)^{-1}$$

where μ = absorption coefficient in air for a certain gamma energy and k = the fraction of primary photons scattered into the pertinent energy window. This coefficient depends not only on the gamma energy but also slightly on air density and moisture content of the air.

The dependance of I(h) on h is shown in fig. 6. It can be approximated within a certain limited range by an exponential function. It is recommended to measure the altitude

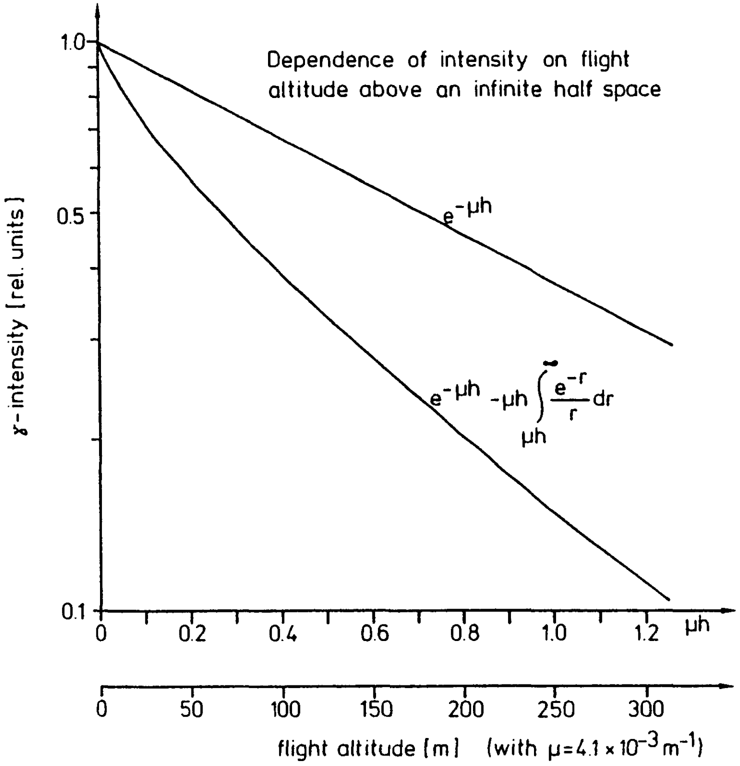

Fig. 6 Altitude dependence of radiation intensity

dependence experimentally. This is done in BGR by vertical ascendine flights of the helicopter from the ground to heights of about 300 m (Sengpiel 1981). Fig. 7 shows results of such flights over different rock units, and the theoretical curve according to equation (6). Due to varying ^{222}Rn-concentrations in the air the altitude dependency curve for U may be distorted. Further one must keep in mind that the theoretical correction to constant altitude above ground is based on the assumption of a homogeneous concentration of radioelements in a flat ground. For areas of rough topography the height dependency of I will be different. These errorss are hardly to be removed.

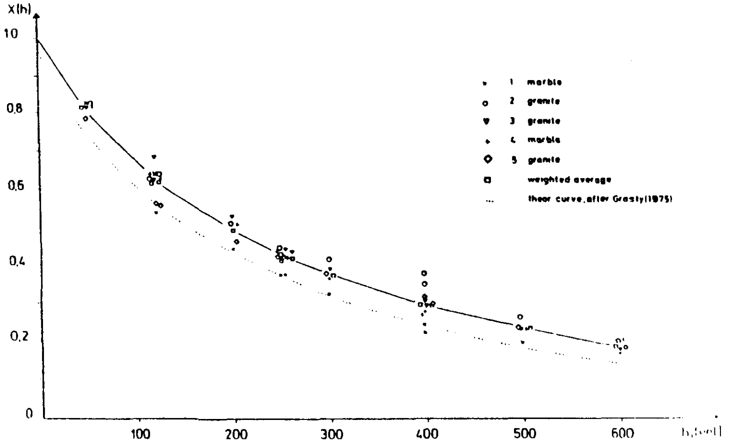

Fig. 7 Experimental results of altitude dependence of gamma

The analog recordings for K, U, and Th along a flight line and the effects of all the processing stages described above are shown in Fig. 8.

4.5. Determination of actual flight-profile

The recorded and processed gamma intensity data still have to be correlated to their exact positions. The geographical coordinates recorded by the Doppler navigation system are correlated for long-term drifts and then combined with the radiometric and others geophysical data .

4.6. Tie lines

The results of all flights of a survey area have to be combined to procedure radiometric contour maps. It is known that small changes in the radiation intensity for flights flown on different days may occur. These changes may be due to different atmospheric conditions like air density and moisture content, different surface conditions caused by rain or snow, varying ^{222}Rn in the air or even instrumental drifts. In order to eliminate such systematic errors and to level the intensities of the individual flights several tie lines with large spacings are flown. A statistical evaluation of the intersection points of measuring lines and tie lines show whether significant differences in radiation level do exist or not. Usually a zero order correction is sufficient.

If there are n intersection points for one group of measuring lines (x-direction) and the tie lines (y-direction) a correction term Δ has to be added to all data of this group. This term Δ will be calculated by the following equation:

$$(7) \qquad \sum_{i=1}^{n} u_i \left(N_{xi} - N_{yi} - \Delta\right)^2 \rightarrow \min$$

N_{xi} and N_{yi} are the count rates of measuring and control profile respectively already corrected as discussed in section 4.1. to 4.4. and u_i are weight factors given by

$$u_i = \frac{1}{\sigma N_{x_i}^2 + \sigma N_{y_i}^2} \tag{8}$$

with N_{xi} and N_{yi} the total errors of the measured count rates for both profiles at the intersection point number i. One obtains

$$\Delta = \bar{N}_x - \bar{N}_y \ ; \quad \sigma\Delta^2 = \frac{1}{\sum u_i} \tag{9}$$

with N_x and N_y the weighted averages of x- and y-profile count rates at the intersection points. The errors σN_{xi} and σN_{yi} which determine the weight factor u_i which represent the "quality" of this particular intersection point are determined not only by counting statistics but also by the error of the navigation. This second part of σN is negligable if both profiles have a rather constant count rate around the intersection point but it can become dominant if the intersection point is located at a steep gradient of the measuring profile.

For a control whether the zero order correction Δ is sufficient the relation

$$\bar{\chi} = \sqrt{\frac{\sum u_i (N_{x_i} - N_{y_i} - \Delta)^2}{n-1}} \approx 1 \tag{10}$$

may be used i.e. after the Δ correction the scatter of the differences is within the experimental errors.

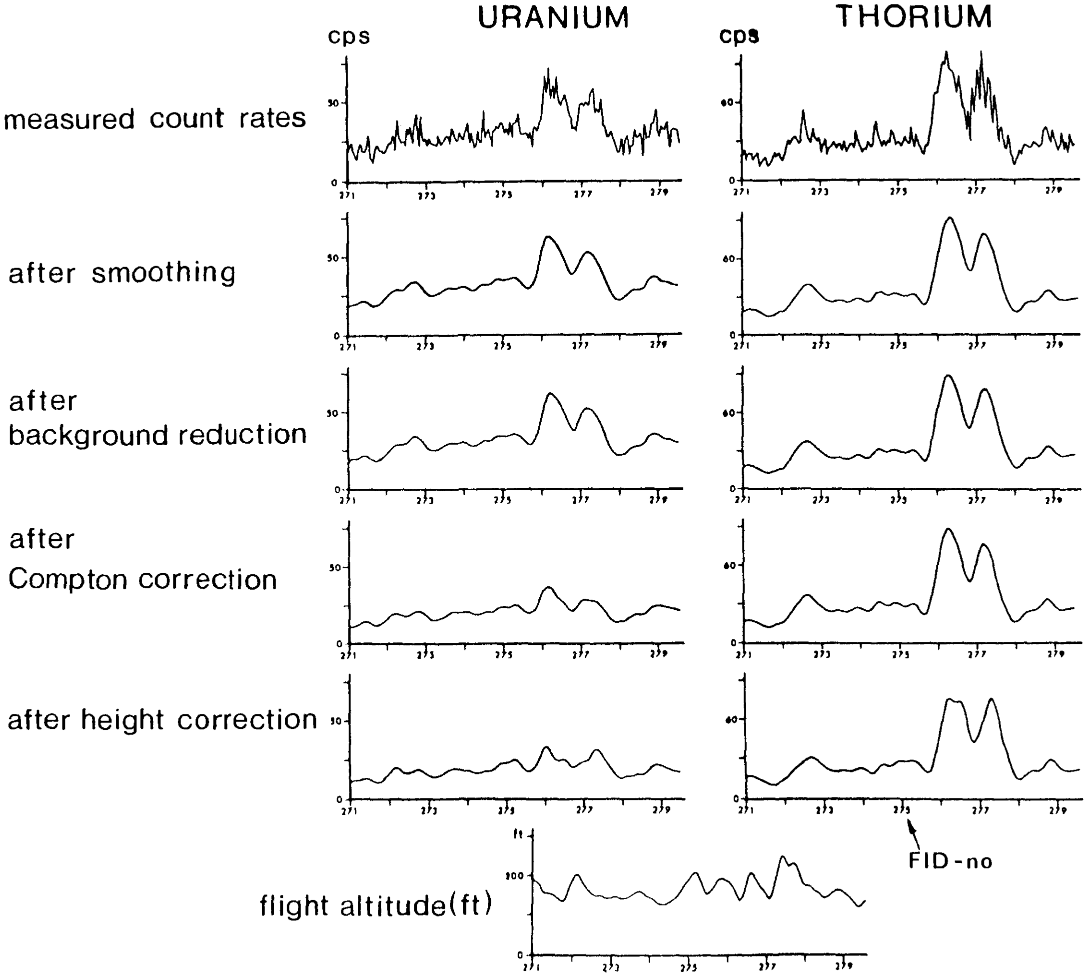

Fig. 8

Example of the effects of the correction processes

4.7. Conversion of counting rates into absolute units

After application of all corrections described in section 4.1. to 4.5. the data are still given in cps for K, U and Th for a constant flight altitude of 200 ft. These count rates are relative units determined by instrumental factors such as size of the NaJ-crystal. It is desireable to convert the count rates into absolute units in order to be able to compare the results obtained by different equipment. The absolute values used are equivalent concentrations of K, U, Th given in % K and ppm U or Th. These equivalent values are based on the model of an infinite half-space of homogeneous concentration. The detector assembly has to be calibrated to convert count rates into eK, eU, eTh concentrations (comp. Lovborg et al. 1971).

The sensitivity of the spectrometer is determined on calibration pads of known concentrations of the radioelements which have a sufficient diameter (>10 m) to provide a 2π-geometry for the detector when the aircraft is placed on the pad. These measurements yield conversion factors of cps into values of concentration for K, U and Th at ground level. These factors then have to be multiplied with factors converting the counting rate calculated for the norm altitude of 200 ft to the counting rate at ground level. The attenuation factors for the different radioelements are found from the results of the ascending flights in the survey area (c.f. fig. 7).

Usually four or more pads are used for calibration

- one 'blank' pad
- one pad with 5-10 % potassium and 'blank' in respect to U and Th
- one pad with 20 to 30 ppm Uranium and 'blank' in respect to K and Th
- one pad with about 50 ppm Th and 'blank' in respect to K and U.

One obtains four sets (one for each pad) of three equations:

$$\begin{aligned} &\text{K -window} : N_K^i = a_{KK}\, C_K^i + a_{UK}\, C_U^i + a_{TK}\, C_T^i + b_K \\ (11)\quad &\text{U -window} : N_U^i = a_{KU}\, C_K^i + a_{UU}\, C_U^i + a_{TU}\, C_T^i + b_U \\ &\text{Th-window} : N_T^i = a_{KT}\, C_K^i + a_{UT}\, C_U^i + a_{TT}\, C_T^i + b_T \end{aligned}$$

where the nine coefficients a_{xy} represent the fraction of radiation from element x- into y-energy window, b_y (y = K,U,T) are the backgrounds in the corresponding energy windows N_y^i the count rates obtained on pad i (i = 0,1,2,3) in the y-energy window and C_y^i the concentration of element y in pad i. The four blocks (i = 0,1,2,3) of equations (11) may be reduced to three blocks subtracting block 0 from block 1, 2, and 3, i.e. eliminating the backgrounds b_K, b_U, b_T.

One obtains for each energy window with

$n_K^1 = N_K^1 - N_n^o$; $c_K^1 = C_K^1 - C_K^o$; $c_U^1 = C_U^1 - C_U^o$ etc.

three equations

$$n_K^{\,1} = a_{KK}\,c_K^{\,1} + a_{UK}\,c_U^{\,1} + a_{TK}\,c_T^{\,1}$$

$$(12)\qquad n_K^{\,2} = a_{KK}\,c_K^{\,2} + a_{UK}\,c_U^{\,2} + a_{TK}\,c_T^{\,2}$$

$$n_K^{\,3} = a_{KK}\,c_K^{\,3} + a_{UK}\,c_U^{\,3} + a_{TK}\,c_T^{\,3}$$

for the three unknowns a_{KK}, a_{UK} and a_{TK} correspondingly one obtains the solutions

$$(13)\qquad a_{KK} = \frac{D_{K1}}{D}\ ;\quad a_{UK} = \frac{D_{K2}}{D}\ ;\quad a_{TK} = \frac{D_{K3}}{D}$$

with the determinate

$$D = \begin{vmatrix} c_K^{\,1} & c_U^{\,1} & c_T^{\,1} \\ c_K^{\,2} & c_U^{\,2} & c_T^{\,2} \\ c_K^{\,3} & c_U^{\,3} & c_T^{\,3} \end{vmatrix}$$

and D_{Ki} is the determinate D where column i is replaced by the vector

$$(14)\qquad Y = \begin{bmatrix} n_K^{\,1} \\ n_K^{\,2} \\ n_K^{\,3} \end{bmatrix}$$

Correspondingly one obtains for U und Th two more sets of three equations with three unknowns each, i.e. one has to determine 9 unknowns which may be written in a matrix scheme

$$(15)\qquad A = \begin{bmatrix} a_{KK} & a_{UK} & a_{TK} \\ a_{KU} & a_{UU} & a_{TU} \\ a_{KT} & a_{UT} & a_{TT} \end{bmatrix}$$

Each of these matrix elements calculated according to equations like (13) is subject to errors caused by twelve experimental data $c_K^{\,i}$, $c_U^{\,i}$, $c_T^{\,i}$ and $n_K^{\,i}$ $(i = 1,2,3)$ and for U and T correspondingly. The twelve error propagation factors can be calculated from elements and subdeterminantes of D and the vector Y (equ. 13 and 14).

The 'sensitivities' (cps/% K, or cps/ppm) aregiven by

$$(16)\qquad S_K = a_{KK}\ ;\ S_U = a_{UU}\ ;\ S_T = a_{TT}$$

and the stripping ratios (equ. 4)

$$(17)\qquad \alpha = \frac{a_{TU}}{a_{TT}}\ ;\quad \beta = \frac{a_{TK}}{a_{TT}}\ ;\quad \gamma = \frac{a_{UK}}{a_{UU}}$$

The equations (12) also may be written as (i = 1,2,3)

$$
\begin{aligned}
& c_K{}^i = a_{KK}' \, n_K{}^i + a_{UK}' \, n_U{}^i + a_{TK}' \, n_T{}^i \\
(18) \quad & c_U{}^i = a_{KU}' \, n_K{}^i + a_{UU}' \, n_U{}^i + a_{TU}' \, n_T{}^i \\
& c_T{}^I = a_{KT}' \, n_K{}^i + a_{UT}' \, n_U{}^i + a_{TT}' \, n_T{}^i
\end{aligned}
$$

where the matrix

$$
(19) \qquad A' = \begin{bmatrix} a_{KK}' & a_{UK}' & a_{TK}' \\ a_{KU}' & a_{UU}' & a_{TU}' \\ a_{KT}' & a_{UT}' & a_{TT}' \end{bmatrix}
$$

is the inverse matrix to A (equ. 15).

The calculation of the errors of the elements of A' is the same as described above. In our case the predominant sources of errors are the uncertainties of the pad concentrations, i.e. a relative calibration of different instruments using the same pads is more precise than a calibration in absolute concentrations.

References

Grasty, R.L., 1975: Uranium measurements by airborne gamm-ray spectrometry. Geophysics, vol. 40, no. 3; Tulsa, Oklahoma.

Hamming, R.W., 1977: Digital Filters. Prentice Hall Signal Processing Series; Englewood Cliffs, New Jersey.

IAEA, 1979: Gamma-ray surveys in uranium exploration. Technical reports series no. 186, International Atomic Energy Agency; Vienna.

Lovborg, L., Christiansen, E.M., Botter-Jensen, L., Kirkegaard, P., 1981: Pad facility for the calibration of gamma-ray measurements on rocks. Riso-R-454. Riso National Laboratory Roskilde, Denmark.

Sengpiel, K.P., 1981: Ausrüstung und Erprobung eines Hubschraubers für geophysikalische Messungen. Final report of search program BMFT NTS 6, archive no. 87 893; BGR Hannover, F.R. Germany.

Tammenmaa, J., Grasty, R.L., Peltoniemi, M., 1976: The reduction of statistical noise in airborne radiometric data. Can. J. Earth Sci. 13, no. 10, 1351.

ABSTRACT

A STANDARD POTASSIUM-URANIUM-THORIUM LOGGING CALIBRATION FACILITY FOR THE PETROLEUM INDUSTRY

Dan M. Arnold
Welex-A Halliburton Company
Houston, Texas, U.S.A.

Spectral gamma ray logs have been used for a number of years to determine the potassium (K), uranium (U), and thorium (Th) content of earth formation penetrated by a borehole. These logs, which are commonly referred to as K-U-Th logs, were initially used in minerals exploration and in bed correlation studies. During the past few years, there has been an expanded usage of K-U-Th logging within the petroleum industry.

The United States Department of Energy operates several facilities which were designed to calibrate K-U-Th logging instruments. The relatively intense radioactive zones and the diameters of boreholes penetrating these zones are more representative of conditions encountered in minerals rather than petroleum exploration.

A K-U-Th logging calibration facility, specifically designed for the petroleum industry, was proposed[1] in 1980. An ad hoc committee, consisting primarily of representatives from petroleum producing and services companies, was formed in 1981 to design and solicit funds for the proposed facility. The facility will be operated under the auspices of the American Petroleum Institute (API) in a manner similar to the existing API neutron and conventional gamma ray logging calibration facilities[2]. The design of the facility has been completed, sufficient funding has been obtained, and it is anticipated that construction of the facility will begin in late 1983.

The proposed K-U-Th logging calibration facility will consist of two cylindrical pits 9.14m (30 ft) in vertical depth and 2.36m (7.75 ft) in diameter. The pits will contain alternating 1.5m (5 ft) thick layers of low activity concrete "barren" zones and concrete layers to which radioactive material has been added. Three radioactive zones will contain known amounts of thorium[3] only, uranium[3] only, and potassium only. Two additional zones will contain mixtures of thorium, uranium, and potassium with relatively low and high total activity. In addition, one pit will contain a 0.15m (0.5 ft) thick high intensity mix zone for determining bed boundary response of logging instruments. Each pit will contain 30cm (12 in), 22cm (8.5 in), and 15 cm (6 in) diameter boreholes which extend 3m (10 ft) below the lowest zone.

This paper will describe the overall configuration of the proposed calibration facility. Specific topics will include:

(a) the intensities of the radioactive zones
(b) criteria for selecting materials used in the radioactive zones
(c) materials used in the base concrete and barren zones
(d) techniques used to obtain homogeneous mixtures
(e) sampling and assaying procedures for raw materials, and for the mixes used to pour the various zones
(f) Monte Carlo transport calculations used to determine the required radial and vertical extent of each zone, and the perturbations introduced by using three boreholes within each pit.

It is felt that the proposed facility will provide an excellent standard for calibrating all K-U-Th instruments for petroleum industry applications.

---

[1] Proposed to the American Petroleum Institute: "Potassium-Uranium-Thorium Calibration Facility", Liang C. Shen, A. B. El-Kareh, R. S. Simpson, and Julie Morris, December 22, 1980.

[2] "API Calibration Facility for Nuclear Logs", William B. Belknap, John T. Dewan, C. V. Kirkpatrick, William E. Mott, A. J. Pearson, and W. R. Rabson, API National Subcommittee on Revision of PR33:" Recommended Practices for Standard Calibration and Form of Nuclear Logs", 1955.

[3] Thorium and uranium ore will be selected on the basis of secular equilibrium.

PROPOSED K-U-Th LOGGING CALIBRATION FACILITY FOR THE PETROLEUM INDUSTRY

Dan M. Arnold
Chairman: Ad Hoc API Committee
Welex, A Halliburton Company
Houston, Texas U.S.A.

I. INTRODUCTION

Spectral gamma ray logs have been used for a number of years to estimate the potassium (K), uranium (U), and thorium (Th) content of earth formations. These logs, which are commonly referred to as K-U-Th logs, were initially used in minerals exploration and in bed correlation studies.

During the past few years, the literature shows that K-U-Th logs have been used by the petroleum industry to determine other important information such as:

(1) oxidation state of the bed at time of deposition
(2) quantity of organic material in sedimentary layers which, together with item (1), leads to source bed identification
(3) depositional environment (i.e. continental versus marine)
(4) water movement in downhole formations which, in turn may indicate fractures, faulting, or permeability
(5) water movement in the borehole region which may indicate channeling or water producing perforations
(6) more accurate shale content determinations
(7) clay typing and marker bed identification

The United States Department of Energy (DOE) has constructed K-U-Th calibration pits at several sites around the country. These pits consist of several layers containing known amounts of potassium, uranium and thorium in sequence. The elemental concentrations and borehole diameters were designed specifically to represent conditions encountered in mineral exploration. In addition, there is no DOE facility within 200 miles of Houston, Texas, which is a major inconvenience for the numerous oil and service companies engaged in K-U-Th logging research and development in the Houston-Harris County, Texas area.

A K-U-Th calibration facility, specifically designed for use by the petroleum industry, was proposed in 1980.[1] It was recommended that the facility be located on the University of Houston Central Campus near the present[2] American Petroleum Institute (API) neutron-conventional gamma ray logging calibration facility.

The API Ad Hoc Committee on K-U-Th Logging Calibration was formed in 1981 to evaluate and possibly expand the scope of the original proposal. The committee consists of representatives from petroleum producing and service companies, the University of Houston, the American Petroleum Institute, and Sandia National Laboratory.

The Committee met on November 20, 1981 to propose a design for the facility. The design proposal was published[3] so that all interested parties could have the opportunity to recommend changes. Numerous suggestions were received. Many of these suggestions have been included in the facility design specifications discussed in the following sections.

II. GENERAL CONSIDERATIONS

As a primary calibration facility for natural gamma-ray spectroscopy tools used in the oil and gas well logging industry, the design and construction of the pits should be governed by the following general considerations:

(1) The radiometric grades of the various zones in the pits and the distribution of the radio-elements in each zone must be well defined. Hence, a thorough sampling and assaying program is intrinsic to the project.

(2) The size of the "hot" zones in the facility must be large enough to exclude external radioactive source material from influencing measurements in the vertical center of any zone. Based on calculations and measurements performed by various groups, zone boundaries should be two feet from the detector. Since most detectors are about one foot long, the height of the hot zones should be five feet.

(3) A zone with a mixture of K, U, and Th at above normal concentrations should be available to test the spectral identification procedures used by the various service companies.

(4) It is desirable to place low activity "barren" zones between the calibration zones to enable bed boundary effects to be assessed. This is in recognition of the differences in bed boundary effects due to the spectral differences of the three species. Barren zones should be made of the same materials as the hot zones except for the radioactive materials used to spike hot zones.

(5) It is recommended that all calibration zones be placed in two pits. The facility will be more easily used with this arrangement.

(6) Access to the facility by service company logging trucks should not be impeded by surrounding structures.

(7) Logging tools with intense neutron sources or strong eccentering devices should be excluded from routine use in this facility. However, it will be desirable to run neutron tools in the facility during the facility characterization process. A delay of several days should be enforced between the use of a neutron tool in the pit and any attempt to calibrate in the facility.

(8) The facility should be kept under water at all times to inhibit radon migration through the cement. Radon migration would especially disturb the measurement of the uranium response.

III. SPECIFICATIONS

A. Physical Geometry of the Pits

The calibration facility will require two pits. Both cylindrical and rectangular designs were considered. Each arrangement has certain advantages and disadvantages. The Committee agreed that either arrangement would be acceptable. Subsequent engineering studies indicated that the cylindrical pit concept would be less costly for the proposed facility location. The rectangular pit concept is discussed in Ref. 3.

Cylindrical Pits

(a) General Description: A sketch of the cylindrical pit concept is shown in Figure 1. The pit consists of a culvert or similar cylindrical form, 7.75' in diameter, set in low activity concrete within a bored hole, and is sealed from the surrounding earth formation. The overall depth of the pit is 30'.

Each pit will contain a series of poured layers or "zones" of "barren" cement, and layers of similar cement into which known amounts of K, U, Th, and mixes of K, U, and Th have been added. Calculations[4] show that zones 5' thick will appear essentially "infinite" in vertical extent to a 12" long gamma ray detector centered within the zone. Each zone should be constructed in a single cement pour. Sources of materials, equilibrium requirements, sampling, assaying techniques, and mixing procedures will be discussed in following Sections.

Each pit will contain three vertical boreholes with nominal diameters of 6", 8.5", and 12". Each borehole will extend below the bottom of the pit into a sealed "rat hole" 10' long and of the same diameter as the borehole. The arrangement of the boreholes is shown in Figure 1. Calculations[4] show that the response of a gamma ray detector, positioned in any of the three boreholes, will not be significantly perturbed by adjacent boreholes radial boundary effects. The boreholes should be lined with very thin cylinders (aluminum or possibly fiberglass/resin containing Al_2O_3 or other material to minimize abrasive wear). These liners will permit the borehole fluid to be changed without contaminating the cement zones. It is felt that very thin liners can be pressure balanced by filling the liners with fluids of density similar to that of cement during the successive zone pores. Some flexibility in the specified borehole diameters can be tolerated in order to use standard O.D. liner material.

(b) Concentrations of Radioactivity: Pit #1 will contain three radioactive zones separated by three barren zones as shown in Figure 2. The upper radioactive zone will be 5' thick and contain ~25ppm uranium in secular equilibrium (Ueg). The middle radioactive zone will be 5' thick and contain ~90ppm Th in secular equilibrium. The lower radioactive zone will be 6" thick and contain a mixture of 5% K, 10ppm Ueq, and 30ppm Th in secular equilibrium

Pit #2 will also contain three radioactive zones separated by three barren zones (see Fig. 3). The upper radioactive zone will be 5' thick and contain 5% K. The middle radioactive zone will be 5' thick and contain a mixture of 1% K, 1 to 2ppm Ueq, and 3-5ppm Th. The lower radioactive zone will be 5' thick and contain a mixture identical to the lower radioactive zone in Pit #1.

(c) Selection of Elemental Concentrations: The concentrations of K, U, and Th will be sufficient to produce "clean" gamma ray spectra with negligible percent contributions from any radioactive materials in the cement carrier. This is extremely important in determining (a) the "stripping" constants and (b) the factors for converting "stripped" count rates to elemental concentrations. Conversely, the radiation intensities within the K, U, and Th zones are sufficiently low so that detector dead time corrections are negligible.

The "hot" and "low" mix zones contain relative and absolute concentrations representative of "hot" shales (~200 API gamma units) and shaly sands (25-40 API gamma units), respectively. The barren zones, which will be assayed, can be used to represent "clean" formations.

The sequence of hot and barren zones can be used to determine bed boundary response of K-U-Th tools. Bed boundary response is a function of gamma ray energy and thus a function of the relative concentrations of K, U, and Th.

The 6" bed of hot mix can be used to establish the response of the tool to thin beds.

B. Overhead Crane Facilities

The overhead crane required to raise and lower logging tools into the pits must meet the following criteria:

(1) It will be necessary to position a logging cable sheave wheel directly above each borehole in each pit.

(2) The crane should be such that a 35' long logging tool can be raised and lowered in each borehole.

(3) The load capacity of the crane should be (a) two tons if only logging tools are used in the borehole or (b) six tons if casing* is to be run in and out of the boreholes.

IV. SOURCE MATERIAL, SAMPLING, AND ASSAYING

In selecting materials to be used in constructing the zones, the following basic criteria should be followed:

(a) The base cement mix, from which all zones are constructed, should be formulated with materials containing very low natural gamma ray activity. Particular care should be taken in selecting the sand.

(b) It is necessary that the sources of thorium and uranium be in or near secular equilibrium.

(c) The compound used as a source of potassium must not be water soluble. This eliminates otherwise attractive compounds such as KCI and K_2SO_4.

A. Source Materials

The following have been suggested as possible source materials:

Uranium:	(1)	Near equilibrated ore - Climax (Colorado)
	(2)	Near equilibrated ore - Ambrosia Lake (New Mexico)
	(3)	Near equilibrated ore - Canon City (Colorado)

---

* Calculations made assuming 35' section of 11-3/4", 60 lb/ft J-55 casing filled with 16 lb/gal mud.

(4) Non-equilibrated ore - Any source (must be completely characterized with respect to uranium and daughter products)

Potassium:
(1) Feldspar - Canon City (Colorado)
(2) Feldspar - Grand Junction (Colorado)
(3) $K_2S_2O_8$
(4) Musgovite - $H_2KAl_3(SiO_4)_3$

Thorium:
(1) Monazite Sand - California
(2) Near equilibrated ore - Canon City (Colorado)

Barren:
(1) Sand**, Wash Frac, 10-20 Mesh and 40 Mesh (Texas Mining Co.)
(2) Cement, White Portland

B. Mixing and Pouring

1. The materials should be dry mixed for eight hours and wet mixed for two hours.
2. Each zone should be constructed from a single pour of 9 yd^3 of cement. The "hot" mix zone (0.5 ft. thick) in Pit #1 and the "hot" mix zone (4.5 ft. thick) in Pit #2 can be constructed from a single pour.
3. Each zone should be allowed to set before the next zone is poured.

C. Sampling and Assaying

1. Grab samples to be taken during dry mixing.
   - 3 samples from different parts of mixer
   - Standard size and weight
   - Count on laboratory Ge(Li) detector to 1% statistics in selected peaks
   - Samples to be within $\pm\sigma$ before adding H_2O
   - Samples every hour until true
2. Samples of Mix During Pour
   - 20 samples ~ ½ liter
   - Allow to set up in closed container
   - Split samples - assay half, archive half
   - Pulverizer and dry-place in closed can for 30 days for radon in-growth
   - Assay redimetrically on well calibrated Ge(Li) or NaI detector
3. Uniformity
   - Less than $\pm 1\sigma$ variation between adjacent intervals
   - Less than $\pm 2\sigma$ variation in all cores and cartons
4. Assaying
   - Pulverized material from each split assayed by two laboratories, minimum. Same method to be employed by each laboratory.
   - Final value for split is average
   - Value for zone is grand average

Arrangements are being made to assay the sample during the mixing and after the pours are completed.

A K-U-Th calibration facility has recently been constructed[5] by Welex in Houston, Texas, using methods similar to those proposed for the API facility. Thorium ore[6], Uranium ore[7], and $K_2S_2O_8$ were used as sources of Th, U, and K, respectively. It was found that these sources met the purity, secular equilibrium, and solubility criteria specified for the API facility. The mixing procedures, again similar to those proposed for the API facility, produced very homogeneous zones. Radiometric scans of the boreholes showed variations in activity of ± 1.5% or less for any given zone.

V. FUNDING AND OPERATION OF THE FACILITY

Based upon the Engineering Design Package, it is estimated that the facility will cost approximately $200,000. This includes the two calibration pits, a small laboratory building, overhead crane facilities, a concrete pad for logging trucks or other heavy equipment, and various other miscellaneous items necessary to complete the facility.

**See Table I

The API has $41,500 in funds allocated for the project. The industry was solicited for the remaining funds necessary to construct the facility. Contributions were solicited on an "equal share" basis, with each organization specifying a maximum contribution. To date, twenty organizations have specified maximum contributions of $168,100, giving a total of $209,600.00 available for the project.

The facility, when completed, will be operated by the University of Houston under the auspices of the American Petroleum Institute. The facility will be open to the public on a daily fee basis. The general terms of the operating agreement[2] will be similar to those used for the existing API neutron and conventional gamma ray calibration facility.

VI. STATUS

The Facilities Planning and Construction Department of the University of Houston is in the process of obtaining construction bids for the project. Once bids have been received, the Committee, the University of Houston, and the American Petroleum Institute will select a contractor.

It is hoped that construction of the facility will begin during the fourth quarter of 1983.

REFERENCES

[1] Proposal to Mr. C.O. Liles, American Petroleum Institute: "Potassium Uranium-Thorium Calibration Facility", Liang C, Shen, A.B. El-Kareh, R.S. Simpson, Julie Norris (University of Houston), December 22, 1980.

[2] "API Calibration Facility for Nuclear Logs," William B. Belknap, John T. Dewan, C.V. Kirkpatrick, William E. Mott, A.J. Pearson, and W.R. Rabson, API National Subcommittee on Revision of RP33: "Recommended Practice for Standard Calibration and Form of Nuclear Logs," 1955.

[3] "API Ad Hoc Committee on K-U-Th Logging Calibration/Recommended Calibration Facility Design," Dan M. Arnold, Chairman, The Log Analyst, Vol. XXIII, No. 2 (March-April), pp. 60-64.

[4] Computer Code SAM-CE, Radiation Shielding Information Center, Oak Ridge National Laboratory, Oak Ridge, Tennessee, U.S.A.

[5] "A Multi-Function Compensated Spectral Natural Gamma Ray Logging System," H.D. Smith, Jr., C.A. Robbins, D.M. Arnold, L.L. Gadeken, and J.G. Deaton, Society of Petroleum Engineers 58th Annual Conference and Exhibition, San Fransisco, CA, October 5-8, 1983, Paper SPE 12050.

[6] Supplier: Mr. Harold Schwartz, 2070 Cedar Avenue, Canon City, Colorado 81212, U.S.A.

[7] Supplier: Cotter Corporation, 502 Fremont County Road, Canon City, Colorado 81212, U.S.A.

TABLE I

Wash Frac Sand

CHEMICAL ANALYSIS (TEXAS MINING COMPANY)
Test Method: ASTM D-2576 - Atomic Absorption Spectrophotometry
Material: Sand

		Elements Found, %							
SIZE	SAMPLE	S_1O_2	Al_2O_3	Fe_2O_3	MgO	CaO	Na_2O	K_2O	T_1O_2
10-20	1	99.12	0.42	0.05	<0.01	0.01	<0.01	0.26	0.01
10-20	2	99.52	0.18	0.09	<0.01	0.02	<0.01	0.10	0.01
10-20	3	99.46	0.22	0.05	<0.01	0.01	<0.01	0.13	0.01
20-40	4	99.60	0.16	0.04	<0.01	0.01	<0.01	0.09	0.01
20-40	5	99.60	0.17	0.05	<0.01	0.01	<0.01	0.10	0.01
20-40	6	99.47	0.23	0.04	<0.01	0.01	<0.01	0.14	0.01
16-100	Ottawa	99.90	0.04	0.02	<0.01	0.01	<0.01	<0.01	<0.01

	Loss on Ignition Test, %					
SAMPLE	TMC 10-20	TMC 20-40	CO_2	OTTAWA 20-30	OTTAWA 16-100	CO_2
1	0.13%	0.09	<0.01	0.03%	0.02%	<0.01
2	0.08%	0.06	<0.01			
3	0.12%	0.10	<0.10			

Fig. 1

CYLINDRICAL PITS
BOREHOLE GEOMETRY

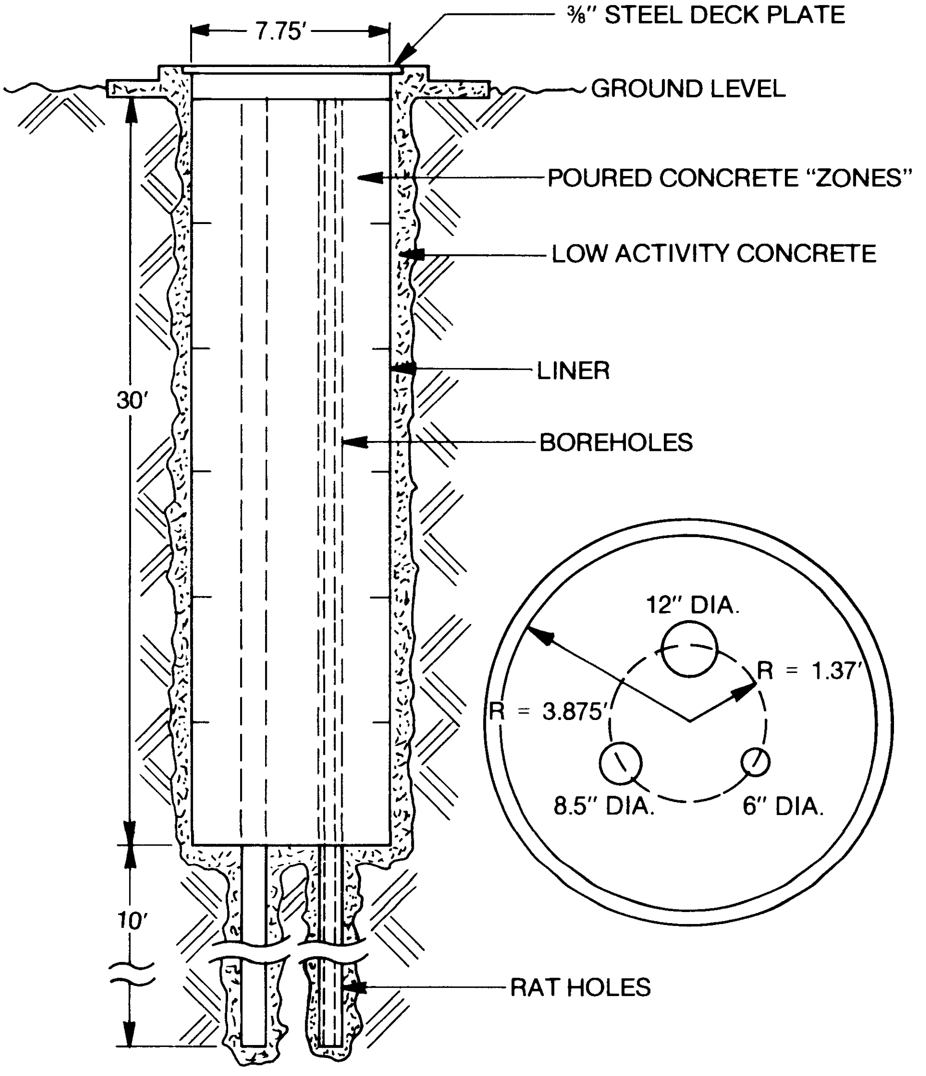

Fig. 2

PIT # 1
ZONE GEOMETRY

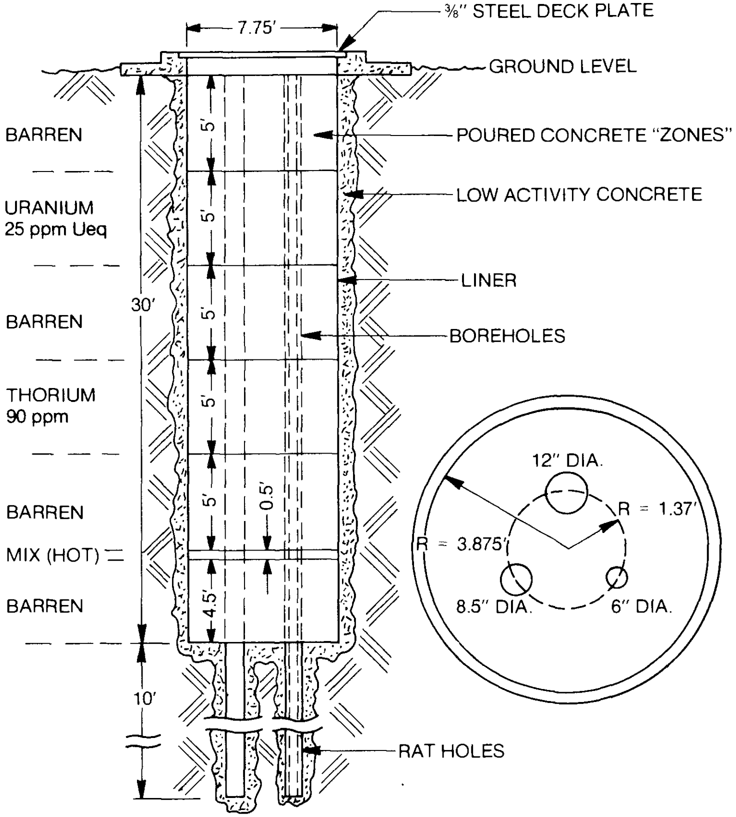

HIGH INTENSITY "HOT" MIX: K = 5%, Ueq = 10 ppm, Th = 30 ppm

Fig. 3

PIT # 2
ZONE GEOMETRY

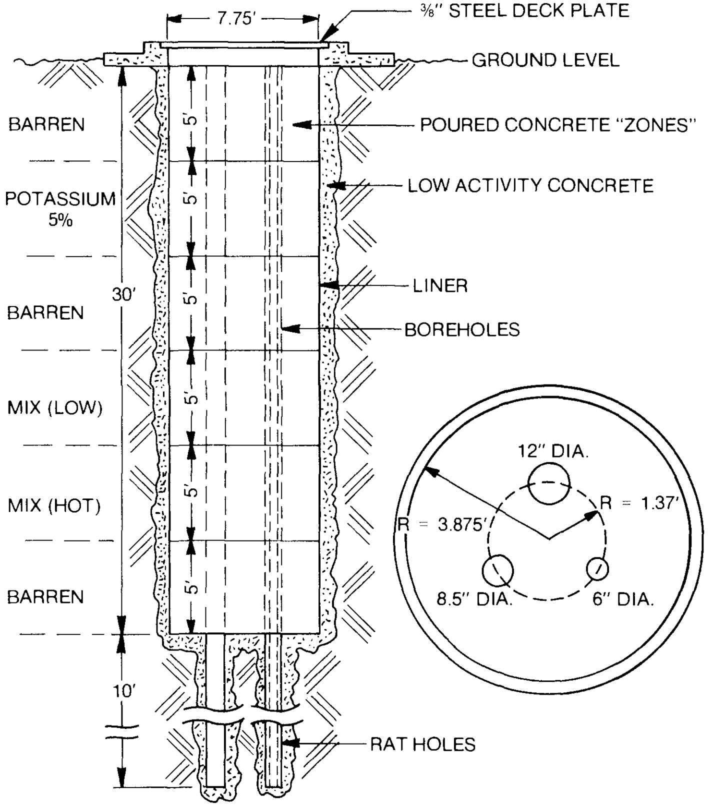

HIGH INTENSITY "HOT" MIX: K = 5%, Ueq = 10 ppm, Th = 30 ppm

LOW INTENSITY "LOW" MIX: K = 1%, Ueq = 1-2 ppm, Th = 3-5 ppm

DETERMINATION OF THE K_2O CONTENT OF MANGANESE ORE BY NATURAL GAMMA-RAY LOGGING

J.A. Aylmer, C. Ceravolo, J. Charbucinski,
P.L. Eisler and S.F. Youl

ABSTRACT

Laboratory static tests on manganese ore, with K_2O content between 0.34 and 3.50 weight percent, were carried out on eight large (200 dm^3) samples to prove the feasibility of a natural gamma technique for determining % K_2O in the ore. The results indicated that K_2O content could be determined with an accuracy (1 σ) of ±0.14% K_2O, based on a net peak area method.

Subsequent tests were carried out at the mine of the Groote Eylandt Mining Company. Using the dynamic logging technique, the results obtained for seventy 0.5 m borehole sections give an accuracy (1 σ) of ±0.16% K_2O. The data analysis was based on total counts from two independent spectral variables.

The results also indicated that, for a heterogeneous ore body, dynamic rather than static logging is the preferred technique for spectral determination of K_2O content.

1. INTRODUCTION

In manganese ores, one of the geochemically significant minerals is cryptomelane ($K_{0.6-0.8}Mn_8O_{16}$), which is of relatively high potassium content. The Groote Eylandt Mining Company Ltd. considered it would be useful to include a borehole logging technique applicable to manganese deposits, which would determine the content of this mineral in the ore. The research for developing this method was undertaken at the Port Melbourne laboratory of the CSIRO Division of Mineral Physics.

The basis for determining cryptomelane was that there are only minor occurrences of potassium-bearing clays and feldspars in the ore. Consequently, there is a strong correlation between the potassium (as % K_2O) and the cryptomelane concentrations [1], so that a technique which measures potassium content would be suitable in this application.

The only method which appeared feasible entailed measuring the count-rate of the 1.46 MeV gamma rays emitted via the beta decay of the naturally occurring radioisotope ^{40}K. This isotope has an effective half-life of 1.28×10^9 y, and a natural abundance of about 0.0118% [2]. The gamma rays are emitted via the electron capture reaction:

$$^{40}K + e^- \rightarrow {}^{40}Ar + \nu + \gamma$$

The first phase of the investigation involved measurements at the CSIRO Port Melbourne laboratories on samples supplied by the Company. The aim of this phase was to establish a range of operating conditions for an appropriate natural gamma-ray technique and to determine the accuracy under laboratory conditions. The second phase was to undertake a field trial at the Company's mine.

2. STATIC LABORATORY INVESTIGATION

2.1 SAMPLES

The potassium content of the eight bulk ore samples supplied for testing (Table 1), varied between 0.34 and 3.50% K_2O by weight on a dry basis. The ore had been crushed prior to delivery and prepared in the laboratory to provide homogeneous samples of average volume, 200 dm^3.

2.2 EXPERIMENTAL

The probe, the sample geometry and the electronic instrumentation used for the measurements are shown schematically in Fig. 1. A 51 × 51 mm NaI(Tl) scintillation crystal was used to detect the gamma rays emitted from the surrounding ore matrix. The analog signals from the detector were processed by a Nuclear Data 4096 channel multi-channel analyser (MCA) for preset counting times of 200 s. At the end of each accumulation phase of the MCA, the spectra were transferred to a DEC PDP8/e minicomputer and stored on magnetic tape for subsequent analysis. A spectral window was preset by software between 1.35 and 1.55 MeV to measure the count-rate of the 1.46 MeV gamma rays emitted by ^{40}K. The total count-rate in the window and the net peak area count-rate due to the 1.46 MeV gamma rays in the specified window were calculated using programs available on the minicomputer.

2.3 RESULTS AND DISCUSSION

The total count-rate in the preset spectral window and the count-rate in the peak above the continuum were both regressed against K_2O

concentration. Cross plots of each of these parameters versus K_2O concentration are shown in Figs. 2 and 3 together with the lines of best fit.

Clearly, the count-rate corresponding to the net peak area is better correlated with the K_2O concentration than the total count-rate in the window. The regression analysis gave an accuracy (1 σ) of 0.14% K_2O for the net peak area method compared with an accuracy of 0.38% K_2O for the total count-rate method. The total count-rate method gave a particularly large residual for one sample which contributed significantly to the large standard deviation obtained with this method.

The occurrence of this large residual can be explained by the variable concentration of other minerals which bear naturally occurring radioisotopes. For example, kaolinitic clay, which has a strong affinity for uranium, thorium and their daughter products, is a significant mineral contaminant of this type. The principle gamma rays emitted by these radionuclides at energies above 1.46 MeV are at 1.60, 1.76, 2.1 and 2.6 MeV. Because the gamma-ray spectra of these photons include a Compton continuum at energies below their respective peak energies, the counts recorded in the 1.35 to 1.55 MeV window will include not only the 1.46 MeV full absorption peak, but also the Compton continua of the gamma rays of higher energy.

3. FIELD TRAILS

3.1 INTRODUCTION

Having established that natural gamma-ray spectrometry provided quantitative values for K_2O in manganese ore under static conditions, a field trial was undertaken at the mine of the Groote Eylandt Mining Company.

To establish the reliability of the method, seven holes of 150 mm diameter, from various representative regions of the mine, were logged by dynamic (continuous) logging. Two of these holes were also logged in the static mode to provide a comparison with the dynamic procedure with respect to both accuracy and the convenience of operation. Data were obtained only for the ore above the water table because the walls of the holes below it were unstable.

Tests were conducted to provide the following information:

(a) The suitability of natural gamma-ray logging for in situ determination of K_2O in manganese ores under field conditions;

(b) The relative merits of static and dynamic logging;

(c) The accuracy of the method using total mine data.

3.2 THE LOGGING PROCEDURES

3.2.1 Instrumentation

a. The Probe

The probe and the uphole instrumentation are shown schematically in Fig. 4. The probe was essentially the same as that used in the static laboratory tests. However, a nose cone fabricated from high density polyethylene was used to protect the end of the probe. Also, a 10 cm lead spacer between the nose cone and the detector was included to provide additional weight which assisted in giving smooth movement of the probe in the borehole.

b. Electronics and Data Processing

The electronics in the probe comprised voltage supplies and a preamplifier which drove 300 m of standard 4-core armoured cable connected with the instrumentation of the Ford F100 logging truck. The relevant electronics in the logging truck consisted of a Canberra 2010 spectroscopy amplifier and a Canberra (Series 30) 1024 channel pulse height analyser (MCA). The MCA was interfaced with a Rockwell AIM65 microcomputer which processed the data transferred from the MCA and provided hard copy output via a printer. The MCA was operated in the "region of interest" mode and thus provided aggregate counts in preset windows and livetime as input parameters for the microprocessor to convert this data into count-rates. For dynamic logging the acquisition/output cycle of the MCA was controlled by a depth-marker generator producing a pulse for each 0.5 m travel of the probe. For static logging, the MCA was operated in a fixed live-time mode.

Spectrum stabilisation was not used in either dynamic or static logging; the response of the 1.46 MeV reference peak in those strata containing relatively low concentrations of K_2O was too weak for effective tracking.

c. Operational Considerations

The zero reference point for logging was the top of the casing in the mouth of the borehole. For the dynamic mode, the logging speed ranged from 0.5 to 0.7 m min^{-1} and the integration time for each 0.5 m split hence varied from 40 to 60 seconds. To ensure uniform movement of the probe, data were collected with the probe moving up the hole. For static logging, the accumulation time was 300 seconds, with the detector positioned at the mid-point of each selected 0.5 m split.

3.3 EXPERIMENTAL DETAILS

a. Spectral Considerations

The static laboratory tests showed that a single variable (the net counts in the peak centred at 1.46 MeV) provided a quantitative measure of the K_2O content. Because the MCA was operated in "region of interest" mode in the field, the net peak area of the 1.46 MeV ^{40}K peak was estimated by setting narrow windows on either side of the total peak window and using these to estimate the background under the peak.

As in the laboratory tests, the gross counts in the ^{40}K total peak window was considered in the analysis. This window includes counts due to the Compton continuum from uranium, thorium and their daughter products (see Section 2.3). In fact, past experience indicted that, for quantitative radiometric analysis of ores, it was necessary to measure all naturally emitted photons of energy above 0.4 MeV [3]. Because the higher energy gamma rays contribute independently to the count-rate in the 1.46 MeV window, the count-rates in windows preset at the higher energies are independent variables in the regression analysis.

For the measurements described in the present paper, five spectral windows were preset to detect gamma rays emitted at 2.62, 2.2, 1.76, 1.46 and 0.6 MeV. The 0.6 MeV window was included in the model because the prominent peak at this energy is actually a Th plus U double peak. Further details concerning these windows are given in Table 2.

b. Theoretical Considerations

In the dynamic logging method, two passes were made in each borehole, both to increase the counting statics for each data point used in the regression analysis and to monitor the correct operation of the instrumentation.

The regression model used for the relationship between the chemical assays and the spectral response variables was represented by the following generalised equation:

$$C = a_0 + a_1X_1 + a_2X_2 + \ldots + a_nX_n$$

where C = the concentration of potassium

$X_1, X_2, \ldots X_n$ = spectral response variables

$a_0, a_1, \ldots a_n$ = regression coefficients

All accuracies quoted are the r.m.s. deviations obtained by regression analysis, between prediction of potassium content by radiometric logging and chemical analysis in 0.5 m strata.

c. Holes used for Logging

Seven holes from three mine areas representing the total mine were included in the dynamic logging programme. To ensure reliability of the regression model, data were only included if at least 20% of drill cuttings was recovered from the split. As a result, 70 data points (0.5 m splits) with a K_2O content varying between 0.18% and 2.34% were available for analysis. Two of these holes were also logged in the static mode, providing 22 data points with a K_2O content varying between 0.33% and 2.34%.

3.4 RESULTS AND DISCUSSION

3.4.1 Dynamic Natural Gamma-Ray Logging

Table 3 shows the correlation structure for the regression model considered. Regression analysis showed that an accuracy of 0.16% K_2O was obtained using 70 data points which represented the mine. The mean potassium content in these 0.5 m strata was 0.67% K_2O. The two independent variables of statistical significance were the total count-rates in the 1.46 and the 2.62 MeV windows. Fig. 5 shows a cross plot of the predicted values of % K_2O against the chemical analyses. The addition of further variables to the regression equation gave no improvement in accuracy. Use of the total count-rate in the 1.46 MeV window as the only independent variable, gave a lesser accuracy of 0.19% K_2O.

Although the most significant variable in the laboratory trials was the net peak area count-rate for the 1.46 MeV gamma rays, an analysis of the data obtained during the field trials showed that this variable was not as significant as that based on the total count-rate in that window. When used alone, the net peak area count-rate gave an accuracy of 0.24% K_2O. This diminished accuracy is probably due to the inadequate counting statistics, obtained in 0.5 m split measurements, for suitably accurate estimation of net peak areas.

3.4.2 Static Gamma-Ray Logging

Two holes were logged in both static and dynamic mode, providing a comparison between the two methods based on 22 data points with a mean K_2O content of 0.94%. Using the two independent variable model from the previous section, both static and dynamic techniques gave an accuracy of 0.18% K_2O.

In general, the static technique would be expected to provide higher accuracy due to longer counting times and hence, better counting statistics. However, since the probe was positioned at the mid-point of each 0.5 m split, its response may not have adequately represented the split K_2O content, due to the heterogeneity of the ore. We had avoided this problem in the laboratory trial by using relatively homogeneous samples of crushed ore.

4. CONCLUSIONS

The static laboratory trials of the natural gamma-ray logging method demonstrated the feasibility of the technique for determining potassium content of maganese ores. Use of the net peak area count-rate for 1.46 MeV gamma rays as the only independent variable for regression analysis, permitted determination of the potassium content with an accuracy of 0.14% K_2O in the bulk samples of mean potassium concentration 1.29% K_2O.

When the technique was applied to dynamic logging in boreholes which were representative of the mine, an accuracy of 0.16% K_2O was obtained for individual 0.5 m strata with a mean potassium content of 0.67% K_2O.

A comparison of the accuracies obtained by static and dynamic logging to determine K_2O contents in 0.5 m splits, showed no statistically significant difference for the two test holes selected. This, together with both the heterogeneity of the Groote Eylandt ore and operational considerations, indicates that dynamic (continuous) logging is the more suitable technique for in situ determinations of K_2O content.

Because impurities in the Groote Eylandt manganese ore do not include alkali fedlspars, micas or other potassium bearing clays, dynamic natural gamma-ray logging for potassium gives an estimate of the cryptomelane content of the ore.

5. ACKNOWLEDGEMENTS

The authors wish to thank the Groote Eylandt Mining Company for supporting this work and for permission to publish this paper.

REFERENCES

1. Frazer, F.W. and Belcher, C.B. Mineralogical Studies of the Groote Eylandt Manganese Ore Deposit; Proc. Aust. I.M.M., No. 254, June 1975, pp 29-36.
2. Lederer, C.M. and Shirley, V.S. Table of Isotopes; 7th Edition (1978). John Wiley and Sons, New York.
3. Aylmer, J.A., Eisler, P.L., Mathew, P.J. and Wylie, A.W., The use of Natural Gamma Radiation for Estimating the Iron Content of Sedimentary Iron Formations Containing Shale Bands; in "Nuclear Techniques in Geochemistry and Geophysics", Proc. of IAEA panel, Vienna, 24-29 Nov., 1974 (IAEA 1976) pp 53-57.

Table 1. Drum samples provided for laboratory testing.

Drum	Rock type	% K_2O
1	Cemented mangan pisolite	1.45
2	Loose mangan pisolite	0.35
3	Lateritic mangite	1.40
4	Minor lateritic siliceous mangite and laterite	0.34
5	Loose mangan oolite	0.66
6	Loose mangan pisolite	0.83
7	Siliceous mangite	1.76
8	Massive mangite	3.50

Table 2. Spectral windows.

Radio element	Th & U	K	Th & U	Th & U	Th
Peak position (MeV)	0.6	1.46	1.76	2.1	2.62
Window width (keV)	60	110	102	330	230

Table 3. Correlations between the regression variables.

0.6 total	1.00						
1.46 total	0.76	1.00					
1.46 net	0.51	0.86	1.00				
1.76 total	0.91	0.61	0.38	1.00			
2.1 total	0.86	0.45	0.23	0.86	1.00		
2.62 total	0.79	0.40	0.20	0.86	0.90	1.00	
% K_2O	0.53	0.88	0.77	0.40	0.22	0.13	1.00
	0.6 total	1.46 total	1.46 net	1.76 total	2.1 total	2.62 total	% K_2O

FIGURE CAPTIONS

Fig. 1. Schematic of instrumentation used for static testing of Groote Eylandt samples.

Fig. 2. Prediction of K_2O in Groote Eylandt samples using the total counts under the 1.46 MeV ^{40}K natural gamma ray peak.

Fig. 3. Prediction of K_2O in Groote Eylandt samples using the net counts under the 1.46 MeV ^{40}K natural gamma ray peak.

Fig. 4. Schematic of instrumentation used for natural gamma-ray logging at Groote Eylandt.

Fig. 5. Comparison of nuclear and chemical determinations for % K_2O.

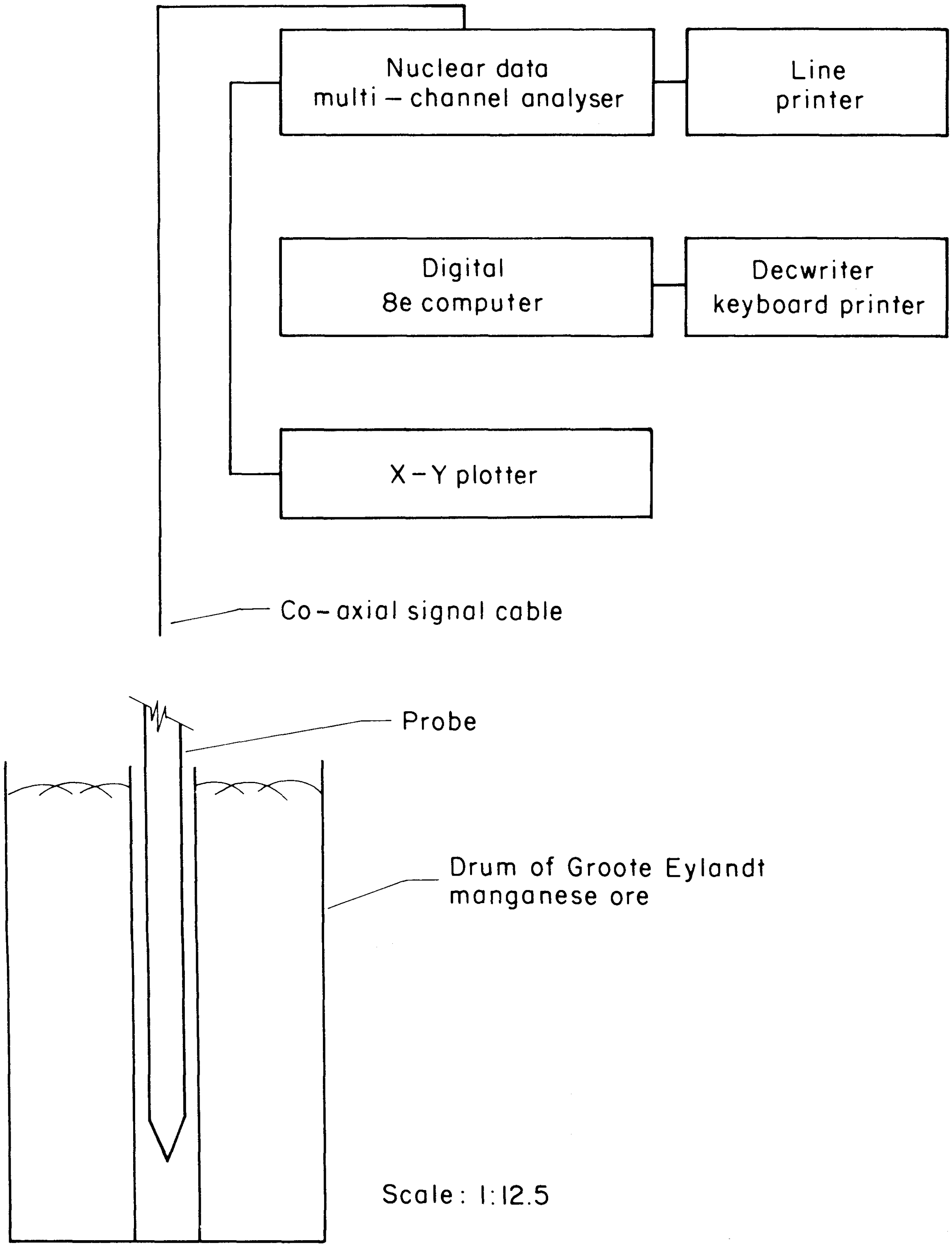
Nuclear data multi – channel analyser
Line printer
Digital 8e computer
Decwriter keyboard printer
X – Y plotter
Co – axial signal cable
Probe
Drum of Groote Eylandt manganese ore
Scale: 1:12.5

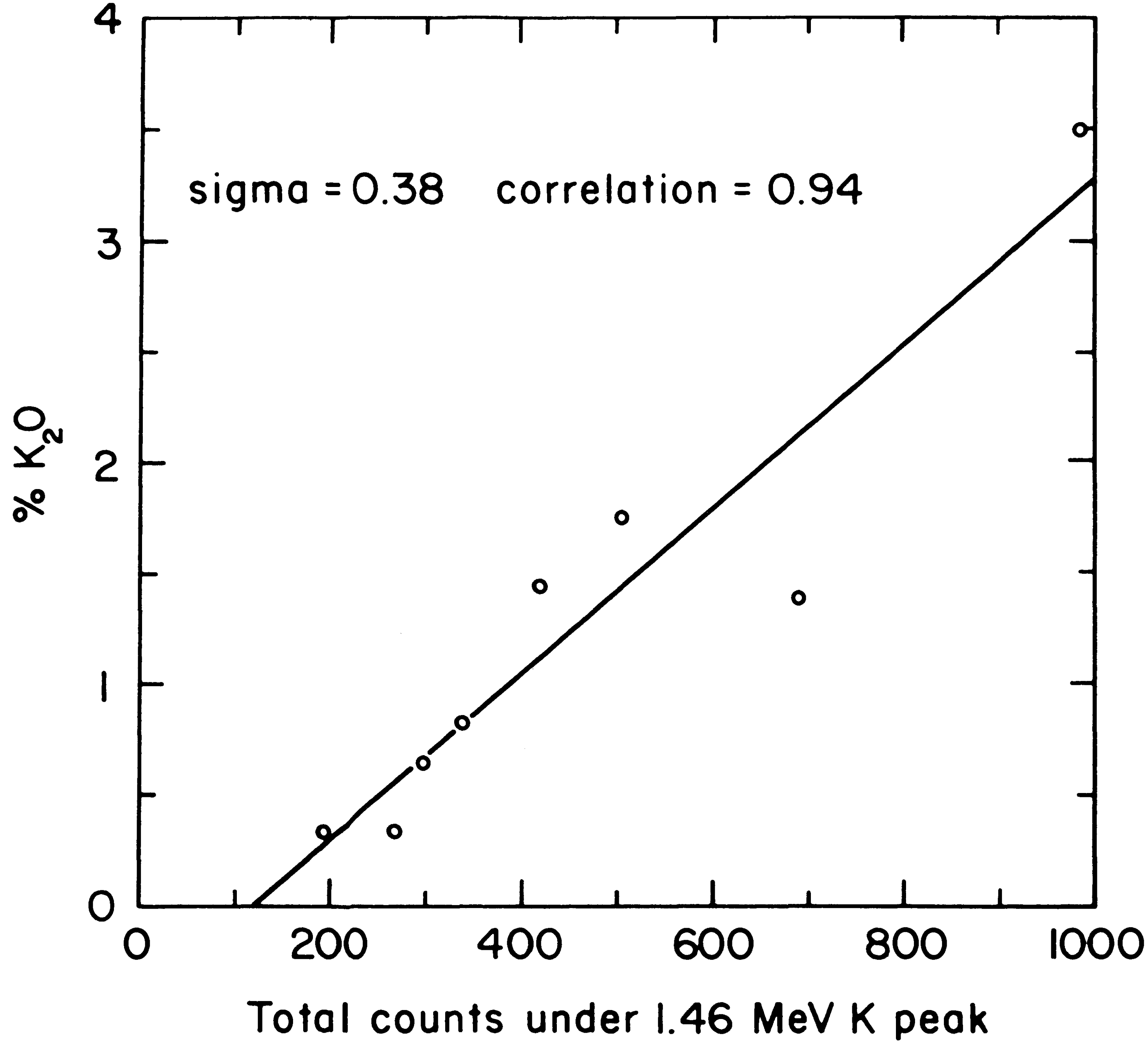
sigma = 0.38 correlation = 0.94
% K_2O
4
3
2
1
0
0
200
400
600
800
1000
Total counts under 1.46 MeV K peak

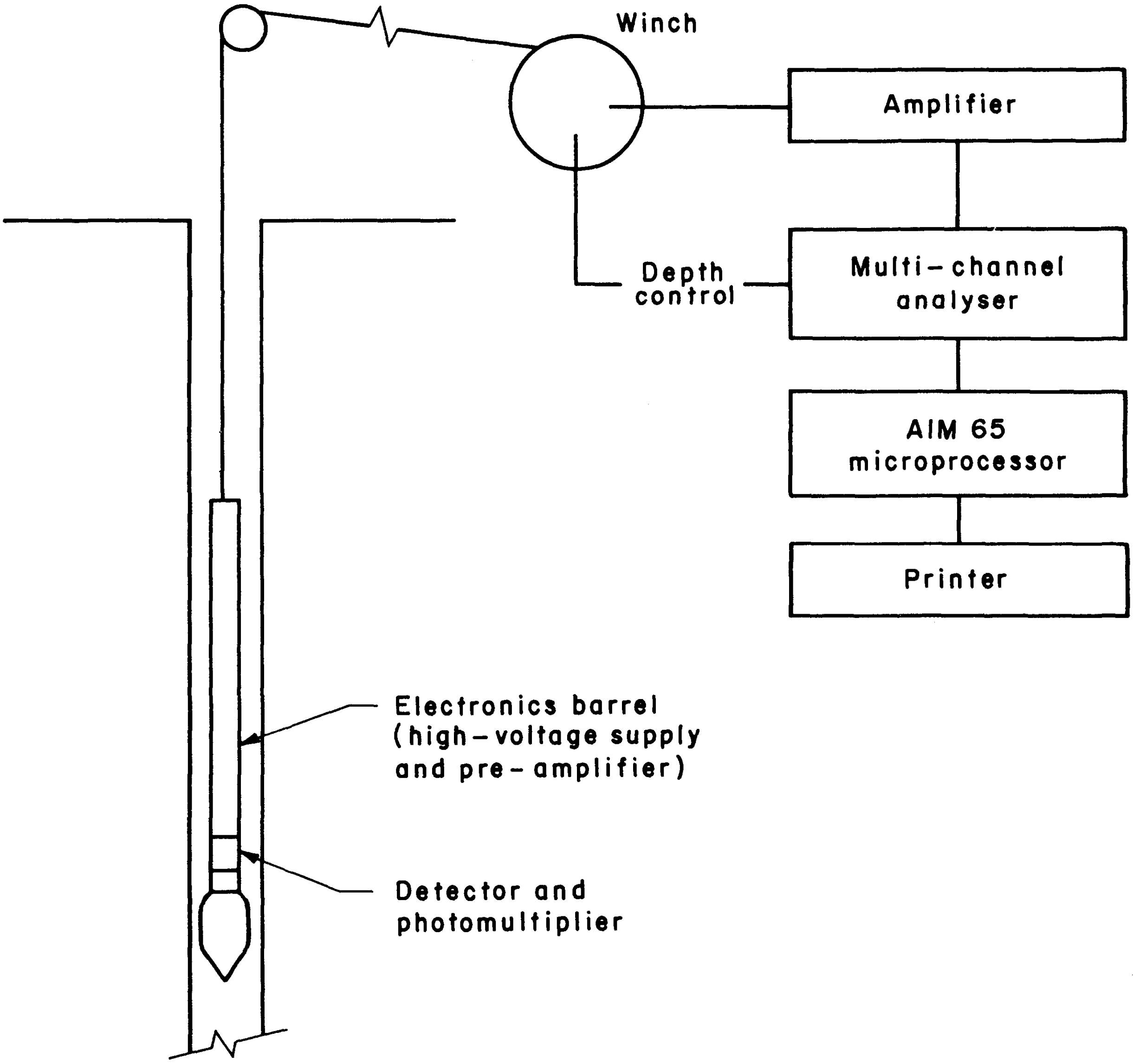
Winch
Amplifier
Multi-channel analyser
Depth control
AIM 65 microprocessor
Printer
Electronics barrel (high-voltage supply and pre-amplifier)
Detector and photomultiplier

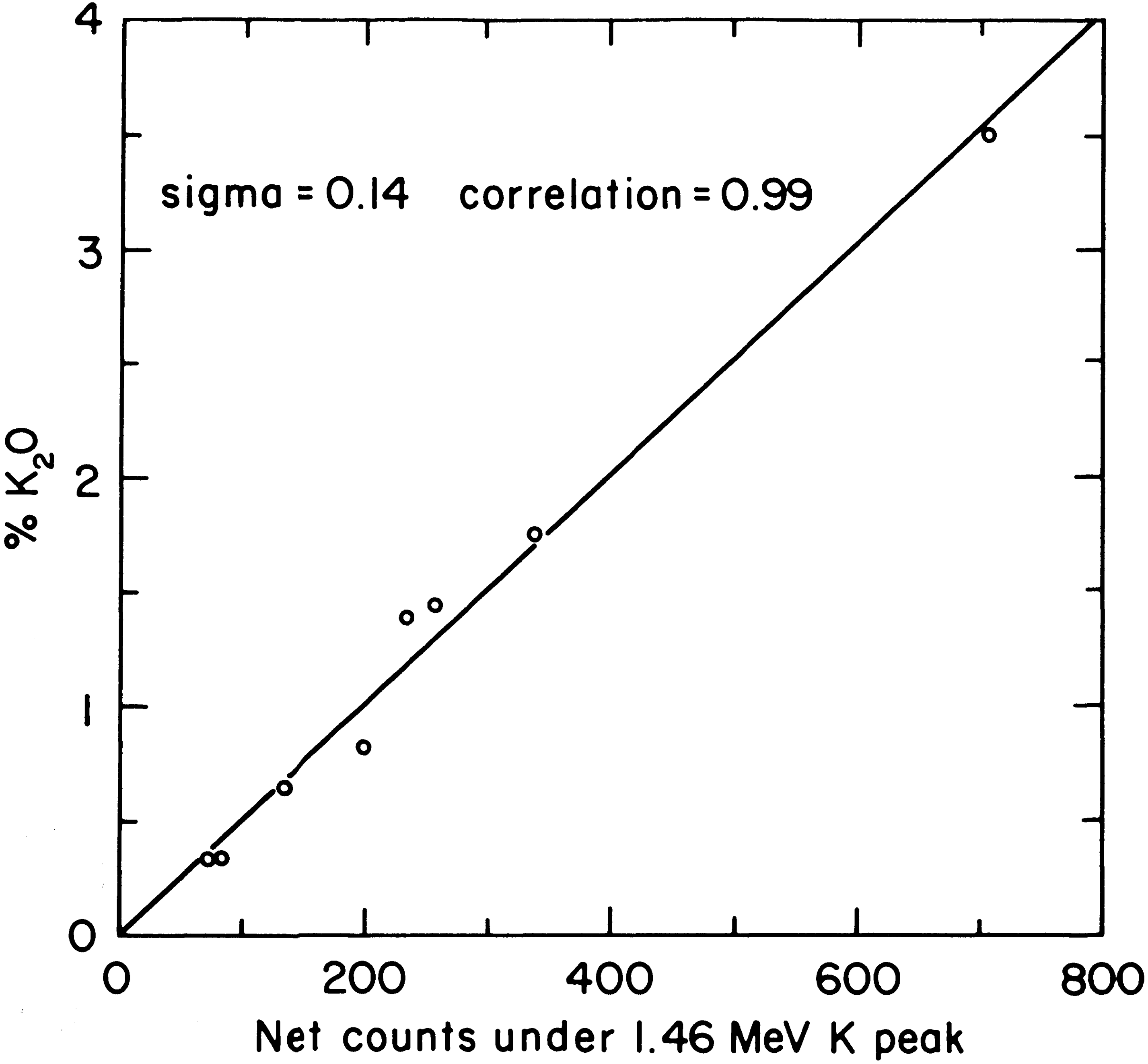
sigma = 0.14 correlation = 0.99
% K_2O
0
1
2
3
4
0
200
400
600
800
Net counts under 1.46 MeV K peak

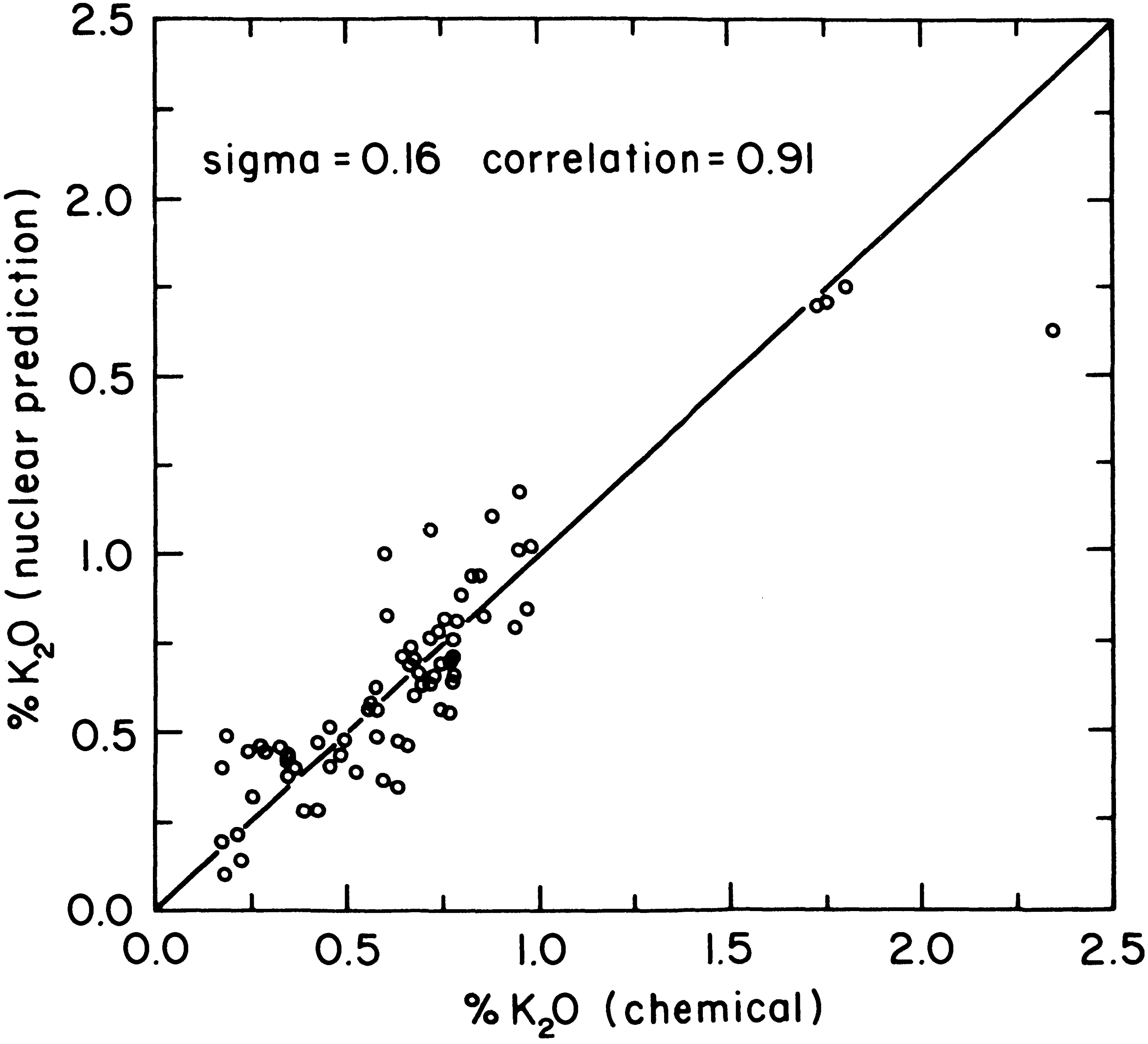
sigma = 0.16 correlation = 0.91
% K$_2$O (nuclear prediction)
% K$_2$O (chemical)
0.0
0.5
1.0
1.5
2.0
2.5
0.0
0.5
1.0
0.5
2.0
2.5

A SIMPLE AND RAPID METHOD OF DETERMINING THE THERMAL NEUTRON ABSORPTION CROSS SECTION OF ROCKS

A. Dydejczyk, J. Gyurcsak and A. Kreft

Institute of Physics and Nuclear Techniques, University of
Mining and Metallurgy, Mickiewicza 30, 30-059 Kraków, Poland

Abstract

A new method of determining the macroscopic thermal neutron absorption cross section of rock samples is described. Due to simplicity and rapidity it is suitable for routine application. The method uses samples of volume of about 1400 cm^3 and a measuring set-up consisting of moderating block, Pu-Be neutron source emitting roughly 5×10^5 n/s, BF_3 proportional counter and ordinary counting equipment. The method has been tested with a set of artificial rock samples. 95% confidence intervals of about 0.27 m^{-1} has been estimated for 2 x 300 s counting times. Results of measurements for several natural rock samples agree with those obtained by pulsed neutron technique.

INTRODUCTION

It is well known that the thermal neutron absorption cross section (Σ_a) of rocks influences various neutron logs [1,2,3]. If it is known, appropriate corrections can be introduced to the interpretation algorithms. Evaluations of Σ_a based on the routine chemical analysis are always more or less underestimated (due to the significant contribution of boron and rare earths to the value of Σ_a whereas these elements are usually omitted in this type of analysis). Therefore, a demand for experimental determining the Σ_a of rocks is announced by log analysts.

Most of methods applied so far to measuring the absorption cross section of rock samples require the use of pulsed neutron generator and other expensive equipment [3,4,5]. Less attention has been paid in the literature to the use of much simpler steady-state methods. The aim of this paper is to show that the steady-state technique can be competitive in respect of rapidity, precision and cost.

DERIVATION OF THE METHOD

Fig.1 shows an experimental arrangement used for determining the concentration of boric acid in water solution [6]. It consists of water-filled steel drum, neutron source emitting 5×10^5 n/s, BF_3 proportional counter and sample container. The sample volume is 2350 cm^3. The source-detector-sample geometry is rigidly defined. Fig.2 shows the results of measurements carried out with the use of this experimental arrangement. Σ_a values attributed to the boric acid concentration are calculated according to the composition and density of the solution. This calibration curve can be used for determining the Σ_a of brines. For Σ_a up to 50 c.u. (1 c.u. = 0.1 m^{-1}) the relative standard deviation below 1 % can be achieved. Thus in the case of brines this simple experimental set-up offers better precision than method using the pulsed neutron technique [3].

Arrangements similar to that shown in Fig.1 can also be used for determining the absorption cross-section of rock samples. However, in this case a serious disadvantage of the method becomes evident. Namely, the detector counting rate depends not only on the Σ_a but also on the scattering and moderating properties of the sample. Therefore, the measuring device of this type requires a seperate calibration practically for each sample to be run. The calibration standards should differ as little as possible from the measured sample excluding Σ_a value. In particular ,they should contain the same amount of hydrogen as an unknown sample. Recently, Tittle and Crawford [7] discussed this problem. To meet the requirement of the same hydrogen content they saturated both standards and unknown sample with the same amount of water.

Instead of combersome calibration procedure used by Tittle and Crawford [7] we propose to measure hydrogen content of the sample and involve it in the Σ_a determination as an normalizing factor. The measuring apparatus based on the neutron thermalization [8,9] is suitable for this purpose. The main idea of the neutron thermalization method is shown in Fig.3. The polyamide block acts as an moderator. A cadmium sheet prevents the thermal diffusion from the polyamide block into the sample and detector space. The sample is irradiated mainly by epithermal neutrons. As the boron counter efficiency follows 1/v law, even single scatterings of epithermal neutrons on hydrogen nuclei of the sample lead to a substantial increase of the detector counting rate. The interactions with heavier nuclei have negligible influence on the detector counting rate. In particular, the gauge response is almost insensitive to changes of Σ_a . An example of the application of the method is shown in Fig. 4.

Making the cadmium sheet removable one can carry out two above mentioned measurements using only one measuring arrangement similar to that shown in Fig. 3(cf Kreft et al [10]). These two measurements give information both on Σ_a and slowing down power. The way of using this information seems to be of secondary importance. At the present stage of the method development we assume that the relation between Σ_a and results of measurements is of the following form:

$$\Sigma_a = a_1 + a_2 I_b + a_3 I_b^2 + a_4 I_{Cd} + a_5 I_{Cd}^2 + a_6 I_b I_{Cd} \qquad (1)$$

where I_b is the counting rate obtained in the case of the sample without cadmium cover, I_{Cd} is the counting rate obtained in the case of the sample covered with cadmium and a_1 - a_6 are coefficients to be found by fitting formula (1) to the experimental data obtained for a set of samples of known Σ_a values. As the assumed formula (1) is linear with respect to coefficients the multiple regression procedure can be applied.

RESULTS

The above mentioned approach has been tested with the set of 49 standards made of three pure components: silica sand, boric acid and water. The resulting Σ_a of the samples varried from 2.6 c.u. to 38 c.u., and hydrogen content varried from 0 to 0.027 g/cm^3. The sample volume was 1425 cm^3. The measuring times 2 x 300 s and the neutron source emitting 5 x 10^5 n/s have been applied. For these conditions the mean 95% confidence interval of 2.7 c.u. for Σ_a determination has been estimated.

We had an opportunity to compare results of assays for three basalt samples with those obtained by Czubek et al. [11] using the pulsed neutron generator technique. Results of this comparison shown in Table 1 appear advantageous for our method.

FINAL REMARKS

Already at the present stage of development the described method of determining the Σ_a appears competitive in all respect in comparison with the pulsed neutron technique. It is expected that the further refinements of the measuring apparatus itself and the shape of the fitted funnction will reduce the uncertainties of Σ_a determinations. The most important is that the calibration carried out with the aid of arbitrary standards seems to be valid for quite other rocks. Due to simplicity and rapidity of the analysis the method is suitable for routine applications.

It would be desirable to can optimize the measuring apparatus with the aid of neutron transport simulation. In this specific case a detailed treatment of the neutron thermalization process would be necessary. However, the available multigroup cross section data files include too less groups for neutron energies below 1 eV to try solve this problem.

ACKNOWLEDGEMENT

The authors are very indebted to Professor J.A.Czubek of Institute of Nuclear Physics in Kraków for the delivery of the basalt samples and valuable discussions.

REFERENCES

1. Majerczyk, J. and Zuber, A.: Radioisotope Instruments in Industry and Geophysics, Vol.2, p.383 (IAEA, Vienna, 1966).
2. Allen, L.S., Mills, W.R., Desai K.P. and Caldwell R.L.: SPWLA 13th Symp. Proc. Paper G, May 7-10 (1972).
3. Czubek, J.A., Drozdowicz,K., Krynicka-Drozdowicz, E., Igielski, A. and Woźnicka, U.: Int. J. Appl. Radiat. Isot. 34, 143 (1983).
4. Antonov, A.V., Granatkin, B.V., Merkulev, A.Yu., Miller, V.V. and Shimelevich Yu.S.: Radioisotope Instruments in Industry and Geophysics, Vol.2, p.139 (IAEA, Vienna, 1966).
5. Allen,L.S. and Mills, W.R.: The Log Analyst 16, No.1, 10 (1975).
6. Kreft, A.: The question of absorption cross section in neutron moisture measurements in Polish , Doctor's Thesis, University of Mining and Metallurgy, Kraków (1974).
7. Tittle, C.W. and Crawford, G.W.: The Log Analyst 24, No.3,12 (1983).
8. Chruściel, E., Gyurcsak, J., Krasowski, R., Kreft, A. and Woźniak, J.: Nuclear Physics Methods in Materials Research, 7th Div. Conf. EPS, p.312 (Darmstadt, 1980).
9. Chruściel, E., Dziunikowski, B., Gyurcsak, J., Kalita, S., Kreft, A., Lenda, A., Przybyłowicz, W. and Woźniak, J.: Integrated instrumental analysis of brown coals in Polish , INT Report No.168/I (1982).
10. Kreft, A., Dydejczyk, A. and Gyurcsak J.: Determining the thermal neutron absorption cross section of rocks, submitted to Int. J. Appl. Radiat. Isot. (1983).
11. Czubek, J.A., Drozdowicz, K., Krynicka-Drozdowicz, E., Igielski, A. and Woźnicka, U.: Thermal neutron absorption cross section measured on rock samples and brines in the Institute of Nuclear Physics, INP Report No. 1223/AP (1983).

TABLE 1. Results of Σ_a measurements for basalts.

Method \ Sample code		S4	S7	S10
Our measurements in c.u./ (g/cm^3)	Σ_a/ρ	7.40	8.23	7.04
	$\Delta_{95\%}$ (•)	1.49	1.64	1.56
Czubek's [11] measurements in c.u./ (g/cm^3)	Σ_a/ρ	7.92	7.78	5.44
	$\sigma(\Sigma_a/\rho)$	1.39	1.15	1.62

(•) $\Delta_{95\%} > 2\sigma$

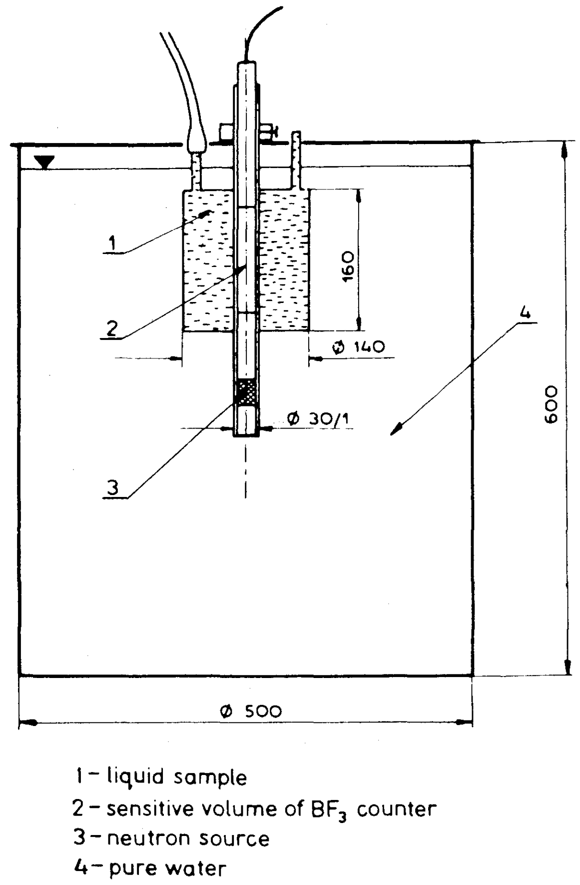

Fig.1. Cross-sectional diagram of apparatus suitable for determining the Σ_a of brines [6].

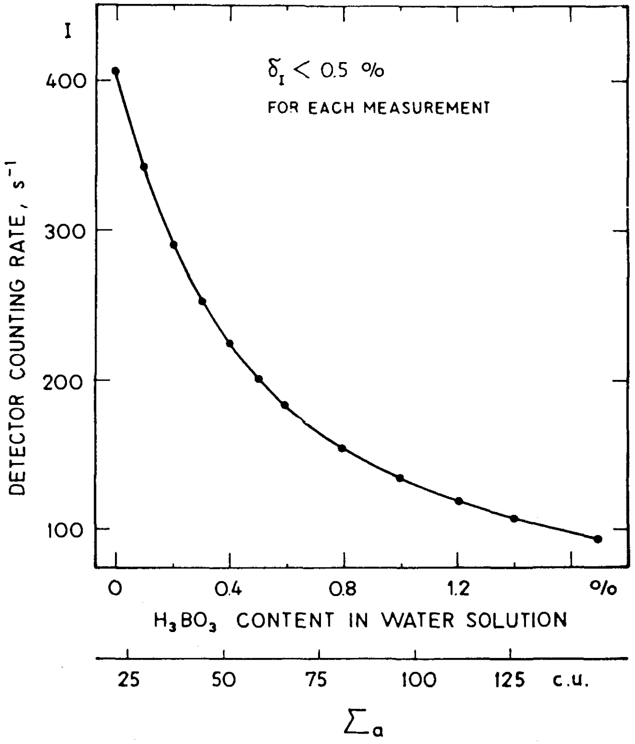

Fig.2. Calibration curve of the apparatus shown in Fig.1 [6].

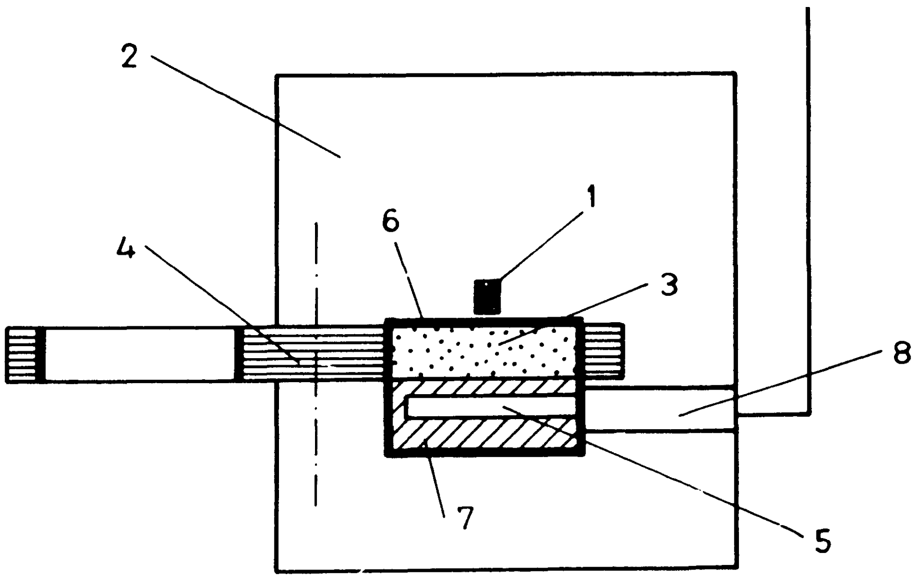

Fig.3. Cross-sectional diagram of apparatus for hydrogen determination [9]. 1 - neutron source, 5 x 10^5n/s; 2 - moderating block; 3 - sample; 4 - sample changer; 5 - BF_3 detector; 6 - cadmium sheet; 7 - graphite reflector; 8 - preamplifier.

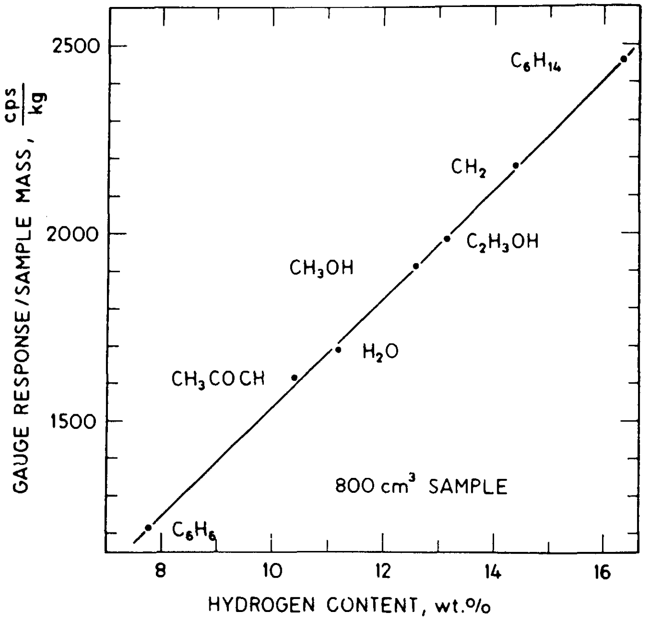

Fig.4. Calibration curve of apparatus shown in Fig.3 obtained for hydrocarbons.

Experimental Determination of Photonuclear Yield Excited by Bremsstrahlung with 20-MeV-Energy

I.N.Ivanov, B.N.Rivkin, Yu.V.Feoktistov, V.V.Filippov
All Union Research Institute of Radiation Engineering, Moscow

To identify elements, optimize analysis conditions in analytical practice, data on different nuclear-reaction yield should be obtained.

The given paper presents results of experimental measurements of yield of nuclides formed under the action of bremsstrahlung and their decay products. This data as well as the data of paper (1) can be used for modelling of gamma-spectrum of induced activity of unspecified samples according to programs described in papers (2-4), and for calculation of detection limits of elements depending on the bremsstrahlung energy and analysis time order.

There were investigated samples containing salts of elements beginning from carbon up to bismuth with exception of technetium, promethium and elements of the eighth group. These samples were irradiated with bremsstrahlung, generated by linear electron accelerator LUE-15A, equipped with 4-mm-thick gold target. The accelerator ensured average electron current of 50 μA at bremsstrahlung energy of 20 MeV. The samples were prepared by mixing of pure or ultra-pure compounds of chemical elements and pure silicon dioxide and were packed in polyethylene containers with internal dimensions as next: diameter -15 mm, height - 40 mm. The average mass of samples was 14.5 g, and element concentration - from 0.1 to 10 wt.%.

Irradiation time for the most part of samples was equal to 10 min and time of measurement of induced gamma-activity - 500 sec. In some cases in order to improve conditions of registration of short-lived activation products, the time of irradiation and measurement was decreased to 30 and 200 s. Time of sample cooling varied from several minutes to several hours depending on the value of induced activity.

To take account of variations of energy and current of the electron accelerator through time, monitors were irradiated simultaneously with the samples. Sodium chloride which was used for the monitors was packed in the same tipe of containers that were used for the samples. Monitoring was made on intensity of gamma-ray-line of nuclide ^{34m}Cl ($T_{\frac{1}{2}}$ = 32.06 min) with energy of 2.128 MeV.

Induced gamma-activity of samples and monitors was registered with the help of spectrometer with 65-cm^3 - volume Ge(Li)-detector. The energy resolution of spectrometer is 3.0 keV at 1.332 MeV gamma-line energy. Geometric conditions of irradiation and registration of induced gamma-activity of the samples is illustrated in Fig. 1, while Fig. 2 presents dependence of absolute registration efficiency of gamma-quanta on their energy for the given detector.

Detector signals were supplied to measuring system based on microcomputer Electronica-60. The equipment was provided with a set of programs ensuring processes of accumulation and processing of spectrometric data. Program GAMMA-F was used for processing of spectrometric data. This program ensured separation of statistically significant photopeaks, calculation of photopeak area and conducting of energy calibration. The statistically significant photopeaks are those the statistical error of whose, when calculating their area, is $\leqslant 30\%$.

Background distribution under the photopeak was determined as follows:

$$B_i = N_L + (N_R - N_L)\Big(\sum_{j=L}^{i} N_j \Big/ \sum_{k=L}^{R} N_k\Big),$$

where B_i - background distribution in i^{th} - channel;

N_i, N_L, N_R - number of registered pulses, accordingly for i^{th} channel and boundary points on low-energy (L) and high-energy (R) slopes of the photopeak.

Nuclides produced in the process of photonuclear reactions and nuclide decay products were identified, on the whole, by the energy of their gamma-irradiation, and in some cases by half-life. Therefore, measurements of sample activity with cooling of up to 7 days were repeated.

Table 1 represents photopeak areas normalized per 50-μA-electron current and reduced to the following time: irradiation - 10 min, cooling - 0, measurement - 500 s. Given in column 7 are values of sample activity normalized per 1% of element for conditions of measurement shown in Fig. 1. Given in column 8 are values of absolute activity normalized per 1 mg of element for point source arranged in the centre of detector end face. These data were obtained after correction for efficiency of the detector, self-absorbtion of gamma rays in the sample and solid angle of registration.

Values of activity in decay chains are given for parent nuclides and calculated by the formula:

$$A_M = \frac{A_D\,(T_M - T_D)}{T_M\,(e^{-0,693\,t_c/T_M} - e^{-0,693\,t_c/T_D})}$$

where A_M, A_D, T_M, T_D - values of activity of parent and daughter nuclides and their half-life periods;

t_c - cooling time.

As a result of identification of photonuclear reaction products, formed from 69 elements under the action of bremsstrahlung with 20 MeV-energy, 227 radioactive nuclides were detected, including 131 nuclide produced from reaction (γ, n), 33 - from reaction (γ, p), 7 - from reaction (γ,2n), 3 - from reaction (γ,α), 15 - from reaction (γ, γ'), 32 - from decay chains and 6 - as a result of production through several channels of nuclear reactions.

Table 1

Nuclide characteristics and yields

Element	Isotope	Abandance, %	Reaction	Half-life	E_γ, keV	A_1	A_2
1	2	3	4	5	6	7	8
C	^{12}C	98,89	$^{12}C(\gamma,n)^{11}C$	20,38 m	511	$2,80.10^4$	$2,57.10^4$
N	^{14}N	99,63	$^{14}N(\gamma,n)^{13}N$	9,97 m	511	$3,70.10^6$	$3,44.10^6$
O	^{16}O	99,76	$^{16}O(\gamma,n)^{15}O$	2,03 m	511	$1,12.10^6$	$1,04.10^6$
F	^{19}F	100	$^{19}F(\gamma,n)^{18}F$	109,8 m	511	$4,21.10^6$	$3,91.10^6$
Na	^{23}Na	100	$^{23}Na(\gamma,n)^{22}Na$	2,6 y	1274	$4,93.10^1$	$1,21.10^2$
Mg	^{25}Mg	10,13	$^{25}Mg(\gamma,p)^{24}Na$	15,005 h	1368	$3,60.10^3$	$1,64.10^4$
	^{26}Mg	11,17	$^{26}Mg(\gamma,p)^{25}Na$	60 s	585,1	$5,33.10^3$	$5,83.10^3$
Si	^{29}Si	4,70	$^{29}Si(\gamma,p)^{28}Al$	2,24 m	1778,7	$8,64.10^4$	$3,51.10^5$
	^{30}Si	3,09	$^{30}Si(\gamma,p)^{29}Al$	6,52 m	1273	$2,58.10^4$	$6,34.10^5$
P	^{31}P	100	$^{31}P(\gamma,n)^{30}P$	2,499 m	511	$2,08.10^7$	$1,92.10^7$
Cl	^{35}Cl	75,53	$^{35}Cl(\gamma,n)^{34m}Cl$	32,06 m	145,7	$1,45.10^6$	$5,20.10^5$
K	^{39}K	93,1	$^{39}K(\gamma,n)^{38}K$	7,71 m	2168	$2,99.10^5$	$1,49.10^6$
Ca	^{43}Ca	0,145	$^{43}Ca(\gamma,p)^{42}K$	12,36 h	1524,6	$1,20.10^1$	$3,58.10^1$
	^{44}Ca	2,06	$^{44}Ca(\gamma,p)^{43}K$	22,6 h	373	$8,77.10^2$	$5,50.10^2$
	^{48}Ca	0,185	$^{48}Ca(\gamma,n)^{47}Ca$	4,55 d	1297,1	$1,08.10^2$	$2,72.10^2$
Sc	^{45}Sc	100	$^{45}Sc(\gamma,n)^{44}Sc$	3,92 h	1156,9	$1,20.10^6$	$2,58.10^6$
			$^{45}Sc(\gamma,n)^{44m}Sc$	2,44 d	271,3	$4,84.10^4$	$2,05.10^4$
			$^{44m}Sc \dashrightarrow ^{44}Sc$	3,92 h	1156,9	$1,78.10^4$	$3,93.10^4$
Ti	^{46}Ti	7,93	$^{46}Ti(\gamma,n)^{45}Ti$	3,09 h	511	$2,48.10^5$	$2,30.10^5$
	^{47}Ti	7,28	$^{47}Ti(\gamma,p)^{46}Sc$	83,80 d	889,2	$5,16.10^1$	$8,90.10^1$
	^{48}Ti	73,94	$^{48}Ti(\gamma,p)^{47}Sc$	3,40 d	159,4	$1,98.10^4$	$6,97.10^3$
	^{49}Ti	5,51	$^{49}Ti(\gamma,p)^{48}Sc$	43,8 h	983,3	$3,29.10^2$	$6,26.10^2$

Table 1, continued

1	2	3	4	5	6	7	8
V	^{51}V	99,76	$^{51}V(\gamma,\alpha)^{47}Sc$	**3.40 d**	159,4	$3,18.10^{2}$	$1,11.10^{2}$
Cr	^{50}Cr	4,31	$^{50}Cr(\gamma,n)^{49}Cr$	41,4 m	152,9	$1,46.10^{5}$	$5,15.10^{4}$
	^{52}Cr	83,76	$^{52}Cr(\gamma,n)^{51}Cr$	27,73 d	320,1	$2,19.10^{3}$	$1,10.10^{3}$
	^{53}Cr	9,55	$^{53}Cr(\gamma,p)^{52}V$	3,76 m	1433,9	$9,20.10^{4}$	$2,60.10^{5}$
Mn	^{55}Mn	100	$^{55}Mn(\gamma,n)^{54}Mn$	312,3 d	834,8	$9,08.10^{2}$	$1,49.10^{3}$
Fe	^{54}Fe	5,84	$^{54}Fe(\gamma,n)^{53}Fe$	8,53 m	377,9	$1,07.10^{5}$	$6,85.10^{4}$
	^{57}Fe	2,17	$^{57}Fe(\gamma,p)^{56}Mn$	2,578 h	846,6	$2,05.10^{3}$	$3,41.10^{3}$
Co	^{59}Co	100	$^{59}Co(\gamma,n)^{58}Co$	70,78 d	810,7	$6,80.10^{3}$	$1,09.10^{4}$
Ni	^{58}Ni	67,88	$^{58}Ni(\gamma,n)^{57}Ni$	36,16 h	1377,6	$3,03.10^{4}$	$8,15.10^{4}$
			$^{58}Ni(\gamma,p)^{57}Co$	271,4 d	122,1	$4,14.10^{3}$	$1,57.10^{3}$
Cu	^{63}Cu	69,09	$^{63}Cu(\gamma,n)^{62}Cu$	9,74 m	1172,7	$3,51.10^{4}$	$7,94.10^{4}$
	^{65}Cu	30,91	$^{65}Cu(\gamma,n)^{64}Cu$	12,71 h	1347	$1,27.10^{3}$	$3,29.10^{3}$
Zn	^{64}Zn	48,89	$^{64}Zn(\gamma,n)^{63}Zn$	38,1 m	669,6	$6,06.10^{5}$	$7,90.10^{5}$
	^{66}Zn	27,81	$^{66}Zn(\gamma,n)^{65}Zn$	244,1 d	1115,5	$3,04.10^{2}$	$6,47.10^{2}$
	^{68}Zn	18,56	$^{68}Zn(\gamma,p)^{67}Cu$	61,88 h	184,5	$2,68.10^{3}$	$9,47.10^{2}$
	^{70}Zn	0,62	$^{70}Zn(\gamma,n)^{69m}Zn$	14,0 h	439,1	$3,99.10^{3}$	$3,11.10^{3}$
Ga	^{69}Ga	60,4	$^{69}Ga(\gamma,n)^{68}Ga$	68,0 m	1077,5	$2,01.10^{5}$	$4,17.10^{5}$
	^{71}Ga	39,6	$^{71}Ga(\gamma,n)^{70}Ga$	21,15 m	173	$5,03.10^{6}$	$1,77.10^{6}$
Ge	^{70}Ge	20,52	$^{70}Ge(\gamma,n)^{69}Ge$	39,05 h	1106,4	$1,06.10^{4}$	$2,26.10^{4}$
	^{73}Ge	7,76	$^{73}Ge(\gamma,p)^{72}Ga$	14,1 h	833,9	$1,20.10^{3}$	$1,97.10^{3}$
	^{74}Ge	36,54	$^{74}Ge(\gamma,p)^{73}Ga$	4,86 h	297,4	$1,52.10^{4}$	$7,14.10^{3}$
	^{76}Ge	7,76	$^{76}Ge(\gamma,n)^{75}Ge$	82,78 m	264,8	$3,22.10^{5}$	$1,34.10^{5}$
			$^{76}Ge(\gamma,n)^{76m}Ge$	48,3 s	139,8	$8,38.10^{5}$	$3,03.10^{5}$
As	^{75}As	100	$^{75}As(\gamma,n)^{74}As$	17,78 d	595,7	$3,63.10^{4}$	$4,07.10^{4}$

Table 1, continued

1	2	3	4	5	6	7	8
Se	^{74}Se	0,87	$^{74}Se(\gamma,n)^{73}Se$	7,1 h	360,9	$2,66.10^{4}$	$1,58.10^{4}$
			$^{74}Se(\gamma,n)^{73m}Se$	39 m	253,8	$7,19.10^{3}$	$2,90.10^{3}$
	^{76}Se	9,02	$^{76}Se(\gamma,n)^{75}Se$	118,45 d	136,6	$1,86.10^{3}$	$6,78.10^{2}$
	^{77}Se ^{78}Se	7,58 23,52	$\left.\begin{array}{l}{}^{77}Se(\gamma,\gamma')\\ {}^{78}Se(\gamma,n)\end{array}\right\}{}^{77m}Se$	17,38 s	162,0	$9,32.10^{5}$	$3,27.10^{5}$
	^{80}Se	49,82	$^{80}Se(\gamma,p)^{79}As$	9,01 m	432,0	$8,28.10^{3}$	$6,27.10^{3}$
			$\left.\begin{array}{l}{}^{79}As \longrightarrow\\ {}^{80}Se(\gamma,n)\end{array}\right\}{}^{79m}Se$	3,91 m	95,5	$6,75.10^{6}$	$3,77.10^{6}$
	^{77}Se	7,58	$^{77}Se(\gamma,p)^{76}As$	26,32 h	559,5	$5,68.10^{2}$	$5,92.10^{2}$
	^{82}Se	9,19	$^{82}Se(\gamma,n)^{81}Se$	18,5 m	289,9	$8,61.10^{4}$	$3,91.10^{4}$
			$^{82}Se(\gamma,n)^{81m}Se$	57,25 m	103,0	$3,13.10^{5}$	$1,51.10^{5}$
			$^{82}Se\ (\gamma,\alpha)^{78}Ge$	87 m	277	$5,18.10^{4}$	$2,25.10^{4}$
Br	^{81}Br	49,46	$^{81}Br(\gamma,n)^{80m}Br$	4,42 h	γ - peaks are not detected		
			$^{80m}Br \longrightarrow {}^{80}Br$	17,4 m	616,9	$4,79.10^{4}$	$5,61.10^{4}$
			$^{81}Br(\gamma,\alpha)^{77}As$	38,83 h	239,1	$8,61.10^{1}$	$3,37.10^{1}$
Rb	^{85}Rb	72,15	$^{85}Rb(\gamma,n)^{84}Rb$	32,77 d	881,5	$1,26.10^{4}$	$2,15.10^{4}$
			$^{85}Rb(\gamma,n)^{84m}Rb$	20,5 m	248,2	$1,22.10^{7}$	$4,85.10^{6}$
	^{87}Rb	27,85	$^{87}Rb(\gamma,n)^{86}Rb$	18,66 d	1076,6	$9,11.10^{2}$	$1,88.10^{3}$
			$^{87}Rb(\gamma,n)^{86m}Rb$	1,017 m	555,9	$9,69.10^{5}$	$9,95.10^{5}$
Sr	^{84}Sr	0,56	$^{84}Sr(\gamma,n)^{83}Sr$	32,4 h	762,5	$1,06.10^{3}$	$1,57.10^{3}$
	^{86}Sr	9,86	$^{86}Sr(\gamma,n)^{85}Sr$	64,73 d	514,0	$2,09.10^{3}$	$1,96.10^{3}$
			$^{86}Sr(\gamma,n)^{85m}Sr$	67,7 m	231,2	$1,05.10^{5}$	$4,02.10^{4}$
	^{87}Sr ^{88}Sr	7,02 82,56	$\left.\begin{array}{l}{}^{87}Sr(\gamma,\gamma')\\ {}^{88}Sr(\gamma,n)\end{array}\right\}{}^{87m}Sr$	2,805 h	388,3	$1,86.10^{6}$	$1,24.10^{6}$
			$^{83}Sr \longrightarrow {}^{83}Rb$	86,2 d	529,2	$1,75.10^{3}$	$1,71.10^{3}$

Table 1, continued

1	2	3	4	5	6	7	8
Y	^{89}Y	100	^{89}Y(γ,n)^{88}Y	106,6 d	898,0	$7,23.10^{3}$	$1,24.10^{4}$
			^{89}Y(γ,γ')^{89m}Y	16,06 s	909,1	$1,62.10^{4}$	$2,83.10^{4}$
Zr	^{90}Zr	51,46	^{90}Zr(γ,n)^{89}Zr	78,43 h	909,1	$9,24.10^{4}$	$1,62.10^{5}$
	^{96}Zr	2,80	^{96}Zr(γ,n)^{95}Zr	64,05 d	756,7	$3,04.10^{2}$	$4,47.10^{2}$
			^{95}Zr$\longrightarrow$^{95}Nb	34,97 d	795,8	$3,69.10^{2}$	$5,51.10^{2}$
Nb	^{93}Nb	100	^{93}Nb(γ,n)^{92m}Nb	10,13 d	934	$2,81.10^{4}$	$5,06.10^{4}$
Mo	^{92}Mo	15,86	^{92}Mo(γ,n)^{91m}Mo	65,5 s	1508	$1,48.10^{5}$	$4,47.10^{5}$
	^{96}Mo	16,53	^{96}Mo(γ,p)^{95m}Nb	3,61 d	235,4	$4,08.10^{2}$	$1,58.10^{2}$
	^{97}Mo	9,46	^{97}Mo(γ,p)^{96}Nb	23,35 h	568,9	$4,59.10^{2}$	$4,88.10^{2}$
	^{98}Mo	23,78	^{98}Mo(γ,p)^{97}Nb	72,1 m	657,9	$2,31.10^{4}$	$2,93.10^{4}$
	^{100}Mo	9,62	^{100}Mo(γ,n)^{99}Mo	66,02 h	181,1	$1,66.10^{4}$	$5,84.10^{3}$
			^{99}Mo$\longrightarrow$^{99m}Tc	6,006 h	140,5	$2,58.10^{5}$	$9,43.10^{4}$
Ru	^{96}Ru	5,68	^{96}Ru(γ,n)^{95}Ru	1,63 h	336,4	$8,36.10^{5}$	$4,46.10^{5}$
			^{95}Ru$\longrightarrow$^{95}Tc	20,0 h	765,7	$5,62.10^{5}$	$8,40.10^{5}$
			^{95}Ru$\longrightarrow$^{95m}Tc	61 d	204,1	$9,74.10^{5}$	$3,54.10^{5}$
	^{98}Ru	2,22	^{98}Ru(γ,n)^{97}Ru	2,89 d	215,7	$2,11.10^{4}$	$7,79.10^{3}$
	^{100}Ru	12,70	^{100}Ru(γ,p)^{99m}Tc	6,006 h	140,5	$1,49.10^{4}$	$5,36.10^{3}$
	^{104}Ru	18,27	^{104}Ru(γ,n)^{103}Ru	39,35 d	497,1	$8,57.10^{3}$	$7,74.10^{3}$
Rh	^{103}Rh	100	^{103}Rh(γ,n)^{102}Rh	207 d	475,0	$2,82.10^{3}$	$2,40.10^{3}$
			^{103}Rh(γ,2n)^{101m}Rh	4,34 d	306,8	$3,03.10^{3}$	$1,44.10^{3}$
Pd	^{102}Pd	0,8	^{102}Pd(γ,n)^{101}Pd	8,5 h	296,3	$1,64.10^{4}$	$1,11.10^{4}$
			^{101}Pd$\longrightarrow$^{101m}Rh	4,34 d	306,8	$8,82.10^{4}$	$4,19.10^{4}$
	^{108}Pd	26,8	^{108}Pd(γ,p)^{107}Rh	21,7 m	302,8	$8,81.10^{4}$	$4,16.10^{4}$

Table 1, continued

1	2	3	4	5	6	7	8
	$^{110}\mathrm{Pd}$	13,5	$^{110}\mathrm{Pd}(\gamma,n)^{109m}\mathrm{Pd}$	4,69 m	188	$2,49.10^{6}$	$8,81.10^{5}$
			$^{110}\mathrm{Pd}(\gamma,n)^{109}\mathrm{Pd}$	13,46 h	γ - peaks are not detected		
			$^{109}\mathrm{Pd}\longrightarrow{}^{109m}\mathrm{Ag}$	39,6 s	88,1	$3,63.10^{4}$	$2,42.10^{4}$
Ag	$^{107}\mathrm{Ag}$	51,35	$^{107}\mathrm{Ag}(\gamma,\gamma')^{107m}\mathrm{Ag}$	44,3 s	93,1	$1,00.10^{5}$	$5,93.10^{4}$
			$^{107}\mathrm{Ag}(\gamma,n)^{106}\mathrm{Ag}$	23,96 m	622,8	$2,37.10^{5}$	$2,82.10^{5}$
			$^{107}\mathrm{Ag}(\gamma,n)^{106m}\mathrm{Ag}$	8,41 d	450,9	$1,07.10^{3}$	$8,63.10^{2}$
	$^{109}\mathrm{Ag}$	48,65	$^{109}\mathrm{Ag}(\gamma,\gamma')^{109m}\mathrm{Ag}$	39,6 s	88,1	$8,13.10^{4}$	$5,43.10^{4}$
			$^{109}\mathrm{Ag}(\gamma,n)^{108}\mathrm{Ag}$	2,41 m	632,9	$9,44.10^{5}$	$1,14.10^{6}$
Cd	$^{106}\mathrm{Cd}$	1,21	$^{106}\mathrm{Cd}(\gamma,n)^{105}\mathrm{Cd}$	55,5 m	961,1	$5,59.10^{3}$	$1,04.10^{4}$
			$^{105}\mathrm{Cd}\longrightarrow{}^{105}\mathrm{Ag}$	41,29 d	280,4	$2,30.10^{5}$	$1,00.10^{5}$
	$^{108}\mathrm{Cd}$	0,88	$^{108}\mathrm{Cd}(\gamma,n)^{107}\mathrm{Cd}$	6,49 h	γ - peaks are not detected		
			$^{107}\mathrm{Cd}\longrightarrow{}^{107m}\mathrm{Ag}$	44,3 s	93,1	$3,47.10^{3}$	$2,05.10^{3}$
	$^{110}\mathrm{Cd}$	12,39	$^{110}\mathrm{Cd}(\gamma,n)^{109}\mathrm{Cd}$	453 d	γ - peaks are not detected		
			$^{109}\mathrm{Cd}\longrightarrow{}^{109m}\mathrm{Ag}$	39,6 s	88,1	$2,41.10^{1}$	$1,61.10^{1}$
	$^{111}\mathrm{Cd}$ $^{112}\mathrm{Cd}$	12,75 24,07	$\left.\begin{array}{l}^{111}\mathrm{Cd}(\gamma,\gamma')\\ ^{112}\mathrm{Cd}(\gamma,n)\end{array}\right\}^{111m}\mathrm{Cd}$	49,1 m	245,3	$1,49.10^{6}$	$5,85.10^{5}$
	$^{113}\mathrm{Cd}$	12,26	$^{113}\mathrm{Cd}(\gamma,p)^{112}\mathrm{Ag}$	3,12 h	616,8	$1,26.10^{3}$	$1,50.10^{3}$
	$^{114}\mathrm{Cd}$	28,86	$^{114}\mathrm{Cd}(\gamma,p)^{113}\mathrm{Ag}$	5,37 h	298,4	$8,24.10^{2}$	$3,86.10^{2}$
	$^{116}\mathrm{Cd}$	7,58	$^{116}\mathrm{Cd}(\gamma,n)^{115}\mathrm{Cd}$	53,46 h	527,9	$1,27.10^{4}$	$1,22.10^{4}$
			$^{115}\mathrm{Cd}\longrightarrow{}^{115m}\mathrm{In}$	4,486 h	336,2	$3,85.10^{4}$	$2,06.10^{4}$
In	$^{113}\mathrm{In}$	4,23	$^{113}\mathrm{In}(\gamma,n)^{112}\mathrm{In}$	14,4 m	617,2	$4,48.10^{5}$	$5,28.10^{5}$
			$^{113}\mathrm{In}(\gamma,n)^{112m}\mathrm{In}$	20,9 m	156,2	$8,46.10^{5}$	$2,97.10^{5}$
			$^{113}\mathrm{In}(\gamma,2n)^{111}\mathrm{In}$	2,802 d	171,3	$7,81.10^{2}$	$2,74.10^{2}$
			$^{113}\mathrm{In}(\gamma,\gamma')^{113m}\mathrm{In}$	99,4 m	391,7	$7,24.10^{4}$	$4,86.10^{4}$

Table 1, continued

1	2	3	4	5	6	7	8
	^{115}In	95,77	$^{115}\text{In}(\gamma,n)^{114m}\text{In}$	49,51 d	191,6	$1,25.10^{4}$	$4,42.10^{3}$
			$^{114m}\text{In}\dashrightarrow{}^{114}\text{In}$	71,9 s	1300	$2,00.10^{1}$	$5,04.10^{1}$
			$^{115}\text{In}(\gamma,\gamma')^{115m}\text{In}$	4,486 h	336,2	$2,17.10^{5}$	$1,17.10^{5}$
Sn	^{112}Sn	0,95	$^{112}\text{Sn}(\gamma,n)^{111}\text{Sn}$	35,3 m	1152,5	$3,40.10^{3}$	$7,52.10^{3}$
			$^{111}\text{Sn}\dashrightarrow{}^{111}\text{In}$	2,802 d	245,3	$1,73.10^{6}$	$6,84.10^{5}$
	^{114}Sn	0,65	$^{114}\text{Sn}(\gamma,n)^{113}\text{Sn}$	115,2 d	γ- peaks are not detected		
			$^{113}\text{Sn}\dashrightarrow{}^{113m}\text{In}$	99,4 m	391,7	$1,31.10^{2}$	$8,80.10^{1}$
	^{116}Sn	14,24	$^{116}\text{Sn}(\gamma,p)^{115m}\text{In}$	4,486 h	336,2	$1,92.10^{3}$	$1,03.10^{3}$
	^{117}Sn	7,57	$^{117}\text{Sn}(\gamma,\gamma')^{117m}\text{Sn}$	14,0 d	158,6	$6,11.10^{3}$	$2,14.10^{3}$
	^{118}Sn	24,01	$^{118}\text{Sn}(\gamma,p)^{117}\text{In}$	44 m	552,9	$3,20.10^{3}$	$3,26.10^{3}$
	^{124}Sn	5,98	$^{124}\text{Sn}(\gamma,n)^{123m}\text{Sn}$	42 m	159,7	$5,48.10^{6}$	$1,92.10^{6}$
Sb	^{121}Sb	57,25	$^{121}\text{Sb}(\gamma,n)^{120}\text{Sb}$	15,89 m	704,0	$3,05.10^{4}$	$4,24.10^{4}$
			$^{121}\text{Sb}(\gamma,n)^{120m}\text{Sb}$	5,76 d	1171,7	$2,72.10^{3}$	$6,18.10^{3}$
	^{123}Sb	42,75	$^{123}\text{Sb}(\gamma,n)^{122}\text{Sb}$	2,714 d	564,0	$1,61.10^{5}$	$1,69.10^{5}$
			$^{123}\text{Sb}(\gamma,n)^{122m}\text{Sb}$	4,2 m	76,1	$3,19.10^{6}$	$3,04.10^{6}$
Te	^{120}Te	0,089	$^{120}\text{Te}(\gamma,n)^{119}\text{Te}$	15,9 h	644,3	$8,53.10^{2}$	$1,05.10^{3}$
	^{122}Te	2,46	$^{122}\text{Te}(\gamma,n)^{121}\text{Te}$	17 d	573,1	$9,05.10^{2}$	$9,67.10^{2}$
			$^{122}\text{Te}(\gamma,n)^{121m}\text{Te}$	154 d	212,2	$6,00.10^{1}$	$2,17.10^{1}$
	^{123}Te	0,87	$^{123}\text{Te}(\gamma,\gamma')\ ^{123m}\text{Te}$	119,7 d	159,0	$1,58.10^{2}$	$5,55.10^{1}$
	^{128}Te	31,79	$^{128}\text{Te}(\gamma,n)^{127}\text{Te}$	9,35 h	417,9	$8,53.10^{3}$	$6,23.10^{3}$
	^{130}Te	34,49	$^{130}\text{Te}(\gamma,n)^{129}\text{Te}$	69,6 m	459,6	$5,33.10^{5}$	$4,36.10^{5}$
			$^{130}\text{Te}(\gamma,n)^{129m}\text{Te}$	33,52 d	696,0	$7,40.10^{1}$	$1,01.10^{2}$
			$^{129m}\text{Te}\dashrightarrow{}^{129}\text{Te}$	69,6 m	459,6	$1,25.10^{2}$	$1,02.10^{2}$
I	^{127}I	100	$^{127}\text{I}(\gamma,n)^{126}\text{I}$	12,93 d	388,6	$4,29.10^{4}$	$2,87.10^{4}$

Table 1, continued

1	2	3	4	5	6	7	8
Cs	^{133}Cs	100	^{133}Cs(γ,n)^{132}Cs	6,475 d	667,5	$2,46.10^{5}$	$3,13.10^{5}$
Ba	^{130}Ba	0,101	^{130}Ba(γ,n)^{129}Ba	2,02 h	1459,3	$3,14.10^{2}$	$9,07.10^{2}$
			^{129}Ba$\longrightarrow$^{129}Cs	32,06 h	371,9	$8,02.10^{3}$	$5,03.10^{3}$
	^{132}Ba	0,097	^{132}Ba(γ,n)^{131}Ba	11,8 d	496,2	$6,10.10^{1}$	$5,40.10^{1}$
			^{132}Ba(γ,n)^{131m}Ba	14,6 m	107	$1,88.10^{4}$	$8,32.10^{3}$
	^{135}Ba	6,59	^{135}Ba(γ,γ')^{135m}Ba	28,7 h	268,2	$6,80.10^{3}$	$2,86.10^{3}$
	^{136}Ba	7,81	^{136}Ba(γ,p)^{135m}Cs	53 m	781	$3,47.10^{2}$	$5,31.10^{2}$
	^{137}Ba	11,32	^{137}Ba(γ,γ')^{137m}Ba	2,552 m	661,6	$5,95.10^{6}$	$7,60.10^{6}$
	^{138}Ba	71,66	^{138}Ba(γ,n)				
	^{134}Ba	2,42	^{134}Ba(γ,n)^{133m}Ba	38,9 h	275,6	$1,13.10^{3}$	$4,86.10^{2}$
Ce	^{136}Ce	0,193	^{136}Ce(γ,n)^{135}Ce	17,76 h	299,9	$2,83.10^{3}$	$1,33.10^{3}$
	^{138}Ce	0,25	^{138}Ce(γ,n)^{137}Ce	9,0 h	447,1	$3,32.10^{2}$	$2,66.10^{2}$
			^{138}Ce(γ,n)^{137m}Ce	34,4 h	254,3	$1,16.10^{2}$	$4,69.10^{1}$
	^{140}Ce	88,48	^{140}Ce(γ,n)^{139}Ce	137,63 d	165,8	$4,66.10^{4}$	$1,64.10^{4}$
			^{140}Ce(γ,n)^{139m}Ce	56,2 s	754,5	$3,79.10^{6}$	$5,58.10^{6}$
	^{142}Ce	11,07	^{142}Ce(γ,n)^{141}Ce	32,50 d	145,4	$1,24.10^{4}$	$4,45.10^{3}$
Pr	^{141}Pr	100	^{141}Pr(γ,n)^{140}Pr	3,39 m	1596,5	$2,42.10^{5}$	$8,00.10^{5}$
			^{141}Pr(γ,2n)^{139}Pr	4,42 h	γ - peaks are not detected		
			^{139}Pr$\longrightarrow$^{139}Ce	137,63 d	165,8	$7,96.10^{4}$	$2,79.10^{4}$
Nd	^{142}Nd	27,13	^{142}Nd(γ,n)^{141}Nd	2,42 d	145,4	$3,02.10^{4}$	$1,08.10^{4}$
			^{142}Nd(γ,n)^{141m}Nd	62,1 s	756,5	$8,79.10^{5}$	$1,29.10^{6}$
	^{148}Nd	5,72	^{148}Nd(γ,n)^{147}Nd	10,98 d	531,0	$1,56.10^{3}$	$1,52.10^{3}$
	^{150}Nd	5,60	^{150}Nd(γ,n)^{149}Nd	1,73 h	211,3	$1,18.10^{6}$	$4,34.10^{5}$
			^{149}Nd$\longrightarrow$^{149}Pm	53,08 h	285,9	$1,16.10^{5}$	$5,15.10^{4}$

Table 1, continued

1	2	3	4	5	6	7	8
Sm	^{144}Sm	3,16	^{144}Sm(γ,n)^{143}Sm	8,83 m	1056,5	$2,93.10^{4}$	$5,96.10^{4}$
			^{143}Sm$\longrightarrow$^{143}Pm	265 d	741,9	$2,03.10^{6}$	$2,98.10^{6}$
	^{152}Sm	26,63	^{152}Sm(γ,p)^{151}Pm	28,40 h	340,1	$6,80.10^{1}$	$3,74.10^{1}$
	^{154}Sm	22,53	^{154}Sm(γ,n)^{153}Sm	46,44 h	103,2	$1,03.10^{5}$	$4,96.10^{4}$
Eu	^{151}Eu	47,77	^{151}Eu(γ,n)^{150}Eu	12,62 h	406,5	$2,40.10^{4}$	$1,69.10^{4}$
	^{153}Eu	52,23	^{153}Eu(γ,n)^{152m_1}Eu	9,3 h	121,7	$1,67.10^{5}$	$6,38.10^{4}$
			^{153}Eu(γ,n)^{152m_2}Eu	96 m	89,5	$6,45.10^{4}$	$4,09.10^{4}$
			^{153}Eu(γ,n)^{152}Eu	13,2 y	121,7	$1,54.10^{2}$	$5,88.10^{1}$
Gd	^{154}Gd	2,15	^{154}Gd(γ,n)^{153}Gd	241,6 d	97,4	$7,10.10^{1}$	$3,81.10^{1}$
	^{160}Gd	21,90	^{160}Gd(γ,n)^{159}Gd	18,6 h	363,3	$1,03.10^{5}$	$6,22.10^{4}$
Tb	^{159}Tb	100	^{159}Tb(γ,n)^{158m}Tb	10,5 s	110	$2,19.10^{5}$	$9,09.10^{4}$
Dy	^{156}Dy	0,052	^{156}Dy(γ,n)^{155}Dy	10,0 h	226,9	$4,59.10^{3}$	$1,72.10^{3}$
			^{155}Dy$\longrightarrow$^{155}Tb	5,32 d	105,3	$1,18.10^{3}$	$5,37.10^{2}$
	^{158}Dy	0,090	^{158}Dy(γ,n)^{157}Dy	8,1 h	326,2	$1,21.10^{4}$	$6,22.10^{3}$
	^{163}Dy	24,97	^{163}Dy(γ,p)^{162}Tb	7,7 m	260 ,0	$5,42.10^{4}$	$2,22.10^{4}$
	^{164}Dy	28,18	^{164}Dy(γ,p)^{163}Tb	19,5 m	389,7	$6,31.10^{3}$	$4,22.10^{3}$
Ho	^{165}Ho	100	^{165}Ho(γ,n)^{164}Ho	29 m	91,4	$1,74.10^{6}$	$1,09.10^{6}$
Er	^{162}Er	0,136	^{162}Er(γ,n)^{161}Er	3,24 h	826,6	$4,86.10^{3}$	$7,87.10^{3}$
			^{161}Er$\longrightarrow$^{161}Ho	2,5 h	103,0	$3,10.10^{2}$	$1,48.10^{2}$
	^{168}Er	27,07	^{168}Er(γ,p)^{167}Ho	3,1 h	346,5	$4,82.10^{2}$	$2,70.10^{2}$
	^{166}Er	33,41	^{166}Er(γ,n)^{165}Er	10,36 h	48,6	$4,25.10^{4}$	$1,76.10^{5}$
Tm	^{169}Tm	100	^{169}Tm(γ,n)^{168}Tm	93,1 d	198,3	$4,15.10^{4}$	$1,49.10^{4}$
			^{169}Tm(γ,2n)^{167}Tm	9,24 d	531,8	$2,77.10^{2}$	$2,69.10^{2}$
			^{167}Tm$\longrightarrow$^{167m}Er	2,28 s	207,8	$1,80.10^{4}$	$6,57.10^{3}$

Table 1, continued

1	2	3	4	5	6	7	8
Yb	^{168}Yb	0,140	^{168}Yb(γ,n)^{167}Yb	17,5 m	176,2	$1,18.10^5$	$4,14.10^4$
			^{167}Yb $\dashrightarrow$ ^{167}Tm	9,24 d	531,8	$1,16.10^4$	$1,13.10^4$
			^{167}Tm $\dashrightarrow$ ^{167m}Er	2,23 s	207,7	$1,11.10^3$	$4,07.10^2$
	^{170}Yb	3,03	^{170}Yb(γ,n)^{169}Yb	30 ,7 d	197,9	$3,63.10^3$	$1,30.10^3$
	^{176}Yb	12,73	^{176}Yb(γ,n)^{175}Yb	4,19 d	396,3	$1,78.10^4$	$1,23.10^4$
Lu	^{175}Lu	97,40	^{175}Lu(γ,n)^{174}Lu	3,31 y	1241,8	$2,60.10^1$	$6,26.10^1$
			^{175}Lu(γ,2n)^{173}Lu	1,37 y	272,0	$2,09.10^2$	$8,93.10^1$
	^{176}Lu	2,60	^{176}Lu(γ,γ')^{176m}Lu	3,68 h	88,3	$1,33.10^4$	$8,92.10^3$
			^{176}Lu(γ,p)^{175}Yb	4,19 d	396,3	$3,80.10^1$	$2,62.10^1$
Hf	^{174}Hf	0,18	^{174}Hf(γ,n)^{173}Hf	24,0 h	123,6	$7,52.10^3$	$2,87.10^3$
	^{176}Hf	5,15	^{176}Hf(γ,n)^{175}Hf	70 d	343,4	$4,53.10^3$	$2,51.10^3$
	^{179}Hf	13,78	^{179}Hf(γ,γ') } ^{179m}Hf	18,67 s	217	$1,80.10^6$	$6,68.10^5$
	^{180}Hf	13,54	^{180}Hf(γ,n) }				
			^{180}Hf(γ,γ')^{180m}Hf	5,5 h	215,5	$1,03.10^3$	$3,80.10^2$
Ta	^{181}Ta	99,99	^{181}Ta(γ,n)^{180m}Ta	8,1 h	57,0	$5,20.10^5$	$1,15.10^6$
			^{181}Ta(γ,p)^{180m}Hf	5,5 h	215,5	$4,86.10^2$	$1,80.10^2$
			^{181}Ta(γ,2n) 179Ta	664,9 d	57,0	$2,10.10^1$	$4,64.10^1$
W	^{180}W	0,135	^{180}W(γ,n)^{179}W	37,5 m	133,9	$1,27.10^3$	$4,56.10^2$
			^{180}W(γ,n)^{180m}W	6,7 m	221,5	$3,28.10^4$	$1,22.10^4$
	^{182}W	26,4	^{182}W(γ,n)^{181}W	120,95 d	58,8	$1,83.10^3$	$3,91.10^3$
	^{183}W	14,4	^{183}W(γ,γ')^{183m}W	5,15 s	107,9	$7,79.10^3$	$3,44.10^3$
	^{186}W	28,4	^{186}W(γ,n)^{185m}W	1,67 m	131,5	$2,87.10^4$	$1,06.10^4$
Re	^{185}Re	37,07	^{185}Re(γ,n)^{184}Re	912 h	792,0	$5,65.10^3$	$3,77.10^3$
	^{187}Re	62,93	^{187}Re(γ,n)^{186}Re	90,64 h	137,1	$1,02.10^5$	$3,73.10^4$
			^{185}Re(γ,2n)183Re	70 d	162,3	$6,98.10^2$	$2,45.10^2$

Table 1, continued

1	2	3	4	5	6	7	8
Os	^{192}Os	41,0	^{192}Os(γ,n)^{191}Os	15,4 d	γ - peaks are not detected		
			^{191}Os$\longrightarrow$^{191m}Ir	4,88 s	129,4	$1,89.10^{5}$	$6,97.10^{4}$
Ir	^{191}Ir	38,5	^{191}Ir(γ,n)^{190}Ir	12,1 d	186,6	$1,06.10^{5}$	$3,74.10^{4}$
	^{193}Ir	61,5	^{193}Ir(γ,n)^{192}Ir	74,02 d	316,5	$2,63.10^{4}$	$1,28.10^{4}$
Pt	^{192}Pt	0,78	^{192}Pt(γ,n) 191Pt	3,0 d	538,9	$9,86.10^{2}$	$9,86.10^{2}$
	^{195}Pt	33,7	^{195}Pt(γ,γ')^{195m}Pt	4,02 d	98,8	$6,46.10^{3}$	$3,34.10^{3}$
	^{198}Pt	7,24	^{198}Pt(γ,n)^{197m}Pt	94,4 m	346,5	$5,75.10^{4}$	$3,22.10^{4}$
			^{197m}Pt$\longrightarrow$^{197m}Au	7,8 s	278,9	$1,58.10^{4}$	$6,87.10^{3}$
			^{198}Pt(γ,n)^{197}Pt	18,3 h	191,5	$3,19.10^{4}$	$1,13.10^{4}$
Au	^{197}Au	100	^{197}Au(γ,n)^{196}Au	6,18 d	355,7	$7,01.10^{5}$	$4,11.10^{5}$
Hg	^{196}Hg	0,146	^{196}Hg(γ,n)^{195m}Hg	40,0 h.	560,2	$3,20.10^{1}$	$3,33.10^{1}$
			^{195m}Hg$\longrightarrow$^{195m}Au	30,5 s	261,8	$2,72.10^{2}$	$1,12.10^{2}$
			^{196}Hg(γ,n)^{195}Hg	9,5 h	779,8	$5,23.10^{2}$	$8,01.10^{2}$
			^{195}Hg$\longrightarrow$^{195m}Au	30,5 s	261,8	$1,27.10^{3}$	$5,22.10^{2}$
	^{198}Hg	10,02	^{198}Hg(γ,n)^{197m}Hg	33,8 h	133,9	$2,95.10^{4}$	$1,08.10^{4}$
			^{198}Hg(γ,n)^{197}Hg	61,4 h	191,5	$1,01.10^{4}$	$3,57.10^{3}$
			^{197}Hg$\longrightarrow$^{197m}Au	7,8 s	278,9	$8,25.10^{2}$	$3,58.10^{2}$
	^{199}Hg	16,34	^{199}Hg(γ,γ')^{199m}Hg	42,6 m	158,4	$1,85.10^{6}$	$6,51.10^{5}$
			^{199}Hg(γ,p)^{198}Au	2,695 d	411,8	$1,00.10^{2}$	$7,18.10^{1}$
	^{204}Hg	6,36	^{204}Hg(γ,n)^{203}Hg	46,76 d	279,2	$1,02.10^{4}$	$4,42.10^{3}$
Tl	^{203}Tl	29,50	^{203}Tl(γ,n)^{202}Tl	12,2 d	439,4	$9,10.10^{4}$	$7,10.10^{4}$
			^{203}Tl(γ,2n)^{201}Tl	73,5 h	167,4	$4,59.10^{3}$	$1,61.10^{3}$
Pb	^{204}Pb	1,55	^{204}Pb(γ,n)^{203}Pb	52,1 h	279,2	$3,47.10^{4}$	$1,51.10^{4}$
			^{204}Pb(γ,γ')^{204m}Pb	66,9 m	911,7	$1,00.10^{2}$	$1,74.10^{2}$
Bi	^{209}Bi	100	^{209}Bi(γ,2n)^{207}Bi	38 y	γ - peaks are not detected		
			^{207}Bi$\longrightarrow$^{207m}Pb	0,8 s	569,7	$1,46.10^{1}$	$1,56.10^{1}$

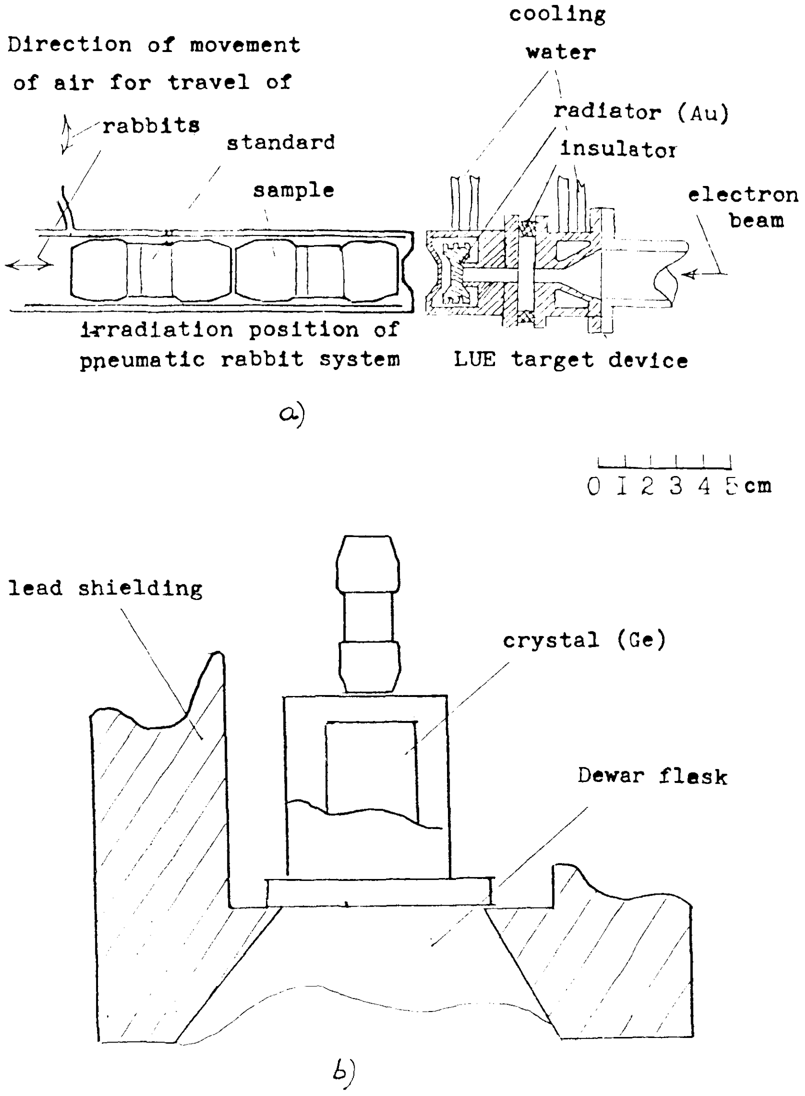

Fig. 1. Geometry of irradiation ("a") and measurement ("b") of samples:

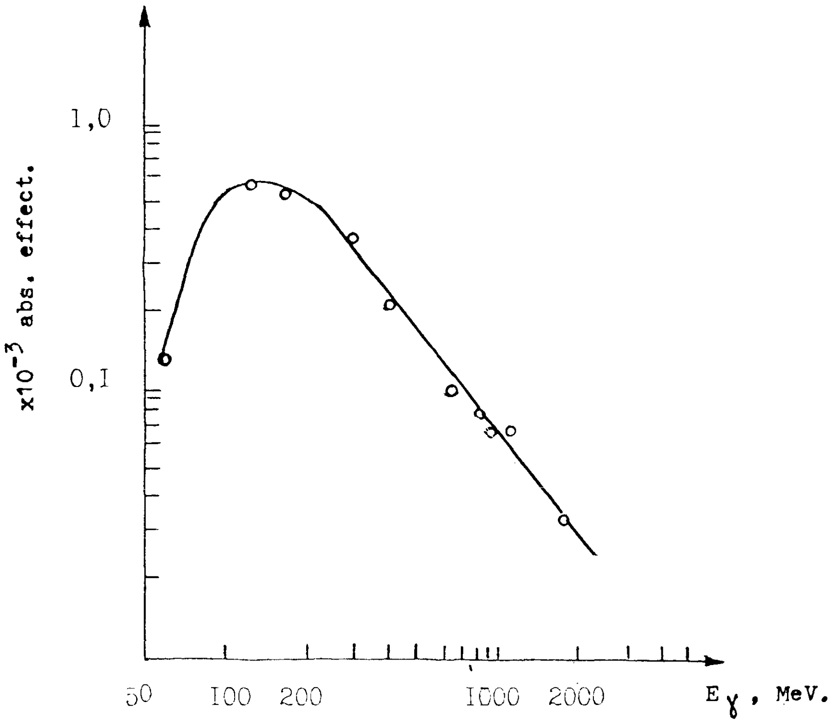

Fig. 2. Dependence of Ge(Li)-detector absolute efficiency on gamma-ray energy

References

1. Esperimentalnoe opredelenie etalonnoi chuvstvitelnosti gamma-aktivatsionnogo analyza. (Experimental determination of standard sensitivity of gamma-activation analysis.) "Sb. Radiatsionnaya tekhnika", vyp. 17, Atomizdat, Moscow (1979), p. 226-234. Auth.: B.V.Anisimov, Yu.N.Bourmistenko, B.N.Rivkin, Yu.V.Feoktistov, V.V.Philippov, A.P.Shpanov.
2. Computer-selected optimization of activation analysis methods. - "J. Radioanal. Chem.", 1977, v. 40, N 1, p. 147, Auth.: Yu.N.Bourmistenko, I.N.Ivanov, V.V.Sviridova, Yu.V.Feoktistov.
3. Choice of a mathematical model of the monoenergetic gamma-ray spectra. - Ibid. p. 155. Auth.: B.V.Anisimov, Yu.N.Bourmistenko, I.N.Ivanov, V.V.Philippov.
4. Matematicheskaya model dlaya approximatsii spectrov gamma-izlucheniaya, poluchennih s pomoshju Ge(Li) detectora. (Mathematical model for approximation of gamma-ray spectra, obtained with the help of Ge(Li)-detector.) "Sb. Radiatsionnaya tekhnika, vyp. 16, (in Russian), Atomizdat, Moscow (1978), p. 166. Auth.: B.V.Anisimov, Yu.N.Bourmistenko, I.N.Ivanov, V.V.Philippov.

On the Sensitivity Evaluation for On-Stream Elemental Analysis using Neutron and Photoactivation Techniques

I.N.Ivanov, E.A.Zakharov, V.A.Kasatkin,
E.R.Kartashev, V.A.Mashinin, Yu.V.Feoktistov,
V.L.Tchulkin
All Union Research Institute of Radiation Engineering,
Moscow

Summary

The paper discusses the data of calculations of neutron and photoactivation effects of moving substances, in particular, bulk materials moving on a conveyor belt and solution streams. The calculated data on minimum detectable concentrations of the various elements are given.

At present neutron and photoactivation techniques become the increasing importance not only for elemental analysis of individual samples, but for continuous analysis of ores, solutions and industrial products. Examples of application of these techniques for on-stream analysis of solutions, ores and coal on a conveyor belt are known [1-2] .

It is possible to select the elements which are appropriate for on-stream activation determination in substances by means of a criterion that we named "rapidity factor" [3] . This factor is expressed by the following formula:

$$F_r = \frac{\sigma_n}{T_{1/2}}$$

where σ_n is activation cross-section per 1 g of the element of interest; $T_{\frac{1}{2}}$ is the half-life of a nuclide produced as a result of the reaction. Practically, the factor F_r evaluates the rate of the activity rise during the irradiation. In paper [3] F_r^* values are tabulated.

However, in F_r factor the geometrical conditions of irradiation and measurement, properties of the radiation and the detector characteristics haven't been taken into account. That's why optimal conditions for analysis may be defined and sensitivity of on-stream determination of various elements of interest may be calculated with improved accuracy by means of the following general expression:

$$N = \Sigma_a m \frac{F}{\lambda} \varepsilon e^{-\lambda t_a} e^{-\lambda t_{tr}} \int_0^{t_a} \varphi(t_a) e^{\lambda t_a} dt_a \int_0^{t_m} K(t_m, \mu, r) e^{-\lambda t_m} dt_m \quad (1)$$

where N is the number of pulses registered by the detector from on-stream activated material; Σ_a is value of macroscopic cross-section of activation; m is the mass of element of interest; F is the flow rate; $\varphi(t_a)$ is the intensity of primary radiation or neutron flux; $K(t_m, \mu, r)$ is the coefficient characterizing the conditions of registration for the induced radiation; ε is the efficiency of registration of the above-mentioned radiation; λ is the decay constant of the nuclide produced; t_a, t_m, t_{tr} are the effective periods of activation, measurement and transportation of substance to be analysed from the position of activation to the position of measurement; r is the distance between the elementary volume of material and the detector.

In this expression the fact is taken into account that each elementary volume of the material when moving by the source of activating radiation is irradiated with the variable neutron or photon flux. The registered value of activity induced is also variable due to the substance motion by the radiation detector and due to the decay of the nuclides during the period of measurement.

On the basis of that formula optimum conditions have been calculated for on-stream activation of solutions (that is, the shape and volume of activation and measurement cells as well as the flow rate have been determined). Besides, optimum conditions have been calculated for on-stream activation analysis of bulk material on the conveyor belt (that is, width and height of the material on the conveyor belt as well as the speed of the conveyor were determined) for various nuclides. In some cases there is a definite discrepancy between the calculated and experimental data by the determining the optimum conditions (for instance, the flow rate for given cell volumes). The discrepancy may be explained by inaccuracies in values of activation cross-sections, decay constants, radiation absorption factors which have been taken for calculations as well as by errors in measurement and calculations of neutron or photon flux density.

The assumption is confirmed by the fact that if the calculated data are normalized per experimental data normalization factor remains constant for the given nuclide and given activation analysis system.

On the basis of formula (1) minimum detectable concentration values have been calculated of on-stream determination of the majority of elements in solution streams or in bulk materials on the moving conveyor belt (see Table 1 and 2).

Table 1

Minimum detectable concentrations of the various elements using on-stream activation of solutions (neutron yield is $5 \cdot 10^8$ n/s, duration of the measurement period is up to 1 h).

Minimum of detectable concentration, mg per l	Thermal-neutron activation	Fast-neutron activation
up to 1	Sc, In, Eu, Rh, Mn, Dy, Hf, Sm, Ag, V, I, Br, Ho, Lu, Au, W, Se, Co, Cu	P, Pr, Br, Sb
1-10	Y, Ga, Al, Cl	Cl, Si, Cu, Cr, Zr
10-100	Ge, Pd, Ir, Te, Yb, As, Mg	F
100-1000	Ba, Re, Nb, La	I, Mg, Mn, Zn, Cl, Na, Ge, Ir, Ag, V

Table 2

Minimum detectable concentrations of the various elements in bulk materials on the moving conveyor belt using neutron activation (neutron yield is 10^9 n/s, duration of the measurement period is up to 1 h.

Minimum of detectable concentrations, %	Thermal-neutron activation	14-MeV-neutron activation	Fast-neutron activation (α,n)-source
10^{-3}	Se, V, Mn, Co, In, Sb, Hf, Ir	-	-
10^{-3}-10^{-2}	Al, Br, I, Pr,W	Si, Cu, Y, Ba, Pr, Hg	-
10^{-2}-10^{-1}	Na, Cu, Se,Ag, Nd, Sm, Dy, Ca, Yb	O, F, Na, Al, P, Cr, Fe,Sb, Br, Ag, Tl, Ba, Ce, Nd	F, Na, Al, Si

The calculation data satisfactorily agree with the experimental data obtained as a result of on-stream neutron activation analysis of solutions containing indium, selenium, aluminium, fluorine and also bulk materials containing aluminium and silicon.

The opportunity of applying the bremsstrahlung generated by the electron accelerator for photoactivation analysis and sorting gold-bearing ores on the conveyor belt has been analysed.

Short half-life of ^{197m}Au ($T_{\frac{1}{2}}$ = 7.8 s) nuclide provides for high rapidity and efficiency of analysis. Relative induced saturation activity has been calculated for ore layers of various width and height on the conveyor belt, the speed of the conveyor being in the range of 0.002 to 0.1 m/s. Results given in paper [4] have been applied for the calculation of yield of ^{197m}Au nuclide produced in the ^{197}Au(γ ,γ')^{197m}Au reaction. The results of calculations demonstrate the most satisfactory agreement with the experimental results.

The calculation of activation effect with application of formula (1) and the formula given in paper [5] have shown that the minimum detectable concentration value for gold is 0.5 g/t, by 8 MeV bremsstrahlung energy, 700 μA electron current, 100 s, registration period duration.

References

1. J.R.RHODES. Radioisotope Neutron Activation for On-Stream Process Analysis. - In: Neutron Sources and Application, CONF-710402, v. III, April,1971.
2. E.R.KARTASHEV, A.S.SHTAN'. Nejtronnye metody nepreryvnogo analiza sostava veshchestva (Continuous neutron activation analysis of substance composition), Atomizdat, Moscow (1978).
3. E.R.KARTASHEV, O.K.NIKOLAENKO, I.A.DANIL'CHENKO e.a. O nekotorykh kriteriyakh ekspressnosti aktivatsionnogo analyza (On some criteria of rapidity of activation analysis), Atom. Energ., 22 (1967) 1, p. 54, 55.
4. L.MEYER-SCHUTZMEISTER, W.L.TELEGDI. Inelastic Scattering of Photons by ^{197}Au, Phys. Rev., 104 (1956), 1, p. 185.
5. Yu.N.BOURMISTENKO, B.N.RYVKIN, Yu.V.FEOKTISTOV e.a. Raschet optimal'noy geometrii oblucheniya obraztsa bol'shoy massy v gamma-aktivatsionnom analize (Calculation of optimal irradiation geometry of large-mass samples for gamma-activation analysis). - V kn. "Voprosy atomnoy nauki i tekhniki". Ser. "Radiatsionnaya tekhnika", vyp. 20, Atomizdat, Moscow (1980), p. 94-104.

Appendices

IAEA Consultants' Meeting on
Nuclear Data for Bore-Hole and Bulk-media Assay
Using Nuclear Techniques

Krakow, Poland
14 - 18 November 1983

CALIBRATION GUIDANCE PROVIDED BY THE INTENSITIES OF URANIUM AND THORIUM GAMMA RAYS

L. Løvborg and S.P. Nielsen
Risø National Laboratory
DK-4000 Roskilde, Denmark

ABSTRACT
(contributed paper)

The internationally adopted calibration procedures for exploration gamma-ray measurements are based on surface and borehole models which are made of concrete with radioactive admixtures. Instrumental sensitivity factors recorded on surface models in a number of countries have demonstrated the difficulty of establishing the calibration grade of uranium-loaded concrete. This difficulty arises from the unknown disequilibrium associated with the possible migration of radon-222 in a porous material. A similar problem does not occur with concrete containing an admixture of thorium or potassium. Natural thorium has a composite emission spectrum of the same complexity as that of uranium with daughters and may serve as a reference element in total-count assays of radiometric uranium grades. The theoretical ratio between the count rates produced by unit equilibrium concentrations of thorium and uranium can be estimated rather easily from transport calculations based on the intensities of the gamma rays in the two decay series. The intensities presently contained in the Evaluated Nuclear Structure Data File (ENSDF) suggest a ratio of 0.41 ppm eU per ppm eTh. This is an almost 15% smaller value than that estimated from the emission spectra which have been used for the calculation of terrestrial exposure rates since 1972.

CALIBRATION GUIDANCE PROVIDED BY THE ABSOLUTE INTENSITIES OF URANIUM AND THORIUM GAMMA RAYS

L. Løvborg and S.P. Nielsen
Risø National Laboratory
DK-4000 Roskilde, Denmark

1. INTRODUCTION

In 1976 a group of IAEA consultants proposed a unit of radioelement concentration for the reporting of total-count gamma-ray measurements in uranium exploration [1]. The unit is known as the "Ur" and is based on the instrument response produced by 1 ppm U in radioactive equilibrium. It is finding increasing acceptance among exploration geologists as an adequate means of removing the ambiguity of instrument readings stated in counts per second.

In principle the calibration of counter probes in terms of the Ur is performed by manufacturing a geological source model which accomodates the field geometry and is loaded with a known concentration of uranium in equilibrium. Over the past decade, large concrete calibration pads and borehole models prepared from naturally radioactive aggregate materials have been installed by survey organisations in a number of countries [2,3]. Monitoring results for several of these facilities substantiate a high potential for calibration error due to the emanation of Rn-222 from a source aggregate of uranium ore [4,5]. A similar error cannot occur with sources constructed from thorium or potassium aggregates. Therefore, if the uranium gamma-ray equivalent of thorium or potassium can be reliably estimated, one or the other of these two radioelements might be a relevant substitution for uranium in the sources required for a world-wide implementation of the Ur.

A potassium concentration of 1% K corresponds to roughly 1 Ur. The exact correspondance is a monotonous function of the energy cut-off for the counter, and this inconvenience excludes total-count calibration with potassium sources [6]. Thorium generates an amplitude spectrum that makes the conversion of 1 ppm Th into Ur almost independent of the energy threshold. The thorium conversion factor is primarily controlled by the gamma and X-ray intensities in the decay series of Th-232, U-238, and U-235. Its numerical value for scintillation probes with threshold settings below 150 keV is 0.4 Ur/ppm Th with a present overall uncertainty of 5%. Improved theoretical knowledge of this auxiliary calibration factor is desirable and may be obtained from gamma-ray transport calculations based on reliable U and Th decay data.

This paper briefly reviews some of the data sources which provide the intensities of the U and Th decay gamma rays. The periodically updated Evaluated Nuclear Structure Data File (ENSDF) is of particular relevance as an input source for the calculation of count rates produced by U and Th.

2. DATA SOURCES

The first reasonably complete and accurate tabulation of the photon emissions in the U and Th decay series was printed in 1969 in a Russian textbook on field gamma-ray spectrometry [7]. A few years later, in 1972, H.L. Beck of the U.S. Health and Safety Laboratory (HASL) published an extensive compilation of gamma and X-rays from the decay of U-238 and Th-232 [8]. An almost simultaneous compilation by Smith and Wollenberg [9] did not include the X-rays, but provided the gamma-ray emissions from U-235 with daughters. Beck's list of photon emissions has been used at HASL and Risø for the calculation of terrestrial gamma-radiation fields and resulting detector responses [10-15]. Other tabulations suited for computerized modelling of radiation measurements are found in NCRP Report No. 58 [16] and Kocher's "Radioactive Decay Data Tables" [17]. These more recent data sources are based on the ENSDF which is maintained by the Nuclear Data Project at Oak Ridge [18].

Table I shows intensities reported in these references for three intense gamma rays from the U-238 daughters, Pb-214 and Bi-214. The table includes a very recent determination by D.G. Olson [19].

TABLE I. Reported intensities of Pb-214 and Bi-214 gamma rays.

Year	Ref.	% Intensity		
		Pb-214 352 keV	Bi-214 609 keV	Bi-214 1765 keV
1969	[7]	37.7	47.1	16.3
1972	[8]	35.0	43.0	14.7
1972	[9]	36.3	42.8	16.7
1978	[16]	34.3 +- 0.9	42.6 +- 1.1	14.6 +- 0.4
1981	[17]	37.2 +- 1.1	46.3 +- 1.2	15.8 +- 0.5
1983	[19]	35.8 +- 0.5	45.0 +- 0.7	15.4 +- 0.2

These selected data, except those from Ref. 19, demonstrate a rather modest improvement in the knowledge of the U emission spectrum over the past fifteen years. The noticeable experimental progress obtained in Ref. 19 indicates that the photon intensities required for the calculation of terrestrial gamma radiation may become determined with 1 or 2% accuracy within the next few years. Some of the intense emissions from Ac-228 in the Th decay series are still very imprecisely known [16,17] and necessitate a particular experimental effort for elucidating the thorium spectrum.

3. CALCULATED GAMMA RADIATION

Direct and scattered gamma radiation calculated for a geological source varies in a proportionate manner with the line intensities assumed in the calculation. Table II shows estimated contributions from U-238 and Th-232 with daughters to the exposure rate one meter above an infinite and plane soil medium. These estimates are from runs with the double-PL transport code GAMP1 and its associated code GFX for the conversion of polynomial flux expansion coefficients into numerical flux or dose [14,20].

TABLE II. Calculated exposure rates at 1 m from 1 ppm U and 1 ppm Th in the ground.

Photon emission data	μR/h	
	U-238	Th-232
Ref. 8	0.62	0.31
ENSDF (1981)	0.65 +- 0.01	0.29 +- 0.01

The first result is based on Beck's 1972 compilation of gamma and X-ray intensities. It is identical to that previously reported by HASL [10] and quoted in the 1977 UNSCEAR report on sources and effects of ionizing radiation [21]. The second result was obtained from the emission data and half-lives contained in an ENSDF tape copy received at Risø in September 1981. Uncertainties ascribed to the ENSDF result were assessed by perturbing the line intensities in accordance with their reported standard deviations.

This example demonstrates that thorium relatively to uranium is a less intensive source of terrestrial gamma radiation than anticipated up to the present. While U radiation calculated from the 1981 update version of the ENSDF is of 1% accuracy, the corresponding Th radiation is only 3% accurate in consequence of the current imprecise knowledge of the Ac-228 gamma rays.

4. THE URANIUM EQIVALENT OF THORIUM

Scintillation counter responses to U and Th radiation can be predicted by incorporating the decreasing counting efficiency with increasing energies in the transport code providing the flux energy spectrum. Calculated uranium and thorium count rates vary sympathetically with the size of the NaI(Tl) detector and the counting geometry and justify the assumption of a constant ratio between readings produced by 1 ppm Th and 1 ppm U [6,22].

Table III shows two computational estimates of the uranium equivalent of thorium. The first value dates from 1976 [15] and is based on the HASL compilation with additional inclusion of the most intensive U-235 gamma rays listed in the 1974 Atomic and Nuclear Data Tables [23]. The second value is from a recent feasibility study on the use of thorium as an admixture for total-count calibration blocks [6]. This study included an experimental determination also presented in Table III.

TABLE III. Suggested values of the U equivalent of Th for scintillation counters.

Estimation method	Photon emission data	ppm U/ppm Th
Calculation (1)	Refs. 8 and 23	0.44
Calculation (2)	ENSDF (1981)	0.41 +- 0.01
Experiment (3)		0.37 +- 0.01
(2) and (3) combined		0.39 +- 0.02

The result obtained from the ENSDF emission data is in reasonable agreement with the experimental determination, and the combined estimate presented in the last row of the table is probably the best one available to-day.

5. CONCLUSION

An overall uncertainty of about 5% on the uranium gamma-ray equivalent of thorium is not acceptable in the use of thorium as a substitution for uranium in total-count calibration sources for the exploration and evaluation of uranium resources. Although an improved future determination might be provided experimentally, the additional availability of a better computational estimate would be very helpful and perhaps just as reliable. A continued updating of the U and Th photon emission data in the ENSDF and other relevant compilations is therefore of great interest to laboratories engaged in research on the calibration of field equipment for radioactivity measurements.

REFERENCES

[1] "Radiometric Reporting Methods and Calibration in Uranium Exploration", Technical Report Series No. 174, International Atomic Energy Agency, Vienna (1976).

[2] KILLEEN, P.G., Geol. Surv. Canada, Econ. Geol. Report 31 (1979) 163.

[3] LØVBORG, L., "Uranium Exploration Methods" (Proc. Symp. Paris), OECD, Paris (1982) 671.

[4] LØVBORG, L., BØTTER-JENSEN, L., KIRKEGAARD, P., Geophys., Vol. 43 (1978) 543.

[5] STROMSWOLD, D.C., GJBX-99 (78), Bendix Field Eng. Corp. (1978).

[6] LØVBORG, L., Risø-R-490, Risø Natl. Laboratory (1983).

[7] KOGAN, P.M., NAZAROV, I.M., FRIDMAN, S.D., "Osnovy gamma spektrometrij prirodnykh shred" (Gamma Spectrometry of Natural Environments and Formations), Atomizdat, Moscow (1969).

[8] BECK, H.L., HASL-262, U.S. Atomic Energy Com. (1972).

[9] SMITH, A.R., WOLLENBERG, H.A., "The Natural Radiation Environment II" (Proc. Conf. Houston, 1972), Vol. 2, ERDA Conf.-720805-P2 (1975) 181.

[10] BECK, H.L., DeCAMPO, J., GOGOLAK, C., HASL-258, U.S. Atomic Energy Com. (1972).

[11] BECK, H.L., "The physical properties of environmental radiation fields and their utility for interpreting aerial measurements" (in Proc. Conf. Am. Nucl. Soc., Las Vegas, 1977).

[12] LØVBORG, L., KIRKEGAARD, P., Nucl. Instrum. Meth., Vol. 121 (1974) 239.

[13] LØVBORG, L., KIRKEGAARD, P., Risø Report 317, Danish Atomic Energy Com. (1975).

[14] KIRKEGAARD, P., LØVBORG, L., J. Computational Phys., Vol. 36 (1980) 20.

[15] LØVBORG, L., KIRKEGAARD, P., CHRISTIANSEN, E.M., "Exploration for Uranium Ore Deposits" (Proc. Symp. Vienna, 1976), International Atomic Energy Agency, Vienna (1976) 217.

[16] "A Handbook of Radioactivity Measurements", NCRP Report No. 58, National Council on Radiation Protection and Measurements, Washington, D.C. (1978).

[17] KOCHER, D.C., "Radioactive Decay Data Tables", Technical Information Center, U.S. Dept. Energy (1981).

[18] EWBANK, W.B., IAEA-TECDOC-232, International Atomic Energy Agency, Vienna (1980).

[19] OLSON, D.G., Nucl. Instrum. Meth., Vol. 206 (1983) 313.

[20] KIRKEGAARD, P., LØVBORG, L., Risø-R-392, Risø Natl. Laboratory (1979).

[21] "Sources and Effects of Ionizing Radiation", United Nations Scientific Committee on the Effects of Atomic Radiation, New York (1977).

[22] "Gamma-Ray Surveys in Uranium Exploration", Technical Report Series No. 186, International Atomic Energy Agency, Vienna (1979).

[23] BOWMAN, W.W., MacMURDO, K.W., "Radioactive Decay Gammas", At. Data Nucl. Data Tables, Vol.13 (1974).

"BULK-MEDIA ASSAY USING NUCLEAR TECHNIQUES IN PORTUGAL"

F.G. Carvalho
Institute of Energy, LNETI,
Sacavem, Portugal

ABSTRACT

Introduction: general description of the instruments and techniques used (XRF, XR Diffraction, PIXE, RBS and NRA). Bulk assay of industrial raw-materials. Soils (including simulation and required nuclear data; instrument development). Radioactive ores: prospection and bulk assay for process control; experience of the Geology and Mining Dept; programmed SSNTD work. Thermal Neutron Activation Work. Difficulties and prospects for future work; fast neutron activation analysis; delayed neutron and prompt gamma ray analysis. The importance of AIEA support.

Appendix 2

IAEA Consultants' Meeting on
Nuclear Data for Bore-hole and Bulk-media Assay
Using Nuclear Techniques
Krakow, Poland
14 - 18 November 1983

List of Participants

EGYPT:

Galal Khalil
Alexandria University
Faculty of Science
Dept. of Physics
Alexandria

FRANCE:

Patrice Dumesnil
IRDI/DEIN
Centre d'Etudes Nucléaires de
Saclay
B.P. N° 2
F-91191 Gif-sur-Yvette

Francoise Massines
SNEAP
26 Avenue des Lilas
Bat. W, Service MPM
64000 PAU

GERMANY, Fed. Rep.:

W. Michaelis
Forschungszentrum Geesthacht GmbH
GKSS, Postfach 1160
D-2054 Geesthacht

I. Wendt
Bundesanstalt für Geowissenschaften und
Rohstoffe
Postfach 51 01 53
D-3000 Hannover 51

HUNGARY:

J. Csikai
Institute of Experimental Physics
Kossuth Lajos University
P.O. Box 105
H-4001 Debrecen

G. Petoe
Institute of Experimental Physics
Kossuth Lajos University
P.O. Box 105
H-4001 Debrecen

JAPAN:

Toshinobu Itoh
Japan Petroleum Exploration Co. Ltd. (JAPEX)
Geothermal Division
2-17-27, Akasaka, Minato-ku
Tokyo 107

NORWAY:

Karen Garder
Institute of Energy Technology
Industrial Chemistry Department
N-2007 Kjeller

POLAND:

J.A. Czubek
Institute of Nuclear Physics
Ul. Radzikowskiego 152
PL-31-342 Krakow

A. Kreft
Institute of Physics and Nuclear Techniques
Academy of Mining and Metallurgy
al. Mickiewicza 30
PL-30-059 Krakow

K. Morstin
Institute of Physics and Nuclear Techniques
Academy of Mining and Metallurgy
al. Mickiewicza 30
PL-30-059 Krakow

K. Przewlocki
Institute of Physics and Nuclear Techniques
Academy of Mining and Metallurgy
al. Mickiewicza 30
PL-30-059 Krakow

UNITED KINGDOM:

C.G. Clayton
Applied Nuclear Geophysics Group
NUTMAQ, Mining Instrumentation
Building 7
AERE Harwell, OXON. OX11 ORA

D. Mellor
British Petroleum Co. Ltd.
Research Centre
Sunbury-on-Thames

R. Peveraro
Britoil PLC
150 St. Vincent Street
Glasgow G2 5LJ, Scotland

L.G. Sanders
NUTMAQ, Mining Instrumentation
Building 7
AERE Harwell, OXON. OX11 ORA

M. Underwood
British Petroleum Co. Ltd.
Research Centre
Sunbury-on-Thames

U.S.S.R.:

E.R. Kartashev
All Union Research Institute of
Radiation Engineering
Varshaveskoje Shosse 46
Moscow

D.A. Kozhevnikov
Gubkin's Moscow Oil Chemical & Gas
Industry Institute (Kathedra GIS)
Minkhiop
Moscow 117296

U.S.A.:

S. Antkiw
Schlumberger-Doll Research
P.O. Box 307
Ridgefield, Conn. 06877

Richard L. Caldwell
Mobil Research and Development Corporation
Research Department, P.O. Box 345100
13777 Midway Road
Farmers Branch, Texas 75234

Frank E. Senftle
U.S. Geological Survey
National Center 12201
Sunrise Valley Drive
Reston, Virginia 22092

VIETNAM:

Tran Dai Nghiep
Institute of Physics
Hanoi

I.A.E.A.:

V. Ferronsky
Director
Division of Research and Laboratories
International Atomic Energy Agency
Wagramerstr. 5, P.O. Box 100
A-1400 Vienna

K. Okamoto
Scientific Secretary
IAEA Nuclear Data Section
Wagramerstr. 5, P.O. Box 100
A-1400 Vienna

J.J. Schmidt
IAEA Nuclear Data Section
Wagramerstr. 5, P.O. Box 100
A-1400 Vienna

Observers:

Guests:

J. Chmielewski (National Atomic Agency, Warsaw)

M. Miesowicz (Academy of Mining and Metallurgy, Krakow

Local observers:

J. Massalski
J. Loskiewicz
A. Zuber
J. Niewodniczanski
S. Kalita
J. Bogacz
K. Drozdowicz
T. Jakiel
M. Konopka
H. Mikolajczyk
W. Przybylowicz